JOURNAL OF BIOLOGICAL REGULATORS & HOMEOSTATIC AGENTS

Volume 33, No. 6, November - December, 2019

CONTENTS

EDITORIAL

FACTORS ADVERSELY INFLUENCING NEURODEVELOPMENT

T.C. THEOHARIDES[1,2,3,4], M. KAVALIOTI[5] and R. MARTINOTTI[6]

[1]Laboratory of Molecular Immunopharmacology and Drug Discovery, Department of Immunology, Tufts University School of Medicine, Boston. MA, USA; [2]Sackler School of Graduate Biomedical Sciences, Tufts University School of Medicine, Boston, MA, USA; [3]Department of Internal Medicine, Tufts University School of Medicine and Tufts Medical Center, Boston, MA, USA; [4]Department of Internal Medicine, Tufts University School of Medicine and Tufts Medical Center, Boston, MA, USA; [5]Graduate Program in Education, Lesley University, Cambridge, MA, USA; [6]Casa di Cura Villa San Marco, Ascoli Piceno, Italy

Received September 6, 2019 – Accepted October 4, 2019

Neurodevelopment has been studied extensively, especially in respect to abuse, anoxia, nutritional status and prematurity/low birth weight. However, less attention has been paid to innate and environmental factors, as well as to inflammatory conditions that may adversely affect neurodevelopment and learning in children. These include heavy metals, herbicides and polyvinyl chlorides (PVCs), mycotoxins, viral infections and Lyme disease-associated pathogens, as well as number of conditions such as chronic inflammatory response syndrome (CIRS) and Mast cell activation syndrome (MCAS). Early recognition of factors/conditions that could interfere with neurodevelopment is critical. Corrective actions, including the use of some unique natural flavonoids, could have lasting beneficial results.

There has been an unexplained increase in children with neurodevelopmental and learning problems (1, 2). Neurodevelopment has been studied extensively. More recently, atopic diseases (3) such as allergies (4, 5), asthma (6), and atopic eczema (7) have been significantly associated with behavioral and learning difficulties, including attention deficit hyperactivity disorder (ADHD) and autism spectrum disorder (ASD). Emotional stress (8, 9) both prenatally (10, 11), as well as in children (12, 13) has also been associated with increased risk of a child developing ADHD or ASD.

Less attention has been paid to innate and environmental factors, as well as inflammatory conditions that may adversely affect neurodevelopment and learning in children (14, 15). These include heavy metals, herbicides and polyvinyl chlorides (PVCs) (Table I), as well as a variety of inflammatory conditions (Table II) such as mold, Lyme disease, viral infections and especially chronic inflammatory response syndrome (CIRS) and mast cell activation syndrome (MCAS).

Recent evidence indicates that inflammation of the brain (8, 16), due to activation of microglia (17, 18) may be involved in neurodevelopment and in the pathogenesis of neuropsychiatric disorders (19, 20) but the reasons are still unknown. We reported that the peptides corticotropin-releasing hormone (CRH)

Key words: autism, brain, mast cells, flavonoids, inflammation, learning, neurodevelopment

Corresponding Author:
Theoharis C. Theoharides, MS, MPhil, PhD, MD
Department of Immunology,
Tufts University School of Medicine,
136 Harrison Avenue, Suite 304,
Boston, MA 02111, USA
Tel.: +1 617 636 6866 - Fax: +1 617 636 2456
e-mail: theoharis.theoharides@tufts.edu

0393-974X (2019)

Table I. *Factors adversely influencing neurodevelopment.*

- Electromagnetic waves
- Heavy metals
  - ✓ Aluminum
  - ✓ Arsenate
  - ✓ Lead
  - ✓ Mercury
- Herbicides
  - ✓ Atrazine
  - ✓ Glyphosate
- Inflammatory cytokines
  - ✓ IL-6, IL-31, IL-33, TNF
- Mitochondrial DNA
- Mycotoxins
  - ✓ Ochratoxin A
- Neuroendocrine disruptors
  - ✓ Polyphenols
  - ✓ Xenoestrogens
  - ✓ Bipsphenol A
  - ✓ Polyvinyl chloride
- Neuropeptides
  - ✓ Neurotensin
  - ✓ Substance P
- Neurotransmitters
  - ✓ Aspartate
  - ✓ Glutamate
  - ✓ Histamine
- Pathogens
  - ✓ Babesia
  - ✓ Bartonella
  - ✓ Borrelia
  - ✓ CMV
  - ✓ EBV
  - ✓ Fungi
- Reactive Oxygen Species
- Toxins
- Venoms
- Xenobiotics

Table II. *Conditions adversely affecting neurodevelopment.*

- Abuse
- Allergies
- Anoxia
- Anxiety disorder
- Asthma
- Attention deficit hyperactivity disorder
- Atopic dermatitis (eczema)
- Avitaminosis
- Chronic inflammatory response syndrome
- Cyclic vomiting syndrome
- Food intolerance
- Hyperthermia
- Hypothyroidism
- Idiopathic urticaria
- Maternal deprivation
- Mastocytosis
- Mast cell activation syndrome
- Multiple chemical sensitivity syndrome
- Neglect
- Non-IgE food allergy
- Nutrition (poor)
- Pediatric acute neuropsychiatric syndrome
- Rhinosinusitis

and neurotensin (NT) are increased in the serum of patients with ASD (21, 22), and can activate human microglia to secrete the pro-inflammatory cytokine IL-1β and chemokine CXCL8 IL-8 (22). These molecules may be produced inside the brain or enter the brain through a disrupted blood-brain barrier (BBB), documented in psychiatric disorders (23) and in ASD (24), due to molecules such as histamine released from brain mast cells (25). Mast cells can stimulate microglia (26) via histamine (27), leading to secretion of pro-inflammatory mediators.

Histamine is secreted from activated mast cells in atopic diseases and mastocytosis (28), but is also found in many foods such as cheese, fermented milk and alcoholic products, nectarines, ripe fruits, sardines, sauerkraut, spinach, spices and tuna. Levels of histamine can build up in patients who have reduced activity of the histamine degrading enzyme diamine oxidase (DAO). Both the activity and the gene expression of DAO can be tested, and DAO can be administered as a dietary supplement that would reduce histamine levels in the intestine. This

approach is complimentary to giving antihistamines, preferably rupatadine (not available in the US, but can be compounded) because it can also inhibit mast cell and eosinophil activation (29) since these cell types are stimulated especially in children exposed to mold (30). However, it should be noted that high doses of antihistamines could interfere with learning and motivation (31).

Natural flavonoids are increasingly discussed as therapeutic agents for neurodegenerative disorders (32, 33). Especially, luteolin (5,7,3´,4´-tetrahydroxyflavone) has potent anti-oxidant, anti-inflammatory (34, 35), anti-allergic (36), and neuroprotective (34) actions including significant improvement of children with ASD (37, 38). The purest (>87%) luteolin, with the greatest oral absorption due to its liposomal formulation in olive kernel extact, is found in the dietary supplements BrainGain®, NeuroProtek®, and Purelut®; a new product will combine luteolin with Ashwagandha, which has anti-anxiety properties (39). We recently showed that the structurally-related methoxyluteolin (5,7,3´,4´-tetramethoxyflavone) is more potent than luteolin (22, 40) and has even better oral absorption (41) but to date has beem formulated only in the anti-inflammatory skin lotion GentleDerm® (42).

Addressing offending conditions and/or minimizing the detrimental effects of suspect molecules as early as possible is of great importance in improving neurodevelopment, cognition and learning in children.

DISCLOSURE**:** TCT is the inventor of US patents No. 7,906,153; No. 8,268,365 and No. 9,050,275 for the treatment of neuroinflammatory conditions.

REFERENCES

1. Leigh JP, Du J. Brief report: forecasting the economic burden of autism in 2015 and 2025 in the United States. J Autism Dev Disord 2015; 12:4135-39.
2. Centers for Disease Control and Prevention. CDC estimates 1 in 59 children has been identified with autism spectrum disorder. 4-30-2018. https://www.cdc.gov/features/new-autism-data/index.html.
3. Theoharides TC, Tsilioni I, Patel AB, Doyle R. Atopic diseases and inflammation of the brain in the pathogenesis of autism spectrum disorders. Transl Psychiatry 2016; 6(6):e844.
4. Lyall K, Van de WJ, Ashwood P, Hertz-Picciotto I. Asthma and allergies in children with autism spectrum disorders: results from the CHARGE Study. Autism Res 2015; 8(5):567-74.
5. Liao TC, Lien YT, Wang S, Huang SL, Chen CY. Comorbidity of atopic disorders with autism spectrum disorder and attention deficit/hyperactivity disorder. J Pediatr 2016; 171:248-55.
6. Kotey S, Ertel K, Whitcomb B. Co-occurrence of autism and asthma in a nationally-representative sample of children in the United States. J Autism Dev Disord 2014; 44(12):3083-88.
7. Billeci L, Tonacci A, Tartarisco G, Ruta L, Pioggia G, Gangemi S. Association between atopic dermatitis and autism spectrum disorders: a systematic review. Am J Clin Dermatol 2015; 16(5):371-88.
8. Angelidou A, Asadi S, Alysandratos KD, Karagkouni A, Kourembanas S, Theoharides TC. Perinatal stress, brain inflammation and risk of autism-Review and proposal. BMC Pediatr 2012; 12(1):89.
9. Theoharides TC, Kavalioti M. Effect of stress on learning and motivation-relevance to autism spectrum disorder. Int J Immunopath Pharmacol 2019; 33:2058738419856760
10. Beversdorf DQ, Manning SE, Hillier A, et al. Timing of prenatal stressors and autism. J Autism Dev Disord 2005; 35(4):471-78.
11. Ronald A, Pennell CE, Whitehouse AJ. Prenatal maternal stress associated with ADHD and autistic traits in early childhood. Front Psychol 2010; 1:223.
12. Rodgers J, Glod M, Connolly B, McConachie H. The relationship between anxiety and repetitive behaviours in autism spectrum disorder. J Autism Dev Disord 2012; 42(11):2404-9.
13. van Steensel FJ, Bogels SM, Perrin S. Anxiety disorders in children and adolescents with autistic spectrum disorders: a meta-analysis. Clin Child Fam Psychol Rev 2011; 14(3):302-17.
14. Ratnaseelan AM, Tsilioni I, Theoharides TC. Effects of mycotoxins on neuropsychiatric symptoms and immune processes. Clin Ther 2018; 40(6):903-17.
15. Rossignol DA, Frye RE. Evidence linking oxidative stress, mitochondrial dysfunction, and inflammation

in the brain of individuals with autism. Front Physiol 2014; 5:150.
16. Hagberg H, Gressens P, Mallard C. Inflammation during fetal and neonatal life: implications for neurologic and neuropsychiatric disease in children and adults. Ann Neurol 2012; 71(4):444-57.
17. Gupta S, Ellis SE, Ashar FN et al. Transcriptome analysis reveals dysregulation of innate immune response genes and neuronal activity-dependent genes in autism. Nat Commun 2014; 5:5748.
18. Koyama R, Ikegaya Y. Microglia in the pathogenesis of autism spectrum disorders. Neurosci Res 2015; 100:1-5.
19. Jones KA, Thomsen C. The role of the innate immune system in psychiatric disorders. Mol Cell Neurosci 2013; 53:52-62.
20. Chavarria A, Alcocer-Varela J. Is damage in central nervous system due to inflammation? Autoimmun Rev 2004; 3:251-260.
21. Tsilioni I, Dodman N, Petra AI et al. Elevated serum neurotensin and CRH levels in children with autistic spectrum disorders and tail-chasing bull terriers with a phenotype similar to autism. Transl Psychiatry 2014; 4:e466.
22. Patel AB, Tsilioni I, Leeman SE, Theoharides TC. Neurotensin stimulates sortilin and mTOR in human microglia inhibitable by methoxyluteolin, a potential therapeutic target for autism. Proc Natl Acad Sci U S A 2016; 113:E7049-E7058.
23. Kealy J, Greene C, Campbell M. Blood-brain barrier regulation in psychiatric disorders. Neurosci Lett 2018;133664.
24. Fiorentino M, Sapone A, Senger S, et al. Blood-brain barrier and intestinal epithelial barrier alterations in autism spectrum disorders. Mol Autism 2016; 7:49.
25. Esposito P, Chandler N, Kandere-Grzybowska K, et al. Corticotropin-releasing hormone (CRH) and brain mast cells regulate blood-brain-barrier permeability induced by acute stress. J Pharmacol Exp Ther 2002; 303:1061-66.
26. Skaper SD, Giusti P, Facci L. Microglia and mast cells: two tracks on the road to neuroinflammation. FASEB J 2012; 26(8):3103-17.
27. Zhang X, Wang Y, Dong H, Xu Y, Zhang S. Induction of microglial activation by mediators released from mast cells. Cell Physiol Biochem 2016; 38(4):1520-31.
28. Theoharides TC, Tsilioni I, Ren H. Recent advances in our understanding of mast cell activation - or should it be mast cell mediator disorders? Expert Rev Clin Immunol 2019; 15(6):639-56.
29. Vasiadi M, Kalogeromitros K, Kempuraj D, et al. Rupatadine inhibits pro-inflammatory mediator secretion from human mast cells triggered by different stimuli. Int Arch Allergy Immunol 2010; 151(1):38-45.
30. Theoharides TC. Mold and immunity. Clin Ther 2018; 40(6):882-84.
31. Theoharides TC, Stewart JM. Antihistamines and mental status. J Clin Psychopharmacol 2016; 36(3):195-97.
32. Jones QR, Warford J, Rupasinghe HP, Robertson GS. Target-based selection of flavonoids for neurodegenerative disorders. Trends Pharmacol Sci 2012; 33(11):602-610.
33. Theoharides TC, Stewart JM, Hatziagelaki E, Kolaitis G. Brain "fog," inflammation and obesity: key aspects of neuropsychiatric disorders improved by luteolin. Front Neurosci 2015; 9:225.
34. Nabavi SF, Braidy N, Gortzi O, et al. Luteolin as an anti-inflammatory and neuroprotective agent: A brief review. Brain Res Bull 2015; 119(Pt A):1-11.
35. Jang S, Kelley KW, Johnson RW. Luteolin reduces IL-6 production in microglia by inhibiting JNK phosphorylation and activation of AP-1. Proc Natl Acad Sci USA 2008; 105(21):7534-39.
36. Weng Z, Patel AB, Panagiotidou S, Theoharides TC. The novel flavone tetramethoxyluteolin is a potent inhibitor of human mast cells. J Allergy Clin Immunol 2015; 135(4):1044-52.
37. Taliou A, Zintzaras E, Lykouras L, Francis K. An open-label pilot study of a formulation containing the anti-inflammatory flavonoid luteolin and its effects on behavior in children with autism spectrum disorders. Clin Ther 2013; 35(5):592-602.
38. Tsilioni I, Taliou A, Francis K, Theoharides TC. Children with autism spectrum disorders, who improved with a luteolin containing dietary formulation, show reduced serum levels of TNF and IL-6. Transl Psychiatry 2015; 5:e647.
39. Theoharides TC, Kavalioti M. Stress, inflammation and natural treatments. J Biol Regul Homeost Agents 2018; 32(6):1345-47.
40. Patel AB, Theoharides TC. Methoxyluteolin Inhibits neuropeptide-stimulated proinflammatory mediator

release via mTOR activation from human mast cells. J Pharmacol Exp Ther 2017; 361(3):462-71.
41. Walle T. Methylation of dietary flavones greatly improves their hepatic metabolic stability and intestinal absorption. Mol Pharm 2007; 4(6):826-32.
42. Theoharides TC. Tolerability and benefit of a tetramethoxyluteolin-containing skin lotion. Int J Immunopath Pharmacol 2017; 30(2):146-51.

EDITORIAL

PRECISION EDITING OF THE GUT MICROBIOTA AMELIORATES CANCER IMMUNOTHERAPY

L. FRANZA, V. CARUSI, G. PARRINELLO and F. PANDOLFI

Immunology and Allergy section, Fondazione Policlinico Universitario A. Gemelli IRCCS -Università Cattolica del Sacro Cuore, Roma, Italy

Received September4, 2019 – Accepted September 30, 2019

In this editorial the authors highlight recent findings which could help design a personalized approach for cancer immunotherapy.

Since the discovery of the ability of T-cells to kill tumor cells, immunotherapy has always been a major aim of immunological studies. In recent years, immunotherapy based on anti PD-1 and anti CTLA-4 antibodies (usually referred to as immune check point therapy, has proven its efficacy in a variety of tumors, including melanoma, renal cell carcinoma, renal cell carcinoma (RCC), non-small cell lung cancer (NSCLC), mismatch-repair deficient colorectal cancer and hematological malignancies. However, the extremely variable response observed in different patients has frustrated the original hopes thus increasing the quest for a personalized approach. More recently, the role of microbiota in shaping the immune response has indicated a new avenue for the study of these complex interactions. In this editorial, we briefly review a few papers in the field that we consider critical achievements obtained in the last 5 years.

Chaput et al. confirmed the importance of specific commensals in both clinical response and toxicity. In a cohort of 26 patients with metastatic melanoma treated with ipilimumab, patients whose baseline microbiota was *Faecalibacterium* rich has longer progression-free survival and overall survival compared to those whose microbiota was *Firmicutes* poor. However, the patients enriched with these commensals also had more frequent occurrence of ipilimumab-induced colitis (1).

Routy et al. studied memory T-cell responses stimulated by PD-1 blockade to explore the association between the gut microbiota and the immune system. The response of CD4+ and CD8+ T cells harvested from the peripheral blood from PD-1-treated NSCLC (n = 27) and RCC (n = 28) patients to specific bacteria was associated with favorable clinical outcome. Higher IFNγ production by $CD4^+$ and $CD8^+$ T cells in response to *A. muciniphila* correlated with prolonged progression-free survival. In contrast, no association was found between clinical outcome and memory T-cell responses against 10 randomly selected commensals (2).

In summary, we suggest that a better understanding of the relationship between the immune system and the microbiota may result in improvement of immunotherapy.

REFERENCES

1. Chaput N, Lepage P, Coutzac C, et al. Baseline gut

Key words: gut microbiota; cancer immunotherapy

Corresponding Author:
Prof. Franco Pandolfi,
Department of Internal Medicine,
Fondazione Policlinico Universitario A. Gemelli IRCCS
Università Cattolica del Sacro Cuore,
Roma, Italy
e-mail: franco.pandolfi@unicatt.it

0393-974X (2019)

DISCLOSURE: ALL AUTHORS REPORT NO CONFLICTS OF INTEREST RELEVANT TO THIS ARTICLE.

microbiota predicts clinical response and colitis in metastatic melanoma patients treated with ipilimumab. Ann Oncol. 2017; 28(6):1368-79. doi:10.1093/annonc/mdx108.

2. Routy B, Le Chatelier E, Derosa L, et al. Gut microbiome influences efficacy of PD-1-based immunotherapy against epithelial tumors. Science 2018; 359(6371):91-97. doi:10.1126/science.aan3706

EDITORIAL

CAR-T CELL THERAPY CAUSES INFLAMMATION BY IL-1 WHICH ACTIVATES INFLAMMATORY CYTOKINE MAST CELLS: ANTI-INFLAMMATORY ROLE OF IL-37

Al. CARAFFA[1], C.E. GALLENGA[2], S.K. KRITAS[3], G. RONCONI[4], P. DI EMIDIO[5] and P. CONTI[6]

[1]School of Pharmacy, University of Camerino, Camerino, Italy; [2]Department of Biomedical Sciences and Specialist Surgery, Section of Ophthalmology, University of Ferrara, Ferrara, Italy; [3]Department of Microbiology and Infectious Diseases, School of Veterinary Medicine, Aristotle University of Thessaloniki, Macedonia, Greece; [4]Clinica dei Pazienti del Territorio, Fondazione Policlinico Gemelli, Rome, Italy; [5]Maxillofacial Surgery, "Mazzini" Hospital, Teramo, Italy; [6]Postgraduate Medical School, University of Chieti, Chieti, Italy

Received August 14, 2019 – Accepted October 15, 2019

Chimeric antigen receptor (CAR) T cells are genetically modified T cells that act against cancer. When CAR-T cells are administered they can trigger inflammatory cytokines and increase toxicity. Interleukin (IL)-1 is the classic cytokine that mediates inflammatory reactions including those that occur in CAR-T-cell therapy. IL-1 also induces IL-33 in mast cells (MCs), amplifying the allergic reaction. IL-37 (ILF7) is an IL-1 family member which binds IL-18 receptor alpha (IL-18Rα) chain and suppresses innate and acquired immunity. IL-37 is an anti-inflammatory cytokine which inhibits pro-inflammatory cytokines including IL-1 and IL-33. Here, we hypothesize that inflammation and toxicity generated in tumor CAR-T therapy could be inhibited by IL-37, contributing to an improvement in the treatment of tumors with CAR-T therapy.

New cancer therapies open new hopes, but their toxicity is still a serious problem to be solved (1). Important adverse occurrences are allergy and inflammation, which can also cause fatal events (2). Chimeric antigen receptor T (CAR-T) has emerged as a new anti-tumor therapy, with the ability to stimulate the immune system (3). CAR-T is a genetically modified engineered receptor that produces a chimeric receptor of artificial T cells used in immunotherapy (4). This T receptor is chimeric because it has the function of binding the antigen and activating T cells, capable of affecting specific proteins.

CAR-T therapy can cause remission in patients with tumors resistant to conventional therapies; but this therapy has turned out to be very toxic by several mechanisms, and it can also affect antigens of normal tissue associated with the tumor and may cause patient death (5). The most important toxicity of CAR-T cells is pro-inflammatory cytokine release (6). These reactions occur after treatment with CAR-T cells, provoking tumor lysis and cytokine release, followed by anaphylaxis syndrome, fever, neurological toxicity, tachycardia, and hypotension (7). In fact, in the serum of patients treated with CAR-T cells a wide variety of inflammatory cytokines are found. The inflammatory reaction produced by the

Key words: CAR-T therapy; cytokines; mast cells; chimeric antigen receptor

Corresponding Author:
Prof. Pio Conti,
Postgraduate Medical School,
University of Chieti,
Viale Unità d'Italia 73, Chieti, Italy
Tel./Fax: +39 0871 574136
e-mail: pconti@unich.it

0393-974X (2019)

DISCLOSURE: ALL AUTHORS REPORT NO CONFLICTS OF INTEREST RELEVANT TO THIS ARTICLE.

cytokines released by the CAR-T cells can activate other immune cells, such as macrophages and mast cells (MCs), which, in turn, produce other pro-inflammatory cytokines, aggravating the situation. Treatment with CAR-T can provoke a systemic inflammatory response mediated by inflammatory cytokines, such as interleukin (IL)-1 and IL-33, in frequent events (8). Therefore, it is important to apply an aggressive anti-inflammatory therapy in patients treated with CAR-T immunotherapy. In this therapy, pro-inflammatory cytokines are produced that activate the immune cells, including macrophages and MCs to produce and release other pro-inflammatory cytokines, aggravating the patient status (8). Macrophages primarily release IL-1 which in turn activates the MCs to generate IL-33, creating an allergic inflammatory phenomenon (9). In addition, IL-18, a cytokine of the IL-1 family polarizes CAR-T cells, provoking an acute inflammatory response, an effect that can be inhibited by IL-37, since it has been demonstrated that this cytokine plays its biological inhibitory role through IL-18 receptor alpha binding (IL-18Rα) (10).

Mast Cells

MCs are bone marrow immune cells derived from hematopoietic stem cells and reside in all the vascularized tissues and serous cavities, where they mature (11). MCs participate in both innate and adaptive immune responses and are a potential source of cytokines/chemokines, which mediate allergic disease (12-13). They can be activated by various molecules through the Toll-like receptors, and IL-1 receptors, without degranulation and without the intervention of IgE (14-15).

In MC pathway activation, intracellular calcium (Ca^{++}) is regulated by PLC, and PKC results in the formation of IP3 and diacylglycerol (DAG). MAPK, ERK, JNK and p38 participate in the transcription of cytokines and subsequently the generation of proteins (11). The production of IL-1 family, is strongly involved in the inflammatory process (16).

IL-1

IL-1 is one of the most important regulators of innate immune responses and participates in numerous inflammatory processes (17). IL-1 is the classic pro-inflammatory cytokine that includes two distinct ligands: IL-1 alpha (IL-1α) and IL-1 beta (IL-1β), which bind the IL-R1 receptor by mediating inflammatory phenomena. IL-1β, which is the most studied, is inducible and is released by the splitting of caspase-1 (17).

The inflammation that is created in CAR-T therapy with the activation of immune cells generates pro-inflammatory cytokines, mainly IL-1 (8). At this point IL-1 causes an inflammatory network by activating other immune cells including the MCs to produce IL-33, which actively participates in the allergic reaction.

IL-33

IL-33 (formerly IL-1F11) is a pro-inflammatory cytokine of the IL-1 family and is produced by several immune cells including macrophages and

Table I. *Organs that may be more frequently affected by toxicity after infusion of pro-inflammatory cytokine-releasing CAR-T cells.*

ORGANS	SOME EFFECTS
Brain	ataxia, headache, tremor, seizures
Blood	neutropenia, thrombocytopenia, lymphopenia
Liver	hyperbilirubinemia, transaminitis
Kidney	acute kidney injury
Lungs	hypoxia, tachypnea
Heart	hypotension, tachycardia

MCs (18). In addition, IL-33 generated by MCs contributes to allergic reactions (19). IL-33 acts through the ST-2 receptor of which there are two types, a transmembrane receptor (ST2L) and a soluble receptor (sST2) (18). IL-33 is released after cellular injury and/or necrosis by alerting. It contributes to inflammatory and allergic states and is expressed in various organs and cells, including lymphoid cells (20).

CAR-T therapy is a new potentially curative method for cancer. However, adverse reactions such as allergic phenomena, where MCs also participate, still remain obstacles to overcome. The generation of IL-33 from MCs and macrophages contributes to the inflammatory and allergic state (20). Therefore, inhibition of this cytokine with IL-37 may be a new strategy for an improvement of CAR-T therapy (21).

Interleukin-37

IL-37 has emerged as an important inhibitor of immune and inflammatory responses, and it has achieved remarkable efficacy in the treatment of inflammatory diseases (22). IL-37 binds to the IL-18R receptor and at low concentrations is capable of inhibiting innate immune reactions, reducing activation of the MyD88 receptor (23). IL-37 is mainly produced by macrophage cells after activation of the toll-like receptors (TLR) which leads to the formation of mature IL-37 through the action of caspase 1. IL-37 could abolish systemic inflammation and neurotoxicity caused by pro-inflammatory cytokines, including IL-1 and IL-33 with prolonged survival. This therapy could offer a new strategy in the treatment with CAR-T. cells.

The gene expression of IL-37 shows an up-regulation of messenger RNA in tumors including melanoma. This enhancement occurs mainly in Treg cells and in granulacites, which probably also include MCs. The up-regulation of IL-37 messenger RNA in tumors indicates a defensive state that the organism uses in neoplasia (24).

The inhibition of IL-1 and IL-33 with IL-37, a new anti-inflammatory cytokine, could be a new therapy, even if the indications of administration are still to be determined. However, treatment with IL-37 which is immune suppressant should be carried out with great care, because it could negatively affect the immune system and may cross-react with the good receptors which are not expressed on tumor cells.

REFERENCES

1. Guedan S, Ruella M, June CH. Emerging cellular therapies for cancer. Annu Rev Immunol 2019; 37:145-71.
2. Kosti P, Maher J, Arnold JN. Perspectives on chimeric antigen receptor T-cell Immunotherapy for solid tumors. Front Immunol 2018; 9:1104.
3. Raulet DH, Vance RE, McMahon CW. Regulation of the natural killer cell receptor repertoire. Annu Rev Immunol 2001;19:291-330. Review.
4. Yang QY, Yang JD, Wang YS. Current strategies to improve the safety of chimeric antigen receptor (CAR) modified T cells. Immunol Lett 2017; 190:201-5.
5. Newick K, O'Brien S, Moon E, Albelda SM. CAR-T Cell therapy for solid tumors. Annu Rev Med 2017; 68:139-52.
6. Brudno JN, Kochenderfer JN. Toxicities of chimeric antigen receptor T cells: recognition and management. Blood 2016; 127(26):3321-30.
7. Bonifant CL, Jackson HJ, Brentjens RJ, Curran KJ. Toxicity and management in CAR-T-cell therapy. Mol Ther Oncolytics 2016; 3:16011.
8. Giavridis T, van der Stegen SJC, Eyquem J, Hamieh M, Piersigilli A, Sadelain M. CAR-T cell-induced cytokine release syndrome is mediated by macrophages and abated by IL-1 blockade. Nat Med 2018; 24(6):731-38.
9. Conti P, Lauritano D, Caraffa A, et al. New insight into systemic mastocytosis mediated by cytokines IL-1β and IL-33: Potential inhibitory effect of IL-37. Eur J Pharmacol 2019; 858:172473.
10. Chmielewski M, Abken H. CAR-T cells releasing IL-18 convert to T-Bet_{high} $FoxO1_{low}$ effectors that exhibit augmented activity against advanced solid tumors. Cell Rep 2017; 21(11):3205-19.
11. Galli SJ, Kalesnikoff J, Grimbaldeston MA, Piliponsky AM, Williams CM, Tsai M. Mast cells as "tunable" effector and immunoregulatory cells: recent advances. Annu Rev Immunol 2005; 23:749-86. Review.

12. Caraffa Al, Gallenga CE, Kritas SK, Ronconi G, Conti P. Impact of mast cells in systemic lupus erythematosus: can inflammation be inhibited? J Biol Regul Homeost Agents 2019; 33(3):669-73.
13. Taracanova A, Tsilioni I, Conti P, Norwitz ER, Leeman SE, Theoharides TC. Substance P and IL-33 administered together stimulate a marked secretion of IL-1β from human mast cells, inhibited by methoxyluteolin. Proc Natl Acad Sci U S A 2018; 115(40):9381-90.
14. Gallenga CE, Pandolfi F, Caraffa Al, et al. Interleukin-1 family cytokines and mast cells: activation and inhibition. J Biol Regul Homeost Agents 2019; 33(1):1-6.
15. Varvara G, Tettamanti L, Gallenga CE, et al. Stimulated mast cells release inflammatory cytokines: potential suppression and therapeutical aspects. J Biol Regul Homeost Agents 2018; 32(6):1355-60.
16. Theoharides TC, Tsilioni I, Bawazeer M. Mast cells, neuroinflammation and pain in fibromyalgia syndrome. Front Cell Neurosci 2019; 13:353.
17. Cavalli G, Dinarello CA. Anakinra therapy for non-cancer inflammatory diseases. Front Pharmacol 2018; 9:1157. doi: 10.3389/fphar.2018.01157.
18. Dinarello CA. An IL-1 family member requires caspase-1 processing and signals through the ST2 receptor. Immunity 2005; 23(5):461-62.
19. Tettamanti L, Kritas SK, Gallenga CE, et al. IL-33 mediates allergy through mast cell activation: Potential inhibitory effect of certain cytokines. J Biol Regul Homeost Agents 2018; 32(5):1061-65.
20. Conti P, Caraffa A, Ronconi G, et al. Mast cells participate in allograft rejection: can IL-37 play an inhibitory role? Inflamm Res 2018; 67(9):747-55.
21. Gugliandolo A, Caraffa AL, Gallenga CE, et al. Mesenchymal stem cells and IL-37: a powerful combination. J Biol Regul Homeost Agents 2019; 33(4):1019-22.
22. Cavalli G, Dinarello CA. Suppression of inflammation and acquired immunity by IL-37. Immunol Rev 2018; 281(1):179-90.
23. Zhan Q, Zeng Q, Song R, Zhai Y, Xu D, Fullerton DA, Dinarello CA, Meng X. IL-37 suppresses MyD88-mediated inflammatory responses in human aortic valve interstitial cells. Mol Med 2017; 23:83-91.
24. Osborne DG, Domenico J, Luo Y, et al. Interleukin-37 is highly expressed in regulatory T cells of melanoma patients and enhanced by melanoma cell secretome. Mol Carcinog 2019; 58(9):1670-79.

EXPRESSION OF SIRT5 PROTEIN IN GASTRIC CANCER CELLS

ZP. WU and HX. FANG

Department of Gastroenterology, The First People's Hospital of Fuyang, Hangzhou, Zhejiang, China

Received May 5, 2019 – September 11, 2019

The purpose of this paper was to investigate the dynamic trend of SIRT5 (Sirtuins 5) protein expression in gastric cancer cells, for which a hypoxic gastric cancer cell line was established. Afterward, the parental gastric cancer cell group and hypo group were designed, and the levels of related proteins and mRNAs were detected by using Western blot along with real-time quantitative fluorescence PCR (RT-PCR). The results showed that the expression of SIRT5 in hypoxic gastric cancer cells increased significantly, which could increase the phosphorylation level of c-MET (hepatocyte growth factor receptor) and promote the migration of gastric cancer cells. When the expression of SIRT5 protein was observed under hypoxic conditions, SIRT5 silencing significantly reduced the migration ability of MGC803/hypo cells. It could be predicted that SIRT5-mediated protein desuccinylation played an important role in promoting the migration of hypoxic gastric cancer cells. Therefore, the migration rate of gastric cancer cells could be affected by controlling the expression of SIRT5 protein, which provides a novel idea for the treatment of gastric cancer in the future.

Gastric cancer is one of the most common malignant tumors, and is the second leading cause of death from malignant tumors worldwide (1). In recent years, epidemiologists have gathered relevant statistics on diseases, believing that the incidence of gastric cancer in developed countries is decreasing yearly. However, in China, which is a developing country, the incidence of gastric cancer has not decreased (2, 3). In recent years, the abnormal cancer cell cycle and differentiation have played a decisive role in malignant tumors. Targeting the cancer cell cycle and differentiation was considered as a new target for cancer treatment. The alteration of related genes would lead to uncontrolled cell cycle and abnormal function, which would result in tumorigenesis (4).

Currently, seven members of the Sirtuins (Sir2-related enzymes, Sirtuins) family have been found, namely SIRT1, SIRT2, SIRT3, SIRT4, SIRT5, SIRT6 and SIRT7, of which SIRT5 is one of the most special members of the Sirtuin protein family. It is located at the mitochondria of the key organelles of cell metabolism. Besides deacetylase activity, SIRT5 also has desuccinylation, de-malonylation and de-glutamylase activities. In addition, it participates in the metabolism of urea cycle as well as fatty acid in mitochondria, and plays an anti-apoptotic and proliferative role through activating cytochrome C (5-7). However, there are few studies on SIRT5, mainly on metabolism, and rarely on tumors (8, 9). SIRT5 targets protein complexes on mitochondrial membrane through its affinity with cardiolipin and

Key words: gastric neoplasms; SIRT5 protein; hypoxia tolerance; cell migration

Corresponding Author:
Dr Zhongping Wu,
Department of Gastroenterology,
The First People's Hospital of Fuyang,
429 Beihuan Road, Fuchun Street,
Hangzhou, 311400, Zhejiang, China
e-mail: wzhongping2010@yeah.net

0393-974X (2019)

promotes respiratory chain function (10). Therefore, the relationships among cell cycle regulatory genes, cell differentiation and tumors have increasingly become the focus of research by biologists.

In conclusion, in order to better understand the mechanism of SIRT5 in gastric cancer, a hypoxic gastric cancer cell line was established through choosing gastric cancer cells MGC803 and BGC823. Furthermore, Western blot and RT-PCR were used to detect the expression of SIRT5 in order to provide new ideas for the treatment of gastric cancer in the future.

MATERIALS AND METHODS

Cell culture

Gastric cancer cells MGC803 and BGC823 were purchased from Shanghai Guandao Bioengineering Co., Ltd., China and cultured in 1640 medium (Shanghai Huashun Biotechnology Co., Ltd., China) containing 6% fetal bovine serum. The cells were incubated at 37°C with 5% CO2 until the logarithmic growth stage. Moreover, MGC803 and BGC823 cells were subcultured until they increased by approximately 90% and were washed with PBS buffer (phosphate buffer saline, Beijing Institute of Biological Products, China) once and covered with trypsin-EDTA (ethylenediamine tetraacetic acid, Shanghai Yaxin Biotechnology Co., Ltd., China) digestion solution. The cells were observed under an inverted microscope (OLYMPUS, Japan) for 3-4 min at 37°C. It could be seen that the cells shed from the bottom of the culture bottle to form a single cell, and the digestion was terminated by adding the complete culture medium. Single cell suspension was prepared through blowing cells by pipette and then reinoculated into the culture flask. The cells in the test seed plate were counted by blood cell counting board.

In order to simulate the hypoxic microenvironment of solid tumors, gastric cancer cell lines MGC803 and BGC823 were cultured at 2% O2 until logarithmic growth phase, and hypoxic resistant gastric cancer cell lines MGC803/hypo and BGC823/hypo were established. Hypoxic tolerant MGC803 (MGC803/hypo) and BGC823 (BGC823/hypo) cells were cultured in 1640 medium containing 10% fetal bovine serum (Biological Industries Corporation, Israel) (Gibco Corporation, USA) and cultured at 37°C, 5% CO2 and 2% O2 incubators. The cells were cultured in the logarithmic growth phase. The conditions and methods of this passage were the same as those of normal oxygen cells.

Cell metastasis and passage experiment

The MGC803, BGC823, MGC803/hypo, BGC823/hypo cells in the logarithmic growth phase were digested and centrifuged. Then they were suspended to a single suspension after adding double non-culture medium, and again suspended to a single suspension. The cell density was adjusted to 10000 cells/pore; 500 μL 2% FBS (fetal bovine serum) was added to the inferior chamber of the Transwell chamber. In addition, 200 μL cell suspension was added to the upper chamber. Attention should be paid to the prevention of bubbles between the culture medium of the lower chamber and the chamber during the operation. After 24 h of incubation, the chamber was taken out, and the culture medium was discarded. PBS was used to rinse it twice, and 400 μL A solution (polyformaldehyde, Beijing Institute of Biological Products, China) was added. After one minute, liquid A (polyformaldehyde) was discarded and liquid B (crystal violet, Beijing Institute of Biological Products, China) was added. After 40 min of dyeing, distilled water was used to gently wash off the floating color, and dry cotton swabs were used to erase the upper unmigrated cells, so as to calculate the migrated cells.

Western blot detection and analysis

After washing the cells three times with pre-cooled PBS buffer, a small amount of RIPA buffer, composed of 50mmol/L Tris-C1 PH8.0, 150mmol/L NaC1, 0.1% SDS, 1% NP-40, 0.5% DOC, 0.02% NaN3, 100ug/ml PMSF (Phenylmethylsulfonyl Fluoride), and 1ug/ml Aprotinin (PMSF and protinin, were added before use; Gibco Company, USA) was added to cover the cell surface. The cells were lysed for 5 min. Afterwards, they were scraped off and transferred to a 1.5 ml EP (Eppendorf) tube by a cell scraper. The cells were centrifuged at 4°C and 13,000rpm for 25 min. Furthermore, the supernatant was abducted and transferred to another 1.5 mL EP tube. All the above operations were carried out at 4°C. 4 μL supernatant was shaken in 1 mL Coomassie Brilliant Blue (PIERCE, USA) prepared previously. The cells were placed in a 96-well plate at a density of 200μL/well after shaking. Each sample was set up with three wells. The absorbance of each well was measured at 570nm

wavelength with an enzyme label. The standard curve (y = ax + b) was drawn. According to the standard curve, the protein concentration of the sample was calculated. Then, SDS-PAGE electrophoresis was carried out, in which the collocation method of concentrated gum and separating gum (Table I). Samples were harvested sequentially (10-30 μg). Electrophoresis was performed at 60V constant voltage. However, when protein samples were inserted into the gel, the voltage was increased to 120 V. After electrophoresis, the gel concentrate was cut off and a PVDF (polyvinylidene fluoride) membrane with suitable size was prepared. The separating glue was placed in the transfer clamp while the PVDF membrane was placed on the separating glue, which was closely connected. The placement order of transfer clips: one layer of sponge, three layers of filter paper, separating glue, PVDF membrane, three layers of filter paper and one layer of sponge. The membrane was rotated for 120 min under 80V constant pressure by wet rotation. Afterwards, it was removed and immersed in 5% skim milk and incubated at room temperature for 1 hour. Furthermore, the antibody was diluted according to manufacturer's instructions, added to 5% skimmed milk, incubated, and shaken at 4°C overnight, after which 1 × TTBS (Tris-Buffered Saline Tween-20) was utilized to wash the membrane 4 times with 10 min each time. The second antibody (Beijing Zhongshan Jinqiao Biotechnology Co., Ltd., China) labeled with horseradish peroxidase (1:2000 dilution) was added and incubated at room temperature for 1 hour. The membrane was washed with 1 × TTBS, 4 times, 10 min each time. The developer solutions A and B (1:1) were mixed and dripped onto the surface of the PVDF membrane evenly. The results were exposed and preserved by a chemiluminescence system of digital multi-functional image enhancement (Shanghai Tianneng Technology Co., Ltd., China).

Real-time quantitative PCR

Cells in the logarithmic growth phase were washed three times with pre-cooled buffer, and then RNA extractant Trizol (Biyun Tian Biotechnology Co., Ltd., China) was added. The cells were blown repeatedly, and RNA was extracted after lysing the cell membrane completely. After 5 min, chloroform 100 μL was added. After 10 min of oscillation, and 15 min of centrifugation (Beijing Fourth Ring Scientific Instrument Factory, China), 150 μL supernatant was removed. Isopropyl alcohol (Biyuntian Biotechnological Technology Co., Ltd., China) was also added at a ratio of 1:1. Furthermore, the supernatant was centrifuged for 10 min at 12,000r/min, and then discarde; 1 mL 75% ethanol was added to the precipitate and centrifuged for 5 min at 12,000r/min, and discarded. After drying the sample, 20 μL DEPC (diethylpyrocarbonate, PIERCE Company, USA) water was added to dissolve the sample. Firstly, the quantitative machine (Zhejiang Lecheng Electrical Appliances Factory, China) was cleaned

Table I. *Formulation of separating glue and concentrating glue.*

Reagent	Separating glue			Concentrating glue
	8%	10%	12%	
ddH20	4.65mL	3.95mL	3.3mL	2.9mL
1M Tris（PH8.8）	2.5mL	2.5mL	2.5mL	0.5M Tris（PH6.8）1.25mL
30% acrylamide	2.65mL	3.35mL	4mL	0.75mL
10% SDS	100μL	100μL	100μL	50μL
10% ammonium persulfate	100μL	100μL	100μL	50μL
TEMED	10μL	10μL	10μL	5μL

and zeroed. The absorbance of RNA at 260 and 280nm was measured to calculate its concentration and evaluate its purity. Total RNA was equaled 500/sample concentration. Moreover, the reverse transcription system was prepared. The reaction time was 2 min at 42°C. 80 μL ddH2O was added to the finished cRNA and maintained at -20°C for use or amplified directly by PCR (ABI Company, USA).

Preparation of protein chip

Cells in the logarithmic growth phase were inoculated into 6-well plates with 3 ×10^5/well. After cell adherence, 1640 medium containing 6% serum was replaced by a double non-culture medium (penicillin-free streptomycin, serum-free), with 2 ml per well. The cell supernatant was harvested after 24 h of starvation treatment. After centrifugation for 10 min at 4000r/min, the supernatant was calibrated and incubated with 1 mL samples on each chip overnight at 4°C, after which the samples on the membrane were removed on the second day. The membrane was cleaned with Buffer I (Shanghai Huashun Biotechnology Co., Ltd., China) and Buffer II (Shanghai Huashun Biotechnology Co., Ltd., China), and then incubated with 1 mL antibody overnight at 4°C. The antibodies on the membrane were then absorbed again. The membrane was again cleaned with Buffer I and Buffer II, and then incubated with 2 mL HRP (horseradish

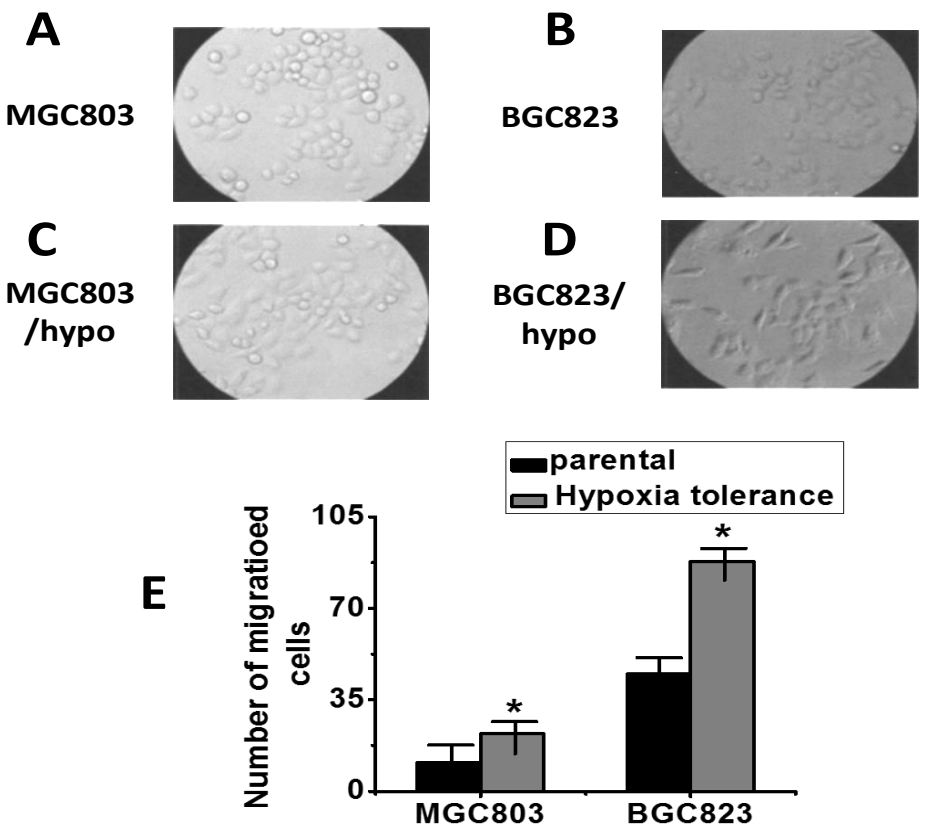

Fig. 1. *Morphological characteristics and migration ability of parental gastric cancer cells and hypoxic resistant gastric cancer cells.* ***A****) Morphological characteristics of parental gastric cancer cell line MGC803; *200* ***B****) Morphological characteristics of parental gastric cancer cell line BGC823; *200* ***C****) Morphological characteristics of hypoxic gastric cancer cell line MGC803/hypo; *200* ***D****) Morphological characteristics of hypoxic gastric cancer cell line BGC823/ hypo; *200* ***E****) Cylindrical chart for measuring the migration ability of parent gastric cancer cells and hypoxic gastric cancer tolerant cells by Transwell method. Compared with parental gastric cancer cells, * $p < 0.05$ indicated statistical significance.*

peroxidase)–Stretavidin (Shanghai Tianneng Technology Co., Ltd., China). Moreover, after overnight at 4°C, the antibodies on the membrane were absorbed again. The membrane was cleaned with Buffer I and Buffer II, and finally, the phenomenon of developing solution (Shanghai Tianneng Technology Co., Ltd., China) was added.

Statistical analysis

All the data were obtained from three independent experiments, which were expressed by the mean± standard deviation (x ± s). SPSS 17.0 statistical software was employed for *t*-test, and $p < 0.05$ indicated statistical significance.

RESULTS

Changes of gastric cancer migration resistance under hypoxia

As seen in Fig. 1, compared with parental gastric cancer cells MGC803 and BGC823, the hypoxic gastric cancer cells MGC803/hypo and BGC823/hypo were long spindle-shaped and loosely structured. The migration ability of parental gastric cancer cells and hypoxic-resistant gastric cancer cells was compared by Transwell method (Fig. 1B). Moreover, it was found that the migration ability of hypoxic-resistant gastric cancer cells MGC803/

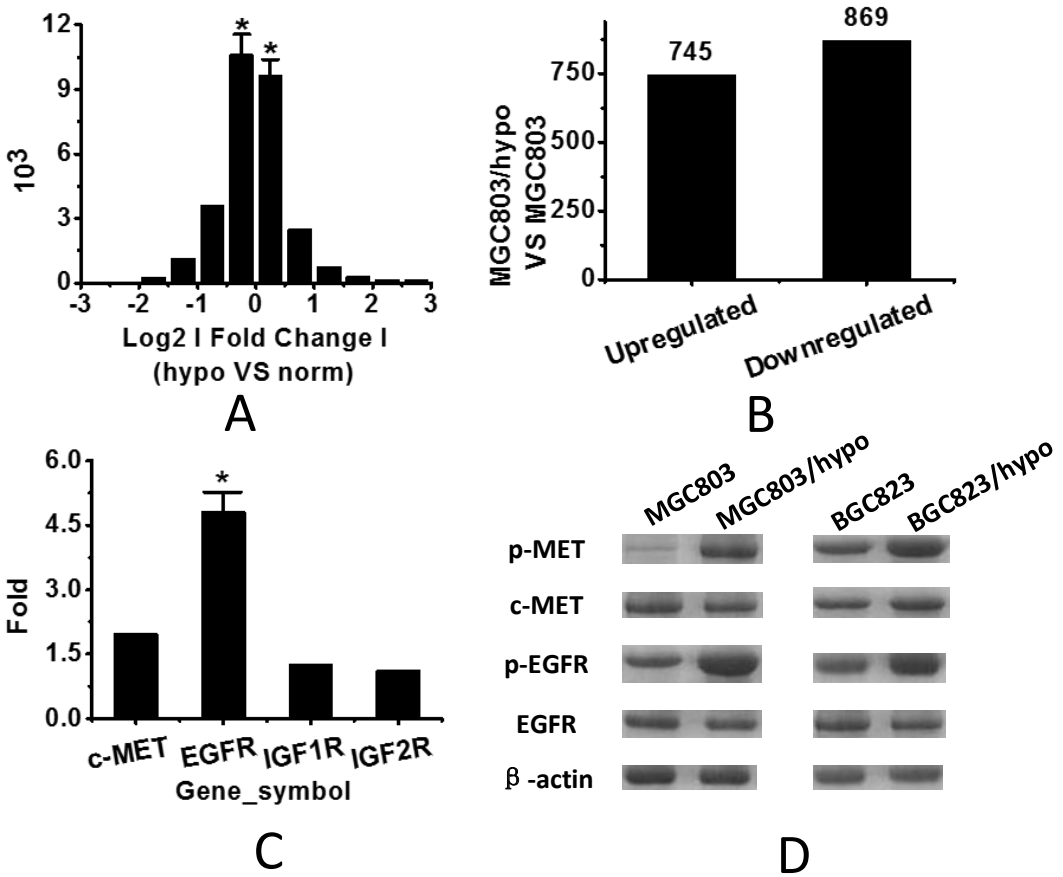

Fig. 2. *The expression level of metastasis-related genes in parental gastric cancer cells and hypoxic-resistant gastric cancer cells.* ***A****) The gene difference between MGC803 and MGC803/hypo cells was detected by expression profiling chip. The graph was a differential multiple histogram (S4 vs S1).* ***B****) Cylindrical maps of gene expression changes in expression profiles;* ***C****) The expression pattern of tyrosine kinase membrane receptor family in the chip;* ***D****) Immunoblotting was used to detect the expression and phosphorylation of hepatocyte growth factor receptor (C-MET) and epidermal growth factor receptor (EGFR) in parental gastric cancer cells (MGC803, BGC823) and hypoxia-resistant gastric cancer cells (MGC803/hypo, BGC823/hypo). The expression level of β-actin protein was internal control. Compared with parental gastric cancer cells, * $p < 0.05$ indicated statistical significance.*

hypo and BGC823/hypo was significantly enhanced. These results indicate that hypoxia promoted the migration of gastric cancer cells.

Hyperphosphorylation of c-MET in gastric cancer cells induced by hypoxia

As shown in Fig. 2, there was significant difference in the gene expression between MGC803 cells and MGC803 cells. In addition, compared with MGC803 cells, 745 genes were up-regulated more than 2 times and 869 genes were down-regulated more than 2 times in MGC803/hypo cells (Fig. 2B). Membrane receptors of tyrosine kinase, such as EGFR, c-MET, as well as IGFR played an important role in the

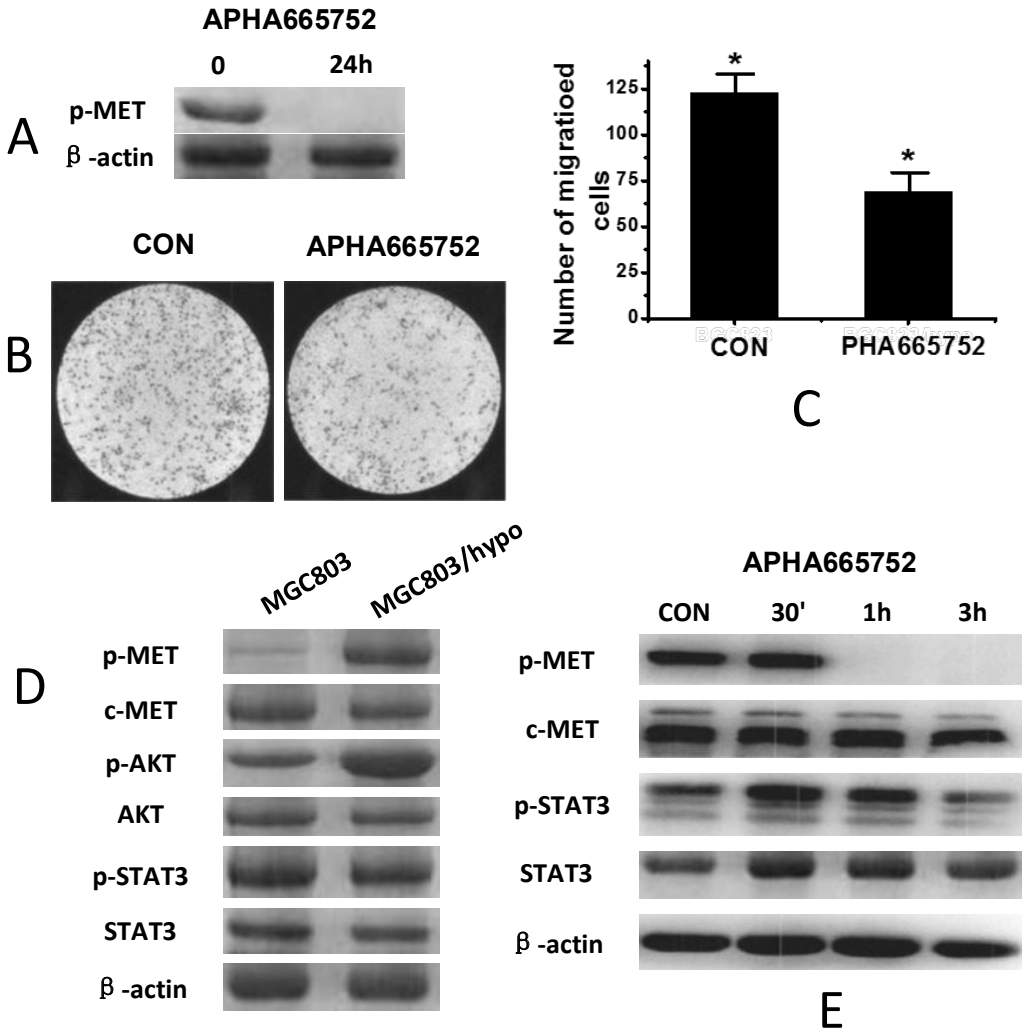

Fig. 3. *Effects of c-MET on the migration of hypoxic gastric cancer cells.* ***A****) Immunoblotting was used to detect the phosphorylation level of c-MET in MGC803/hypo cells treated with c-MET inhibitors for 24 hours.* ***B****) After the treatment of MGC803/hypo cells with c-MET inhibitors, transwell was used to detect the migration ability of MGC803/hypo cells. (Ventricular field of vision * 200 times)* ***C****) After treatment of MGC803/hypo cells with c-MET inhibitors, transwell was used to detect cell migration (cell number histogram)* ***D****) Immunoblotting was used to detect the expression and phosphorylation of hepatocyte growth factor receptor (c-MET), protein kinase B (AKT), signal transduction and transcription activator 3 (STAT3), and p-actin was used as control group.* ***E****) Immunoblotting assay was used to detect the expression and phosphorylation of hepatocyte growth factor receptor (c-MET), signal transduction and transcription activator 3 (STAT3), and the expression of β-actin was the control group. Compared with parental gastric cancer cells, *p<0.05 indicated statistical significance.*

proliferation and metastasis of tumors. Furthermore, the expression of these membrane receptors in MGC803/hypo cells was up-regulated 2-4-fold, and the expression of EGFR was the most significant (Fig. 2C). The expression and phosphorylation of these membrane receptor proteins in parental gastric cancer cells (MGC803 and BGC803) and hypoxic tolerant cells (MGC803/hypo and BGC823/hypo) were detected by utilizing Western blot. The results showed that these membrane receptor proteins in hypoxic gastric cancer cells MGC803 and BGC823 were only slightly up-regulated or unchanged, while the levels of p-EGFR and p-MET, especially p-MET, increased significantly. These results pointed out that c-MET activation may be one of the reasons for the enhanced migration of hypoxic-resistant gastric cancer cells.

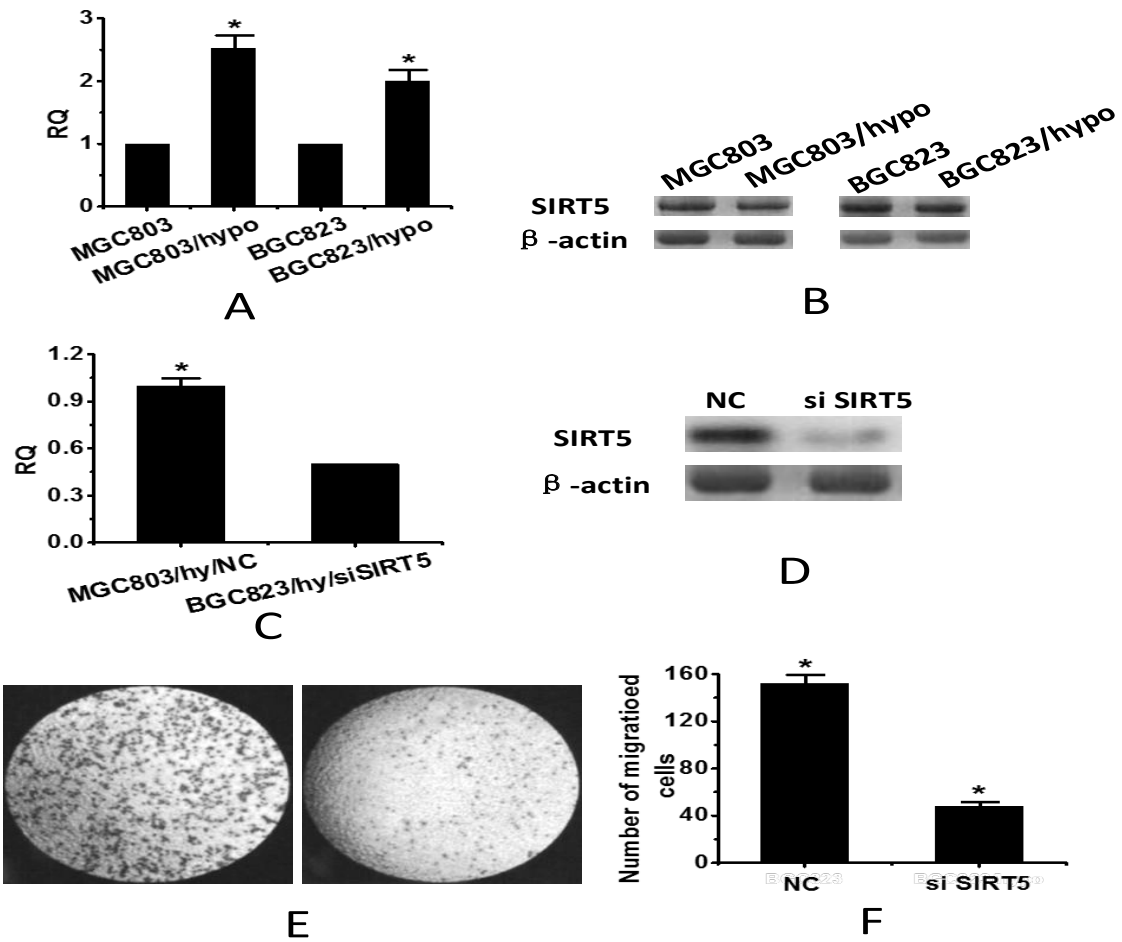

Fig. 4. *The expression level of SIRT5 in hypoxic gastric cancer cells and its effect on cell migration.* ***A)*** *RTPCR was used to detect the expression level of mRNA in SIRT5 in parental and hypoxic gastric cancer cells (MGC803, BGC823).* ***B)*** *The expression of SIRT5 protein in parental and hypoxic gastric cancer cells (MGC803, BGC823) was detected through Western blotting.* ***C)*** *After SIRT5 was silenced instantaneously, the expression of SIRT5 was detected by RT-PCR.* ***D)*** *Western blot was used to detect the expression of SIRT5 in hypoxic gastric cancer cells.* ***E)*** *Transwell was used to detect the migration ability of hypoxic gastric cancer cells, and the ventricular field of vision of Transwell was × 10 times).* ***F)*** *Cylindrical chart of cell count for detection of migration ability of hypoxic gastric cancer cells by Transwell. Compared with parental gastric cancer cells, * $p < 0.05$ indicated statistical significance.*

C-MET activation promotes migration of hypoxic gastric cancer cells

The migration ability of MGC803/hypo cells treated with c-MET inhibitor PHA665752 for 24 h was significantly inhibited by PHA665752 (Fig. 3 A-C). The expression levels of c-MET protein and phosphorylation in MGC803 and MGC803/hypo cells along with their downstream signals could be obtained by utilizing immunoblotting (Fig. 3D). The results showed that the levels of c-MET, AKT and STAT3 (signal transducer and activator of transcription 3) protein did not change significantly. In addition, although the phosphorylation levels of c-MET and STAT3 increased significantly, those of AKT did not change significantly. From Fig. 3E, it can be seen that when MGC803/hypo cells were treated with PHA665752 for 0, 30 min, 1 h and 3 h, the downstream ERK and STAT3 signaling pathways were detected through Western blotting. It was found that the phosphorylation of c-MET was completely inhibited when PHA665752 acted for 1 hour, and the phosphorylation of STAT3 downstream was inhibited when PHA665752 acted for 3 h. These results suggested that c-MET/STAT3 pathway plays an important role in promoting the migration of gastric cancer cells under hypoxia.

Effects of the SIRT5 expression on migration of gastric cancer cells under hypoxia

The expression of SIRT5 was up-regulated by 2.52 times (Fig. 4 A,B). The expression levels of SIRT5 in hypoxic gastric cancer cells MGC803/hypo and BGC823/hypo were significantly higher than those in parental gastric cancer cells MGC803 and BGC823/hypo by utilizing RT-PCR along with Western blot. The role of SIRT5 in tumor metastasis could be obtained, and SIRT5 was found to be silent instantaneously (Fig. 4 C, D). Furthermore, Transwell could be used to detect the migration ability of hypoxic gastric cancer cells. The results showed that SIRT5 silencing significantly reduced the migration ability of MGC803/hypo cells. These results proposed that hypoxia can induce SIRT5 expression and promote the migration of gastric cancer cells.

DISCUSSION

Hypoxia promotes tumor metastasis through the transcriptional mechanism of HIFs. In addition, abnormal post-translational modification of protein plays a major role in hypoxia promoting tumor metastasis (11). Furthermore, it has been found that hypoxia can inhibit glycosylation of integrin alpha 3 through blocking glycoprotein translocation to cell membrane and promoting tumor cell migration (12). In this study, a hypoxia-tolerant gastric cancer cell line was successfully established and it was demonstrated that c-MET played an important role in promoting hypoxia-induced migration of gastric cancer cells. To further explore the mechanism of hypoxia-induced c-MET activation, it was found that the SIRT5 expression level was significantly increased in hypoxic gastric cancer cells, which could increase the phosphorylation level of c-MET and promote the migration of gastric cancer cells. Therefore, this study provided a new method to further clarify the mechanism of c-MET activation induced by chronic hypoxia.

SIRT5 is not only a deacetylase, but also a desuccinylating acylase (13). Succinylation is a new post-translational modification, in which succinyl-CoA covalently binds succinyl groups to lysine residues of protein by enzymatic or non-enzymatic methods, and plays an important role in the biological processes of apoptosis, aging, and fat as well as energy metabolism (14-16). In this study, the expression of SIRT5 in hypoxic gastric cancer cells MGC803/hypo and BGC823/hypo was significantly higher than that in parental gastric cancer cells by utilizing RT-PCR and Western blot. Through comparing the panacetylation level and pansuccinylation level of parental gastric cancer cells along with hypoxic tolerant cells before and after silencing SIRT5, it was found that SIRT5 can reduce the expression of SIRT5 in hypoxic gastric cancer cells. Furthermore, the level of succinylation and its migration were promoted which suggested that SIRT5-mediated protein desuccination plays an important role in promoting the migration of hypoxic gastric cancer cells. Therefore, the results of this study further demonstrate that hypoxia can induce

the SIRT5 expression and promote the metastasis of gastric cancer, where c-MET/STAT3 pathway plays an important role.

In conclusion, this study indicates that SIRT5-mediated protein desuccinylation plays an important role in promoting migration of hypoxic gastric cancer cells. Therefore, the migration of gastric cancer cells can be controlled by regulating the expression of SIRT5 protein, which provides a new idea for the treatment of gastric cancer in the future.

REFERENCES

1. Karimi P, Islami F, Anandasabapathy S, Freedman ND, Kamangar F. Gastric cancer: descriptive epidemiology, risk factors, screening, and prevention. Cancer Epidemiol Biomarkers Prev 2014; 23(5):700-13.
2. Zong L, Abe M, Seto Y, Ji J. The challenge of screening for early gastric cancer in China. Lancet 2016; 388(10060):2606.
3. Strong VE, Wu AW, Selby LV, et al. Differences in gastric cancer survival between the U.S. and China. J Surg Oncol 2015; 112(1):31-7.
4. Qu Y, Dang S, Hou P. Gene methylation in gastric cancer. Clin Chim Acta 2013; 424:53-65.
5. Rardin MJ, He W, Nishida Y, et al. SIRT5 regulates the mitochondrial lysine succinylome and metabolic networks. Cell Metab 2013; 18(6):920-33.
6. Chen XF, Tian MX, Sun RQ, et al. SIRT5 inhibits peroxisomal ACOX1 to prevent oxidative damage and is downregulated in liver cancer. EMBO Rep 2018; 19(5): e45124.
7. Chen L, Wang H, Gao F, et al. Functional genetic variants in the SIRT5 gene promoter in acute myocardial infarction. Gene 2018; 675:233-39.
8. Yang X, Wang Z, Li X, et al. SHMT2 desuccinylation by SIRT5 drives cancer cell proliferation. Cancer Res 2018; 78(2):372-86.
9. Wang F, Wang K, Xu W, et al. SIRT5 Desuccinylates and activates pyruvate kinase M2 to block macrophage IL-1β production and to prevent DSS-induced colitis in mice. Cell Rep 2017; 19(11):2331-44.
10. Zhang Y, Bharathi SS, Rardin MJ, et al. SIRT5 binds to cardiolipin and regulates the electron transport chain. J Biol Chem 2017; 292(24):10239-49.
11. Hsu YC, Hsieh YH, Liao CC, Chong LW, Lee CY, Yu YL, Chou RH. Targeting post-translational modifications of histones for cancer therapy. Cell Mol Biol (Noisy-le-grand) 2015; 61(6):69-84.
12. Ren Y, Hao P, Law SK, Sze SK. Hypoxia-induced changes to integrin α 3 glycosylation facilitate invasion in epidermoid carcinoma cell line A431. Mol Cell Proteomics 2014; 13(11):3126-37.
13. Du Y, Hu H, Hua C, Du K, Wei T. Tissue distribution, subcellular localization, and enzymatic activity analysis of human SIRT5 isoforms. Biochem Biophys Res Commun 2018; 503(2):763-69.
14. Zhang Y, Bharathi SS, Rardin MJ, et al. SIRT5 Binds to Cardiolipin and Regulates the Electron Transport Chain. J Biol Chem 2017; 292(24):10239-49.
15. Xu L, Che X, Wu Y, et al. SIRT5 as a biomarker for response to anthracycline-taxane-based neoadjuvant chemotherapy in triple-negative breast cancer. Oncol Rep 2018; 39(5):2315-23.
16. Chang L, Xi L, Liu Y, Liu R, Wu Z, Jian Z. SIRT5 promotes cell proliferation and invasion in hepatocellular carcinoma by targeting E2F1. Mol Med Rep 2018; 17(1):342-49.

EFFECTS OF PROGESTERONE RECEPTOR ON PROLIFERATION OF UTERINE LEIOMYOMA CELLS

S. LIAO, HN. MI, LY. CHAI and HN. WANG

Department of Gynaecology, The People's Hospital of Putuo, Zhoushan, Zhejiang, China

Received May 16, 2019 – Accepted October 2, 2019

In order to study the mechanism of the effect of progesterone receptor on the growth of primary uterine leiomyoma cells, the primary cells were extracted from uterine leiomyoma cells and identified by immunohistochemistry (IHC). Mitochondrial progesterone receptor-positive [PR-M(+)], mitochondrial progesterone receptor-negative [PR-M(-)], progesterone receptor A (PR-A) and progesterone receptor B (PR-B) were screened by Western blotting. Different concentrations of Mifepristone (MIF), a progesterone receptor antagonist, were used to interfere with PR-M(+) and PR-M(-) cell lines, respectively. Proliferation and apoptosis of PR-M(+) and PR-M(-) cell lines were detected by tetramethylazolyl blue method and flow cytometry, respectively. The expression of Caspase-3 and B-cell lymphoma 2 (Bcl-2) protein was detected by Western blotting. The results showed that the growth of PR-M(+) and PR-M(-) uterine leiomyoma cells was inhibited with the increase of MIF concentration. Furthermore, the proliferation inhibition rate and apoptosis rate were gradually increased. However, the expression of Caspase-3 protein on progesterone receptor M increased, while the expression of Bcl-2 decreased. Moreover, progesterone could induce progesterone receptor M to up-regulate apoptotic protein Caspase-3 and down-regulate anti-apoptotic protein Bcl-2, thus it could inhibit the apoptosis of primary cultured uterine leiomyoma cells and promote the proliferation of leiomyoma cells.

Uterine leiomyoma is one of the most common benign tumors in female genital organs, which usually affects middle-aged women (1, 2). It is harmful to female reproductive health, leading to infertility and even cancer (3-5). The mitochondrial progesterone receptor (PR-M) was found in the mitochondrial extracorporeal membrane at the beginning of the 20th century. Unlike traditional PR-A and PR-B, PR-M only has a truncated hinge region and a ligand binding region (6-8). Compared with normal uterine smooth muscle tissues, the expression of PR-M, PR-A and PR-B in uterine leiomyoma increases significantly (9), suggesting that PR-M may promote growth of leiomyoma. Some scholars have shown that progesterone can up-regulate the expression of Bcl-2 in uterine leiomyoma cells (10). It has been shown that progesterone receptor agonists can promote cell apoptosis by down-regulating Caspase-3 in human uterine leiomyoma cells (11). It is hypothesised that PR-M may play a role in leiomyoma growth through certain proliferation and apoptosis pathways.

At present, the pathogenesis of uterine leiomyoma and the mechanism of drugs for this disease are not clear. Therefore, in this study, the primary cells were extracted from uterine leiomyoma, and different concentrations of mifepristone were

Key words: progesterone receptor; uterine leiomyoma; cell proliferation; primary culture

Corresponding Author:
Dr Haina Wang,
Department of Gynaecology,
The People's Hospital of Putuo,
No.19, Donggang Wenkang Street,
Zhoushan, 316100, Zhejiang, China.
e-mail: wanghaina_putuo111@163.com

0393-974X (2019)

used to interfere with PR-M positive cell lines and detect the proliferation and apoptosis of cells. This study aimed to explore the effect of progesterone receptor on uterine leiomyoma in order to deepen the understanding of PR-M function and provide a scientific basis for clinical treatment of uterine leiomyoma.

MATERIALS AND METHODS

Subjects

Ten patients (aged 30-45 years; average 38±3.68 years) with simple hysteromyoma who underwent abdominal myomectomy or laparoscopic hysterectomy in The People's Hospital of Putuo (January 2018-July 2018) were randomly selected. The patients had not received steroid hormone therapy within the six month prior to surgery, and they did not have sex hormone-related complications. The protocol of this experiment was approved by the ethics committee of The People's Hospital of Putuo, and the informed consent documents were obtained from the patients.

Primary cell culture and identification

During surgery, uterine leiomyoma of the patients were removed and three blocks of uterine leiomyoma tissues near the margin (about 1 cm^3 in volume) were immediately taken and put into Dulbecco's modified eagle medium (DMEM, 4°C) containing bis-antibodies. Uterine leiomyoma tissues were immersed in a phosphate buffer solution (PBS) containing bis-resistance (Beijing Institute of Biological Products, China), and then washed three times after immersion for 5 min. Subsequently, tissue pieces were shredded and placed in a centrifugal tube, and 0.25% collagenase type I was added (equivalent to 3 times of the volume of tissue pieces; Shanghai Bohu Biotechnology Co., Ltd., China).

Afterwards, the centrifuge tube was placed in a 37°C water bath for 3 h, and whipped with pasteurized straw (Shanghai Jingan Biotechnology Co., Ltd., China). When the tissue pieces became smaller and the collagenase solution became turbid (15 min each time), complete medium was added to stop the digestion. A stainless-steel cell sieve (200 mesh) was employed for filtration. The filtrate was centrifuged for 5 min (1000 rpm) and the supernatant was discarded. After adding the complete medium, it was cultured at 37°C, 5% CO_2 (Shanghai Santeng Instrument Co., Ltd., China). After 24 h, the cells were changed after adherence, and then they were changed once every 3 days. When the fusion rate reached 80%, the cells were digested and passaged with 0.25% trypsin-Ethylenediaminetetraacetic acid (EDTA) (Shanghai Yaxin Biotechnology Co., Ltd., China). Morphological characteristics of the cells were observed under an inverted phase contrast microscope (Leica, Germany).

After the cells were transferred to the third generation, they were digested and suspended with trypsin (Sichuan Shunsheng Pharmaceutical Co., Ltd., China), and then dropped on the cover slide of a 6-well plate. When the cell confluence reached 80%, the culture medium was discarded. Afterwards, the cover slide was taken out and placed on the slide. Furthermore, polyformaldehyde (4%; Haisaobao Biotechnology Co., Ltd., China) was dropped on the slide and washed with PBS 30 min later. Subsequently, the Biotin-labeled secondary antibody solution (Guangzhou Yijin Biotechnology Co., Ltd., China) was added and cultured at room temperature for 2 h in the absence of light and then washed with PBS three times. Finally, diaminobenzidine (DAB) (Jin Ruibo Biological Technology Co., Ltd., Xiamen, China) was added to dye the cells for observation under a microscope. Hematoxylin (Shanghai Xinyu Biotechnology Co., Ltd., China) was utilized to re-dye for several seconds and then the neutral gum (Shanghai Yantuo Biotechnology Co., Ltd., China) was used to seal the film for preservation.

Growth of uterine myoma cells

The second generation of cultured uterine leiomyoma cells were digested, centrifuged and counted. Cells were inoculated onto a 96-well plate at a density of $1x10^4$ cells/well. The growth and morphological changes of cells were observed using an inverted microscope. The absorbance was measured at a wavelength of 450 nm by the Molecular Devices (Molecular Devices, LLC. San Jose, CA, USA) every 24 h after inoculation. After repeating the measurement three times, the average value was calculated and the cell growth curve was drawn.

Detection of the progesterone receptor expression by Western blot

The cultured third-generation uterine fibroid cells on the 6-well plate were taken from the incubator, the medium was discarded, and the cells were washed 3 times

with PBS, and dried with a filter paper. Then, 100 μL of cold cracking buffer (Shanghai Biyuntian Biotechnology Co., Ltd., China) which was prepared in advance was added. It was placed on an ice box and pipetting guns were employed to blow cells (for 5 min/time) to break them down completely. The supernatant was discarded by centrifugation (14000g/min) for 5 min using a high-speed centrifuge (Anhui Zhongke Zhongjia Co., Ltd., China).

BCA protein kit was used for quantitative analysis of protein concentration in samples. The diluted protein samples were added to 96-well labeled plates, each plate had three parallel holes, and 100 μL BCA working fluid was added to mix them completely, then put in a 37°C water bath for 30 min. The absorbance at 562 nm was measured by a Micro plate Reader (Multiskan GO; Thermo Scientific, USA) and the standard curve was drawn, then the protein concentration of the sample was calculated. 25 μL of Sample protein was mixed with 5×protein buffer (SDS-PAGE Sample Loading Buffer, a modified 5-fold protein concentration buffer with bromophenol blue as dye) (4:1; Xi'an Hutt Biotechnology Co., Ltd., China) and boiled in water for 10 min, then cooled on ice. The first well was filled with a 5 μL protein marker (Shanghai Bogu Biotechnology Co., Ltd., China) and a 15 μL 1 Lording buffer (Beijing Norborad Technology Co., Ltd., China). In the remaining wells, protein samples were added. Concentrated gel electrophoresis (80 V) was performed for 30 min and separation gel electrophoresis (120 V) was conducted for 90 min. When the protein was electro-transferred to NC membrane (nitrocellulose filter membrane), it was sealed with skimmed milk powder (5%) (Shanghai Huashun Biotechnology Co., Ltd., China) for 1 h. TBST (Tris Buffer Solution Tween) buffer (Beijing Baiaolebo Technology Co., Ltd., China) was rinsed three times. An anti-dilution solution was added (PR, progesterone receptor) rabbit-derived polyclonal antibody, 1:800) (Shanghai Yubo Biological Technology Co., Ltd., China). It was maintained at 4°C overnight, and then fluorescent secondary antibody diluent was added (sheep anti-rabbit IgG, 1:4000) (Nanjing Shengxing Biotechnology Co., Ltd., China). After 2 h, it was washed with TBST buffer. Odyssey dual-color infrared fluorescence imaging system (LI-COR, USA) was utilized to scan, save and calculate the gray value of protein bands. Breast cancer cell lines (T47-D; Shanghai Fengshou Biotechnology Co., Ltd., China) were classified into positive control group. PR-M(+) (progesterone receptor positive), PR-M(-) (progesterone receptor negative), PR-A (progesterone receptor A) and PR-B (progesterone receptor B) cell lines were screened.

Thiazolyl blue tetrazolium bromide (MTT) assay for cell proliferation

The cells were inoculated into a 96-well plate at a cell density of $1x10^3$ cells/well and added into DMEM medium (100 μl/well; Beijing Baierdi Biotechnology Co., Ltd., China). After 24 h of starvation culture, PR-M(+) and PR-M(-) groups were added to different concentrations of

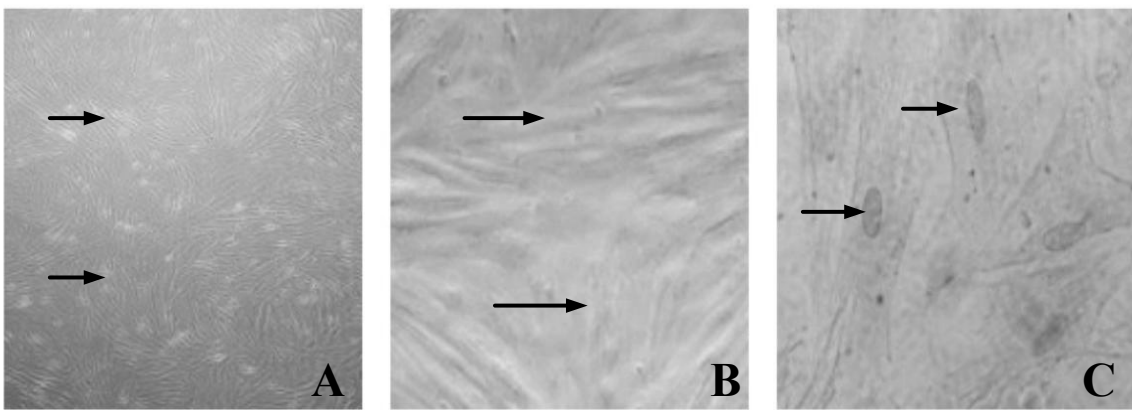

Fig. 1. *Morphology of leiomyoma cells under an inverted microscope. **A**) Morphology of uterine leiomyoma cells under a 100×microscope; **B**) Morphology of uterine leiomyoma cells under a 400× microscope; **C**) Identification of uterine smooth muscle cells by immunohistochemical DAB staining under a 100 × microscope)*

mifepristone (MIF) (Hubei Gedian Renfu Pharmaceutical Co., Ltd., China): 0mol/L, 1 x 10^{-6} mol/L, 1 x 10^{-5} mol/L, and 1 x 10^{-4} mol/L, respectively. MTT solution 150 μL/well (Shanghai Heart Language Biotechnology Co., Ltd., China) was added and placed in an incubator for 4 h. The absorbance was measured at a wavelength of 450 nm by enzyme labeling. The DMEM medium and MTT solution were mixed uniformly at a ratio of 2:3 as blank group. The inhibition rate was calculated according to the formula: absorbance = (OD of control group – OD of experimental group)/(OD of control group – OD of blank group)*100%. The control group was cultured with 0 mol/L MIF, while the experimental group was cultured with 1 x 10^{-6} mol/L, 1 x 10^{-5} mol/L and 1 x 10^{-4} mol/L MIF, respectively.

Detection of apoptosis by flow cytometry

The cell density was 2x10^5 cells/well. The PR-M(+) group and PR-M(-) group were divided into four groups. Different concentrations of MIF were added to 0 mol/L, 1 x10^{-6} mol/L, 1 x10^{-5} mol/L, and 1 x10^{-4} mol/L, respectively. After 48 h of incubation, the supernatant was discarded and cells were rinsed with PBS (at 4°C) twice (500 r/min, 5 min/time) by centrifugation. At room temperature, 100 μL Binding Buffer (Hangzhou Beiwo Medical Technology Co., Ltd., China) suspension, 5 μL Annexin V (Shanghai Ruishi Biotechnology Co., Ltd., China) and 5 μL Propidium Iodide (PI) (Nanjing Institute of Bioengineering, China) were added; 10 min later, 40 μL Binding Buffer was added. The mixture was homogenized and detected by flow cytometry (EPICS XL/XL-MCL; Beckman Kurt Company, USA).

Detection of Caspase-3 and Bcl-2 expression levels by Western blot

Uterine leiomyoma cells (logarithmic growth phase) were inoculated into a cell culture flask at a density of 1x10^5 cells/well. Different concentrations of MIF including 0 mol/L,1 x10^{-6} mol/L, 1 x10^{-5} mol/L and 1 x10^{-4} mol/L were added, and three parallel samples were set up. After 24 h, the culture medium was discarded the cells were washed three times with PBS along with RIPA (Radio Immunoprecipitation Assay) pyrolysis solution (Shanghai Jinsui Biotechnology Co., Ltd., China). After centrifugation at 4°C for 10 min (12000 r/min), the supernatant was absorbed. Concentrated gel electrophoresis (80 V) was performed for 30 min and separation gel electrophoresis (120 V) was conducted for 90 min. When protein was electro-transferred to NC membrane, it was sealed with skimmed milk powder (5%) (Shanghai Huashun Biotechnology Co., Ltd., China) for 1 h. Caspase-3 monoclonal antibody 0.1 ug/mL (Xi'an Jiacheng Biotechnology Co., Ltd., China) and Bcl-2

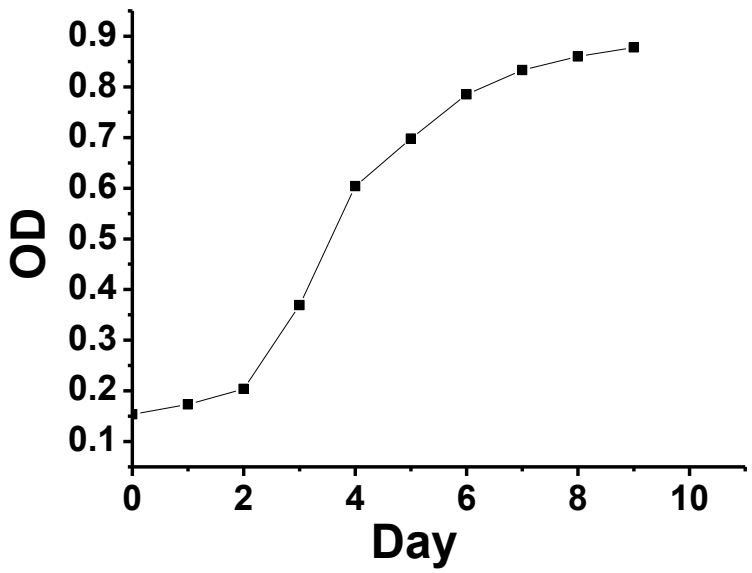

Fig. 2. *Growth curve of uterine leiomyoma cells.*

monoclonal antibody 0.1 ug/mL (Shanghai Wanjiang Biotechnology Co., Ltd., China) were added to the NC film and placed in the refrigerator overnight. Next day, sheep anti-rabbit IgG labeled with red fluorescence (dilution ratio 1:4000) was added, followed after 2 h by was washing three times with PBS.

Statistical analysis

Data processing and analysis were performed using SPSS21.0 statistical software. Quantitative data consistent with normal distribution were described by mean ± standard deviation. Comparison between the two groups was performed by two independent samples *t*-test or rank sum test. The comparison of different group rates was performed by *chi*-squared test. $P < 0.05$ indicated significant difference.

RESULTS

Primary cell identification

After 24 h of inoculation, the cells adhered to the wall and grew slowly, showing a long fusiform or irregular shape which was observed under an inverted microscope. Then they were left to continue

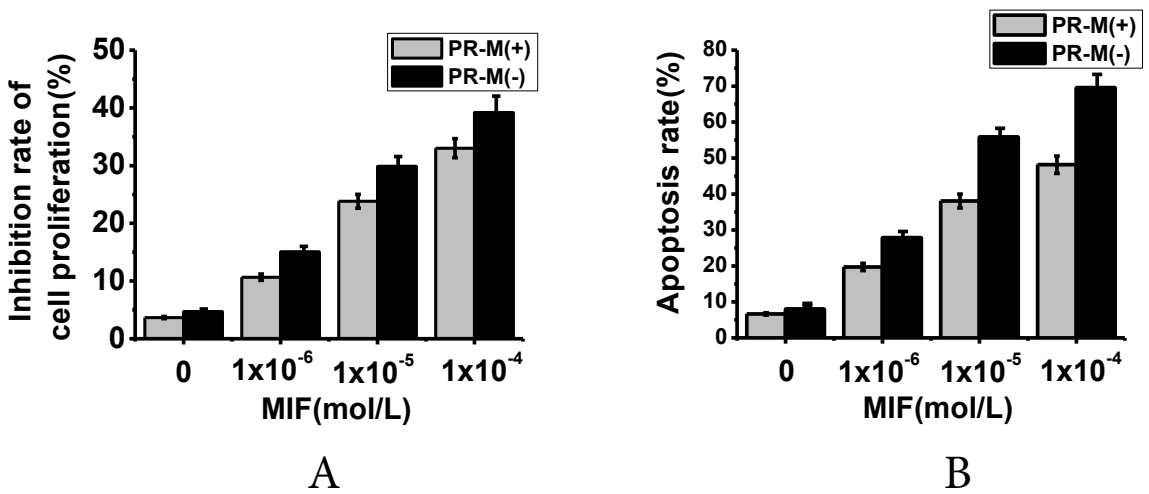

Fig. 3. *Effects of different concentrations of MIF on the cell proliferation inhibition rate and apoptosis rate.* ***A****) Inhibition rate of proliferation;* ***B****) Rate of apoptosis.*

Table I. *Effects of different concentrations of MIF on the cell proliferation inhibition rate*

MIF(mol/L)	PR-M(+)(%)	PR-M(-)(%)
0	3.67±0.30	4.72±0.85
1×10^{-6}	10.66±1.17*	15.03±1.27*
1×10^{-5}	23.81±2.65*	29.87±3.01*
1×10^{-4}	33.01±3.58*	39.19±3.98*

*($\bar{x}$±s, *p <0.05)*

Table II. *Effects of different concentrations of MIF on the apoptosis rate.*

MIF(mol/L)	PR-M(+)(%)	PR-M(-)(%)
0	6.66±0.51	8.00±0.79
1×10^{-6}	19.73±1.38*	27.87±2.05*
1×10^{-5}	38.06±2.83*	55.83±2.92*
1×10^{-4}	48.15±3.06*	69.54±3.59*

($\bar{x}\pm s$, $^{*}p<0.05$)

Table III. *Results of protein expression levels of Caspase-3 and Bcl-2 .*

MIF(mol/L)	Caspase-3	Bcl-2
0	0.82±0.01	1.19±0.01
1×10^{-6}	1.25±0.01*	1.00±0.01*
1×10^{-5}	1.44±0.01*	0.81±0.02*
1×10^{-4}	1.71±0.02*	0.49±0.02*

($\bar{x}\pm s$, $^{*}p<0.05$)

proliferation. The morphology of primary uterine leiomyoma cells is shown in Fig. 1. After one week of growth, the number of uterine leiomyoma cells reached a peak, as shown in Fig. 1 A and B, which showed the typical characteristics of smooth muscle cell growth, that was, "peak-valley" growth. Fig. 1C shows the result of immunohistochemical DAB staining. Smooth muscle actin was positive with brown filamentous structure in the cytoplasm.

Drawing of the growth curve of uterine leiomyoma cells

Based on the growth of passaged uterine leiomyoma cells, it could be observed that the initial 24-48 h were the growth latency period. After 48 h of inoculation, the cells grew rapidly and proliferated. This was the logarithmic growth phase. The seventh day was the plateau, and cell monolayer was formed. The overall curve of cell growth which was "S"-shaped is shown in Fig. 2,.

MTT method

As shown in Table I and Fig.3A, the MIF concentration increased, and the inhibition rates of cell proliferation in PR-M(+) and PR-M(-) groups increased with the blank control group (MIF 0 μmol/L). The same concentration of MIF was applied to PR-M(+) and PR-M(-) groups, and the inhibition rate of cell proliferation in PR-M(+) group was smaller than that in PR-M(-) group.

Flow cytometry

As shown in Table II and Fig. 3B, the MIF concentration increased, and the apoptosis rates of PR-M(+) and PR-M(-) cells increased with the blank control group (MIF 0 μmol/L). The same concentration of MIF was applied to the PR-M(+) group and PR-M(-) group. The apoptosis rate of PR-M(+) group was less than that of PR-M(-) group.

Detection of the progesterone receptor expression by Western blot

Expressions of PR-M(+), PR-M(-), PR-A and PR-B cell lines were detected by Western blot. The

scanning results of Odyssey dual-color infrared fluorescence imaging system are shown in Fig. 4A. T-47D breast cancer cell line, which was used as positive control group, expressed PR-M, PR-A and PR-B simultaneously. PR-M(+) cell lines expressed PR-M but not PR-A, and PR-B. PR-M(-) cell lines expressed PR-A and PR-B but not PR-M.

Detection of Caspase-3 and Bcl-2 protein expression

In protein immunoblotting, the results of protein expression levels are shown in Table III and Fig. 4B. As the concentration of MIF increased, the expression of Caspase-3 (pro-apoptotic protein) increased, and the expression of Bcl-2 (anti-apoptotic protein) decreased, compared with the blank control group.

DISCUSSION

MIF is a progesterone antagonist with a structure similar to steroid hormones and has a strong affinity for progesterone receptors (12-14). MIF was initially used to prevent early pregnancy and has been used in recent years for the treatment of diseases such as uterine leiomyoma (15). In this study, an *in-vitro* uterine leiomyoma cell model was successfully established, which could increase the cell extraction rate and cell number through shortening the time required for surgical specimens to be transported to the laboratory and rapid cleaning of the uterine leiomyoma cells. Using primary cultured uterine leiomyoma cells, PR-M, PR-A and PR-B cell lines with high protein expression were detected by Western blotting, and PR-M(+) cells were screened out. The strain was used as the experimental group specimen, and the PR-M(-) cell strain was used as the control group specimen. Moreover, the T47D breast cancer cell strain was used as the positive control, which was a specific antibody that simultaneously expressed PR-M, PR-A as well as PR-B cells. Different concentrations of MIF were used to intervene in PR-M(+) uterine leiomyoma cells. It could be concluded from the test results that the proliferation inhibition rate and apoptosis rate of both groups increased with the increase of MIF

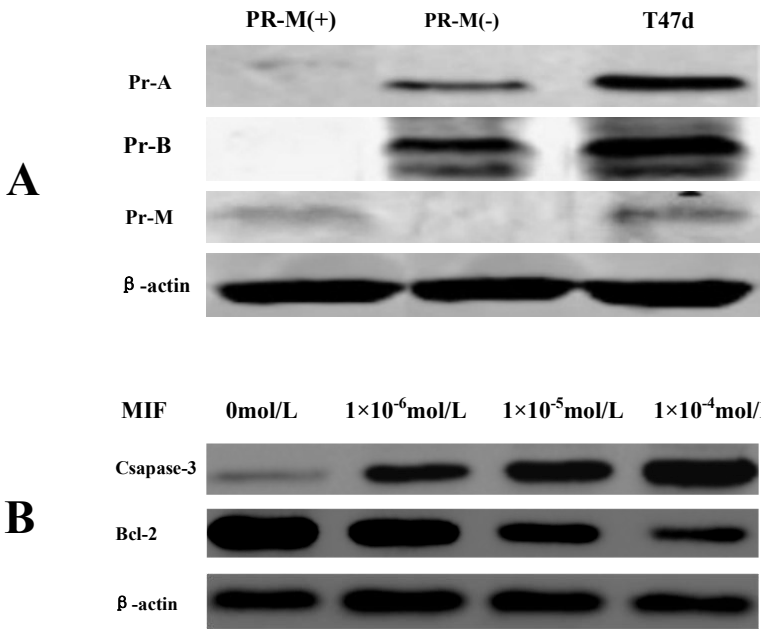

Fig. 4. ***A)*** *Western blot results of progesterone receptor. T-47D breast cancer cell line was the positive control group, and beta-actin was the internal parameter index of antibody.* ***B)*** *Results of Caspase-3 and Bcl-2 protein expressions at different concentrations of MIF.*

concentrations. According to the results of Western blotting, as the concentration of MIF increased, the expression of Caspase-3 protein increased while the expression of Bcl-2 decreased, which was statistically different from the blank control group.

Bcl-2 is a gene that inhibits apoptosis and is an important regulator of mitochondria-related apoptosis release, which plays a key role in apoptosis (16-18). The results of this study demonstrated that progesterone receptors inhibit cell apoptosis by inhibiting the expression of Bcl-2 gene, thereby promoting the proliferation of uterine leiomyoma cells.

In summary, in the development of uterine leiomyoma disease, progesterone receptor M can inhibit the apoptosis of uterine leiomyoma cells and promote cell proliferation, which may be achieved through up-regulating the pro-apoptotic protein Caspase-3 and down-regulating the anti-apoptotic protein Bcl-2. This effect of the progesterone receptor M can be inhibited by a progesterone receptor antagonist (mifepristone).

REFERENCES

1. Segars JH, Al-Hendy A. Uterine leiomyoma: new perspectives on an old disease. Semin Reprod Med 2017; 35(6):471-72.
2. Islam MS, Ciavattini A, Petraglia F, Castellucci M, Ciarmela P. Extracellular matrix in uterine leiomyoma pathogenesis: a potential target for future therapeutics. Hum Reprod Update 2018; 24(1):59-85.
3. Nicolaus K, Bräuer D, Sczesny R, Lehmann T, Diebolder H, Runnebaum IB. Unexpected coexistent endometriosis in women with symptomatic uterine leiomyomas is independently associated with infertility, nulliparity and minor myoma size. Arch Gynecol Obstet 2019; 300(1):103-8.
4. Borah BJ, Laughlin-Tommaso SK, Myers ER, Yao X, Stewart EA. Association between patient characteristics and treatment procedure among patients with uterine leiomyomas.Obstet Gynecol 2016; 127(1):67-77.
5. Zepiridis LI, Grimbizis GF, Tarlatzis BC. Infertility and uterine fibroids. Best Pract Res Clin Obstet Gynaecol 2016; 34:66-73.
6. Price TM, Dai Q. the role of a mitochondrial progesterone receptor (PR-M) in progesterone action. Semin Reprod Med 2015; 33(3):185-94.
7. Feng Q, Crochet JR, Dai Q, Leppert PC, Price TM. Expression of a mitochondrial progesterone receptor (PR-M) in leiomyomata and association with increased mitochondrial membrane potential. J Clin Endocrinol Metab 2014; 99(3):E390-9.
8. Feng Q, Crochet JR, Dai Q, Leppert PC, Price TM. Expression of a mitochondrial progesterone receptor (PR-M) in leiomyomata and association with increased mitochondrial membrane potential. J Clin Endocrinol Metab 2014; 99(3):E390-9.
9. Tsigkou A, Reis FM, Lee MH, et al. Increased progesterone receptor expression in uterine leiomyoma: correlation with age, number of leiomyomas, and clinical symptoms. Fertil Steril 2015; 104(1):170-75.
10. Yin P, Lin Z, Cheng YH, et al. Progesterone receptor regulates Bcl-2 gene expression through direct binding to its promoter region in uterine leiomyoma cells. J Clin Endocrinol Metab 2007; 92(11):4459-66.
11. Xu Q, Takekida S, Ohara N, et al. Progesterone receptor modulator CDB-2914 down-regulates proliferative cell nuclear antigen and Bcl-2 protein expression and up-regulates caspase-3 and poly(adenosine 5'-diphosphate-ribose) polymerase expression in cultured human uterine leiomyoma cells. J Clin Endocrinol Metab 2005; 90(2):953-61.
12. Kannan A, Bhurke A, Sitruk-Ware R, et al. Characterization of molecular changes in endometrium associated with chronic use of progesterone receptor modulators: ulipristal acetate versus mifepristone. Reprod Sci 2018; 25(3):320-28.
13. Chabbert-Buffet N, Kolanska K, Daraï E, Bouchard P. Selective progesterone receptor modulators: current applications and perspectives. Climacteric 2018; 21(4):375-79.
14. Sarvilinna N, Unkila-Kallio, Härkki P, Tiitinen A, Heikinheimo O.Selective progesterone receptor modulators: new possibilities for gynecologic hormone therapy. Duodecim 2017; 133(1):27-33.
15. Arora D, Chawla J, Kochar SPS, Sharma JC. A randomized control trial to assess efficacy of Mifepristone in medical management of uterine fibroid. Med J Armed Forces India 2017; 73(3):267-73.
16. Yin P1, Lin Z, Cheng YH, et al.Progesterone receptor

regulates Bcl-2 gene expression through direct binding to its promoter region in uterine leiomyoma cells.J Clin Endocrinol Metab 2007; 92(11):4459-66.

17. Kim KW, Jin UH, Kim DI,et al. Antiproliferative effect of Scutellaria barbata D. Don. on cultured human uterine leiomyoma cells by down-regulation of the expression of Bcl-2 protein. Phytother Res 008; 22(5):583-90.
18. Courtoy GE, Donnez J, Marbaix E, Barreira M, Luyckx M, Dolmans MM. Progesterone receptor isoforms, nuclear corepressor-1 and steroid receptor coactivator-1 and B-cell lymphoma 2 and Akt and Akt phosphorylation status in uterine myomas after ulipristal acetate treatment: a systematic immunohistochemical evaluation. Gynecol Obstet Invest 2018; 83(5):443-54.

INFLUENCE OF THE Klotho/FGF23/Egr1 SIGNALING PATHWAY ON CALCIUM-PHOSPHORUS METABOLISM IN DIABETIC NEPHROPATHY AND THE INTERVENTION OF SHENYUAN GRANULES

X-R. ZOU[1,2], L-R. ZHAN[3], L. CHEN[3], Q-H. LONG[3], J. YUAN[1,2,3], L. WANG[1,2,3] and X-Q. WANG[1,2]

[1]Department of Nephrology, Hubei Provincial Hospital of Traditional Chinese Medicine, Wuhan, Hubei, China; [2]Department of Nephrology, Hubei Province Academy of Traditional Chinese Medicine, Wuhan, Hubei, China; [3]First Clinical College, Hubei University of Chinese Medicine, Wuhan, Hubei, China

Received May 16, 2019 – Accepted November 11, 2019

This study aimed to explore the effects of Shenyuan granules on the Klotho/FGFR23/Egr1 signaling pathway and calcium-phosphorus metabolism in diabetic mice models with impairment of renal function. Streptozotocin-induced diabetic nephropathy (DN) mice models were randomly divided into three groups: Shenyuan granules group (n=10), model control group (n=10), and blank control group (n=10). Corresponding drugs were given by gavage for 8 weeks. Blood glucose and serum creatinine (SCr), urea nitrogen (BUN), calcium (Ca), phosphorus (P) and mLAB were detected before and after administration. Moreover, RT-qPCR was performed to detect the expression of CYP24 and CYP27 mRNA in kidney tissue. Blood FGF23 was detected by ELISA. Western-blot and immunohistochemistry were performed to detect the expressions of Klotho, FGFR1, Egr1, CYP24, CYP27, ERK1/2 and p-ERK1/2. Compared with the blank control group, in the model control group serum FGF23,P, SCr and 24-hour proteinuria levels increased (P<0.05), serum Ca significantly decreased (P<0.05), expressionss of Egr1, CYP24, CYP27 and p-ERK1/2 were up-regulated (P<0.05), and the expressions of Klotho and FGFR1 were down-regulated (P<0.05). After treatment, compared with the model control group, in the Shenyuan granule group serum FGF23, P, SCr levels decreased (P<0.05), serum Ca increased (P<0.05), expressions of Egr-1, CYP24, CYP27 and p-ERK1/2 were down-regulated (P<0.05), and the expressions of Klotho and FGFR1 were up-regulated (P<0.05). Shenyuan granules may partly intervene in the expressions of CYP24 and CYP27 through the Klotho/FGF23/Egr1 signaling pathway, thereby improving calcium and phosphorus metabolism and alleviating renal injury in diabetic nephropathy.

Globally, the incidence of metabolic diseases such as diabetes mellitus is rapidly increasing (1). With the high incidence of diabetes, the number of patients with diabetic nephropathy (DN) is also on the increase (2). In China, DN has become the primary cause of end-stage renal disease (3), and more than 50% of DN patients die from cardiovascular diseases (4), therefore DN has become a serious public health concern. Calcium deposition is a characteristic of vascular media calcification, and arteriosclerosis with medial calcification is a key cause of cardiovascular complications in DN (5). Therefore, it is of great significance to pay attention to and strengthen the study of vascular calcification mechanism related to

Key words: diabetic nephropathy; Klotho; calcium-phosphorus metabolism;Shenyuan granules

Corresponding Author:
Dr Xiao-Qin Wang,
Department of Nephrology, Hubei Provincial Hospital of Traditional Chinese Medicine, No. 856 of Luoyu Road, Hongshan District, Wuhan, Hubei 430074, China
Tel.: +86 10 8774 8220 - Fax: +86 10 8774 8220
e-mail: wangxq55wxq@163.com

0393-974X (2019)

DISCLOSURE: ALL AUTHORS REPORT NO CONFLICTS OF INTEREST RELEVANT TO THIS ARTICLE.

abnormal calcium and phosphorus metabolism in DN for the prevention and treatment of cardiovascular complications of diabetes mellitus. Traditional Chinese medicine (TCM) has been playing an important role in the prevention and treatment of DN with its unique advantages of multi-target and multi-level intervention. In our previous study, Shenyuan Granules, a traditional Chinese medicine (TCM) prescription, was used to improve calcium and phosphorus metabolism in rat models by regulating the Klotho (Kl)/FGF23 signaling pathway (6). The present study intended to further observe the mechanism of Kl signaling pathway affecting calcium and phosphorus metabolism and vascular calcification in DN and the effect of intervention with Chinese medicine on vascular calcification in DN.

MATERIALS AND METHODS

Thirty specific-pathogen free (SPF) grade C57BL/6 male mice, seven weeks old and weighing 16-22g, were purchased from Hubei Laboratory Animal Research Center, with license SCXK (Hubei) 2015-0018, certificate number: 42000600015155. The temperature of the feeding environment ranged within 20-24°C, and humidity ranged within 10-40%. The mice were provided with free access to food and water.

Shenyuan Granules, a Chinese herbal medicine compound, was prepared in the Preparation Center of Hubei Traditional Chinese Medicine Hospital (Astragalus, *Herba Epimedii* and Rhubarb are the main constituents, approval number: Hubei Medicine Z20113155); Trizol was purchased from Beijing Aidlab; streptozotocin (STZ) was purchased from SIGMA; RNA first strand cDNA synthesis kit and All-in-one quantitative real-time PCR (qPCR) Mix were purchased from Genecopoeia (USA); Rabbit anti-FGFR1, rabbit anti- early growth response gene 1 (Egr1), rabbit anti-CYP24 and rabbit anti-CYP27 were purchased from Wuhan Proteintech Group, Inc.; Rabbit anti-Kl was purchased from Abcam (UK); Mouse anti-β-actin was purchased from Wuhan Boster Biotechnology, Ltd.; Roche Biochemical kit was purchased from Roche (Swiss); Mouse fibroblast growth factor-23 (FGF23) enzyme-linked immunosorbent assay (ELISA) kit was purchased from Abcam (UK).

Modeling and grouping

The mice underwent adaptive feeding for 10 days, then mouse models were established. STZ was dissolved in a citric acid buffer with a pH of 4.5, then a single intraperitoneal injection was given to mice at a rate of 150 mg/kg. After three days, blood glucose was continuously measured through tail vein blood sampling for three days, where the blood glucose was always higher than 16.7 mmol/L. Continuous detection revealed that urinary microalbumin (mALB) increased, suggesting the models were successfully established. Mice with successful modeling were divided into two groups using a random number table: model control group (n=10) and Shenyuan granules group (n=10). In addition, a blank control group (n=10) was set up, in which mice were intraperitoneally injected with an equal volume of citric acid buffer. The dosage for mice was converted by body surface coefficient: Shenyuan Granules were fully dissolved in distilled water into a 0.5g/ml suspension, the dosage of intragastric administration was 4.55 g/Kg/day, the volume of intragastric administration was 0.2-0.3 ml, daily. Mice in the blank control group and model control group were orally fed with corresponding volumes of distilled water according to body weight. Intragastric administration lasted for eight weeks.

Collection and treatment of specimens

Before administration, blood samples were taken from the tail tips to detect blood glucose, and blood was taken from the tail vein for future use. After eight weeks of drug intervention, mice in all groups were placed in separate metabolic cages and fasted without water deprivation. The total 24-hour urine volume was determined using a urine collection tube, centrifuged, and supernatant was obtained to measure the 24-hour urinary mALB. At the end of the experiment, the eyeballs of the mice in all groups were taken for blood collection. The blood was left standing for 40 min, then centrifuged at 4,000 rpm for 10 min, serum was obtained, and serum creatinine, urea nitrogen, calcium and phosphorus levels were measured. The mice were sacrificed, then the abdominal cavity was opened and the kidneys were taken, the capsule was removed, then tissues were stored at -80°C for future use. A Roche fully automatic biochemical analyzer was used to detect blood glucose, blood urea nitrogen, creatinine, serum calcium, phosphorus and urine mALB.

Enzyme-linked immunosorbent assay

Blank wells and tested sample wells were set up respectively, and standards were diluted and loaded. Tested sample wells on the enzyme labeled plate received 40 µl of sample diluent then received 10 µl of the sample to be tested, and the wells were sealed with a plate-sealing membrane, then the samples were incubated at 37°C for 30 min. The 30-fold concentrated detergent was diluted with distilled water for future use. The plate-sealing membrane was removed; the liquid was discarded then dried out. Detergent was added to each well, left standing for 30 s, then discarded, this procedure was carried out five times, and samples were dried by patting. 50 µl of FGF23 enzyme labeled reagent was added to each well, except for the blank well. Incubation and washing operations were performed as before. During development, each well received 50 µl of chromogenic agent A, then received 50 µl of chromogenic agent B, was shaken gently to mix, then placed in the dark and developed at 37°C for 15 min. 50 µl of stop solution was added to each well to terminate the reaction; under this condition, the blue color immediately turned to yellow color.

Fluorescence quantitative PCR detection

100 mg of renal tissue was added with corresponding 1 ml of Trizol, and the total RNA was extracted from kidney tissues in all groups according to the manufacturer's instructions. 2 µl of total RNA was added to 200 µl of DEPC·ddH_2O, and its purity and concentration were determined using a UV spectrophotometer. After the examination, reverse transcription was performed. The reverse transcription system (20 µl) was selected. The reaction conditions were as follows: 25°C for 5 min, 50°C for 15 min, 85°C for 5 min, and 4°C for 10 min. Reverse transcription product cDNA was diluted five times, according to the manufacturer's instructions, then the corresponding primers, qPCR Master Mix and ultra-pure water were added for configuration of the 20-µl system. The reaction conditions were 50°C for 2 min, 95°C for 10 min, 95°C for 5 s, and 60°C for 30 s, with a total of 40 cycles performed. A dissolution curve was drawn within 60-95°C and 0.5°C/s. The final data were analyzed using $2^{-\Delta\Delta Ct}$. Primer Premier 5.0 software was used to design the primer sequence (Table I).

Western blot

Approximately 100 mg of the kidney tissue was obtained, to which a protein lysis solution was added, then the mixture was homogenized, repeatedly homogenized on ice to crush the tissue as much as possible for full lysis, centrifuged and supernatant was obtained, then the protein of kidney tissue was obtained. Some protein samples were diluted and the protein concentration was determined. Electrophoresis gel was prepared, and 50 µg of the total protein sample was obtained which underwent electrophoresis for approximately 1.5 h. Gel was taken out, target bands were cut according to the markers, filled with transfer buffer, then transferred onto membrane in the transmembrane groove. Polyvinylidene fluoride (PVDF) membrane was immersed in Tris-Buffered Saline and Tween 20 (TBST) containing 5% dried skimmed milk, and sealed on a shaking table at room temperature for 2 h. The corresponding first antibodies were diluted with a blocking solution, to allow the PVDF membrane to be immersed in incubation solution with the first antibodies and left standing overnight at 4°C. Redundant first antibodies were washed out, and the corresponding horseradish peroxidase (HRP)-labeled secondary antibody was diluted with blocking solution (diluted at 1:50000), to allow the PVDF membrane to be immersed in incubation solution with the secondary antibodies, then incubated on a shaking table at 37°C for 2 h. Redundant secondary antibodies were washed out, developed and exposed. The gel analysis system was used to analyze and calculate the gray value of the film.

Immunohistochemical analysis

Kidney tissues were dehydrated, treated with xylene till they became transparent, dipped in wax and embedded, prepared in paraffined sections and baked, then dewaxed. Sectioned tissue was added with prepared 3% hydrogen peroxide to block endogenous peroxidase, incubated at room temperature for 15 min, rinsed with phosphate buffered saline (PBS) for 3 min in triplicate, to which the first antibodies, polymer adjuvants, were added, then HRP-labeled IgG polymer and diaminobenzidine (DAB) color developing solution and Harris hematoxylin for re-staining, dehydrated and sealed, then underwent microscopic examination and photographed.

Statistical analysis

Data were analyzed using statistical software SPSS l7.0. Measurement data were expressed in mean ± standard

deviation (x±SD). Comparison among groups was conducted using analysis of variance (ANOVA). Means were compared using ANOVA, and the homogeneity of variance was tested using the Levene method. Pairwise comparison was carried out using the least significant difference (LSD) test and Tamhane method. $P<0.05$ was considered statistically significant.

RESULTS

Biochemical indicators and detection of serum FGF23 level by ELISA

After mice in all groups were treated for eight weeks, compared with the blank control group, the levels of blood glucose, microalbumin, serum phosphorus and creatinine in the model control group and Shenyuan granules group were higher. Compared with the model control group, the levels of blood glucose, microalbumin, serum phosphorus and creatinine in the Shenyuan granules group were lower. Compared with the blank control group, the blood calcium level in the model control group and Shenyuan granules group was lower. Compared with the model control group, the blood calcium level in the Shenyuan granules group was higher. The difference in blood urea nitrogen (BUN) among groups was not statistically significant. ELISA results revealed that, compared with the blank control group, the levels of serum FGF23 in the model control group and Shenyuan granules group were significantly higher. Compared with the model control group, the level of serum FGF23 in the Shenyuan granules group was significantly lower (Table II).

Detection of CYP24 and CYP27 mRNA expression in renal tissue by fluorescence quantitative PCR

Compared with the blank control group, the mRNA expressions of CYP24 and CYP27 in the kidneys

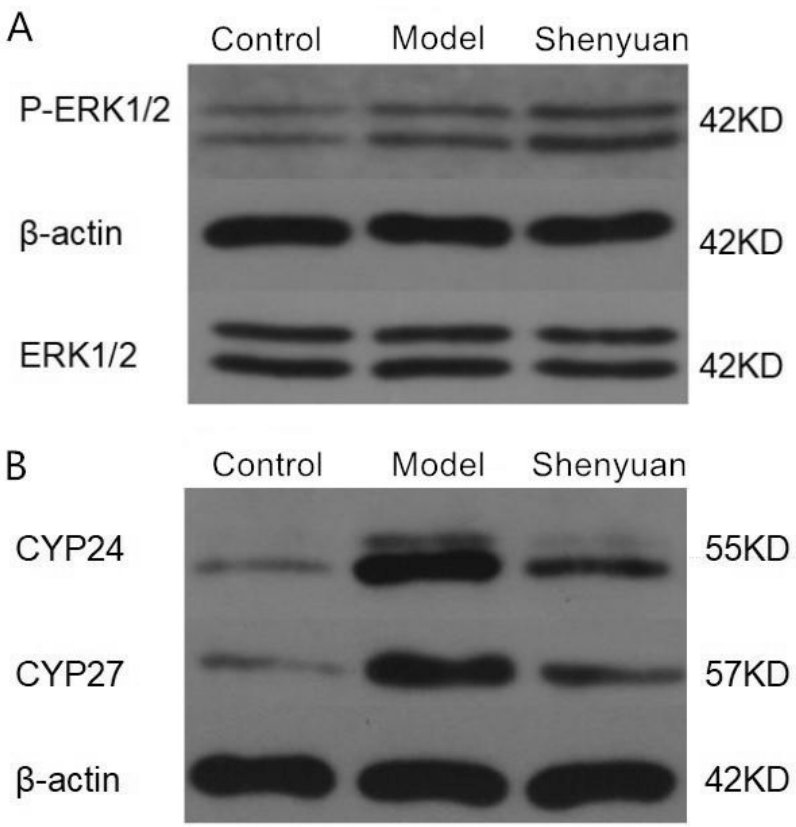

Fig. 1. *Detection of CYP24, CYP27, ERK1/2 and p-ERK1/2 protein expression in the kidney of mice in all groups by Western blot.*

of mice in the model control group and Shenyuan granules group were up-regulated. Compared with the model control group, the mRNA expressions of CYP24 and CYP27 in the kidneys of mice in the Shenyuan granules group were down-regulated (Table III).

Detection of CYP24, CYP27, ERK1/2 and p-ERK1/2 protein expression in the kidneys by Western blot

Compared with the blank control group, the protein expressions of p-ERK1/2, CYP24 and CYP27 in the kidneys of mice in the model control group and Shenyuan granules group were up-regulated. Compared with the model control group, the protein expressions of p-ERK1/2, CYP24 and CYP27 in the kidneys of mice in the Shenyuan granules group were down-regulated. The difference in ERK1/2 among groups was not statistically significant (Table IV, Fig. 1).

Detection of the expressions of Kl, FGFR1 and Egr1 in the kidneys of mice in all groups by immunohistochemistry

Immunohistochemical results of mice in all groups were analyzed. The results revealed that, compared with the blank control group, the dyeing intensities of Kl and FGFR1 in the kidneys of mice in the model control group decreased, while the dyeing intensities of Kl and FGFR1 in the kidneys of mice in the Shenyuan granules group increased. Compared with the model control group, the dyeing intensities of Kl and FGFR1 in the kidneys of mice in Shenyuan granules group increased more significantly. Compared with the blank control group, the dyeing intensities of Egr1 in the kidneys of mice in the model control group and Shenyuan granules group increased. Compared with the model control group, the dyeing intensity of Egr1 in the kidneys of mice in the Shenyuan granules group decreased (Table V, Fig. 2).

DISCUSSION

Kl has receptor, ligand and enzyme functions and was originally thought to be a gene associated with aging and. Furthermore α-Kl is mainly secreted by the distal tubular epithelial cells of the kidney, is expressed in the kidney and can be involved in regulating the

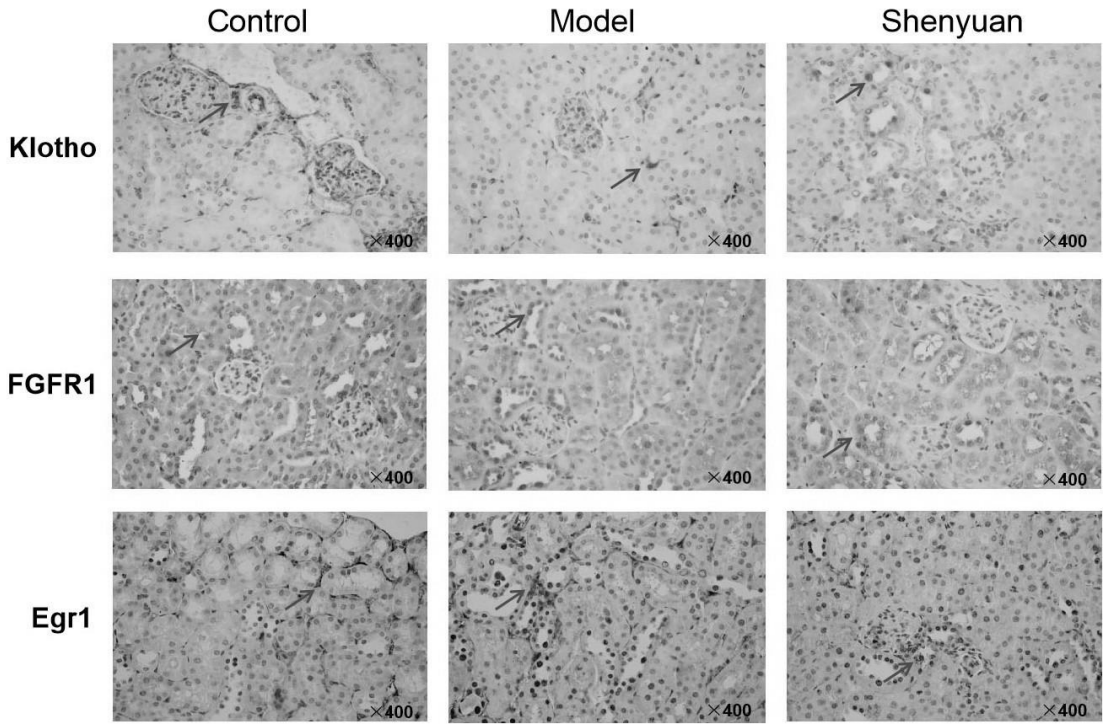

Fig. 2. *Immunohistochemical results of Klotho, FGFR1 and Egr1 in the kidney of mice in all groups.*

metabolism of minerals such as calcium and phosphorus (7). When Kl expression is defective, serum soluble Kl is insufficient, then patients present with obvious arteriosclerosis and vascular calcification (8). FGF23 regulated by Kl is secreted by skeletal cells (9), has the functions of regulating the content of active vitamin D and the metabolism of calcium and phosphorus in the kidney (10, 11). Phosphorylated α-Kl by extracellular signal-regulated protein kinase (ERK) binds to FGFR1 to form a receptor, then binds to FGF23 to form a functional protein complex to induce change in the expression of the Egr1, enhances the coding of the 24-hydroxylase (CYP24) gene, inhibits the expression of the 1α-hydroxylase (CYP27B1) gene to promote the degradation of $1,25(OH)_2VitD_3$ on the one hand and reduce the formation of $1,25(OH)_2VitD_3$ on the other

Table I. *RT-qPCR Main primers.*

Primer	Primer sequence
CYP24	Mus CYP24 F: 5'- CAAATCGATGAGCTGCGTGA-3' Mus CYP24 R: 5'- TGTTTTGATGGCCGCAATGA-3'
CYP27	Mus CYP27B1 F: 5'- GAAGGTGAAGCTGCGATGAG -3' Mus CYP27B1 R : 5'- TCAGAGTGGAGTGCAGTCTG -3'
β-actin	Mus β-actin F:5'-CACGATGGAGGGGCCGGACTCATC-3' Mus β-actin R:5'-TAAAGACCTCTATGCCAACACAGT-3'

Table II. *Detection results of blood biochemistry, urinary microalbumin and FGF23 in mice of each group after 8 weeks of treatment(x±s).*

Group	n	Blood glucose (mmol/L)	Blood calcium (mmol/L)	Blood phosphorus (mmol/L)	Urea nitrogen (mmol/L)	Serum creatinine (umol/L)	Urinary microalbumin (ug/ml)	Blood FGF23 (ug/L)
Blank control group	10	6.9±1.4	2.4±0.1	2.6±0.2	9.0±1.0	21.1±3.3	22.1±2.4	144.6±18.9
Model control group	10	28.4±5.6*	2.2±0.2*	3.5±1.0*	10.1±1.9	34.7±5.7*	105.3±12.9*	191.3±19.7*
Shenyuan granules group	10	25.6±4.3*	2.3±0.1*$^{\Delta}$	2.8±0.3*$^{\Delta}$	9.0±1.6	28.1±3.4*$^{\Delta}$	68.9±6.3*$^{\Delta}$	166.8±24.3*$^{\Delta}$

*Note: Compared with blank control group,*P<0.05; Compared with model control group, $^{\Delta}$P<0.05.*

Table III. *Detection of CYP24 and CYP27 mRNA expression in mice by RT-PCR(x±s).*

Group	CYP24/β-actin	CYP27/β-actin
Blank control group	1.01±0.10	1.061±0.17
Model control group	1.49±0.36*	1.751±0.40*
Shenyuan granules group	1.30±0.26*$^{\Delta}$	1.352±0.20*$^{\Delta}$

*Note: Compared with blank control group,*P<0.05; Compared with model control group, $^{\Delta}$P<0.05.*

Table IV. *Expression of CYP24, CYP27, ERK1/2 and p-ERK1/2 in mice of each group by Western Blot(x±s).*

Group	CYP24/β-actin	CYP27/β-actin	ERK1/2/β-actin	p-ERK1/2/β-actin
Blank control group	0.19±0.04	0.12±0.06	0.52±0.05	0.16±0.03
Model control group	0.91±0.06*	0.71±0.11*	0.50±0.04	0.35±0.07*
Shenyuan granules group	0.47±0.08*$^{\Delta}$	0.34±0.09*$^{\Delta}$	0.51±0.04	0.25±0.03*$^{\Delta}$

*Note: Compared with blank control group,*P<0.05; Compared with model control group, $^{\Delta}$P<0.05.*

Table V. *Quantitative results of immunohistochemical optical density of Klotho, FGFR1 and Egr1 in kidneys of mice in each group (x±s).*

Group	Klotho	FGFR1	Egr1
Blank control group	0.0020±0.0012	0.0057±0.0009	0.0036±0.0020
Model control group	0.0012±0.0009*	0.0044±0.0009*	0.0099±0.0039*
Shenyuan granules group	0.0037±0.0015*$^{\Delta}$	0.0073±0.0014*$^{\Delta}$	0.0051±0.0050*$^{\Delta}$

*Note: Compared with blank control group,*P<0.05; Compared with model control group, $^{\Delta}$P<0.05.*

hand (12-14). The human body maintains the balance of calcium-phosphorus metabolism in such positive and negative feedback regulations. But in the course of chronic kidney disease, when the expression of Kl, a synergistic receptor, is decreased, then FGF23 cannot bind to the corresponding Kl/FGFR1 complex receptor, resulting in the accumulation of FGF23 in the body (15). Studies have revealed that, in human DN, with the decrease in Kl gene expression, the concentration of serum FGF23 was significantly increased, which was accompanied by abnormal metabolism of active vitamin D and calcium and phosphorus (16, 17).

In the present study, in kidney tissue of DN mice, the protein expression of Kl and FGFR1 decreased, the protein expression of p-ERK1/2 increased, serum level of FGF23 increased, and the expression of Egr1 increased, increasing the expression of downstream CYP24 mRNA and protein. Additionally, the feedback expression of CYP27 mRNA and protein increased, ultimately, causing disorder of calcium-phosphorus metabolism, hypocalcemia and hyperphosphatemia. But after the intervention of Shenyuan granules, a TCM prescription, in the kidney, the protein expression of Kl and FGFR1 increased, serum level of FGF23 decreased, and the protein expression of Egr1 was inhibited, then the expression of downstream CYP24 mRNA and protein were down-regulated, and CYP27 mRNA and protein were concurrently inhibited. Finally, the disorder of serum calcium-phosphorus metabolism was improved, and microalbuminuria and renal injury were alleviated.

Shenyuan granules are a preparation formed through long-term clinical application summary and optimization in our department of the hospital. It is prepared with selected Astragalus, *Herba Epimedii* and Rhubarb. Our previous study on chronic renal failure in model rats revealed that, with the progress of chronic kidney disease, the expression of Kl in the kidney decreased, blood calcium, phosphorus and bone metabolism disorders, and Shenyuan granules could improve calcium-phosphorus metabolism and renal function by up-regulating the expression of Kl in the kidney (6). A study of DN model mice revealed that up-regulation of the expression of miR-199b-5p inhibited

the expression of Kl in the kidney, while Shenyuan granules could up-regulate Kl by inhibiting miR-199b-5p, finally improving calcium and phosphorus and bone metabolism (18).

Diabetic complications, especially DN, are common conundrums in the medical profession today. Cardiovascular calcification in DN is closely correlated to the disorders of calcium-phosphorus metabolism. In the present study, the regulatory mechanism of calcium-phosphorus metabolism based on the Kl/FGF23/Egr1 signaling pathway in DN mice were further explored, and the result revealed that Shenyuan granules might improve DN calcium-phosphorus metabolism and vascular calcification by interfering with this signaling pathway, providing a new target for the prevention and treatment of DN complications.

ACKNOWLEDGEMENTS

This study was funded by the National Science Foundation of China (81874439).

REFERENCES

1. Kahn SE, Cooper ME, Del Prato S. Pathophysiology and treatment of type 2 diabetes: perspectives on the past, present, and future. Lancet 2014; 383:1068-83.
2. Xu Y, Wang L, He J, et al. 2010 China Noncommunicable Disease Surveillance Group. Prevalence and control of diabetes in Chinese adults. Jama 2013; 310:948-59.
3. Zhang L, Long J, Jiang W, et al. Trends in chronic kidney disease in China. N Engl J Med 2016; 375:905-906.
4. Fernandez-Fernandez B, Ortiz A, Gomez-Guerrero C, Egido J. Therapeutic approaches to diabetic nephropathy--beyond the RAS. Nat Rev Nephrol 2014; 10:325-46.
5. Thompson B, Towler DA. Arterial calcification and bone physiology: role of the bone-vascular axis. Nat Rev Endocrinol 2012; 8:529-43.
6. Zou XR, Wang XQ, Wang CJ, Yuan J, Zhu SZ. Effect of Shen'an granule on KLOTHO gene expression in kidney tissue of rats with renal osteopathy. J Clin Nephrol 2013; 13:282-85.
7. Hum JM, O'Bryan LM, Tatiparthi AK, et al. Chronic hyperphosphatemia and vascular calcification are reduced by stable delivery of soluble klotho. J Am Soc Nephrol 2017; 28:1162-74.
8. Kim H, Kang E, Oh Y, et al. The association between soluble klotho and cardiovascular parameters in chronic kidney disease: results from the KNOW-CKD study. BMC Nephrol 2018; 19:51.
9. Eswarakumar VP, Lax I, Schlessinger J. Cellular signaling by fibroblast growth factor receptors. Cytokine Growth Factor Rev 2005; 16:139-49.
10. Kuro-O M, Moe OW. FGF23-alphaKlotho as a paradigm for a kidney-bone network. Bone 2017; 100:4-18.
11. Wang XQ, Zou XR, Zhang YC. From "kidneys govern bones" to chronic kidney disease, diabetes mellitus, and metabolic bone disorder: a crosstalk between traditional chinese medicine and modern science. Evid Based Complement Alternat Med 2016; 2016:4370263.
12. Urakawa I, Yamazaki Y, Shimada T, et al. Klotho converts canonical FGF receptor into a specific receptor for FGF23. Nature 2006; 444:770-74.
13. Nabeshima Y, Imura H. α-Klotho: A regulator that integrates calcium homeostasis. Am J Nephrol 2008; 28:455-64.
14. Xu P, Guan MP, Bi JG, Wang D, Zheng ZJ, Xue YM. High glucose down-regulates microRNA-181a-5p to increase pro-fibrotic gene expression by targeting early growth response factor 1 in HK-2 cells. Cell Signal 2017; 31:96-104.
15. Tan SJ, Smith ER, Holt SG, Hewitson TD, Toussaint ND. Soluble klotho may be a marker of phosphate reabsorption. Clin Kidney J 2017; 10:397-404.
16. Takahashi H, Komaba H, Takahashi Y, et al. Impact of parathyroidectomy on serum FGF23 and soluble klotho in hemodialysis patients with severe secondary hyperparathyroidism. J Clin Endocrinol Metab 2014; 99:652-58.
17. Lee EY, Kim SS, Lee JS, et al. Soluble a-Klotho as a Novel Biomarker in the Early Stageof Nephropathy in Patients with Type 2 Diabetes. PLOS ONE 2014; 9:1-8.
18. Zhan LR, Wang XQ, Zou XR, et al. Effect of Shenyuan granule on kidney of diabetic mice study on MicroRNA-199b-5p and calcium and phosphorus metabolism. Zhongguo Zhongyiyao Danganguan 2017; 35:2819-23.

miR-1290 PROMOTES PROLIFERATION AND SUPPRESSES APOPTOSIS IN ACUTE MYELOID LEUKEMIA BY TARGETING FOXG1/SOCS3

Y. SUN[1,2], X-L. JU[1], D. LI[3], P-P. ZHOU[1], X. LI[1] and R-H. LUO[2]

[1]Department of Pediatrics, Qilu Hospital, Shandong University, Jinan, Shandong Province, China;
[2]Department of Pediatrics, Taian City Central Hospital, Taian, Shandong Province, China;
[3]Laboratory of Cryogenic Medicine, Qilu hospital, Shandong University, Shandong Province, China

Received May 8, 2019 – Accepted November 7, 2019

Acute myeloid leukemia (AML) is an invasive hematological malignancy of which the mechanism is still unknown. MicroRNAs (miRNAs) act as critical controllers of target gene expression at post-transcriptional level. MiR-1290 is found to abnormally express in multiple cancers, however, its role in AML is still unknown. In this study, the mRNA and protein expression levels of related genes were determined by quantitative reverse transcription-polymerase chain reaction (qRT-PCR) and Western blot. Luciferase assay was used to verify the target genes of miR-1290. In addition, the cell proliferation, cell cycle and apoptosis of HL-60 and KG-1 cells were detected by Counting Kit-8 (CCK-8) and flow cytometry assay, respectively. Our results showed that the expression of miR-1290 was increased in AML *in vivo* and *in vitro*. Gain and loss of function experiments by transfection of miR-1290 mimics or miR-1290 inhibitors into HL-50 and KG-1 cells indicated that miR-1290 significantly promoted cell proliferation and inhibited cell apoptosis. Furthermore, Forkhead-box gene 1 (FOXG1) and Suppressor of cytokine signaling 3 (SOCS3) were verified to be the target genes of miR-1290. Overexpression of FOXG1 or SOCS3 inhibited cell proliferation and induced cell apoptosis in HL-50 and KG-1 cells. Moreover, knockdown of miR-1290 inhibited cell proliferation and promoted apoptosis, whereas these effects were reversed by silencing of FOXG1 or SOCS3 in HL-50 and KG-1 cells. In conclusion, miR-1290 promoted proliferation and suppressed apoptosis in AML by targeting FOXG1 and SOCS3, which might provide a therapeutic target for AML.

Acute myeloid leukemia **(**AML) is a common invasive hematological malignancy and is characterized by expansion of clonal myeloid blasts in the bone marrow and blood (1). The development of AML is generally driven by leukemia stem cells. Although the target genes driving the development of AML have been investigated, the treatment and survival rate of AML remain unsatisfactory. Therefore, it is still crucial to find new gene targets and further investigate the pathogenesis of AML.

MiRNAs are a series of endogenous, conserved small non-coding RNAs with a length of 20-25 nucleotides (2). The biological function of miRNA is mainly to regulate tumor pathogenesis by binding to the 3'-UTRs of target genes and inhibiting gene expression (3). Currently, miRNAs

Key words: MiR-1290; proliferation; apoptosis; AML; FOXG1; SOCS3

Corresponding Author:
Dr Xiuli Ju,
Department of Pediatrics, Qilu Hospital,
Shandong University, No. 107 Cultural West Road,
Lixia district, Jinan, Shandong province, China
Tel.: +86 0531 82169215
e-mail: xiulijufgh@163.com

0393-974X (2019)

DISCLOSURE: ALL AUTHORS REPORT NO CONFLICTS OF INTEREST RELEVANT TO THIS ARTICLE.

have been reported to be abnormally expressed in AML patients and involved in the development of AML (4, 5). MiR-449a inhibits AML cell growth, migration and invasion (6). A previous study demonstrated that upregulation of miR-96 inhibits cell proliferation in AML (7). Moreover, miR-628 inhibits the proliferation of AML cells and may serve as a therapeutic target in AML (8). Given that the miRNAs play crucial roles in AML, the function of other miRNAs in AML requires further investigation.

MiR-1290 is observed to be abnormally expressed in multiple cancers (9-11). In esophageal squamous cell carcinoma cells, miR-1290 promotes cell proliferation, migration and invasion by targeting the negative regulation of nuclear factor 1/X (NFIX) expression (12). In gastric cancer cells, miR-1290 promotes the proliferation and migration by targeting FOXA1 (13). In DNA-mismatch-repair-deficient colon cancer cells, miR-1290 enhances 5-FU chemotherapy resistance by targeting hMSH2 (14). In acute lymphoblastic leukemia cells, miR-1290 is up-regulated and involved in antineoplastic activity by targeting insulin-like growth factor binding protein 3 (IGFBP3) (15). However, the role of miR-1290 in AML remains unknown.

In this study, we found that miR-1290 was up-regulated in AML. Knockdown of miR-1290 inhibited the proliferation of HL-60 and KG-1 cells and promoted apoptosis, whereas these effects were reversed in HL-60 and KG-1 cells transfected with miR-1290 mimics. According to the prediction of TargetScan, FOXG1 and SOCS3 were the two targets of miR-1290. Luciferase reporter assay showed that miR-1290 could bind to the FOXG1/SOCS3 3'-UTRs and inhibit FOXG1/SOCS3 expression. These results provide a new perspective for understanding the pathogenesis of AML, and suggest that miR-1290 has the potential to be a novel therapeutic target for treatment of AML.

MATERIALS AND METHODS

Cell culture and transfection

Human AML cell line HL-60 was purchased from Zhongqiaoxinzhou company (ZQ0433; China) and the KG-1 cell line was purchased from and ATCC (ATCC Cell Bank, USA). HL-60 cells were cultured in Iscove's Modified Dulbecco's Medium (IMDM; Hyclone, USA) containing 20% fetal bovine serum (FBS, Gibco, USA) in a 37°C humidified incubator with 5% CO_2. KG-1 cells were cultured in Roswell Park Memorial Institute (RPMI; Gibco, USA) 1640 medium containing 10% FBS and 1% penicillin-streptomycin with 5% CO_2 at 37°C.

MiR-1290 mimic (miR-1290), mimic NC (Control), miR-1290 inhibitor or NC inhibitor were purchased from Ribobio company (Guangzhou, China). These biological molecules were transfected into HL-60 and KG-1 cells by Lipofectamine 2000 reagent (Invitrogen).

NC inhibitor or miR-1290 inhibitor together with siFOXG1 or siSOCS3 were co-transfected into HL-60 and KG-1 cells by Lipofectamine 2000 reagent (Invitrogen). The PCR product of FOXG1 or SOCS3 were inserted into pcDNA3.1 plasmid to construct the overexpression plasmids for FOXG1 or SOCS3. At the same time, the pcDNA3.1 plasmid (Vector) was regarded a control.

The sequences of these biological molecules were as follows: miR-1290 mimics (sense 5'-UGGAUUUUUGGAUCAGGGA-3', antisense 5'-CCUGAUCCAAAAAUCCAUU-3'), mimic NC (sense 5'-UUCUCCGAACGUGUCACGUTT-3', antisense 5'-ACGUGACACGUUCGGAGAATT-3'), has-miR-1290 inhibitor (sequence 5'-UCCCUGAUCCAAAAAUCCA-3') and NC inhibitor (sequence 5'-CAGUACUUUUGUGUAGUACAA-3'). siFOXG1-1#: 5'-GGACCAGACTGTAAGTGAA-3'; siFOXG1-2#:5'- GCCCTTCAGTTCAGGTACA-3'; siSOCS3-1#: 5'-CAGUAUGAUGCUUUAAAG-3'; siSOCS3-2#: 5'-GCTTCGACTGTGTACTCAA-3'; si-NC: 5'- UUCUCCGAACGUGUCACGU-3'.

Patient samples

This study was conducted in accordance with the Declaration of Helsinki. Bone marrow (BM) samples were obtained from 60 AML patients and 60 healthy donors at Qilu hospital, Shandong University. The written informed consents were obtained from the subjects, and the use of clinical specimens was determined and approved by the Qilu Hospital, Shandong University.

Quantitative Real-time PCR

Total RNAs were extracted from cells by using TRIzol™ Plus RNA Purification Kit (12183555, Invitrogen, USA).

The cDNAs were synthesized by reverse transcriptase (D2680A, Takara, Japan). qRT-PCR was performed by SYBR Premix Ex TaqTM II (RR820A, Takara, Japan). The relative expression level of target genes was calculated with $2^{-\Delta\Delta Ct}$ method. The sequences of primers were listed as follows: FOXG1-F: 5'-GAGCGACGACGTGTTCATC-3', FOXG1-R 5'-GCCGTTGTAACTCAAAGTGCTG-3'; SOCS3-F: 5′-TCGCCACCTACTGAACCCTC-3′, SOCS3-R: 5′-TGGTCCAGGAACTCCCGAAT-3′; U6-F: 5'-GTGCTCGCTTCGGCAGCACATATAC-3', U6-R: 5'-AAAAATATGGAACGCTCACGAATTTG-3; GAPDH-F: 5'-CGGAGTCAACGGATTTGGTCGTAT-3' andGAPDH-R:'-AGCCTTCTCCATGGTGGTGAAGAC-3'

CCK-8 assay

The cell proliferation was detected by using CCK-8 assay (C0038, Beyotime, China). Breifly, the transfected HL-60 or KG-1 cells were seeded into a 96-well plate, and grown at 37°C in 5% CO_2. The cell proliferation was evaluated at 24, 48, 72 and 96 h time-points. The detection of absorbance (450 nm) was carriedout using a microtiter plate reader (Molecular Devices, USA).

Flow cytometry analysis

After transfection, the cell cycle and cell apoptosis were analyzed by flow cytometry using a FlowSight flow cytometer (Merck Millipore, USA). The cell cycle was examined by staining cell with a Cell Cycle Analysis Kit (PK-CA577-K920, Promocell, Germany). The cell apoptotic rates were determined by using Annexin V-FITC Apoptosis Detection Kit (C1062S, Beyotime, China).

Luciferase reporter assay

The binding sites of wild type FOXG1 3'-UTR or SOCS3 3'-UTR with miR-1290 were inserted into the pmiR-GLO vector. And the miR-1290 mimic or miR-NC and FOXG1 3'-UTR-WT, SOCS3 3'-UTR-WT, FOXG1 3'-UTR-MUT or SOCS3 3'-UTR-MUT were co-transfected into HEK-293T cells by using Lipofectamine 2000. Then, the luciferase activities were analyzed by Luciferase reporter system (Promega, USA).

Western blot

Equal amounts of proteins extracted from cells were separated by 10% sodium dodecyl sulfate-polyacrylamide gel electrophoresis (SDS-PAGE) and then transferred onto polyvinylidene fluoride (PVDF) membranes (Beyotime, China). Then, the membranes were blocked with 5% skim milk and incubated with different primary antibodies, including CyclinD1 antibody (dilution 1:500; ab134175, Abcam, UK), p21 antibody (dilution 1:200; AP021, Beyotime), Bcl-2 antibody (dilution 1:500; ab117115, Abcam, UK), Bax antibody (dilution 1:500; ab32503, Abcam, UK), Cleaved caspase-3 antibody (dilution 1:500; ab2302, Abcam, UK) or GAPDH antibody (dilution 1:5000; 60004-1-Ig, Proteintech, USA) overnight at 4°C. Afterwards, the membranes were incubated with secondary antibodies, including Goat Anti-Rabbit IgG (dilution 1:5000; ab6721, Abcam, UK) or Goat Anti-mouse IgG (dilution 1:5000; ab6789, Abcam, UK) at room temperature for 1 h. Proteins were quantified by chemiluminescent HRP substrate (WBKLS0500, Millipore). The relative protein expressions were then calculated with GAPDH used as control.

Statistical analyses

All statistical analyses were performed using GraphPad Prism 7.0. Differences between groups in this study were analyzed by one-way analysis of variance or *t*-test. Results are expressed as mean ± standard deviation with three repeats for each experiment. $P < 0.05$ was considered statistically significant.

RESULTS

MiR-1290 expression was upregulated in AML bone marrow tissues and cells

The results from qRT-PCR uncovered that the expression of miR-1290 was evidently increased in AML bone marrow tissues (n=60) compared with the healthy bone marrow tissues (n=60) (Fig. 1A). Meanwhile, to investigate the correlation between miR-1290 expression and the survival rate of patients, sixty AML patients were divided into 2 groups: High miR-1290 (n=32) group and Low miR-1290 (n=28) group, based on the median expression of miR-1290 in AML bone marrow tissues. The results revealed that the increased miR-1290 expression in AML bone marrow tissues was related with a lower rate of survival (Fig. 1B). Moreover, the expression of miR-1290 was also upregulated in AML cells, including HL-60, KG-1 and Kasumi-1 cells.

Next, the clinical implication of miR-1290 was investigated. The results showed that miR-1290 expression was related to white blood cell (p=0.001), hemoglobin (p=0.023), platelet (p=0.002) and blasts in BM (p=0.011) in 60 AML patients. However, some features were not associated to miR-1290 expression (FAB subtype, complete remission, age and gender, Table I). Then multivariable Cox

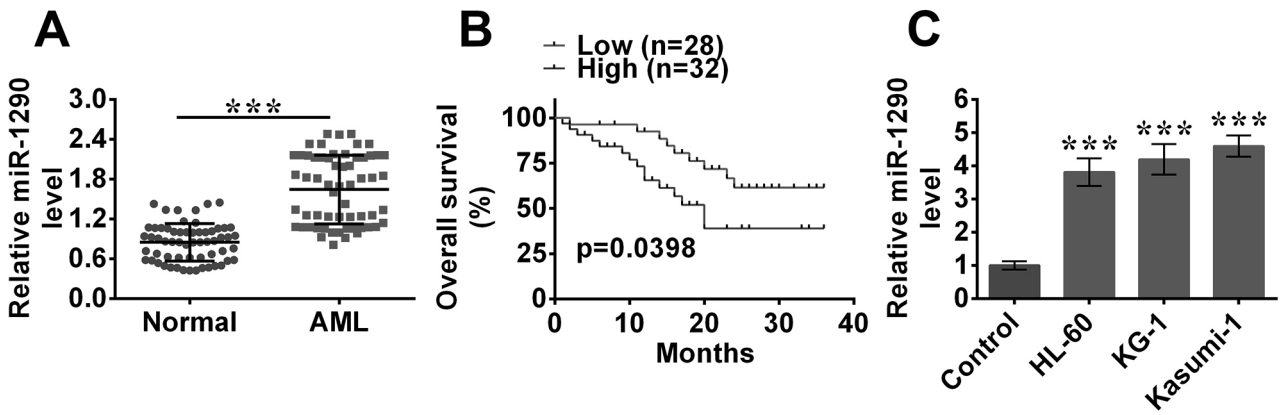

Fig. 1. *Relative expression of miR-1290 in AML bone marrow tissues and cells. **A**) Relative expression of miR-1290 in AML bone marrow tissues and healthy bone marrow tissues measured by qRT-PCR. **B**) The patients were classified into two groups according to miR-1290 expression. **C**) Relative expression of miR-1290 in AML cell lines and hMSCs. (NC) measured by qRT-PCR. **E**) The expression of CyclinD1, p21, Bcl-2, Bax, Cleaved caspase-3 were determined by western blot in HL-60 and KG-1 cells. *p<0.05, **p<0.01, ***p<0.001.*

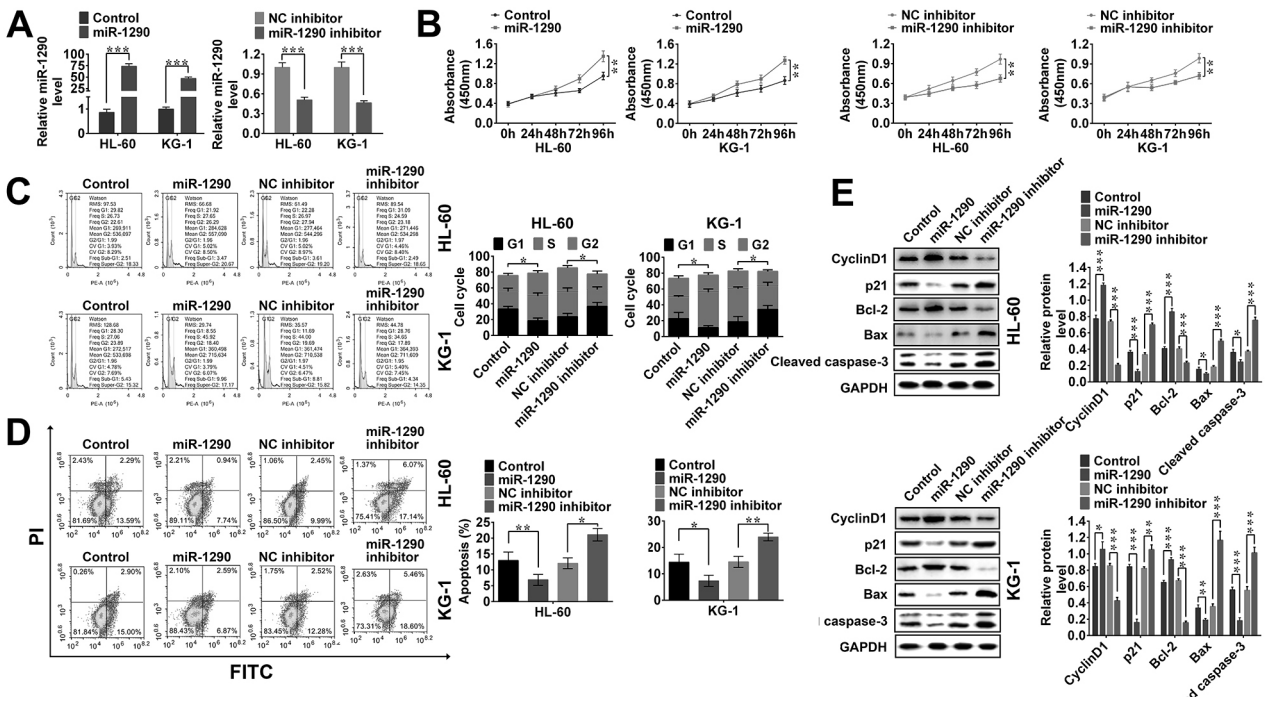

Fig. 2. *MiR-1290 induced cell proliferation but inhibited cell apoptosis. **A**) MiR-1290 expression was detected after transfection in HL-60 and KG-1 cells by qRT-PCR. **B**) CCK-8 assays were used to detect cell proliferation of HL-60 and KG-1 cells after transfection. **C**) Cell cycles of HL-60 and KG-1 cells after transfection was detected by flow cytometry. **D**) Cell apoptosis of HL-60 and KG-1 cells after transfection was assessed by flow cytometry. **D**) The expression of CyclinD1, p21, Bcl-2, Bax and Cleaved caspase-3 were measured by Western blot. All experiments were repeated three times. *P<0.05, **P<0.01, ***P<0.001.*

regression analysis was used to further determine the impact of clinicopathological features and expression of miR-1290 on the overall survival of patients with AML. The results indicated that miR-1290 expression [the exponent of B (Exp (B) = 6.419, 95% confidence interval (CI): 1.523-27.061, P = 0.011] was an independent prognostic factor for AML (Table 1).

MiR-1290 promoted cell proliferation and inhibited cell apoptosis in AML cells

MiR-1290 inhibitor was transfected into HL-60 and KG-1 cells for silencing the miR-1290 expression, and miR-1290 mimic was transfected into HL-60 and KG-1 cells for overexpressing miR-1290 (Fig. 2A). The CCK-8 assay results showed that knockdown of miR-1290 inhibited cell proliferation, while overexpression of miR-1290 promoted cell proliferation (Fig. 2B). The effects of miR-1290 on HL-60 or KG-1 cell cycles and cell apoptosis were examined by flow cytometry. The results indicated that overexpressing miR-1290 decreased the G1-phase cells population, whereas increased the S phase cell population in HL 60 and KG-1 cells compared with the control group. While, knockdown of miR-1290 increased the G1-phase cells, whereas decreased the S-phase cells in HL 60 and KG-1 cells compared to NC inhibitor cells (Fig. 2C). In addition, the flow cytometry results showed that the cell apoptosis was inhibited by overexpressing of miR-1290, whereas increased by knockdown of miR-1290 in HL-60 and KG-1 cells (Fig. 2D). Finally, the expressions of cell cycle and cell apoptosis related proteins including CyclinD1, p21, Bcl-2, Bax and Cleaved caspase-3 were examined by Western blot. Overexpression of miR-1290 increased the expression of CyclinD1 and Bcl-2, while inhibited the expression of p21, Bax and cleaved caspase-3 in HL-60 and KG-1 cells. However, the results were opposite in miR-1290 knockdown HL-60 and KG-1

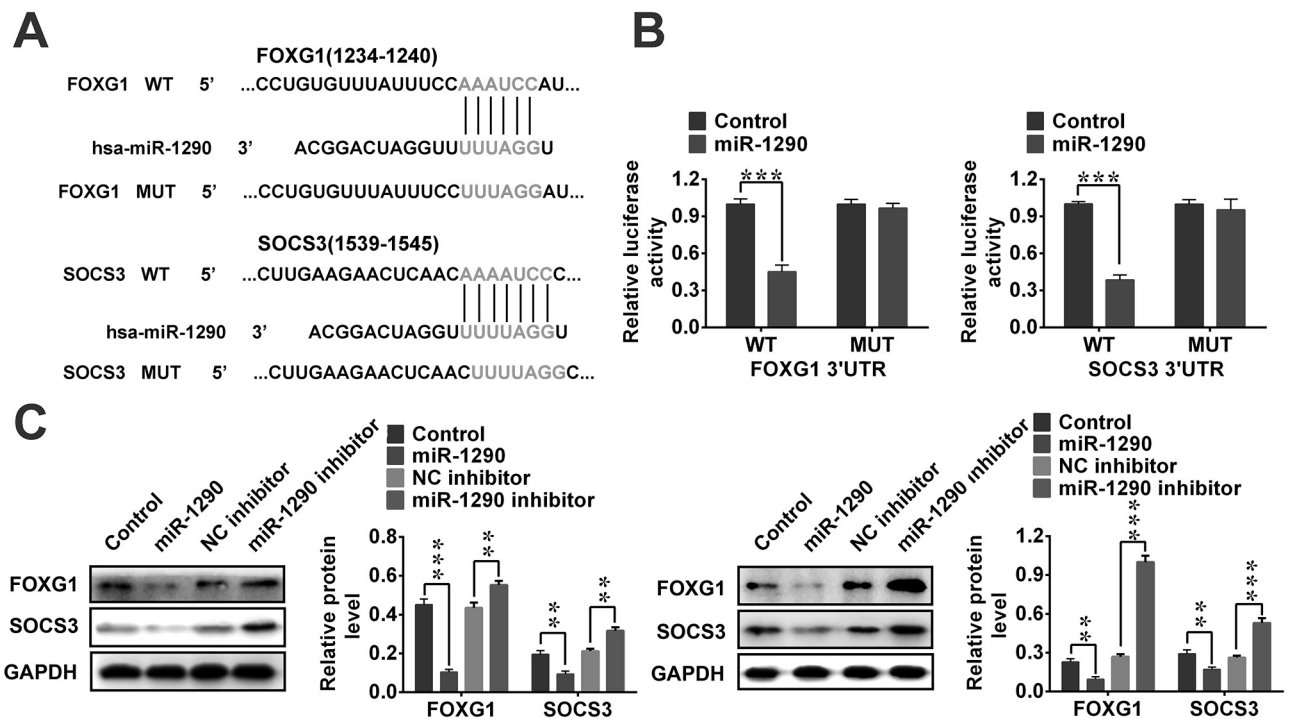

Fig. 3. *Both FOXG1 and SOCS3 were the target genes of miR-1290 in HL-60 and KG-1 cells.* ***A****) Diagrammatic sketch of the binding sites for FOXG1 and SOCS3 3'-UTRs in miR-1290.* ***B****) The luciferase assays were performed in HEK-293T cells co-transfected with FOXG1 3'-UTR-WT or SOCS1 3'-UTR-WT and miR-1290 mimics, or FOXG1 3'-UTR-MUT or SOCS1 3'-UTR-MUT and miR-1290 mimics.* ***C****) MiR-1290 regulated the protein levels of FOXG1 and SOCS3 directly in HL-60 and KG-1 cells. **P<0.01, ***P<0.001.*

Table I. *Clinicopathological variables of 60 patients with newly diagnosed AML divided into low (n=28) and high (n=32) miR-1290 expression groups*

Clinicopathological variables	No. of patients	miR-1290 expression		*P*-value
		Low (n=28)	High(n=32)	
Age				0.128
≤60	28	16	12	
＞60	32	12	20	
Gender				0.405
Male	33	17	16	
Female	27	11	16	
WBC, $X10^9$/l				0.001
＜10	34	22	12	
≥10	26	6	20	
HGB, g/dl				0.023
＜80	35	12	23	
≥80	25	16	9	
PLT, $X10^9$/l				0.002
＜50	36	11	25	
≥50	24	17	7	
Blasts in BM, %				0.011
＜50	26	17	9	
≥50	34	11	23	
FAB subtype				0.233
M1/M2	24	8	16	
M4/M5	32	18	14	
Other	4	2	2	
Complete remission				0.694
Yes	22	11	11	
No	38	17	21	

WBC: white blood cell; HGB: hemoglobin; PLT, platelet

Table II. *Cox multivariate analyse of factors for overall survival in AML patients*

Variables in the equation								
							95.0% CI for Exp (B)	
	B	SE	Wald	df	Sig.	Exp(B)	Down	Up
Group	1.859	0.734	6.415	1	0.011	6.419	1.523	27.061
Age	-1.147	0.635	3.263	1	0.071	0.317	0.091	1.102
Gender	0.733	0.721	1.033	1	0.309	2.081	0.506	8.556
WBC	-1.405	0.575	5.973	1	0.015	0.245	0.08	0.757
HGB	0.677	0.575	1.387	1	0.239	1.969	0.638	6.078
PLT	-2.15	0.912	5.551	1	0.018	0.117	0.019	0.697
BiBM	-0.794	0.66	1.446	1	0.229	0.452	0.124	1.649
Fs	0.072	0.679	0.011	1	0.916	1.075	0.284	4.068
Cr	-1.406	0.67	4.397	1	0.036	0.245	0.066	0.912

cells (Fig. 2E). Therefore, we concluded that miR-1290 promoted cell proliferation, and inhibited cell apoptosis in HL-60 and KG-1 cells.

FOXG1 and SOCS3 were identified as the target genes of miR-1290

It is well known that miRNAs participate in post-transcriptional regulation of target downstream genes. To assess the underlying mechanism of the effect of miR-1290 on HL-60 and KG-1 cells, bioinformatics analysis was used to predict target genes for miR-1290. According to the prediction from TargetScan, the binding sites of FOXG1 and SOCS3 3'-UTRs within miR-1290 were shown in Fig. 3A. Then luciferase reporter assay confirmed that the luciferase activities of cells co-transfected with FOXG1 3'-UTR-WT or SOCS3 3'-UTR-WT and miR-1290 were significantly decreased compared with cells co-transfected with FOXG1 3'-UTR-WT or SOCS3 3'-UTR-WT and mimic NC (Fig. 3B). However, the luciferase activities remained unchanged when co-transfected with the FOXG1 3'-UTR-MUT or SOCS3 3'-UTR-MUT and miR-1290 mimic. As shown in Figure.3C, the expressions of FOXG1 and SOCS3 were upregulated by knockdown of miR-1290, while inhibited by overexpression of miR-1290 in HL-60 and KG-1 cells.

FOXG1 and SOCS3 inhibited proliferation and promoted apoptosis of HL-60 and KG-1 cells

To demonstrate that effects of FOXG1 and SOCS3 on the cell proliferation and cell apoptosis, the related siRNAs and overexpression plasmids were transfected into HL-60 and KG-1 cells. The siNC, siFOXG1-1#, siFOXG1-2#, siSOCS3-1# or siSOCS3-2# were transfected into HL-60 and KG-1 cells to down regulate of FOXG1 or SOCS3 respectively. The pcDNA3.1 plasmid (Vector), pcDNA3.1-FOXG1 plasmid or pcDNA3.1-SOCS3 plasmid were transfected into HL-60 or KG-1 cells to overexpress FOXG1 or SOCS3. qRT-PCR and Western blot analysis results showed that the mRNA and protein expression levels of FOXG1 and SOCS3 were significant increased by overexpression plasmids or decreased after transfection with siRNAs (Fig. 4, A and B). Furthermore, the effects of FOXG1 and SOCS3 on cell proliferation and apoptosis were examined by CCK-8 and flow cytometry assays. Overexpression of FOXG1 and SOCS3 inhibited the cell proliferation, while knockdown of FOXG1 and SOCS3 promoted cell proliferation in HL-60 and KG-1 cells (Fig. 4C). Moreover, the cell cycle analysis showed that overexpression of FOXG1 or SOCS3 arrested cells in the G1-phase, whereas downregulation of FOXG1 or SOCS3 by siFOXG1 or siSOCS3 increased S-phase cells (Fig. 4D). Moreover, the cell apoptosis rate was significantly increased by overexpression of FOXG1 or SOCS3, while inhibited by knockdown of FOXG1 or SOCS3 (Fig. 4E). Finally, overexpression of FOXG1 or SOCS3 decreased the expression levels of CyclinD1 and Bcl-2, while increased the expression levels of p21, Bax and Cleaved caspase-3 in HL-60 and KG-1 cells (Fig. 4F). Downregulation of FOXG1 or SOCS3 in HL-60 and KG-1 cells had the opposite effects (Fig. 4F). Thus, these findings indicated that FOXG1 and SOCS3 inhibited proliferation and promoted apoptosis in HL-60 and KG-1 cells.

Mir-1290 promoted cell proliferation and inhibited cell apoptosis via targeting FOXG1 and SOCS3 in HL-60 and KG-1 cells

Lastly, we explored the function of miR-1290/FOXG1/SOCS3 axis in HL-60 and KG-1 cells. As shown in Fig. 5A, the proliferation of HL-60 and KG-1 cells was inhibited by transfection of miR-1290 inhibitors, whereas the inhibition was reversed by transfection of siFOXG1 or siSOCS3. As shown in Fig. 5B, downregulation of miR-1290 by its inhibitor in HL-60 and KG-1 cells increased the G1 phase cells. However, downregulation of FOXG1 or SOCS3 reversed this effect (Fig. 5B). Similarly, the miR-1290 inhibitor-induced cell apoptosis was reversed by knocking down of FOXG1 or SOCS3 in HL-60 and KG-1 cells (Fig. 5C). Moreover, the expression levels of p21, Bax and Cleaved caspase-3 were increased by miR-1290 inhibitors, while inhibited by co-transfection of miR-1290 inhibitors and siFOXG1 or siSOCS3. The expression levels of CyclinD1 and Bcl-2 were inhibited by miR-1290 inhibitors, while increased by co-transfection of miR-1290 inhibitors and siFOXG1 or siSOCS3

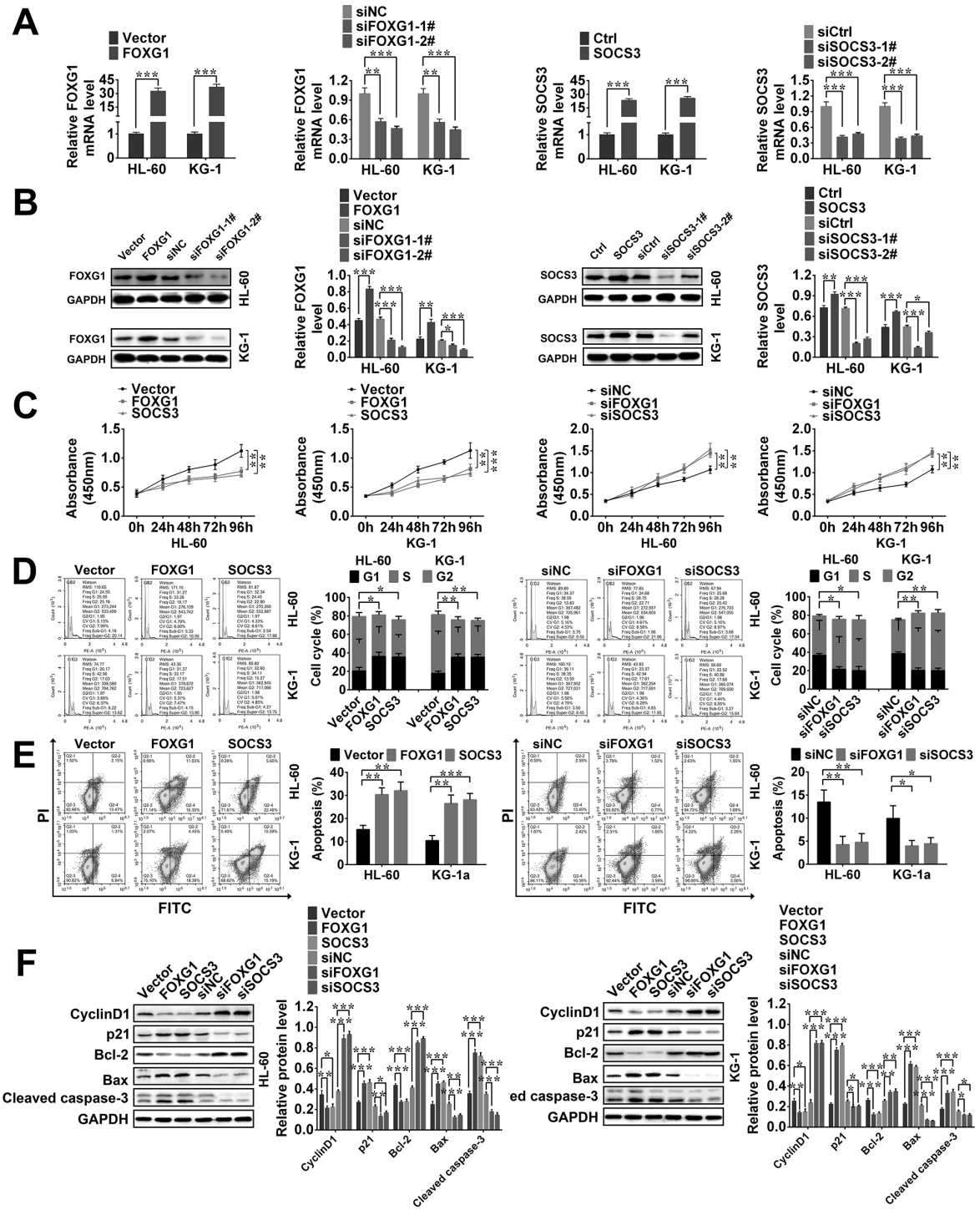

Fig. 4. *FOXG1 and SOCS3 inhibited proliferation and induced apoptosis in HL-60 and KG-1 cells. The HL-60 and KG-1 cells were transfected with siFOXG1-1#, siFOXG1-2#, siNC, Vector, FOXG1, siSOCS3-1#, siSOCS3-2# or SOCS3. A) The mRNA levels of FOXG1 and SOCS3 were detected after transfection in HL-60 and KG-1 cells by qRT-PCR.* ***B****) The expression levels of FOXG1 and SOCS3 were detected after transfection in HL-60 and KG-1 cells by western blot.* ***C****) CCK-8 assays were used to detect cell proliferation of HL-60 and KG-1 cells after transfection.* ***D****) Cell cycles of HL-60 and KG-1 cells after transfection was detected by flow cytometry.* ***E****) Cell apoptosis of HL-60 and KG-1 cells after transfection was assessed by flow cytometry.* ***F****) The expression of CyclinD1, p21, Bcl-2, Bax and Cleaved caspase-3 were measured by western blot after transfection. All experiments were repeated three times. *P<0.05, **P<0.01, ***P<0.001.*

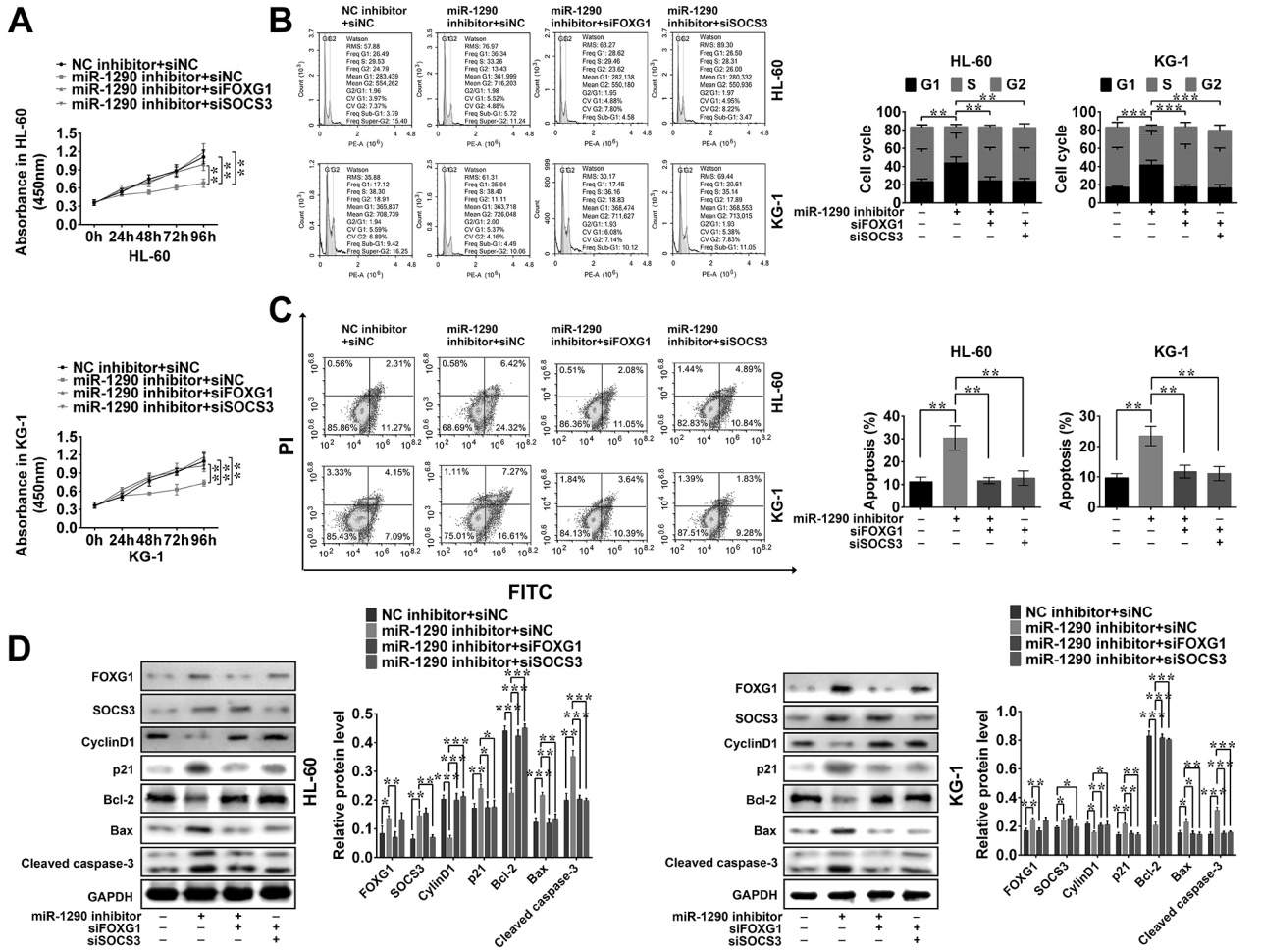

Fig. 5. *MiR-1290 promoted cell proliferation but inhibited cell apoptosis via targeting FOXG1 and SOCS3 in HL-60 and KG-1 cells. The HL-60 and KG-1 cells were co-transfected with miR-1290 inhibitors and siFOXG1 or siSOCS3 (**A**) CCK-8 assay was used to determine cell proliferation after transfection. **B-C**) The cell cycle and cell apoptosis were detected by flow cytometry assay in HL-60 and KG-1 cells after transfection. **D**) The expression of CyclinD1, p21, Bcl-2, Bax and Cleaved caspase-3 were assessed by Western blot after transfection. *P<0.05, **P<0.01, ***P<0.001.*

(Fig. 5D). Therefore, these findings suggested that miR-1290 promoted proliferation and suppressed apoptosis in acute myeloid leukemia by targeting FOXG1/SOCS3.

DISCUSSION

AML is a heterogeneous disease and its mechanism is still unknown. Our study focused on analyzing the role of miR-1290 in AML cells. Our results showed that the expression of miR-1290 was significantly increased *in vivo* and *in vitro* in AML models. This finding increased the interest in the analysis of the function of miR-1290 in AML cells, with particular focus on its effect on cell proliferation and apoptosis. After transfection of miR-1290 mimics into HL-50 and KG-1 cells, miR-1290 significantly promoted proliferation and inhibited cell apoptosis. In addition, FOXG1 and SOCS3 were identified as target genes of miR-1290 in HEK-293T cells. Further results demonstrated that overexpression of FOXG1or SOCS3 inhibited cell proliferation and promoted cell apoptosis in HL-50 and KG-1 cells. Moreover, the miR-1290 inhibitors-induced changes of cell proliferation and apoptosis were reversed by downregulation of FOXG1 or SOCS3 in HL-50

and KG-1 cells. Taken together, all these findings suggested that miR-1290 promoted cell proliferation and inhibited cell apoptosis via targeting FOXG1 and SOCS3 in HL-50 and KG-1 cells, which may provide therapeutic targets for AML treatment.

Accumulating evidence showed that abnormal expression of miRNAs was related with a variety of diseases, including AML (16). MiR-1290 is elevated in pancreatic cancer, colorectal cancer and lung adenocarcinoma (9, 17, 18). In the present study, the expression of miR-1290 in tissues of AML patients was up-regulated compared with normal tissues. Yan L et al. have demonstrated that miR-1290 promotes the proliferation, migration and invasion of glioma cells by targeting LHX6 (19). It has been reported that miR-1290 affects the proliferation and invasion of non-small cell lung cancer (NSCLC) cells by targeting interferon regulatory factor 2 (IRF2) (20). In lung adenocarcinoma, miR-1290 promotes cell proliferation by targeting SOCS4 (21). Therefore, miR-1290 may contribute to development of various cancers and diseases via regulation of cell proliferation, migration or invasion. Similarly, we found that miR-1290 mimics promoted the cell proliferation, and inhibited cell apoptosis in HL-60 and KG-1 cells, while its inhibitor showed the opposite effect. To investigate how the miR-1290 affected cell proliferation and apoptosis, the bioinformatics analysis indicated that FOXG1 and SOCS3 were the target genes of miR-1290.

FOXG1 is a transcription factor, which belongs to the forkhead family and is reported to be involved in telencephalon development. As p21 expression increases, down-regulation of FOXG1 inhibits cell proliferation (22). In glioma cells, FOXG1 promotes cell proliferation and inhibits cell apoptosis (23). SOCS3 is a negative regulator of JAK-STAT pathway. Overexpression of SOCS3 attenuates cell proliferation and enhances cell apoptosis in lymphoma and Osteoarthritis (24, 25). In the current study, miR-1290 could bind to FOXG1 and SOCS3 3'-UTRs in HL-60 and KG-1 cells. More interestingly, knocking down of FOXG1 or SOCS3 promoted cell proliferation but inhibited cell apoptosis, while overexpression of FOXG1 or SOCS3 had the opposite effect. Further study demonstrated that the changes in cell proliferation and apoptosis caused by miR-1290 inhibitor were reversed by si-FOXG1 or si-SOCS3. Therefore, we concluded that miR-1290 promoted proliferation and suppressed apoptosis in AML by targeting FOXG1/SOCS3. MiR-1290 expression inhibits cell growth in NSCLC *in vivo* (20). Xiao X et al. have pointed out that miR-1290 promotes tumor growth, invasion and metastasis *in vivo* (21). Despite these, there are still more *in vivo* studies needed to be carried out in the future on miR-1290 function in AML.

In conclusion, this study demonstrated that the miR-1290 was up-regulated in AML patients. Moreover, miR-1290 mimics promoted cell proliferation and inhibited apoptosis in HL-60 and KG-1 cells by targeting FOXG1 and SOCS3. Therefore, these results provided novel insights into the vital role of miR-1290 in AML, which might provide a therapeutic strategy for AML treatment.

REFERENCES

1. Estey EH. Acute myeloid leukemia: 2013 update on risk-stratification and management. Am J Hematol 2013; 88:318-27.
2. Bartel DP. MicroRNAs: genomics, biogenesis, mechanism, and function. Cell 2004; 116:281-97.
3. Malan-Muller S, Hemmings SM, Seedat S. Big effects of small RNAs: a review of microRNAs in anxiety. Mol Neurobiol 2013; 47:726-39.
4. Garzon R, Volinia S, Liu CG, et al. MicroRNA signatures associated with cytogenetics and prognosis in acute myeloid leukemia. Blood 2008; 111:3183-89.
5. Mi S, Lu J, Sun M, et al. MicroRNA expression signatures accurately discriminate acute lymphoblastic leukemia from acute myeloid leukemia. Proc Natl Acad Sci U S A 2007; 104:19971-76.
6. Zhang Y, Zhang C, Min D. Ailanthone up-regulates miR-449a to restrain acute myeloid leukemia cells growth, migration and invasion. Exp Mol Pathol 2019; 108:114-20.
7. Hu N, Chen L, Wang C, Zhao H. MALAT1 knockdown inhibits proliferation and enhances cytarabine chemosensitivity by upregulating miR-96 in acute myeloid leukemia cells. Biomed Pharmacother 2019; 112:108720.

8. Chen L, Jiang X, Chen H, Han Q, Liu C, Sun M. microRNA-628 inhibits the proliferation of acute myeloid leukemia cells by directly targeting IGF-1R. Onco Targets Ther 2019; 12:907-19.
9. Li A, Yu J, Kim H, et al. MicroRNA array analysis finds elevated serum miR-1290 accurately distinguishes patients with low-stage pancreatic cancer from healthy and disease controls. Clin Cancer Res 2013; 19:3600-610.
10. Kim G, An HJ, Lee MJ, et al. Hsa-miR-1246 and hsa-miR-1290 are associated with stemness and invasiveness of non-small cell lung cancer. Lung Cancer 2016; 91:15-22.
11. Endo Y, Toyama T, Takahashi S, et al. miR-1290 and its potential targets are associated with characteristics of estrogen receptor alpha-positive breast cancer. Endocr Relat Cancer 2013; 20:91-102.
12. Mao Y, Liu J, Zhang D, Li B. MiR-1290 promotes cancer progression by targeting nuclear factor I/X(NFIX) in esophageal squamous cell carcinoma (ESCC). Biomed Pharmacother 2015; 76:82-93.
13. Lin M, Shi C, Lin X, et al. sMicroRNA-1290 inhibits cells proliferation and migration by targeting FOXA1 in gastric cancer cells. Gene 2016; 582:137-42.
14. Ye L, Jiang T, Shao H, et al. miR-1290 Is a biomarker in DNA-mismatch-repair-deficient colon cancer and promotes resistance to 5-fluorouracil by directly targeting hMSH2. Mol Ther Nucleic Acids 2017; 7:453-64.
15. Zhou W, Wang S, Ying Y, Zhou R, Mao P. miR-196b/miR-1290 participate in the antitumor effect of resveratrol via regulation of IGFBP3 expression in acute lymphoblastic leukemia. Oncol Rep 2017; 37:1075-83.
16. Diaz-Beya M, Brunet S, Nomdedeu J, et al. MicroRNA expression at diagnosis adds relevant prognostic information to molecular categorization in patients with intermediate-risk cytogenetic acute myeloid leukemia. Leukemia 2014; 28:804-12.
17. Imaoka H, Toiyama Y, Fujikawa H, et al. Circulating microRNA-1290 as a novel diagnostic and prognostic biomarker in human colorectal cancer. Ann Oncol 2016; 27:1879-86.
18. Saito M, Shiraishi K, Matsumoto K, et al. A three-microRNA signature predicts responses to platinum-based doublet chemotherapy in patients with lung adenocarcinoma. Clin Cancer Res 2014; 20:4784-93.
19. Yan L, Cai K, Sun K, Gui J, Liang J. MiR-1290 promotes proliferation, migration, and invasion of glioma cells by targeting LHX6. J Cell Physiol 2018; 233:6621-29.
20. Jin JJ, Liu YH, Si JM, Ni R, Wang J. Overexpression of miR-1290 contributes to cell proliferation and invasion of non small cell lung cancer by targeting interferon regulatory factor 2. Int J Biochem Cell Biol 2018; 95:113-20.
21. Xiao X, Yang D, Gong X, Mo D, Pan S, Xu J. miR-1290 promotes lung adenocarcinoma cell proliferation and invasion by targeting SOCS4. Oncotarget 2018; 9:11977-88.
22. Chan DW, Liu VW, To RM, et al. Overexpression of FOXG1 contributes to TGF-beta resistance through inhibition of p21WAF1/CIP1 expression in ovarian cancer. Br J Cancer 2009; 101:1433-43.
23. Chen J, Wu X, Xing Z, et al. FOXG1 Expression is elevated in glioma and inhibits glioma cell apoptosis. J Cancer 2018; 9:778-783.
24. Li XD, Li XM, Gu JW, Sun XC. MiR-155 regulates lymphoma cell proliferation and apoptosis through targeting SOCS3/JAK-STAT3 signaling pathway. Eur Rev Med Pharmacol Sci 2017; 21:5153-59.
25. Gui T, He BS, Gan Q, Yang C. Enhanced SOCS3 in osteoarthiritis may limit both proliferation and inflammation. Biotech Histochem 2017; 92:107-14.

ASCORBIC ACID ENHANCES BONE PARAMETER EXPRESSION IN HUMAN GINGIVAL MESENCHYMAL STEM CELLS

F. DIOMEDE[1], G.D. MARCONI[1], M. SERRONI[1], G. PIZZICANNELLA[2], O. TRUBIANI[1] and J. PIZZICANNELLA[2]

[1]Department of Medical, Oral and Biotechnological Sciences, Chieti, Italy; [2]ASL02 Lanciano-Vasto-Chieti, Chieti, Italy

Received July 21, 2019 – September 27, 2019

Ascorbic acid (AS), also known as vitamin C or ascorbate, is an essential dietary nutrient which plays a vital role in biological processes through various different mechanisms, in particular for the biosynthesis of collagen. The aim of the study was to establish the possibility of enhancing the osteogenic differentiation potential by manipulating the cellular micro-environment, through AS supplementation in human gingival mesenchymal stem cells (hGMSCs) at different concentrations, such as 60 and 90 µg/mL, for three weeks. Human GMSCs are considered a stem cell population, easily obtainable and displaying a remarkable immunotherapeutic potential and regenerative repair expression. Osteogenic differentiation level induced from AS was assayed by histochemical characterization, using light microscopy through Alizarin red S staining. The transcript levels of Collagen 1A1 (COL1A1), runt-related transcription factor 2 (RUNX2), bone morphogenetic protein 2/4 (BMP2/4), osteopontin (OPN) and osteonectin (SPARC) were determined by quantitative RT-PCR. Protein expression of COL1A1, RUNX2, BMP2/4, OPN, SPARC were studied trough Western blotting and confocal laser scanning microscopy (CLSM). Our results demonstrate that AS supports osteogenic differentiation in stem cells from gingiva niche as shown by osteogenic marker upregulation and by *de novo* production of calcium phosphate deposits as revealed by Alizarin red S staining. In summary, the results of the current study provide evidence that hGMSCs undergo osteogenic differentiation with AS treatment, for that reason AS could be a promising candidate for the prevention and healing of bone-related diseases.

Bone is a specialized, highly dynamic connective tissue, in which pre-osteoblasts, osteoblasts, osteocytes, osteoclasts, and blood vessels play a key role in the maintenance of its homeostasis. In the past two decades, several studies have been carried out to understand the processes that regulate physiological bone turnover during lifetime (1, 2). In particular, during aging, bone diseases, such as osteopaenia and osteoporosis, cause a structural deterioration of tissue that can affect bone functional properties associated with an increased risk of fractures and representing a major global health problem that affects people all over the world (3). For these reasons, several drugs have been developed but they do not offer an effective solution, because they do not completely reduce the incidence of fractures and decline of functionality (4).

Nowadays, there is a growing interest in the development of alternative natural molecules that can contribute to the replacement and repair of injured

Key words: ascorbic acid; human gingival mesenchymal stem cells; osteogenic markers

Corresponding Author:
Prof. Oriana Trubiani,
Department of Medical,
Oral and Biotechnological Sciences,
Via dei Vestini, 31,
66100 Chieti, Italy
e-mail: trubiani@unich.it

0393-974X (2019)

bone tissue. Ascorbic acid (AS) is an important antioxidant and cofactor which is involved in the development, function and maintenance of several cell types in the body such as adipocytes, myoblast, chondroblasts, odontoblasts and osteoblasts (5). Current evidence suggests that AS is involved in collagen matrix synthesis. Several studies have shown that the addition of AS to cultured osteoblast-like cells stimulates the initial deposition of a collagenous extracellular matrix followed by the induction of specific genes associated with the osteoblast phenotype, such as alkaline phosphatase and osteocalcin (6).

AS, during the differentiation process of mouse calvaria-derived MC3T3-EI cells, promotes the induction of collagen matrix formation (5). Mesenchymal stem cells (MSCs), which were first identified in the bone marrow, can also now be obtained from various tissues, such as fat, synovial membrane, muscle, skin, trabecular bone, articular cartilage, and oral cavity (7-9). MSCs are able to differentiate into osteoblasts, chondroblasts, myoblasts, adipoblasts, myocardium and skin (10, 11). Human gingival MSCs (hGMSCs) are a novel type of pluripotent MSCs that exhibit self-renewal, multipotent differentiation potential and immunomodulatory capacities (12, 13). hGMSCs have attracted great attention due to their easy isolation, high proliferative capacity, homogeneity, stable phenotype and, notably, the fact that they maintain a normal karyotype and telomerase activity during prolonged culture (14). Therefore, hGMSCs are considered to be an optimal candidate cell source for tissue engineering and cell-based therapies. In the present study, we evaluated the effect of AS treatment at different concentrations (60 and 90 µg/mL) on hGMSCs, in terms of proliferation and osteogenic differentiation. Mainly, the effects were evaluated of AS treatment on osteogenic marker modulation such as Collagen 1A1 (COL1A1), Runt-related transcription factor 2 (RUNX2), bone morphogenetic protein 2 (BMP2), osteopontin (OPN) and osteonectin (SPARC), to evaluate the potential role of AS in the development of novel therapeutic strategies that could support bone tissue homeostasis.

MATERIALS AND METHODS

The present study was approved by the Ethics Committee of the Medical School, "G. d'Annunzio" University, Chieti, Italy (number 266/April 17, 2014). Informative consent before enrolment in the study was signed from all subjects.

Cell culture

To obtain hGMSCs, the gingival tissue was collected by a procedure previously described (10). Healthy patients scheduled to remove the third molar for orthodontic purpose were enrolled in the study. Tissue explants were cultured in Petri dish with Mesenchymal stem cells growth medium chemically-defined (MSCGM-CD) (Lonza, Basel, Switzerland) (15). The medium was replaced with a fresh one every two days. After two weeks of culture, cells spontaneously migrated from tissue explants. All experiments were performed with cells at 2nd passage.

Experimental design

Cells at 2nd passage were divided into four experimental groups: CTRL: hGMSCs cultured with basal medium (MSCGM-CD); AS 60 µg/mL: hGMSCs treated with AS at a concentration of 60 µg/mL; AS 90 µg/mL: hGMSCs treated with AS at a concentration of 90 µg/mL; and DIFF OSTEO: hGMSCs cultured with osteogenic differentiation medium as reported hereafter. For osteogenic differentiation, cells were cultured in osteogenic differentiation medium (Lonza) for three weeks. The osteogenic differentiation and the effects of AS were then evaluated.

Cell proliferation and viability assay

Cell proliferation was evaluated through MTT assay, as previously reported (16). $2x10^3$ cells per well were seeded into 96-well plates in medium volume of 200 µL to test all experimental groups at different endpoints, 24, 48 and 72 h. 20 µL of MTT (Promega, Milan, Italy) solution were added to each well. Absorbance at 490 nm was measured with a reference wavelength of 630 nm (17).

Cell viability was assessed by trypan blue exclusion test. For this purpose all samples were incubated with trypan blue solution at the same endpoint used for MTT testing (24, 48 and 72 h) and subsequently analysed with Burker's chamber at inverted light microscopy, as previously described (18).

Osteogenic differentiation evaluation

Evaluation of calcium deposition and ECM mineralization was obtained by Alizarin Red S (ARS) staining assay performed after 6 weeks. Cells were washed with PBS, fixed in 10% (v/v) formaldehyde (Sigma-Aldrich, Milan, Italy) for 30 min and washed twice with abundant dH_2O prior to addition of 0.5% Alizarin red S in H_2O, pH 4.0, for 1 h at room temperature. After cell incubation under gentle shaking, cells were washed with dH_2O four times for 5 min. For staining quantification, 800 µL 10% (v/v) acetic acid was added to each well. Cells incubated for 30 min were scraped from the plate, transferred into a 1.5 mL vial and vortexed for 30 s. The obtained suspension, overlaid with 500 µL mineral oil (Sigma-Aldrich), was heated to 85°C for 10 min, then transferred to ice for 5 min, carefully avoiding opening the tubes until fully cooled, and centrifuged at 20,000× g for 15 min (19). In addition, 500 µL of the supernatant were placed into a new 1.5 mL vial and 200 µL of 10% (v/v) ammonium hydroxide was added (pH 4.1–pH 4.5). Furthermore, 150 µL of the supernatant obtained from cultures were read in triplicate at 405 nm by a spectrophotometer (Synergy HT, BioTek, Bad Friedrichshall, Germany).

Confocal laser scanning microscope (CLSM) analysis

For immunofluorescence detections, cells grown on 8-well chamber slides were fixed using 4% paraformaldehyde diluted in 0.1M sodium phosphate buffer (PBS, Lonza). After the fixation step, cells were permeabilized with 0.5% Triton X-100 in PBS for 10 min, followed by blocking with 5% skimmed milk in PBS for 30 min (20). Primary antibodies used for immunofluorescence were purchased from Santa Cruz Biotechnology (Santa Cruz Biotechnology, Santa Cruz, CA, USA). COL1A1 (1:200, Santa Cruz Biotechnology, Santa Cruz, CA, USA), RUNX2 (1:100, Santa Cruz Biotechnology), BMP2/4 (1:200, Santa Cruz Biotechnology), OPN (1:200, Santa Cruz Biotechnology) and SPARC (1:250, Santa Cruz Biotechnology) were used as primary antibodies. Then cells were incubated by Alexa Fluor 568 red fluorescence conjugated goat anti-rabbit as secondary antibodies (1:200, Molecular Probes, Invitrogen, Eugene, OR, USA). Alexa Fluor 488 phalloidin green fluorescence conjugate (1:400, Molecular Probes) was used to mark the cytoskeleton actin. After immunofluorescence labelling cells were washed and incubated with TOPRO (1:200, Molecular Probes) for 1 h at 37°C (15). Samples were observed under Zeiss LSM800 confocal system (Zeiss, Jena, Germany). All the experiments were performed in triplicate.

Western blot analysis

Proteins (30 µg) derived from all experimental groups were processed as previously reported (21). All antibodies used for Western blot were purchased from Santa Cruz Biotechnology. After protein separation, saturated sheets were incubated overnight at 4°C with COL1A1 (1:200, Santa Cruz Biotechnology), RUNX2 (1:1000, Santa Cruz Biotechnology), BMP2/4 (1:750, Santa Cruz Biotechnology), OPN (1:750, Santa Cruz Biotechnology), SPARC (1:1000, Santa Cruz Biotechnology) and β-Actin (1:1000, Santa Cruz Biotechnology) (22). Then samples were washed and incubated in secondary antibody diluted 1:1000 in 1x TBS, 5% milk, 0.05% Tween-20. Protein specific bands were visualized by means of the ECL method (23).

Gene expression

Total RNA was isolated from all experimental groups used in the present study through the RNeasy Plus Universal Mini Kit (Qiagen, Valencia, CA, USA). ABI PRISM 7900 HT Sequence Detection System (Applied Biosystems, Foster City, CA, USA) was used for qPCR of studied markers (COL1A1 Hs00164004_m1; RUNX2 Hs00231692_m1; BMP2/4 Hs00154192_m1; OPN Hs00959010_m1; SPARC Hs00234160_m1; ThermoFischer, Milan, Italy). Beta-2 microglobulin (B2M Hs00187842_m1, Hs99999907_m1; ThermoFischer) was used for template normalization (24). Comparative $2^{-\Delta\Delta Ct}$ relative quantification method was used to analyze the mRNA expression.

Statistical analysis

Graph Pad Prism 5.0 (GraphPad Software, La Jolla, CA, USA) was used to perform the statistical evaluation. Student's *t*-test was used to analyze the differences between the groups. The obtained results are reported as means ± SEM. A P-value <0.05 was considered statistically significant.

RESULTS

Ascorbic acid effects on cell proliferation and viability

To evaluate cell proliferation and viability, MTT and Trypan blue assay were performed on all considered samples. Cells treated with AS 60 µg/mL and AS 90 µg/mL showed no significant differences when compared to the CTRL and to the DIFF OSTEO samples (Fig. 1).

Ascorbic acid effects on the osteogenic differentiation

To evaluate the osteogenic differentiation process Alizarin red S staining was performed on all samples after three weeks of culture. Calcium deposits, stained in red were visible in AS 90 µg/mL and in DIFF OSTEO samples when compared to the CTRL and to the AS 60 µg/mL, indicating that a high concentration of AS showed some effect on osteogenic commitment (Fig. 2A-D). Bar graphs showed the quantitative results of the *in-vitro* staining (Fig. 2E).

Ascorbic acid treatment modulates the osteogenic markers in hGMSCs

Immunofluorescence staining was performed to evaluate the expression of markers related to the osteogenic differentiation. All considered markers, COL1A1, RUNX2, BMP2/4, OPN and SPARC, showed an increase expression in differentiated cells (DIFF OSTEO) and in cells treated with AS 90 µg/mL, when compared to the untreated cells (CTRL) and with cells treated with a lower concentration of AS (AS 60 µg/mL) (Fig. 3).

Ascorbic acid treatment modulates genes and proteins related to the osteogenic commitment

COL1A1, RUNX2, BMP2/4, OPN and SPARC are osteogenic markers related to the differentiation process. To evaluate their expression RT-PCR analyses were performed. The mRNA levels of COL1A1, RUNX2, BMP2/4, OPN and SPARC increased in AS 90 µg/mL and DIFF OSTEO (Fig. 4A). In particular, the obtained data confirmed the expression of related proteins evidenced by immunofluorescence (Fig. 4B).

DISCUSSION

Skeletal regeneration is often initiated by a traumatic episode that involves damage to the bone, which often includes the periosteum, bone marrow spaces, and surrounding soft tissues (25). Trauma, such as fracture or surgical cutting and drilling, causes a physiological disruption of the mineralized tissue matrix, death of many types of cells, and interruption of the local blood supply (26). Nowadays, stem cells that combine a capacity for self-renewal with the ability to initiate multiple differentiation cascades, resulting in the generation of cells with specialized functions are attracting great interest, in particular for bone regeneration and homeostasis.

Deficiencies in AS can lead to conditions such as scurvy, which, among other ailments, causes bleeding gums, bone pain and impaired wound healing. This work examined the functional importance of vitamin C related to the development and maintenance of bone tissues. Analysis of several epidemiological and *in-vivo* studies regarding the effect of vitamin C showed a positive effect on bone health. Overall, vitamin C exerts a positive effect on trabecular bone formation by influencing expression of bone matrix genes in osteoblasts. Recent studies on the molecular pathway for vitamin C actions that include direct effects of vitamin C on transcriptional regulation of target genes by influencing the activity of transcription factors and by epigenetic modification of key genes involved in skeletal development and maintenance have been discussed. AS can be considered an essential dietary nutrient required for various biological functions, including the biosynthesis of collagen (27). AS used in basal concentrations showed an antioxidant role as a water□soluble factor. At pharmacologic or increased doses, AS is also known to act as a prooxidant *in vitro*. Antioxidant AS reduces oxidizing substances, such as hydrogen peroxide (28). AS used at the appropriate dose could potentially function as a preventative therapy for heterotopic ossification through the same mechanism used by radiation therapy, without the harmful risks or side effects (29). In the current study, we evaluated the biological response of hGMSCs to AS at 60 and 90 µg/mL after three weeks of culture.

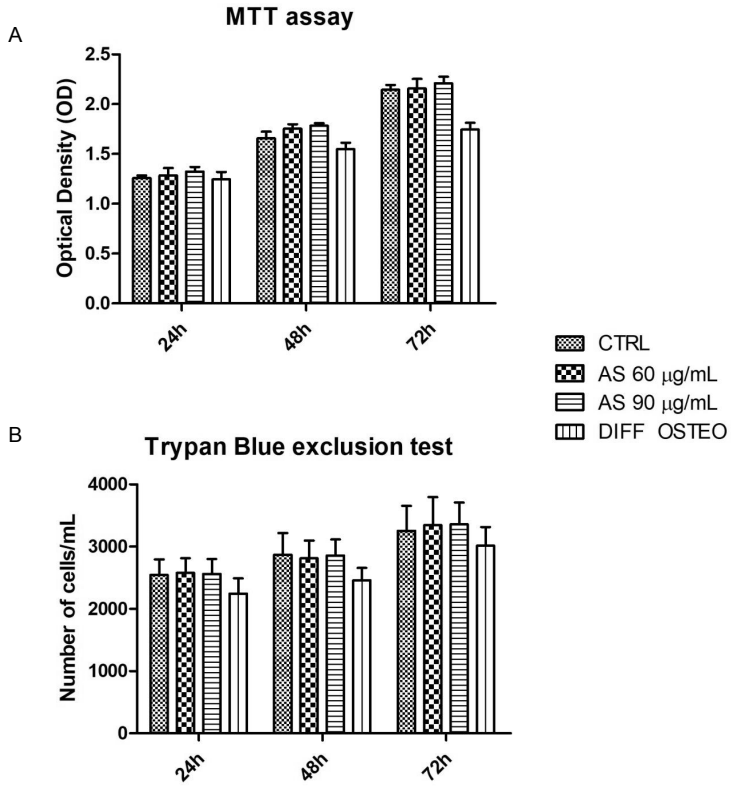

Fig. 1. *Cell proliferation and viability.* ***A)*** *MTT assay.* ***B)*** *Trypan blue exclusion test. Treatment with AS 60µg/mL and AS 90µg/mL showed no statistical differences in terms of cell proliferation and viability after 24, 48 and 72 h of culture.*

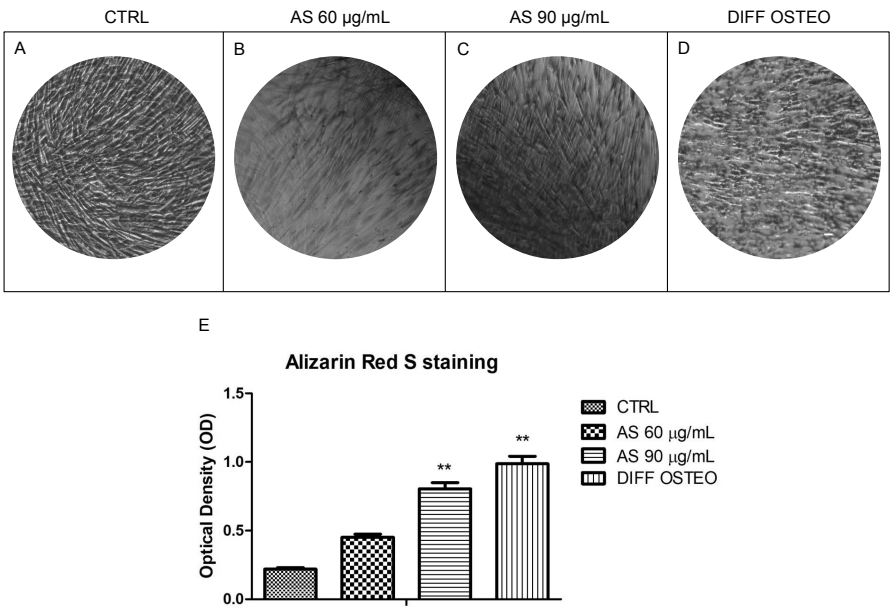

Fig. 2. *Osteogenic differentiation. Alizarin red S staining was used to evaluate the calcium depositions in (****A****) CTRL, (****B****) AS 60 µg/mL, (****C****) AS 90 µg/mL and (****D****) DIFF OSTEO by means of inverted light microscopy.* ***E)*** *Quantitative analysis of Alizarin red S staining was performed by measuring the absorbance of Alizarin red S at 562 nm. The results are expressed as mean – standard deviation (SD) (n = 3). **, $p < 0.01$ was recognized to be significant. Scale bar: 20 µm. Mag: 10X.*

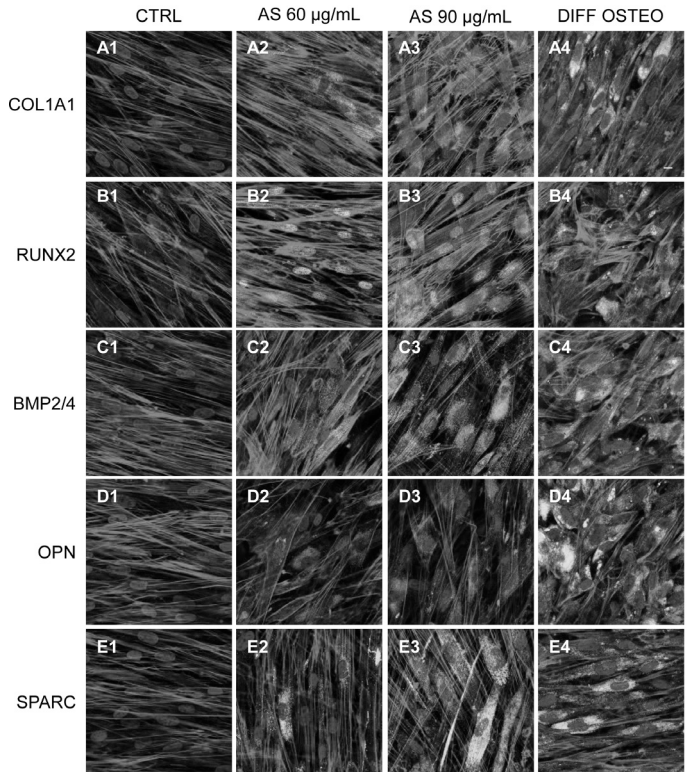

Fig. 3. *Immunofluorescence detection. Expression of COL1A1 in (A1) CTRL, (A2) AS 60µg/mL (A3) AS 90µg/mL and (A4) DIFF OSTEO. Expression of RUNX2 in (B1) CTRL, (B2) AS 60µg/mL (B3) AS 90µg/mL and (B4) DIFF OSTEO. Expression of BMP2/4 in (C1) CTRL, (C2) AS 60µg/mL (C3) AS 90µg/mL and (C4) DIFF OSTEO. Expression of OPN in (D1) CTRL, (D2) AS 60 µg/mL (D3) AS 90µg/mL and (D4) DIFF OSTEO. Expression of SPARC in (E1) CTRL, (E2) AS 60µg/mL (E3) AS 90µg/mL and (E4) DIFF OSTEO. Scale bar: 10 µm. Mag: 63X.*

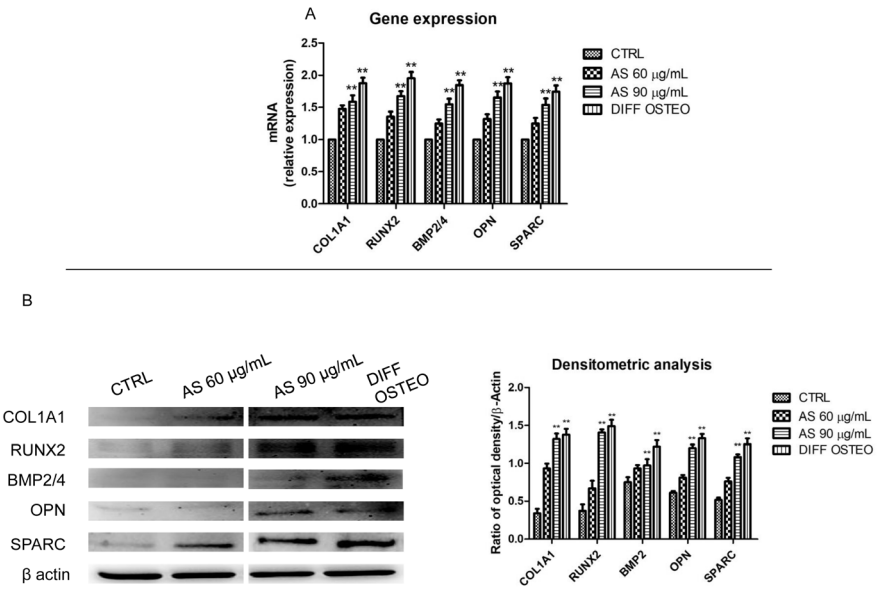

Fig. 4. *Gene expression. **A**) RT-PCR showed the expression of mRNA levels in CTRL, AS 60µg/mL, AS 90µg/mL and DIFF OSTEO of specific osteogenic related markers. **B**) Western blot analysis of COL1A1, RUNX2, BMP2/4, OPN and SPARC and their densitometric analysis using the expression ratios of β actin used as housekeeping protein.*

Alizarin red S staining indicated that the extent of mineralization was higher in the hGMSC cultures in presence of osteogenic medium compared to cultures supplemented with AS. The mRNA levels of several classic osteogenic genes, such as COL1A1, RUNX2, BMP2/4, OPN and SPARC, were analyzed in presence of AS. RUNX2 is a transcriptional factor essential for the activation of osteoblast-associated genes, and therefore is an important early indicator of osteoblast differentiation and bone formation (30). RUNX2 directly activates the transcription of genes such as Collagen type I, Osteopontin (OPN) or Osteonectin (SPARC).

In our experiments it was possible to detect that after three weeks of cultures the expression profile of RUNX2 was mainly upregulated in presence of differentiated medium in respect to samples treated with 60 and 90 μg/mL of AS. These data demonstrate that AS works as an osteogenic inductor in hGMSCs, but other cofactors are necessary for a complete differentiative pathway. The expression of SPARC, a non-structural glycoprotein secreted by osteoblasts, shows the identical trend of RUNX2 after three week in osteogenic differentiated culture conditions compared to AS-treated samples. The mRNA level of osteogenic-related markers is also confirmed by Western blot analysis. This protein binds calcium in bone, has an affinity for collagen and is also involved in cell-matrix interactions (31).

However, given that SPARC is more strongly expressed during the early stages of osteogenesis (i.e. during the proliferative and matrix deposition periods (32), our results may suggest that in the presence of the AS, osteogenic differentiation process was accelerated relative to the control groups. Upregulation of non-collagenous proteins, such as OPN and SPARC, with an important role in osteogenesis, confirmed the osteogenesis-promoting effect of the AS on hGMSCs. OPN codes for one of the most predominant non-collagenous proteins in bone extracellular matrix produced by osteoblasts, and it also promotes cell adhesion to the bone surface (33). OPN regulates cell–matrix interactions and signaling through binding to integrin- and CD44-receptors (34). Integrins are a family of heterodimeric transmembrane glycoproteins mediating cell-cell matrix and cell-cell adhesion, migration, proliferation and survival (35). Likewise, receptors of OPN integrins and CD44 also expressed in host stromal cells and in hGMSCs (36). OPN, which plays an important role in the regulation of vessel regeneration, is produced by mature osteoblasts during the bone formation process and is recognized as a major marker of osteogenic differentiation (37). During bone resorption, OPN is reported to be involved in the attachment of osteoclasts, and during bone mineralization plays a key role in osteogenesis and in the regulation of the crystal size (38).

Collagen 1A1, known as an early marker of osteoprogenitor cells, is considered fundamental for extracellular matrix synthesis (27), and in our study, COL1A1 was upregulated in DIFF OSTEO and AS 90 μg/mL.

Based on these results, validated through multiparametric analyses, we can conclude that AS is an antioxidant natural molecule which promotes osteogenesis, resulting in faster bone tissue formation in gingival-derived stem cells and can assume a strategic role in physiological and healthy bone remodelling.

REFERENCES

1. Diomede F, Gugliandolo A, Cardelli P, et al. Three-dimensional printed PLA scaffold and human gingival stem cell-derived extracellular vesicles: a new tool for bone defect repair. Stem Cell Res Ther 2018; 9:104.
2. Diomede F, D'Aurora M, Gugliandolo A, et al. A novel role in skeletal segment regeneration of extracellular vesicles released from periodontal-ligament stem cells. Int J Nanomed 2018; 13:3805-25.
3. Diomede F, D'Aurora M, Gugliandolo A, et al. Biofunctionalized scaffold in bone tissue repair. Int J Mol Sci 2018; 19. doi: 10.3390/ijms19041022.
4. Khosla S, Hopbauer LC. Osteoporosis treatment: recent developments and ongoing challenges. Lancet Diabetes Endo 2017; 5:898-907.
5. Franceschi RT, Iyer BS, Cui YQ. Effects of ascorbic-acid on collagen matrix formation and osteoblast differentiation in murine Mc3t3-E1 cells. J Bone

Miner Res 1994; 9:843-54.
6. Franceschi RT, Young J. Regulation of alkaline-phosphatase by 1,25-Dihydroxyvitamin-D3 and ascorbic-acid in bone-derived cells. J Bone Miner Res 1990; 5:1157-67.
7. Gugliandolo A, Diomede F, Cardelli P, et al. Transcriptomic analysis of gingival mesenchymal stem cells cultured on 3D bioprinted scaffold: A promising strategy for neuroregeneration. J Biomed Mater Research A 2018; 106:126-37.
8. Trubiani O, Toniato E, Di Iorio D, et al. Morphological analysis and interleukin release in human gingival fibroblasts seeded on different denture base acrylic resins. Int J Immunopathol Pharmacol 2012; 25:637-43.
9. Di Nisio C, De Colli M, di Giacomo V, et al. A dual role for beta1 integrin in an in vitro Streptococcus mitis/human gingival fibroblasts co-culture model in response to TEGDMA. Int Endod J 2015; 48:839-49.
10. Diomede F, Gugliandolo A, Scionti D, et al. Biotherapeutic effect of gingival stem cells conditioned medium in bone tissue restoration. Int J Mol Sci 2018; 19. doi: 10.3390/ijms19020329.
11. De Colli M, Zara S, di Giacomo V, et al. Nitric oxide-mediated cytotoxic effect induced by zoledronic acid treatment on human gingival fibroblasts. Clin Oral Investig 2015; 19:1269-77.
12. Mitrano TI, Grob MS, Carrion F, et al. Culture and characterization of mesenchymal stem cells from human gingival tissue. J Periodontol 2010; 81:917-25.
13. Zhang Q, Shi S, Liu Y, et al. Mesenchymal stem cells derived from human gingiva are capable of immunomodulatory functions and ameliorate inflammation-related tissue destruction in experimental colitis. J Immunol 2009; 183:7787-98.
14. Diomede F, Zini N, Pizzicannella J, et al. 5-Aza Exposure improves reprogramming process through embryoid body formation in human gingival stem cells. Front Genet 2018; 9:419.
15. Pizzicannella J, Diomede F, Merciaro I, et al. Endothelial committed oral stem cells as modelling in the relationship between periodontal and cardiovascular disease. J Cell Physiol 2018; 233:6734-47.
16. Diomede F, Zingariello M, Cavalcanti M, et al. MyD88/ERK/NFkB pathways and pro-inflammatory cytokines release in periodontal ligament stem cells stimulated by Porphyromonas gingivalis. Eur J Histochem 2017; 61:2791.
17. Diomede F, Merciaro I, Martinotti S, et al. miR-2861 is involved in osteogenic commitment of human periodontal ligament stem cells grown onto 3D scaffold. J Biol Regul Homeost Agents 2016; 30:1009-18.
18. Cavalcanti MF, Maria DA, de Isla N, et al. Evaluation of the proliferative effects induced by low-level laser therapy in bone marrow stem cell culture. Photomed Las Surg 2015; 33:6101-6.
19. Ballerini P, Diomede F, Petragnani N, et al. Conditioned medium from relapsing-remitting multiple sclerosis patients reduces the expression and release of inflammatory cytokines induced by LPS-gingivalis in THP-1 and MO3.13 cell lines. Cytokine 2017; 96:261-72.
20. Pizzicannella J, Gugliandolo A, Orsini T, et al. Engineered extracellular vesicles from human periodontal-ligament stem cells increase VEGF/VEGFR2 expression during bone regeneration. Front Physiol 2019; 10:512.
21. Giacoppo S, Thangavelu SR, Diomede F, et al. Anti-inflammatory effects of hypoxia-preconditioned human periodontal ligament cell secretome in an experimental model of multiple sclerosis: a key role of IL-37. FASEB J 2017; 31:5592-608.
22. Trubiani O, Ballerini P, Murmura G, et al. Toll-like receptor 4 expression, interleukin-6,-8 and Ccl-20 release, and Nf-Kb translocation in human periodontal ligament mesenchymal stem cells stimulated with Lps-P-gingivalis. Eur J Inflamm 2012; 10:81-89.
23. Mammana S, Gugliandolo A, Cavalli E, et al. Human gingival mesenchymal stem cells (GMSCs) pre-treated with vesicular Moringin nanostructures as a new therapeutic approach in a mouse model of spinal cord injury. J Tissue Eng Regen Med 2019; 13:1109-21.
24. Pizzicannella J, Cavalcanti M, Trubiani O, Diomede F. MicroRNA 210 mediates VEGF upregulation in human periodontal ligament stem cells cultured on 3D hydroxyapatite ceramic scaffold. Int J Mol Sci 2018; 19.

25. Plotkin LI, Bruzzaniti A. Molecular signaling in bone cells: Regulation of cell differentiation and survival. Adv Protein Chem Struct Biol 2019; 116:237-81.
26. Scioli MG, Bielli A, Gentile P, Cervelli V, Orlandi A. Combined treatment with platelet-rich plasma and insulin favours chondrogenic and osteogenic differentiation of human adipose-derived stem cells in three-dimensional collagen scaffolds. J Tissue Eng Regen Med 2017; 11:2398-410.
27. Ferrazzo PC, Niccoli S, Khaper N, Rathbone CR, Lees SJ. Ascorbic acid diminishes bone morphogenetic protein 2-induced osteogenic differentiation of muscle precursor cells. Muscle Nerve 2019; 59:501-8.
28. Casciari JJ, Riordan NH, Schmidt TL, Meng XL, Jackson JA, Riordan HD. Cytotoxicity of ascorbate, lipoic acid, and other antioxidants in hollow fibre in vitro tumours. Br J Cancer 2001; 84:1544-50.
29. Lee A, Amin NP. Radiation therapy for heterotopic ossification prophylaxis. StatPearls. Treasure Island (FL) 2019.
30. Huang W, Yang S, Shao J, Li YP. Signaling and transcriptional regulation in osteoblast commitment and differentiation. Front Biosci 2007; 12:3068-92.
31. Llacua LA, Faas MM, de Vos P. Extracellular matrix molecules and their potential contribution to the function of transplanted pancreatic islets. Diabetologia 2018; 61:1261-72.
32. Matta C, Szucs-Somogyi C, Kon E, et al. Osteogenic differentiation of human bone marrow-derived mesenchymal stem cells is enhanced by an aragonite scaffold. Differentiation 2019; 107:24-34.
33. Florencio-Silva R, Sasso GRD, Sasso-Cerri E, Simoes MJ, Cerri PS. Biology of bone tissue: structure, function, and factors that influence bone cells. Biomed Res Int 2015; 2015:421746.
34. Zhang X, Xu W. Neutrophils diminish T-cell immunity to foster gastric cancer progression: the role of GM-CSF/PD-L1/PD-1 signalling pathway. Gut 2017; 66:1878-80.
35. Zhao H, Chen Q, Alam A, et al. The role of osteopontin in the progression of solid organ tumour. Cell Death Dis 2018; 9:356.
36. Diomede F, Rajan TS, Gatta V, et al. Stemness Maintenance Properties in Human Oral Stem Cells after Long-Term Passage. Stem Cells Int 2017; 2017:5651287.
37. Ganss B, Kim RH, Sodek J. Bone sialoprotein. Crit Rev Oral Biol Med 1999; 10:79-98.
38. McKee MD, Nanci A. Osteopontin: an interfacial extracellular matrix protein in mineralized tissues. Connect Tissue Res 1996; 35:197-205.

POTENTIAL ROLE OF MAGNETIC RESONANCE BRAIN RELAXOMETRY IN VETERINARY MEDICINE: A PRELIMINARY STUDY

F. DEL SIGNORE, M. VIGNOLI, G. MARRUCHELLA, F. SIMEONI, R. TAMBURRO, G. ASTE and F. DE PASQUALE

University of Teramo, Piano D'Accio, Teramo, Italy

Received May 25, 2019 - Accepted September 9, 2019

Magnetic Resonance (MR) is a non-invasive modality of choice for the evaluation of brain morphology, with superior performance as compared to other techniques. However, MR images are typically assessed qualitatively, thus relying on the experience of the involved radiologist. This may lead to errors of interpretation in the presence of subtle alterations and does not exploit the full potential of this technique as a quantitative diagnostic tool. To this end Magnetic Resonance Relaxometry (MRR), which is able to quantitively characterize the tissues under investigation through their relaxation rates, seems extremely promising. Many studies assessed the feasibility of relaxometry as a diagnostic tool in human brain disorders, with the most promising results obtained in the evaluation of neurodegenerative diseases and in the oncologic field. However, despite such extensive literature in human medicine, due to the lack of standardized protocols and the need of high-field MRI scanners, to date few studies have been performed on companion animals. In this work, first we describe relaxometry applications in human neuropathology and their possible extension to companion animals both in the experimental and clinical fields. Then, we present two experiments performed on a typical standard clinical scanner operating at 0.25 T to show that, despite the low field intensity, this technique may be promising even in the clinical setup. We tested the relaxometry protocol in a phantom study and then applied it to a real clinical case study. The results showed that this protocol used on a phantom led to a higher contrast, as compared to the standard approach. Furthermore, when applied to a real case study, this protocol revealed brain lesions undetected by the standard technique which were confirmed by a histopathological examination. These preliminary results are encouraging and support the development of this approach as an advanced diagnostic tool even in a clinical setting where low field MRI scanners are typically employed.

Relaxometry refers to a Magnetic Resonance Imaging (MRI) quantitative technique developed to estimate the relaxation times of the tissues under investigation. This approach is an emerging and promising technique which aims at exploiting the full potentiality of MRI as a quantitative diagnostic tool (1). In fact, although MR is the modality of choice for the evaluation of brain morphology, as compared to CT (2), images are typically assessed qualitatively, thus relying on the experience of involved radiologists. This has severe drawbacks (e.g. errors of interpretation in presence of subtle alterations and unfeasibility of multi-center studies) which are overcome with MR Relaxometry (MRR) where individual contrast mechanisms (e.g. T1, T2 and T2*) of the tissues under investigation are

Key words: brain; magnetic resonance; relaxometry; dog; cat

Corresponding Author:
Francesca Del Signore DVM,
University of Teramo,
Piano D'Accio,
64100, Teramo, Italy
Tel.: +39 3409736807
e-mail: fdelsignore@unite.it

0393-974X (2019)

isolated and quantified (1, 3). Such mechanisms and the basic MRR concepts are summarized in the next section.

Several applications of MR relaxometry to human medicine have been reported, e.g. in the oncologic field, epilepsy and neurodegenerative disorders (4-10), however, in veterinary medicine, few studies have been performed on brain disorders affecting canine and feline patients. For feline species, the first study was performed by Kamman et al. to assess whether T1 and T2 relaxation times could characterize brain edema experimentally induced in feline brains (11). They showed that there was a linear correlation between water content and T1 and T2 relaxation times. The second study, performed on cats at 4.7 T, investigated T2 abnormalities in case of experimentally inoculated glioma (12). It was shown that at the time of maximal tumor growth and edema spread, a tissue differentiation was possible through MRR parameter maps (12). Regarding canine species, in addition to experimental studies (13), in a recent study (14) the authors tried to quantitatively detect hippocampal abnormalities in epilepsy to be used in the veterinary practice. The results suggest that individual analysis might be a suitable method to prove hippocampal involvement in epileptic dogs (14).

After what has been illustrated regarding MRR applications in human medicine, the fundamental question is 'can we perform MRR by adopting standard clinical scanners to obtain new clinical insights in veterinary medicine?' We believe that this is the real challenge for MRR to become an advanced diagnostic tool.

In this work, firstly we introduced the above MRR parameters, e.g. T1 and T2. Secondly, we discussed the current literature on this topic in canine and feline species and the possible applications based on human medicine, where this technique has been largely tested. Thirdly, we report an original phantom-based study to explore the feasibility of this approach using the typical experimental setup available in the clinical field. The aim is to assess whether MRR can be useful to differentiate tissues which cannot be detected by the standard clinical scans. This allowed us to test the potentiality of the MRR protocol which was then applied to a second experiment where we studied the brain of an euthanized dog in order to test whether it was possible to identify lesions which had been undetected by the standard T1/T2 weighted images. Finally, these findings were validated by a histopathology study. Notably, our preliminary tests were performed with a low field scanner (operating at 0.25 T) since this is typically employed in the vast majority of veterinary facilities (15).

MATERIALS AND METHODS

MRR relaxation times T1 and T2

In conventional MRI, the tissue contrast is obtained by adjusting the sensitivity of the acquired signal to differences in the tissue T1, T2 and T2* characteristic relaxation times (T1, T2 and T2*-weighted images) (1). Since T1, T2 and T2* are influenced by local biophysical structure and biochemical environment, alterations in T1 and T2 can be associated with disease (e.g. edema, tumor invasion and axonal de-myelination) or other biological processes such as neuro/development-degeneration-plasticity, learning and aging (3, 16). Therefore, to obtain information on tissue structure and function in a quantitative manner (and theoretically independent of scanner hardware and sequence parameters) MRR extracts the relaxation times from the MRI data (1). This is achieved through the adoption of a model describing the MRI signal evolution as a function of the relaxation parameters and a fitting procedure to estimate from the acquired signals, T1, T2 and T2* (1). Many T1/T2w images have to be repeatedly acquired to sample the recovery/decay of the MR signals corresponding to the acquisition through either Inversion Recovery (IR)- or Spin Echo (SE)-based sequences (1). For the T1 estimation, although both IR and SE can be adopted, in this study, an SE sequence was adopted for two reasons. Firstly, the SE acquisitions are faster than IR and this is a fundamental aspect in veterinary medicine since the patients are anesthetized and a long general anesthesia is dangerous. Secondly, SE sequences can be adopted by varying a single parameter (Repetition Time TR) that is accessible to the user in all standard scanners/software. On the contrary, to adopt IR sequences for relaxometry, the standard scanner software needs to be modified in order to give access to other parameters such as the Inversion Time (TI) to the user. Once the final T1/T2 map is obtained this can be overlaid to the anatomical

MRI data to spatially localize the eventual brain lesions.

The typical acquisition and analysis pipeline are shown in Fig. 1. Despite this technique being promising, it is not without disadvantages. For example, common sources of error are due to residual or incoherent transverse magnetization and movement artifacts (3). In fact, beyond bulk motion, physiological motion, including blood flow, can also induce subtle artifacts and bias in T1 and T2 values (3). Furthermore, accelerated measurement techniques, usually adopted to speed up the acquisition time, generally use small flip angle radiofrequency pulses to sample the magnetization which are characterized by a low signal to noise ratio (SNR). To increase the SNR, as an example, systems based on multichannel detection can be used.

Moreover, the subject motion due to the longer scanning time of MRR as compared to standard MRI, lead to important artifacts affecting the final T1/T2 maps. This can be particularly problematic in multi-slice acquisitions, where the slice selection may result inaccurate due to differences of times, echo times or flip angles (1). Notably, this aspect can be minimized in veterinary medicine thanks to the general anesthesia.

Experiment 1 – Phantom study

The basic idea behind this experiment was to compare the minimum contrast detectable through a T1-based approach with what can be evidenced with an MRR technique. Data was acquired from two phantoms (P1 and P2) composed of NaCl 0.9% solution (B. Brown, Melsungen, Germany) doped with different concentrations of a contrast agent (CA), namely Magnegita (Gadopentetate dimeglumine 500µmol/ml, Agfa HealthCare Imaging Agents GmbH, Köln, Germany). P1, filled with 5 µmol of CA, represented the reference, and thus remained constant throughout the experiment. In P2, instead, the concentration of the CA was gradually varied in order to consider three separate conditions. The MR data were acquired by means of an Esaote Vetscan Grande scanner operating at 0.25 T equipped with a NeuroCoil 2 (Esaote S.PA, Genova, Italy). In each condition, two sets of MRI data were acquired. The "clinical" dataset (CLI), i.e. obtained with clinical sequences, was acquired by an SE T1w sequence with standard typical settings on a dorsal plane (TR = 200 ms, TE = 26 ms, FOV = 210x210 mm^2, slice thickness = 2 mm, Gap =0 mm, Matrix 384x368, Number of acquisition-NEX =2). The second dataset, related to the relaxometry and denoted by 'REL', was acquired with an ad-hoc developed protocol consisting of repeated acquisitions of SE T1w images corresponding to a variable TR in the range [150, 900] ms with the same other parameters setting. The first interval [150 800] ms was sampled every 50 ms, while the interval [800 900] ms was sampled every 100 ms. This selective sampling represented a compromise to allow a denser sampling in the most rapid part of the relaxation curve while saving some acquisition time. For the data analyses, these consisted of fitting the acquired signals with a two-parameter model by means of an unconstrained minimization based on derivative-free method (17). These analyses were performed by means of in-house developed codes in MATLAB (MATLAB and Statistics Toolbox Release 2015b, The MathWorks, Inc., Natick, Massachusetts, USA).

Experiment 2 – Single case study

In this case, the protocol developed in Experiment 1 was applied to a real clinical case. A 9 year-old male German shepherd was referred to our hospital because of anorexia and vomiting; atopic dermatitis treated with cyclosporine and *Escherichia coli* (*E. coli*) multiresistent cystitis were recorded in the patient history. Left head tilt and bilateral nystagmus were observed during physical examination. Soon after the referral, rapid worsening of clinical conditions occurred, and euthanasia was elected by the owner; a post mortem MRI of the brain was performed. All the procedures were performed with the owner's compliance. Sequences T1w, T2w and FLAIR were acquired in different planes with the same scanner and coil used in Experiment 1. Sequences SE T1w, FSE REL T2w and FAST FLAIR were acquired with the settings as follows. For SE T1w transverse scan: TR= 1350 ms, TE= 26 ms, Matrix 320 x 288 and FOV 240 x 240 mm^2, for SE T1w sagittal plane: TR=1500 ms, TE=26, Matrix 384x 240 and FOV 180x180 mm^2, for the FSE REL T2w sagittal sequence: TR= 7780, TE= 90 ms, FOV 250x250 mm^2, Matrix 400x352, for FSE REL T2W: TR= 8640, TE= 90, Matrix 488x352 and FOV 260x260 mm^2, for FLAIR dorsal scan: TR=6670, TE=90 ms, FOV 230x230 mm^2, Matrix 288x224 and Number of Acquisition- NEX =1. Slice thickness = 3 mm and Gap=0.4 mm were set for all the sequences and Number of Acquisition - NEX

=2 for all T1w and T2w sequences. The MRR protocol was then applied to the central 2 mm sagittal slice in order to obtain a representative sampling of the brain while limiting the long acquisition time as compared to 3D multi-slice approach. During the acquisition, a set of SE T1w images corresponding to a variable TR in the range [50, 1100] ms were acquired. The first interval [50 300] ms was sampled every 150 ms, while the interval [350 1100] ms was sampled every 50 ms. Data analysis was performed with the same analysis steps described for Experiment 1. In order to validate the MRR results and thus to assess the nature of these lesions, necropsy and the histopathological analysis were performed. The entire brain was collected, fixed in 10% neutral buffered formalin, embedded in paraffin and routinely processed for histopathological investigations. In particular, 4-µm thick sections were stained with hematoxylin and eosin and observed under a light microscope (model ECLIPSE E600W, Nikon, Japan).

RESULTS

Experiment 1

In this experiment, three separate scenarios were considered. Firstly, we studied a control condition where P1 and P2 have a significant different concentration of CA, 5 *vs* 3 µmol, respectively. In this case, as can be seen in Fig. 2, where T1w images are reported, the contrast in the 'CLI' data is sufficient to clearly distinguish P1 (Fig. 2A) from P2 (Fig. 2B). A visual inspection by an expert radiologist can easily identify such difference. The idea was then to decrease the difference in the concentration between P1 and P2 to check whether there is a condition where this difference is so small that in the 'CLI' data P1 and P2 cannot be distinguished while in the 'REL' data these result separated. We started from a control condition where the P1 and P2 CA concentrations were identical (Fig. 2 C-D). In this case, no evident contrast can be observed between P1 and P2 from 'CLI' data. On 'REL' data the estimation of T1 was run. As an example, Fig. 3 demonstrates the comparison between the evolution of the acquired and the predicted signal (dashed line) based on the estimated parameters. A good agreement between the acquired and predicted signal can be noted, thus suggesting a successful fitting procedure. The obtained T1 maps are shown in Fig. 2 E-F and, as expected, also in this case the visual inspection did not reveal significant differences in the two phantoms. To quantify these observations, in Table I mean values (µ) and standard errors (Standard Error of the Mean- SEM) are compared of the 'CLI' signals and T1 values. To quantify the contrast, the absolute value of the percentage variation between the two phantoms defined as $\Delta = (\mu_1 - \mu_2)/\mu_1$ are shown (Table I). In this case, the same percentage variation was observed between P1 and P2 both from 'CLI' and 'REL' data. This confirms that no artefactual higher contrast, as expected, is obtained from T1 maps.

Table I. *Phantom study - same contrast agent concentration.*

	Clinical Signal Values (au) µ±SEM (ms)	**T1 Map values µ±SEM (ms)**
P1	1074±1	56.3±0.8
P2	1110±1	58.0±0.8
Δ%	3%	3%

mparison between clinical and T1 values from phantoms with the same contrast medium centration. As expected, no significant differences are obtained in both CLI and REL data.

Table II. *Phantom study - different contrast agent concentration (0.5 µmol).*

	Clinical Signal Values µ± SE**M (au)**	**T1 Map Values** µ± SE**M (ms)**
P1	1082±1	57.2±0.7
P2	1092±2	49±1
Δ%	1%	12% **

*Comparison between clinical and T1 values from phantoms corresponding to different CA concentrations (P1: 5 µmol and P2: 5.5 µmol). A significant increase in the contrast is obtained in REL as compared to CLI data. The percentage variation (Δ) is twelve times higher and a t-test reveals a statistically significant difference in REL data (** p <0.01).*

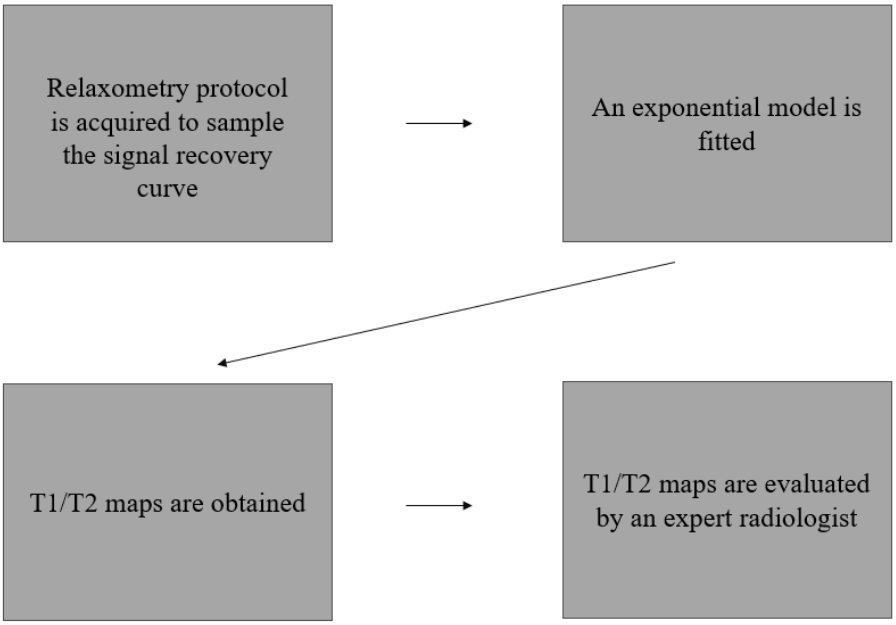

Fig. 1. *Summary scheme illustrating the pipeline to perform MRR studies.*

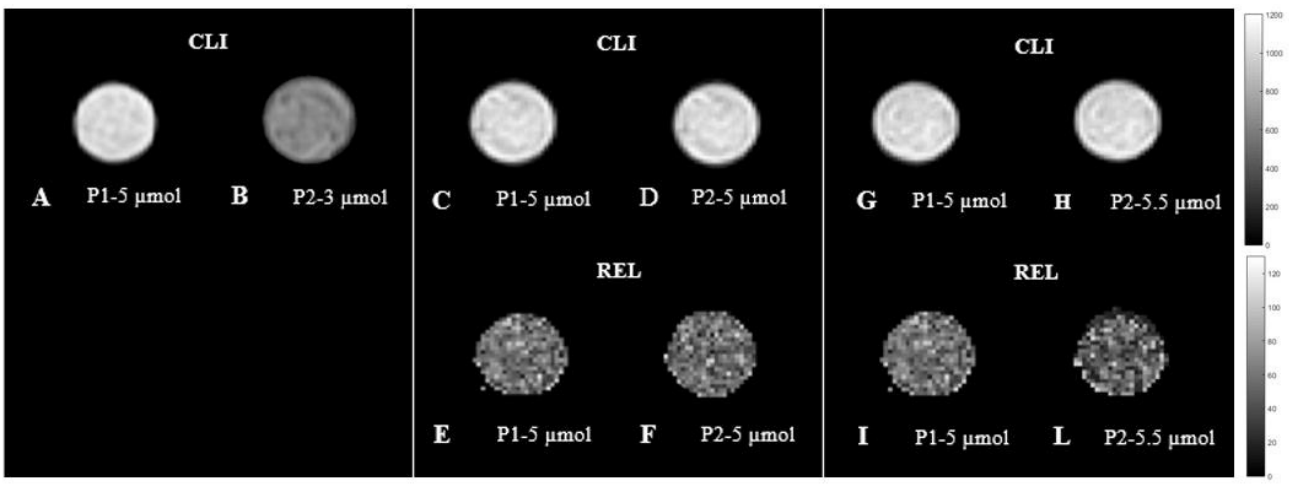

Fig. 2. *Comparison between the Clinical (CLI) and Relaxometry (REL) results. On the right, color bars indicating the signal intensity expressed in au for CLI and in ms for T1 maps.* ***A***, ***B****) Comparison between CLI data acquired with a SE-T1w dorsal scan on phantom P1 doped with 5 µmol of CA (A) and on phantom P2 doped with 3 µmol of CA (B); it can be noted the high contrast in signal difference between P1 and P2 clearly identifiable by visual inspection.* ***C-F****) CLI data acquired with a SE-T1w dorsal scan on phantom P1 and P2 doped with 5 µmol of CA (C, D) and REL data showing T1 maps obtained from P1 and P2 (E, F); in both T1w and T1 maps no visual difference can be detected; this is an important check on the false positives.* ***G-L****) CLI data acquired with T1w dorsal images of P1 filled with 5 µmol of CA (G), CLI data of P2 filled with 5.5 µmol of CA (H) and respective T1 maps (I-L); while from T1w images no difference can be detected, the T1 map of P2 is clearly darker than P1. This difference is statistically significant ($p<0.01$) and consistent with the underlying physics, i.e. increasing CA concentration we expect T1 to progressively decrease.*

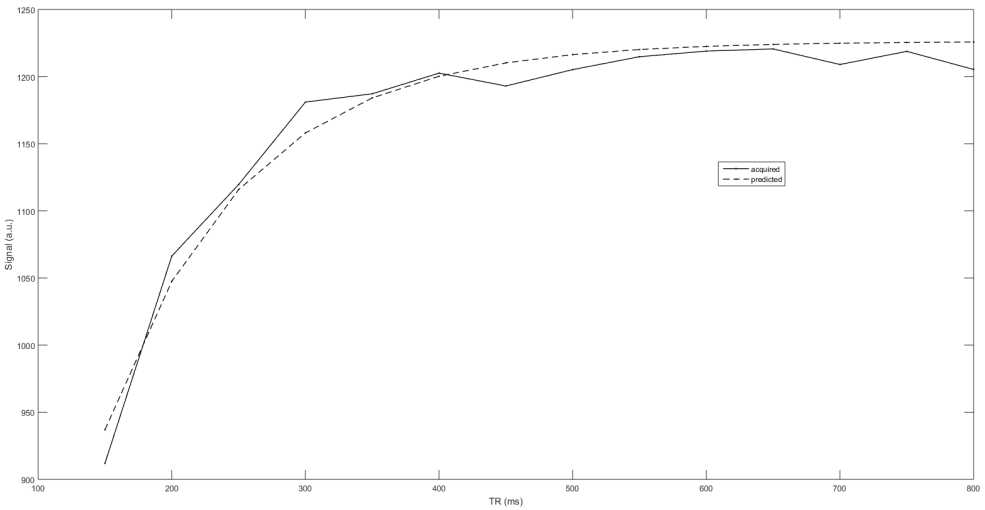

Fig. 3. *As a representative example, the results of the fitting procedure for a voxel are shown. Good agreement can be noted between the acquired (solid line) and predicted (dashed line) signal by the model based on the estimated T1 and proton density.*

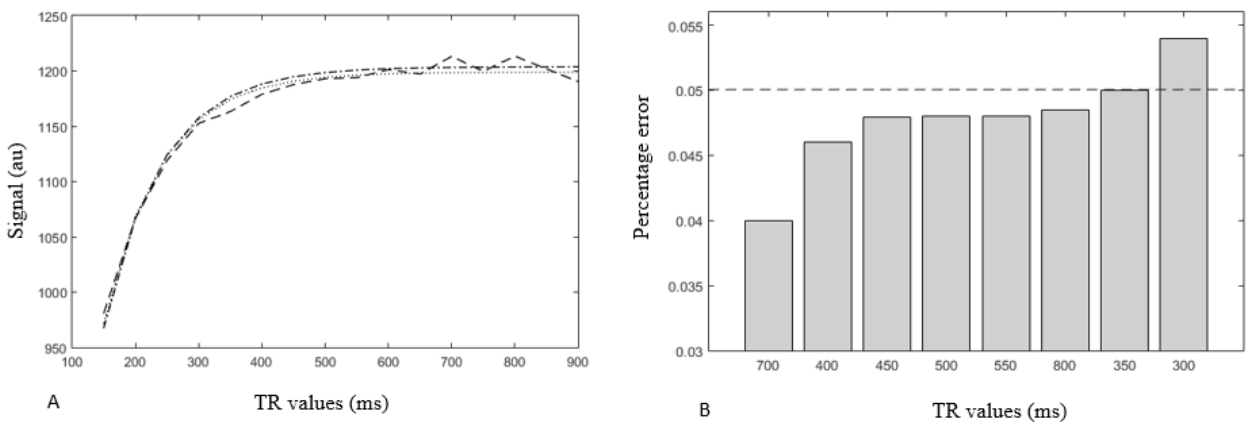

Fig. 4. ***A)*** *As an example, the MR signal predicted by the two-parameter model using the original 15 TR values from the 'true' T1 estimate (dashed-dotted line). The dotted line rshows the signal obtained from the same model with the T1 estimated. The dotted line shows the signal computed from the T1 estimate obtained using only 8 TR values.*
B) *The incremental percentage error is reported as a function of the TR values iteratively removed from the model. It can be noted that the adopted threshold (5%) is exceeded at TR = 300 ms.*

In the next scenario (Fig. 2 G-L), the CA concentration was increased in P2 to 5.5 µmol (P1 CA concentration fixed to 5 µmol). As seen in Fig. 2 G-H, no contrast is apparent from a visual inspection from 'CLI' data. This is confirmed by the values reported in Table II where the average values in P1 and P2 are not statistically different, as revealed by a *t*-test, and the percentage change is around 1%. This supports the evidence of a negligible contrast in 'CLI' data between P1 and P2. On the other hand, as shown in Fig. 2 I-L (REL data), some contrast is evident between P1 and P2 from the visual inspection. It can be noted that T1 values in P2 are smaller. This is correct, since the higher the CA concentration, the lower T1 values (as expected by the physic properties of the CA itself in shortening T1 relaxation time (18). This is confirmed by the values reported in Table II. The mean values are significantly different (** $p<0.01$) and the percentage change is twelve times larger than in the 'CLI' data. Therefore, in this case, the contrast obtained in the T1 map is one order of magnitude higher than with the standard MRI procedure. These results are promising in showing that a higher contrast can be achieved with MRR, revealing potential subtle differences among tissues that the standard approach could not detect.

However, an important limitation, especially in the clinical field, relates to the large acquisition time required by the MRR protocol. As matter of fact, in the above analysis, a set of 15 TR values was used in order to estimate a reliable T1 map. This leads to a total acquisition time of 90 minutes that might result prohibitive in clinical settings. Therefore, we tried to quantify the stability of the T1 estimate corresponding to a smaller and 'optimal' subset of the TR values. The general idea is to compute the distance between the T1 values obtained from all TRs and from a subset of them. Then, such distance was minimized as a function of the set of TR explored. Initially, the T1 mean and standard deviation reported Table I for phantom P1 was considered as a reference. By means of a Gaussian distribution based on these values, 200 T1 values were sampled. Then, by inputting such values in the two-parameter model adopted in this study (see above), 200 MR signals were simulated. Finally, some noise estimated in the background of the 'real' acquired data was added. The standard deviation of the acquired signals was estimated and then noise sampled from a Gaussian distribution was added

Table III. *MRI* vs *advanced MRI.*

	MRI	**ADVANCED MRI**
ADVANTAGES	Non-invasive No X-Rays Greater contrast in soft tissues respect on CT Multiple sequences-different contrasts	Non-invasive Quantitative and objective Evidence of undetectable lesions with qualitative scans No extra costs in term of diagnostic tools Signal analysis performed off-line
DISADVANTAGES	Longer scan protocol respect on CT General anesthesia necessary for pets	Longer scan protocols respect on MRI Extra skills for radiologists to analyze maps Errors in relaxation times estimation

Summary of advantages and disadvantages of the application of relaxometry compared to clinical studies.

with mean zero and such standard deviation. In Fig. 4A (broken line) an example a simulated signal is shown. Then the fitting procedure was run. Initially, all the TR values were used and the corresponding T1 estimates were adopted as reference ('true') values. In Fig. 4A, is an example of a signal simulated form a 'true' T1 value (dashed-dotted line). Then, one TR value was removed and the 200 T1 estimates were repeated. This was carried out for all the possible TR values and every time the percentage error between the 'true' and the estimated T1 values was computed. Afterwards, the TR leading to the smallest error was selected. If such value was smaller than 5%, that value was removed from the subset of TR considered. This procedure was repeated for the next TR value to be removed and it stopped when the cumulative percentage error reached 5%. Seven TR values obtained, namely [700 400 450 500 550 800 350] could be removed, see Fig. 4B where the cumulative error is reported. As an example, in Fig. 4A (dotted line) the signal simulated from the model when these 7 TR values were removed (in Fig. 4B the T1 estimate obtained from the 'reduced' model was used in the complete model, i.e. using all the TR values, for display reasons).

These results are encouraging, showing that with the smaller number of TR values obtained the quality of the estimate is still acceptable. Notably the acquisition time reduces from 90 to 40 minutes.

Experiment 2

In the real case study, in T2w and T1w images, slightly hyperintense lesions were detected at the level of pons and medulla oblongata in every scan (Fig. 5, solid white arrows) and in both T1w and T2w scans the fourth ventricle was barely visualized

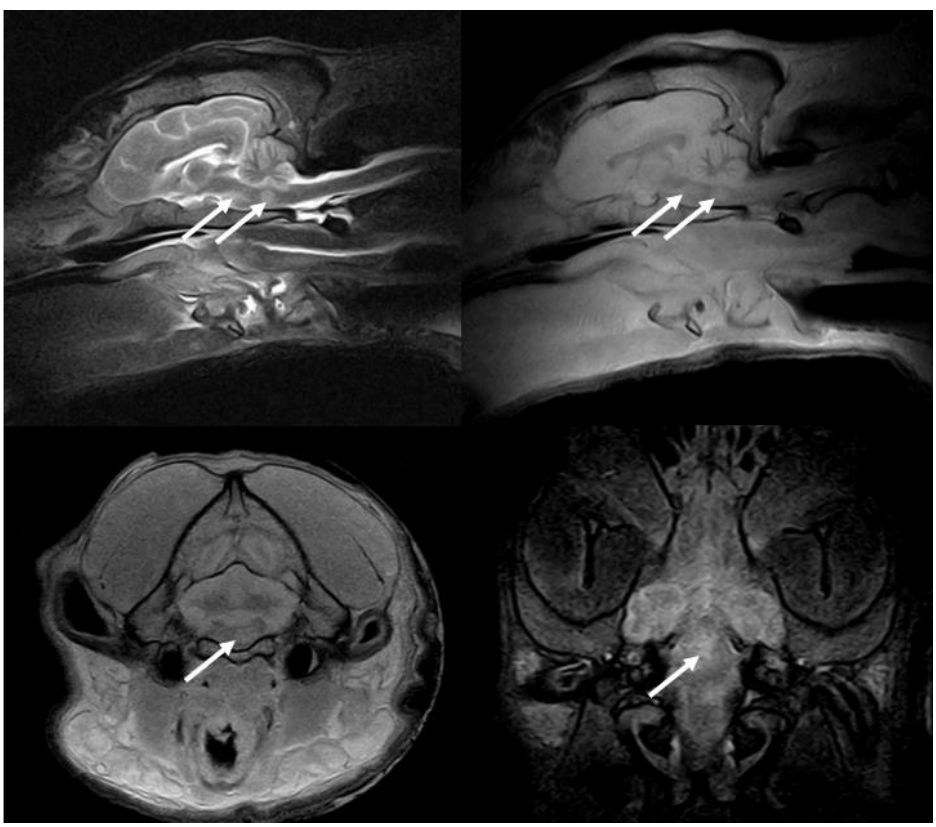

Fig. 5. ***A)*** *FSE REL T2w sagittal scan;* ***B)*** *SE T1w sagittal scan;* ***C)*** *SE T1w transverse scan;* ***D)*** *dorsal FAST FLAIR scan. White solid arrows point at hyperintense lesions at the level of pons and medulla oblongata evident in every scan acquired. The fourth ventricle is not evident.*

(Fig. 5 A-B). These lesions were suspected to be inflammatory or vascular. In the sagittal and transverse T2w image of the cerebellum (Fig. 6 A-B), a slight hyperintense lesion was detected. Notably, this lesion was not evident in T1w images (Fig. 6C, solid white arrows). Furthermore, it can be noted that, at the level of the pons and the medulla oblongata, hyperintense areas are present both in T1w and T2w images (Fig. 6 D-F, solid white arrows). Of note, in the T1 map, some additional hyperintense regions were observed in the area usually occupied by the fourth ventricle and at the level of the cerebellar parenchyma (Fig. 6 D-F, solid black arrows). These observations are in line with the histopathological study. The brain sections to be sampled were identified by comparing the sagittal images with the transversal ones (Fig. 6G - white line). Within the sampled area (reported in Fig. 6H – white square), grossly and scattered hemorrhages were identified at the level of the pons, medulla oblongata, cerebellar vermis and parenchyma (Fig. 6I, white solid and dashed arrows). Histologically, foci of acute vasculitis and fibrinoid necrosis were observed at the same level (Fig. 7A, solid white arrow). Necrotic-hemorrhagic areas, mainly infiltrated by polymorphonuclear cells, were also observed in the surrounding parenchyma and, notably, a large hemorrhagic area was evident within the white matter of the cerebellum (Fig. 7B,

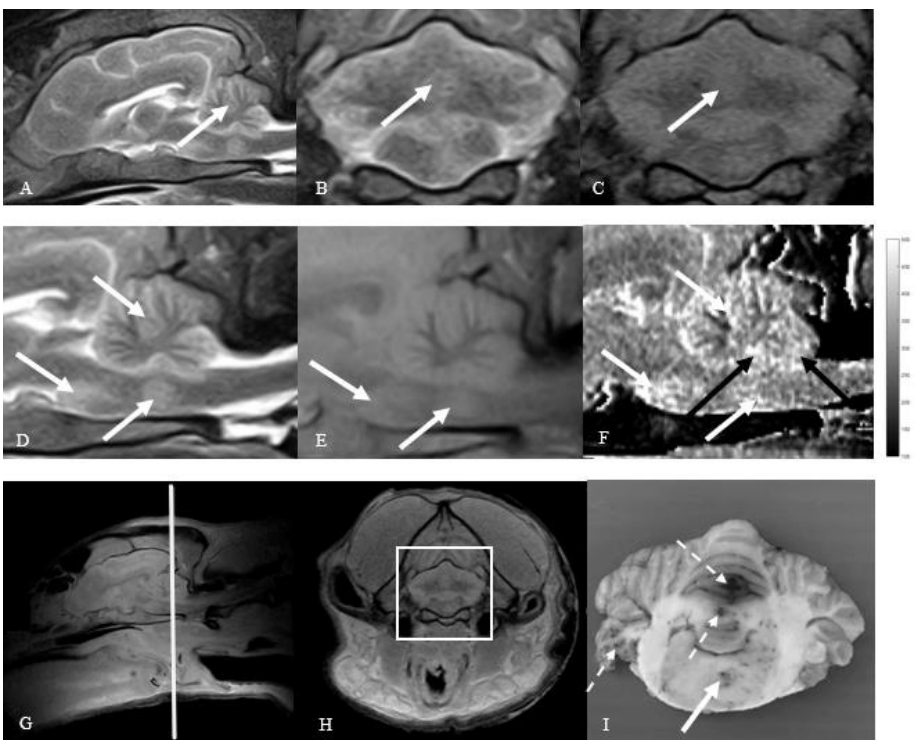

Fig. 6. ***A)*** *FSE REL T2w sagittal scan;* ***B)*** *FSE REL T2w transverse scan;* ***C)*** *SE T1w transverse scan. White solid arrows point at the cerebellar hyperintense lesion detected in T2w images; notably, at the same level, no abnormalities are visible in T1w image.* ***D-F)*** *Comparison between the T2w sagittal image (D), the T1w sagittal image (E) and T1 map of pons, medulla oblongata and cerebellum (F); white solid arrows point at hyperintense lesions at the level of pons, medulla oblongata and cerebellar evidenced by both T1 map and clinical scans. In the T1 map, black solid arrows point at hyperintense areas at the level of cerebellar parenchyma and at the level of the area surrounding the fourth ventricle not detected by clinical scans. On the right of T1 map, the color bar of the signal is demonstrated. G-I) correspondence between MRI data and corresponding anatomical sections used for the histopathological study; in T1w sagittal section (G), the white line represents the transverse section of vermis cerebelli and medulla oblongata that has been sampled for histological examination, evidenced by the white square (H); in the transverse anatomical section (I) scattered hemorrhages can be observed at the level of cerebellar parenchyma (dashed white arrows) and of the medulla oblongata (solid white arrow).*

solid white arrow). Therefore, histopathological examination confirmed the presence of cerebellar lesions barely detected by clinical T1w scans, and the nature of the lesion was consistent with what was suspected after MRI examination.

The detection of brain lesions related to vasculitis is of interest. While in human medicine this condition is currently detected with high field scanners (19), little information is available on the pathologic mechanisms that result in this disorder in dogs (20); in veterinary medicine few reports are available on this condition, none of which describe MRI findings (20-23).

DISCUSSION

Nowadays, in veterinary medicine, few relaxometry studies have been to investigate canine and feline brain disorders and the application of this technique in the clinical practice. In this study, we report preliminary results obtained both on phantoms and real data experiments performed with a low field scanner. We obtained that, in phantoms, MRR can reach a higher contrast than in clinical scans. Notably, when applied to a real clinical case, as compared to the clinical protocol, MRR was able to characterize better cerebellar abnormalities that were confirmed by histopathological examinations. These results are encouraging, although this work was performed only post-mortem, and the contribution of post-mortem abnormalities in MRR must be thoroughly investigated in successive studies.

In general, to develop advanced techniques, such as MRR, in veterinary medicine it may be useful to improve diagnosis/treatments of brain diseases, as in human medicine, especially in cases of disorders causing only subtle changes (e.g., hepatic encephalopathy or distemper encephalitis) that can be easily missed without an adequate resolution scanning and careful interpretation (24). However, this technique presents some disadvantages that makes its widespread application difficult, such as a long acquisition time in patients under general anesthesia (see Table III for a summary of the main drawbacks of this approach). In this work, to show the potentiality of this approach in the typical clinical setup, we used the standard equipment typically provided in the clinical field. To reduce the large acquisition time, we adopted SE sequences (faster than typically employed IR) and we optimized

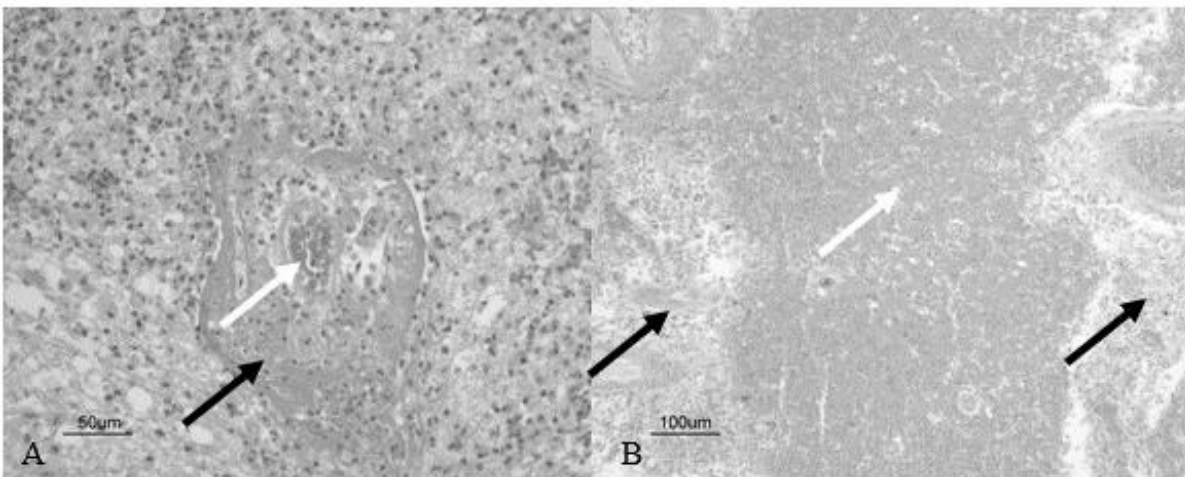

Fig. 7. *Histological examination of medulla oblongata and vermis cerebelli.* ***A)*** *Medulla oblongata: a blood vessel (solid white arrow) is surrounded by the deposition of hyaline, "fibrinoid" material (solid black arrow). The presence of a mixed inflammatory infiltrate is also evident. Haematoxylin and eosin stain. Final magnification: x 200.* ***B)*** *vermis cerebelli: a large haemorrhagic area (solid white arrow) is present within the white matter of the cerebellum (solid black arrow). Hematoxylin and eosin stain. Final magnification: x 100.*

the number of TR employed through a simulation study. Furthermore, while anatomic sections for histopathological analysis are usually performed in the transversal plane, we computed the T1 map in a sagittal slice to acquire as much cerebral parenchyma as possible with a single acquisition protocol, limiting as much as possible post mortem deterioration artifacts.

It must be stressed that typically in human medicine as well as in animal model studies (25) MRR is typically performed with high field scanners (≥1.5 T), while in veterinary facilities the magnetic fields employed are in the order of a few hundred mTs (15). This limits the spatial resolution and in general the possible applications of this technique. To overcome this limitation, a possible approach could be the use of cross-modality co-registration approaches suitable to co-register single or a few slices from an image obtained by a modality (e.g. the histopathological image) to a volume obtained by another modality with different spatial resolution (e.g. the T1-maps) (26,27).

In conclusion, MRR is a useful technique currently applied to human brain disorders, however, in veterinary medicine the literature is limited but increasing, with recent MRR studies performed on neurological (14) and orthopedic fields (28). In line with these works, the results reported here suggest that this technique may be promising and pave the way for further studies on MRR as an advanced diagnostic tool to be associated with routine clinical scans. In future studies, this technique might be applied in case of inflammatory/infectious or metabolic disorders (e.g distemper encephalitis, hepatic encephalopathy) to detect subtle lesions and on epileptic patents to clarify some aspects of this condition that are still under debate.

REFERENCES

1. Cheng HL, Stikov N, Ghugre NR, Wright GA. Practical medical applications of quantitative MR relaxometry. J Magn Reson Imaging 2012; 36:805-24.
2. Robertson ID. Magnetic resonance imaging features of brain disease in small animals. In Thrall D. Veterinary Diagnostic Radiology, ed Saunders, Elsevier. St. Luis, 2013; p. 204.
3. Deoni SC. Quantitative relaxometry of the brain. Top Magn Reson Imaging 2010; 21:101-13.
4. Blystad I, Warntjes JBM, Smedby O, Lundberg P, Larsson EM, Tisell A. Quantitative MRI for analysis of peritumoral edema in malignant gliomas. Plos One 2017; 12(5):e0177135.
5. Chen H, Yu GL, Wang JT, Li F, Li GM. Application of T2 relaxometry in lateralization and localization of mesial temporal lobe epilepsy and corresponding comparison with MR volumetry. Acta Radiol 2016; 57:1107-13.
6. Sato S, Iwasaki M, Suzuki H, et al. T2 relaxometry improves detection of non-sclerotic epileptogenic hippocampus. Epilepsy Res 2016; 126:1-9.
7. Gillmann C, Coras R, Rossler K, Doerfler A, Uder M, Blumcke I, Bäuerle T. Ultra-high field MRI of human hippocampi: Morphological and multiparametric differentiation of hippocampal sclerosis subtypes. Plos One 2018; 13(4):e0196008.
8. Steenwijk MD, Vrenken H, Jonkman LE, Daams M, Geurts JJ, Barkhof F, Pouwels PJ. High-resolution T1-relaxation time mapping displays subtle, clinically relevant, gray matter damage in long-standing multiple sclerosis. Mult Scler J 2016; 22:1279-88.
9. Dean DC, Hurley SA, Kecskemeti SR, et al. Association of amyloid pathology with myelin alteration in preclinical alzheimer disease. Jama Neurol 2017; 74:41-49.
10. Pyatigorskaya N, Sharman M, Corvol JC, et al. High nigral iron deposition in LRRK2 and Parkin mutation carriers using R2*relaxometry. Mov Disord 2015; 30:1077-84.
11. Kamman RL, Go KG, Berendsen HJC. Nuclear magnetic resonance relaxation in experimental brain edema: effects of water concentration, protein concentration, and temperature. Magn Reson Med 1988; 6:265-74.
12. Hoehnberlage M, Tolxdorff T, Bockhorst K, Okada Y, Ernestus RI. In vivo nmr t(2) relaxation of experimental brain-tumors in the cat - a multiparameter tissue characterization. Magn Reson Imaging 1992; 10:935-47.
13. Samsonov A, Alexander AL, Mossahebi P, Wu CY, Duncan ID, Field AS. Quantitative MR imaging of two-pool magnetization transfer model parameters

in myelin mutant shaking pup. NeuroImage 2012; 1390-98.
14. Lorincz BA, Anson A, Csebi P, et al. Novel approach to magnetic resonance imaging of epileptic dogs-t2 relaxometry of the brain with emphasised hippocampus. Acta Vet Hung 2017; 65:185-97.
15. Konar M, Lang J. Pros and cons of low-field magnetic resonance imaging in veterinary practice. Vet Radiol Ultrasound 2011; 52(1 Suppl 1):S5-S14
16. Paus T, Collins DL, Evans AC, Leonard G, Pike B, Zijdenbos A. Maturation of white matter in the human brain: A review of magnetic resonance studies. Brain Res Bull 2001; 54:255-66.
17. Lagarias JC, Reeds JA, Wright MH, Wright PE. Convergence properties of the Nelder-Mead simplex method in low dimensions. SIAM J Optim 1998; 9:112-47.
18. Owen M. Radiographic, computed tomography and magnetic resonance imaging contrast media. In Thrall D. Veterinary Diagnostic Radiology, ed Saunders, Elsevier. St. Luis, 2013; p. 104.
19. Razek AAKA , Alvarez H, Bagg S, Refaat S, Castillo M. Imaging Spectrum of CNS Vasculitis. Radioraphics 2014; 34:873-94.
20. Swann JW, Priestnall SL, Dawson C, Chang YM, Garden OA. Histologic and clinical features of primary and secondary vasculitis: a retrospective study of 42 Dogs (2004-2011). J Vet Diagn Invest 2015; 27(4):489-96.
21. Crawford MA, Foil CS. Vasculitis: clinical syndromes in small animals. Compend Contin Educ Pract 1989; 11:400-415.
22. Snyder PW, Kazacos EA, Scott-Moncrieff JC, HogenEsch H, Carlton WW, Glickman LT, Felsburg PJ. Pathologic features of naturally occurring juvenile polyarteritis in beagle dogs. Vet Pathol 1995; 32:337-45.
23. Sasaki M, Pool R, Summers BA. Vasculitis in a dog resembling isolated angiitis of the central nervous system in humans. Vet Pathol 2003; 40:95-97.
24. Rusbridge C, Long S, Jovanovik J, et al. International Veterinary Epilepsy Task Force recommendations for a veterinary epilepsy-specific MRI protocol. BMC Vet Res 2015; 11:194.
25. Heiland S, Sartor K, Martin E, Bardenheuer HJ, Plaschke K. In vivo monitoring of age-related changes in rat brain using quantitative diffusion magnetic resonance imaging and magnetic resonance relaxometry. Neurosci Lett 2002; 334:157-60.
26. Guidotti R, Sinibaldi R, De Luca C, et al. Optimized 3D co-registration of ultra-low- field and hig field magnetic resonance images. Plos One 2018; 13(3):e019389020182018.
27. Sinibaldi R, Conti A, Sinjari B et al., Multimodal 3D imaging based on μMRI and μCT techiniques bridges the gap with histology in visualization of the bone regeneration process. J Tissue Eng Regen Med. 2018; 12(3):750-61.
28. Pownder SL, Hyashi K, Caserto BG, Breghner RE, Norman ML, Potter HG, Koff MF. Quantitative magnetic resonance imaging and histological comparison of normal canine menisci. Vet Comp Orthop Traumatol 2018; 31(6):452-57.

REAL-TIME PCR DETECTION OF THE EFFECT OF POSTWEANING ON THE EXPRESSION OF CYTOKINES AND NF-κB IN PIGLETS

L. TURIN, R. TORINESI and G. PASTORELLI

Department of Veterinary Medicine (DIMEVET), University of Milan, Milan, Italy

Received August 6, 2019 – Accepted October 14, 2019

Pig weaning involves radical changes, which affect health, behavior and performance. Weaning stress dramatically impacts the porcine immune system. This study aimed to evaluate the expression of different cytokines and nuclear factor kappa B (NF-κB) in growing postweaning pigs. Forty piglets weaned at 28 days of age, with an average starting weight of 10.12±0.28 kg were considered for the analysis (time 0) and followed up for 28 days (time 1). Growth performance, skin lesions, cytokines and NF-κB expression were measured. The results showed an increased expression of two cytokines with pro-inflammatory effect, interleukin (IL)-8 and interferon-gamma (IFN-γ), a cytokine with anti-inflammatory effect, IL-4, and a cytokine with both pro- and anti-inflammatory effects, IL-6. An effect of time was observed for body lesions. Compared to females, male piglets had higher levels of all cytokines tested (IL-1β, IL-6, IL-8, IL-10, TNF-α, IL-4) except IFN-γ. Also NF-κB resulted expressed higher in males compared to females. In conclusion, this study demonstrated that weaning in piglets is associated with increased expression of inflammatory cytokines.

In pig farms, piglets are weaned between 21 and 28 days after birth, at a much earlier age than what would be expected in a natural environment. The immediate postweaning period is the most critical stage in the life cycle of piglets. They have to adapt to changes in the feed regime and in the environment, in a period when the animal still has an immature immune system and low digestive capacities, besides a precarious intestinal microbiota (1).

The innate immune system represents the first line of defense of the animal. It elicits its functions through two mechanisms: on one hand, the recruitment and activation of cellular components, including macrophages, neutrophils, natural killer cells and dendritic cells; on the other hand, the secretion of extracellular mediators, such as cytokines and chemokines (2). The cells of the innate immune system are responsible for the release of these extracellular mediators, including pro- and anti-inflammatory cytokines, such as interleukin (IL)-1β, IL-2, IL-4, IL-6, IL-8, IL-10, IL-12, tumor necrosis factor (TNF)-α, interferon (IFN)-α, IFN-γ and transforming growth factor (TGF)-β (3). Their production is triggered in response to several stimuli and it alters cell behavior, activating a downstream signaling cascade that involves nuclear factor kappa B (NF-κB), which stimulates or inhibits the expression of different genes with the aim of coordinating the inflammatory process (4).

In neonatal piglets, the immune system is under-developed, therefore, their survival depends on colostrum ingestion, which provides immunoglobulins to the newborn, generating the so-called lactogenic immunity (5). The intake of sow's milk influences the

Key words: pig, postweaning, cytokine, nuclear factor-κB

Corresponding Author:
Lauretta Turin,
Department of Veterinary Medicine (DIMEVET),
University of Milan,
via Celoria 10, 20133 Milan, Italy
Tel.: +39 02 50318090
e-mail: lauretta.turin@unimi.it

0393-974X (2019)

maturation of the immune system of the piglet and is fundamental for the newborn to develop an efficient capacity to sense and intervene against pathogens (6). After weaning, piglets' immune system is still immature, but they cannot rely on the passive immunity from mother's milk anymore, as they rapidly pass to solid feed (1). The exposure to the appropriate microbiota plays a fundamental role in the maturation of the immune system and it influences the defensive responses in later life, since an altered microbial environment could increase the susceptibility to infections, other than the likelihood of allergic diseases (7).

Only little is known about the development of innate immunity in swine and the evolution of immune cells in newborn piglets. Grierson *et al.* (8) studied the changes in the immune cells (monocytes, B cells and T cells) of piglets from birth, and followed-up their increase along with the age. These cells are able to respond to antigenic and inflammatory agents even if the immune system is not fully developed (9).

Pié *et al*. (10) quantified the expression of some inflammatory cytokines in the intestine and in the colon of piglets, and Li *et al.* (11) studied the modification of inflammatory cytokines in the skeletal muscle. Nevertheless, to our knowledge, there is no other relevant evidence regarding the natural production of pro- and anti-inflammatory cytokines in piglets, describing the different expression of these mediators throughout the animal's growth. Cytokines are extremely important in the induction and regulation of the immune responses; in fact, when the animal is infected by a pathogen, the expression of cytokines is up- or down-regulated (12). In this study, we quantified the expression of a selected panel of cytokines, in order to cover Th1 and Th2 types of response, considering both pro- and anti-inflammatory cytokines. In addition, we investigated the expression of NF-κB, implied in the regulation of both innate and adaptive immunity (13).

MATERIALS AND METHODS

Animals

The study was conducted in accordance with the Declaration of Helsinki, and the protocol was approved by the Ethics Committee of Animal Welfare of the University of Milan (OPBA_10_2018) according to the EU Directive 2010/63/EU.

A total of forty weaned (LW-L x Talent Topics) piglets (28 days old), 20 castrated males and 20 females, weighing 10.12±0.28 kg, were used in this study.

The animals were individually identified, divided into 4 pens (10 pigs/pen) and reared in environmentally controlled rooms (average temperature 26°C and relative humidity 60%). Each pen measured 1.5 m wide × 1.5 m long. Animals were fed *ad libitum* a commercial diet to meet the requirements for all nutrients. Individual piglet's weight at day 0 (time 0) and day 28 (time 1) and pen feed consumption were recorded, the average daily gain (ADG) and feed conversion ratio (FCR) were calculated.

Skin lesions were assessed by one trained observer the first day (baseline level day 1), and subsequently once a week for a total of 5 observations (at days 1, 7, 14, 21 and 28). Pigs were encouraged to stand up in order to make the body more clearly visible. The total amount of lesions on one side of the pig for each one of the five regions (ears, front, middle, hind-quarters and legs) defined in the Welfare Quality® (Welfare Quality® Consortium, 2009, Lelystad, Netherlands) were recorded. Each region was scored as 'a' (up to 4 lesions), 'b' (5–10 lesions), or 'c' (11–15 lesions) and regions with more than 15 lesions were recorded. Then, each pig was scored using a 0-to-2 scale, where 0 corresponded to a pig having the full body classified as 'a', 1 to a pig having any body region with an individual score 'b', and/or a maximum of one region scored as 'c', and 2 to a pig having at least two body regions or more classified as 'c', or at least one body region with more than 15 lesions.

Collection of blood samples

At the beginning (time 0) and at the end of the study (time 1), blood samples were drawn by cranial vena cava puncture prior to the morning feeding from 12 animals (total number of samples = 12 for each time-point). The blood was collected in 3 different vacutainer glass tubes (5 ml) containing 3 different anticoagulants, heparin, EDTA, a gel and clot activator (Becton and Dickinson, Milan, Italy), and immediately transported to the laboratory. Plasma and serum were separated from blood samples by centrifugation (3,500 x g for 15 min at 4°C) and stored at –18°C until use.

Tests for porcine reproductive and respiratory syndrome virus

Serum samples were tested for the presence of

antibodies against Porcine Reproductive and Respiratory Syndrome Virus (PRRSV) using a commercially available enzyme-linked immunosorbent assay (ELISA) (HerdChek; IDEXX Laboratories, Westbrook, Maine, USA) and confirmed by RT-PCR.

Buffy coat preparation, RNA extraction, reverse transcription and Real-Time PCR assays

Concentrated leukocytes, referred to as buffy coat, were isolated from EDTA-collected blood according to a method previously described (14). Briefly, 4 ml of blood was mixed with 6 ml of red blood cell lysis buffer (1.4 M NH_4Cl, 0.1 M KHCO, 3.5 mM EDTA, pH 8) and vigorously shaken for 15 min. After centrifugation at 300 x g for 5 min at 4°C, the supernatant was discarded, and the white blood cells were resuspended in 4 ml of ice-cold red blood cell lysis buffer. The tubes were vortexed and centrifugated at 300 x g for 5 min at 4°C. Supernatant was discarded and 4 ml of room temperature phosphate buffered saline (PBS, containing 137 mM NaCl, 2.7 mM KCl, 10 mM Na_2HPO_4 $2H_2O$, 2 mM KH_2PO_4, pH 7.4) was added. The samples were again vortexed and centrifugated at 300 x g for 5 min at 4°C. The supernatant was discarded, and the pellet was resuspended directly in 1 ml of RNAzol® (Sigma-Aldrich, St. Louis, MO, USA) for the following RNA purification.

Total RNA was purified from the samples by the RNAzol® method. All samples were homogenized in 1 ml of RNAzol® by multiple pipetting up and down and subsequently processed for RNA isolation, rigorously applying the manufacturing protocol. The RNA pellet was dissolved in sterile nuclease-free water and stored at -80°C until use. The purity and concentration of total RNA were assessed using a spectrophotometer (BioPhotometer, Eppendorf, Hamburg, Germany) at 260 nm wavelength. About 1 μg of total RNA from each specimen was reverse transcribed into cDNA in a 25 μl final volume using the High Capacity cDNA Archive kit with random hexamers (incubation at 25°C for 10 min, followed by 37°C for 60 min, and inactivation at 95°C for 5 min) (Applied Biosystems, Foster City, CA, USA) (15). The cDNA obtained was utilized in optimized Real-Time PCR assays with the 7000 Sequence Detection System (Applied Biosystems, Foster City, CA, USA) (16) to quantify the expression of cytokines and NF-κB. Porcine specific primer pairs were designed using the swine genome sequences available in the NCBI nucleotide sequences database as template (gi:288782229

Table I. *Oligonucleotides used to quantify gene expression in Real-Time quantitative PCR assays.*

Primer	Nucleotide sequence (5' to 3')
Swine β-actin Forward	CTCCTTCCTGGGCATGGAG
Swine β-actin Reverse	GAGTTGAAGGTGGTCTCGTGG
Swine IL-1β Forward	ACGGTGACAACAATAATGACCTGT
Swine IL-1β Reverse	CAAGGTCCAGGTTTTGGGTG
Swine IL-4 Forward	AGCATGGCAAACATGACCTG
Swine IL-4 Reverse	CAAAGTGCTCTTCTTGGCTTCA
Swine IL-6 Forward	AGCTATGAACTCCCTCTCCACAAG
Swine IL-6 Reverse	AGGGAGAAGGCGACTGGACT
Swine IL-8 Forward	TGCCTTCTTGGCAGTTTTCCT
Swine IL-8 Reverse	TGGGGTCCACTCTCAATCACT
Swine IL-10 Forward	CTCTGCTGGAGGACTTTAAGGG
Swine IL-10 Reverse	TCTCTGACAAGGCTTGGCAAC
Swine TNF-α Forward	CTCAAACCTCAGATAAGCCCGT
Swine TNF-α Reverse	CGGCTTTGACATTGGCTACAA
Swine IFN-γ Forward	GCCAGGCGCCCTTTTTTA
Swine IFN-γ Reverse	CTCTCCTCTTTCCAATTCTTCAAAAT
Swine NF-κB Forward	AACAGCAGATGGCCCATACC
Swine NF-κB Reverse	TTTCACTAGATGCGCCAGGG

for IL-1β, gi:100525739 for IL-4, gi:399500 for IL-6, gi:396880 for IL-8, gi:397106 for IL-10, gi:397086 for TNF-α, gi:47522725 for IFN-γ, gi:751869 for NF-κB). All reactions were carried out in duplicate and, to correct for variations of extracted mRNA amounts and cDNA synthesis efficiency, and as endogenous control, quantitative Real-Time PCR assays were also performed on each sample with primers for the porcine housekeeping gene β-actin (gi:112980806). The free software BLAST accessible on PubMed website was utilized for gene sequence seeking and alignment. All the primers were designed with Primer Express software (Applied Biosystems, Foster City, CA, USA) crosswise exons in order to prevent genomic DNA contamination. Primers were custom synthesized by Invitrogen (Carlsbad, CA, USA); their sequences are reported in Table I.

Quantitation was achieved by application of an algorithm to the data analyzed by the software of the 7000 Detection System (Applied Biosystems, Foster City, CA, USA). The expression of each gene was normalized utilizing the calculated β-actin cDNA expression (mean) of the same sample and run. Data are expressed in Arbitrary Units.

Statistical analysis

The following analyses were performed with SPSS software (SPSS/PC Statistics 18.0, SPSS Inc., Chicago, IL, USA). All data were analyzed using the ANOVA procedure with time and sex as main effects. The distribution of skin lesions into the three severity classes were reported as relative frequency percentage.

Data were deemed significant at $P<0.05$ and a trend was noted when $P<0.1$.

RESULTS

Growth performance and body lesions

The average body weight of the piglets at 28 days was 24.66±0.3 kg, with an average daily gain (ADG) of 538 g and gain feed equal to 0.75. No significant difference between males and females was observed.

No morbidity nor mortality was registered throughout the entire observation period and the good health status of piglets was confirmed by the negative results obtained in tests for PRRSV.

An effect of time was observed for body lesions, showing at day 28 a percentage reduction of score 0 associated to an increase of scores 1 and 2. Results for body lesions expressed as percentage are presented in Fig. 1.

Cytokines and NF-κB expression

The expression levels of cytokines and NF-κB are summarized in Table II.

A significant time effect was observed for the majority of the analyzed cytokines, indeed, at time 1 an increased expression of IL-4, IL-6, IL-8 and IFN-γ ($P<0.05$) (Fig. 2) was shown compared to time 0; also the expression of TNF-α augmented, although not in a statistically significant manner. On

Table II. *Effect of time and sex on the expression of cytokines and NF-κB (mean ± standard error) in postweaning piglets expressed in Arbitrary Units.*

	Time (T)		Sex (S)		P	
	0	1	M	F	T	S
IL-1β	9.56±0.80	8.61±0.74	10.45±0.55	7.72±0.78	n.s.	0.011
IL-4	3.11±1.62	8.52±2.17	7.24±2.19	4.39±1.88	0.049	n.s.
IL-6	10.33±1.11	13.87±0.51	13.47±0.57	10.81±1.24	0.015	0.050
IL-8	7.44±0.68	9.43±0.67	9.71±0.63	7.16±0.64	0.027	0.006
IL-10	9.45±0.49	9.08±0.61	10.21±0.43	8.33±0.52	n.s.	0.014
TNF-α	9.26±0.98	10.19±0.65	11.09±0.59	8.36±0.86	n.s.	0.019
IFN-γ	6.23±1.62	11.22±1.20	8.71±1.91	8.74±1.23	0.012	n.s.
NF-κB	6.12±0.39	5.71±0.55	6.77±0.41	5.09±0.40	n.s.	0.007

n.s.: not significant

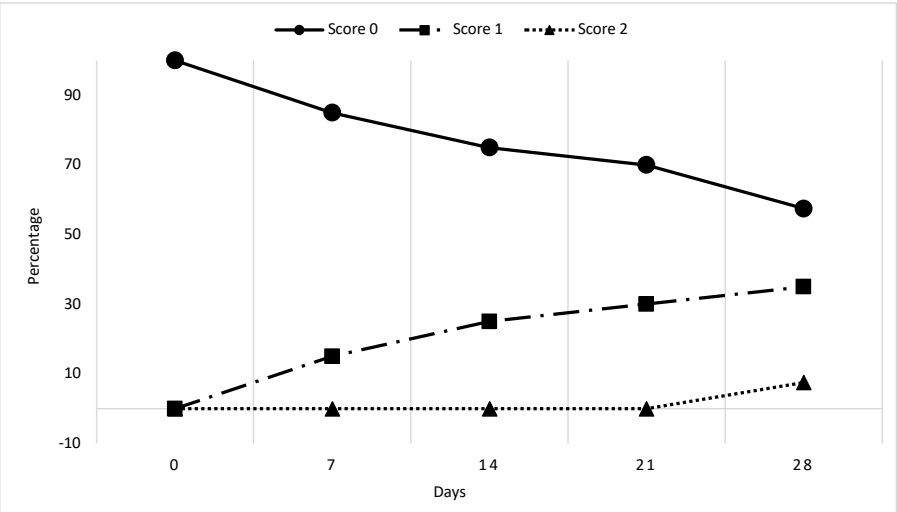

Fig. 1. *Skin lesions expressed as percentage in piglets during the 28-day observation period.*

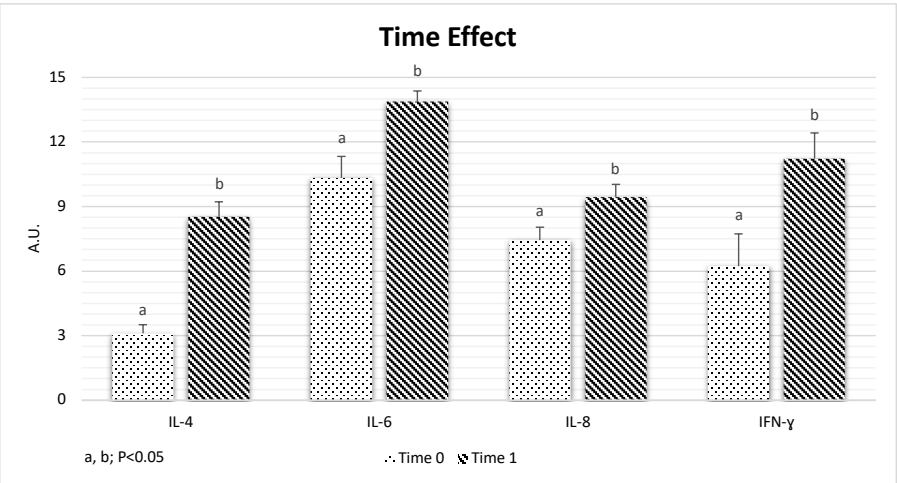

Fig. 2. *Impact of time on the expression of cytokines and NF-κB in piglets (P<0.05).*

the contrary, the expression of IL-1β, IL-10 and NF-κB slightly decreased.

Sex impacted the expression of some genes, showing higher values in male pigs than in females, in particular, it was significant for IL-8 and NF-κB ($P<0.01$) and for IL-1β, IL-6, IL-10 and TNF-α ($P<0.05$) (Fig. 3); also IL-4 expression resulted higher in males than in females, although not in a statistically significant manner. The expression level of IFN-γ resulted similar in males and females.

DISCUSSION

The present study demonstrated that weaning in piglets is associated with inflammation. Indeed, an upregulation of IL-4, IL-6, IL-8 and IFN-γ mRNA levels occurred during the 4 weeks postweaning. During the naturally stressful period corresponding to weaning, piglets are exposed to environmental insults which have a negative effect on their health, welfare and performance. The origin of stress may

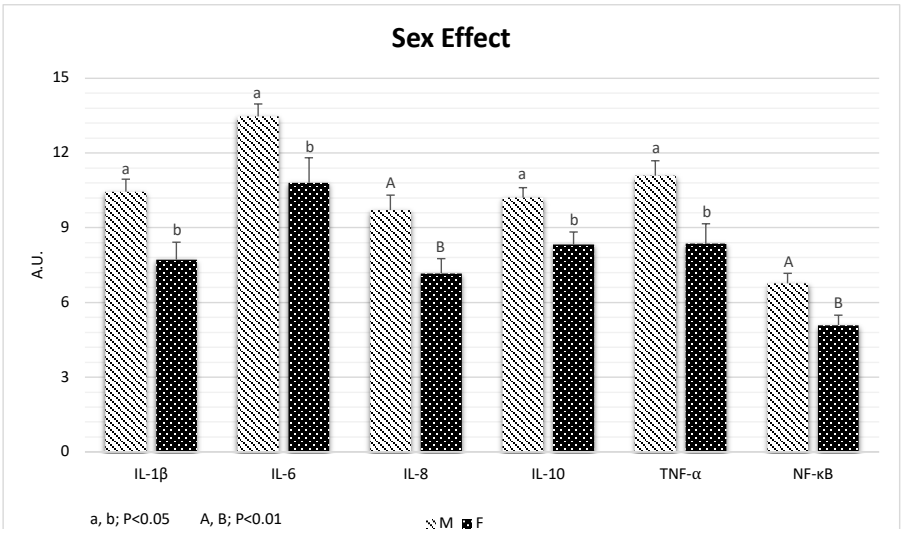

Fig. 3. *Impact of sex on the expression of a selected panel of cytokines and NF-κB in piglets (P<0.05).*

be weaning itself, combination of different litters, movement to another area, housing conditions, and diet changes, which may lead to a reduced feed intake, poor performance and increased susceptibility to diseases (1, 11). Therefore, weaning causes high adaptive pressure at the behavioral and physiological levels (17). In this context, cytokines, which play a pivotal role in the regulation of the immune system, may be markers of an activated response. The balance of pro- and anti-inflammatory cytokines varies according to the individual health status. Stress is recognized to have a significant impact on cytokine expression (18).

As reported in the result section, piglet health status was good during the 4 weeks after weaning, with growth performance in line with data commonly registered in pig farms.

Skin lesions are usually provoked by fighting, which takes place at the time of weaning, when pigs are mixed together. Moreover, stress, fasting, extended lairage time and environmental circumstances may negatively impact pigs' behavior, leading to augmented skin damage (19). The conflicts are also worsened when pigs are comparable in terms of dominance ability, which causes visible skin lesions (20).

In the present study we observed an increased percentage of scores 1 and 2 (Fig. 1) after 21 and 28 days of the experimental trial, corresponding approximately to 20-25 kg body weight range; space allowance was lower than recommended by EU Council Directive 2001/88/EC in this weight class (European Community, 2001 amending directive 91/630/EEC).

Newborn pigs are protected for the first weeks of their life by the immunoglobulins contained in the sow's colostrum and milk. After weaning, young pigs can no longer rely on mother's milk, but their immune system is not yet completely developed. Moreover, it is greatly influenced by the wide range of microbial and dietary/environmental antigens, being also affected by deficiencies and excesses of specific nutrients in the pig's new diet (21-23).

Recent studies have inspected the impact of piglets' weights on the development of the immune system during the first weeks of life. Results suggest that the maturation of the immune system could be compromised in low weight gain (LWG) piglets, with a reduced abundancy of immune cells in the animals. Moreover, the expression of IL-6 resulted significantly lower in LWG piglets, whereas TNF-α production increased. Finally, the expression of signaling pathways involved in the recognition of PAMPs and expression of cytokines, such as NF-κB, was found to be downregulated in LWG piglets (9).

As soluble molecules secreted by immune cells, cytokines are fundamental for the immunological communication. In swine, as in other mammals, leukocytes are the major cells producing cytokines, crucial for the innate and adaptive immune responses (4). Hence, the analysis of cytokine expression indicates the functionality of immune cells in physiological and pathological circumstances (24). Modifications in the cytokine pattern have been found during pig weaning, as a result of major dietary and environmental changes or after microbial infections. However, only a few authors have studied the gene expression of a wide panel of cytokines in piglets immediately after weaning, but in specific tissues (10-11). The present study investigated the expression pattern of pro- and anti-inflammatory cytokines as well as NF-κB in postweaning piglets by measuring messenger RNA by Real-Time RT-PCR assays.

An upregulation of leukocyte gene expression for the majority of the cytokines assayed was found for both Th1 (TNF-α, IFN-γ) and Th2 (IL-4, IL-6), pro-inflammatory (IL-8, TNF-α, IFN-γ), anti-inflammatory cytokines (IL-4) and with both pro- and anti-inflammatory effects (IL-6 and TNF-α). The upregulation may be explained as a consequence of a wide range of specific and nonspecific stimuli, including feed changes, disclosure to a large number of piglets, and aggressions (10). Conversely, in our study, the expression of IL-1β and IL-10 decreased in the postweaning period. In absence of data about the expression of these cytokines in blood leukocytes of postweaning pigs, we found reports of an increased production of both Th1 and Th2 cytokines in rodents, along with conflicting report, some of which describe a decrease in the expression levels of IL-1β and IL-10 in blood or other tissues (25-26). Discrepancies in results are explainable with inflammation being the outcome of the balance between pro- and anti-inflammatory cytokines. The mRNA expression of cytokines changes with the site studied. We tested the expression in concentrated leukocytes.

A slight downregulation was found for the expression of the regulatory factor NF-κB, crucial for the modulation of the cytokine gene transcription. In mammals, the active form of NF-κB is a dimer, composed of p50 (NF-κB1) and p65 (RelA) subunits (13); for this reason, we analyzed the NF-κB1 subunit.

Our study showed the impact of gender on the expression of some genes, showing higher values in males than in females for the majority of genes, namely IL-1β, IL-4, IL-6, IL-8, IL-10, TNF-α and NF-κB. The expression level of IFN-γ resulted similar in males and females. It is well established that sex impacts the expression of inflammatory mediators in different species (27-28). Data reported by Benini and colleagues (27) demonstrated a different immune response between men and women; TNF-α production was reported to be lower in women than in men, probably due to the inhibitory properties of estrogens elicited on inflammatory gene expression (29). We can hypothesize a similar mechanism in piglets, where hormonal differences are detected between males and females from the fetal stage (30).

In conclusion, the results of our research indicated that weaning in piglets is associated with increased expression of inflammatory cytokines, explainable with the numerous changes occurring in diet and environment, including the exposure to potential disease-causing agents. Further studies are needed to delineate the influence of such stressors on inflammatory cytokine expression pattern.

ACKNOWLEDGEMENT

This research was supported by the University of Milan, Linea 2, 2017.

REFERENCES

1. Gu Y, Song Y, Yin H, et al. Dietary supplementation with tributyrin prevented weaned pigs from growth retardation and lethal infection via modulation of inflammatory cytokines production, ileal FGF19 expression, and intestinal acetate fermentation. J Anim Sci 2017; 95:226-38. doi:10.2527/jas2016.0911.
2. Šinkora M, Butler JE. The ontogeny of the porcine immune system. Dev Comp Immunol 2009; 33:273-83. doi:10.1016/j.dci.2008.07.011.
3. Edwards JC, Everett HE, Pedrera M, et al. $CD1^-$ and $CD1^+$ porcine blood dendritic cells are enriched

for the orthologues of the two major mammalian conventional subsets. Sci Rep 2017; 7:40942. doi:10.1038/srep40942.

4. Turin L, Riva F. Toll-like receptor family in domestic animal species. Crit Rev Immunol 2008; 28:513-38.
5. Salmon H, Berri M, Gerdts V, Meurens F. Humoral and cellular factors of maternal immunity in swine. Dev Comp Immunol 2009; 33:384-93. doi:10.1016/j.dci.2008.07.007.
6. Nguyen TV, Yuan L, Azevedo MSP, Jeong K, Gonzalez AM, Saif LJ. Transfer of maternal cytokines to suckling piglets: in vivo and in vitro models with implications for immunomodulation of neonatal immunity. Vet Immunol Immunopathol 2007; 117:236-48. doi:10.1016/j.vetimm.2007.02.013.
7. Inman CF, Haverson K, Konstantinov SR, et al. Rearing environment affects development of the immune system in neonates. Clin Exp Immunol 2010; 160:431-39. doi:10.1111/j.1365-2249.2010.04090.x.
8. Grierson SS, King DP, Tucker AW, et al. Ontogeny of systemic cellular immunity in the neonatal pig: correlation with the development of postweaning multisystemic wasting syndrome. Vet Immunol Immunopathol 2007; 119:254-68. doi:10.1016/j.vetimm.2007.06.004.
9. Lessard M, Blais M, Beaudoin F, et al. Piglet weight gain during the first two weeks of lactation influences the immune system development. Vet Immunol Immunopathol 2018; 206:25-34. doi:10.1016/j.vetimm.2018.11.005.
10. Pié S, Lallès JP, Blazy F, Laffitte J, Sève B, Oswald IP. Weaning is associated with an upregulation of expression of inflammatory cytokines in the intestine of piglets. J Nutr 2004; 134:641-47. doi:10.1093/jn/134.3.641.
11. Li F, Li Y, Tan B, et al. Alteration of inflammatory cytokines, energy metabolic regulators, and muscle fiber type in the skeletal muscle of postweaning piglets. J Anim Sci 2016; 94:1064-72. doi:10.2527/jas.2015-9646.
12. Van Reeth K, Van Gucht S, Pensaert M. In vivo studies on cytokine involvement during acute viral respiratory disease of swine: troublesome but rewarding. Vet Immunol Immunopathol 2002; 87:161-68. doi:10.1016/s0165-2427(02)00047-8.
13. Baldwin ASJ. The NF-κB and IκB proteins: new discoveries and insights. Annu Rev Immunol 1996; 14:649-81. doi:10.1146/annurev.immunol.14.1.649.
14. Boddicker RL, Koltes JE, Fritz-Waters ER, et al. Genome-wide methylation profile following prenatal and postnatal dietary omega-3 fatty acid supplementation in pigs. Anim Genet 2016; 47:658-71. doi:10.1111/age.12468.
15. Riva F, Rahman MM, Ceciliani F, Russo S, Tribbioli G, Lecchi C. TIR8 receptor expression in bovine tissues. Vet Immunol Immunopathol 2010; 136:65-70. doi:10.1016/j.vetimm.2010.02.009.
16. Turin L, Tribbioli G, Invernizzi P, Grati FR, Crema S, Laible G, Riva F. Fetal microchimerism in normal and embryo transfer bovine pregnancies. Vet Res Commun 2007; 31(S1):205-7. doi:10.1007/s11259-007-0095-3.
17. Pastorelli G, Rossi R, Guarino M, Borgonovo F, Candotti P, Corino C. Livestock precision farming and the kit radicaux libres test: two simple approaches to detect variation in piglets' behaviour and welfare. J Agric Sci 2016; 8:44-55. doi:10.5539/jas.v8n3p44.
18. Salak-Johnson JL, McGlone JJ. Making sense of apparently conflicting data: stress and immunity in swine and cattle. J Anim Sci 2007; 85(Suppl):E81-E88.
19. Dokmanovic M, Ivanovic J, Janjic J, Boskovic M, Laudanovic M, Pantic S, Baltic MZ. Effect of lairage time, behaviour and gender on stress and meat quality parameters in pigs. Anim Sci J 2017; 88:500-6. doi:10.1111/asj.12649.
20. Andersen IL, Andenaes H, Bøe KE, Jensen P, Bakken M. The effects of weight asymmetry and resource distribution on aggression in groups of unacquainted pigs. Appl Anim Behav Sci 2000; 68:107-20. doi:10.1016/S0168-1591(00)00092-7.
21. Scrimshaw NS, SanGiovanni JP. Synergism of nutrition, infection, and immunity: an overview. Am J Clin Nutr 1997; 66:464S-77S.
22. Rochell SJ, Alexander LS, Rocha GC, Van Alstine WG, Boyd RD, Pettigrew JE, Dilger RN. Effects of dietary soybean meal concentration on growth and immune response of pigs infected with porcine reproductive and respiratory syndrome virus. J Anim Sci 2015; 93:2987–97. doi:10.2527/jas2014-8462.
23. Stokes CR. The development and role of microbial-host interactions in gut mucosal immune

development. J Anim Sci Biotechnol 2017; 8:12. doi: 10.1186/s40104-016-0138-0.

24. Kirthika P, Ali MA, Behera P, Subidhi PK, Tolenkhomba TC, Gali JM. Dynamics of cytokine gene expression in peripheral blood mononuclear cells in indigenous and exotic breeds of pigs in India. Anim Sci J 2017; 88:1794-800. doi:10.1111/asj.12827.
25. Corsi-Zuelli F, Fachim HA, Loureiro CM, et al. Prolonged periods of social isolation from weaning reduce the anti-inflammatory cytokine IL-10 in blood and brain. Front Neurosci 2019; 12:1011. doi:10.3389/fnins.2018.
26. Vázquez E, Gil A, García-Olivares E, Rueda R. Weaning induces an increase in the number of specific cytokine-secreting intestinal lymphocytes in mice. Cytokine 2000; 12:1267-70.
27. Benini R, Numes PRP, Orsatti CL, Portari GV, Orsatti FL. Influence of sex on cytokines, heat shock protein and oxidative stress markers in response to an acute total body resistance exercise protocol. J Exerc Sci Fit 2015; 13:1-7. doi:10.1016/j.jesf.2014.10.002.
28. Queen AE, Moerdyk-Schauwecker M, McKee LM, Leamy LJ, Huet YM. Differential expression of inflammatory cytokines and stress genes in male and female mice in response to a lipopolysaccharide challenge. Plos One 2016; 11:1-13. doi:10.1371/journal.pone.0152289.
29. Ershler WB, Keller ET. Age-associated increased interleukin-6 gene expression, late-life diseases, and frailty. Annu Rev Med 2000; 51:245-70. doi:10.1146/annurev.med.51.1.245.
30. Goxe B, Prunier A, Remy JJ, Salesse R. Ontogeny of gonadal luteinizing hormone and follicle-stimulating hormone receptors in the fetal pig and related changes in gonadotropin and testosterone secretion. Biol Reprod 1993; 49:609-16. doi:10.1095/biolreprod49.3.609.

INTERLEUKIN-2-MEDIATED STAT-5 EXPRESSION LEVELS IN $CD8^+CD25^+$ REGULATORY T CELLS: THE RELEVANCE FOR ASTHMA

M. EUSEBIO[1], L. KRASZULA[1], M. KUPCZYK[2], P. KUNA[2] and M. PIETRUCZUK[1]

[1]Department of Laboratory Diagnostics, Medical University of Lodz, Poland; [2]Department of Internal Medicine, Medical University of Lodz, Poland

Received July 18, 2019 – Accepted October 17, 2019

Preliminary studies demonstrated the potential role of $CD8^+CD25^+$ T regulatory cells (Tregs) in asthma. However, published data with regard to the relevance of signaling pathways that govern Tregs homeostasis are limited and conflicting. The first aim of this study was to characterize the phosphorylation of STAT-5 in $CD8^+CD25^+$ Tregs. The second aim was to investigate the ability of $CD8^+CD25^+$ Tregs from patients and controls to respond to interleukin (IL)-2 treatment *in vitro*. Twenty-five healthy subjects (NC) and 50 patients with either severe (SA) or mild-moderate (MA) asthma were enrolled in the study. STAT-5 phosphorylation was detected in purified $CD8^+CD25^+$ Tregs from healthy and asthma subjects, indicating that STAT-5 has a role in their pathobiology. At baseline, asthma cases had either significantly lower [(SA=4.5±5% *vs* NC=26±25%, $P < 0.001$) and (MA=10±7.5% *vs* NC=26±25%, $P < 0.001$)] or higher [(SA=54±58.5% *vs* 26±25%, $P < 0.01$) and (MA=71±74.5% vs 26±25%, $P < 0.01$) proportion of Tregs expressing pSTAT-5 than controls. In contrast to healthy subjects, $CD8^+CD25^+$ Tregs from asthma subjects had either increased ($pSTAT\text{-}5^{high}$) or decreased ($pSTAT\text{-}5^{low}$) phosphorylated STAT-5 levels within individual cells. These data suggest that the alteration in STAT5 phosphorylation level might be associated with asthma and is a potential molecular basis of skewed $CD8^+CD25^+$ Treg differentiation. IL-2 treatment of cells from severe asthma subjects increased the proportion of cells expressing high level of pSTAT-5 while it decreased the proportion of those expressing low level of pSTAT-5. Strikingly, IL-2 increased the proportions of both subsets from mild-moderate asthma subjects. These findings demonstrate that altered IL-2-mediated STAT-5 phosphorylation within individual circulatory $CD8^+CD25^+$ Tregs may be associated with asthma and disease severity.

Asthma is a multifactorial syndrome characterized by the activation and migration of various immune cells to the inflamed bronchial mucosa. Despite increasing awareness of asthma, its pathogenesis has not been fully established. It is known that peripheral blood $CD8^+CD25^+$ T regulatory cells (Tregs) may play a pathogenic role in asthma. Asthma death was associated with increased percentage of peripheral $CD8^+CD25^+$ T cells in the airways (1). The precise mechanisms underlying the peripheral homeostasis of this subset is unclear, nevertheless, some evidence suggests that homeostasis and function of Tregs are maintained by signaling pathways that are activated through several cytokines and related receptors. Increasing evidence suggests that a family of tyrosine kinases known as Janus kinases (JAKs) collaborates with related transcription factors, known as STATs (signal transducers and activators of transcription)

Key words: T-regulatory cells; asthma, $CD8^+CD25^+$ Tregs; STAT-5; interleukin (IL)-2

Corresponding Author:
Makandjou-Ola Eusebio, MD, PhD
Department of Laboratory Diagnostics,
II Chair of Internal Medicine,
Medical University of Lodz,
Kopcinski 22 str., 90-153 Lodz, Poland
Tel.: +48 42 677 69 83 - Fax: +48 42 678 28 33
e-mail: eusemak@yahoo.com

0393-974X (2019)

DISCLOSURE: ALL AUTHORS REPORT NO CONFLICTS OF INTEREST RELEVANT TO THIS ARTICLE.

to maintain the appropriate number of Treg cells. Likewise, other published data have reported that Interleukin (IL)-2 signaling cascade helps to maintain the appropriate quality and quantity of human Tregs (2) at the periphery. Furthermore, it has been previously reported that this cytokine signaling molecule induces the activation and phosphorylation of a great array of protein tyrosine kinases, namely JAK-1 and JAK-3. This preliminary event results in the activation of the receptor-associated JAK subunit, and serves as a precursor for the phosphorylation of the latent cytosolic STAT subunits. Phosphorylated STATs are thereafter translocated to the nucleus where they bind specific DNA sequences to regulate the transcription of target genes, which control cellular survival. The STAT pathway regulates the molecular events underlying a variety of biological processes including T-cell activation and differentiation (3), therefore, it is probable that STAT protein family inhibits or enhances autoimmune and allergic responses (4). Recent studies have demonstrated that the pathogenic implication of cytokines in immunological disorders relies on the JAK-STAT signaling pathway (5). Dysregulation of this signaling pathway partially caused by alteration of either γc or Jak3 subunits was linked to immunodeficiency (6). Signal transducers and activators of transcription 5 (STAT-5) have been reported to play a critical role in the proliferation of various cells including eosinophils (7) and mast cells (8). Furthermore, a cytokine signaling through STAT-5 has been shown to regulate the peripheral homeostasis of $CD4^+CD25^+$ Treg cells in mice (9). Some previous studies have shown that IL-2 enhances the survival of $CD4^+CD25^+$ Tregs (10). Others highlight some similarities between human $CD8^+CD25^+$ thymocytes and $CD4^+CD25^+$ Tregs (11). The significance of IL-2-mediated STAT phosphorylation for T cell survival and proliferation has prompted the investigation of this pathway in asthma. Studies in this context are extremely scarce or conflicting.

The first aim of the study was to characterize the phosphorylation of STAT-5 in $CD8^+CD25^+$ Tregs The second aim was to investigate the ability of $CD8^+CD25^+$ Tregs from patients and controls to respond to IL-2 treatment *in vitro*.

MATERIALS AND METHODS

Study subjects

Fifty patients with allergic asthma (AA) as defined by the Global Initiative for Asthma (GINA) guidelines and 25 gender- and age-matched controls (NC) were enrolled in this study. The diagnosis of asthma was confirmed by pulmonologists based on evidence of variable airway obstructions according to The Global Initiative for Asthma (GINA 2008) guidelines. Patients were divided into the severe asthma (SA) (n = 25) and mild-moderate asthma (MA) (n = 25) groups (Table I). They were treated based on European Network for Understanding Mechanisms of Severe Asthma (ENFUMOSA) guidelines. Atopy was evaluated based on skin prick tests or evidence of increase specific serum IgE. Patients with severe asthma required treatment with either high dose of inhaled steroids, long acting ß-agonists for at least 1 year. Patients with mild-moderate asthma received daily inhaled steroids in combination with symptomatic therapy. Subjects without evidence of allergic or infectious diseases served as controls.

All participants underwent a standard check-up including a questionnaire related to their general health status. In addition, all subjects with clinical symptoms of asthma filled in an Asthma Control Questionnaire. Furthermore, all participants provided written informed consent before enrolment in the study. The study was approved by the ethics committee, in accordance with the Declaration of Helsinki and good clinical practice guidelines (RNN/17/09/KE).

Assessment of asthma and its severity

Pulmonary function tests were performed using a calibrated spirometer as recommended by the American Thoracic Society/European Respiratory Society guidelines. The best of three reproducible loops was recorded for the study. The forced expiratory volume in first second (FEV_1), forced vital capacity (FVC) and the ratio of FEV_1/FVC were recorded for the differential diagnosis of asthma. Patients also underwent skin-prick tests to common allergens, and methacholine tests, and specific serum immunoglobulin E (IgE) was measured. Atopy was defined as at least one positive skin-prick test against the most common allergens and its degree was assessed based on total serum IgE levels as previously described. Allergen polysensitization was determined based on sensitization to more than 2 allergen-specific

IgEs, regardless of the allergen class. Patients with initially impaired lung function values were excluded from the challenge test. Bronchodilator and steroid drugs were discontinued 24 h before the challenge test.

Isolation of peripheral blood mononuclear cells

Peripheral blood samples were collected in EDTA vacutainer tubes, between 7–9 a.m. after 12 h of fasting and processed immediately. Briefly, peripheral blood mononuclear cells (PBMCs) were freshly isolated from peripheral buffy coats by standard Ficoll-Hypaque high-density gradient centrifugation (2500 g, 30 min).

Cell purification

After enrichment of PBMCs, $CD8^+$ T cells were isolated using biotinylated human CD8 T lymphocyte enrichment cocktail and BD™ IMag magnetic field according to the manufacturer's instructions. Cells were incubated with saturating amounts of antibodies at a ratio of 5 µl per 1 x 10^6 cells, for 15 min at 4°C. Thereafter, streptavidin particles were added at a concentration of 5 µl of particles for every 1 x 10^6 total cells and incubated for 30 min at 4°C. To maintain high purity using the Miltenyi MACS system, cells were passed through two LS columns placed on BD™ IMag magnetic field. The purity of the enriched $CD8^+$ T cells was over 90% and 93% for all samples. $CD8^+$ T cell fraction was subsequently incubated for 15 min with CD25-coated magnetic beads conjugated to anti-CD25 mAb (Miltenyi Biotec, mouse IgG1), followed by incubation with anti-human $CD25^{PE}$ mAb (Miltenyi Biotec, clone 4E3, Mouse IgG2b, k). Cells were passed through two LD columns placed on BD™ IMag magnetic field. The purity of $CD8^+CD25^+$ T cell was > 97% as assessed by flow cytometry.

In vitro *cell activation*

Next, the ability was evaluated of $CD8^+CD25^+$ Tregs from healthy and asthma subjects to respond directly to IL-2 stimulation *in vitro* in the absence of any other co-stimuli such as T Cell Receptor (TCR) activation. Specifically, the activation of the downstream signaling molecule, STAT-5, and the expression of the pSTAT-5 on the surface of $CD8^+CD25^+$ Treg cells before and after short term *in-vitro* stimulation were quantified. Firstly, the patients and healthy subjects were analyzed for the expression pattern of phosphorylated STAT-5 (pSTAT-5). For quantitative analysis, freshly isolated $CD8^+CD25^+$ T cells (1x10^6 cells/100µl) were cultured in complete RPMI medium containing 10% fetal bovine serum, 20 mM Hepes buffer, non-essential amino acids, sodium pyruvate, 2 mM L-glutamine, 100 µg/ml streptomycin and 100 units/ml penicillin (Sigma-Aldrich) supplemented with 10ng/ml recombinant human IL-2 (R & D SYSTEMS) for 15 min. The cells were incubated for 72 h in 24-well flat bottom sterile plates (Thermo Fisher Scientific Inc) at 37°C in a 5% CO_2-humidified atmosphere.

Table I. *Clinical and demographic characteristics of the study population.*

Parameters	SA	NC	MA
Number	25	25	25
Sex (Female/Male)	13/12	12/13	12/13
Age (yr±SD)	48±14	48.5±14.5	42±13
Disease duration (yr±SD)	16±8.7	NC	10±6.3
Atopy	Yes	No	Yes
Predicted FEV1(%±SD)	67±15.98	96.6±4	87.71±16.2

SA: Severe asthma; MA: Mild-to-moderate asthma; NC: Healthy controls; FEV1: forced expired volume in 1 s; NA: Not applicable

Flow cytometry analysis

Activated or non-activated $CD8^+CD25^+$ T cells were fixed with Buffer Cytofix (BD Bioscience). To increase the cell membrane permeability to anti-STAT5, 500 µl BD Perm Buffer III Phosflow (BD Bioscience) was added to the suspension which was vortexed and incubated for 30 min on ice. ($1x10^6$/100µl) cells were incubated for 30 min at 4°C with anti-human $CD8^{AmCyan}$ mAb (BD Biosciences, clone SK1, Mouse IgG1, k), and anti- human $CD25^{FITC}$ mAb (BD Biosciences, clone M-A251, Mouse IgG1, k). For intracellular staining, cells were incubated with anti-human anti-STAT5-conjugated PE (BD Biosciences, clone 236A/E7, Mouse IgG1, k) for 45 min at 4°C. Labeling of phosphorylated STAT-5 was carried out in accordance with the BD™ Phosflow Protocol. Cells were washed twice and analyzed using a BD Biosciences FACS Canto II flow cytometer and FACS DIVA software.

Statistical analyses

The Mann-Whitney U test and Kruskal-Wallis analysis were used to assess statistical differences between the study and control groups. A Spearman correlation test was performed to analyze the association between the forced expiratory volume in one second FEV_1 (% predicted) and the percentage of $pSTAT\text{-}5^+$ T cells. Data were expressed as median and interquartile range (IQR) which is the difference between the third and first quartiles. A p-value less than 0.05 was considered significant. Calculations were performed by the statistical software package Statistica (Stat Soft, Polska).

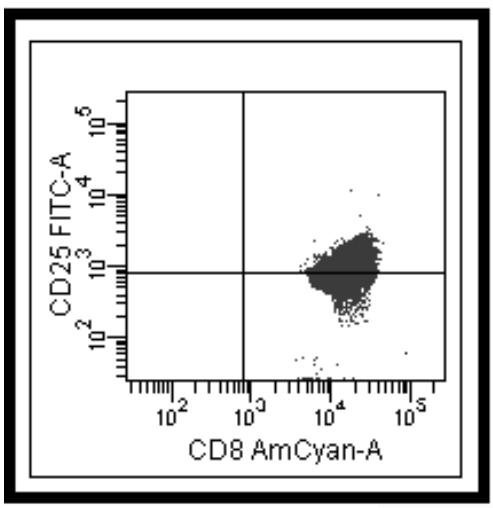

Fig. 1. *Representative flow cytometric analysis of $CD8^+CD25^+$ Tregs from fresh peripheral blood of asthma and healthy subjects. $CD8^+CD25^+$ T cells were gated from $CD8^+$ lymphocytes. An isotype control FMOs (fluorescence minus one)was used to set the positive gates. The same gates were used for data analysis of each asthma subject and healthy control. Variable pSTAT5 expression levels were detected in $CD8^+CD25^+$ Tregs from all subjects.*

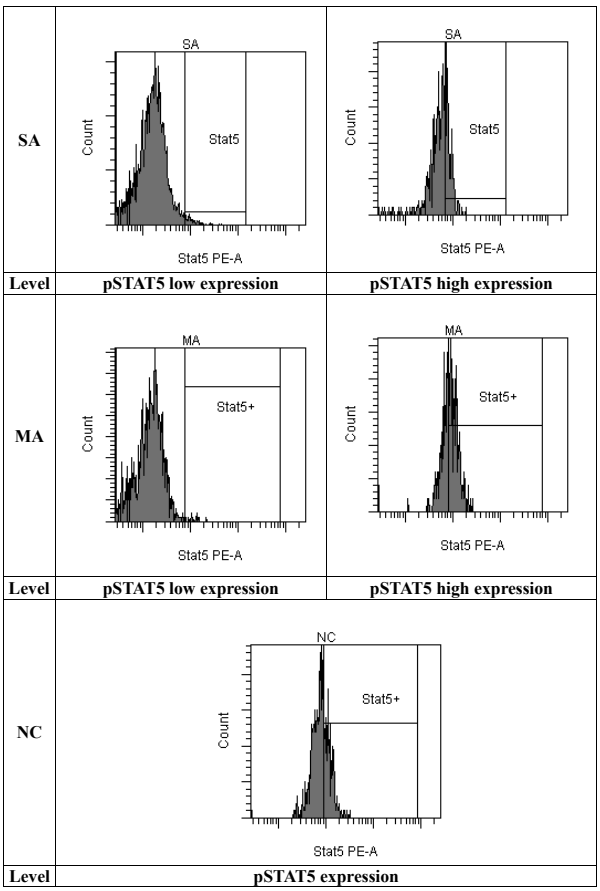

Fig. 2. *Representative histograms illustrating pSTAT-5 expression. Cells were isolated from the peripheral blood and cultured in RPMI with IL-2 for 72 hours. Cells were fixed, permeabilized, and flow cytometry performed using antibodies against CD8, CD25, and phosphorylated STAT-5 (pSTAT-5).*

RESULTS

The clinical and demographic data of the study population are presented in Table I.

Circulatory $CD8^+CD25^+$ Tregs express pSTAT-5

The existence of data suggesting the implication of STAT5 in $CD25^+CD4^+$ Treg homeostasis prompted

our attempt to characterize the phosphorylation of STAT-5 in peripheral blood $CD8^+CD25^+$ Tregs in an *ex-vivo* model and flow cytometry (Fig. 1). Variable pSTAT5 expression levels were detected in $CD8^+CD25^+$ Tregs from all subjects (Fig. 2). Asthmas had either significantly lower [(SA=4.5±5% *vs* 26±25%, $P < 0.001$) and (MA=10±7.5% *vs* 26±25%, $P < 0.001$)] (Fig. 3) or higher [(SA=54±58.5% *vs* 26±25%, $P < 0.01$) and (MA=71±74.5% *vs* 26±25%, $P < 0.01$) (Fig.3) proportion of Tregs expressing pSTAT-5 than healthy controls.

Stratification of each asthma phenotype into high and low STAT-5 profiles

Baseline analysis allowed stratification of each asthma group, based on the extent of STAT-5 expression in $CD25^+CD8^+$ Tregs. $CD8^+CD25^+$ Tregs from asthma subjects had either increased ($pSTAT\text{-}5^{high}$) (Fig. 4) or decreased (Fig. 3) ($pSTAT\text{-}5^{low}$) phosphorylated STAT-5 levels within individual cells. Patients with high-STAT-5 profile had higher levels of pSTAT-5 [(SA=54±58.5) and (MA=71±74.5)] compared with the control group (NC= 26±25) (Fig. 4) whereas those with low-pSTAT-5 profile had lower pSTAT-5 expression level [(SA=4.5±5) and (MA=10±7.5)] (Fig. 3) than the control group (NC= 26±25).

Strikingly, the proportion of cells expressing low level of pSTAT-5 was lower in the severe asthma group than in the mild-to-moderate group (SA=4.5±5% *vs* MA=10±7.5%, $P< 0.001$) (Fig. 3). Likewise, the proportion of cells expressing high level of pSTAT-5 expression was lower in the severe asthma group than in those from mild-to-moderate group (SA=54±58.5% *vs* MA=71±74.5%, $P< 0.001$) (Fig. 4).

IL-2 had pleiotropic effects on $CD8^+CD25^+$ Tregs expressing low or high pSTAT-5

IL-2 treatment of cells from severe asthma subjects increased the proportion of cells expressing high level of pSTAT-5 while it decreased the proportion of those expressing low level of pSTAT-5. Strikingly, IL-2 increased the proportions of both subsets from mild-to-moderate asthma subjects. After stimulation, statistically significant differences were noted among the asthma groups ($p<0.001$). Likewise, we observed statistically significant differences between the control and mild-to-moderate or severe asthma groups. In each case, p was lower than 0.001 (Figs. 3 and 4). IL-2

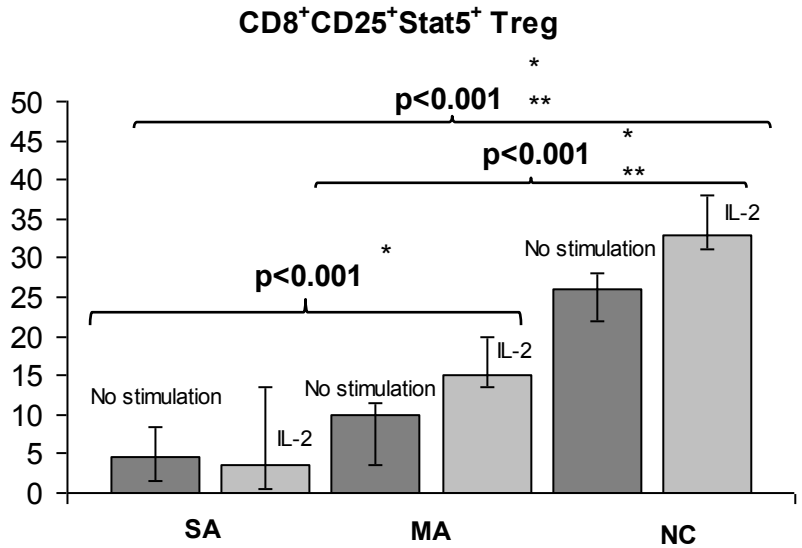

Fig. 3. *$CD8^+CD25^+$ T cells from asthma patients have decreased pSTAT-5 levels ($pSTAT\text{-}5^{high}$) as compared to healthy subjects. Cells were isolated from the peripheral blood of asthma subjects and controls. They were cultured in RPMI media supplied with IL-2 for 72 hours and analyzed as described in methods. Data are expressed as median percentages±interquartiles and are representative of three independent experiments. Significance was determined by * significant difference after stimulation and ** significant difference without stimulation; NS: no significance.*

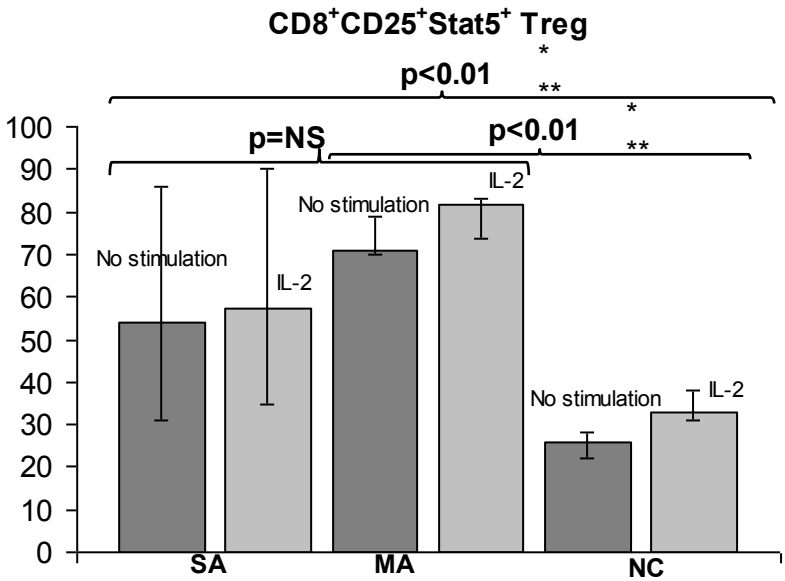

Fig. 4. *$CD8^+CD25^+$ T cells from asthma patients have increased pSTAT-5 levels ($pSTAT\text{-}5^{high}$) as compared to healthy subjects. Cells were isolated from the peripheral blood of asthma subjects and controls and were cultured in RPMI media supplied with IL-2 for 72 hours and analyzed as described in methods. Data are expressed as median percentages±interquartiles and are representative of three independent experiments. Significance was determined by * significant difference after stimulation and ** significant difference without stimulation; NS: no significance.*

stimulation increased the proportion of $CD25^+CD8^+$ Tregs expressing low or high pSTAT-5 in the control group (NC= 26±25) *vs* (NC= 33±34.5) (Figs. 3 and 4).

IL-2 increased the proportion of Tregs with high pSTAT-5 expression in the asthma groups

IL-2 increased the frequencies of $CD25^+CD8^+$ Tregs expressing high STAT-5 level in the asthma subgroups [(SA=54±58.5) *vs* (SA=57.5±62.3) and [(MA=71±74.5) *vs* (MA=81.5±78) subgroups (Fig. 3). At baselines and after stimulation, statistically significant differences were observed between controls and mild-to-moderate or severe asthma groups, In each case, *p* was lower than 0.01 (Fig. 4). IL-2 stimulation increased $STAT\text{-}5^+CD25^+CD8^+$ Treg frequencies in the control group (NC= 26±25) *vs* (NC= 33±34.5) (Figs. 3 and 4).

IL-2 decreased the proportion of Tregs with low pSTAT-5 expression in the severe asthma subgroup

IL-2 decreased the frequencies of $CD25^+CD8^+$ Tregs expressing low STAT-5 level in the severe asthma subgroup [(SA=4.5±5) *vs* (SA=3.5±7). In contrast, IL-2 stimulation increased this parameter in mild-to-moderate asthma [(MA=10±7.5) *vs* (MA=15±16.5)] subgroup. At baseline state, there were statistically significant differences in the proportion of $CD25^+CD8^+$ Tregs expressing low STAT-5 level between controls and mild-to-moderate ($p<0.001$) or severe ($p<0.001$) asthma groups.

DISCUSSION

STAT-5 phosphorylation was detected in cells purified from peripheral blood of healthy and asthma subjects. These findings indicate that the development and expansion of human $CD8^+$ $CD25^+$ Tregs is mediated by activation of STAT-5, as previously reported (12). However, they contradict previous studies suggesting that STAT-5 activation is not required for cell development (13). Aberrant STAT-5 phosphorylation has been described in chronic inflammation (14). Our study extends this preliminary data by showing that pSTAT-5 expression significantly differed between the group of healthy subjects, and those with mild-to-moderate or severe asthma. This observation corroborates with a

previous study which described the implication of the STAT-5 signaling in IgE-mediated inflammation (15) and lung diseases (16). We also argued that immune phenotyping by flow cytometry may provide a better insight of intracellular signaling pathways involved in immunological disorders. The baseline analysis of patients and controls revealed two specific patterns of pSTAT-5 expression within individual $CD8^+CD25^+$ Tregs. Some cells expressed high pSTAT-5 levels (pSTAT-5 high) while others expressed low pSTAT-5 levels (pSTAT-5 low). This observation corroborates with previous studies that demonstrated distinct STAT5 thresholds among innate lymphoid subsets (17). Collectively, our results indicate that despite being expressed by all $CD8^+CD25^+$ Tregs, different STAT5 signaling thresholds regulate these cells. Our study supports previous hypothesis of cell-specific requirements of STAT signaling in T cells (18). Our results also corroborate with previous findings suggesting that STAT-5 regulates human $CD8^+$ T-cell function in a dose-dependent manner (19). The differential intracellular pSTAT-5 expression patterns could reflect the difference in the STAT-5 intra-cellular signaling patterns in asthma. Therefore, our observations lend support to other studies suggesting the implication of different molecular pathomechanisms in asthma (20). Furthermore, our results are in agreement with a previous study suggesting that differential STAT-5 phosphorylation by various subsets can help discriminate between healthy and disease states (21). Another main finding from this study was that IL-2 plays a role in STAT-5 activation, as previously suggested (22). Specifically, flow cytometry analysis of the IL-2-mediated STAT-5 signaling demonstrated that circulatory $CD8^+CD25^+$ Treg cells from asthma subjects could phosphorylate STAT-5 at a higher or lower level than those from controls. The pleitropic effects of IL-2 on STAT-5 phosphorylation in $CD8^+CD25^+$ Tregs lend support to previous studies which highlighted the redundant role of IL-2 on STAT-5-mediated proliferation of lymphocytes (23). More importantly, our study showed that IL-2 increased the proportion of some proliferating $CD8^+CD25^+$ Tregs which express high levels of the transcription factor STAT-5. This finding is consistent with previous reports indicating that $CD8^+$ T-cell proliferation is partially driven by IL-2. Our observation corroborates the results of previous studies suggesting that IL-2 induces STAT5 phosphorylation (24). Our observations are also in agreement with previous studies suggesting that altered cytokine signaling in T cells might play a role in asthma (25). Despite remarkable progress in understanding and managing asthma, the continuous increase in the number of asthma patients with steroid-resistance or insensitivity remains a challenge. Our study may provide better insights into the regulatory mechanisms driving this phenomenon. IL-2 treatment of cells from severe asthma subjects increased the proportion of cells expressing high levels of pSTAT-5 while it decreased the proportion of those expressing low level of pSTAT-5. Moreover, IL-2 increased the proportions of both subsets from mild-to-moderate asthma subjects. This observation is in agreement with previous studies suggesting that IL-2 mediated STAT5 phosphorylation has a role in asthma and may be relevant to steroid insensitivity (26).

Taking all together, we showed that alteration in IL-2 mediated-STAT-5 phosphorylation level may be associated with asthma and is a potential molecular basis of skewed $CD8^+CD25^+$ Treg differentiation. Further studies investigating the clinical relevance of these STAT-5 phosphorylation levels may provide new approaches to identifying asthma phenotypes and endotypes.

ACKNOWLEDGEMENT

This work was supported by the Polish Academy of Sciences grant KBN nr N N402 517339.

REFERENCES

1. O'Sullivan S, Cormican L, Faul JL, Ichinohe S, Johnston SL, Burke CM, Poulter LW. Activated, cytotoxic CD8 (+) T lymphocytes contribute to the pathology of asthma death. Am J Respir Crit Care Med 2001; 164 (4):560-64.
2. Attridge K, Walker LS. Homeostasis and function of regulatory T cells (Tregs) in vivo: lessons from TCR-transgenic Tregs. Immunol Rev 2014; 259(1):23-39.
3. Stabile H, Scarno G, Fionda C, Gismondi A, Santoni A, Gadina M, Sciumè G. JAK/STAT signaling in regulation of innate lymphoid cells: The gods before the guardians. Immunol Rev 2018; 286 (1):148-59.
4. Pfitzner E, Kliem S, Baus D, Litterst CM. The role of STATs in inflammation and inflammatory diseases.

Curr Pharm Des 2004; 10 (23):2839-50.
5. Banerjee S, Biehl A, Gadina M, Hasni S, Schwartz DM. .JAK-stat signaling as a target for inflammatory and autoimmune diseases: current and future prospects. Drugs 2017; 77 (11):1261.
6. Ghoreschi K, Laurence A, O'Shea JJ. Janus kinases in immune cell signaling. Immunol Rev 2009; 228(1):273-87.
7. Buitenhuis M, Baltus B, Lammers JW, Coffer PJ, Koenderman L. Signal transducer and activator of transcription 5a (STAT5a) is required for eosinophil differentiation of human cord blood-derived CD34+ cells. Blood 2003; 101(1):134-42.
8. Shelburne CP, McCoy ME, Piekorz R, et al. Stat5: an essential regulator of mast cell biology. Mol Immunol 2002; 38(16-18):1187-91.
9. Antov A, Yang L, Vig M, Baltimore D, Van Parijs L. Essential role for STAT5 signaling in CD25+CD4+ regulatory T cell homeostasis and the maintenance of self-tolerance. J Immunol 2003; 171(7):3435-41.
10. Hall BM. CD4+CD25+ T regulatory cells in transplantation tolerance: 25 years on. Transplantation 2016; 100 (12):2533-47.
11. Cosmi L, Liotta F, Lazzeri E, et al. $CD8^+CD25^+$ thymocytes share phenotypic and functional features with $CD4^+CD25^+$ regulatory thymocytes. Blood 2003; 102(12):4107-14.
12. Passerini L, Allan SE, Battaglia M, et al. STAT5-signaling cytokines regulate the expression of FOXP3 in CD41CD251 regulatory T cells and CD41CD252 effector T cells. Int Immunol 2008; 20(3):421-31.
13. Zamorano J, Wang HY, Wang R, Shi Y, Longmore GD, Keegan AD. Regulation of cell growth by IL-2: role of STAT5 in protection from apoptosis but not in cell cycle progression. J Immunol 1998; 160 (7):3502-12.
14. Franceschini D, Paroli M, Francavilla V, et al. PD-L1 negatively regulates CD4+CD25+Foxp3+ Tregs by limiting STAT-5 phosphorylation in patients chronically infected with HCV. J Clin Invest 2009; 119(3):551-64.
15. Pullen NA, Barnstein BO, Falanga YT, et al. Novel mechanism for Fc {epsilon} RI-mediated signal transducer and activator of transcription 5 (STAT5) tyrosine phosphorylation and the selective influence of STAT5B over mast cell cytokine production. J Biol Chem 2012; 287(3):2045-54.
16. Kanai T, Jenks J, Nadeau KC. The STAT5b pathway defect and autoimmunity. Front Immunol 2012; 3:234.
17. Villarino AV, Sciumè G, Davis FP, et al. Subset- and tissue-defined STAT5 thresholds control homeostasis and function of innate lymphoid cells. J Exp Med 2017; 214(10):2999-3014.
18. Dabitao D, Hedrich CM, Wang F, Vacharathit V, Bream JH. Cell-Specific Requirements for STAT Proteins and Type I IFN Receptor Signaling Discretely Regulate IL-24 and IL-10 Expression in NK Cells and Macrophages. Immunol 2018; 200 (6):2154-64.
19. Nivarthi H, Prchal-Murphy M, Swoboda A, et al. Stat5 gene dosage in T cells modulates CD8+ T-cell homeostasis and attenuates contact hypersensitivity response in mice. Allergy 2015; 70(1):67-79.
20. Lötvall J, Akdis CA, Bacharier LB, et al. Asthma endotypes: a new approach to classification of disease entities within the asthma syndrome. J Allergy Clin Immunol 2011; 127(2):355-60.
21. Teofili L, Martini M, Cenci T, et al. Different STAT-3 and STAT-5 phosphorylation discriminates among Ph-negative chronic myeloproliferative diseases and is independent of the V617F JAK-2 mutation. Blood 2007; 110(1):354-59.
22. Beadling C, Ng J, Babbage JW, Cantrell DA. Interleukin-2 activation of STAT5 requires the convergent action of tyrosine kinases and a serine/threonine kinase pathway distinct from the Raf1/ERK2 MAP kinase pathway. EMBO J 1996; 15(8):1902-13.
23. Lockyer HM, Tran E, Nelson BH. STAT5 is essential for Akt/p70S6 kinase activity during IL-2-induced lymphocyte proliferation.J Immunol 2007; 179(8):5301-8.
24. Huss DJ, Mehta DS, Sharma A, et al. *In vivo* maintenance of human regulatory T cells during CD25 blockade. J Immunol 2015; 194(1):84-92.
25. Gernez Y, Tirouvanziam R, Nguyen KD, Herzenberg LA, Krensky AM, Nadeau KC. Altered phosphorylated signal transducer and activator of transcription profile of CD4+CD161+ T cells in asthma: modulation by allergic status and oral corticosteroids. J Allergy Clin Immunol 2007; 120(6):1441-48.
26. Goleva E, Kisich KO, Leung DY. A Role for STAT5 in the pathogenesis of IL-2-induced glucocorticoid resistance. J Immunol 2002; 169(10):5934-40.

LETTER TO THE EDITOR

CORRELATIONS OF PLACENTAL ABRUPTION WITH OTHER COMPLICATIONS OF PREGNANT WOMEN AND INFLAMMATORY FACTORS IN AMNIOTIC FLUID

H. ZHANG[1] and M. LI[2]

[1]Department of Reproductive, Guangxi Medical University, Nanning, Guangxi, China;
[2]Department of Reproductive Center, The First Affiliated Hospital of Guangxi Medical University, Nanning, Guangxi, China

Received June 20, 2019 – Accepted August 30, 2019

To the Editor,

Placental abruption (PA), a pregnancy complication, has a high incidence rate, unknown cause and rapid development, seriously endangering the safety of mothers and infants (1). Multiple factors, such as vasculopathy and changes of the blood coagulation system, in pregnant women can cause PA (2). Studies have found that matrix metalloproteinases (MMPs) play an important role in placental development, while the inflammatory cytokines, including tumor necrosis factor-α (TNF-α) and interleukins (ILs), can regulate the activity of MMPs (3). This study explored the correlations of PA with gestational hypertension (GH) and other complicated diseases and analyzed the risk factors for PA as well as the relationship between PA and the inflammatory factors in amniotic fluid, which is of great significance for diagnosing and treating the disease at early stage as well as improving the prognosis of pregnant and lying-in women and perinatal infants.

MATERIALS AND METHODS

Patients

A total of 80 pregnant women aged 22-35 (median 25 years) diagnosed with PA in the Obstetrics and Gynaecology Department of our hospital between March 2017 and March 2018 were selected as the study group, and they were divided into three subgroups: grade I, II and III based on disease conditions. Furthermore, 80 pregnant women aged 21-34 years (median 23 years) without PA in the same period were enrolled as the control group. The diagnosis and grading of PA were based on international guidelines. General information and age in the two groups were comparable. Before the study, all the women signed an informed consent. This study was approved by the ethics committee of The First Affiliated Hospital of Guangxi Medical University.

Detection indicators

Under sterile conditions, 5 mL of amniotic fluid was taken from each patient and centrifuged. The supernatant obtained was conserved at -20°C until testing. A Multiskan FC fully-automatic microplate reader (Thermo Fisher Scientific, USA) was used to determine the levels of TNF-α, IL-6, IL-8 and MMP-9. Pearson correlation analysis of the relationship between the severity of PA and the inflammatory factors was carried out, and the risk factors for PA were analyzed. The Apgar score was assessed in both groups, and the cases of low-birth-weight neonates, neonatal asphyxia and dead fetuses were counted, respectively.

Key words: placental abruption, complications, inflammatory factors, correlations

Corresponding Author:
Dr Mujun Li,
Department of Reproductive Center,
The First Affiliated Hospital
of Guangxi Medical University,
No 6 ShuangYong Road, Nanning, 530021, Guangxi, China
e-mail: limujun0771@126.com

0393-974X (2019)

Statistical analysis

IBM Statistical Product and Service Solutions (SPSS) 20.0 software was used for statistical analysis. The measurement data were expressed as mean ± standard deviation, and *chi*-squared test was employed to compare the countable data. Pearson correlation analyses were performed between two variables. $p \leq 0.05$ suggested that differences were statistically significant. Logistic regression analysis was performed using the Binnsary Logistic process of SPSS. The variables for the diagnosis of PA were screened, the logistic regression equation was obtained, and new variables of individual body prediction values were generated in the SPSS worksheet. The ROC (receiver operating characteristic) process was used to predict the individual variables. The other variables were used as test variables, and the clinical diagnosis results were used as state variables for ROC curve analysis.

RESULTS

Comparisons between the two groups

In the PA group, there were higher incidence rates of other complications, such as GH [18% (PA group) *vs* 6% (non-PA group)], gestational diabetes (9% *vs* 3%), fibroid (10% *vs* 5%) and premature rupture of membranes (PROM) (14% *vs* 4%) than those in the non-PA group, and GH was the most prevalent complication.

According to analysis results, the levels of TNF-α (314.5±78.9), IL-6 (266.5±62.4) and IL-8 (290.2±71.3) in amniotic fluid of the PA group were significantly higher than those in the non-PA group (111.6.5±60.5 for TNF-α, 180.5±51.1 for IL-6 and 172.2±56.7 for IL-8) ($p<0.05$), indicating that the inflammatory response occurs in the body of the PA pregnant women.

Table I. *Changes in the expression of the inflammatory factors and MMP-9 among cases with different degrees of PA*

Indicator	Grade III n=25	Grade II n=20	Grade I n=35
TNF-α	382.5±58.9※※#	240.3±62.2※	158.5±51.2
IL-6	266.5±62.4※※#	190.6±58.9※	101.3±42.3
IL-8	310.2±57.7※※#	223.3±58.6※	168.9±60.2
MMP-9	511.3±78.6※※#	312.3±50.5※	177.3±68.1

Note: ※※$p<0.01$ vs grade I PA subgroup, #$p<0.05$ vs grade II PA subgroup.

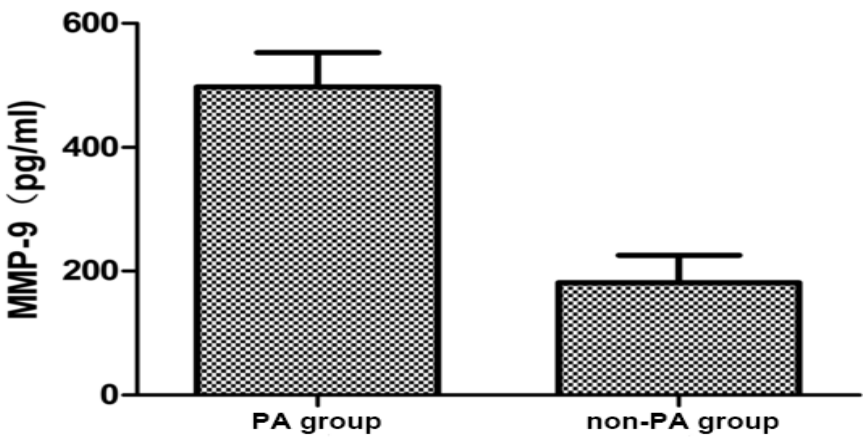

Fig. 1. *Comparison of the level of MMP-9 between the two groups.*

Table II. *Analyses on the risk factors for PA*

Factor		B	Wald	*p*	Odd ratio (OR)	95% confidence interval (CI)
Placenta previa	Yes No	1.499	5.011	0.033	5.221	1.562-9.566
GH	Yes No	1.083	5.434	0.012	4.662	1.112-8.789
PROM	Yes No	1.321	5.128	0.025	4.987	1.323-9.011
Abnormal amniotic fluid volume	Yes No	0.426	4.116	0.029	35.85	1.238-1.998

The level of MMP-9 in amniotic fluid of the PA group was significantly higher than that in the non-PA group ($p<0.05$), indicating decreased fetal membrane strength of PA pregnant women (Fig. 1).

Furthermore, as PA aggravated, the levels of inflammatory factors and MMP-9 gradually increased in the order of grade III PA > grade II PA > grade I PA, and the inter-group differences were significant ($p<0.01$, or $p<0.05$) (Table I).

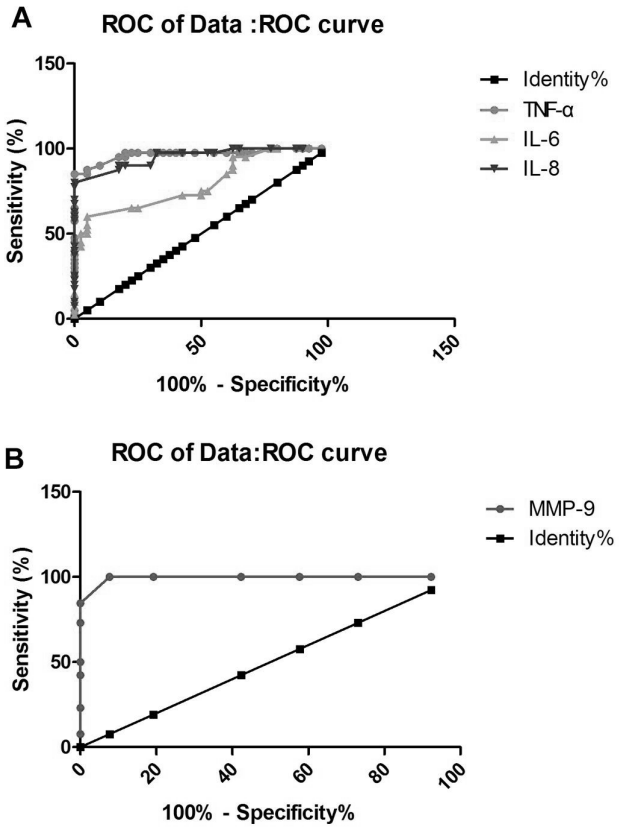

Fig. 2. *ROC curve. **A**) ROC curve of inflammatory factors; **B**) ROC curve of MMP-9.*

Correlation analysis of inflammatory indexes in diagnosis of placental abruption

The ROC curves of various biochemical indicators TNF-α, IL-6, IL-8 and MMP-9 are shown in Fig. 2A and B. The area under the ROC curve of each variable was 0.9663, 0.8969, 0.9509 and 0.9941 ($p<0.01$) (Fig. 2A and B). The point on the top left of the curve in the graph was selected and the sensitivity and specificity were calculated according to the sensitivity and specificity of each possible cut point in the statistical result. The highest value was the critical value.

Moreover, Pearson correlation analysis revealed that GH, placenta previa, abnormal amniotic fluid volume and PROM were identified as the risk factors for PA (Table II).

Adverse fetal outcomes between the two groups

The comparisons of adverse fetal outcomes in both groups revealed that the PA group had higher incidence rates of low-birth-weight neonates, neonatal asphyxia and death than the control group, and the Apgar score was (8.09±0.98) points, which was significantly lower than that in the non-PA group [(9.49±0.76) points] ($p<0.05$).

DISCUSSION

The main pathological features of PA are basal

decidual bleeding and formation of hematoma, and the perinatal mortality of PA is 10-20% (4). This study showed that the pregnant women in the PA group had higher incidence rates of other complications than those in the non-PA group, which is consistent with reports in the literature (5, 6).

A variety of factors can lead to PA (7, 8), including the age of pregnant women, smoking, hypertension. In this study, GH, placenta previa, abnormal amniotic fluid volume and premature rupture of membranes were the risk factors for PA.

In recent years, the roles of inflammatory factors, such as IL-6, IL-8, and TNF-α, in PA have attracted widespread attention (9, 10). Furthermore, inflammatory factors can improve the activity of MMP-9 (11). In this study, it was found that levels of IL-6, IL-8, TNF-α and MMP-9 in amniotic fluid of PA pregnant women were significantly higher than those in the control group, and grade I, II and III PA pregnant women had gradually increased levels of inflammatory factors and MMP-9 with the aggravation of the disease, demonstrating the synergistic roles of inflammatory factors and MMP-9 in PA development. In addition IL-6, IL-8, TNF-α and MMP-9 are associated with PA, which can be used as an indicator for clinical prediction of PA.

In conclusion, monitoring the changes of TNF-α, IL-6, IL-8 and MMP-9 in amniotic fluid of pregnant women helps the early diagnosis of PA and sub-clinical infection, and is critical for improving the prognosis of pregnant and lying-in women and perinatal infants.

ACKNOWLEDGEMENTS

This work was supported by Chongzuo Science and Technology Tackling (15111005 and 17111307).

REFERENCES

1. Salihu HM, Bekan B, Aliyu MH, Rouse DJ, Kirby RS, Alexander GR. Perinatal mortality associated with abruptio placenta in singletons and multiples. Am J Obstet Gynecol 2005; 193:198-203.
2. Sheiner E, Shoham-Vardi I, Hallak M, et al. Placental abruption in term pregnancies: clinical significance and obstetric factors. J Matern Fetal Neonatal Med 2003; 13:45-49.
3. Chen J, Khalil RA. Matrix metalloproteinases in normal pregnancy and preeclampsia. Prog Mol Biol Transl Sci 2017; 148:187-65.
4. Tikkanen M. Placental abruption: epidemiology, risk factors and consequences. Acta Obstet Gynecol Scand 2011; 90:140-49.
5. Sholl JS. Abruption placentae: clinical management innonacute cases. Am J Obstet Gynecol 1987; 156:40-51.
6. Veerbeek JH, Hermes W, Breimer AY, et al. Cardiovascular disease risk factors after early-onset preeclampsia, late-onset preeclampsia, and pregnancy-induced hypertension. Hypertension 2015; 65:600-606.
7. Tikkanen M. Placental abruption: epidemiology, risk factors and consequences. Acta Obstet Gynecol Scand 2011; 90:140-49.
8. Boisramé T, Sananès N, Fritz G, Boudier E, Aissi G, Favre R, Langer B. Placental abruption: risk factors, management and maternal-fetal prognosis. Cohort study over 10 years. Eur J Obstet Gynecol Reprod Biol 2014; 179:100-104.
9. Babine RE, Bender SL. Molecular recognition of protein-ligand complexes: applications to drug design. Chem Rev 1997; 97:1359-472.
10. Roh CR, Oh WJ, Yoon BK, Lee JH. Up-regulation of matrix metalloproteinase-9 in human myometrium during labour: a cytokine-mediated process in uterine smooth muscle cells. Mol Hum Reprod 2000; 6:96-102.
11. Weiss A, Goldman S, Shalev E. The matrix metalloproteinases (MMPS) in the decidua and fetal membranes. Front Biosci 2007; 12:649-59.

LETTER TO THE EDITOR

CHANGES IN SERUM LEVELS OF IGF-1, GHRELIN AND NESFATIN-1 AND CLINICAL SIGNIFICANCE AFTER TREATMENT WITH RECOMBINANT HUMAN GROWTH HORMONE IN CHILDREN WITH IDIOPATHIC SHORT STATURE

D-D. WANG, M. SUN, X. WANG and Y-Y. CHENG

Department of Pediatrics, Hebei General Hospital, Shijiazhuang, China

Received June 4, 2019 – August 30, 2019

To the Editor,

Short stature is defined as a height that is more than 2 standard deviations (SDs) below the mean for age, sex, and population (1), and idiopathic short stature (ISS) is one of the most common types. ISS has unknown causes, with no growth hormone deficiency or growth retardation caused by other endocrine, genetic and metabolic diseases, chromosomal abnormalities, various chronic diseases and malnutrition (1). In 2003, the US Food and Drug Administration (FDA) approved the use of growth hormone for treatment of ISS in children whose height is more than 2.25 SDs below the mean for age and sex without evidence of underlying disease or growth hormone deficiency (GHD) (2). Therefore, subcutaneous injection of recombinant human growth hormone (rhGH) is currently a clinically recognized treatment for ISS. Subsequent FDA approval of rhGH treatment for children with ISS validated the notion that if rhGH treatment is effective at increasing height in children without GHD, then the etiology of short stature is not relevant in deciding who is entitled to treatment (3). Controversy was raised regarding the effectiveness of rhGH in treatment of ISS, since ISS showed no GHD indications. In addition, individual differences exist in rhGH efficacy in treatment of ISS, which may be related to serum factors involved in growth and development, such as IGF-1, ghrelin and nesfatin-1. Hence, in this study, we compared the serum levels of IGF-1, ghrelin, and nesfatin-1 in children with ISS and normal height, and analyzed the relationship between the clinical efficacy of rhGH and the changes of serum factor levels, and discussed its significance in the diagnosis and treatment of ISS.

MATERIALS AND METHODS

Study subjects

This study was approved by the ethics committee of Hebei People's Hospital. Written informed consents by the guardians of the patients were obtained to participate this study. A total of 36 children with ISS, who were treated in the Child Care Clinic of Hebei People's Hospital from 2016 to 2017, were included into the study. These children were assigned to the ISS group (21 boys and 15 girls), and their ages ranged within 3-7 years. Inclusion criteria for the patients: height lower than the standard height for children with matched age, gender, resident region and race by more than 2 SDs; having undergone growth hormone (GH) provocation tests with two different drugs (insulin and clonidine), and revealed that the peak value of GH was more than 10 ng/ml; no previous treatment with GH; normal height and body weight at birth. Exclusion criteria:

Key words: idiopathic short stature; recombinant human growth hormone; IGF-1; ghrelin; nesfatin-1

Corresponding Author:
Dr Ya-Ying Cheng,
Department of Pediatrics, Hebei General Hospital,
No. 348 of Heping Street, Xinhua District,
Shijiazhuang 050051, China
Tel.: +86 013503312606 - Fax: +86 0311 85988140
e-mail: chengyy521034@163.com

0393-974X (2019)

growth hormone deficiency and other types of abnormal growth and development, such as Turner syndrome and Labor syndrome; preterm birth; endocrine diseases, nutritional diseases, mental disorders and chromosomal abnormalities. In addition, 20 healthy children (12 boys and 8 girls) with normal height, who underwent physical examination in our hospital, were randomly selected as the control group. Differences in age, gender, eating habits, living environment and lifestyle between these two groups were not statistically significant.

Routine examinations were performed on all the selected children, including blood analysis, urine analysis, fecal analysis, liver function examination, renal function examination, hepatitis B virus detection, thyroid function monitoring, cortisol detection, pituitary MRI and electrocardiogram examination. The complaints, birth history, feeding history, and family history, history of head trauma, time of onset of slow growth, and annual growth velocity (GV) of height of these children were recorded in detail. Furthermore, the lifestyle, eating and sleeping habits, sports practiced, intelligence development and learning, and the height of parents were investigated.

Collection of clinical data

The height, weight, BMI, and GV of children at the initial visit were recorded. Height, weight, BMI and GV of the ISS group at 3 and 6 months after treatment with rhGH were recorded in a specially designed medical record of short stature in the child health care clinic of our hospital.

Measurement of serum factors

Four ml of fasting venous blood was collected from children in the control group (one time point) and ISS group (three time points: before treatment, three and six months after rhGH treatment). Then, the collected samples were centrifuged to obtain the serum and preserved at -70°C for further testing. The serum IGF-1 levels were measured by immunoluminescence (Roche E-601 electrochemiluminescence immunoanalyzer). The serum levels of ghrelin and nesfatin-1 were measured by enzyme-linked immunosorbent assay (ELISA) (Shenzhen NeoBioscience Biotechnology Co., Ltd. and Wuhan Boster Biotechnology, Ltd).

Statistical analysis

Statistical analysis was conducted using SPSS 21.0 software. All data were tested for homogeneity of variance and normal distribution. Measurement data in normal distribution were expressed as mean ± standard deviation ($\bar{x}$±SD). Comparisons between the means were carried out by independent sample *t*-tests. The correlation between two factors was evaluated using Pearson's correlation test. $P<0.05$ was considered statistically significant.

RESULTS

Comparisons between the ISS group and control group

Before treatment of rhGH in the ISS group, height and GV were significantly decreased, serum IGF-1 level was significantly decreased while serum ghrelin level was significantly increased, compared with the control group (Table I).

Height, GV, IGF-1 were significantly increased while ghrelin significantly decreased when compared between pre-treatment, 3-month post-treatment and 6-month post-treatment of rhGH in children with ISS (Table II).

In children with ISS, before treatment with rhGH, serum IGF-1 level was positively correlated with height (r=0.610, $P<0.001$), serum ghrelin level was negatively correlated with height (r=-0.405, $P=0.014$) and weight (r=-0.498, $P=0.002$), and serum nesfatin-1 level was negatively correlated with weight (r=-0.393, $P=0.018$) (Fig. 1).

GV at three months after treatment (GV3) was positively correlated with serum IGF-1 level before treatment with rhGH in children with ISS (r=0.618, $P<0.001$), but was not significantly correlated with serum ghrelin and nesfatin-1 levels (Fig. 2).

DISCUSSION

Although FDA approved rhGH for the treatment of children with ISS in 2003, its curative effect remains controversial (2). In this study, the height and GV of ISS children significantly increased at three and six months after rhGH treatment, which is consistent with results in the relevant literature (4).

IGF-1 mediates growth by promoting the effect of GH. The present study revealed that serum IGF-1 level was significantly lower in children with ISS, which is consistent with other reports (5). Unlike

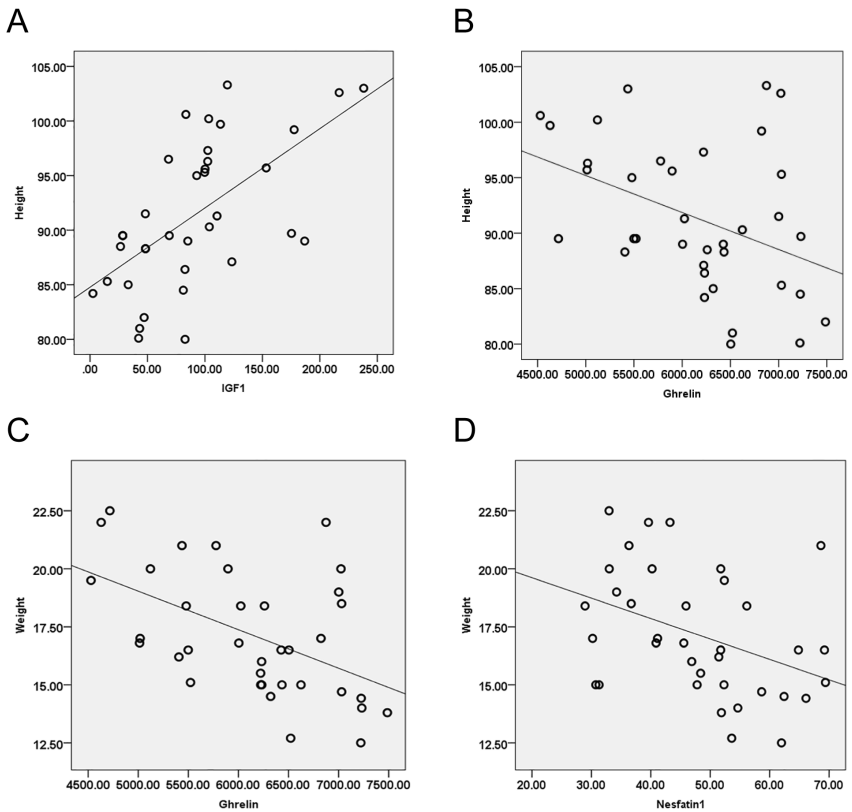

Fig. 1. *Correlation between serum IGF-1, ghrelin and height, and between ghrelin, nesfatin-1 and weight.*

Table I. D*ata of weight, height, BMI, IGF-1, ghrelin, nesfatin-1 and other indicators in the observation ISS group and control group.*

Index	**Control group（n=20）**	**ISS group（n=36）**	***P***
Gender (male/ female)	11/9	21/15	0.919
Age (years old)	4.45±1.43	4.50±1.03	0.890
Gestational age (weeks)	38.66±1.20	38.58±1.21	0.815
Birth Weight (kg)	303±0.45	3.12±0.39	0.429
Weight (kg)	19.21±4.27	17.10±2.74	0.056
GV ($cm \cdot year^{-1}$)	6.39±0.68	3.51±0.67	0.002
BMI ($kg \cdot m^{-2}$)	20.15±2.85	20.41±1.49	0.656
IGF-1 ($ng \cdot ml^{-1}$)	161.54±84.64	91.84±56.15	0.030
Ghrelin ($pg \cdot ml^{-1}$)	4933.43±232.91	6098.29±804.76	0.013
Nesfatin-1 ($pg \cdot ml^{-1}$)	45.67±12.01	48.08±12.09	0.476

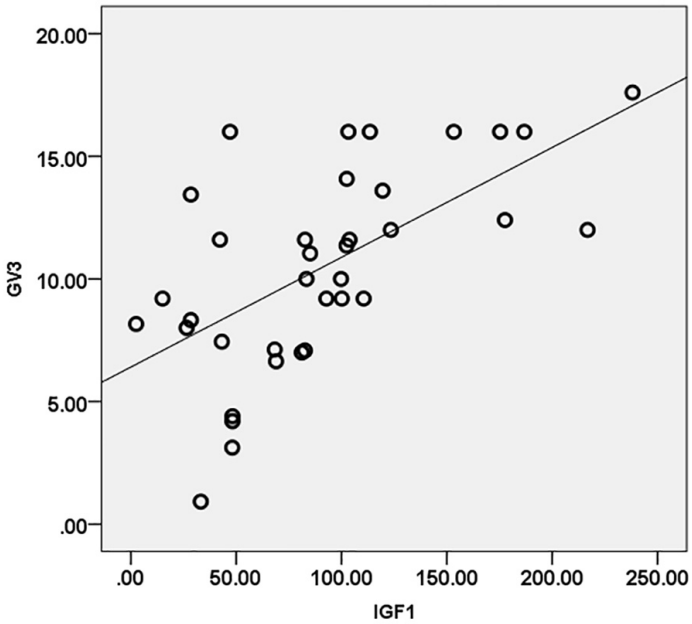

Fig. 2. *Positive correlation between GV3 and pre-treatment serum IGF-1 in patients with ISS.*

Table II. *Changes of anthropometrics and serum IGF-1, ghrelin, nesfatin-1 before and after the treatment with rhGH in ISS.*

Index	**Time Point**		
	Before treatment	After 3 months	After 6months
Height (cm)	91.39±6.70	94.02±6.65[a]	97.81±7.33[ab]
Weight (kg)	17.10±2.74	17.90±2.61	18.36±2.76
GV (cm/year)	3.51±0.67	10.48±4.07[a]	12.82±2.93[ab]
BMI (kg/m2)	21.41±1.49	20.26±2.14	19.87±2.09
IGF-1 (ng/ml)	91.84±56.15	148.16±67.98[a]	192.36±85.76[ab]
Ghrelin (pg/ml)	6098.29±804.76	4725.78±866.89[a]	3995.09±777.76[ab]
Nesfatin-1 (pg/ml)	48.08±12.09	43.87±13.08	42.56±10.86

[a]P<0.05 vs before treatment; [b]P<0.05 vs after treatment for 3 months

GH, IGF-1 does not have the characteristics of pulse secretion and circadian rhythm, therefore it can be an appropriate biomarker to diagnose children with ISS. Results of the correlation between IGF-1 and height suggested that rhGH could promote height growth by increasing IGF-1 levels, which is consistent with previous studies (6, 7). In addition, relationship of GV3 and IGF-1 showed that monitoring the level of IGF-1 can also reflect the sensitivity of rhGH (8, 9).

Ghrelin promotes the release of GH by binding with its receptors. Higher ghrelin in the ISS group is consistent with other studies (10). Negative correlation of serum ghrelin and height and weight of the ISS group indicated that there might be ghrelin resistance or abnormal Ghrelin signaling in ISS children. Decrease of ghrelin after rhGH treatment suggested that exogenous GH could downregulate the level of ghrelin.

Negative correlation between serum nesfatin-1 and weight in children with ISS, suggested that nesfatin-1 inhibited food intake and reduced weight which is in accordance with a previous study (11). Hence, Nesfatin-1 might affect the growth of children by regulating food intake.

In the present study, only changes in relevant indexes of 36 ISS children within six months after treatment were examined. Hence, a larger cohort and prolonged follow-up are needed in the future.

ACKNOWLEDGEMENTS

This study was funded by the Nature fund of Hebei province (No. H2014307057); key project of health and family planning commission in Hebei province (No. 20170256).

REFERENCES

1. Cohen P, Rogol AD, Deal CL, Saenger P, Reiter EO, Ross JL, Chernausek SD, Savage MO, Wit JM; 2007 ISS Consensus Workshop participants. Consensus statement on the diagnosis and treatment of children with idiopathic short stature: a summary of the Growth Hormone Research Society, the Lawson Wilkins Pediatric Endocrine Society, and the European Society for Paediatric Endocrinology Workshop. J Clin Endocrinol Metab 2008; 93:4210-17.
2. Cohen LE. Idiopathic short stature: a clinical review. JAMA 2014; 311:1787-96.
3. Allen DB. Growth promotion ethics and the challenge to resist cosmetic endocrinology. Horm Res Paediatr 2017; 87:145-52.
4. Kim HS, Yang SW, Yoo HW, et al. efficacy of short-term growth hormone treatment in prepubertal children with idiopathic short stature. Yonsei Med J 2014; 55:53-60.
5. Stawerska R, Czkwianianc E, Smyczyńska J, Hilczer M, Lewiński A. Nutritional status in short stature children is related to both Ghrelin and insulin-like growth factor I concentrations. J Pediatr Gastroenterol Nutr 2017; 64:812-17.
6. Cheng YY, Zhao XM, Cai BP, Ma LN, Yin JY, Song GY. Nesfatin-1 in newborns: relationship with endocrine and metabolic and anthropometric measures. J Pediatr Endocrinol Metab 2012; 25:727-32.
7. Im M, Kim YD, Han HS. Effect of growth hormone treatment on children with idiopathic short stature and idiopathic growth hormone deficiency. Ann Pediatr Endocrinol Metab 2017; 22:119-24.
8. Inzaghi E, Cianfarani S. The challenge of growth hormone deficiency diagnosis and treatment during the transition from puberty into adulthood. Front Endocrinol (Lausanne) 2013; 4:34.
9. Kriström B, Lundberg E, Jonsson B, Albertsson-Wikland K; study group. IGF-1 and growth response to adult height in a randomized GH treatment trial in short non-GH-deficient children. J Clin Endocrinol Metab 2014; 99:2917-2924.
10. Stawerska R, Smyczyńska J, Czkwianianc E, Hilczer M, Lewiński A. High concentration of ghrelin in children with growth hormone deficiency and neurosecretory dysfunction. Neuro Endocrinol Lett 2012; 33:331-39.
11. Oh-I S, Shimizu H, Satoh T, et al. Identification of nesfatin-1 as a satiety molecule in the hypothalamus. Nature. 2006; 443(7112):709-12.

LETTER TO THE EDITOR

A NEWLY DISCOVERED CASE OF PROGRESSIVE MUSCULAR DYSTROPHY CAUSED BY EXON DELETION MUTATION OF DUCHENNE MUSCULAR DYSTROPHY GENE 12-28

BT. LI[1*], JX. CHEN[2*], HA. LI[1] and XY. HUANG[1]

[1]Department of Pediatrics, Hainan Maternal and Child Health Hospital, Haikou, China;
[2]Department of Medical Care Center, Hainan General Hospital, Haikou, China

Received April 1, 2019 – Accepted August 30, 2019

[*]These authors contributed equally to this study

To the Editor,

Duchenne muscular dystrophy (DMD) is a genetic muscular system disease characterized by progressive muscular atrophy. The cDNA encodes dystrophin, the mutation of which causes complete deletion of the protein and leads to progressive muscular dystrophy (1).The diagnostic points of DMD include recessive inheritance of X-linkage and progressive development of disease. The early manifestation is the weakness of the two lower limbs, duck step, Gowers sign (+), squatting difficulty and hypertrophy of the gastrocnemius muscle. With the increase of age, weakness of the upper limbs and wing-like scapulae appear. Lastly, joint contracture and deformity of the spine occur. The creatine kinase of serum increases significantly. The electromyogram and muscle biopsy show myogenic damage. The main diagnostic method of DMD is gene detection showing exon deletion, a repeat, a small mutation or a point mutation. The condition of DMD is complex, which suggests that multi-disciplinary comprehensive treatment should be taken at different stages of the disease (2). Researchers have found different deletions on the exons of DMD gene by gene detection, but the presented case of muscular dystrophy is DMD gene exon 12-28 heterozygous deletion mutation, which reports a newly discovered deletion mutation.

Case description

A 5-year-old boy was admitted to our hospital due to "abnormal enzymes for three years". Three years previously, the patient's abnormal enzyme index (ALT, 479 U/L) was found through a preoperative examination of "cryptorchidism". Then, the patient was treated with some oral traditional Chinese medicine. However, the entropy index did not decline. The patient often felt tired after doing exercise and was without regular treatment. The present clinical results were: ALT, 315 U/L; AST, 335 U/L; CK, 10170 U/L; CK-MB, 221 U/L. Furthermore, the patient was G1P1 and full-term delivery, and his growth and development were obviously behind those of the peers. His family members did not have a similar morbidity. The patient was conscious and mentally responsive. The heart, lung and abdominal examination revealed no abnormalities. The bilateral gastrocnemius muscles were slightly hypertrophied, lower limb muscle strength was level four, upper limb muscle strength was normal. Furthermore, upper and lower limb muscle tension was normal. The patient had duck step and Gower sign (+). The bilateral bicep and tricep

Key words: muscular dystrophy; creatine kinase; MLPA gene analysis

Corresponding Author:
Dr Xiao-Yan Huang,
Department of Pediatrics,
Hainan Maternal and Child Health Hospital,
No. 75 Longkun South Road, Qiongshan District, Haikou 570206, China
Tel.: +86 0898 36689605 - Fax: +86 0898 36689190
e-mail: xyhdr_123@163.com

0393-974X (2019)

reflexes were normal. Both knee and Achilles tendon reflexes were also normal. The bilateral Brudzinski, Kernig and Babinski signs were all negative. The right scrotum did not touch the testicles. There were no abnormalities in the MRI scan and DWI of the brain. Hepatobiliary, spleen and pancreatic ultrasonography suggested thickening parenchyma of the liver. Electromyography, Epstein-Barr virus, cytomegalovirus, antinuclear antibody, ceruloplasmin, troponin I, amino terminal brain sodium precursor, and erythrocyte sedimentation rate were not abnormal. On the 1st day of hospitalization: ALT was 396 U/L, AST was 429 U/L, CK was 10,898 U/L, CK-MB was 383 U/L, and LDH was 1,321 U/L. Furthermore, the patient was treated with monoammonium glycyrrhizinate, B vitamins and some symptomatic supportive care during hospitalization. On the 9th day of hospitalization: ALT was 498 U/L, AST was 651 U/L, CK was 25,349 U/L, CK-MB was 482 U/L, LDH was 1,652 U/L, and the zymogram index significantly increased. Genomic DNA was extracted from peripheral blood leukocytes using standard protocol and DMD gene deletions and duplications were tested by multiplex-ligation-dependent-probe-amplification (MLPA) (SALSA P034 and SALSA P035, MRC-Holland). MLPA analysis surprisingly demonstrated exons 12-28 deletion mutation of DMD gene (Fig. 1), and the diagnosis of muscular dystrophy was finally made. An informed written consent was given by the patient's parents, who was well informed about participation in scientific publication.

DISCUSSION

The dystrophin gene includes 79 exons, mainly expressed in skeletal muscle and myocardium (3). The deletion mutation is the most common type of mutation in the dystrophin gene, while the two major deletion regions are the central region (including the 45th to 55th exons) and the 5' end of the gene (including the 2nd-20th exons) (4). Deletion mutations can affect the structure and function of dystrophin, and can also cause defects in skeletal muscle cell membranes and leakage of intracellular phosphokinase.

In China, 60% children with DMD have gene deletion mutations (5). In this case, the DMD gene exons 12-28 deletion mutation was found through the genetic examination with the use of MLPA technology (6, 7). MLPA is a reliable technology for quantitative analysis of the copy number in clinical diagnosis of genetic diseases. Our finding via MLPA is a newly discovered deletion mutation which the HGMD Professional Edition Database has not previously reported. In 2018, Josef et al. reported a woman with DMD gene exons 12-29 deletion. The mutations of this woman were not identical to the child reported in our case (8).

Clinically, glucocorticoid drugs and supportive therapies are often used to improve the symptoms of the disease, but these cannot change its final outcome (9). Since DMD is directly caused by defects of the DMD gene, with the in-depth study

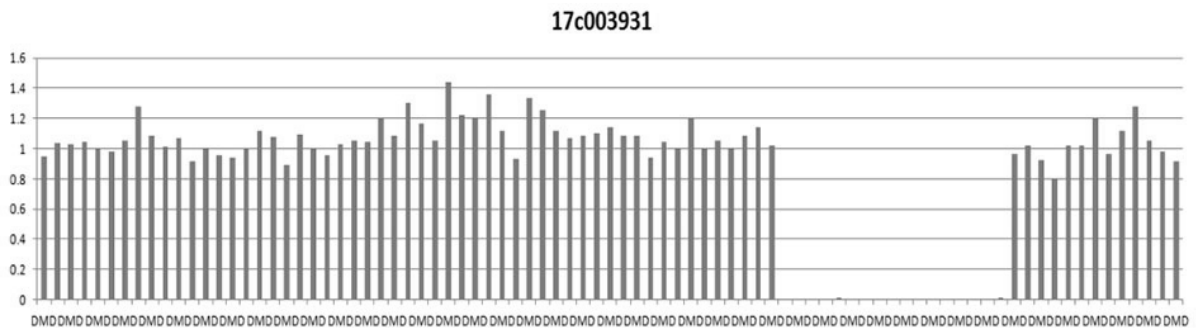

Fig. 1. *Multiplex-ligationdependent-probe-amplification result showing the absence of exon 12-28 in the patient.*

of gene therapy, gene replacement therapy, such as adeno-associated virus (AAV)-mediated DMD gene transduction and Utrophin upregulation strategies, has been developed for DMD patients (10). In addition, short palindromic repeat sequence gene editing technology with regular cluster spacing has also become a research hotspot (11, 12).

In conclusion, this case adds a novel deletion in DMD gene in human. In clinical work, it is necessary to be alert for DMD, which can be early diagnosed by neuromuscular disease genes analysis.

REFERENCES

1. Li T, Wu D, Hou QF, et al. Efficiency of multiplex ligation-dependent probe amplification combined with short tandem repeat linkage analysis for the prenatal diagnosis for Duchenne muscular dystrophy. Zhonghua Yi Xue Yi Chuan Xue Za Zhi 2013; 30:40-44.
2. Chinese Medical Association Neurology Branch, Neuromuscular Group of the Chinese Medical Association Neurology Branch, Electrophysiology and Clinical Neurophysiology Group of the Chinese Medical Association Neurology Branch. Guidelines for the diagnosis and treatment of large-scale muscular dystrophy in China. Chin J Neurol 2016; 49:17-20.
3. Zhu HY, Wu LQ, Liang DS, Xia JH. Progress of DMD gene, mutations and mutation detection technology. Basic Clinl Med 2005; 25:975-81.
4. Du Q, Liu Y, Tian L, Zhang L, Du R, Zhu Y, Zhu J. Detection of dystrophin gene mutation in a Chinese pedigree affected with Duchenne muscular dystrophy. Zhonghua Yi Xue Yi Chuan Xue Za Zhi 2014; 31:733-36.
5. Li X,Zhao L, Zhou S, et al. A comprehensive database of Duchenne and Becker muscular dystrophy patients (0-18 years old) in East China. Orphanet J Rare Dis 2015; 10:5.
6. Luce LN, Dalamon V, Ferrer M, Parma D, Szijan I, Giliberto F. MLPA analysis of an Argentine cohort of patients with dystrophinopathy: Association of intronbreakpoints hot spots with STR abundance in DMD gene. J Neurol Sci 2016; 365:22-30.
7. Ji X, Zhang J, Xu Y, et al. MLPA Application in Clinical Diagnosis of DMD/BMD in Shanghai. J Clin Lab Anal 2015; 29:405-41.
8. Josef F, Claudia S, Birgit F, Desiree DS, Klaus W. Muscular and cardiac manifestations in a Duchenne-carrier harboring a dystrophindeletion of exons 12-29. Intractable Rare Dis Res 2018; 7:120-25.
9. Gloss D, Moxley RT 3rd, Ashwal S, Oskoui M. Practice guideline update summary: Corticosteroid treatment of Duchenne muscular dystrophy: Report of the Guideline Development Subcommittee of the American Academy of Neurology. Neurology 2016; 86:465-42.
10. Dong QC, Chen HM, Jin X. A review of gene therapy for Duchenne muscular dystrophy. Zhongguo Dang Dai Er Ke Za Zhi 2018; 20:691-96.
11. Young CS, Mokhonova E, Quinonez M, Pyle AD, Spencer MJ. Creation of a novel humanized dystrophic mouse model of duchenne muscular dystrophy and application of a CRISPR/Cas9 gene editing therapy. J Neuromuscul Dis 2017; 4:139-45.
12. Lattanzi A, Duguez S, Moiani A, et al. Correction of the Exon 2 Duplication in DMD Myoblasts by a Single CRISPR/Cas9 System. Mol Ther Nucleic Acids 2017; 7:11-19.

LETTER TO THE EDITOR

ROLE OF YAP AND TAZ EXPRESSIONS IN PATHOLOGICAL SCARS

J. CHEN[1] and HB. LUO[2]

[1]Department of Dermatology, Zhuji People's Hospital of Zhejiang Province, Zhuji, Zhejiang Province, China; [2]Department of Dermatology, The First Affiliated Hospital of Zhejiang Chinese Medical University, Hangzhou, Zhejiang Province, China

Received May 16, 2019 – Accepted September 13, 2019

To the Editor,

A scar refers to the changes in appearance and histopathology of healthy skin tissues induced by wounds, which is an inevitable result of human wound repair (1). Once the growth of scars exceeds a specific limit, various complications may occur, such as appearance destruction and functional disorders, bringing agony to patients (2). Researchers suggested that the features of pathological scars were excessive proliferation and insufficient apoptosis of fibroblasts, while the Hippo signaling pathway could regulate the proliferation and apoptosis of cells to control the size of organs (3-5). The key factors of the Hippo signaling pathway included yes—associated protein (YAP) and Transcriptional coactivator with PDZ-binding motif (TAZ). Studies indicated that YAP regulated cell proliferation and apoptosis through controlling transduction of intracellular signals and expressions of downstream genes (6-8). Therefore, it was speculated that YAP and TAZ were closely related to the onset and development of pathological scars.

Currently, pressure therapy has been accepted as a treatment for keloid globally, but its mechanism is still obscure. Therefore, the expression levels of YAP and TAZ in keloid and wound surface repair were explored in this study to provide a theoretical basis of the mechanism of scars and provide new ideas and methods for the clinical treatment of pathological scars.

MATERIALS AND METHODS

Animals

A total of 10 adult New Zealand white rabbits (purchased from Xi'an Dilepu Biological Resources Development Co., Ltd., China) (male and female) weighing 2.5-3.0kg were used in the study. All rabbits were kept in separate cages with natural illumination and were fed with standard chow and had free access to food and water. The room temperature was controlled at 20-26°C, and humidity at 40-50%. The adaptive feeding continued for two weeks. The animal experiments were conducted under the International Animal Protection and Management Regulations and the protocol was approved by ethics committee of Zhuji People's Hospital of Zhejiang Province.

Grouping

The left ears of all ten rabbits were classified into group A, and the right ears of all ten rabbits were classified into group B. The ears of the rabbits were sterilized, and all the rabbits were anesthetized under strict aseptic conditions via ear vein injection of sodium pentobarbital (3%, 1.5mg/Kg) (Shanghai Xin-yu Biotechnology Corporation, China).

The left ear group (group A): Using a puncher (Hunan Yuanxiang Biological Technology Co., Ltd., China), a total of 3 whole-layer wounds with a skin defect of about

Key words: YAP; pathological scar; Hippo signaling pathway; fibroblast

Corresponding Author:
Dr Hongbin Luo,
Department of Dermatology,
The First Affiliated Hospital
of Zhejiang Chinese Medical University,
No.54 Youdian Road, Hangzhou, Zhejiang Province, China
e-mail: luo_hongbin1219@163.com

0393-974X (2019)

DISCLOSURE: ALL AUTHORS REPORT NO CONFLICTS OF INTEREST RELEVANT TO THIS ARTICLE.

0.6 cm in diameter were created at the cartilage side of the left ear of each rabbit.

The right ear group (group B): Using a puncher, a total of 3 whole-layer wounds with a skin defect of about 1 cm in diameter were created at the cartilage side of the right ear of each rabbit.

The wounds penetrated the perichondrium and the distance between adjacent wounds was greater than 1 cm. In addition, the hemostasis at the wound surface and the edge of wound was maintained through thermal coagulation. In order to prevent the rabbits from licking their wounds and affecting the experiment, their ears were tied back. All rabbits had access to the same type of feed. At 7 days after the operation, the clamps were removed. At 14 and 30 days after the operation, wound tissues were collected from the upper end and the middle part of the ears, respectively, as experimental samples. Finally, the remaining wound tissues were collected at 60 days after the operation for subsequent analysis.

Morphological changes of the samples with Hematoxylin-Eosin (H&E) staining

The scar tissue samples were fixed with neutral formalin (10%, Wuhan Boster Biotechnology Corporation, China) for 12 h, conventionally dehydrated by gradient alcohol, and incubated with pure trichloromethane (Sinopharm Chemical Reagent, China) at 15°C until they became transparent and were then embedded in paraffin and rinsed with running water. Afterwards, the samples were serially sectioned to the thickness of 4 μm, stained with a Hematoxylin-Eosin (HE) staining solution (Shanghai Zheng-mao Biotechnology, China) and mounted with neutral resin (Shanghai Yan-tuo Biotechnology, China). The sample sections were placed under an inverted phase contrast microscope (Leica, Germany) to observe and acquire the images of morphological characteristics of the cells.

Tissue YAP distribution with immunohistochemistry staining

The sections were deparaffinized, immersed in 3% hydrogen peroxide for 10 min in the dark, and rinsed 3 times with distilled water. Afterwards, the sample sections were placed into a 0.01M citrate buffer (pH6.0, Wuhan Boster Biotechnology Corporation, China) and heated to boiling in a microwave oven. Once the sections were completely cooled, they were washed three times with PBS (phosphate buffered saline, Beijing Institute of Biological Products, China) and blocked with a 5% BSA (bovine serum albumin) blocking solution (Shanghai Wei-ao Biotechnology, China) for 30 min. In the next step, the samples of the left ear group were incubated for 1 h at 37°C with 0.01M phosphate buffer, while the samples of the right ear group were incubated with a diluted solution of goat anti-rabbit YAP polyclonal antibody and goat anti-rabbit TAZ polyclonal antibody (1:100 dilution, Beijing Applygen Gene Technology, China) under the same conditions. Then, the samples were rinsed 3 times with PBS, and incubated for 30 min at 37°C with a diluted solution of rat anti-goat IgG secondary antibody (Nanjing Sheng-xing Biotechnology, China). They were then rinsed 3 times with PBS, incubated for 30 min at 37°C with an SABC (Strept Avidin Biotin-peroxidase Complex) immunohistochemistry staining reagent (Wuhan Boster Biotechnology Corporation, China), and rinsed 3 times with PBS. Afterwards, the samples were counterstained with DAB (diaminobenzidine) (Xiamen Jin-rui-bo Biotechnology, China) and placed under an inverted microscope to observe the results of color development. Finally, the sections were dehydrated by gradient alcohol, made transparent with xylene, and mounted with neutral balsam, while the images of the samples were acquired under the microscope.

Detection of the YAP/TAZ expression with Western blot

In the next step, the protein concentration of the sample was determined using a BCA (bicinchoninic acid) assay (Beijing Bai-ao Lai-bo Technology, China) following the manufacturer's instructions. Based on the molecular weight of the target protein, a 10% separation gel, which was made of 1.9 mL of deionized water, 1.7 mL of 30% acrylamide (Jiangxin Biochemical Corporation, China), 1.3 mL of 1.5 M Tris-HCl (pH8.8, Beijing Solarbio Science & Technology, China), 50 μL of 10% SDS (sodium dodecyl sulfate) (Beijing Solarbio Science & Technology, China), 0.05 mL of 10% ammonium persulfate (Shaanxi Bao-hua Technology, China), and 2 μL of TEMED (Tetramethylethylenediamine, Shanghai Sangon Biotech, China), and a 5% stacking gel, which was made of 1.4 mL of deionized water, 0.33 mL of 30% acrylamide, 0.25 mL of 1M Tris-HCl (pH6.8), 20 μL of 10% SDS, 20 μL of 10% ammonium persulfate, and 2 μL of TEMED, were prepared. The samples of tissue lysate were loaded onto the gel (20μL/well) and resolved via electrophoresis for

60 min at 100-120V. Then, the resolved protein bands were blotted onto an NC membrane (nitrocellulose filter membrane) for 1 h at 400mA and 300V, and the membrane was subsequently blocked for 30 min with a blocking solution (a 7:2:1 ratio of ultra-pure water : Blocker A : Blocker B). They were rinsed 3 times with distilled water, and incubated overnight at 4°C with diluted solutions of rabbit anti-human YAP (Shanghai Gu-yan Biotechnology, China), rabbit anti-human P-YAP (Wuhan Hua-mei Bioengineering, China), rabbit anti-human TAZ (Shanghai Sangon Biotech, China), and rabbit anti-human-actin (Shanghai Zhen-yu Biotechnology, China) primary antibodies. Then, the membrane was rinsed 3 times with a tri-n-propylamine buffer solution and incubated at room temperature for 1 h with the secondary antibody. It was then rinsed 3 times each with the tri-n-propylamine buffer solution and distilled water, and developed for 30 min with 1 mL of a colorimetric solution in the dark. It was rinsed 3 times again with distilled water, and dried using a filter paper. Finally, membrane images were acquired using an Odyssey Infrared Imaging System (LI-COR, USA) to calculate the gray values of protein bands.

Statistical analysis

SPSS 21.0 statistical software was used for data processing and analysis. All quantitative data with a normal distribution were expressed as mean ± standard deviation. Intra-group comparisons were carried out by independent sample *t*-test or rank sum test. Inter-group comparisons were made isomg *Chi*-squared test.

RESULTS

Hematoxylin-Eosin staining

On the 14th day after surgery, the H&E staining showed a large number of fibroblasts in the granulation tissues accompanied by inflammatory cell infiltration and capillary proliferation. On the 30th postoperative day, a large number of orderly arranged fibroblasts accompanied by capillary proliferation were observed in the samples of group A, while the number of fibroblasts in the samples of group B was greater than that of group A. In addition, the secretion sedimentation of extracellular matrix was also observed. Compared to the 30th day after operation, the scar area and the number of fibroblasts in the samples of both group A group B were significantly lower on the 60th postoperative day, along with more obvious sedimentation of collagen, indicating that the keloid in group B was

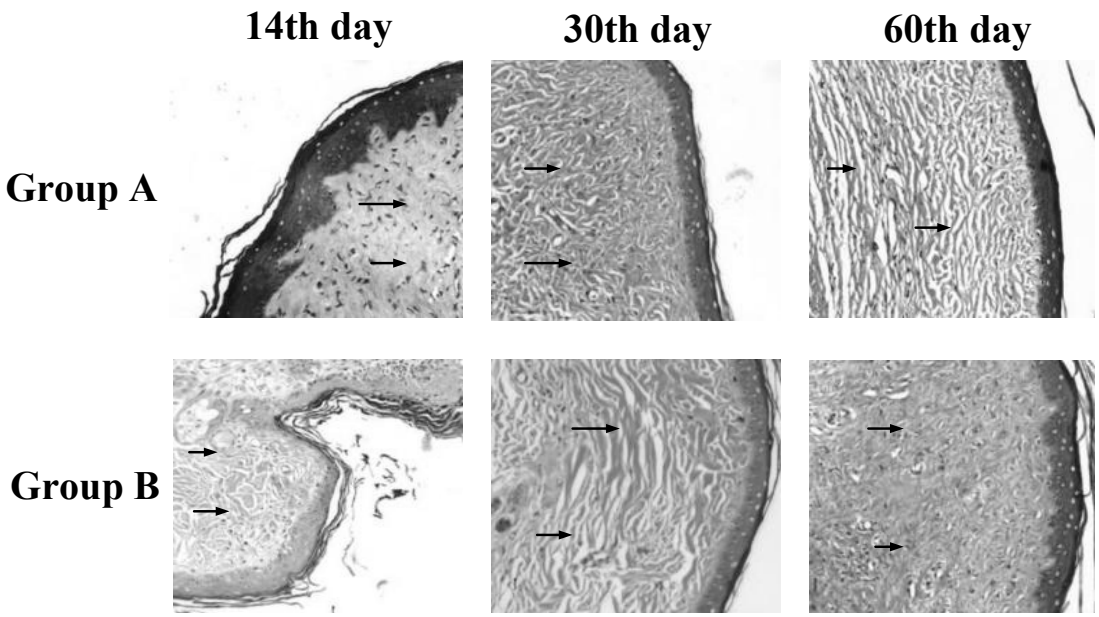

Fig. 1. *Results of H&E staining under an inverted microscope (cell morphological changes in groups A and B on the 14th, 30th and 60th days after operation, respectively)*

more serious compared with that in group A. The experimental results are shown in Fig. 1.

YAP and TAZ immunohistochemical staining

The immunohistochemistry staining showed that on the 14th day after operation, a small number of YAP positive particles was present in the nuclei of fibroblasts, and the number of YAP positive particles in group B was greater than that in group A. On the 30th postoperative day, the number of YAP positive particles in both groups A and B was higher than that observed on the 14th day, and these particles were mainly distributed in the nuclei of fibroblasts. At the same time, the number of YAP positive particles in group B was higher than that in group A. On the 60th day after operation, the number of YAP positive particles in group A was not much different from that observed on the 30th day, while the number of YAP positive particles in group B was higher than that in group A and the number of YAP positive particles observed on the 30th day. Finally, the YAP positive particles in group B were mainly distributed in the nuclei of fibroblasts. The experimental results are shown in Fig. 2.

The immunohistochemical staining results of TAZ are shown in Fig.3. On the 14^{th} day, a small number of TAZ positive particles were observed, and there were more TAZ positive particles in group B than in group A. On the 30^{th} day, there were more TAZ positive particles in groups A and B compared to the 14^{th} day, and there were more TAZ positive particles in group B than in group A. On the 60^{th} day, the amount of TAZ positive particles observed in group A were not significantly different from those observed on the 30^{th} day; there were more TAZ positive particles in group B on the 60^{th} day compared to the 30^{th} day and group A.

YAP/TAZ protein expressions

The Western blot in Fig.4 shows that the YAP expression in group B was significantly higher than that in group A ($^{*}P<0.01$). Similarly, the TAZ expression in group B was significantly higher than that in group A ($^{*}P<0.01$).

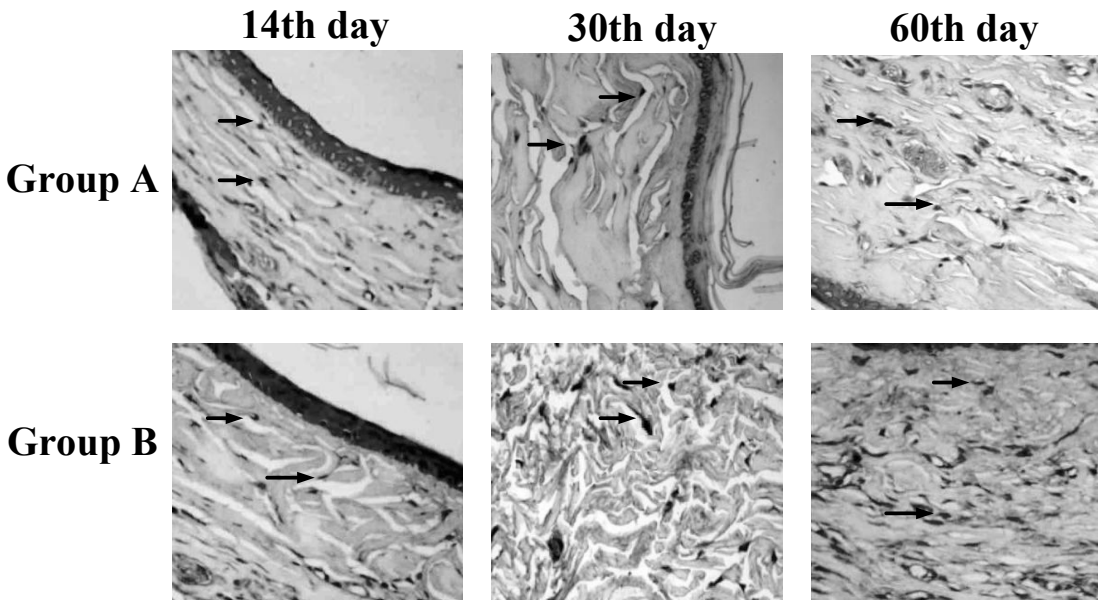

Fig. 2. *Results of YAP immunohistochemical staining (YAP distributions in tissues in groups A and B on the 14^{th}, 30^{th} and 60^{th} days after operation)*

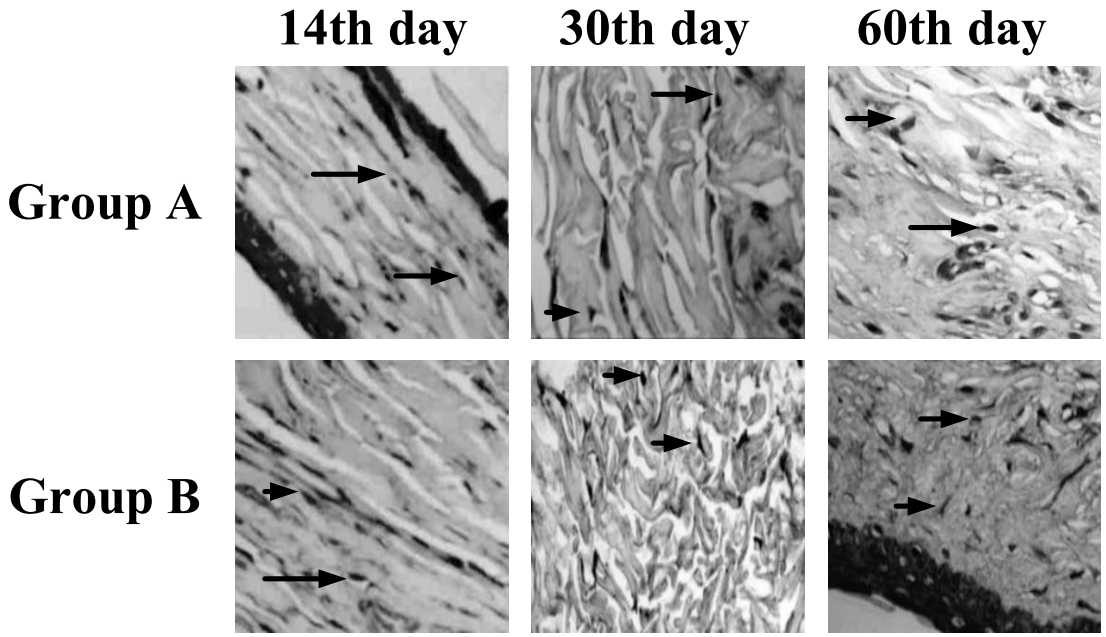

Fig. 3. *Results of TAZ immunohistochemical staining (TAZ distributions in tissues in groups A and B on the 14th, 30th and 60th days after operation, respectively)*

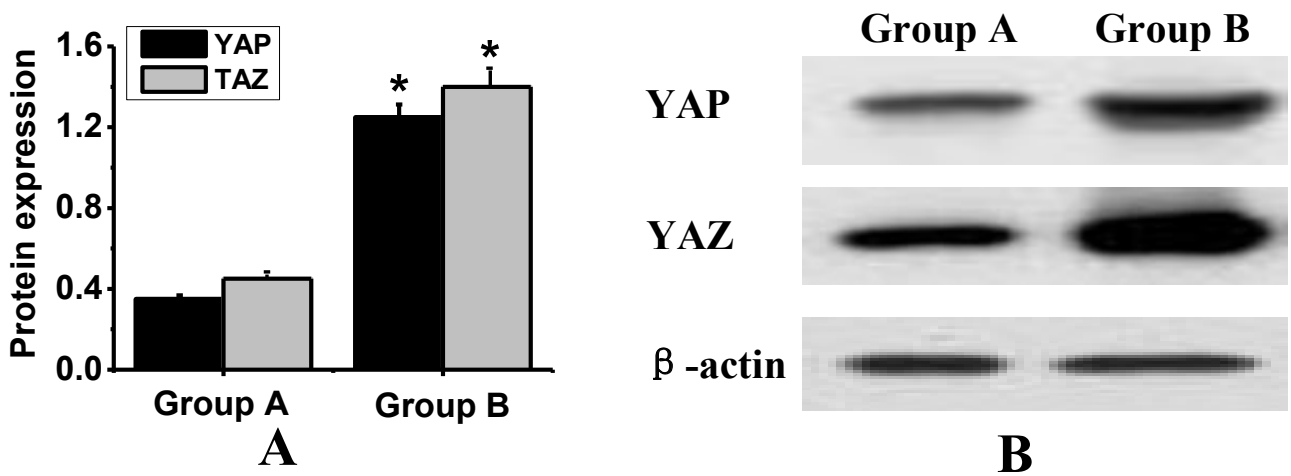

Fig. 4. *YAP/TAZ expressions. **A**) Expression of YAP/TAZ; **B**) Western blot (β-actin was used as the internal reference)*

DISCUSSION

Fibroblasts are the major cell components of loose connective tissues. The unique property of fibroblasts is that they could help repair the damaged skin and reduce the effects of aging on the skin (9, 10). The models of pathological scars of rabbit ears were established; in addition, the distributions of YAP/TAZ and the morphological changes during the process of wound repair to scar formation were observed on the 14th, 30th, and 60th days, respectively. For H&E staining, it was observed that there were more fibroblasts in the right ear group than in the left ear group, and the keloid in the right ear group was more severe than that in the left ear group. On the 30th day, the scar was still in formation, and the fibroblasts in both groups increased significantly compared to the 14th day. On the 60th day, the scar in

the left ear group began to shrink, and the fibroblasts decreased compared to the 30th day. The keloid in the right ear group continued to grow, and the fibroblasts increased.

YAP/TAZ is the crucial protein molecules of the Hippo signaling pathway that regulates the downstream factors. If the Hippo signaling pathway is blocked, YAP/TAZ will be over-expressed, which promotes cell growth and proliferation and inhibits cell apoptosis (11, 12). By immunohistochemical staining of rabbit ears, it was observed that during the scar formation process, the amount of YAP and TAZ positive particles in the right ear group was much greater than that in the left ear group. On the 30th day, the positive particles in both groups were significantly increased compared to the 14th day. On the 60th day, the positive particles in the left ear group barely increased compared to the 30th day, while the amount of positive particles in the right ear group was still increasing. The expression levels of YAP/TAZ were determined by Western blot. The results showed that the expression of YAP/TAZ in the right ear group was significantly higher than that in the left ear group.

In summary, the active mechanism of scar formation is excessive proliferation of fibroblasts induced by the initiation of YAP/TAZ activity in the Hippo signaling pathway.

REFERENCES

1. Berman B, Maderal A, Raphael B. Keloids and hypertrophic scars: pathophysiology, classification, and treatment. Dermatol Surg 2017; 438(S1):S3-S18.
2. Ghazawi FM, Zargham R, Gilardino MS, Sasseville D, Jafarian F. Insights into the pathophysiology of hypertrophic scars and keloids: how do they differ? Adv Skin Wound Care 2018; 31(1):582-95.
3. Varelas X. The Hippo pathway effectors TAZ and YAP in development, homeostasis and disease. Development 2014; 141(8):1614-26.
4. Hayashi S, Yokoyama H, Tamura K. Roles of Hippo signaling pathway in size control of organ regeneration. Dev Growth Differ 2015; 57(4):341-51.
5. Boopathy GTK, Hong W. Role of Hippo Pathway-YAP/TAZ Signaling in Angiogenesis. Front Cell Dev Biol 2019; 7:49.
6. Mannaerts I, Leite SB, Verhulst S. The Hippo pathway effector YAP controls mouse hepatic stellate cell activation. J Hepatol 2015; 63(3):679-88.
7. Flinn MA, Jeffery BE, O'Meara CC, Link BA. Yap is required for scar formation but not myocyte proliferation during heart regeneration in zebrafish. Cardiovasc Res 2019; 115(3):570-77.
8. Rognoni E, Walko G. The roles of YAP/TAZ and the hippo pathway in healthy and diseased skin. Cells 2019; 8(5):411.
9. Chun Q, ZhiYong W, Fei S, XiQiao W. Dynamic biological changes in fibroblasts during hypertrophic scar formation and regression. Int Wound J 2016; 13(2):257-62.
10. Hsieh SC, Wu CC, Hsu SL, Yen JH. Molecular mechanisms of gallic acid-induced growth inhibition, apoptosis, and necrosis in hypertrophic scar fibroblasts. Life Sci 2017; 179:130-38.
11. Kim CL, Choi SH, Mo JS. Role of the hippo pathway in fibrosis and cancer. Cells 2019; 8(5):468.
12. Hansen CG, Moroishi T, Guan KL. YAP and TAZ: a nexus for Hippo signaling and beyond. Trends Cell Biol 2015; 25(9):499-513.

LETTER TO THE EDITOR

OLMESARTAN/VALSARTAN INDUCED GIANT ACHROMATIC CUTANEOUS MELANOMA: "MODIFIED" ONE-STEP SURGICAL APPROACH WITH FAVOURABLE OUTCOME

G. TCHERNEV[1,2] and I. TEMELKOVA[1,2]

[1]Department of Dermatology, Venereology and Dermatologic Surgery, Medical Institute of Ministry of Interior (MVR), Sofia, Bulgaria; [2]Onkoderma- Clinic for Dermatology, Venereology and Dermatologic Surgery, Sofia, Bulgaria

Received July 28, 2019 – Accepted September 13, 2019

To the Editor,

We present the case of a 74-year-old woman with arterial hypertension, diabetes mellitus, chronic kidney failure, gout and hypothyroidism. The patient was hospitalized for surgical removal of cutaneous tumor in the area of the right foot (Fig. 1a). The patient is familiar with and informed about her participation in the study and has signed informed consent. According to anamnestic data, the patient had a pigmented melanocytic nevus in the right foot area in 2012. In 2018 the lesion began crustily and progressively to increase in size. In a more detailed anamnestic history and according to the attached documentation for arterial hypertension the patient had taken olmesartan 10 mg x 1/daily from July 2017, but the onset of the olmesartan therapy is unknown; according to the patient's data its duration had been approximately 2-3 years (before July 2017). Subsequently, in the period July 2017 - September 2018, the patient passed to medication with valsartan with 320mg x1/ day. In October 2018 the drug was replaced with a combination preparation containing amlodipine/ valsartan 5 mg/160mg 2 x 1/per day, which the patient also accepted at the time of hospitalisation. In the framework of the dermatological examination on the medial part of the right foot, the presence of exophytic achromatic tumour formation with an erosive surface adjacent to a nevus-like lesion was observed (Fig. 1a). According to the patient, the transformation of the nevus to the tumour lesion presented in the past coincided with the onset of sartan therapy. Based on clinical and historical data, there was a suspicion of drug-induced giant acral cutaneous melanoma based on acquired acral located melanocytic nevus (Fig. 1a). MRT examination of the right foot was carried out with the conclusion of a superficial neoplastic cutaneous process without bone involvement (Fig. 1 b-c). Preoperative ultrasound measurement of tumor thickness was performed with tumor thickness significantly greater than 4 mm. Ultrasound diagnosis did not detect evidence for pathologically increased locoregional (inguinal) lymph nodes. The chest radiography was normal, and the abdominal ultrasound found liver steatosis, chronic pyelonephritis and left kidney cyst. Additionally, LDH (163.0 U / l) and protein S-100 were tested, which were in the reference range. Based on the preoperative ultrasound data for a tumor over 4 mm thick and the lack of pathologically

Key words: drug induced melanoma; sartans; olmesartan induced skin cancer; olmesartan induced melanoma; on step melanoma surgery

Corresponding Author:
Prof. Georgi Tchernev,
Department of Dermatology,
Venereology and Dermatologic Surgery,
Medical Institute of Ministry of Interior (MVR),
General Skobelev 79, 1606 Sofia, Bulgaria
e-mail: georgi_tchernev@yahoo.de

0393-974X (2019)

DISCLOSURE: ALL AUTHORS REPORT NO CONFLICTS OF INTEREST RELEVANT TO THIS ARTICLE.

enlarged lymph nodes, a decision was made to conduct a one-step melanoma surgery (OSMS) with a wider field of surgical safety without removal of the sentinel lymph node. The lesion was removed by an oval offset with a safety margin of 1.5 cm in all directions according the rules of ″modified″ one-step melanoma surgery (OSMS) in view of the patient's desire for a better cosmetic result and an optimal recovery of the defect (anamnestic diabetes mellitus/ proximity to dorsalis pedis artery) following a signed operational agreement. The surgical defect was left for secondary healing, with reverdin plastics/flap being planned at a later stage (Fig. 1e). The post-operative histological examination of a removed tumor formation revealed nodular giant achromatic melanoma above 9 mm thick with ulcerations, and the subsequent immunohistochemical study confirmed the diagnosis of melanoma. Staging was performed, which showed melanoma stage IIC (T4bN0M0). PET scan, regular ultrasound control of the lymph nodes over a period of time and discontinuation of angiotensin receptor blocker therapy were planned.

Compared to AJCC recommendations for a thickness over 4 mm, the determination and removal of a draining lymph node is not mandatory and is recommended only in cases of preoperatively enlarged lymph nodes (1). Independently from this, surgical interventions are always two-primary

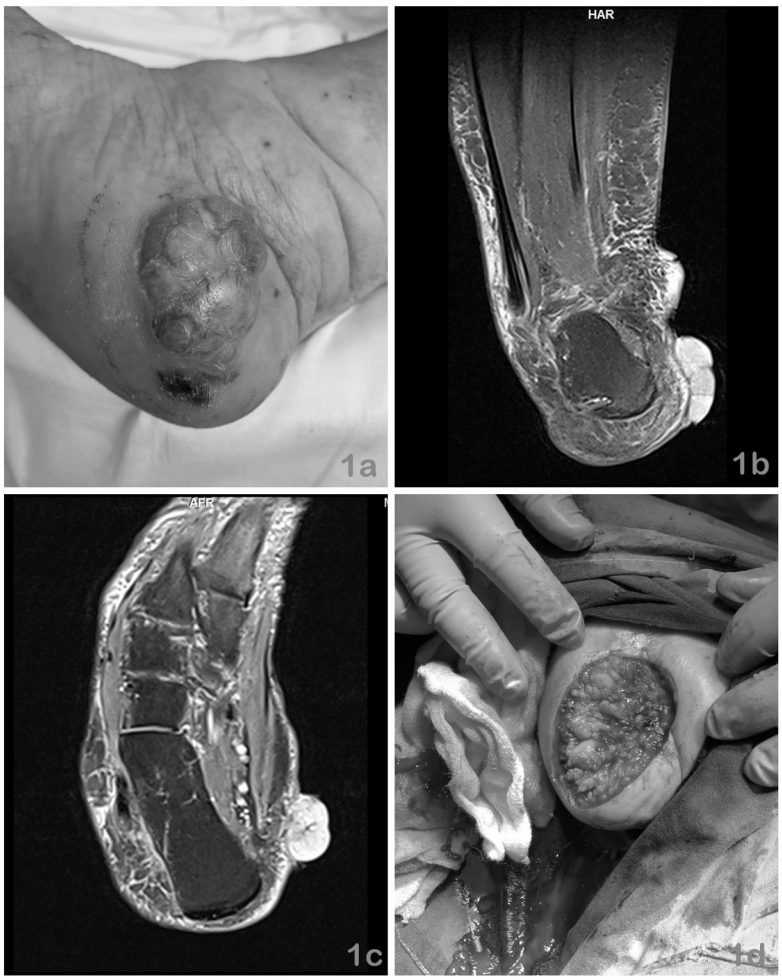

Fig. 1. ***a)*** *Clinical picture: giant tumour formation, located next to hyperpigmented macula in area of the right sole.* ***b-c)*** *Preoperative MRT: superficial neoplastic cutaneous process in the medial part of the right foot.* ***d)*** *Intraoperative view: elliptical excision of the lesion.*

excision with 0.5 cm in all directions and re-excision with an additional field of operative safety, depending on the postoperative histologically established tumor thickness (1). The advantages of OSMS/ modified OSMS in this case are i) the performance of preoperative ultrasound measurement of tumor thickness and subsequent choice of the correct safety margin, and ii) the need of a only one surgical intervention with a direct surgical safety field (2 cm at a thickness over 4 mm/OSMS rules) with the possibility for modification according to the patient's individual desire for a better aesthetic result (surgical margin from 1.5 cm in all directions with the purpose of creating optimal healing process, because of diabetes mellitus/diabetic polyneuropathy, microangiopathy) (2).

In previous papers we presented the possibility of drug induction of carcinogenesis as well as the development of melanoma based on the intake of angiotensin receptor blockers (valsartan and irbesartan) (4-8). We present a new case/or the second case of probable olmesartan/valsartan-induced giant acral achromatic melanoma, developing on the basis of acral located melanocytic nevus, considering/ examining the modified OSMS method as the most appropriate treatment approach.

REFERENCES

1. Swetter S, Tsao H, Bichakjian C, et al. Guidelines of care for the management of primary cutaneous melanoma. J Am Acad Dermatol 2019; 80(1):208-50.
2. Tchernev G, Temelkova I. Comparative analysis of the "scholastic" recommendations of the AJCC From 2011 for the surgical treatment of cutaneous melanoma with the newly suggested guidelines for OSMS from the Bulgarian Society For Dermatologic Surgery! Open Access Maced J Med Sci 2018; 6(12):2369-72.
3. Tchernev G, Temelkova I, Stavrov K. One Step Melanoma Surgery (OSMS) without using ultrasonography for preoperative tumour thickness measurement? - "A question that sometimes drives me hazy: am I or are the others crazy!" Open Access Maced J Med Sci 2018; 6(6):1085-90.
4. Tchernev G, Temelkova I. Drug-induced melanoma: irbesartan induced cutaneous melanoma! first description in the world literature! Open Access Maced J Med Sci 2019;7(1):114-16.
5. Tchernev G, Temelkova I. Irbesartan induced cutaneous melanoma! Second case in the medical literature! Open Access Maced J Med Sci 2019;7(1):121-23.
6. Tchernev G, Temelkova I. Valsartan induced melanoma?! First description in medical literature! Open Access Maced J Med Sci 2018;6(12):2378-2380.
7. Tchernev G, Temelkova I. Additional 4 cases of valsartan/irbesartan-induced melanomas? J Biol Regul Homeost Agents 2019; 33(3):911-912.
8. Tchernev G, Temelkova I. Valsartan/hydrochlorothiazide induced prostate carcinoma in a patient who subsequently developed melanoma. J Biol Regul Homeost Agents 2019; 33(4):1125-27.

JOURNAL OF BIOLOGICAL REGULATORS & HOMEOSTATIC AGENTS Vol. 33, no. 6, 1779-1782 (2019)

LETTER TO THE EDITOR

ANTI-HYPERTENSIVE AND ANTI-OXIDATIVE IMPACT OF PROBIOTIC CULTURES IN CHEDDAR CHEESE

M.A. UR REHMAN[1], M.A. MURTAZA[1*], I. HAFIZ[2], M.A. SHABBIR[3], R. ARSHAD[3] and M.A. FAROOQ[4]

[1]Institute of Food Science and Nutrition, University of Sargodha, Sargodha, Pakistan; [2]Department of Chemistry, University of Sargodha, Sargodha, Pakistan; [3]National Institute of Food Science and Technology, University of Agriculture, Faisalabad, Pakistan; [4]School of Food Science and Engineering, South China University of Technology, Guangzhou, China

Received May 27, 2019 – September 19, 2019

To the Editor,

Public awareness about diet and health have increased the demand for functional foods. Many food products, including cheese, yogurt, frozen fermented dairy desserts, ice cream, dried yogurt (frozen) and fruit juices, are being marketed with probiotic strains to ensure health. Probiotic foods have been associated with certain health benefits in cancer, high blood cholesterol, lactose intolerance, diarrhea and immunity disorders (1).

In dairy products, a supportive environment is provided to probiotic strains for their proper growth and viability. Cheddar cheese is characterized with higher pH, more solid and fat consistency and higher buffering capacity as compared to yoghurt and other fresh fermented dairy products. Therefore, it has the most effective probiotic delivery system to gastrointestinal tract (2). In Cheddar cheese, during storage, a series of biochemical reactions takes place including glycolysis, citrate catabolism, lipolysis and proteolysis. These reactions are responsible for flavor development and metabolism of fatty acids and amino acids resulting in peptide formation. During proteolysis, different bioactive peptides are generated that are particular protein fragments which express hormone- or drug-like activity in the human body. Therapeutic potential of bioactive peptides is associated with their high bio-functionality and bio-specificity to targets, low levels of toxicity, structural diversity and less accumulation in body tissues (3).

The composition and sequence of inherent amino acids are the base of peptide activity. Milk-based bioactive peptides include bioactivities such as opioid, anti-thrombotic, anti-hypertensive, immune-modulating, anti-oxidative, anti-microbial, anti-cancer, mineral reserving and growth inducing functions (4). Thus, keeping in mind the potential benefits of probiotic Cheddar cheese, this study was designed to characterize the *in-vitro* anti-oxidant and anti-hypertensive activities of the water soluble extracts from probiotic Cheddar cheese.

MATERIALS AND METHODS

Raw Buffalo milk was purchased from a local dairy market in Sargodha-Pakistan. Cheddar cheese starter cultures (*L. Lactis subsp. Cremoris* and *L. Lactis subsp. Lactis*) and *Lactobacillus acidophilus*, and *Bifidobacterium bifidum* (probiotic cultures) were purchased from Chr. Hansen Ireland Ltd. (Ireland). The

Key words: bioactive peptides; probiotics; anti-oxidant; anti-hypertensive

Corresponding Author:
Mian Anjum Murtaza, PhD
Institute of Food Science and Nutrition,
University of Sargodha,
Sargodha, 0100, Pakistan
Tel.: +92 300 6625503
e-mail: anjum.murtaza@uos.edu.pk

0393-974X (2019)

rennet (chymosin) of 50000 u/G strength was bought from Pharm Chemical Co., Ltd. China.

Three samples of probiotic Cheddar cheese were prepared, including one control (Mesophilic Cheddar cheese starter cultures only) and two with probiotic strains (La: Mesophilic cheese starter + *Lb. acidophilus* and Bb: Mesophilic cheese starter + *Bifidobacterium bifidum*). Cheddar cheese was developed according to the method described by Rehman et al. (5) with some modifications. Ripening of the cheese was carried out at 6-8°C for 180 days. Probiotic Cheddar cheese was analyzed for physico-chemical analysis (moisture, fat, protein, ash, pH, acidity, salts and mineral content), organic acid determination, quantification of proteolysis, texture profile analysis, bacterial survival in cheese and sensory evaluation in the period 60 to 180 days.

Quantification of proteolysis

The method of Rulikowska et al. (6) was used to quantify proteolysis in probiotic Cheddar cheese during ripening after 30 day intervals using high performance liquid chromatography (HPLC). An aliquot of 20 mL was injected into Shimadzu liquid chromatograph (LC-10 AT VP Series, Shimadzu Corporation, Kyoto, Japan) with a UV/Vis detector at 214 nm (Shimadzu Corporation, Kyoto, Japan).

Anti-oxidant and anti-hypertensive activities of peptides

The scavenging activities of water soluble peptide extract were evaluated according to the method described by Apostolidis et al. (7). Anti-hypertensive activity was assayed based on the release of hippuric acid in hippuryl-histidyl-leucine (HHL) catalyzed by angiotensin converting enzyme (ACE). The activity was measured by a spectrophotometer at the wavelength of 228 nm (8).

Statistical analysis

The resultant data was analyzed statistically by using Minitab statistical package at $p<0.05$ confidence level and Tukey's test was used for multiple comparisons between means values.

RESULTS

Quantification of proteolysis

Table 1-2 showed that The ripening period and probiotic cultures havd highly significant ($p < 0.01$) impact on the water soluble nitrogen (WSN) as percentage of total nitrogen (TN) and total free amino acids (TFAA) (Tables I, II). Proteolysis in probiotic Cheddar cheese samples was quantified at 0, 30 and 60 days of ripening at 8°C by determination of WSN/TN and TFAA. The ratio of WSN to TN and free amino acid in all samples increased progressively, but the maximum increase in WSN was observed in the Cheddar cheese containing *Lactobacillus acidophilus*, whereas the sample containing *Bifidobacterium bifidum* showed the maximum free amino acids on the 60th day of the ripening period.

Anti-oxidative activity of peptides

A highly significant ($p<0.01$) effect of the ripening period and treatments was observed on the anti-oxidative activity of bioactive peptides (Table III). Anti-oxidative activity of water soluble extracts of probiotic Cheddar cheese samples was accessed at 60, 120 and 180 days of ripening. Maximum anti-oxidative activity (37.2%) was found in probiotic Cheddar cheese containing *Lactobacillus acidophilus* while the control sample showed the lowest anti-oxidative activity on 180th day of ripening.

Anti-hypertensive activity

ACE inhibitory peptides are claimed to decrease the vasoconstrictor peptide level, therefore they have a tendency to modulate blood pressure and impart an anti-hypertensive effect. The results presented in Table IV indicate that the ripening period and probiotic cultures have a highly significant ($P<0.01$) impact on the ACE-inhibitory activity of bioactive peptides. During the ripening, probiotic Cheddar cheese containing *Bifidobacterium bifidum* showed the highest (101.7%) ACE inhibitory activity compared to the control.

DISCUSSION

The increase in proteolytic activity may be due to the probiotic strains that have higher casein hydrolytic ability, which contribute to the release of more water soluble peptides. However, during ripening, the increase in nitrogen content was due

Table I. *Water soluble nitrogen (%) in Cheddar cheese during proteolysis.*

Treatment	Storage			Means
	0	30	60	
Control	5.18±0.19	8.49±0.16	11.91±0.40	8.53±0.98B
La	5.80±0.17	8.93±0.23	12.85±0.47	9.19±1.03A
Bb	5.24±0.15	8.74±0.08	12.67±0.44	8.88±1.08AB

Table II. *FAA content (%) in Cheddar cheese during proteolysis.*

Treatment	Storage			Means
	0	30	60	
Control	1328.0±21.9	1738.3±67.3	2204.3±24.0	1756.9±128.4D
La	1559.7±21.1	1922.0±39.8	2510.0±25.4	1997.2±139.3C
Bb	1650.0±28.3	2020.3±27.4	2639.0±130.5	2103.1±149.5AB

Table III. *Anti-oxidant capacity of probiotic Cheddar cheese.*

Treatment	Storage (days)			Means
	60	120	180	
Control	8.7±0.43	28.6±1.10	33.5±1.16	23.6±2.17
La	12.7±1.55	31.6±0.97	37.2±1.03	27.2±2.16
Bb	10.2±0.45	31.2±1.27	34.9±1.53	25.4±2.23

Table IV. *Anti-hypertensive capacity of probiotic Cheddar cheese.*

Treatment	Storage (days)			Means
	60	120	180	
Control	54.3±1.12	76.0±1.28	88.8±1.72	73.0±2.29E
La	71.7±1.36	87.5±1.43	99.6±1.30	86.3±1.89D
Bb	74.7±1.39	90.1±1.07	101.7±1.10	88.8±1.80C

to the continuous breakdown of casein into smaller peptides and amino acid fractions. This breakdown is facilitated by starter cultures, non-starter lactic acid bacteria (NSLAB), certain enzymes and residual rennet. One study also concluded that the nitrogen content tended to increase with the ripening period due to the continuous breakdown of casein by the action of starter cultures, non-starter lactic acid bacteria (NSLAB), certain enzymes and residual rennet (9). Moreover, certain strains, including *L. acidophilus, L. casei*, and *L. paracasei,* are reported to release minute quantities of peptides and free amino acids (FAA) due to their proteolytic nature.

Anti-oxidative peptides are capable of inhibiting the formation of free radicles. The degree of ripening and the rate of soluble peptide production in cheeses are directly related to the anti-oxidative activity (10). The anti-oxidative activity of peptides is due to phenolic amino acids, such as tyrosine or phenylalanine, or the presence of Leu-Leu-Pro-His-His within the peptide sequence. The anti-oxidative activity and peptide sequence relationship leads to the formation of extremely effective anti-oxidative peptides that could potentially be used in various food applications (11).

Several studies have confirmed that ACE

inhibitory activity of water soluble cheese extracts are influenced by the ripening period. During one study, higher ACE-inhibitory activities of probiotic adjuncts were noted as compared to control cheese after few weeks of ripening at 4 and 8ºC. Moreover, it has been reported that total peptide levels in cheese extracts increased approximately five-fold over four weeks of ripening (12).

ACKNOWLEDGEMENTS

The authors are grateful to the Higher Education Commission of Pakistan for providing funds and the Department of Biological Systems and Engineering, University of Wisconsin Madison, USA, for providing some research facilities and technical support.

REFERENCES

1. Altahir MOE, Elgasim EA, Ahmed IAM. Ripening of Sudanese braided (Muddaffara) cheese manufactured from raw or pasteurized milk: Effect of heat treatment and salt concentration on the physicochemical properties. Int J Food Sci 2014; Article ID 698263: 1-7.
2. Martinez-Villaluenga C, Penas E, Frias. Bioactive peptides in fermented foods, production and evidence for health effects. Elsevier Inc. 2017.
3. Mohanty DP, Mohapatra S, Misra S, Sahu PS. Milk derived bioactive peptides and their impact on human health. A review. Saudi J Biol Sci 2016; 23:577-83.
4. Sah BNP, Vasiljevic T, McKechnie S, Donkor ON. Antioxidative and antibacterial peptides derived from bovine milk proteins. Crit Rev Food Sci Nutr 2018; 58:726-40.
5. Rehman SU, McSweeney PLH, Banks JM, Brechany EY, Muir DD, Fox PF. Ripening of Cheddar cheese made from blends of raw and pasteurized milk. Int Dairy J 2000; 10:33-44.
6. Rulikowska A, Kilcawley KN, Doolan IA, Alonso-Gomez M, Nongonierma AB, Hannon JA, Wilkinson MG. The impact of reduced sodium chloride content on Cheddar cheese quality. Int Dairy J 2013; 28:45-55.
7. Apostolidis E, Kwon YI, Shetty K. Inhibitory potential of herb, fruit, and fungal-enriched cheese against key enzymes linked to type 2 diabetes and hypertension, Innov Food Sci Emerg Technol 2007; 8:46-54.
8. Cushman DW, Cheung HS. Spectrophotometric assay and properties of the angiotensin-converting enzyme of rabbit lung. Biochem Pharmacol 1971; 20:1637-48.
9. Adouard N, Magne L, Cattenoz T, Guillemin H, Folign B, Picque D, Bonnarme P. Survival of cheese-ripening microorganisms in a dynamic simulator of the gastrointestinal tract. Food Microbiol 2016; 53:30-40.
10. Kesenkaş H, Gursoy O, Ozbaş H. Kefir. Fermented Foods Health and Disease Prevention 2017; 339-61.
11. Nazari F, Delborde Y, Karimitabar Z, Ranjbar A, Alikhani MY. Antioxidant Effect of Lactobacillus acidophilus as a probiotic at different time intervals. Avicenna. J Clin Microbiol Infection 2016; 3:10-12.
12. Mushtaq M, Gani A, Masoodi FA. Himalayan cheese (Kalari/Kradi) fermented with different probiotic strains: In vitro investigation of nutraceutical properties. LWT 2019; 104:53-60.

LETTER TO THE EDITOR

EFFECTS OF TRANSIENT RECEPTOR POTENTIAL CHANNEL 1 ON CARDIAC FIBROSIS IN SALT-SENSITIVE HYPERTENSIVE RATS

Z. YU[1] and Y. CHEN[2]

[1]Department of Cardiology, Affiliated Hangzhou First People's Hospital, Zhejiang University School of Medicine, Hangzhou, China; [2]Department of Neurology, Affiliated Hangzhou First People's Hospital, Zhejiang University School of Medicine, Hangzhou, China

Received April 4, 2019 – Accepted September 19, 2019

To the Editor,

High salt diets are taken as a dangerous factor of hypertension. The increased blood pressure caused by high salt diets is known to develop hypertension (1). Ventricular remodeling and cardiac fibrosis are the main pathophysiological characteristics of cardiovascular disease (CVD). A recently conducted research reported that a high salt diet affects renal fibrosis through adjusting the expression levels of endothelin and transforming growth factor beta-1 (TGF-β1)/Smad pathway (2). Another study indicated that high salt may adjust the level of Rho-associated protein kinase (ROCK), thereby influencing the myocardium fibrosis (3). Transient receptor potential (TRP) channels are important mediators of sensory signals with marked effects on cellular functions and signaling pathways (4) and are also commonly expressed in major organs of the human body (5). Similarly, Ca^{2+} plays a significant role in maintaining physiological functions of the cardiovascular system. Together with other membrane receptors and ion channels, TPR channels simultaneously adjust the concentration of Ca^{2+} in cells (6). The abnormality of ion channels is related to SSH to some extent, however, the relationship between TRPC1 and SSH, TRPC1, and cardiac fibrosisstill remains elusive. Therefore, this study aimed to explore the correlation between CVD, SSH, and TRPC.

MATERIALS AND METHODS

Animals

A total of 32 male specific pathogen-free (SPF) Wistar rats (age, 7 weeks old; body weight, less than 250 g) were purchased from SPF (Beijing) Biotechnology Co., Ltd. All rats were fed under a temperature of (25±1) °C, a relative humidity of (50±3) %, and a 12h-12h light-dark cycle. The experiment started after 1-week adaptation. The administration and treatment of rats during this study were in accordance with the regulations for the protection of experimental animals and the protocol was approved by ethics committee of Affiliated Hangzhou First People's Hospital.

Establishment of animal models

After 1-week adaptive feeding, 32 male Wistar rats were randomly divided into a control group (Group C, n=8) and a high-salt group (n=24). The basic blood pressure of the rats was measured. Rats in Group C were given normal diet (0.5% NaCl) for 14 weeks. By referring to the feeding method of human salt-sensitive hypertension (7, 8), rats in the high-salt group were fed by 8% NaCl.

Key words: salt-sensitive hypertension; TRCP1; cardiac fibrosis; ventricular remodeling

Corresponding Author:
Dr Yan Chen,
Department of Neurology,
Affiliated Hangzhou First People's Hospital,
Zhejiang University School of Medicine,
No. 261 Huansha Road, Hangzhou, 310066, China
e-mail: chenyan_hz01@126.com

0393-974X (2019)

After 8-week feeding, those rats whose systolic blood pressure (SBP) increased by more than 10% (and ≥ 140 mmHg) were initially subdivided into SSH group (n=11). Additionally, the rats were fed by 0.3% NaCl for another 2 weeks, and those rats whose SBP decreased by more than 5% compared with the value at the 8th week were classified into SSH group (Group A, n=7). The remaining 4 rats were removed from the study. After 8-week feeding, rats left in the high-salt group (non-SSH rats, n=13) were fed by high-salt diets for 2 consecutive weeks. Those rats whose SBP increased by less than 5% compared with the basic blood pressure (and < 140 mmHg) were classified into a salt-resistant normotensive (SRN) group (Group B, n=7). The remaining 6 rats were eliminated from the data analysis. Rats in both Group A and Group B were fed with high-salt diets for 4 consecutive weeks. The SBP was measured every 2 weeks, and the average of three measurements was taken. After 14 weeks, the body weight of rats in different groups was as follows: Group A, 449.92±57.28 g; Group B, 413.53±18.37 g; and Group C, 381.22±50.18 g.

The formula of the rat feed was barley flour, dried cabbage, soy flour, yeast, bone meal, cornflour, bran, and fish meal, which were purchased from Jiangsu Xietong Pharmaceutical Bio-engineering Co., Ltd., China.

Sample collection

At the end of the 14th week of feeding, the data related to rat samples were collected. The rats were anesthetized with 7% chloral hydrate solution through intraperitoneal injection. The fur in the thoracoabdominal area of the rat was shaved for operation. The thoracic cavity and the abdominal cavity of the rat were then cut open and the hearts were excised rapidly and were immediately placed in an ice-cold phosphate-buffered saline (PBS). Fat tissues around the heart were also eliminated. Both the left and right ventricular myocardium with the size of approximately 0.5 cm^3 were cut and placed in the EP tubes. The tubes were then maintained at -80□ until use for Western blot analysis; samples of rat blood (0.5 cm^3) were taken from the tail vein; 24 h later, tissues were embedded in paraffin for immunohistochemistry analysis.

Masson's trichrome staining

The paraffin block was placed in the microtome for preparation of sectioning, which was treated by the Masson staining kit (Beijing Leagene Biotech, China) according to themanufactuer's instructions. After standard dewaxing, the tissue sections were dyed with celestine blue for 3 min, washed, and stained with hematoxylin and eosin (H&E) for 3 min. Then, the sections were differentiated by acid ethanol for 2 s, and were then washed with running water for 10 min. Next, the sections were dyed with Ponceau-Fuchsin solution for 6 min and were then washed with double distilled water. The sections were soaked in a phosphomolybdic acid solution for 2 min. Afterwards, the upper solution was discarded. The sections were dyed with aniline blue for 5 min, and soaked in the weak acid solution for 2 min. Next, the sections were dehydrated by gradient ethanol, processed with xylene till transparent, sealed with neutral balsam, and dried in the air. The staining effects were observed under an optical microscope. The collagen fiber was blue, the muscle fiber was red, and the nucleus was blue purple.

Immunohistochemistry

The tissue was sectioned on a paraffin microtome at 4 μm thickness. Then, the sections were pit onto glass slides and placed in an oven and baked for 1 h at 60°. Afterwards, the sections were dewaxed, hydrated, and soaked in 3% hydrogen peroxide solution for inactivation of endogenous enzyme. After that, the sections were washed with PBS three times 3 min each time. Next, the tissue sections were blocked with goat serum for 40 min at room temperature. The TRP channel-1 antigen (Sigma, USA) was diluted in a ratio of 1:500. Then, the diluted solution was dripped onto the tissue sections. The sections were incubated overnight at 4°C. Next day, the incubated sections were taken out and baked at 37° for 30 min. Later, the sections were washed three times with PBS solution for 3 min each time. The tissue sections were dripped with Streptavidin Peroxidase Immunohistochemistry reagent (Beijing ZSGB Biotechnology, China) for the immunohistochemistry and then incubated for 30 min at room temperature. Then, the sections are washed thrice with PBS for 3 min each time. The tissue sections were dripped with horseradish peroxidase streptavidin for the immunohistochemistry and incubated for 15 min at 37°C. The 3,3'-diaminobenzidine (DAB) was diluted at a ratio of 1:50 and dripped onto the tissue sections. Then, the tissue sections were observed under a microscope; 10 s later, as soon as the dark brown color at the targeted

spot was observed, the sections were immediately rinsed with double distilled water to terminate the reaction. Next, the tissue sections are washed for 15 min with tap water. Afterwards, the sections were re-stained with H&E, gradient dehydrated, processed till they became transparent, and sealed. Image-Pro Plus 6.0 software was applied to analyze the images. The mean optical density (MOD) on each image was calculated by Image-Pro Plus 6.0 software, and the average of MOD for 5 images from different views of one section was considered as the MOD of the section.

Western blot

The total protein extraction kit (Shanghai Kalang Biotechnology, China) was used for extraction of the total protein. The Bicinchoninic Acid (BCA) protein assay kit was used for drawing the standard protein curve. DU-800 was employed to detect the light-absorbency and calculate the protein content of each sample under a wavelength of 562nm. The protein content was adjusted in accordance with the result, and the sample was stored at -80°C. The sample protein solution was mixed with 2×sampling buffer of an equal volume and underwent 100°C denaturalization for 3~5min. Then, the protein was separated by SDS-PAGE (7.5% separating gel and 5% stacking gel) (WB gel production reagent kit, Shanghai Beyotime Biotechnology, China). After electrophoretic separation, the protein was transferred at a constant voltage to Polyvinylidene Fluoride (PVDF) membranes. In accordance with the molecular weight of the pre-stained standard protein, the targeted protein-membrane under the molecular weight was cut and enclosed with 3% Bovine Serum Albumin (BSA) for 1.5 h. Each membrane was incubated with the primary antibody formulated by blocking solution (TRPC1 antibody, mouse anti-human type I collagen antibody, mouse anti-human type III collagen antibody, Chondrex, USA) at 4°C overnight. Afterward, the membranes were washed three times with PBS-Tween-20, 10 min each time. After addition of the horseradish peroxidase (HRP)-labeled secondary antibody formulated by the blocking solution, the membranes were incubated at room temperature for 1 h. Consequently, the protein membranes were washed, added with the exposure solution, and placed under the exposer for development. Gray values of the developed WB membranes were detected and analyzed by Image Lab 4.0, and protein expressions of different groups were compared.

Statistical analysis

All the data were analyzed with SPSS 21.0 software (IBM, Armonk, NY, USA), and they were expressed as mean ± standard deviation ($\bar{x}\pm s$). For inter-group comparison, one-way analysis of variance was applied, and $P<0.05$ was considered statistically significant.

Table I. *Variations in the blood pressure of rats.*

Experimental Period	Group A	Group B	Group C
0 Weeks	130.26±5.13	127.53±9.65	125.76±5.22
2 Weeks	132.46±8.24	129.14±7.73	126.35±8.16
4 Weeks	154.16±12.17*&	122.53±11.37	121.13±6.46
6 Weeks	146.11±8.36&	136.51±12.27	127.63±7.18
8 Weeks	155.74±10.26*&	124.27±7.36	125.26±8.02
10 Weeks	125.14±9.13#	129.67±6.25	121.27±10.11
12 Weeks	151.22±8.53*&	121.59±13.77	122.98±6.42
14 Weeks	164.14±10.64*&	126.03±10.16	117.26±6.38

*Note: *P<0.01, comparison between Group A and Group C. &P<0.01, comparison between Group A and Group B. #P<0.01, comparison of the blood pressure at 10 weeks and 8 weeks.*

RESULTS

Variations in the blood pressure among the three groups of rats are shown in Table I. There was no significant difference in blood pressure between Group C and Groups A and B before the high-salt diet (P>0.05). After 8 weeks of high-salt feeding, there was no significant difference in the SBP of rats between Group B and Group C (P>0.05). However, compared with Group C, the SBP of rats in Group A increased significantly (P<0.01). After 2 weeks of salt reduction feeding in Group A, the SBP of rats was significantly reduced compared with before (after 8 weeks of high-salt feeding) (P<0.01). Then rats in Groups A and B continued to receive 8% NaCl high-salt diet for another 4 weeks, and those in Group C received normal diet until the 14th week. At the end of the 14th week, the caudal arterial SBP of rats in Group A increased significantly compared with Group C (P<0.01). There was no significant difference in caudal arterial SBP between Group B and Group C (P>0.05). The caudal arterial SBP of rats in Group A increased significantly compared with Group B (P<0.01).

Masson's trichrome staining (Fig. 1) showed that collagen fibers in the myocardium were increased in

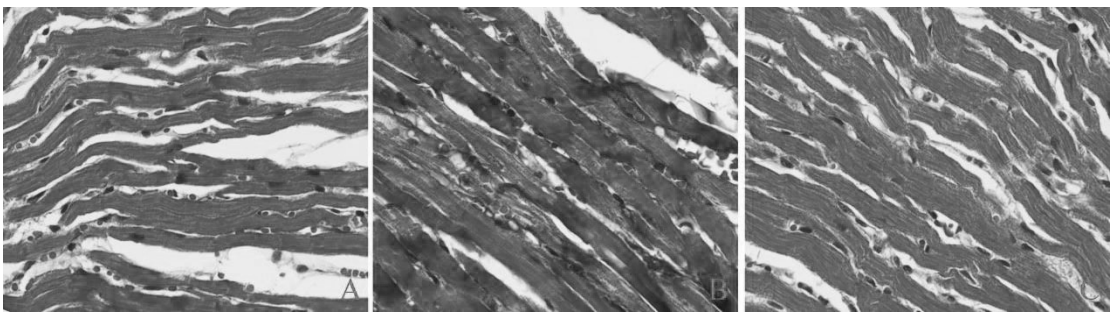

Fig. 1. *Myocardium collagen expressions of rats in each group. **A**) Group A; **B**) Group B; **C**) Group C. (×400)*

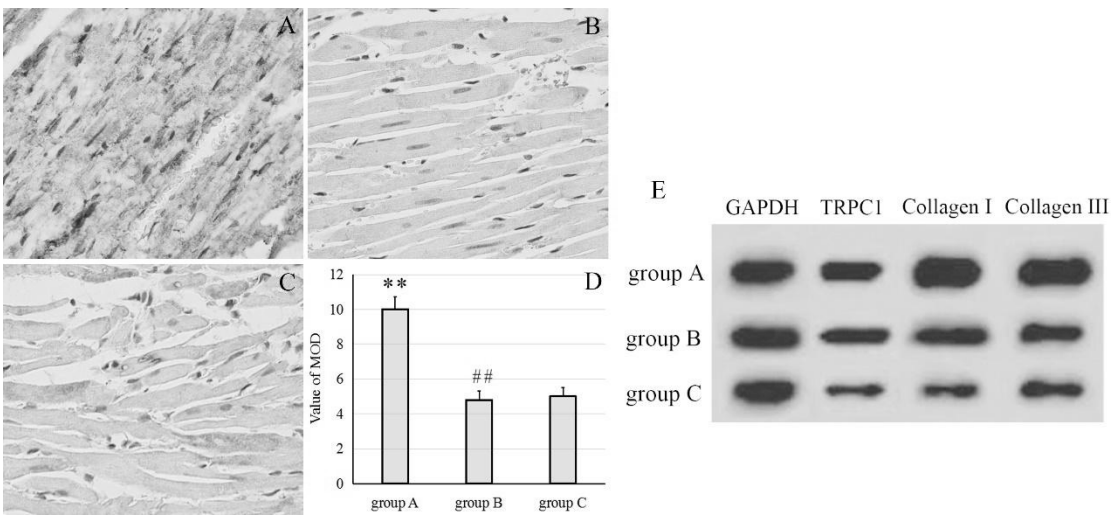

Fig. 2. *The immunohistochemistry results of rats in each group. **A**) Immunohistochemistry image for Group A; **B**) immunohistochemistry image for Group B; **C**) immunohistochemistry image for Group C; **D**) immunohistochemistry results for each group; **E**) The expressions of myocardium TRPC1, Collagen I, and Collagen III in each group. **P<0.01, comparison between Group A and Group C. ##P<0.01, comparison between Group B and Group A.*

Group A compared with Group C, while they were decreased in Group B compared with Group A; however, there was no significant difference between Group B and Group C.

Immunohistochemistry

Compared with Group B (4.81±0.53) and Group C (5.02±0.51), the expression of TRP channel-1 in the myocardium of Group A (10.02±0.71) was notably increased (Group A *vs* Group C, P<0.05; Group A *vs* Group B, P<0.05). However, there was no remarkable difference between Group B and Group C in terms of the expression of TRP channel-1 in the myocardium (P>0. 05) (Fig. 2A-D).

Expressions of TRPC1, Collagen I, and Collagen III

Western blot was used to detect the expression levels of TRPC1 in the myocardium. Compared with Group C, the TRPC1 expression of Group A increased significantly (P<0.01); however, fed by high-salt feeds, the myocardium TRPC1 expression of Group B decreased sharply compared with that of Group A (P<0.01). No significant difference was found between Group B and Group C in terms of TRPC1 expressions (P>0.05) (Fig. 2E; Table II). Therefore, the expression levels of TRPC1 was related to the salt-sensitivity instead of sodium concentration in the diet.

Furthermore, the expression levels of myocardium Collagen I and Collagen III of Group A increased sharply compared with that of Group B and C (Group A *vs* Group C, P<0.05; Group A *vs* Group B, P<0.05).

DISCUSSION

The World Health Organization (WHO) suggests that the daily salt intake should be 6 g; however, in most places in China, the daily salt intake of residents far exceeds the standard which could be one of the factors that cause the high incidence and low disease control rate of hypertension in China. Moreover, high-salt diet and salt-sensitivity is an independent dangerous factor of hypertensive target organ damage. Due to the individual difference of salt-sensitivity, the risk of stroke and CVD of salt-sensitive individuals increases sharply under a high-salt diet (9, 10). However, the mechanisms of SSH attacks and SSH target organ damage are complicated and not yet completely explained.

In the present study, the myocardium TRPC1 expression level of rats in Group A increased after being fed with high-salt diet, while compared with Group A, the TRPC1 expression level of rats in Group B was relatively low regardless of the last 4-week high-salt feeding. Therefore, this further proves that the high expression level of TRPC1 is related to salt-sensitivity. Results of the experiment show that the myocardium TRPC1 expression level of SSH rats sharply increases, which may be related to the level of myocardium fibrosis.

In summary, TRPC1 may participate in myocardium fibrosis in SSH rats.

Table II. *The relative expression levels of myocardium TRPC1, Collagen I, and Collagen III in each group.*

Groups	Group A	Group B	Group C
TRPC1	0.98±0.06**	0.51±0.05##	0.53±0.05
Collagen I	1.69±0.21**	0.69±0.18##	0.71±0.11
Collagen III	1.48±0.37*	0.91±0.14#	0.83±0.06

*Note: *P<0.05, comparison between Group A and Group C. #P<0.05, comparison between Group B and Group A. **P<0.01, comparison between Group A and Group C. ##P<0.01, comparison between Group B and Group A.*

REFERENCES

1. Komatsu R. Salt-sensitive hypertension in circadian clock-deficient Cry-null mice involves dysregulated adrenal Hsd3b6. Nat Med 2010; 16(1):67-74.
2. Feng W, Chen B, Xing D, et al. Haploinsufficiency of the transcription factor Ets-1 is renoprotective in Dahl salt-sensitive rats. J Am Soc Nephrol 2017; 28(11):3239-50.
3. Liu S, Liu LX, Zhang YL, et al. Cardiac ablation of SOCS3 aggravates DOCA-salt-induced hypertrophic remodeling by activation of Gp130-dependent signaling in mice. Cell Physiol Biochem 2018; 47(1):140-50.
4. Wang Y, Wang DH. A novel mechanism contributing to development of Dahl salt–sensitive hypertension role of the transient receptor potential vanilloid Type 1. Hypertension 2006; 47(3):609-14.
5. Ma Y, Sugiura R, Koike A, Ebina H, Sio SO, Kuno T. Transient receptor potential (TRP) and Cch1-Yam8 channels play key roles in the regulation of cytoplasmic Ca2+ in fission yeast. PLoS One 2011; 6(7):e22421.
6. Zhang B, Jiang J, Yue Z, et al. Store-Operated Ca2+ Entry (SOCE) contributes to angiotensin II-induced cardiac fibrosis in cardiac fibroblasts. J Pharmacol Sci 2016; 132(3):171-80.
7. He FJ, Macgregor GA. Salt and sugar: their effects on blood pressure. Pflugers Arch 2015; 467(3):577-86.
8. Ueda K, Nishimoto M, Hirohama D, et al. Renal dysfunction induced by kidney-specific gene deletion of Hsd11b2 as a primary cause of salt-dependent hypertension. Hypertension 2017; 70(1):111-18.
9. Polonia J, Monteiro J, Almeida J, Silva JA, Bertoquini S. High salt intake is associated with a higher risk of cardiovascular events: a 7.2-year evaluation of a cohort of hypertensive patients. Blood Press Monit 2016; 21(5):301-6.
10. Borah PK, Sharma M, Kalita HC, et al. Salt-sensitive phenotypes: A community-based exploratory study from northeastern India. Natl Med J India 2018; 31(3):140-45.

LETTER TO THE EDITOR

EXPLORATION OF THE RELATIONSHIP BETWEEN DNA METHYLTRANSFERASE 1 AND LUNG CANCER SCREENING

DG. YIN[1], B. YAN[1] and K. FENG[2]

[1]Department of Thoracic Surgery, Xixi Hospital, Hangzhou, China; [2]Department of Thoracic Surgery, First Hospital, Fuyang District, Hangzhou, China

Received May 16, 2019 – Accepted October 2, 2019

To the Editor,

One of the most common malignant tumors in the world is lung cancer (1), of which non-small cell lung cancer (NSCLC) accounts for more than 80%, mainly including adenocarcinoma, squamous cell carcinoma (SCC), large cell carcinoma (LCC) and adenosquamous carcinoma (ASC). In fact, its morbidity and mortality are among the highest in the world, and its treatment is still dominated by surgery (2). The role of epigenetics in the occurrence and development of non-small cell lung cancer has been given increasing attention by researchers (3).

In recent years, along with the progress of molecular biology, genetics and other disciplines, epigenetics has become the focus of studies on lung cancer, including genomic DNA methylation, non-coding RNA regulation (miRNA) and histone modification (4). DNA methylation has played an important role in the progression of lung cancer (5). The correlation between DNA methylation and histone modification in gene silencing has been indicated, suggesting that treatment with DNMT and histone deacetylase (HDAC) inhibitors can restore the expression of silenced genes (6, 7). Moreover, some researchers have found that combined treatment of HDAC and DNMT inhibitor 5-Aza can inhibit cell proliferation in lung cancer cells (8).

In order to better understand the relationship between DNMTI and lung cancer cell screening in NSCLC, human lung adenocarcinoma cell lines A549 and H838 were selected as experimental samples. The samples were grouped according to different treatment methods, and then the expression level of DNMI was detected by relevant methods, so as to provide new ideas for possible clinical application.

MATERIALS AND METHODS

Cell culture and passage

Human lung adenocarcinoma cell lines A549 and H838 were purchased from Shanghai Jianglin Biotechnology Co., Ltd., China. The cell strain to be resuscitated was taken out from the crycontainer (Santn Instrument Co., Ltd, China), and quickly placed in a 37°C water bath, and the cryotube was continuously shaken to rapidly thaw the liquid which was then sucked into a 1.5 mL centrifuge tube and centrifuged at 1000 r/min for 5 min. After this, the supernatant was discarded, and the sediment in the tube was suspended in fresh medium. After being blown, suspended cells were inhaled into the culture flask, and placed in an incubator for cultivation after adding fresh medium to 4 mL. The culture dish was removed from the cell culture incubator (Santn Instrument Co., Ltd, China) and placed under a microscope to observe whether the cells were completely detached. After the cells were detached, the culture dish was placed on a sterile table again,

Key words: non-small cell lung cancer (NSCLC), DNMT1, A549 cell line, H838 cell line, cell proliferation

Corresponding Author:
Dr Kan Feng,
Department of Thoracic Surgery, First Hospital,
NO. 429 Beihuan Road,
Fuchun Town,
Fuyang District, Hangzhou, 311400, China
e-mail: fengkan1yy@126.com

0393-974X (2019)

DISCLOSURE: ALL AUTHORS REPORT NO CONFLICTS OF INTEREST RELEVANT TO THIS ARTICLE.

and 5 mL of the medium was aspirated by a disposable pipette to stop the digestion of the cells. These cells were continuously blown with a pipette about 50 times to uniformly disperse the cells. Ten mL of the medium was added to each of the prepared 5 culture dishes. Then, 1 mL dispersed cells were added to each culture dish. When the procedures above were completed, all culture dishes were timed and placed in a cell culture chamber.

Extraction of the total protein from cells

All the cells from which the protein was to be extracted were taken out of the cell culture incubator and placed on ice. The cells were then rinsed with PBS (phosphate buffered saline). After the cells were clean, 500 μL buffer was added. The cells were placed on an ice box at room temperature, and about half an hour later, 300 μL cell lysate was taken by a pipette and placed in a centrifuge tube. After the cells were lysed, the cells were scraped with a spatula and placed in a centrifuge tube, and then centrifuged for 10 min. The supernatant was removed with a 100 μL pipette (GeneCopoeia, China) and placed in a new centrifuge tube, which was finally placed in a cryocontainer at -80°C to prevent degradation of the cells at 4°C. The standard curve of cells was drawn, and 200 μL of BCA (bicinchoninic acid) working fluid was added to each well of the plate in accordance with the proportion. The sampled Elisa plate was placed in a 4°C incubator for 30 min, and then measured to read the absorbance at 570 nm. The protein standard curve was drawn based on the data obtained. The true sample protein concentration was obtained by the absorbance value of the sample at 570 nm and the standard regression equation calculated by the data.

Extraction of total DNA from cells

The cells were centrifuged for 5 min using the boiling method, and 300 μL sterile water was added to suspend the cells. The nucleic acid extract was added to the cells and boiled at a high temperature for 20 min. Centrifugation was carried out again according to the above-mentioned centrifugation conditions, the supernatant was taken after centrifugation, and electrophoresis was performed. The configured sample was added into 30 μL prepared Conversion Reagent solution (Shanghai Xinyu Biotechnology Co., Ltd, China), mixed and placed in the PCR instrument. 600 μL 1M-BindingBuffer was added to the mixture and mixed in the adsorption column (Molecular Devices, USA). Centrifugation was carried out for 30 s at 12,000 rpm. Finally, the liquid in the tube was discarded, and the adsorption column was recovered with a new collection tube; 200 μL M-Wash Buffer solution (Shanghai Xinyu Biotechnology Co., Ltd, China) was sucked out with a pipette and placed into the adsorption column in the collection tube. After centrifugation, the liquid was discarded and the adsorption column was put back into the collection tube. The adsorption column in the collection tube was placed in another centrifugal tube, and 10 μL M-Elution Buffer solution with a pH of 8.5 was absorbed by pipette into the center of the adsorption membrane. The solution was left at room temperature for about 2 min. After centrifugation for 1 min, the DNA was collected and stored at -20°C.

Detection of the DNMT1 gene expression in non-small cell lung cancer cells by RT-PCR

The lung cancer cell lines A549 and H838 in logarithmic growth phase were divided into four groups: control group, 5-Aza group, MS-275 (Entinostat) group and combined treatment group (5-Aza and MS-275). Epigenetic treatment was performed on each group of NSCLC cells according to the treatment requirements. The concentration of both drugs (5-Aza and MS-275) was 0.5 μmol/L. Total RNA for each group was extracted by Trizol method. 2 μg total RNA was used as the template, and the reverse transcription reaction system was prepared according to the instructions of Bestar qPCR RT Kit. The total system was 20 μL, and the first chain of cDNA was synthesized. The reaction conditions of the PCR (Nanjing Sunshine Biotechnology Co., Ltd, China) were as follows: 94°C for 2 min, 94°C for 20 s, 58°C for 20 s, 72°C for 20 s, 40 cycles. The conditions for the melting curve analysis: the temperature of 62-95°C. Three experiments were repeated for each set of samples. An Agilent Stratagene fluorescence quantitative PCR instrument Mx3000P was used for the fluorescence quantitative PCR experiment. The sequence of the target gene was: DNIT1 gene length: 143bp, the primer sequence: 5-AGGACTAGTTCTGCCCTCCC-3 (upstream), 5-ACAGCTTCATGTCAGCCAAG-3 (downstream);

β-actin gene length: 216bp, the primer sequence: GGCATCCTCACCCTGAAGT (upstream), GGGATAGCACAGCCTGGAT (downstream).

50 μL PCR amplification reaction system was prepared as shown in Table I. After the reaction was completed, 5 μL of the amplified product was subjected to 2% agarose gel electrophoresis analysis.

Determination of the protein concentration of bicinchoninic acid (BCA)

The cell culture medium was aspirated and the cells were washed 3 times with PBS (Beijing Institute of Biological Products, China). The cells were gently scraped off with a cell curette, and this sediment was dissolved in PBS, which was then transferred to an Eppendorf (EP) tube, and placed on ice. The collected cells were centrifuged at 3000 r/min for 5 min, and the supernatant was discarded. Cell lysate was prepared at a ratio of Radio Immunoprecipitation Assay (RIPA)/ Phenylmethanesulfonyl fluoride (PMSF) = 100/1, and lysate was prepared on the spot. After the cell lysate became clear, the EP tube was placed in a 4°C centrifuge at 12000 r/min for 15 min. The supernatant (i.e., the lysed protein) was transferred to a new EP tube and immediately used or stored at -80°C. The protein standard and BCA working solution were configured, and the standard was added to the standard well of a 96-well plate at 0, 1, 2, 4, 8, 12, 16, and 20 μL and supplemented with PBS to 20 μL/well; 2 μL of the sample to be tested was added to the well of a 96-well plate, and PBS was added to make up to 20 μL; 200 μL of BCA working solution was added to each well and incubated at 37°C for about 20-30 min. The absorbance of each well was measured using a microplate reader, and then the concentration of the sample protein to be tested was calculated according to the equation.

Table I. *PCR amplification reaction system.*

Component	Volume
2 × PCR Taq mix	25 μL
Primers (10μM)	2.0 μL (F/R)
DNA	3 μL
H_2O	18 μL
Total	50 μL

Detection of proteins of DWMT1 gene and related tumor suppressor gene in NSCLC by Western blot

After the cell lines A549 and H838 were fully grown in the cell culture dish, they were digested with trypsin to collect the cells. DNIT1 and total protein of tumor suppressor gene were extracted respectively. Then, the total protein was quantified, sodium dodecyl sulfate polyacrylamide gel electrophoresis (SDS-PAGE) was performed, in which wet transfer was mainly used. DNMT1 wet transfer conditions were as follows: current size 250 mA, time 120 min. After the wet transfer, the prepared polyvinylidene difluoride (PVDF) membrane (Shanghai Yaxin Biotechnology Co., Ltd, China) was used for membrane transfer. With this in mind, Coomass Brilliant Blue can be used for staining to observe the efficiency of protein transfer. Then, 10 mL Tris-Buffered Saline Tween-20 (TBST) (Shanghai Huashun Biotechnology Co., Ltd, China), and prepared skim milk were used for sealing for about 1 h. Then, the membrane was washed 3 times with TBST for about 10 min each time. DNMT1 and primary antibody of tumor suppressor protein (Nanjing Sunshine Biotechnology Co., Ltd, China) was added, and then cultured overnight at room temperature. On the second day, the primary antibody was incubated, and then the secondary antibody (Nanjing Sunshine Biotechnology Co., Ltd, China) was added and shaken for 1 h at room temperature on a shaker. After the secondary antibody was incubated, the membrane was washed three times with TBST for 5 min each time. Electrochemiluminescence (ECL) fluorescence coloration, 100 μL pipette gun, gun head and other items were placed in a dark room for exposure, and fixing and developing solution (Leica, Germany) were used for film-developing to observe the experimental results. Finally, the gel image (Leica, Germany) was used to process the experimental data and obtain the protein gray value.

Growth of NSCLC cell lines after epigenetic treatment by CCK-8

Two cell lines with good logarithmic growth were selected for epigenetic therapy according to the above groups. After treatment, cells were collected at different times and added to the culture medium for one day. After the synchronization step was completed, the cells were added to the 96-well plate. In each sample, three auxiliary wells were set, and unsampled wells were replenished

with other solutions. After this, the 96-well plate was placed in a cell culture box, which was then taken out and observed every 24 h for 6 consecutive days. Methyl thiazolyl tetrazolium (MTT) reagent was added to each observation well and then cultured. After almost 4 h, the original medium was removed and 200 μL of dimethyl sulfoxide (DMSO) solution was added to each well, and then these cells were fully dissolved. The absorbance was detected with a microplate analyzer. Finally, the graph was drawn according to the obtained data.

Statistical analysis

All data of the experimental results were represented by x±s, analysis of variance (ANOVA) and *t*-test were used for data processing, and all data were analyzed by SPSS software.

RESULTS

Analysis of the transcriptional expression of DNMT1 in NSCLC cells treated with 5-Aza and MS-275

As shown in Fig.1, the 5-Aza group, MS-275 group and combined treatment group were treated for 5 days respectively, and the expression level of DNMIT1 gene in non-small cell lung cancer cells was detected by RT-PCR. As shown in Fig.1A, the transcription expression levels of DNMT1 in the 5-Aza group and MS-275 group were significantly lower than those in the control group ($P<0.05$). The transcription expression level of DNMT1 was significantly decreased in the 5-Aza and MS-275 combination treatment group, which was significantly different from the control group ($P<0.01$). According to Fig.1B, in H838 cells, the transcription expression levels of DNMT1 in the 5-Aza group and MS-275 group were significantly lower than those in the control group ($P<0.05$). However, the transcription expression level of DNMT1 was significantly decreased in the combined treatment group, which was significantly different from the control group ($P<0.01$). Therefore, for the total amount of RNA extracted from the control group, 5-Aza group, MS-275 group, and the combination treatment group, the combination treatment of 5-Aza and MS-275 significantly reduced the mRNA expression level of DNMT1 gene.

Analysis of the recovery expression of tumor suppressor genes in NSCLC cells after epigenetic treatment

The expression level of tumor suppressor gene (RASSF1A, ASC, APC) protein after epigenetic treatment in non-small cell lung cancer cells was detected by Western blot. The electrophoresis and

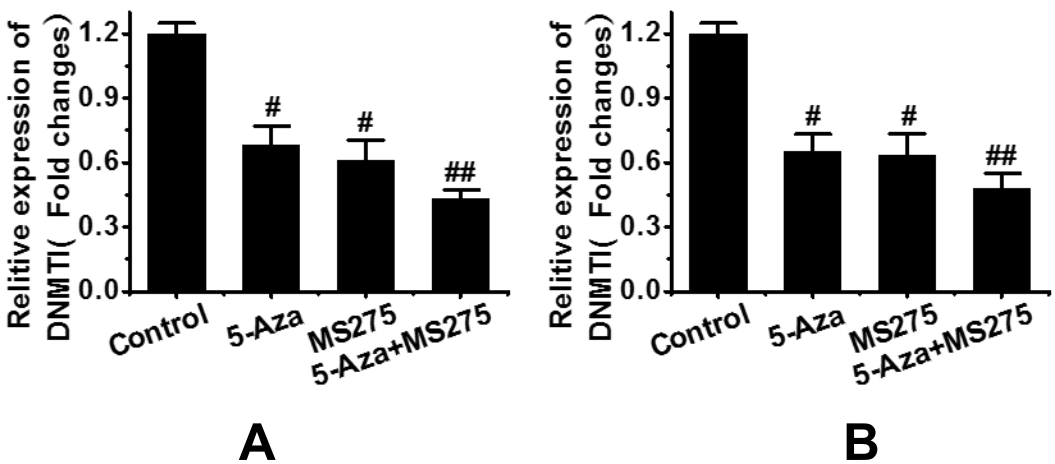

Fig. 1. *The transcriptional expression of DNMT1 in non-small cell lung cancer cells after treatment with 5-Aza and MS-275.* ***A****) A549 cells;* ***B****) H838 cells; (compared with the control group, # $P<0.05$ indicates significant difference, and ## $P<0.01$ indicates very significant difference)*

histogram were obtained, and are shown in Fig. 2. As can be concluded from Fig. 2A and B, the protein expression of tumor suppressor gene RASSF1A in A549 cells gradually increased after the epigenetic treatment, with statistical difference ($P<0.05$). According to Fig. 2C and D, the expression of tumor suppressor gene RASSF1A and APC protein in H838 cells also showed an increasing trend ($P<0.05$), while there was no significant change in the expression of tumor suppressor gene ASC ($P > 0.05$).

Analysis on the inhibitory effect of non-small cell lung cancer cells after epigenetic treatment

The expression levels of genes which were obtained by CCK-8 after epigenetic treatment of A549 and H838 cell line are shown in Fig.3. As demonstrated in Fig. 3A, the expression levels of A549 cell lines in the control group, 5-Aza group, MS275 group and the combined treatment group all showed an increasing trend as the number of days of experimental culture increased. However, the increasing trend of 5-Aza group, MS275 group and the combined treatment group was lower than that of the control group, and the reduction effect was the most obvious in the combined treatment group, so the group with the best inhibitory effect was the combined treatment group. In Fig. 3B, the expression levels of H838 cell lines in the control group, 5-Aza group, MS275 group and the combined treatment group all showed an increasing trend as the number of days of experimental culture increased, whereas the increasing trend of 5-Aza group, MS275

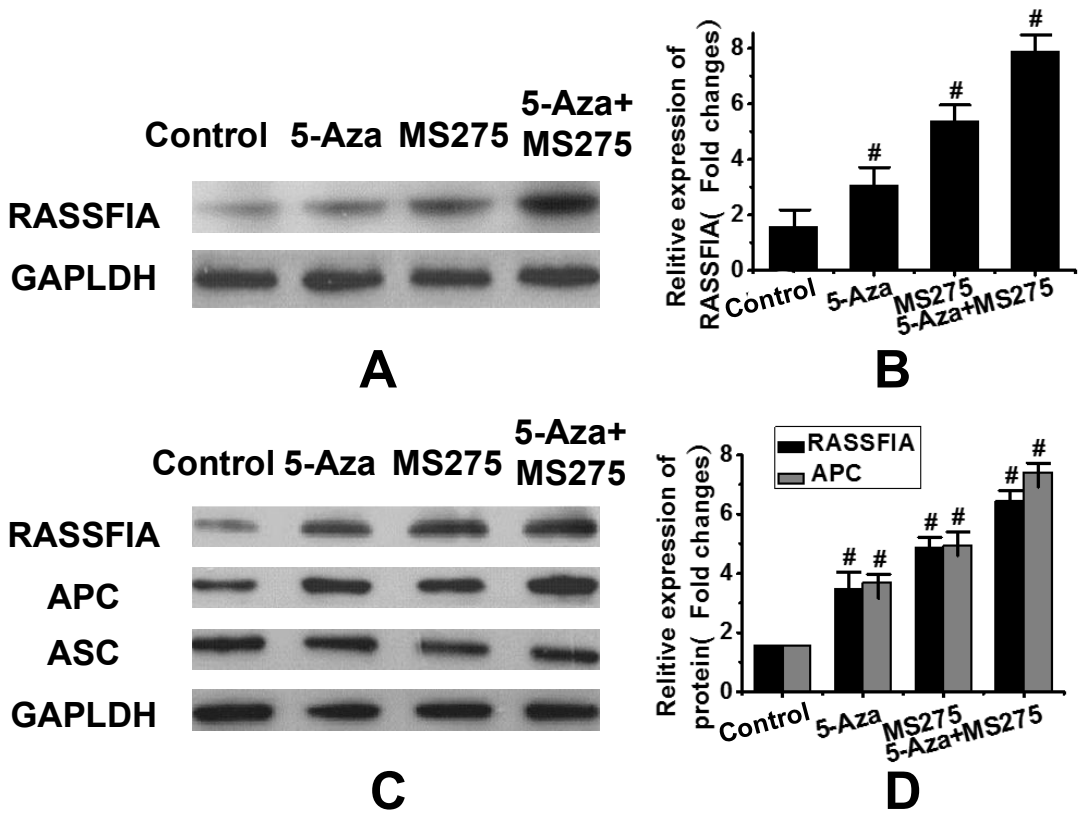

Fig. 2. *Analysis results of the recovery expression of tumor suppressor genes after epigenetic treatment in non-small cell lung cancer cells. **A)** Western blot analysis of tumor suppressor gene expression in A549 cells; **B)** Histogram of the tumor suppressor gene protein expression level of A549 cells; **C)** Western blot analysis of the tumor suppressor gene expression in H838 cells; **D)** Histogram of the expression level of tumor suppressor gene protein in H838 cells (compared with the control group, # $P<0.05$ indicated significant difference)*

group and the combined treatment group was slower than the control group, and the slowing effect was the most obvious in the combined treatment group. Therefore, the group with the best inhibitory effect was the combination therapy group.

DISCUSSION

Hypermethylation of tumor suppressor gene in tumor cells inhibits gene expression, resulting in uncontrolled cell cycle and canceration (9). Some researchers have suggested that DNMT1 was involved in the process of cell transformation and tumorigenesis (10). In this study, the total amount of RNA extracted from the four groups was analyzed by RT-PCR, and it was found that the combined treatment of 5-Aza and MS-275 significantly reduced the mRNA expression level of DNMT1 gene compared with the control group or the individual medication group.

Many experimental studies have proved that gene therapy targeting DNMT1 has a certain effect on tumor cells (11). Whether this change has occurred in NSCLC cell lines has not been clearly demonstrated (12). In this study, Western blot analysis showed that the protein expression of tumor suppressor gene RASSF1A increased gradually after epigenetic treatment in A549 cells ($P<0.05$), and the protein expression of tumor suppressor gene RASSF1A and APC increased gradually in H838 cells ($P<0.05$), while the expression of tumor suppressor gene ASC showed no significant change. The CCK-8 method showed that the combination treatment group had the most obvious mitigating effect compared with the other groups. Therefore, it is hypothesised that the combined epigenetic treatment of 5-Aza and MS-275 can significantly reduce the expression of DNMT1 in non-small cell lung cancer cells and activate the expression of related cancer suppressor genes, so as to restore the function of cancer suppressor genes and inhibit the growth and proliferation of lung cancer cells.

To sum up, it can be hypothesised that DNMT1 can be used as a sensitive marker for the epigenetic treatment of lung cancer, providing experimental evidence for later clinical surgery.

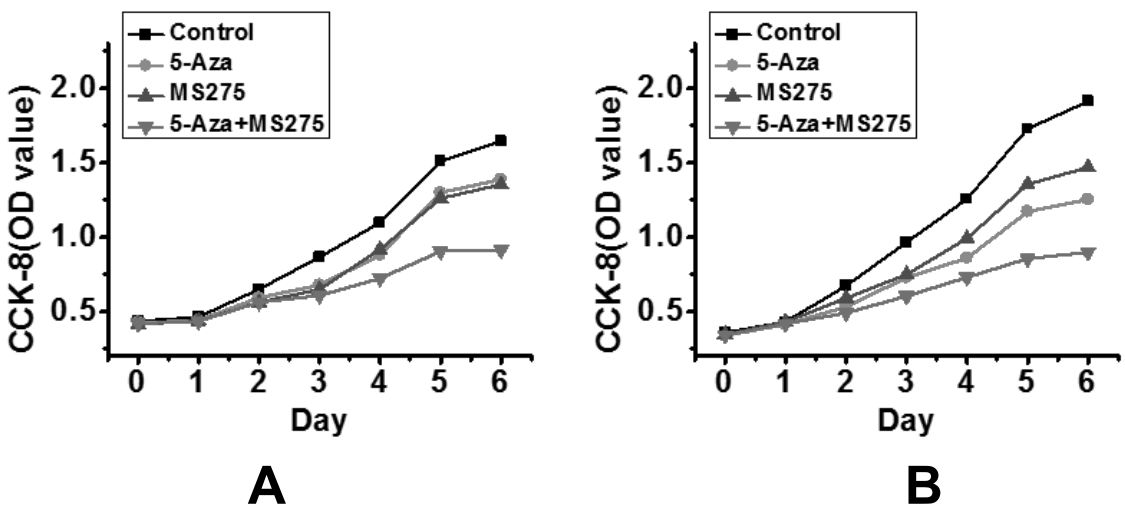

Fig. 3. *Histogram of inhibition effects of A549 cells and H838 cells on non-small cell lung cancer cells after epigenetic treatment.* ***A****) A549 cells;* ***B****) H838 cells).*

REFERENCES

1. Malhotra J, Malvezzi M, Negri E, La Vecchia C, Boffetta P. Risk factors for lung cancer worldwide. Eur Respir J 2016; 48(3):889-902.
2. Akhurst T. Staging of non-small-cell lung cancer. PET Clin 2018;13(1):1-10.
3. Ansari J, Shackelford RE, El-Osta H. Epigenetics in non-small cell lung cancer: from basics to therapeutics. Transl Lung Cancer Res 2016; 5(2):155-71.
4. O'Leary K, Shia A, Schmid P. Epigenetic regulation of EMT in non-small cell lung cancer. Curr Cancer Drug Targets 2018; 18(1):89-96.
5. Di Paolo A, Del Re M, Petrini I, Altavilla G, Danesi R. Recent advances in epigenomics in NSCLC: real-time detection and therapeutic implications. Epigenomics 2016; 8(8):1151-67.
6. Vendetti FP, Rudin CM. Epigenetic therapy in non-small-cell lung cancer: targeting DNA methyltransferases and histone deacetylases. Expert Opin Biol Ther 2013; 13(9):1273-85.
7. Fuks F, Burgers WA, Brehm A, Hughes-Davies L, Kouzarides T. DNA methyltransferase Dnmt1 associates with histone deacetylase activity. Nat Genet 2000; 24(1):88-91.
8. Chu BF, Karpenko MJ, Liu Z, et al. Phase I study of 5-aza-2'-deoxycytidine in combination with valproic acid in non-small-cell lung cancer. Cancer Chemother Pharmacol 2013; 71(1):115-21.
9. Yanagawa N, Tamura G, Oizumi H, Takahashi N, Shimazaki Y, Motoyama T. Promoter hypermethylation of tumor suppressor and tumor-related genes in non-small cell lung cancers. ancer Sci 2003; 94(7):589-92.
10. Feng Y, Wang J, Wu Y, Feng X, Yu Y. [Protein expressions of HDAC1 and DNMT1 in non-small-cell lung cancer and its clinical significance]. Zhonghua Yi Xue Za Zhi 2014; 94(8):596-8.
11. Kwon YM, Park JH, Kim H, et al. Different susceptibility of increased DNMT1 expression by exposure to tobacco smoke according to histology in primary non-small cell lung cancer. J Cancer Res Clin Oncol 2007; 133(4):219-26.
12. Suzuki M, Yoshino I. Aberrant methylation in non-small cell lung cancer. Surg Today 2010; 40(7):602-7.

JOURNAL OF BIOLOGICAL REGULATORS & HOMEOSTATIC AGENTS Vol. 33, no. 6, 1797-1801 (2019)

LETTER TO THE EDITOR

STARRING ROLE OF ACETYLCHOLINESTERASE FROM MEDICINAL PLANTS ON LACTATE DEHYDROGENASE PRODUCTION IN CYTOTOXIC HEPATIC CELLS

UMM-E-HABIBA[1], KHALIL-UR-REHMAN[1], N. JAHAN[2] and M. SHAHID[1]

[1]Department of Biochemistry, University of Agriculture, Faisalabad, Pakistan; [2]Department of Chemistry, University of Agriculture, Faisalabad, Pakistan

Received May 8, 2019 – Accepted October 2, 2019

To the Editor,

Acetylcholinesterase (AChE) is an enzyme that hydrolyzes the acetylcholine (ACh) in cholinergic synapse and converts it into acetate and choline. AChE also participates in cell differentiation and development of different tissues. Acetylcholine has two receptors, muscarinic and nicotinic that promote differentiation, proliferation, apoptosis and cytoskeleton organization of the cells during phases of cell cycle (1). Hyper production of acetylcholine intriguingly increases the Ca^{2+} influx and diverse activation of molecules such as Ras-mitogen-activated protein kinase, phosphatidylinositol 3-kinase-Akt, protein kinase C and c-Src through muscarinic and nicotinic receptors and resulting cell proliferation and apoptosis occur (2).

Due to exposure to pesticides and chemicals, acetylcholine level is increased in hepatic cells that ultimately induce more differentiation and proliferation of cells and, as a result, hepatocellular carcinoma occurs (3). Therefore, AChE enzyme is needed to breakdown the extra acetylcholine produced as a result of environmental insults like chemicals and toxins etc. The plants which show minimum inhibition of AChE enzyme are supposed to have more hepatoprotective activity. Lactate dehydrogenase (LDH) is a cytotoxicity marker of cells that is normally involved in glucose metabolism pathway. Liver is the major organ involved in glucose metabolism pathways like gluconeogenesis. When hepatic cells are treated with toxicants then they become swollen and necrotic and, as a result, more LDH is released from the hepatic cells (4). To achieve this objective, toxicological evaluation of selected medicinal plants was carried out through hemolytic and thrombolytic activities and then AChE inhibition activity of these plants was accomplished. Sibsequently, *in vitro* liver slice culture assay was performed to measure the level of LDH released from hepatic cells against hepatotoxicity induced by carbon tetrachloride.

MATERIALS AND METHODS

Collection and extractions of plants

The selected parts of plants were collected from the Faisalabad region and identified by the plant taxonomist Department of Botany, University of Agriculture Faisalabad, Pakistan as shown in Table I. The extraction of selected parts of plants was performed in methanol through maceration at 37°C and then lyophilized. After that each plant concentration 500 µg/mL was prepared from dry plant extracts for the study.

Key words: hepatoprotective; hemolysis; cytotoxicity; acetylcholinesterase; hepatocellular carcinoma

Corresponding Author:
Dr Umm-e-Habiba,
Clinico-Medical Biochemistry Lab,
Department of Biochemistry,
University of Agriculture,
Faisalabad, 38000, Pakistan
e-mail: habibaakram518@gmail.com

0393-974X (2019)

Hemolytic activity

For hemolytic activity, fresh blood was taken and centrifuged at 2000 rpm for 3 min. Afterward the centrifugation pellet was taken and washed three times with chilled (4°C) phosphate buffer saline of pH 7.4. The washed red blood cells were suspended in 20 mL chilled phosphate buffer saline and kept on ice to perform hemolytic activity. In micro centrifuge tubes 20 µL of each plant sample and 180 µL of diluted blood cell suspension were taken and incubated at 37°C for 30 min with shaking (80 rev/min). After incubation these samples were immediately placed on ice for 5 min and then centrifuged at 3000 rpm for 5 min. After centrifugation 100 µL supernatant of each sample was taken and diluted with 900 µL of chilled phosphate buffer saline. The absorbance of these diluted samples were noted at 576 nm. Triton X-100 was used as a positive control and phosphate buffer saline as a negative control. Percentage hemolysis was calculated using the formula:

Hemolysis (%) = (Absorbance of sample-Absorbance of negative control/ Absorbance of positive control) × 100

Thrombolytic activity

For thrombolytic activity, 500 µL of blood was put into pre-weighed micro centrifuge tubes and incubated for 45 min at 37°C. After incubation, serum was removed and the tubes were weighed again with blood clots and used for thrombolytic activity. 100 µL of each plant sample was put into the blood clot-containing tubes and incubated at 37°C for 90 min. After incubation, dissolved clots were removed carefully from the tubes and weighed again. The difference in weight of the tubes before and after clot lysis was calculated and expressed in terms of % clot lysis. Distilled water and streptokinase were used respectively as negative and positive control.

Acetylcholineterase (AChE) inhibition assay

In vitro acetylcholinesterase inhibitory activity of medicinal plants was executed following the method described by Rahman and Choudhary (2001). Sodium phosphate (0.1 M) buffer of pH 7.8 was prepared first and then 10 mM solution of Ellman's Reagent (DTNB) and 14 mM solution of acetylthiocholine (ATCI) were perpared in sodium phosphate buffer and distill water, respectively. After preparing the solutions, 120 µL sodium phosphate buffer and 20 µL of each plant extract were put into a microplate and incubated at 25°C for 15 min. Subsequently, 10 µL of DTNB and 10 µL of ATCI solutions were added to the mixture and again incubated for 10 min and then absorbance of the colored product was taken at 412 nm by ELISA reader. Galantamine (10 µM) was used as a positive control. The percentage inhibition of AChE was calculated by the formula:

AChE Inhibition (%) = (1 – Abs. of sample/Abs. of control) × 100

In-vitro hepatoportective activity through liver slice culture assay

The hepatoprotective potential of selected medicinal plants was explored by liver slice culture model which was prepared after slight modification (6). For this purpose 20-22 liver slices from prepared liver slice culture model were put into capped glass tubes that contained 2 mL Krebs – Ringer – Hepes (KRH media). The liver slices were then incubated at 37°C for 30 min on a water bath shaker. After incubation, the KRH medium was replaced with fresh 2 mL KRH medium with 500µg/mL of each plant extract, and ascorbic acid (10 mM) was used as a reference standard. The liver slices with plant extratcs were incubated for 1 h at 37°C and then 1 mL of CCl_4 (40 mM) was added to each glass tube to induce heaptotoxcity and again incubated for 2 h on a water bath shaker at 37°C. In this period of 2 h, liver slices were aerated every 10 minutes with oxygen by removing the caps of the glass tubes. After incubation, culture medium was collected to measure the Latate dehydrogenase (LDH) level, which was the cytotoxic marker of liver injury. For the measurement of lactate dehydrogenase, commerical LDH cytotoxicity assay kit II Abcam (ab65393) was used. To calcutae the percentage cytotoxicity of LDH released from liver slices the formula used was:

Cytotoxicity (%) = [(Test sample Abs – Low control Abs)/(Low control Abs – High control Abs)] × 100

Here, "Test samples $_{Abs}$" showed incubated liver slices with both plant extract and 40 mM CCl_4, "High control $_{Abs}$" showed incubated liver slices with 40 mM CCl_4 only and "Low control $_{Abs}$" indicated incubated liver slices with KRH medium only.

Statistical analysis

Hemlytic and thrombolytic activites of plants were expressed as mean±SD. The results of AChE inhibition

Table I. *Details of selected medicinal plants with their parts used.*

Botanical name	Family	Common name	Selected parts of plants	Voucher number
Ficus religiosa	Moraceae	Peepul tree	Leaves	804-2-17
Cassia fistula	Fabaceae	Amaltas	Leaves	804-3-17
Ziziphus jujuba	Rhamnaceae	Unaab	Fruit	804-5-17
Phyllanthus emblica	Phyllanthaceae	Aamla	Fruit	804-6-17
Ocimum basilicum	Lamiaceae	Niazboo	Seeds	804-8-17

Table II. *Percentage hemolysis and clot lysis of medicinal plants.*

Medicinal plants	Hemolysis (%)	Clot lysis (%)
F. religiosa	14±1.5*	4±1.33*
C. fistula	12±0.56*	3±5.73*
Z. jujuba	23±0.31*	9±0.38*
P. emblica	16±1.06*	10±3.82*
O. basilicum	30±0.45*	12±0.57*
Negative control	1.8±0.24*	2.5±0.58 *
Positive control	83±1.83	99±14.56

** indicates significant difference with positive control*

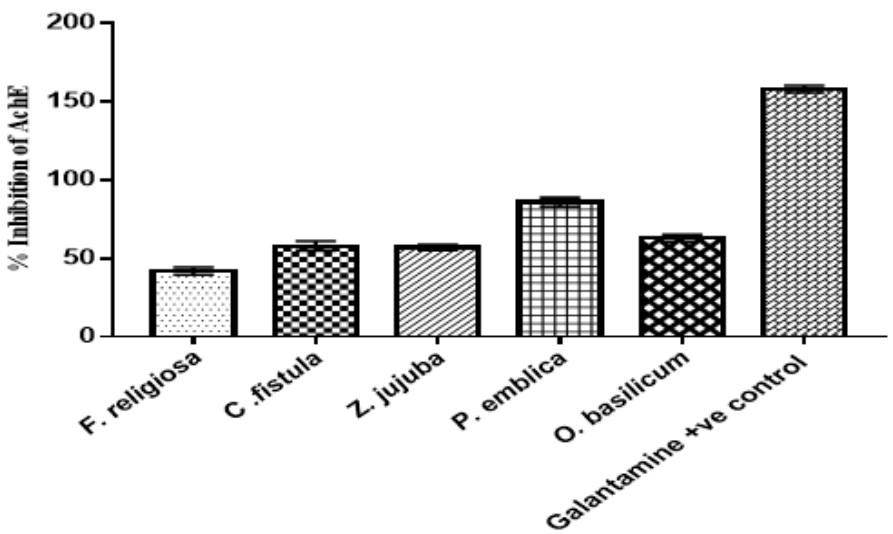

Fig. 1. *Percentage inhibition of AChE activity in medicinal plants.*

assay and liver slice culture assay were analyzed through One-way ANOVA Tukey's multiple comparison test by using Graph pad prism 7.

RESULTS

Among all the studied plants, *C. fistula* showed minimum percentage of hemolysis 12±0.56 and clot lysis 3±5.73 as compared to positive control that exhibited maximum parentage of hemolysis (83±1.83) and clot lysis (99±14.56). On the other hand, in *O. basilicum* high percentages of hemolysis and clot lysis were observed 30±0.45 and 12±0.57, respectively as described in Table II. *In vitro* AChE activity was expressed in terms of percentage inhibition of acetylcholinesterase and plants that showed minimum percentage inhibition of enzyme were considered best in terms of hepatoprotective potential. It was observed from graphical presentation (Fig. 1) that *F. religiosa* showed significantly ($p<0.05$) low percentage inhibition 42±2.4 of AChE, while in *P. emblica* highest percentage inhibition 86±2.8 of AChE was observed as compared to positive control galantamine (95±2.3).

After determination of AChE activity of selected medicinal plants, their hepatoprotective potential was evaluated through liver slice culture assay. In this assay, release of lactate dehydrogenase was measured in terms of percentage cytotoxicity against hepatotoxicant CCl_4. Among all the studied plants *F. religiosa* possessed (14±1.32) maximum significant ($p<0.05$) hepatoprotective potential in terms of least percentage cytotoxicity as compared to the high control group (72±3.40) that received only CCl_4 intoxication. Whereas *F. religiosa* exhibited non-significant ($p>0.05$) hepatoprotective potential in comparison with the standard control group (17±1.87) that received ascorbic acid with hepatotoxicant CCl_4. On the other hand, comparison of *P. emblica* and the standard group showed significant difference 31±1.088 and 17±1.87, respectively, in percentage cytotoxicity that indicated minimum hepatoprotective potential of this plant (Fig 2). Overall comparison of percentage inhibition of AChE and cytotoxicity among all the studied plants indicated that *Ficus religiosa* possessed more hepatoprotective potential due to minimum inhibition of AChE.

DISCUSSION

Owing to the increase of resistance against pathogenic microbes and existing antibiotics, the demand for natural herbal remedies is increasing rapidly for the treatment of several diseases (7). Since ancient times, medicinal plants have been shown to possess remarkable potential against numerous diseases and are a highly valuable source of pharmaceutical drugs. However, before using medicinal plants for any treatment it is necessary to find out their effects on cells. Therefore, in the present study, hemolytic and thrombolytic activities of five different plants were

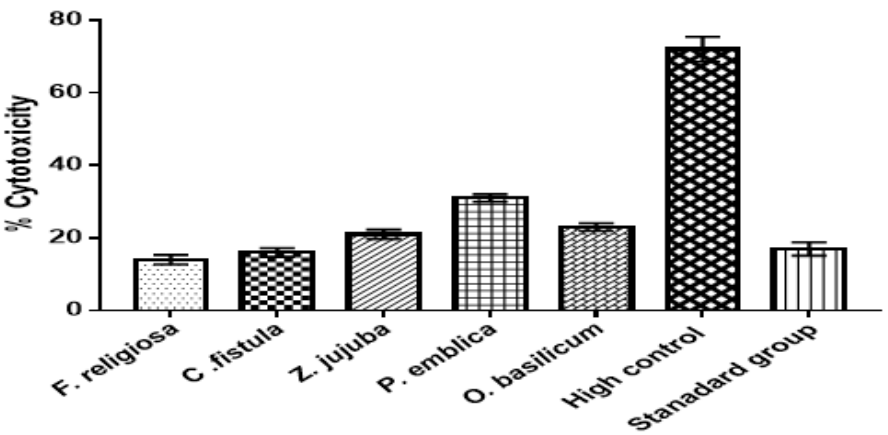

Fig. 2. *Trend of percentage cytotoxicity of medicinal plants in terms of LDH released*

carried out on human erythrocytes to find out which plants showed minimum toxic effects and which were considered best and safe.

The natural antioxidants of medicinal plants reduced oxidative stress that increased due to imbalance of reactive metabolites that ultimately disrupted the homeostasis of the body (8). In case of oxidative damage, necrosis and proliferation of the hepatic cells more lactate dehydrogenase is produced that eventually increases cytotoxicity (9). On the other side a certain level of neurotransmitter acetylcholine controlled by AChE plays a crucial role in cell survival, differentiation and proliferation (10). A variable amount of AChE is present in hepatic cells and in the absence of this enzyme more acetylcholine is accumulated and increased cell proliferation and differentiation by downregulation of p27 and cyclin proteins. The hyper production of acetylcholine induced hepatotoxicity and ultimately hepatocellular carcinoma (11, 12).

The obtained results of the present study indicated that *F. religiosa* has more AChE activity and hepatoprotective potential in terms of least percentage cytotoxicity due to minimum LDH release as compared to the other plants studied. The outcomes of the present research are in agreement with the study of Perez-Aguilar et al. (2015) in which they found that AChE activity decreased in cancer cells due to hyper production of acetylcholine that induced more proliferation and differentiation of the cells.

Therefore it was concluded that medicinal plants which have high AChE activity possess more hepatoprotective potential due to a decrease in LDH and are ultimately beneficial to combat against liver diseases which are prone to be carcinogenic.

ACKNOWLEDGEMENTS

This study was funded by the Office of Research Innovation & Commercialization (ORIC), University of Agriculture Faisalabad. The authors thank ORIC for financial support.

REFERENCES

1. Resende RR, Alves AS, Britto LR, Ulrich H. Role of acetylcholine receptors in proliferation and differentiation of P19 embryonal carcinoma cells. Exp Cell Res 2008; 314(7):1429-43.
2. Resende R, Adhikari A. Cholinergic receptor pathways involved in apoptosis, cell proliferation and neuronal differentiation. Cell Commun Signal 2009; 27:7-20.
3. Nazam N, Shaikh S, Lone MI, Sharma M, Ahmad W. Combined in silico and in vivo studies shed insights into the acute acetylcholinesterase response in rat and human brain. Biotechnol Appl Biochem 2015; 62(3):407-15.
4. Vatakuti S, Schoonen WG, Elferink ML, Groothuis GM, Olinga P. Acute toxicity of CCl4 but not of paracetamol induces a transcriptomic signature of fibrosis in precision-cut liver slices. Toxicolo In Vitro 2015; 29 (5):1012-20.
5. Rahman AU, Choudhary MI. Bioactive natural products as a potential source of new pharmacophores a theory of memory. Pure Appl Chem 2001; 73(3):555-60.
6. Wormser U, Ben ZS. The liver slice system-an in vitro acute toxicity test for assessment of hepatotoxins and their antidotes. Toxicol In Vitro 1990; 4(4-5):449-51.
7. Kumar HC, Ramesh A, Kumar JNS, Ishaq BM. A review on hepatoprotective activity of medicinal plants. Inter J Pharma Sci Res 2011; 2:501-15.
8. Palanisamy V, Shanmugam S, Balakrishnan S. An improvement in hepatoprotective activity by herbal drug combination. Middle-East J Sci Res 2014; 21(9):1454-59.
9. Kabiri N, Ahangar-Darabi M, Setorki M, Rafieian-Kopaei M. The effect of silymarin on liver injury induced by thioacetamide in rats. J Herb Med Pharmacol 2013; 2(2):29-33.
10. Shen JX, Qin D, Wang H, et al. Roles of nicotinic acetylcholine receptors in stem cell survival/ apoptosis, proliferation and differentiation. Curr Mol Med 2013; 13(9):1455-64.
11. Perez-Aguilar B, Vidal CJ, Palomec G, et al. Acetylcholinesterase is associated with a decrease in cell proliferation of hepatocellular carcinoma cells. Biochimica Biophy Acta 2015; 1852 (7):1380-87.
12. Bruix J, Colombo M. Hepatocellular carcinoma: current state of the art in diagnosis and treatment. Best Pract. Res Clin Gastroenterol 2014; 28(5):751.

LETTER TO THE EDITOR

LIVER FAILURE PROMOTES GASTROINTESTINAL DYSFUNCTION BY CHANGING CHOLINERGIC AND NITRERGIC NERVES AND CAJAL INTERSTITIAL CELLS IN GASTRIC ANTRUM

JZ. ZHU[1], TT. ZHAO[2,3], YY. CHEN[2,3], R. ZHANG[2], JK. WANG[4], SH. ZHANG[5,6] and KC. LIU[2,3]

[1]Department of Hepatal-Gastroenterology, Meng chao Hepato-biliary Hospital of Fujian Medical University, Fuzhou, China; [2]Institute for Laboratory Medicine, 900 Hospital of the Joint Logistics Team, Dongfang Hospital, Fuzhou, Fujian, China; [3]School of Medicine, Xiamen University, Xiamen, Fujian, China; [4]School of Life Science, Xiamen University, Xiamen, Fujian, China; [5]School of Life Sciences, Central South University, Changsha, Hunan, China; [6]School of Life Sciences, University of Dundee, Nethergate, Dundee, Scotland, UK

Received June 10, 2019 – Accepted October 4, 2019

To the Editor,

Patients with liver failure often exhibit obvious symptoms of gastrointestinal dysfunction, such as nausea, vomiting, and abdominal distension, which seriously affect their quality of life. However, how gastrointestinal dysfunction occurs in these patients remains elusive. The regulation of gastrointestinal function is influenced by neurohumoral factors, inflammatory mediators, intestinal flora imbalance, endotoxemia, nitric oxide, and nitric oxide synthase. For example, inflammatory mediators, such as interleukins and interferons, can inhibit the feeding center, thereby decreasing appetite and weakening gastrointestinal motility. Moreover, intestinal flora imbalance can lead to gastrointestinal mucosal lesions, bacterial translocation, increased endotoxin absorption, and gastrointestinal dysfunction.

Liver failure can be caused by many factors, one of which is infection with viral hepatitis (1, 2). The mortality rate of liver failure is up to 50−90% (3). Previous studies have shown that gastrointestinal dysfunction is closely correlated with liver failure (4). Currently, the pathogenesis of gastrointestinal dysfunction in relation to liver failure remains elusive, therefore, it is important to explore its underlying mechanism. Here, we established a rat model of liver failure to study the relationships between liver failure and gastrointestinal dysfunction and to dissect the underlying physiological mechanism of gastrointestinal dysfunction, including alterations to cholinergic nerves, nitrergic nerves, and interstitial Cajal cells (ICCs) in the myenteric plexus of gastric antrum.

MATERIALS AND METHODS

Dextran blue-2000 (Cat No. DB-2000) was purchased from Pharmacia company (USA), NAPDH (Cat No. N6505) and NBT (Cat No. N6639) were both purchased from Sigma, and the rabbit anti-human polyclonal c-kit antibody was purchased from Beijing Zhongshan Biotechnology. All other reagents used in this study were

Key words: liver failure; gastric antrum; interstitial cells

Corresponding Author:
Dr Kuancan Liu,
900 Hospital of the Joint Logistics Team,
Dongfang Hospital, Institute for Laboratory Medicine,
No 156 at Xi-er Huan North Road, Fuzhou, Fujian, 350025, China
Tel.: +86 591 22859490 - Fax: +86 591 83732129
e-mail: liukuancan@163.com

0393-974X (2019)

of analytical grade. Wistar rats were purchased from Shanghai Experimental Animal Center (Shanghai, China), and the experiments on rats were approved by the Medical Ethics Committee of Meng chao Hepatobiliary Hospital, Fujian Medical University (No. 2015-10).

Animal models of acute liver failure

Wistar rats (50% males and 50% females) weighing 200−250 g and of clean grade were selected for animal model production. Forty rats were randomly divided into a normal control group (n = 20) and a liver failure model group (n = 20). The model of acute liver failure was established according to the method determined by a previous study (1). The model group was induced with an intraperitoneal injection of 350 mg/kg thioacetamide, which was repeated 24 h later. The control group was intraperitoneally injected with the same dose of aseptic saline, which was repeated 24 h later. Thioacetamide was prepared with normal saline to reach a concentration of 40 g/L.

Gastric motility test in rats

Dextran blue-2000 (2%, DB-2000, Pharmacia company) was used as a gastrointestinal marker for the gastric motility test. Each group of rats was injected into the stomach with 0.4 ml 2% DB-2000 20 min before laparotomy. Specimens were collected after intraperitoneal injection of 1% pentobarbital sodium (30 mg/kg). Rats were cut along the large curved side and the stomach was taken from the pylorus sphincter, the pigment residue in the stomach was fully washed with 4 ml deionized water. This was followed by centrifugation at 3500 rpm for 15 min. The absorbance of the supernatant was measured with a 721-A spectrophotometer at 620 nm. The mean values of absorbance from the model and control group were calculated as the relative rate of residual gastric pigment in each sample.

Histochemical staining of acetylcholinesterase

The Karnovsky-Roots method was used for histochemical staining of acetylcholinesterase (AchE) in the myenteric plexus of gastric antrum. Gastric antrums were treated with 10% formaldehyde and 1% calcium chloride solution at 4°C overnight and then were rinsed with distilled water for 5 min, cut into 0.5×0.5 cm pieces, and placed in 0.01 M PBS solution. The longitudinal muscle layer was stripped with forceps and placed in a solution composed of acetylthiocholine iodide (5 mg), acetic acid buffer (6.5 ml, 0.1 M, pH 5.5), sodium citrate (0.5 ml, 0.1 M), copper sulfate (1 ml, 30 mM), and distilled water (1 ml) for 10 min. This was followed by washing with distilled water, lamination, dehydration, transparent, and sealing.

NADPH-d histochemical staining (nitric oxide synthase)

Gastric antrums were rinsed with distilled water for 5 min, cut into 0.5×0.5 cm pieces, and placed in 0.01 M PBS solution; the longitudinal muscle layers were gently peeled off with forceps. The stripped longitudinal myometriums were washed twice with 0.02 M paraformaldehyde phosphate buffer (pH 7.2−7.6) and then placed in 0.02 M PBS (pH 7.4−7.6) solution composed of 0.1 g/L NADPH, 0.2 g/L NBT (Sigma Company), and 30 g/L Triton X-100 for 20 min; the reaction was blocked with PBS solution. This was followed by washing with distilled water, lamination, dehydration, transparent, and sealing.

c-kit immunocytochemistry staining of ICCs

Gastric antrums were fixed with 4% paraformaldehyde solution for 24 h, dehydrated by alcohol gradients, and embedded in paraffin. The sections were baked at 60°C for 4 h, dewaxed in xylene and alcohol, rinsed with tap water, and incubated with 3% H_2O_2 at room temperature for 10 min to eliminate endogenous peroxidase activity. These sections were rinsed with distilled water, soaked in PBS for 5 min, blocked with 5% normal goat serum at room temperature for 10 min, incubated with 1:100 rabbit anti-human polyclonal c-kit antibody at 4°C overnight, and rinsed with PBS three times for 5 min. The sections were then incubated with 50 µl of secondary antibody, which was diluted to 1:100 and labeled with biotin, at 37°C for 30 min and then washed with PBS three times for 5 min. The sections were then incubated with 50 µl of streptomycin, which was labeled with horseradish peroxidase and diluted to 1:100, at 37°C for 30 min and then washed with PBS three times for 5 min. This was followed by washing with tap water, re-dyeing, dehydration, and sealing. The results were observed under a light microscope after adding DAB for 5 min.

Tissue specimen (ICC) preparation for electron microscopy

Gastric antrums were fixed with 3% glutaraldehyde, washed with 2% PBS, fixed with 1% osmium acid for

Table I. *Result of histochemical staining of AChE and NOS in gastric antral myenteric plexus (density %) (n =20)*

	Control group	Model group
AChE	5.58±0.86	4.21±0.49**
NOS	5.91±1.36	6.79±1.12**

** indicates P<0.05; ** indicates P<0.01*

1 h, washed with 2% PBS, dehydrated with alcohol gradients and acetone, and soaked and polymerized with resin. These samples were cut into ultrathin sections (70 nm), which were stained with 1% uranium acetate and lead citrate. The sections were observed with a Philips S-206 transmission electron microscope (TEM) at 1500× magnification.

Image analysis

Image analysis was performed with the MAS-5 image analysis system. The sections that underwent both AchE and nitric oxide synthase (NOS) staining under the same condition were selected for further analysis, and five visual fields were selected with a light microscope with a 200× magnification. The distribution of the positively stained neurons in the myenteric plexus was observed. The images were scanned into a computer, the basic statistical area and the gray value was set up, the non-positive part was filtered out to obtain the positive expression area, and the density of positive expression was obtained after computer analysis.

Statistical analysis

Differences between groups were compared using analysis of variance for repeated measurements. All statistical analyses were performed using SPSS 16.0 statistical software. Data were presented as mean±SD (standard deviation). Statistical significance between the two groups was calculated with the unpaired Student's *t*-test. A P value < 0.05 was considered significant.

RESULTS

The model for acute liver failure was established using thioacetamide, and the rates of production and reproducibility were high. In the model group, three rats died within 24 h after the second injection, and the remaining rats were observed for up to 72 h. Moreover, compared with the control

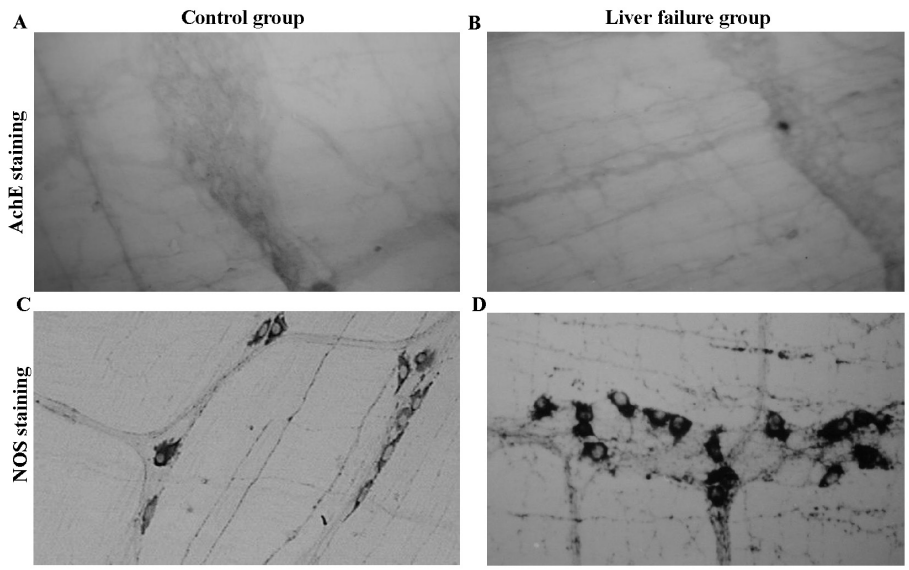

Fig. 1. *Liver failure affects AchE- and NOS-positive neurons in the myenteric plexus of gastric antrum. A) AchE-positive nerves in the myenteric plexus of gastric antrum are significantly reduced after liver failure. The image was enlarged 200-fold. B) NOS-positive nerves in the myenteric plexus of gastric antrum are significantly increased after liver failure. The image was enlarged 200-fold.*

group, obvious symptoms including lethargy, slow reactions, low food intake, and abdominal bulging appeared. Furthermore, the liver in the model group was congested and enlarged, some hemorrhaging was found on the surface of the liver capsule, the structure of the liver was destroyed, and the lobule was also disrupted. Hepatocytes in the model group showed obvious edema, balloon-like degeneration, infiltration of inflammatory cells occurred in the portal area, and patchy and focal necrosis of hepatocytes could also be found.

Liver failure promotes gastrointestinal dysfunction

Compared with the control group, the residual rate of gastric pigment in the model group with liver failure was significantly increased (163±25.68 *vs* 100±18.93, $P < 0.01$), suggesting that gastric emptying was significantly delayed and that gastric motility was significantly impaired in the model group.

Liver failure affects AchE- and NOS-positive neurons in the myenteric plexus of gastric antrum

AchE is the hydrolase for acetylcholine and

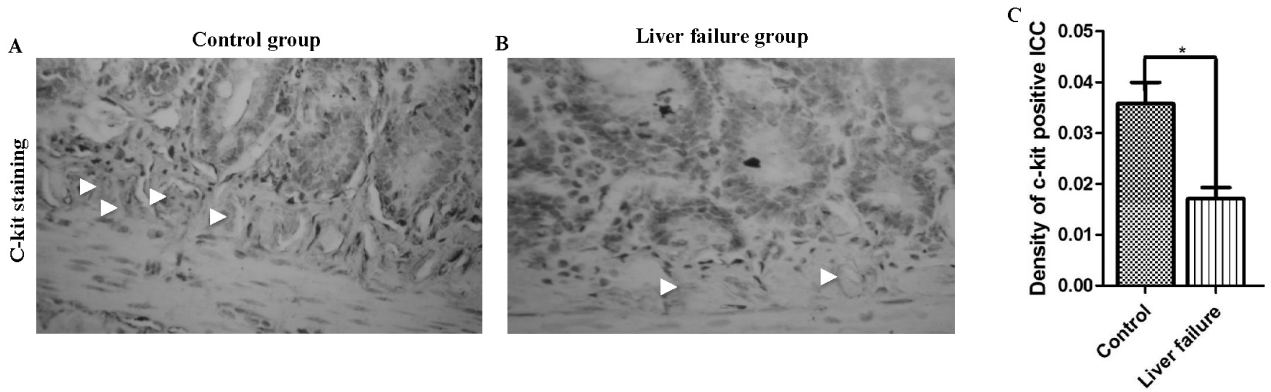

Fig. 2. *The density of c-kit-positive ICCs in gastric antrum was impaired upon liver failure.* ***A)*** *c-kit-positive ICCs in the control group. The image was enlarged 200-fold.* ***B)*** *c-kit-positive ICCs in the model group (white arrows). The image was enlarged 200-fold, and white arrows here indicates the c-kit positive ICC.* ***C)*** *The density of c-kit-positive ICCs in gastric antrum of the model group is lower than that in the control group. * P < 0.05, ** P < 0.01, *** P < 0.001 vs control, and the error bars indicate the mean±standard deviation (SD).*

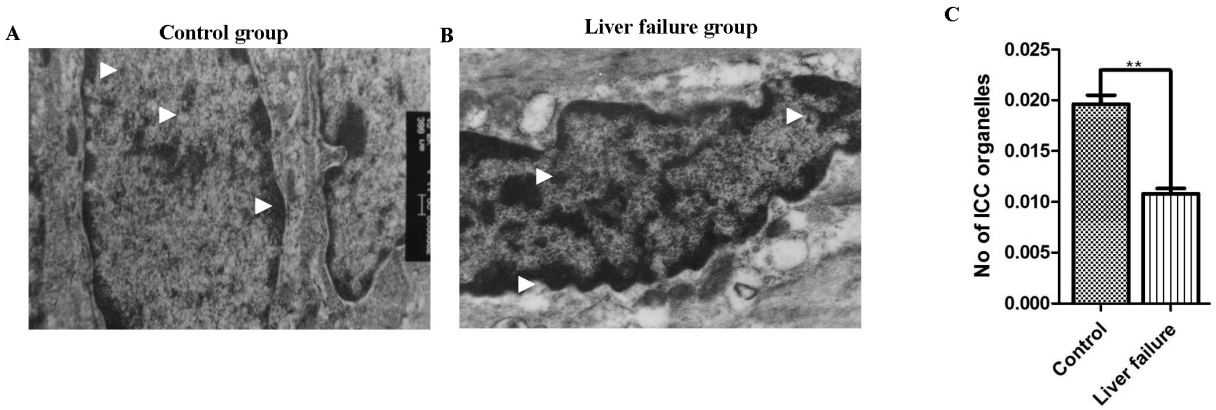

Fig. 3. *The number of organelles in ICCs in the gastric antrum are decreased upon liver failure.* ***A)*** *The ultrastructure of ICCs in the control group. The image was enlarged 1500-fold.* ***B)*** *The ultrastructure of ICCs in the model group (white arrows). The image was enlarged 1500-fold, and white arrows here shows the ultrastructural structure of ICC.* ***C)*** *The number of organelles in ICCs in the model group was decreased compared with that of the control group. * P < 0.05, ** P < 0.01, *** P < 0.001 vs control, and the error bars indicate the mean±standard deviation (SD).*

is an effective method for tracing acetylcholine in cells. Positive sites of AchE exhibited brownish red precipitation after histochemical staining. In the myenteric plexus of the gastric antrum, we found that AchE-positive nerve fibers exhibited a reticular distribution; more AchE-positive neurons were found scattered in the ganglion. However, compared with the control group, the number of AchE-positive nerves in the myenteric plexus of the gastric antrum was significantly decreased in the model group. Moreover, AchE-positive neurons were sparse and their staining was weak and AchE-positive nerve fibers were also sparse and thinner in the model group (Fig. 1, Table I, $P < 0.01$). The decrease of gastrointestinal function in the model group was correlated with the reduced number of cholinergic neurons in the myenteric plexus of gastric antrum.

Nitric oxide (NO) is a neurotransmitter in the nitrergic nervous system. NOS is the pivotal enzyme for NO synthesis, and NOS neurons are widely distributed in the gastrointestinal tract. Previous studies have shown that a variety of diseases and urgent gastrointestinal dysfunction were always accompanied by changes in the nitrergic nervous system (5), suggesting that the nitrergic nervous system plays pivotal roles in gastrointestinal function. NOS histochemical staining resulted in positive blue and purple sites. NOS-positive nerve fibers exhibited a reticular distribution in the myenteric plexus of gastric antrum, whereas NOS-positive neurons were scattered in the ganglion. In the control group, we observed a network of NOS-positive nerve fibers in the stomach and round or oval NOS-positive neurons in the ganglion with blue cytoplasm. However, in the model group, we observed a disordered arrangement of NOS-positive nerves in the myenteric plexus of gastric antrum; the NOS-positive nerves in the gastric antrum were thicker, the number of NOS-positive neurons was increased, and the staining was stronger (Fig. 1, Table I, $P < 0.01$).

Liver failure impairs the density of c-kit-positive ICCs in the gastric antrum

Immunohistochemical staining exhibited brownish yellow c-kit-positive round- or irregular-shaped ICCs, which were distributed between the layers of circular and longitudinal muscles. Additionally, we found that c-kit-positive ICCs exhibited weaker staining and were less abundant in the model group. Image analysis revealed that the density of c-kit-positive ICC in the gastric antrum of the model group was significantly lower than that of the control group (Fig. 2 A-C, $P < 0.05$).

ICC organelles were decreased in the model group

To further understand how liver failure promotes gastrointestinal dysfunction, ultrastructural observation of ICCs in rat gastric antrum was performed with TEM. ICCs were mainly distributed in muscle and exhibited gap junctions with smooth muscle cells and nerve fiber endings. Our study also revealed that c-kit immunohistochemical staining could reflect the distribution of ICCs, which were colored brownish yellow. The shape of these cells was mostly round or irregular, and they were distributed between the layers of circular and longitudinal muscle. Moreover, in the model group, c-kit staining in the gastric antrum was weaker and demonstrated that the number of ICCs in this group was lower than that in the control group.

The ultrastructure of ICCs was further analyzed with TEM. The model group exhibited an altered ultrastructure of ICCs. ICCs in the control group also exhibited large nuclei and little cytoplasm as well as abundant mitochondria, endoplasmic reticulum, and ribosomes. In the model group, ICCs were consistently swollen or atrophied (and thus of distorted shapes), with expanded and fragmented endoplasmic reticulum, swollen and vacuolated mitochondria, fewer organelles, and cytoplasmic vacuoles. The interactions between ICCs and other cells including nerves or smooth muscle cells were decreased, and the junction structures between them were destroyed compared with those of the control group. The number of ICC organelles in the gastric antrum of the model group was significantly lower than that of the control group (Fig. 3 A-C, $P < 0.01$).

DISCUSSION

Cholinergic nerves are one of the most important factors for studying gastrointestinal dynamic diseases

(6). Acetylcholine, an excitatory neurotransmitter released by cholinergic nerves, plays an important role in the regulation of gastrointestinal motility (7). In our study, we directly observed AchE with the Karnovsky-Roots method, and the results showed that whole mount stretch preparation can clearly display cholinergic nerves in the myenteric plexus of gastric antrum. Moreover, a typical network distribution of AchE-positive nerves was found in the myenteric plexus of gastric antrum in the control group, and more AchE-positive nerve cells were found in the ganglion. However, in the model group, the number of cholinergic neurons was lower in the myenteric plexus of gastric antrum, and their nerve fibers were thinner with weaker staining.

NADPH diaphorase, a histochemical marker of NOS, has been widely used for NOS localization, and we analyzed the gastric myenteric plexus using NADPH histochemical staining and whole mount stretch preparation. Intriguingly, we found that the decreased gastrointestinal function in the model group was related to the increased number of nitrergic neurons in the myenteric plexus of gastric antrum.

Previously, the basic electrical rhythm was found in ICCs of the gastrointestinal tract (8). ICCs have been demonstrated to initiate slow wave activity in gastrointestinal smooth muscle, promote the transmission caused by electrical activity, regulate neurotransmitter function, and regulate the immunomodulatory effect (9, 10). The occurrence of a variety of gastrointestinal motility diseases was closely correlated with changes in ICCs (11). Furthermore, ICCs in the gastric body and antrum of diabetic mice were significantly decreased, especially at the distal area of gastric antrum (12). Similarly, ICCs in the gastrointestinal tract of diabetic patients were significantly decreased and exhibited an altered ultrastructure (13, 14). ICCs express c-kit, a receptor of tyrosine protein kinase, and thus c-kit expression could serve as a marker for gastrointestinal ICCs (15). In the model group, c-kit staining in the gastric antrum was weaker and demonstrated that the number of ICCs in this group was lower than that in the control group, and the model group exhibited an altered ultrastructure of ICCs. This suggests that the decreased gastrointestinal function in the model group may be related to the decreased number and destruction of ICCs in the gastrointestinal tract.

ACKNOWLEDGEMENTS

This work was supported by the scientific research program of Fuzhou city (No, 2011-S-69-3), the National Natural Science Foundation of China (No. 81772994), the International Collaborative Project of Fujian Province (No. 2017I0014) and the Program for the Top Young Innovative Talents of Fujian Province (No. 2016RCLKC).

REFERENCES

1. Sedhom D, D'Souza M, John E, rustgi V. Viral hepatitis and acute liver failure: still a problem. Clin Liver Dis 2018; 22:289-300.
2. Chen Z, Diaz G, Pollicino T, et al. Role of humoral immunity against hepatitis B virus core antigen in the pathogenesis of acute liver failure. Proc Natl Acad Sci U S A 2018; 115:E11369-E11378.
3. Katoonizadeh A, Laleman W, Verslype C, Wilmer A, Maleux G, Roskams T, Nevens F. Early features of acute-on-chronic alcoholic liver failure: a prospective cohort study. Gut 2010; 59:1561-69.
4. Kalaitzakis E. Gastrointestinal dysfunction in liver cirrhosis. World J Gastroenterol 2014; 20:14686-95.
5. Groneberg D, Lies B, Konig P, et al. Cell-specific deletion of nitric oxide-sensitive guanylyl cyclase reveals a dual pathway for nitrergic neuromuscular transmission in the murine fundus. Gastroenterology 2013; 145:188-96.
6. Kobayashi H, Li Z, Yamataka A, Lane GJ, Yokota H, Watanabe A, Miyano T. Acetylcholinesterase distribution and refractory constipation - a new criterion for diagnosis and management. Pediatr Surg Int 2002; 18:349-53.
7. Zheng LF, Wang ZY, Li XF, et al. Reduced expression of choline acetyltransferase in vagal motoneurons and gastric motor dysfunction in a 6-OHDA rat model of Parkinson's disease. Brain Res 2011; 1420:59-67.
8. Barajas-Lopez C, Berezin I, Daniel EE, Huizinga JD. Pacemaker activity recorded in interstitial cells of Cajal of the gastrointestinal tract. Am J Physiol

1989; 257:C830-35.
9. Huizinga JD, Robinson TL, Thomsen L. The search for the origin of rhythmicity in intestinal contraction; from tissue to single cells. Neurogastroenterol Motil 2000; 12:3-9.
10. Ward SM, Beckett EA, Wang X, Baker F, Khoyi M, Sanders KM. Interstitial cells of Cajal mediate cholinergic neurotransmission from enteric motor neurons. J Neurosci 2000; 20:1393-403.
11. Jain D, Moussa K, Tandon M, Culpepper-Morgan J, Proctor DD. Role of interstitial cells of Cajal in motility disorders of the bowel. Am J Gastroenterol 2003; 98:618-24.
12. Ordog T, Takayama I, Cheung WK, Ward SM, Sanders KM. Remodeling of networks of interstitial cells of Cajal in a murine model of diabetic gastroparesis. Diabetes 2000; 49:1731-39.
13. Kim ER, Kim KM, Lee JY, et al. The clue of Interstitial Cell of Cajalopathy (ICCpathy) in human diabetic gastropathy: the ultrastructural and electrical clues of ICCpathy in human diabetic gastropathy. Exp Toxicol Pathol 2012; 64:521-26.
14. Iwasaki H, Kajimura M, Osawa S, Kanaoka S, Furuta T, Ikuma M, Hishida A. A deficiency of gastric interstitial cells of Cajal accompanied by decreased expression of neuronal nitric oxide synthase and substance P in patients with type 2 diabetes mellitus. J Gastroenterol 2006; 41:1076-87.
15. Burns AJ, Herbert TM, Ward SM, Sanders KM. Interstitial cells of Cajal in the guinea-pig gastrointestinal tract as revealed by c-Kit immunohistochemistry. Cell Tissue Res 1997; 290:11-20.

JOURNAL OF BIOLOGICAL REGULATORS & HOMEOSTATIC AGENTS Vol. 33, no. 6, 1811-1813 (2019)

LETTER TO THE EDITOR

DOES RUOCCO'S HYPOTHESIS ON IMMUNOCOMPROMISED CUTANEOUS AREA POTENTIATE THE EARLY SURGICAL REMOVAL OF CUTANEOUS BENIGN LESIONS AS ADEQUATE PREVENTION?

G. TCHERNEV and I. TEMELKOVA

Onkoderma- Clinic for Dermatology, Venereology and Dermatologic Surgery, Sofia, Bulgaria

Received September 24, 2019 – Accepted October 10, 2019

To the Editor,

We present the case of a 79-year-old man referred to our Department for the appearance of a large tumoral lesion on the abdominal wall with a duration of 5-6 months (Fig. 1a-b). According to the patient, during this period the tumour progressively increased in size, including the left inguinal region. In the dermatological examination, a giant tumour with pink color, covering the lower abdomen and left inguinal region, was observed (Fig. 1a-b). The patient gave an informed consent to publish his case report.

Additionally, the presence of comedone, which was formed more than eight years ago, in the right part of the tumour lesion was visualized during the clinical examination (Fig. 1a-b). After a thorough and detailed anamnestic record, the affected area was found to be a comedo, mechanically manipulated many times over the last 10 years. Based on clinical and anamnestic data it was initially thought to be a comedo-associated/induced inflammatory reaction, such as paniculitis or folliculitis. In the differential diagnostic aspect, the following was considered: primary cutaneous B-cell lymphoma, primary cutaneous T-cell lymphoma, Merkel cell carcinoma, giant metastasis of unknown primary tumor, or per continuitatem spread of tumorous lesion with primary pelvic or intra-abdominal localization and susbsequent secondary cutaneous involvement. Paraclinical studies showed elevated erythrocyte sedimentation rate (ESR) values (54mm/h), CRP (54.15 mg/l), monocytosis data (11.7%), dyslipidemia and slightly decreased Hgb (132g/L) and Hct (0.385L/L). A biopsy was taken for a histological examination, which showed evidence of a massive lymphocyte infiltration of the skin and subcutis large cells with abundant cytoplasm as well as a large round-ovoid nuclei (Fig. 1c), thus determining a large cell B-cell non-Hodgkin's lymphoma. Subsequent immunohistochemical studies found positive cell expression for CD20 (Fig. 1d), with single stromal cells expressing CD3, MUM1 positive expression of stromal plasma cells and no expression of CD30. The MRI examination of the pelvis showed evidence of soft pelvic edema, conglomerates of pathologically enlarged lymph nodes with restriction of the diffusion bilaterally inguinal and at the level of aortic bifurcation, concluding the presence of malignant pelvic lymphadenopathy. Data on the malignant nature of the bilateral inguinal lymph nodes were also confirmed on the basis of ultrasound diagnosis. Further to clinical, histological, immunohistochemical and instrumental data, the diagnosis of comedo-associated giant cutaneous CD20 (+) B-cell non-Hodgkin's lymphoma in the

Key words: immunocompromised cutaneous area (ICA); comedo-associated B cell lymphoma; Ruocco's hypothesis; surgical removal; benign lesions; prevention

Corresponding Author:
Prof. Dr. Georgi Tchernev,
Department of Dermatology,
Venereology and Dermatologic Surgery,
Medical Institute of Ministry of Interior (MVR),
General Skobelev 79, 1606 Sofia, Bulgaria
e-mail: georgi_tchernev@yahoo.de

0393-974X (2019)

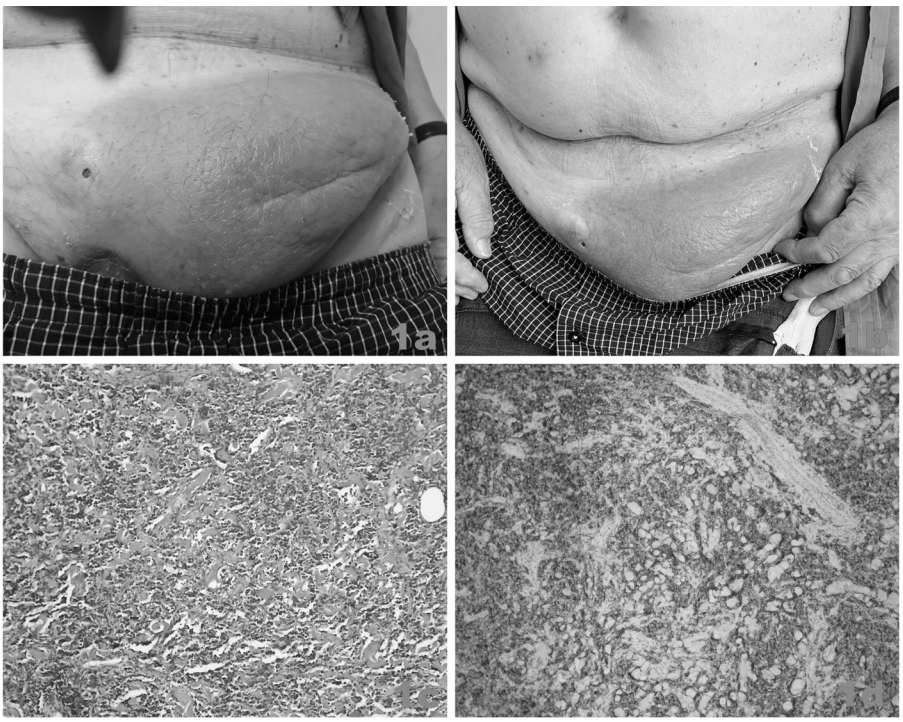

Fig. 1. ***a,b)*** *Clinical view: giant tumor formation with pink color covering the lower abdomen and left inguinal region.* ***c)*** *Histological examination: HE staining- massive lymphocyte infiltration of skin and subcutis large cells with abundant cytoplasm and large round-ovoid nuclei.* ***d)*** *Immunohistochemical study - positive cell expression for CD20.*

abdominal area, arising from recurrent mechanical irritation of comedones in the past, was diagnosed. The performed staging identified B-cell lymphoma stage I (T1bN1M0). Initial chemotherapy was planned in order to prevent the so-called cytokine-release syndrome and subsequently to switch to a systemic therapy with Rituximab.

We present a case where we describe the possibility of developing B-cell lymphoma based on the concept of ‚locus minoris resistentiae' (lmr) or immunocompromised cutaneous area (ICA) (3). In accordance with this model, previously injured cutaneous sites, as in the case of mechanical irritation of simple comedone for example, may become areas for the outbreak of opportunistic infections, tumors, and immune reactions (3). According to the ICA theory, even after a long period of time and the disappearance of the causing event, the affected district may appear clinically normal, but its immune behavior is often compromised forever (2). Based on the model proposed by Ruocco et al. for ICA-defined clinical events, these can selectively damage and immunologically mark the cutaneous area they act upon, as in the case described, such an event being the mechanical treatment of comedone (2). This line of conception actually regards it as a form of "acquired immune dysregulation" (4).

The open controversial question in this case remains whether the early surgical eradication of lesions initially benign in nature would have a preventive effect on the development of neoplasms in the future. We share the hypothesis that the accurate identification of new inducers of Lmr/ICA would lead to an increase in the number of surgical excisions performed in benign early-stage skin lesions, which would, however, reduce the future development of malignant tumors, including skin lymphomas.

REFERENCES

1. Caccavale S, Kannangara AP, Ruocco E. The immunocompromised cutaneous district and the necessity of a new classification of its disparate causes. Indian J Dermatol Venereol Leprol 2016; 82(2):227-29.
2. Ruocco V, Brunetti G, Puca R, Ruocco E. The immunocompromised district: a unifying concept for lymphoedematous, herpes-infected and otherwise damaged sites. J Eur Acad Dermatol Venereol 2009; 23(12):1364-73.
3. Piccolo V, Baroni A, Russo T, Schwartz R. Ruocco's immunocompromised cutaneous district. Int J Dermatol 2016; 55(2):135-41.
4. Lo Schiavo A, Ruocco E, Gambardella A, O'Leary R, Gee S. Granulomatous dysimmune reactions (sarcoidosis, granuloma annulare, and others) on differently injured skin areas. Clin Dermatol 2014; 32(5):646-53.

LETTER TO THE EDITOR

ANTI-INFLAMMATORY AND ANALGESIC EFFECTS OF ELEUTHEROSIDE E IN ALCOHOLIC BEVERAGE

YC. LIU[1], YJ. YANG[2], MS. CHEN[2], Z. WANG[1], YH. CHEN[3], YF. ZHANG[3], YM. SHAN[3] and B. YU[3]

[1]Jing Brand Co., Ltd. Daye, Hubei Province, China; [2]Hubei Provincial Key Lab for Quality and Safety of Traditional Chinese Medicine Health Food, Daye, Hubei Province, China; [3]Jing Brand Research Institute, Daye, Hubei Province, China

Received August 8, 2019 – Accepted October 7, 2019

To the Editor,

Herbal liqueurs, such as Jägermeister, Becherovka and Jing liquor, are widely popular in the world and are considered to have certain health care effects because of their active pharmaceutical ingredients, but most of them are not verified by experiment. Rheumatoid arthritis (RA), which is characterized by pain, swelling and the destruction of joints, is one of the most prevalent chronic inflammatory joint diseases (1). Medicinal liquors such as Zhui-Feng liquor containing *Acanthopanax senticosus* are considered to have effect of anti-rheumatoid arthritis in traditional Chinese medicine. Eleutheroside E (EE) is the main active ingredient of senticosus, which was confirmed to be able to alleviate arthritis in collagen-induced arthritis mice model by suppressing inflammatory cytokine release (2). This research aimed to verify the anti-inflammatory and analgesic effects of EE in alcoholic beverage.

MATERIALS AND METHODS

EE was dissolved in 15% vol alcohol, the low/middle/high doses of treated groups were converted from 100/300/1000 $mg.L^{-1}$ EE, respectively, and prepared for the gavage doses for animals (0.2 ml per 10 g.bw).

Ninety SPF male Kun Ming (KM) mice (18–22 g) were provided by the Hubei Provincial Key Lab for Quality and Safety of Traditional Chinese Medicine Health Food. The mice were randomized into six groups: control group (distilled water), alcohol group (15% ethanol), positive group (dexamethasone acetate), and EE low/middle/high dose groups. All groups received intragastric administration of 0.2 ml per 10 g/bw of their respective treatment once a day for 14 days, except the positive group. The positive group mice were administered dexamethasone acetate 6 mg/kg p.o. from day 8 to 14. At day 14, mice were fasted for 12 h, 60 min after the final administration, 1% Evans blue was injected through the tail intravenously (0.1 ml/10 g.bw), and then acetic acid (0.6%) was administered by intraperitoneal injection (0.1 ml/10 g.bw) for peritoneal effusion. Mice were sacrificed 20 min later, and abdominal exudatives were collected by 4 ml normal saline peritoneal lavage. After 3000 r/min centrifugation for 15 min, the optical density of the supernatant was measured using a spectrophotometer at 590 nm. The change

Key words: eleutheroside E; alcohol; anti-inflammatory; analgesic; antiarthritic

Corresponding Author:
Mo-Si Chen,
Hubei Provincial Key Lab for Quality
and Safety of Traditional Chinese Medicine Health Food,
Daye Avenue 169, Daye, Hubei, 435100, China
Tel.: +86 0714 8855631 - Fax: +86 0714 8770541
e-mail: ccmmss@sina.com

0393-974X (2019)

in blood capillary permeability was presented as the OD value (3).

Xylene-induced mouse ear edema

Animals were randomized into six groups and treated as above, and ear edema analysis in mice was performed using a method described in previous studies (3). Briefly, 60 min after the final administration, each animal received 20 µl of xylene on the anterior and posterior surface of the right ear, and the left ear was considered as a negative control. Twenty min later, mice were sacrificed, and both ears were sampled with a punch (5 mm diameter) and weighed. The extent of ear edema was evaluated by the weight difference between the right and the left ear biopsies of the same animal.

Carrageenan-induced paw edema test

Male Wistar rats were randomized into six groups and treated as above, but in the positive group, rats were administered dexamethasone acetate 0.05 ml/10 g.bw intraperitoneal injection only once before the test. On the 14th day, 60 min after the final administration, each rat was given a subcutaneous injection of 0.1 ml freshly prepared carrageenan suspension (1% w/v) in the right hind paw. The degree of swelling = final paw volume – initial paw volume, was calculated every hour for 6 h (4).

Acetic acid-induced abdominal writhing test

KM mice were randomized into six groups and treated as above, but in the positive group, rats were administered 300 mg/kg aspirin via intragastric administration from day 8 to 14. On the 14th day, all the mice received intraperitoneal acetic acid solution (10 ml/kg, 0.6%) 60 min after the final administration, and the time when the abdominal writhes/constrictions appeared (latent period) was recorded for a period of 15 min (5).

Formalin-induced paw licking test

KM mice were randomized into six groups and treated as above. On the 14th day, animals received a subplantar injection of 20 µl (5%) formalin solution into the right hind paw 60 min after the final administration. Subsequently, the total time of paw licking was observed during the initial (0–5 min) neurogenic phase and late (15–35 min) inflammatory phase after formalin injection. The experiment was performed under strict conditions of no disturbance that may affect the animal's response (5).

Adjuvant-induced arthritis animal models and treatment

The adjuvant-induced arthritis (AIA) Wistar rat models were prepared according to a previous report (6), which was induced by a single injection of 0.1 mL of Freund's complete adjuvant (FCA) into the plantar skin of the right hind paw.

Twelve rats without FCA treatment were used as the normal control group. The AIA rats were divided into six groups (n=12 per group): negative control group (distilled water), alcohol group (15% ethanol), positive group (dexamethasone acetate), and EE low/middle/high dose groups. All groups received intragastric administration of 0.2 ml/10 g.bw once a day for 28 days, except the positive group. The animals in the positive group were administered dexamethasone acetate 1.5 mg/kg via intraperitoneal injection once every three days. After day 28, the rats were fasted for 12 hours and sacrificed by drawing blood from the femoral artery. Blood serum was collected, and the levels of the inflammatory cytokines (IL-1β, IL-6, TNF-α)/anti-inflammatory cytokines (IL-2, IL-10) and IgG were analyzed by an enzyme-linked immunosorbent assay. The fresh ankle joint of the right hind paw was obtained and prepared separately for paraffin sections. After staining with hematoxylin and eosin, the sections were photographed for the analysis of pathology by histopathologic examination. Histopathological scores were determined using a semiquantitative scale of 0 (normal), 1 (mild synovitis), 2 (severe synovitis), 3 (synovitis with chondrogenesis), and 4 (synovitis with bone destruction) (7).

The study was approved by the ethics committee of Hubei Provincial Key Lab for Quality and Safety of Traditional Chinese Medicine Health Food (No.: JB-EC-20180220) and meets the requirements of the Regulations on the Administration of Experimental Animals in Hubei Province as well as the requirements of the Universal Declaration on Animal Welfare.

Statistical analysis

The results were presented as the mean±S.E.M., statistical comparison of data was performed by one-way analysis of variance (ANOVA) when the data conformed to normal distribution, and the Wilcoxon rank sum test was used when data did not comply with the normal distribution; $p<0.05$ was considered significant.

RESULTS

Anti-inflammatory effects

The capillary permeability was represented by the amount of Evans blue that extruded into the peritoneal cavity, which was measured by the OD value of the abdominal exudatives. In this study, the OD value of the control group was markedly increased by the influence of acetic acid. When compared with the control group, treatment with a low/middle/high dose of alcoholic solution containing EE produced a dose-dependent inhibitory effect on capillary permeability, which demonstrated that EE could alleviate inflammatory exudation.

The ear edema was represented as the ear edema index, which was assessed as the weight increase of the right ear over the left ear. The application of xylene in the mouse ears resulted in a significant increase in ear weight in the control group, and compared

Table I. *Effect of alcoholic solution containing EE on the acetic acid-induced abdominal writhing test.*

Group	Dose	Latent period (min)	Times of abdominal writhes
Control group	Normal saline	5.69±1.85	14.57±9.09
Aspirin group	300 $mg.kg^{-1}$	9.03±2.78*	2.22±2.28*
Alcohol group	15% Ethanol	6.04±2.75	11.50±7.78
EE group	100 $mg.L^{-1}$	5.73±2.72	11.15±9.30
	300 $mg.L^{-1}$	5.81±1.90	9.46±6.06
	1000 $mg.L^{-1}$	5.81±2.41	6.36±4.80*

** $p<0.05$ compared with the control group*

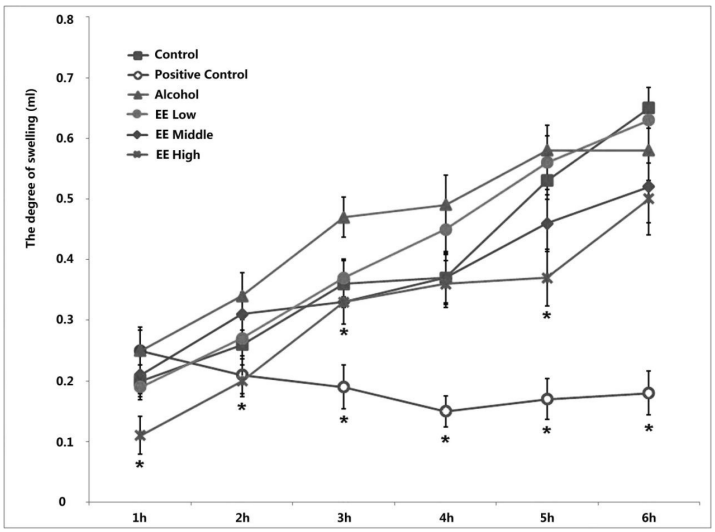

Fig. 1. *Effect of EE on carrageenan-induced paw edema. * $p<0.05$ compared with the control group.*

with the control group, animals in the EE-treated (100/300/1000 mg.L^{-1}) groups showed a significant inhibition of ear edema. The results demonstrated that administration of EE decreased xylene-induced inflammatory swelling.

As illustrated in Fig. 1, the subcutaneous injection of carrageenan (1.0 mg/paw) induced a noticeable mechanical hypernociception, and treatment with dexamethasone significantly reduced swelling. The systemic administration of the EE 1000 mg.L^{-1} produced a significant reduction of the mechanical hypernociceptive response at 1h, 2h, 3h and 5h after the injection.

The acetic acid-induced abdominal writhing test is a nonspecific procedure for the determination of analgesia, results showed that the reference standard drug aspirin produced a greater inhibitory effect, and in the test groups treated with a low/middle/high dose of alcoholic solution containing EE, an inhibition of the abdominal writhes were observed. Significant analgesic activity was recorded at the middle dose compared to the control group, as depicted in Table I.

The formalin-induced pain paradigm is a well-recommended biphasic procedure for the determination of antinociceptive activity (5). The first phase is for the initial 5 min (neurogenic phase), and the second phase takes 20 to 30 min (inflammatory phase). The experimental result (Fig. 2) showed that alcoholic solution containing EE significantly decreased paw licking in both the neurogenic and inflammatory phases of the formalin-induced paw-licking test in mice. Statistics indicate that EE significantly inhibited both phases, while the positive control drug aspirin only inhibited the second phase, and the alcohol group (15% ethanol) was not affected. Thus, the antinociceptive potential might be due to involvement of both peripheral and central pathways.

Antiarthritic activity in vivo

As shown in Fig. 3, compared with the arthritis model group, the levels of the inflammatory cytokines IL-6 and IgG in the EE groups were obviously decreased, and the level of the anti-inflammatory cytokine IL-10 in the EE high dose group was obviously increased. Treatment with EE did not influence the levels of IL-1β, IL-2 or TNF-α in the arthritis model rats.

The effects of alcoholic solution containing EE on the histopathological changes are presented in Fig. 4. The rats were sacrificed on day 28 after induction of AIA, and ankle joints were subjected to histopathological examination. As shown in Fig. 4A, intense inflammatory cell infiltration consisting of lymphocytes, macrophages and eosinophils, synovial thickening, and significant proliferation of synovial tissue and fibrous tissue were observed in the model group, whereas the normal control group displayed

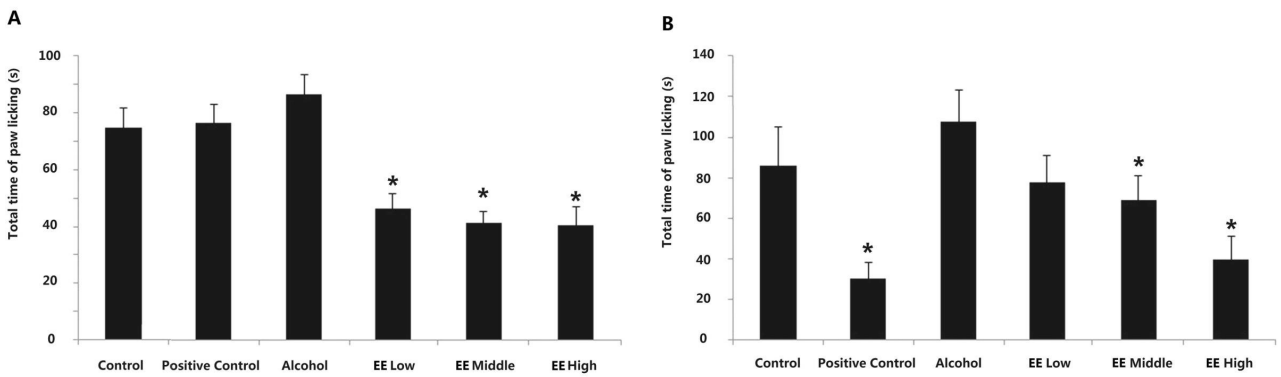

Fig. 2. *Effect of EE on the neurogenic pain phase (**A**) and inflammatory pain phase (**B**) of the formalin-induced paw licking test. * $p<0.05$ compared with the control group.*

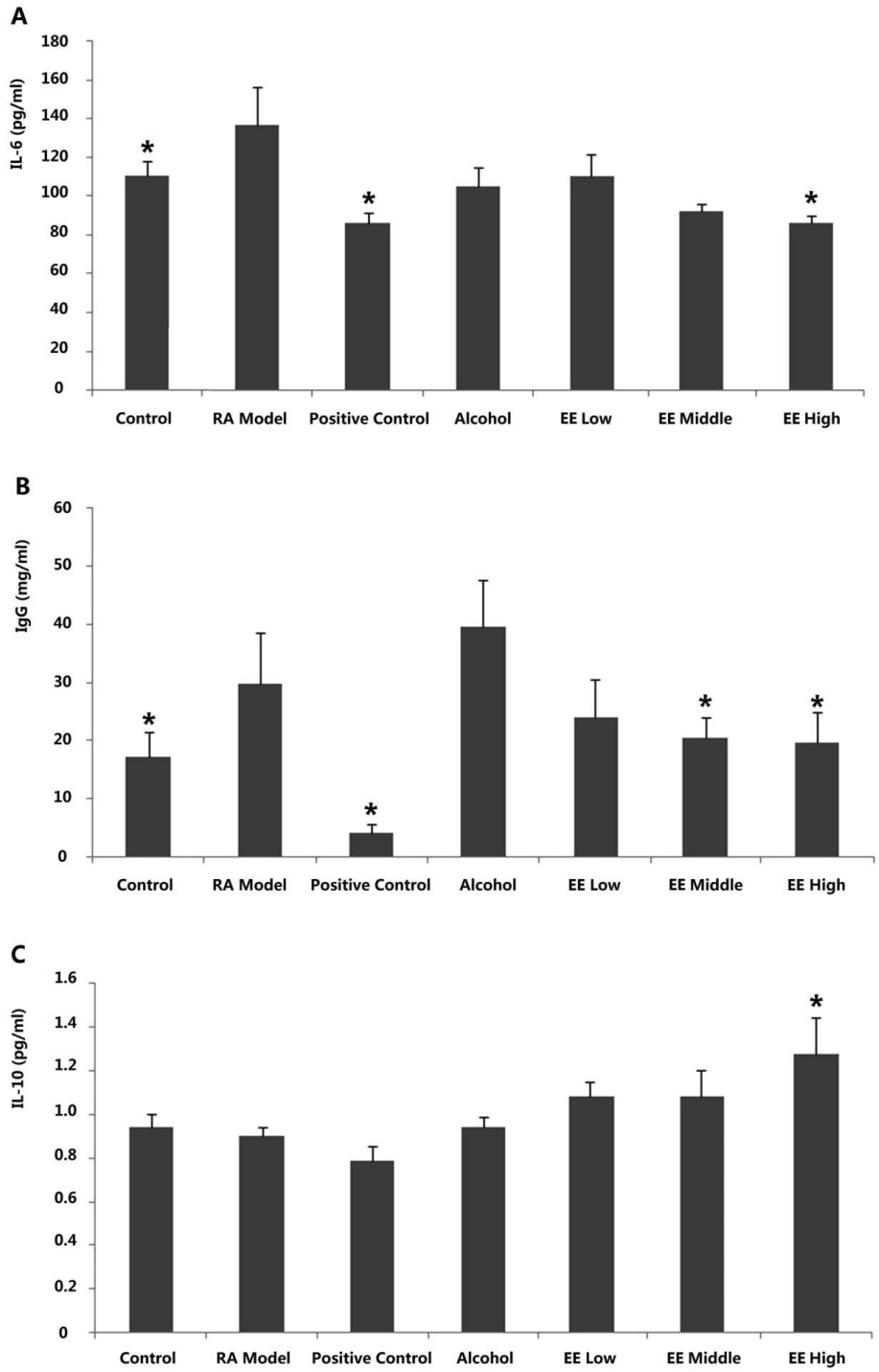

Fig. 3. *Effect of EE on the levels of the inflammatory cytokines IL-6 (**A**), IgG (**B**) and IL-10 (**C**) in vivo. * $p<0.05$ compared with the rheumatoid arthritis (RA) model group.*

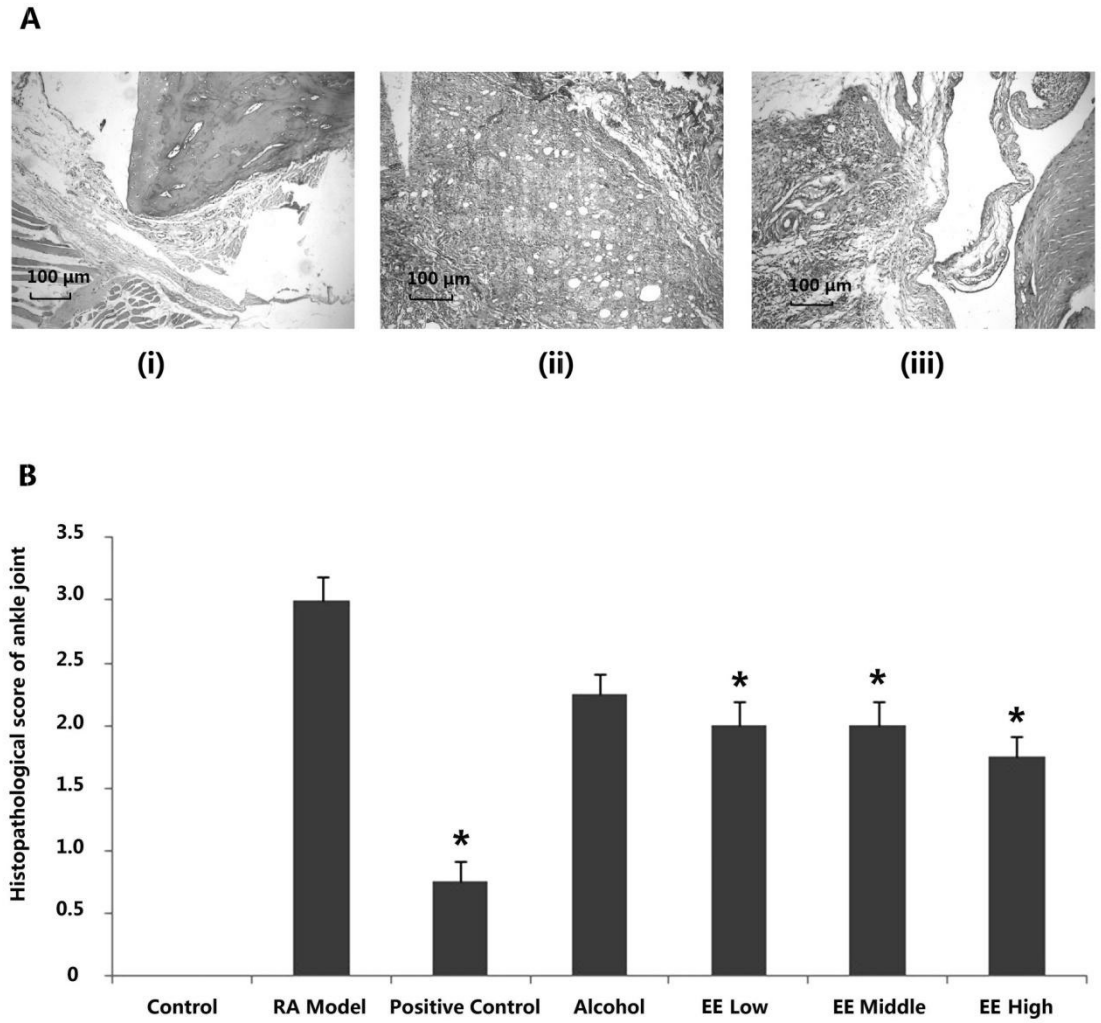

Fig. 4. ***A)*** *Pathological sections of the (i) control group, (ii) rheumatoid arthritis (RA) model group, and (iii) RA model group treated by alcoholic solution containing EE.* ***B)*** *Histopathological scores of the ankle joint pathological degree in each group. *p<0.05 compared with the rheumatoid arthritis (RA) model group.*

no inflammatory cell infiltration. Treatment with EE or dexamethasone resulted in a significant reduction in these symptoms. As indicated in Fig. 4B, the scores for the four indicators in the EE and dexamethasone groups were less than those of the model group, thus indicating an obvious therapeutic effect of EE.

DISCUSSION

The relationship between RA and alcohol consumption is unclear. The protective effect of alcohol on developing RA was supported by some researchers through systematic reviews and meta-analyses (8), but other studies did not support a causal inverse association between alcohol intake and RA occurrence (9). The antiarthritic activities of the ethanol extracts of specific herbs were supported by pharmacological experimental evidence (10). Alcoholic solution containing EE could alleviate inflammatory exudation and edema, demonstrating it had an anti-acute inflammatory effect. Alcoholic solution containing EE inhibited the abdominal writhes induced by acetic acid intraperitoneal injection and significantly decreased the paw licking

in both the neurogenic and inflammatory phases of the formalin-induced paw licking test in mice, demonstrating its analgesic effect, while the alcohol control group had no significant effect.

Inflammatory cytokines, including IL-10, IL-6, IL-1, IL-1β and TNF-α, are involved in the pathogenesis of RA by inducing the infiltration of immune cells into lesion areas, stimulating the release of proteinases to degrade cartilage, and upregulating the expression of proinflammatory genes (11, 12). Our experiments showed that alcoholic solution containing EE had the effect of anti-adjuvant arthritis in the rat model, which could inhibit foot swelling and synovial inflammatory lesions. The mechanism may be due to the nonspecific anti-inflammatory effect of EE, which could downregulate the serum proinflammatory cytokines (IL-6, IL-1β, TNF-α) and serum IgG levels, upregulate the anti-inflammatory cytokines (IL-10, IL-2) in RA model rats, but the pharmacological action needs to be proven in long-time consumer groups of alcoholic beverage containing EE.

ACKNOWLEDGEMENT

The authors would like to thank Professor Nan Zeng, Chengdu University of Traditional Chinese Medicine.

REFERENCES

1. Smolen JS, Aletaha D, Koeller M, Weisman MH, Emery P. New therapies for treatment of rheumatoid arthritis. Lancet 2007; 370:1861-74.
2. He C, Chen X, Zhao C, Qie Y, Yan Z, Zhu X. Eleutheroside E Ameliorates Arthritis Severity in Collagen-Induced Arthritis Mice Model by Suppressing Inflammatory Cytokine Release. Inflammation 2014; 37:1533-43.
3. Li CW, Wu XL, Zhao XN, et al. Anti-Inflammatory Property of the Ethanol Extract of the Root and Rhizome of Pogostemon cablin (Blanco) Benth. Scientific World Journal 2013; 2013:434151.
4. Shah SM, Shah SM. Phytochemicals, antioxidant, antinociceptive and anti-inflammatory potential of the aqueous extract of Teucrium stocksianum bioss. BMC Complement Altern Med 2015; 15:351.
5. Khan H, Saeed M, Gilani AU, Khan MA, Dar A, Khan I. The antinociceptive activity of Polygonatumverticillatum rhizomes in pain models. J Ethnopharmacol 2010; 127:521-7.
6. Zheng Z, Sun Y, Liu Z, Zhang M, Li C, Cai H. The effect of curcumin and its nanoformulation on adjuvant-induced arthritis in rats. Drug Des Devel Ther 2015; 9:4931-42.
7. Fouda AM, Berika MY. Evaluation of the effect of hydroalcoholic extract of Zingiber officinale rhizomes in rat collagen-induced arthritis. Basic Clin Pharmacol Toxicol 2009; 104:262-71.
8. Scott IC, Tan R, Stahl D, Steer S, Lewis CM, Cope AP. The protective effect of alcohol on developing rheumatoid arthritis: a systematic review and meta-analysis. Rheumatology (Oxford) 2013; 52:856-67.
9. Bae SC, Lee YH. Alcohol intake and risk of rheumatoid arthritis: a Mendelian randomization study. Z Rheumatol 2018; 9:12.
10. Zhang Q, Yu Y, Li J, et al. Anti-arthritic activities of ethanol extracts of Circaea mollis Sieb. & Zucc. (whole plant) in rodents. J Ethnopharmacol 2018; 225:359-66.
11. McInnes IB, Schett G. The pathogenesis of rheumatoid arthritis. N Engl J Med 2011; 365:2205-19.
12. Lin B, Zhao Y, Han P, et al. Anti-arthritic activity of Xanthium strumarium L. extract on complete Freund's adjuvant induced arthritis in rats. J Ethnopharmacol 2014; 155:248-55.

JOURNAL OF BIOLOGICAL REGULATORS & HOMEOSTATIC AGENTS Vol. 33, no. 6, 1823-1828 (2019)

LETTER TO THE EDITOR

LC-MS/MS ANALYSIS REVEALS PLACENTAL DIFFERENTIAL EXPRESSION OF CHORIONIC SOMATOMAMMOTROPIN HORMONE/HUMAN GROWTH HORMONE IN PREGNANCIES WITH GESTATIONAL DIABETES MELLITUS

S. ASHRAF[1,2], N. ROOHI[1], S. ALYAS[1,3], S. ILYAS[1] and Y. ASHRAF[1]

[1]Physiology/Endocrinology Laboratory, Department of Zoology, University of the Punjab, Lahore, Punjab, Pakistan; [2]Department of Biological Sciences, Purdue University, West Lafayette, IN, USA; [3]Institute of Molecular Biology and Biotechnology (IMBB), The University of Lahore, Punjab, Pakistan

Received August 30, 2019 – Accepted October 10, 2019

To the Editor,

Pregnancy has been associated with a diabetogenic environment, characterized by hyperinsulinemia and hyperglycemia (1). Placenta is the functional interface which develops between mother and fetus to secrete and transport growth factors and hormones, with obvious physiological effects. Several maternal adaptations to pregnancy are facilitated by placenta (2).

Hyperglycemia in pregnancy causes insulin resistance in late pregnancy which is a physiological adaptation to shunt adequate amounts of nutrient supplies to the fetus by limiting maternal glucose uptake. During normal pregnancy there is about 50% reduction in insulin-mediated glucose uptake and approximately 200-250% increase in maternal insulin secretion to control glycaemia. Placenta secretes hormones to develop insulin resistance in the maternal physiological environment in order to meet the significant demand of energy and nutrients for fetal growth, which requires around 80% of glucose as energy source (3). Two important hormones which have been attributed to help maternal physiology adapt to pregnancy are the human somatomammotrophin hormone (CSH1) and the human placental growth hormone (hGH) (4).

CSH1 and hGH increase up to 30-fold during pregnancy and tend to enhance beta cell proliferation to increase insulin secretion from pancreas. hPL-mediated increase in insulin level during pregnancy results in insulin resistance (IR) (5). Placental GH also regulates insulin-like growth factor-I (IGF-I) in the maternal body. Moreover, GH also stimulates lipolysis, gluconeogenesis and maternal issue anabolism, as well as influencing placental development, maternal adaptation to pregnancy and fetus growth (6). Available data suggest that placental CSH/GHs hormones are important for adapting the maternal physiological environment to pregnancy, and incidence of GDM may be attributed to the overexpression of these hormones.

MATERIALS AND METHODS

Seven pregnant females complicated with gestational diabetes mellitus (GDM) were recruited for the GDM group. GDM was diagnosed on the basis of International Association of Diabetes and Pregnancy Study Groups (IADPSG) criteria. To minimize age-dependent variations, women of same age group (30-35) were selected for study. The control group comprised of seven age-matched healthy pregnant females with normal glucose tolerance during pregnancy. Categorical parameters (age, BMI, gravidity

Key words: pregnancy; gestational diabetes mellitus; placenta, chorionic somatomammotropin hormone; human growth hormone; insulin resistance

Corresponding Author:
Dr Samina Ashraf,
Physiology/Endocrinology Laboratory,
Department of Zoology, University of the Punjab,
Lahore, 54590, Punjab, Pakistan
Tel.: +923371437368
e-mail: saminaash89@gmail.com

0393-974X (2019)

and parity), fasting glycemia and glycated hemoglobin (HbA1c) were recorded and compared between the study groups. Exclusion criteria were pregestational diabetes, type 2 diabetes diagnosed at first trimester, endocrine disorders, renal diseases, drugs and/or alcohol abuse, or other major medical disorders that could interfere with maternal glucose regulation. The exclusion criteria for both GDM and control groups also included hypertensive disorders, assisted reproductive technology treatment, smoking habits, chemical addiction, multiple pregnancies, fetal congenital abnormalities and hypothyroidism/ hyperthyroidism.

This study was approved by the ethics committee of The "University of the Punjab", Lahore. An informed written consent was provided by all participants in the study.

Sample collection and preparation

All placental tissue samples were collected soon after the term caesarean section, in order to avoid possible effects of labor-induced alterations in samples. Immediately after section four different intact placental cotyledons were selected to get approximately 4 cm^3 sized placental villi. Maternal decidual layer was removed carefully and samples were washed with ice cold buffer multiple times to remove excess of blood. Washed samples of placenta were taken from the hospital to the Physiology/Endocrinology laboratory, Department of Zoology, using liquid nitrogen.

A total of 500 mg tissue was disrupted in liquid nitrogen and ground using pestle and mortar with continuous addition of liquid nitrogen to get a powdered form. This powdered sample was dissolved in 1 mL lysis buffer consisting of urea, thiourea, CHAPS, DTT, IPG buffer, PMSF and protease inhibitor. The sample in the lysis buffer was homogenized to obtain a uniform suspension and then incubated on ice for 1 h. After incubation samples were centrifuged for 30 min at 14000 rpm to remove all the debris from samples. Afterwards centrifugation supernatant was collected by removing contaminating constituents in the sample. The supernatant was stored at -80°C for protein extraction.

The protein concentration in samples was estimated by the most rapid and sensitive Bradford method. This method employs Coomassie blue dye G250 which binds with sample proteins and gives maximum absorbance at 595nm wavelength. After quantification the proteins were resolved on gel using 2 dimensional gel electrophoresis

Table I. *Clinical characteristics of gestational diabetes mellitus patients under investigation.*

Clinical parameters	NGT (N=7)	GDM (N=7)	p value	Percentage difference
Age	31.30±0.57	32.05±0.65	0.4	2↑
HbA1c (%)	5.77±0.12	8.97±0.35	< 0.0001***	55↑
BMI (kg/m²)	26.03±0.36	28.21±0.90	0.04*	8↑
FPG (mmol/l)	4.47±0.17	5.01±0.13	0.02*	12↑
1-hr PLG (mmol/l)	6.30±0.17	9.68±0.19	< 0.0001***	53↑
2-hr PLG (mmol/l)	5.20± 0.15	8.52±0.11	< 0.0001***	63↑
Gravidity	1.85±0.14	2.00±0.30	0.68	8↑
Parity	1.85±0.14	1.71±0.18	0.55	8↓

*NGT: Normal glucose tolerance; GDM: Gestational diabetes mellitus; HbA1c: Glycosylated hemoglobin; BMI: Body mass index; FPG: Fasting plasma glucose; PLG: Post load glycemia; ↑increase; ↓Decrease; * significant at P<0.05; *** significant at P<0.001.*

technique. This technique relies on two steps: the first is "first Dimension" which separates proteins based on their isoelectric points (pI), followed by SDS-PAGE in the second dimension which separates proteins based on their molecular weight.

Readystrip IPG strips (Bio-Rad, 17cm, linear, 4-7 pH) were used to perform iso-electric focusing on The PROTEAN® IEF cell (Bio-Rad). Sample for Iso-electric focusing was prepared in rehydration buffer using thiourea, urea, DDT, CHAPS, ampholyte and bromophenol blue. The final concentration was 250 µg protein/300µL of sample. Mineral oil (3 ml) was used after loading the sample in the IPG strip tray to prevent evaporation during rehydration. Rehydration was carried out at 50 V for 12 h and IEF was carried out at 20°C using 10000 V, 40-60000 Vhr. After IEF completion, the IPG strips were removed from the tray and equilibrated with 2% DTT in SDS buffer for 15 min to denature proteins. After incubating in DTT buffer, the strips were incubated in 2.5% IAA SDS buffer for 15 min for alkylation.

Second dimension gel electrophoresis was carried out using PROTEAN II XL Cell (Bio-Rad). 12% polyacrylamide gel was prepared and poured into the inner glass plates of the electrophoresis cell. After polymerization of the gel, the IPG strip was transferred to the gel top. The IPG strip was mounted on gel with the help of 0.5% (w/v) low melting point agarose with bromophenol blue. The standard protein marker (10 ul) was loaded on the "+ ive" end of the IPG strip. The electrophoresis chamber was filled with running buffer containing tris, glycine and SDS. Initially, the gel was allowed to run at 16 mA for approximately 1 h. Afterwards, the current was increased to 35 mA for rest of the duration. The gel was removed from the electrophoresis plates and transferred into a fixative solution and left overnight. Gel was stained using Coomassie brilliant blue G250. Destaining solution was used to destain the gel on a shaker.

All the gels from normal glucose tolerance (NGT) and GDM groups were visualized for differentially expressed spots. Four spots showing upregulation in all the GDM patients in comparison with controls were cut from gels and subjected to LC-MS/MS analysis for protein identification. Samples were then analyzed by LC-MS/MS analysis using the Agilent 1260 Infinity high performance liquid chromatography HPLC system. Peptides were then loaded onto a ProtID-Chip-150 C18 column and separated with a linear gradient of water/acetonitrile/ formic acid.

Statistical analysis

Spectra were analyzed to identify proteins of interest using Mascot sequence matching software [Matrix Science] with MSPnr100 database. Homo sapiens uniprot data was used to match the sequence of our identified proteins. Melanie 2D Gel Analysis Software was used to determine the percentage of area covered by each of the fractions. The data was analyzed statistically using Student's *t*-test.

RESULTS

To prevent possible intrusion from insulin or metformin, only diet-controlled GDM females were enrolled in the study. The physician recommended a customized nutrition plan to all the GDM patients, considering their gestational age, physical activity levels and pre-pregnancy BMI. Age, BMI, HbA1c, fasting glycaemia, 1 h post-load and 2 h post-load glycemic levels were measured for all the subjects under investigation. There was a significantly higher level of glycosylated hemoglobin in GDM-diagnosed women as compared to those of the NGT group. Higher values of HbA1c above the recommended range in late pregnancy are positively correlated with incidence of GDM. Significantly higher BMI was also shown to be associated with GDM patients. Increased BMI develops visceral adiposity which results in insulin resistance. Fasting plasma glucose and OGTT results showed significant elevation in glucose level, indicating hyperglycemic environment in GDM-diagnosed mothers. The clinical characteristics of GDM as well as NGT groups are reported in Table I.

LC-MS/MS

Four spots in the GDM group showing abundance through 2DE gels in placentas of gestational diabetes mellitus patients were subjected to LC-MS/MS analysis. Three spots were identified as uncharacterized protein spots. The scores of these three protein hits were too low to identify them as well characterized proteins, therefore, here only one spot which showed higher Mascot score is discussed. This spot showed protein hits for two proteins, CSH1_HUMAN

Chorionic somatomammotropin hormone 1 and GH1_HUMAN Growth hormone 1 variant 1 (Table II).

Human somatomammotrophin hormone/growth hormone variant 1 spot in 2DE gels was visualized using Melanie software. Raw volume (%) of hCSH/hGH1 spot in comparable groups was measured using Melanie 2D gel analysis software tools (Fig. 1A). Using Graph Pad Prism software (version 6), Student *t*-test revealed 3.1-fold up regulation ($P \leq 0.001$) of hCSH/hGH1 spot in GDM patients when compared to the NGT control group (Fig. 1B).

Table II. *Mascot search result shows protein hits for chorionic somatomammotropin hormone and growth hormone 1.*

Mascot search results	Protein hit 1	Protein hit 2
Protein ID	P0DML2	Q6IYF1
Protein name	Chorionic somatomammotropin hormone	HUMAN Growth hormone 1
Score	436	170
Nominal mass (M_r)	25289	25145
Calculated Pi	5.34	5.29
Protein sequence coverage	53%	18%

Pi: Isoelectric point

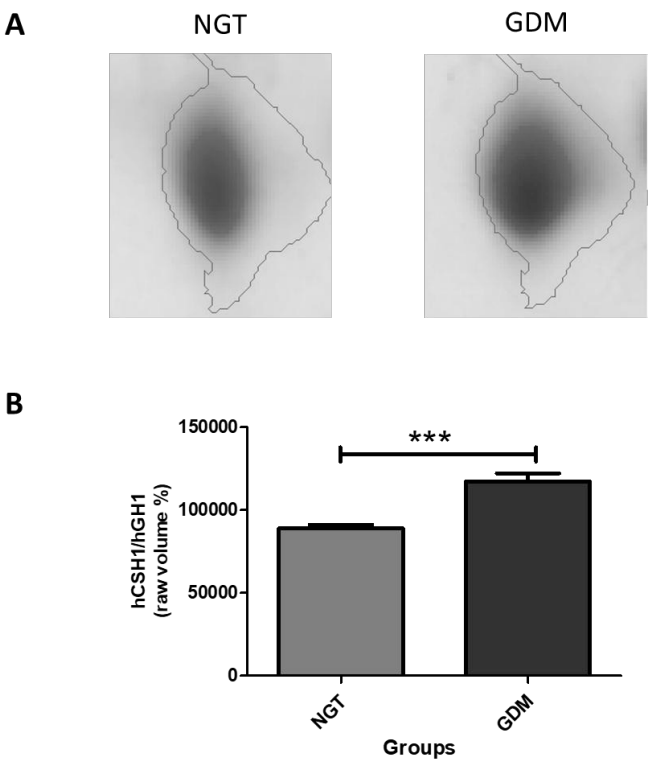

Fig. 1. *hCSH/hGH1 up-regulation in GDM placenta tissue revealed by 2-DE gel analysis (**A**) Raw volume (%) of hCSH/hGH1 spot in comparable groups (B). Values are Mean ± SEM. ***significance at P ≤ 0.001.*

DISCUSSION

Placental tissue produces several hormones and cytokines during pregnancy. Overexpression of hPL and hPGH in pregnant females leads to hyperinsulinemia hence, insulin resistance (7, 8). Results of our study show upregulation of a protein cluster spot consisting of CSH1 and hGH1. Several studies indicate the role of both these hormones in pathophysiology of GDM.

During the second half of pregnancy, human placental lactogen level rises about 10-fold. CSH1 has a somatotropic effect on fat tissues which leads to increased lipolysis, resulting in free fatty acids (FFA) in maternal circulation. This increased FFA level interferes with the insulin-mediated glucose entry through GLUT4 into cells. Hence, CSH1 works as an antagonistic to insulin, decreasing glucose uptake by cells and increasing the insulin level in blood which, ultimately, leads to insulin resistance in pregnant females. Moreover, CSH1 and hGH1 work synergistically to stimulate production of IGF and modulate metabolism by increasing higher amounts of glucose and amino acids to fetus (9).

Maternal fat is another reason for the increase in the expression levels of CSH1 and hGH1 because fat deposits reduce plasma adiponectin which, in turn, stimulates these hormones secretions (10). This increased chorionic somatotropin level can induce β-cell replication which eventually causes IR (11). Increased IR promotes hyperglycemia. Increased glucose content in circulation leads to fetal weight gain. Maternal CSH increases β-cell proliferation in the maternal pancreas, and elevated insulin production helps to compensate maternal IR and defend the body against the complications associated with GDM (12). Higher placental levels of CSH1/hGH1 in our study group might also have interfered with the translocation of GLUT4 transporter through phosphorylation of IRS-1, resulting in poor glycemic control, hence leading to pathogenesis of GDM. Managing overexpressed hPL/hPGH hormones during pregnancy might be helpful in preventing onset of GDM.

ACKNOWLEDGEMENTS

This work was supported by funds released by the Higher Education Commission, Pakistan. We thank the Higher Education Commission Pakistan for providing funds for this study.

REFERENCES

1. Ngala RA, Fondjo LA, Gmagna P, Ghartey FN, Awe MA. Placental peptides metabolism and maternal factors as predictors of risk of gestational diabetes in pregnant women. A case-control study. PLOS ONE 2017; 12:e0181613.
2. Napso T, Yong HEJ, Lopez-Tello J, Sferruzzi-Perri AN. The role of placental hormones in mediating maternal adaptations to support pregnancy and lactation. Front Physiol 2018; 9:1091.
3. Barbour LA, Shao J, Qiao L, et al. Human placental growth hormone causes severe insulin resistance in transgenic mice. Am J Obstet Gynecol 2002; 186:512-17.
4. Männik J, Vaas P, Rull K, Teesalu P, Laan M. Differential placental expression profile of human Growth Hormone/Chorionic Somatomammotropin genes in pregnancies with pre-eclampsia and gestational diabetes mellitus. Mol Cell Endocrinol 2012; 355:180-87.
5. Barbour LA, McCurdy CE, Hernandez TL, Kirwan JP, Catalano PM, Friedman JE. Cellular Mechanisms for Insulin Resistance in Normal Pregnancy and Gestational Diabetes. Diabetes Care 2007; 30:S112-S19.
6. Velegrakis A, Sfakiotaki M, Sifakis S. Human placental growth hormone in normal and abnormal fetal growth. Biomed Rep 2017; 7:115-22.
7. Buchanan TA, Xiang AH. Gestational diabetes mellitus. J Clin Invest 2005; 115:485-93.
8. Hd M, Zeck W, Russell A. Placental growth hormone, fetal growth and the IGF axis in normal diabetic pregnancy. Curr Diabetes Rev 2009; 5:1-5.
9. Chyad M, Faris Shalayel MH. Pathophysiology of Gestational Diabetes Mellitus: The Past, the Present and the Future," in Gestational Diabetes, M. Radenkovic, Ed. InTech, 2011.
10. McDonald EA, Wolfe MW. Adiponectin attenuation

of endocrine function within human term trophoblast Cells. Endocrinology 2009; 150:4358–65.

11. Freemark M, Isabelle A, Don F, Phyllis D, Ann P, Emmanuel O, Will K. Targeted deletion of the prl receptor: effects on islet development, insulin production, and glucose tolerance. Endocrinology 2002; 143:1378-85.
12. Freemark M. Placental hormones and the control of fetal growth. J Clin Endocrinol Metab 2010; 95:2054-57.

JOURNAL OF BIOLOGICAL REGULATORS & HOMEOSTATIC AGENTS Vol. 33, no. 6, 1829-1835 (2019)

LETTER TO THE EDITOR

DIAGNOSTIC ACCURACY OF COMPUTED TOMOGRAPHY-GUIDED NONCOAXIAL CUTTING NEEDLE TRANSTHORACIC LUNG BIOPSIES AND THE ASSOCIATED PNEUMOTHORAX

M. KUKU LJAN[1], D. MILETIĆ[1], E. MRŠIĆ[2], E. OŠTARIJAŠ[2], A. MRŠIĆ[2] and I. ŠOŠA[3]

[1]Department of Radiology, Clinical Hospital Rijeka, Rijeka, Croatia; [2]Faculty of Medicine, University of Rijeka, Rijeka, Croatia; [3]Department of Forensic Medicine and Criminalistics, Faculty of Medicine, University of Rijeka, Rijeka, Croatia

Received August 27, 2019 – Accepted October 11, 2019

To the Editor,

Transthoracic needle biopsy is a preferred radiological method for diagnostics of pulmonary lesions. It has achieved great popularity due to its low invasiveness, precise sample collection, and high diagnostic accuracy. The diagnostic accuracy reported for needle biopsy ranges from 77% to 96% (1).

Cutting needle biopsy provides a tissue sample suitable for cytological and pathological analysis. Computed tomography (CT) is the most common modality used for guidance of pleural, mediastinal, and peripheral lung lesion biopsies. CT reveals anatomic structures and characterizes the lesion, allows path planning that minimizes passage through the lung parenchyma, bullae, fissures or vessels. All of these characteristics are necessary for planning the best and the safest approach to the lesion.

The most common minor complications of CT-guided transthoracic biopsy of lung lesions are pneumothorax and pulmonary hemorrhage. The incidence of pneumothorax, according to the latest meta-analysis, ranges from 22.2% to 28.6%, while the incidence of pulmonary hemorrhage ranges from 13.4% to 23.8%. The rate of major complications such as pneumothorax requiring intervention, hemothorax, air embolism, needle tract seeding, and death is 5.7% (1, 2).

The first objective of this study was to determine the diagnostic accuracy achieved with our biopsy technique. The second objective was to determine the incidence of pneumothorax and chest tube placement among our patients. The third objective of this study was to evaluate the association between individual potential risk factors and the development of pneumothorax. The identification of risk factors is extremely important because, among other reasons, it allows deficiencies of the techniques to be addressed. Furthermore, if the risk of complications for the individual patient is unacceptably high, it is necessary to use alternative methods of diagnosis.

MATERIALS AND METHODS

Patients

This retrospective study included 436 patients who underwent a CT-guided cutting needle biopsy at our institution, due to an etiologically unclear lung lesion, from January 2008 to January 2019. All patients had a single or multiple focal lung lesions with paracentral or peripheral localization, which presented on a CT scan as

Key words: biopsy; pneumothorax; radiology; risk factors; thorax

Corresponding Author:
Asst Prof. Ivan Šoša MD, Ph.D.
Department of Forensic Medicine and Criminalistics,
Faculty of Medicine, University of Rijeka,
Braće Branchetta 20, 51 000 Rijeka, Croatia
Tel.: +385916996969
e-mail: ivan.sosa@medri.uniri.hr

0393-974X (2019)

a nodule or a consolidation, with a diameter greater than 15 mm. Prerequisites for this diagnostic method were signed informed consent, valid coagulation test (not older than 7 days), and the patient`s cooperation. Functional pulmonary tests were not a mandatory part of our biopsy protocol. All patients in this study were hospitalized at the Department of Pulmonology ("Daily hospital") on the day of the biopsy.

Methods

In all the patients, a single needle transthoracic cutting biopsy was performed under CT-guidance (Somatom Sensation 16 and Somatom Definition AS (128)). The patient`s position during the biopsy depended on the location of the lesion (prone, supine, left and right lateral position). During the biopsy, only the segment of the chest in which the lesion was localized was scanned. The puncture site was subcutaneously injected with local anesthetic (2 ml of 2% lidocaine) immediately before the intervention. After the skin incision, all biopsies were performed with an 18-gauge or 16-gauge cutting needle, 10 or 15 cm in length. A 16-gauge cutting needle was used only for lesions that were in direct contact with the pleura and had a diameter greater than 30 mm. There was only one pleural pass while performing the biopsy of lesions that were not in direct contact with the pleura.

Biopsies were planned to avoid major blood vessels and bronchi, as well as fissures and bullae if possible. The biopsy needle was led to the target lesions step by step. After each step, a CT scan was performed to check the position of the needle. Before any manipulation of the needle and before scanning, the patient was asked to stop breathing. Finally, the obtained tissue sample was sent for pathological analysis and its imprint for cytological analysis. To control and evaluate possible complications, the entire thorax was scanned by CT. After the biopsy, patients returned to the Department of Pulmonology. If pneumothorax was documented by the control CT scan, patients with no signs of respiratory insufficiency were treated conservatively and monitored by chest radiogram after 24 hours. If there was no significant increase in the pneumothorax, the patients were released from the hospital with the recommendation to be strictly stationary and report to the pulmonologist examination after 7 days, or earlier if they experienced shortness of breath or chest pain.

The pneumothorax size was determined by measuring the distance between the visceral pleura and chest wall on the control axial CT scan using an electronic ruler on workstation MSCT devices. The longest measured distance was recorded and used in this study. The pulmonary hemorrhage was defined as parenchymal bleeding in the needle track path observed on the control CT-scan after the procedure.

Risk factors for developing pneumothorax and hemorrhage during CT-guided transthoracic needle biopsy were divided into three groups (patient-related, lesion-related, and procedure-related). The first group included factors related to the patient, such as age, gender and patient`s position during the biopsy. The second group included factors related to lung lesion, such as localization, size, and depth. The third group included factors related to the biopsy method, such as the duration of the intervention and the pleura-needle angle.

The lesion localization (upper, lower, and middle lung lobe) was determined based on the chest CT performed before the intervention. The lesion size was determined by measuring the largest diameter in all three planes (axial, coronal, and sagittal) using an electronic ruler on workstation MSCT devices. The depth of the lesion was determined by the trajectory of the needle during the biopsy, a defined distance of the points in which the needle penetrates the pleura and the edge of the lesion. If the needle was fully displayed on the axial CT slices, measuring the distance between these points was carried out on these slices. If the needle was not visible, the specified distance was measured using multiplanar reconstruction. The duration of the transthoracic needle biopsy was determined by the time interval elapsed since the moment the biopsy needle penetrated the pleura until the moment the needle was removed from the thorax. The angle at which the biopsy needle penetrated the pleura was measured on CT sections. The medio-lateral deflection of the needle from the perpendicular was measured from the axial CT sections. Hereafter, the deflection is referred to as the medio-lateral angle. The angle was measured as follows: a tangential line was drawn from the point where the needle penetrated the pleura and marked with the letter "A". Through the same point, a line was drawn perpendicularly to the tangential line and marked with the letter "B". The angle between the intrathoracic part of the biopsy needle and

line "B" corresponded to the angle at which the needle penetrated the pleura during the transthoracic biopsy. These angles were measured by electronic protractor on the workstation MSCT devices.

The final diagnosis of biopsied lesions was one of the three categories: malignant, benign, and inconclusive results. The criteria for malignancy were positive pathological and/or cytological results of malignancy after TTB or surgical resection, and the regression findings on the follow-up radiological examination after completion of oncologic therapy. Malignant findings were divided into primary and secondary malignancies. In the aforementioned, the primary site was labeled as determined or undetermined. Patients who met the criteria for malignancy were included in the group with true positive (TP) results. If the biopsy findings showed a malignancy, but the lesion on the follow-up CT regressed or remained stable, the patients would be included in the group with false positive (FP) results.

The criteria for a benign diagnosis (non-specific pneumonia, tuberculosis, fibrotic mass or scar, neurinoma, and hamartoma) were pathological and/or cytological results of benign entities and if the lesion regressed with conservative medical treatment or remained the same. Patients with these mentioned findings were counted in the group with true negative (TN) results.

The third diagnostic category included inconclusive findings (atypical cells or non-representative samples) when malignancy was suspected but undiagnosed. In this group of patients, when the CT findings and clinical course indicated malignant lung disease, the diagnosis was confirmed by pathological results after repeated bronchoscopy or open surgical biopsy. Patients who met the criteria for inconclusive findings were included in the false negative (FN) group. All patients were clinically monitored with control non-invasive radiological methods (chest radiographs or chest CT) for a period of 2-12 months.

Based on the division of patients in groups of TP, TN, FP and FN results, we calculated the sensitivity, specificity, diagnostic accuracy, positive and negative predictive values by using standard formulas: sensitivity = TP/(TP + FN); specificity = TN/(TN + FP); diagnostic accuracy = (TN + TP)/(TN+TP+FN+FP); positive predictive value (PPV) = TP/(TP + FP); and negative predictive value (PNV) = TN/(TN + FN).

Statistical analysis

Patient data were collected from a hospital information system (WIN BIS), while TTB information was gathered from the ISSA application. Percentages, means, medians and standard deviations were calculated from descriptive statistical methods. Gathered data were processed using IBM SPSS Statistics (version 25). Differences between the two groups were calculated using the non-parametric Mann-Whitney U-test. To determine differences between groups of patients, the data were expressed in terms of frequencies using the chi-square test; while the correlation between the used variables was calculated using Spearman's correlation coefficient. Differences were considered significant when the *p*-value was below 0.05.

RESULTS

A total of 436 patients, 289 (66.3%) men and 147 (33.7%) women, were included in the study. The youngest patient was 25 years old and the oldest was 90. The mean age of our patients was 67.62±11.16 years. Pneumothorax occurred in 115 patients or 26.4%. 94 (21.6%) patients had a pneumothorax thickness of 20 mm, and 18 patients (4.1%) had a pneumothorax thickness of 21-40 mm. Only three (0.7%) patients had a pneumothorax thickness greater than 40 mm. One patient (0.2%) required chest tube placement. All patients with maximal pneumothorax thickness of 20 mm were discharged from the hospital within 24 hours of the biopsy. Of the 18 patients who had pneumothorax thickness of 21-40 mm, 12 patients were kept in the hospital because they were elderly or their place of residence was not well connected with other major centers. As a precaution, three patients with pneumothorax thickness wider than 40 mm were kept in the hospital for observation. Hospitalization did not last longer than 7 days for all 15 patients. Out of the total number of biopsies, 37 (8.5%) resulted in pulmonary hemorrhage, four (0.92%) patients experienced hemoptysis and no patient had hemothorax.

The size of the pulmonary lesion was based on the longest measured diameter, which ranged from 15-170 mm (median = 50.69±25.45mm). Our results indicated that there was a statistically significant difference in the size of the lesion between the group

in which pneumothorax occurred (median = 38 mm) and the group of patients without pneumothorax (median = 51 mm) (U = 13353.5; $p < 0.001$; Fig. 1A). Also, the results of the Mann-Whitney U-test indicated a statistical difference between the incidence of pulmonary hemorrhage and the lesion size, as hemorrhage was more frequent in patients with a smaller diameter lesion (U = 4678.0; $p < 0.001$; Fig. 1B).

Lesion depth was determined by the needle trajectory during a biopsy, a defined distance between the points where the needle penetrated the pleura and the lesion edge. The distance was 0 mm in 217 patients, meaning the lesion was in direct contact with the surface of the visceral pleura. The remaining 219 patients had pulmonary lesions at distances from the surface of the pleura ranging from 4-77 mm (median = 12.88±15.82 mm). We found a big difference in the pneumothorax rate between patients with a 0 mm lesion distance and all the others. The pneumothorax rate was higher in patients with distances greater than 0 mm ($\chi 2$ = 98.827; df = 1; $p < 0.001$). Therefore, direct pleura-lesion contact can be considered as a protective factor for pneumothorax. There was an irregular distribution of tumor depth; therefore, this difference was tested by the Mann-Whitney U-test. The results indicated a significantly higher rate of pneumothorax in patients with target lesion located at a greater distance from the surface of the pleura (U = 6564.5; $p < 0.001$).

Regarding the size of pneumothorax, Spearman test showed statistically significant correlation between the depth of the lesion and the size of the pneumothorax (ρ = 0.523; $p < 0.001$) while Mann-Whitney U-test indicated a significant difference in the size of pneumothorax between group of patients with 0 mm lesion distance and those with lesions located at greater distance from pleura (U = 13610.0; $p < 0.001$). In addition, the results of the Mann-Whitney U-test showed a significantly higher rate of pulmonary hemorrhage in patients with a greater pleura-lesion distance (U = 3080.0; $p < 0.001$).

Duration of the needle biopsy was the period from pleural penetration until needle extraction. All interventions were performed between 5 s and 16.25 min, and the average time was 2.88±3.2 min. Mann-Whitney U-test showed a higher rate of pneumothorax in the group of patients with a longer duration of the procedure (U = 13892.5; $p < 0.001$; Fig. 1C). To assess the difference between the duration of the procedure in the groups of patients with and without pulmonary hemorrhage, the results of the Mann-Whitney U-test indicated a significantly higher incidence of hemorrhage in patients with longer duration of the intervention (U = 4932.0; $p = 0.001$).

It is important to emphasize that in this study the number of pleural penetrations, during the biopsy, was not considered as a possible risk factor for pneumothorax, since a single pleural penetration was performed when the deeper lesions were biopsied.

The next examined variable was the patient`s position during the intervention. There was a statistically significant difference between the rate of pneumothorax and a certain placement of patients. The difference was significant in the group of patients placed in the prone position (lower pneumothorax rate) and supine position (higher pneumothorax rate) (χ^2 = 7.860; df = 3; $p < 0.05$).

The frequency of pneumothorax after CT-guided transthoracic needle biopsy was not statistically significantly different between the genders, different pleura-needle angle or localizations of the lesions (χ^2-test; $p > 0.05$). Our study did not determine any connection between the incidence of pneumothorax and patient`s age, nor did it determine the connection between the size of pneumothorax and different lesion localizations or patient`s positions (Mann-Whitney U-test; $p > 0.05$). Moreover, there was no positive correlation between the size of pneumothorax and pleura-needle angle, duration of procedure or size of the lesion (Spearman correlation; $p > 0.05$).

According to the literature, intrapulmonary hemorrhage may be a protective factor for the development of pneumothorax, effectively sealing the biopsy tract. In this study, 17 (45.9%) patients with pulmonary hemorrhage presented also with pneumothorax, so we cannot conclude with certainty that hemorrhage was a protective factor for pneumothorax.

Diagnoses were established based on pathological and/or cytological analysis of samples obtained by

Table I. *Pathologic/cytologic findings for 436 biopsies.*

Pathologic/cytologic finding	No of Patients	%
Primary malignancy	**292**	**67**
Adenocarcinoma	155	35.6
Squamous cell carcinoma	75	17.2
Non-small cell carcinoma	41	9.4
Small cell carcinoma	14	3.2
Large cell carcinoma	2	0.5
Mesothelioma	1	0.2
Hemangiopericytoma	3	0.7
Sarcomatoid carcinoma	1	0.2
Secondary malignancy – determined primary site	**52**	**12**
Neuroendocrine tumors	9	2.1
Colon adenocarcinoma	7	1.6
Renal cell carcinoma	6	1.4
Breast adenocarcinoma	4	0.9
Transitional cell carcinoma	3	0.7
Hodgkin lymphoma	3	0.7
Melanoma	3	0.7
Leiomyosarcoma	2	0.5
Endometrial adenocarcinoma	2	0.5
Non-Hodgkin lymphoma	2	0.5
Thymoma	2	0.5
Plasmacytoma	2	0.5
Osteosarcoma	1	0.2
Thyroid carcinoma	1	0.2
Eccrine carcinoma	1	0.2
Adenoid cystic carcinoma	1	0.2
Mucoepidermoid carcinoma	1	0.2
Synovial sarcoma	1	0.2
Carcinoid tumors	1	0.2
Secondary malignancy - undetermined primary site	**8**	**1.8**
Metastatic adenocarcinoma	5	1.1
Undifferentiated carcinoma	3	0.7
Benign lesions	**62**	**14.2**
Tuberculosis	3	0.7
Solitary fibrous tumor	2	0.5
Hamarthoma	1	0.2
Neurinoma	2	0.5
Organizing fibrosis or scar	5	1.1
Fibroma	1	0.2
Bronchiolitis obliterans organizing pneumonia	4	0.9
Nonspecific inflammation	44	10.1
Inconclusive findings (atypical cells and non-representative samples)	**22**	**5**

Table II. *Measures of diagnostic accuracy.*

Diagnostic contribution	N/%
True positive	352
False positive	0
True negative	62
False negative	22
Sensitivity	94.12 (352/374)
Specificity	100 (62/62)
Positive predictive value	100 (352/352)
Negative predictive value	73.81 (62/84)
AUROC[1]	0.95 (±SD= 0.06)

[1]*area under the receiver operating characteristics*

transthoracic biopsies from all 436 patients in our study and are shown in Table I. All patients were followed-up for 2 to 12 months to check the diagnostic accuracy. The diagnosis was determined in 414 patients (94.95%). Malignant disease (TP results) was identified in 352 patients (80.73%); while, 62 patients (14.22%) had benign lesions (TN results). In this study were no FP results. There were 22 (5%) inconclusive findings of atypical cells or non-representative samples, which were categorized as FN results since the diagnosis was not determined by TTB. The final diagnosis of malignancy was based on specific malignant results from TTB (n = 352), open surgical procedure (n = 14), and repeated bronchoscopy (n = 8). The final diagnosis of benign entity (n = 62) was made based on specific benign results from TTB and the follow-up imaging. The measures of diagnostic accuracy are reported in Table II.

The diagnostic accuracy, sensitivity, specificity, positive and negative predictive values of TTB were 95%, 94,1%, 100%, 100%, and 73.8%, respectively.

DISCUSSION

The diagnostic accuracy, sensitivity, specificity, PPV, and NPV were 95%, 94.1%, 100%, 100%, and 73.8%, suggesting a very high diagnostic yield. Similarly to the literature (1, 4-6), specificity and PPV were 100% due to zero FP findings. The sensitivity of the mentioned studies ranged from 92% to 97.3%, and diagnostic accuracy from 92.9% to 97.7%. NPV in the recent studies ranged from 78.6% to 93.3%, which was slightly higher than our results. NPV was

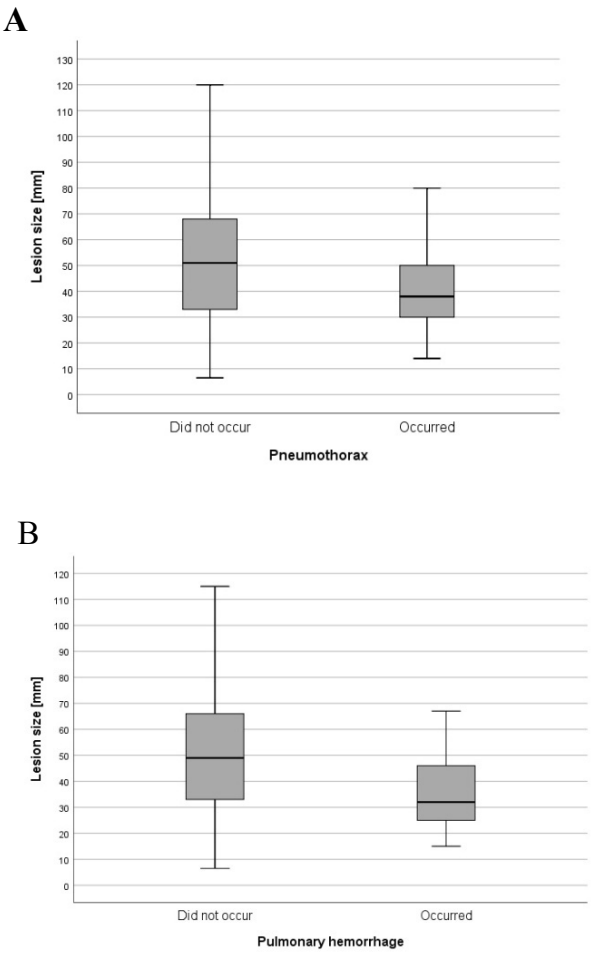

Fig. 1. *Statistically significant difference between the lesion size and the incidence of (**A**) pneumothorax and (**B**) pulmonary hemorrhage..*

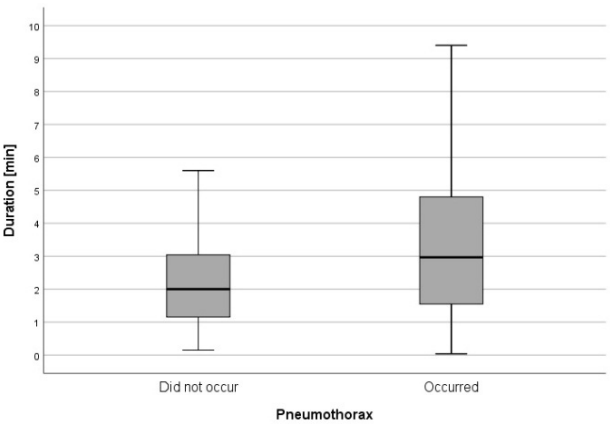

Fig. 2. *Statistically significant difference between the duration of the procedure and the incidence of pneumothorax.*

lower in our study due to the diagnostic failure of 22 (5%) FN findings. The incidence of pneumothorax in this study was 26.4%, while it varied in different studies. Some studies (3-8) reported the incidence lower than 20%, whereas others (1, 9-12) from 20 to 30%. In our study, one patient with pneumothorax (0.9%) required chest tube placement. Two studies (4, 5) reported incidence below 1%. In addition, most authors (1, 3, 6, 7, 9, 12) reported the incidence of chest tube placement in the range from 1 to 11%. The rate of pulmonary hemorrhage in our study (8.5%) was substantially lower than results (8.5 - 45.4%) of recent studies (1, 4-7, 10, 11), only a few (3, 8, 9, 12) reported an even lower rate. We found that complications were more frequent in patients with smaller diameter lung lesions. Similar results were published by different authors (1, 10, 11), while two studies (6, 7) contradicted these results. Also, we found a higher rate of pneumothorax in the group of patients with a longer duration of the procedure, as did Li et al. (7). Analyzing the relationship between the lesion depth and the occurrence of complications, the results suggested a higher incidence when the pleura-lesion distance was greater. These results were consistent with the literature (1, 5, 6, 8, 10-12). In the present study, nearly 50% (217/436) of biopsied lesions were in contact with pleura, which may be the reason for the low incidence of complications. In addition, the results of this study showed a statistically significant correlation between the lesion depth and the pneumothorax size; which, as far as we know, no author of recent literature has reported. A detailed assessment of risk factors and anticipation of possible complications are significant for successful biopsy.

REFERENCES

1. Wattanasatesiri T, Puntu W, Vithitsuvanakul N. Influencing factors of pneumothorax and parenchymal haemorrhage after CT-guided transthoracic needle biopsy: single-institution experience. Pol J Radiol 2018; 83:379-88.
2. Heerink WJ, de Bock GH, de Jonge GJ, Groen HJM, Vliegenthart R, Oudkerk M. Complication rates of CT-guided transthoracic lung biopsy: meta-analysis. Eur Radiol 2017; 27:138-48.
3. Lee HY, Lee IJ. Assessment of independent risk factors of developing pneumothorax during percutaneous core needle lung biopsy: focus on lesion depth. Iran J Radiol 2016; 13:30929.
4. Tian P, Wang Y, Li L, Zhou Y, Luo W, Li W. CT-guided transthoracic core needle biopsy for small pulmonary lesions: diagnostic performance and adequacy for molecular testing. J Thorac Dis 2017; 9:333-43.
5. Yang W, Sun W, Li Q et al. Diagnostic accuracy of CT-guided transthoracic needle biopsy for solitary pulmonary nodules. PLoS One 2015; 10:0131373.
6. Wang Y, Li W, He X, Li G, Xu L. Computed tomography-guided core needle biopsy of lung lesions: Diagnostic yield and correlation between factors and complications. Oncol Lett 2014; 7:288-94.
7. Li GC, Fu YF, Cao W, Shi YB, Wang T. Computed tomography-guided percutaneous cutting needle biopsy for small (≤ 20 mm) lung nodules. Medicine (Baltimore) 2017; 96:8703.
8. Xu C, Yuan Q, Chi C et al. Computed tomography-guided percutaneous transthoracic needle biopsy for solitary pulmonary nodules in diameter less than 20 mm. Medicine (Baltimore) 2018; 97:0154.
9. Aktaş AR, Gözlek E, Yılmaz O et al. CT-guided transthoracic biopsy: histopathologic results and complication rates. Diagn Interv Radiol 2015; 21:67-70.
10. Aktas AR, Gozlek E, Yazkan R, et al. Transthoracic biopsy of lung masses: Non technical factors affecting complication occurrence. Thorac Cancer 2015; 6:151-8.
11. Nour-Eldin NE, Alsubhi M, Naguib NN, et al. Risk factor analysis of pulmonary hemorrhage complicating CT-guided lung biopsy in coaxial and non-coaxial core biopsy techniques in 650 patients. Eur J Radiol 2014; 83:1945-52.
12. Schulze R, Seebacher G, Enderes B, Kugler G, Fischer JR, Graeter TP. Complications in CT-Guided, semi-automatic coaxial core biopsy of potentially malignant pulmonary lesions. Rofo 2015; 187:697-702.

LETTER TO THE EDITOR

IMPACT OF REPRODUCTIVE IMMUNIZATION CONDITIONING ON RECURRENT SPONTANEOUS ABORTION

FX. MU[1], Y. JIANG[1], H. WU[1], QX. YOU[1] and LG. XIONG[2]

[1]Department of Integrated TCM & Western Medicine Department, Southwest Hospital, Army Medical University, Chongqing, China; [2]Departmentof Immunoreproductive Clinic, Hubei Hospital of Traditional Chinese Medicine Affiliated to Hubei University of Traditional Chinese Medicine, Wuhan, China

Received April 15, 2019 – Accepted October 14, 2019

To the Editor

In healthy female individuals, spontaneous abortion brings pain, bleeding or massive hemorrhage, and significantly damages their health (1). Clinically, the incidence of spontaneous abortion is approximately 15~25%, 80% of which are early abortions occurring before the 12th week of gestation (2). Recurrent spontaneous abortion (RSA) refers to the occurrence of two or more spontaneous consecutive abortions before 20 weeks of gestation when the fetus weighs less than 500g. The incidence of RSA is approximately 2-5% (3, 4). Currently, the causes of RSA include genetic factors, uterus lesions, endocrine dyscrasia, immunological factors, and infectious factors. Moreover, in more than half RSA cases the causes remain unknown and are termed as unclear recurrent spontaneous abortion (URSA) (5). CD4+CD25+ T Regulate Cells (Tregs) are a type of suppressive cells derived from thymus. By secreting cytokine IL-10, Treg cells can suppress Thl-associated cell inflammation (6). IL-10 can trigger the generation of Treg cells. The positive feedback between Treg cells and IL-10 is one of the most important factors inducing maternal-fetal immune tolerance and maintaining pregnancy (7). Therefore, the immune state of URSA may affect the maintenance of pregnancy and embryo nidation. Using mice as the subjects, this study was designed to comparatively analyze the impact of reproductive immunization conditioning on RSA, to provide a new approach for future clinical treatment.

MATERIALS AND METHODS

Animals

A total of 24 SPF female CBA/J mice and 28 male DBA/2 mice (8~10 weeks old, weighing 18-22g) were purchased from Beijing Huafukang Biotechnology Co., Ltd., China. All mice were housed under a 12-hour light and dark cycle and allowed free access to food and water. The temperature was controlled at 22±2°C and the humidity was 40-60%. The experimental mice were allowed 1 week of acclimation prior to intervention. The protocol was approved by the ethics committee of Southwest Hospital, Army Medical University, and the experiment also followed the regulations of the State Science and Technology Commission on the management of laboratory animals.

Establishment of an abortion mouse model

Twenty-four female CBA/J mice were mated with 28 male DBA/2 mice in cages, and the pregnant CBA/J

Keywords: recurrent spontaneous abortion; inflammation; IL-7; Treg cell; signal channel

Corresponding Author:
Dr Ligui Xiong,
Department of Immunoreproductive Clinic,
Hubei Hospital of Traditional Chinese Medicine
Affiliated to Hubei University of Traditional Chinese Medicine,
No.360 Zhongshan Road, Wuhan City, 430061, Hubei Province, China
e-mail: xiong_liguimed1@163.com

0393-974X (2019)

female mice were set as the classic abortion mouse model (8). Twenty-four female CBA/J mice randomly mated with 12 male DBA/2 and BABL/c mice in cages. CBA/JXBABL/c caged CBA/J pregnancy was set as a normal pregnant rat model. The mice were randomly divided into a control group (normal pregnant mice, n=8), a normal pregnant mice + IL-7 group (intravenous injection of IL-7 blocker to normal pregnant mice) (n=8), normal pregnant mice + IL-7Ra group (intravenous injection of IL-7Ra blocker to normal pregnant mice) (n=8). CBA/JXDBA/2 caged female CBA/J pregnant mice were defined as URSA model mice. They were randomly divided into a control group (abortion mice, n=8), abortion mice + IL-7 group (n=8) and abortion mice + IL-7Ra group (n=8). According to the experimental design, different interventions were carried out. After the cages were merged together, the vaginal plug was checked. CBA/J mice were reared separately after vaginal plug and it was recorded as 1st day of pregnancy. On the 3rd day of pregnancy (embryo nidation period), animals in the normal pregnant mice + IL-7 group were injected with IL-7 through the caudal veins, with a dosage of 15μL/per mouse/per day. Mice in the normal pregnant mice + IL-7Ra group were injected with IL-7Ra blocker through caudal veins, with a dosage of 25mg/per mouse/per day for 3 consecutive times. The drugs (IL-7/IL-7Ra blockers) or the same type of lgG was not used in the control group.

On the 14th day of pregnancy, mice in each group were sacrificed by cervical dislocation. Abdominal skin and subcutaneous tissues were separated. After separation of uterus and ovary, the fetal placenta was removed from the implantation site. The complete amniotic sac, placenta and mouse embryos were normal. If the amniotic sac or placenta was incomplete or the embryo was not formed, it was deemed abnormal. The number of absorbed embryos and normal embryos in each group was counted and recorded.

Flow cytometry analysis

Mice in each group were sacrificed and soaked in 75% alcohol. Then, they were placed on sterile surgical dressings. The skin of each mouse was cut open. The mouse spleen was obtained and placed on a 230 mesh stainless steel screen. The spleen was ground to collect the cell homogenate, which was the spleen cell suspension. Next, the mouse spleen lymphocytes were isolated by using the Ficoll-Hypaque density gradient centrifugation method (the Ficoll method). Finally, the cells were added with pre-cooled flow cell staining buffer (2 mL) and centrifuged at 1000 rpm for 8 min. The supernatant was discarded. Then, the cells were added with 1 mL of stationary liquid and membrane-breaking solution (BD Corporation, USA) and incubated for 30 min in the dark. Next, the cells were added with 2 mL of 1×membrane-breaking buffer solution and centrifuged at 1,000 rpm for 8 min. The supernatant was discarded (repeated twice). The cells were added with 500 μL of FACS Buffer for resuspension and stored at 4°C. The number of cells was measured and recorded by a flow cytometer (BD Corporation, USA) within 24 h.

Real-time PCR

For RT-PCR, 100 mg cryopreserved decidual tissues were cut and placed in a mortar for 3 min. Then, a 100 mesh screen was used for filtration to prepare single cell suspension, and the lymphocyte isolate was absorbed into a centrifugal tube. After centrifugation at 2,000 rpm and 24°C for 20 min, cells at the lymphocyte layer were collected. Normal saline of four times the volume was added, fully mixed and centrifugated (repeated twice). Then, using the RNA extraction kit, the RNA solution was harvested. The spectrophotometer was used to read the absorption values at 260 and 280 nm. The ratio of 260mm/280nm in RNA solution was RNA purity, and the ratio ranged from 1.8 to 2.0. The obtained RNA solution was stored at -80°C for subsequent use.

Primers of target gene sequences

The Foxp3 gene was 181bp in length, and the primer sequence was F-end ACAGAAGCAGCGTCAGTACC; R-end CGGGGTATTTTICGCAAGGC;

The RORγt was 169bp in length, and the primer sequence was F-end TCACATCACCCCGTCATTGG; R-end CTCCACGACTGCCCATCATT;

The GAPDH gene was 158bp in length, and the primer sequence was F-end GTCAAGGCTGAGAACGGGAA; R-end AAATGAGCCCCAGCCTTCTCC.

As shown in Table I, a 20 μL reaction system for reverse transcription was formulated. The procedure of reverse transcription was PCR (BIO-RAD, USA) at 42°C for 30 min and 4°C for 10 min. The cDNA obtained from reverse transcription could be directly used for following

PCR or stored at -80°C for later use.

An ABI PCR (ABI Corporation, USA) was used for detecting the expression of target mRNAs. Each sample was detected using 3 duplicate wells. During the process of PCR, the samples were denatured for 10 s at 95°C, annealed for 31 s at 60°C, and extended for 50 s at 68°C (40 cyclesin total).

Bicinchoninic acid (BCA) protein assay

The tissue samples obtained from the above operation were lysed in a Radio Immunoprecipitation Assay (RIPA) cracking solution 0.9 mL RIPA solution per 0.1 g of tissue (Beyotime Biotechnology, China) and then homogenized on ice. The cerebral tissue samples were cracked for 45 min to isolate total protein of the samples. Then, the cracking solution was transferred into a 2 mL Eppendorf (EP) tube using a liquid transfer instrument (GILSON, Finland). The EP tube was incubated on dry ice (-80°C) for 30-minand centrifuged (4°C, 12,000r/min×20min). Afterward, the supernatant was collected to determine the protein concentration using a BCA protein assay kit (Boster Biological Technology Co. Ltd, China) according to the kit instruction.

Western blotting to detect target protein expressions

Firstly, the concentration of the protein samples was measured. Then, the loading buffer was added to the supernatant sample protein in each pore, and the samples were boiled. Then, they were placed in the sodium dodecyl sulfate (SDS)-polyacrylamide gel for electrophoresis for about 1 h. Afterwards, the proteins were transferred onto a nitrocellulose (NC) membrane using the wet method under a 100V constant voltage. 1.5 h later, the membrane was rinsed with TBST buffer, blocked for 60 min by a blocking solution (20 mL TBST, 0.75g BSA, 3 spoons of skimmed milk powder) at room temperature. The mouse-derived monoclonal antibody (Beyotime Biotechnology, China) was used as the primary antibody and incubated overnight at 4°C. On the next day, the membrane was rinsed by PBS for 5 min×twice and incubated for 1 h at room temperature with the rabbit anti-mouse polyclonal antibody as the secondary antibody (1:5,000 dilution) under shaking. Afterward, the membrane was washed by PBS for 15 min×4 times and analyzed by an imaging system (Image Pro Plus) (BIO-RAD, USA) to calculate the gray value of protein bands and their relative expression using β-actin as the control.

Statistical analysis

All experimental data were processed by SPSS21. Based on different conditions, one-way ANOVA or *chi*-squared test was used for testing. $P<0.05$ was considered statistically significant.

Table I. *Reaction system*

	Component	Volume
A	Total RNA	2 μL
	5×first-strand Buffer	4 μL
	M-Mu LV Reverse Transcriptase (200U/μL)	0.8 μL
	Oligo dT Primer (50μM)	2 μL
	dNTP Mixture (10mM each)	2 μL
	RNase Inhibitor (40U/μL)	0.5 μL
	RNase Free dH_2O	up to 50 μL
B	2×Super SYBR premixture	9 μl
	PCR Forward Primer (10μM)	0.5 μl
	PCR Reverse Primer(10μM)	0.5μl
	cDNA	4μl
	RNase Free dH_2O	up to 20 μl

***A)** reverse transcription; **B)** real-time PCR*

RESULTS

Result of the fetal resorption rate

It can be seen from Fig. 1 that the fetal resorption rate of the normal control group was 11.4%. After the injection with IL-7 through the caudal vein, the fetal resorption rate was increased to 20% ($P<0.05$). After the injection with IL-7Ra, the fetal resorption rate was increased slightly to 13.4% ($P>0.05$). Finally, the fetus resorption rate in the abortion group was 14.4% ($P<0.05$).

Flow cytometry analysis of Th17 and Treg cells

The percentages of Th17 (CD4+IL-17A+/CD4+) and Treg (CD4+CD25 high Foxp3+/CD4+) cells in the spleen blood samples of normal pregnant mice were 1.43±0.27% and 4.83±0.19%, respectively (Fig. 2). After the injection with IL-7, the percentages of Th17 and Treg cells in the peripheral blood of normal pregnant mice were 4.27±0.18% and 3.54±0.24%, respectively. After the injection with IL-7Ra, the percentages of Th17 and Treg cells in the peripheral blood of the normal pregnant mice+IL-7Ra group were 1.79±0.13% and 4.53±0.24%, respectively. The statistical analysis showed that after the injection with IL-7, the number of inflammatory Th17 cells in the normal pregnant mice was significantly increased while the number of Treg cells was significantly decreased ($P<0.05$). However, after the injection with IL-7Ra through the caudal vein, the number of Th17 and Treg cells in the normal pregnant mice was not significantly different compared with that in the control group of normal pregnant mice ($P>0.05$). In the abortion mice group, the percentages of Th17 and Treg cells in the blood of spleen were 4.68±0.21% and 2.69±0.21%, respectively. After the injection with IL-7Ra, the percentages of Th17 and Treg cells in the peripheral blood of abortion mice were 5.23±0.21% and 1.87±0.15%, respectively, which were not significantly different compared with those in the control group of abortion mice. Finally, the percentages of Th17 and Treg cells in the peripheral blood of IL-7Ra abortion mice were 2.25±0.23% and 4.98±0.17%, respectively, and were obviously different from those of the control group of abortion mice ($P<0.05$).

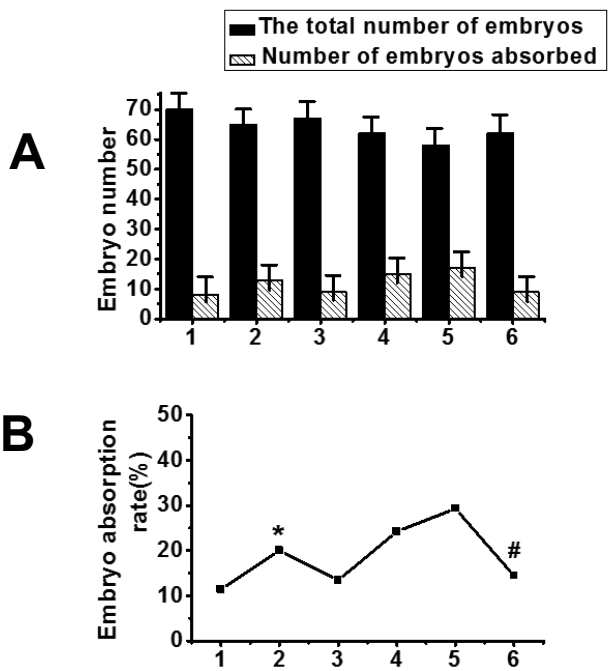

Fig. 1. *Statistical chart of the fetus resorption rate. 1: the normal control group of pregnant mice; 2: the normal pregnant mice +IL-7 group; 3: the normal pregnant mice +IL-7Ra group; 4: the control group of abortion mice; 5: the abortion mice +IL-7 group ; 6: the abortion mice +IL-7Ra group.* ***A****) number of embryos;* ***B****) fetus resorption rate. Compared with the control group of normal pregnant mice, *P<0.05 was of statistical significance; compared with the control group of abortion mice and the abortion mice +IL-7 group, #P<0.05 was of statistical significance; n=8*

IL-7/IL-7R signal pathway on the maternal-fetal interface of mice

It can be seen from Fig. 3A that the R2 of standard curve of BCA protein concentrations was 0.99979. The results of Western blotting showed the protein expression of IL-7, IL-7R, Foxp3 and IL-17A in the 6 groups showed that the expression of IL-17A and Fox3 in the normal mice + IL-7 group was significantly higher than that in the group of normal pregnant mice (Fig. 3 B, C and D). Furthermore, the expression of IL-17A and Fox3 in the decidua of the normal pregnant mice +IL-7 group was increased and was significantly different from that in the normal control group. Moreover, no obvious difference was observed between the

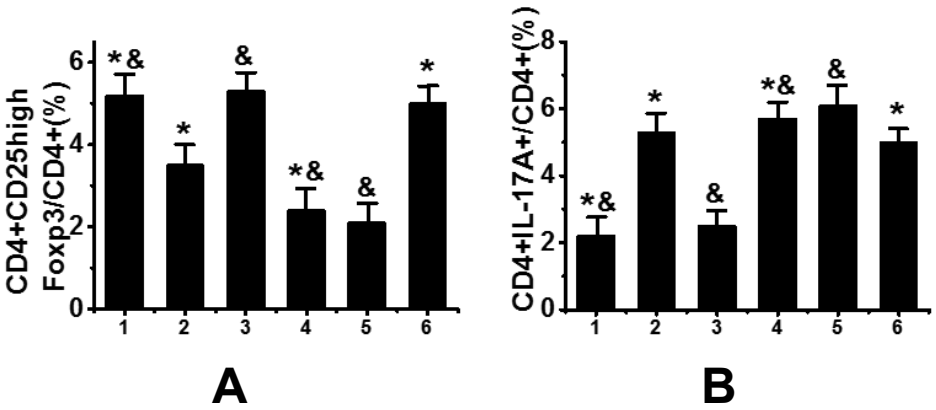

Fig. 2. *Test results of cells in each group. **A)** Th17 cells; **B)** Treg cells. Compared with normal pregnant mice, *P<0.05 was of statistical significance; compared between two groups, &P<0.05 showed no statistical significance; n=8.*

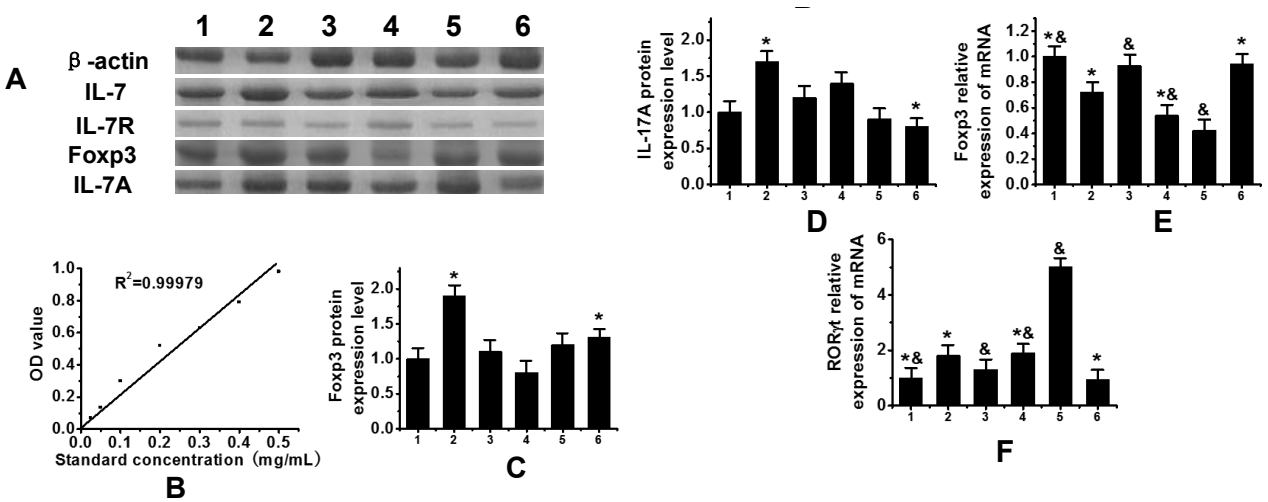

Fig. 3. C*hart of protein and mRNA of genes regulating the IL-7/IL-7R signal pathway on the maternal-fetal interface of mice. **A)** Standard curve of BCA protein concentration assay; **B)** protein expressions of IL-7, IL-7R, Foxp3 and IL-17A detected by Western-Blots; **C)** Foxp3 protein expressions; **D)** IL-17A protein expressions; **E)** Foxp3 mRNA expressions; **F)** RORγt mRNA expressions; compared with the control group of normal pregnant mice, *P<0.05 was of statistical significance; compared between two groups, &P<0.05 was of no statistical significance, n=8*

control group and the normal pregnant mice +IL-7Ra group. In the abortion mice +IL-7 group, the expression level of IL-17A was relatively high while the expression level of Foxp3 was relatively low, and the results were not significantly different from those in the abortion mice group. In the +IL-7Ra group, the expression level of +IL-17A was relatively low while the expression level of Foxp3 was relatively high (P<0.05). It can be seen from Fig. 3 E and F that in the normal pregnant +IL-7 group, the mRNA expression of Foxp3 was significantly different from the mRNA expression of RORγt in the control group of normal pregnant mice, indicating an increased rate of abortion (P<0.05). After the injection with IL-7Ra, the relevant gene expression of the normal pregnant mice +IL-7Ra group was not significantly different from that of the control group of normal pregnant mice. The gene expression of the abortion

mice control group was significantly different from that of the control group of normal pregnant mice ($P<0.05$). Compared with that in the control group of abortion mice, the results in the abortion mice +IL-7 group and the abortion mice +IL-7Ra group were significantly different ($P<0.05$).

DISCUSSION

In this study, it was found that after IL-7 was injected into the tail vein of normal pregnant mice, the control group increased ($P < 0.05$) compared with normal pregnant mice, but there was no significant difference after IL-7Ra injection. The abortion mice group also had significant difference ($P < 0.05$). It was found that IL-7 may induce inflammation and promote local embryo absorption, leading to abortion, while blocking this signaling pathway can inhibit the occurrence of abortion.

In normal pregnancy, the expression level of IL-7 is relatively low and the expression level of IL-7R is increased in partial deciduas. However, URSA patients showed an opposite trend (10, 11). In this study, flow pattern analysis and Western blot assay showed that there was significant difference compared with the abortion mice group. There was significant difference between abortion mice + IL-7 group and abortion mice control group. There was significant difference between abortion mice + IL-7Ra group and abortion mice control group ($P < 0.05$). Therefore, blocking the signal pathway of IL-7 and decreasing the secretion of Th17-related cytokines can reduce the local inflammatory effect and inhibit the occurrence of abortion.

In summary, it was found that the risk of recurrent abortion could be reduced by adding IL-7Ra/IL-7 during pregnancy. This study provides a new idea for the treatment of recurrent abortion.

REFERENCES

1. Barišić A, Pereza N, Hodžić A, Kapović M, Peterlin B, Ostojić S. Functional single nucleotide polymorphisms of matrix metalloproteinase 7 and 12 genes in idiopathic recurrent spontaneous abortion. J Assist Reprod Genet 2017; 34(3):365-71.
2. Zhao X, Jiang Y, Wang L, Li Z, Li Q, Feng X. Advances in understanding the immune imbalance between T-lymphocyte subsets and NK cells in recurrent spontaneous abortion. Geburtshilfe Frauenheilkd 2018; 78(7):677-83.
3. Ye SL, Gu XK, Tao LY, Cong JM, Wang YQ. Efficacy of different treatment regimens for antiphospholipid syndrome-related recurrent spontaneous abortion. Chin Med J (Engl)2017;130(12):1395-99.
4. Kaur R, Gupta K. Endocrine dysfunction and recurrent spontaneous abortion: An overview. Int J Appl Basic Med Res 2016; 6(2):79-83.
5. Hashemi M, Mokhtari M, Khazaeian S, Bahari G, Rezaei M, Nakhaee A, Taheri M. Evaluation of HLA-G 14-bp ins/del and +3142G>C polymorphisms with susceptibility to recurrent spontaneous abortion. Taiwan J Obstet Gynecol 2017; 56(3):276-80.
6. Zhang Y, Wu YY, Qiao FY, Zeng WJ. Association between p53 Polymorphismat Codon72 and recurrent spontaneous abortion. J Huazhong Univ Sci Technolog Med Sci 2016; 36(3):402-405.
7. Lv S, Yu J, Xu X. A comparison of effectiveness among frequent treatments of recurrent spontaneous abortion: A Bayesian network meta-analysis. Am J Reprod Immunol 2018; 80(1):e12856.
8. Li X, Yin M, Gu J, Hou Y, Tian F, Sun F. metabolomic profiling of plasma samples from women with recurrent spontaneous abortion. Med Sci Monit 2018; 24:4038-45.
9. Farhan HM, Abu-Gabal K, Katta M, Ibrahim R. Evaluation of the adenosine deaminase (ADA) G22A gene polymorphism with recurrent spontaneous abortion among Egyptian patients. Cent Eur J Immunol 2017; 42(3):281-86.
10. Luan X, Kang X, Li W, Dong Q. An investigation of the relationship between recurrent spontaneous abortion and memory T follicular helper cells. American Am J Reprod Immunol 2017; 78(5):e12714.
11. Hodžić A, Lavtar P, Ristanović M, Novaković I, Dotlić J, Peterlin B. Genetic variation in the CLOCK gene is associated with idiopathic recurrent spontaneous abortion. PLoS One 2018; 13(5):e0196345.

LETTER TO THE EDITOR

EXPRESSION OF MATRIX METALLOPROTEINASE IN CHOLESTEATOMA EPITHELIUM OF PATIENTS WITH CHOLESTEATOMA OTITIS MEDIA

GX. MI[1], Y. NING[2], K. SUN[3], LL. TAO[1], XF. MA[1] and LQ. WANG[1]

[1]Department of Otolaryngology, Hongqi Hospital Affiliated to Mudanjiang Medical University, Mudanjiang, Heilongjiang, China; [2]Office of International Exchange and Cooperation, Mudanjiang Medical University, Mudanjiang, Heilongjiang, China; [3]Department of Biology, Mudanjiang Medical University, Mudanjiang, Heilongjiang, China

Received April 8, 2019 - Accepted October 16, 2019

To the Editor,

Many theories have been proposed to explain the mechanism underlying the formation of cholesteatoma of the middle ear (CME). In recent years, a number of scholars have conducted numerous studies. Ohashi et al. (1) analyzed 37 patients with otitis media accompanied by middle ear effusion, and their results indicated that the level of soluble VCAM-1 in the effusion of atopic patients was significantly higher than that of non-atopic patients, which played a more important role in the pathogenesis of OME in atopic patients. Nishizawa et al. (2) studied the localization of periosteum proteins in ear specimens collected from patients and experimental animals with eosinophilic otitis media (EOM). The authors showed positive immune staining of periosteal proteins in the middle ear section, along with the immune response induced by periosteal proteins in animal models. These results played important roles to further study VCAM-1 and periosteum proteins in CME. In addition, it is also believed that MMP must remain active in the process of angiogenesis, otherwise it will not be completed (3). TIMP-1 (tissue inhibitor of metalloproteinases-1) can affect the formation of new blood vessels. by inhibiting the activity of MMP (4). Generally, the mixture of TIMP and MMP at a ratio of 1:1 is used to inhibit MMP activity (5). When the MMP/TIMP value is increased, the balance is broken, which may lead to invasion or metastasis of tumors (6). In this study, the expression of MMP-1 and MMP-2 in the epithelia of cholesteatoma was detected, and the correlation between MMP-1 and MMP-2 is discussed.

MATERIALS AND METHODS

Subjects

A total of 46 CME patients admitted to Hongqi Hospital Affiliated to Mudanjiang Medical University from August 2017 to January 2019 were randomly selected to collect their intraoperative specimens. According to the standard of "Otolaryngology Diagnosis" for grading of the severity of hearing loss, average bone conduction thresholds of 500, 1000 and 2000 Hz were used in this study to calculate the level of hearing loss: 26 to 40 db for mild deafness (+), 41 to 55 db for moderate deafness (+ +), 56 to 70 db for moderately severe deafness (+ + +), 71 to 90 db for severe deafness (+ + + +), and above 90 db for profound deafness (+ + + + +). According to these criteria, the patients were divided into two groups: 15 cases in the group of + to ++, and 31 cases in the group of + + + to + + + + +. Furthermore, the degree of CME-induced invasion and

Key words: matrix metalloproteinases; chronic otitis media of cholesteatoma; bone destruction; invasion

Corresponding Author:
Dr Leqiu Wang,
Department of Biology,
Mudanjiang Medical University,
No.5 Tongxiang, Mudanjiang 157011,
Heilongjiang, China
e-mail: wangleqiumdju00@163.com

0393-974X (2019)

bone destruction was divided into four groups according to the Saleh's evaluation criteria (7) for the invasion ability of cholesteatoma epithelia and findings of intraoperative observation: no obvious osteon destruction was deemed as grade I; incus or malleus destruction was deemed as grade II; incus and stirrup vandals were deemed as grade III; and the destruction of incus, malleus, papillae, and/or sigmoid sinus plates was deemed as grade IV. According to these criteria, 15 cases of patients were allocated into the group of I-II, while 31 cases of patients were allocated into the group of III-IV. The expression of MMP-1 and MMP-2 in the cholesteatoma epithelia of three different sites, i.e., tympanum, tympanum sinus and mastoid, was analyzed by the S-P method. Signed informed consent was obtained from all patients and this study was approved by the Ethics Committee of Hongqi Hospital Affiliated to Mudanjiang Medical University.

Pure tone audiometry

Air and bone conduction thresholds of all patients were detected by professional audiologists according to the standard method. The background noise was 28dB(A) in the sound insulation room. A Danish Madson audiometer was employed, with ISO standard zero-level calibration. Air conduction thresholds of the patients were examined first, and the bone conduction headphones were pressed against the mastoid process for determination of bone conduction thresholds. The other ear with masking indications was shielded by conventional methods, and then the standard method was followed for the test. If the average hearing thresholds was 100dB, profound deafness was defined.

Surgical procedures

The patients were placed in a supine cephalic position and local anesthesia was applied. The intraarticular or posterior incision was made under the otoscope, and granulation tissues and cholesteatoma lesions in the ethmoid area of the temporal bone, tympanic antrum or upper tympanic chamber were completely removed. If it was difficult to thoroughly clean the cholesteatoma around the small bone or granulation, the incus and malleus head was cut off to remove the lesions. If the stapes structure was complete, autologous incus or malleus or papillary cortical bone was used to reconstruct the ossicular chain. The upper tympanic chamber, tympanic antrum, mastoid cavity and facial nerve recess were closed and filled. An appropriate size of temporalis muscle fascia was taken to repair the periosteum, and the external auditory canal flap was returned to cover the mastoid process and external auditory canal. When granulation tissues were injured or bleeding during the operation, a 1% adrenergic cotton ball was used to stop the bleeding, and antibiotic ear drops were given after the operation.

Hematoxylin-eosin staining

Tissue sections were dewaxed with xylene, hydrated with gradient alcohol and rinsed with sterile water. Hematoxylin staining droplets were added to the specimens and incubated for 5–15 min. Then, 1% hydrochloric acid alcohol was used for 1-2 min of differentiation, and the slices were rinsed under sterile running water before they were impregnated with an eosin dye solution for 2-5min. They were then dehydrated, made transparent and sealed in pellets.

Immunohistochemistry

Tissue sections were dewaxed with xylene, hydrated with gradient alcohol, rinsed with sterile water, repaired with an EDTA (ethylene diamine tetraacetic acid) repair solution (Beijing Zhongshan Jinqiao Biotechnology Co., Ltd, China) and washed three times with PBS for 5 min each. After adding the primary antibody, the tissue sections were incubated at 4°C for more than 10 h before they were washed three times with phosphate buffered saline (PBS) for 5 min each. After adding the secondary antibody dropwise (DAKO, Denmark), the tissue sections were incubated at room temperature for 50 min. BS buffer was used as a negative control. Finally, 50 μL colorant (DAB, Dako REAL™ EnVision™ Detection System, Peroxidase/DAB+) was dripped onto each section before it was observed under a light microscope. When there were specific staining results for the specimens but the background was not stained, the sections were rinsed with running tap water, and soaked in a hematoxylin solution for 3 min. After rinsing with tap water again, they were differentiated for 10 s, and rinsed with tap water again. The sections were then dehydrated, made transparent and sealed in pellets.

Result determination

According to the range and strength of the stained

color signal, the samples with brown-yellow particles in the cells were considered as positive, and the expression results of MMP-1 and MMP-2 were divided into negative (-), weakly positive (+), positive (++) and strongly positive (+++) groups, respectively. In each field of view, the number of cells showing yellow and brown-yellow granules was counted and the percentage in total cell number was taken as the positive expression rate. Five fields were randomly selected for each section, and the average was taken as the final result. If the positive cell rate was ≤ 10%, the section was negative (-); if the positive cell rate was > 10% - 25%, the section was weakly positive (+); if the positive cell rate was >25% - 50%, the section was positive (++); and if the positive cell rate was >50%, the section was strongly positive (+++).

Statistical analysis

Data in this study were analyzed with SPSS 19.0 statistical software, and measurement data were expressed as mean ± standard deviation ($\bar{x} \pm s$). The positive expression rates in two samples were compared by *chi*-squared test and Spearman correlation test. The test level was set as $\alpha = 0.05$, and $P<0.05$ was considered statistically significant.

RESULTS

Expressions of MMP-1 and MMP-2 in the epithelia of cholesteatoma

The tissue sections were observed under the microscope, and it was found that the immunoreactive substances positive for MMP-1 and MMP-2 proteins were precipitated on the cell membrane and cytoplasm. The signals mainly located in the epithelium of cholesteatoma, and a small amount of inflammatory cells in the subepithelial matrix also

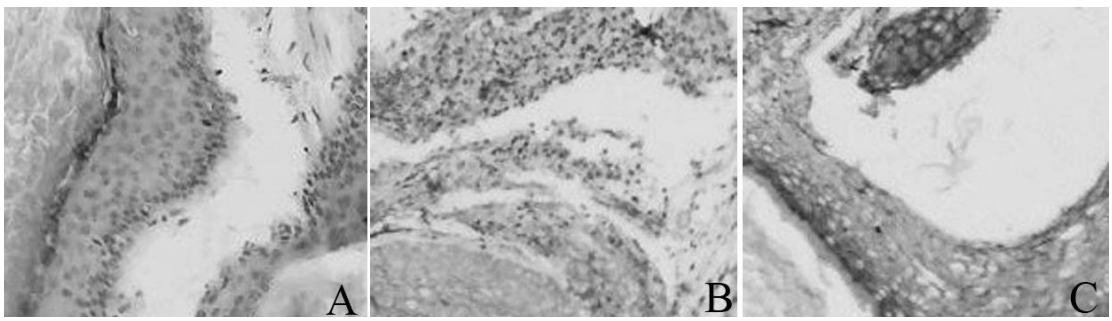

Fig. 1. *Test results. **A**) H&E staining of cholesteatoma epithelium; **B**) strongly positive expressions of MMP-1 in cholesteatoma epithelium; **C**) strongly positive expressions of MMP-2 in cholesteatoma epithelium) (×200)*

Table I. *Expressions of MMP-1 and MMP-2 in cholesteatoma tissues of patients of different genders and ages*

Attribute		Expressions of MMP-1				P value	Expressions of MMP-2				P value
		-	+	++	+++		-	+	++	+++	
Age	≤60 years	6	5	14	6	0.814	4	4	8	15	0.912
	>60 years	2	2	6	5		1	2	4	8	
Gender	Male	4	6	11	6	0.604	2	4	7	14	0.933
	Female	4	1	9	5		3	2	5	9	

expressed MMP-1 and MMP-2 proteins, as shown in Fig. 1.

Expressions of MMP-1 and MMP-2 under different conditions

Among the 46 CME patients in this study, there were 27 males and 19 females. In addition, 31 were ≤60 years old and 15 were > 60 years old. Statistical analysis of MMP-1 and MMP-2 expressions in cholesteatoma showed that age and gender had no effect on their expression in cholesteatoma, as shown in Table I.

This study collected 15 cases of tympanum samples, 18 cases of tympanum sinus samples and 13 cases of mastoid process samples, respectively. The results showed that the different sites of sampling had no effect on the expression of MMP-1 and MMP-2 in the epithelium of cholesteatoma. In addition, the expressions of MMP-1 and MMP-2 in the epithelium of colostomy with different hearing loss and different degree of bone destruction were statistically different ($P<0.05$). With the aggravation of hearing loss, their expressions were higher. With the aggravation of bone destruction, their expressions were also higher, as shown in Table II.

Correlation analysis of MMP-1 and MMP-2 expressions

Spearman rank correlation analysis was conducted on the expression of MMP-1 and MMP-2 in the cholesteatoma epithelium, and the results were $r=0.815$ and $P<0.05$, indicating that the expression of MMP-1 and MMP-2 in cholesteatoma was positively correlated with each other, as shown in Table III.

Table II. *Relationship between MMP-1/MMP-2 expressions and the sampling sites in cholesteatoma as well as expressions of MMP-1 and MMP-2 in patients with different degrees of hearing loss and bone destruction*

Location		Expressions of MMP-1				P	Expressions of MMP-2				P
		-	+	++	+++		-	+	++	+++	
Tympanum		4	1	6	4	0.839	2	2	5	6	0.712
Tympanic antrum		2	4	8	4		2	4	4	8	
Mastoid		2	2	6	3		1	0	3	9	
Hearing loss	+~++	8	4	3	0	0.003	5	4	4	2	0.004
	+++~+++ +	0	3	17	11		0	2	8	21	
Destruction level	I ~ II stage	7	4	4	0	0.002	5	3	5	2	0.005
	III ~ IV stage	1	3	16	11		0	3	7	21	

Table III. *Correlation analysis of MMP-1 and MMP-2 expressions in CME*

MMP-1	MMP-2				Total
	-	+	++	+++	
-	5	3	0	0	8
+	0	3	4	0	7
++	0	0	8	12	20
+++	0	0	0	11	11
Total	5	6	12	23	46

DISCUSSION

CME is not a malignant tumor and does not show metastasis and other characteristics of malignant tumors, although it has an invasive property similar to that of malignant tumors (8). The results of this study showed that the expression of MMP-1 in the epithelium of cholesteatoma was increased. Recent studies have shown (9, 10) that the proliferation of malignant tumor cells is usually accompanied by abnormal expressions of MMP-1, which is related to the blood supply and metastasis of tumors. It has been found that the metastasis of gastric cancer cells in the digestive system depends on the activation of MMP-2 precursor (11). It was also found that MMP-2 is involved in tumor vascular invasion and metastasis. The results of this study showed that the positive expression of MMP-2 in cholesteatoma tissues became higher and stronger when the hearing loss and sclerotin damage became more severe.

In addition, the results of this study showed that MMP-1 and MMP-2 were correlated with the degree of otosteon damage. Moreover, the expressions of MMP-1 and MMP-2 in CME were positively correlated with each other. Therefore, it was hypothesized that CME must be involved in the process of bone destruction and hearing damage, and both MMP-1 and MMP-2 exerted synergistic effects in the pathogenesis of CME by jointly promoting bone invasion and hearing damage. In this study, it was also found that MMP-1 and MMP-2 were not expressed in epithelial cells and only expressed in stromal cells. Therefore, it can be considered that CME-induced bone destruction and hearing damage play an important role in stromal cells. In patients with increased expressions of MMP-1 and MMP-2, the degree of bone destruction and hearing loss is also increased. Therefore, it can be hypothesized that, as secreted by stromal cells, activated MMP-1 and MMP-2 act directly on surrounding tissues and bone matrix to exert their unique clinical effects.

ACKNOWLEDGEMENTS

This work was supported by Hongqi Hospital Scientific Research Fund Science and Technology Project (2018HQ-30); Research Projects of Basic Scientific Research Expenses in Heilongjiang Provincial Institutions of Higher Learning 2018(2018-KYYWFMY-0068).

REFERENCES

1. Ohashi Y, Nakai Y, Tanaka A, Kakinoki Y, Washio Y. Soluble adhesion molecules in middle ear effusions from patients with chronic otitis media with effusion. Clin Otolaryngol Allied Sci 1998; 23(3):231-34.
2. Nishizawa H, Matsubara A, Nakagawa T, et al. The role of periostin in eosinophilic otitis media. Acta Otolaryngol 2012; 132(8):838-44.
3. Misra S, Fu AA, Puggioni A, et al. Increased shear stress with upregulation of VEGF-A and its receptors and MMP-2, MMP-9, and TIMP-1 in venous stenosis of hemodialysis grafts. Am J Physiol Heart Circ Physiol 2008; 294(5):H2219-30.
4. Schmidt M, Grünsfelder P, Hoppe F. Up-regulation of matrix metalloprotease-9 in middle ear cholesteatoma – correlations with growth factor expression in vivo?. Eur Arch Otorhinolaryngol 2001; 258(9):472-76.
5. Muller M, Trocme C, Lardy B, Morel F, Halimi S, Benhamou PY. Matrix metalloproteinases and diabetic foot ulcers: the ratio of MMP-1 to TIMP-1 is a predictor of wound healing. Diabet Med 2008; 25(4):419-26.
6. Fan YZ, Zhang JT, Yang HC, Yang YQ. Expression of MMP-2, TIMP-2 protein and the ratio of MMP-2/TIMP-2 in gallbladder carcinoma and their significance. World J Gastroenterol 2002; 8(6):1138-43.
7. Saleh HA, Mills RP. Classification and staging of cholesteatoma. Clin Otolaryngol Allied Sci 1999; 24(4):355-59.
8. Yang X, Li X, Ma M, et al. [Expression of transforming growth factor-beta 1 matrix metalloproteinase-1 and its inhibitor in human middle ear cholesteatoma]. Zhonghua Er Bi Yan Hou Ke Za Zhi 2002; 37(2):121-23.
9. Grimm M, Lazariotou M, Kircher S, et al. MMP-1 is a (pre-)invasive factor in Barrett-associated esophageal adenocarcinomas and is associated with positive lymph node status. J Transl Med 2010; 8:99.
10. Qazi H, Shi ZD, Tarbell JM. Fluid shear stress regulates

the invasive potential of glioma cells via modulation of migratory activity and matrix metalloproteinase expression. PLoS One 2011; 6(5):e20348.

11. Kamata I, Ishikawa Y, Akishima-Fukasawa Y, et al. Significance of lymphatic invasion and cancer invasion-related proteins on lymph node metastasis in gastric cancer. J Gastroenterol Hepatol 2009; 24(9):1527-33.

LETTER TO THE EDITOR

CURCUMIN PROTECTS RAT H9C2 CARDIOMYOCYTES AGAINST DOXORUBICIN TOXICITY BY MODULATING OXIDATIVE STRESS AND APOPTOSIS

Q. LIU[1*], JW. YUAN[1*], F. ZHANG[1], F. QIAO[2], XF. SUI[3] and CH. LIU[4]

[1]Department of Cardiovascular Medicine, The First Affiliated Hospital of Jiamusi University, Jiamusi City, Heilongjiang Province, China; [2]Department of Thoracic Surgery, The First Affiliated Hospital of Jiamusi University, Jiamusi City, Heilongjiang Province, China;[3]Geriatrics Department, The First Affiliated Hospital of Jiamusi University, Jiamusi City, Heilongjiang Province, China;[4]Department of Physical Examination Center, The First Affiliated Hospital of JiamusiUniversity, Jiamusi City, Heilongjiang Province, China

Received September 1, 2019 – Accepted October 16, 2019

[*]These authors contributed equally to this work

To the Editor,

In recent years, the high incidence of the tumor and the extensive use of chemotherapeutic agents led to an increased incidence of chemotherapy-induced cardiotoxicity. Chemotherapy-induced cardiomyopathy has become the leading cause of drug-induced cardiomyopathy (1). According to the Food and Drug Administration (FDA), more than 1 million chemotherapy-induced adverse events occurred in 2014 in the United States. As a representative drug of anthracyclines, doxorubicin is widely used in the treatment of various human tumors (2). The toxicity and side effects of doxorubicin are usually dose-dependent and can only be detected after the accumulation of a specific dose (3, 4). Nevertheless, the mechanism underlying doxorubicin-induced cardiomyopathy is still not fully understood, although oxidative stress is suspected of playing a significant role (5).

Curcumin extracted from turmeric (*Curcuma longa L*. Family: Zingiberaceae) has been shown to exert anti-inflammatory, antioxidant, and anti-tumor effects in the treatment of a variety of diseases (6, 7). Inflammation is thought to play an essential role in the development of cardiovascular diseases, and the anti-inflammatory property of curcumin can, therefore, be used in the treatment of these diseases. Recent studies showed that curcumin exerts a protective effect on different organs due to its antioxidant and anti-inflammatory properties (8, 9). Because curcumin can exert anti-inflammatory, anti-oxidative, and anti-apoptotic effects, it is assumed that curcumin may prevent doxorubicin-induced myocardial cell damage by inhibiting doxorubicin-induced oxidative stress and apoptosis. This study intends to evaluate the protective effect of curcumin against doxorubicin toxicity in cardiomyocytes.

MATERIALS AND METHODS

Grouping

An H9C2 rat cardiomyocyte cell line was purchased from Beijing Bio-RAD life science development Co., Ltd., China. The H9C2 cardiomyocytes were divided

Key words: curcumin; H9C2 cardiomyocytes; cell viability; doxorubicin

Corresponding author:
Dr Chunhui Liu,
Department of Physical Examination Center,
The First Affiliated Hospital of JiamusiUniversity,
Jiamusi City, 154002,
Heilongjiang Province, China
e-mail: liuchdoctor01@163.com

0393-974X (2019)

into 5 groups and cultured for 12 h with the following treatments: Control group: H9C2 cells without any treatment; Doxorubicin-induced cardiotoxicity group: H9C2 cells were treated with 10 μmol/L doxorubicin; Low-dose curcumin group: H9C2 cells were treated with 5 μmol/L curcumin and 10 μmol/L doxorubicin; Medium-dose curcumin group: H9C2 cells were treated with 20 μmol/L curcumin and 10 μmol/L doxorubicin; High-dose curcumin group: H9C2 cells were treated with 35 μmol/L curcumin and 10 μmol/L doxorubicin.

The concentration of doxorubicin and curcumin used in the experiment were chosen after testing the cytotoxic effects of different levels of doxorubicin curcumin on H9C2 cells.

Cell survival rate

Before starting the experiment, the effect of curcumin and doxorubicin on H9C2 cells viability was tested by ((3-(4,5-dimethylthiazol-2-yl)-2,5-diphenyltetrazolium bromide) tetrazolium reduction) (MTT) assay as follows. H9C2 cells grown in the log phase were collected and counted to prepare cell suspensions in a high glucose medium. The effect of curcumin (5, 10, 20, 35, 75, 100 μmol/L) and of doxorubicin (1, 5, 10, 15, 20, 25 μmol/L) on cell viability was evaluated and compared with the untreated group. The cells were incubated for 12 h in a 5% CO_2 atmosphere at 37□. Then, 10 μL of 5 mg/mL MTT solution was added and incubated for 4 h. After culture, the absorbance (OD value)was measured at 490 nm using a plate reader. The rate of cell survival was calculated as follows: cell survival rate = (OD value in the experimental group - OD value in the blank group) / (OD value in the control group - OD value in the blank group) × 100%.

Determination of LDH, MDA levels and SOD activity

LDH level was determined using a lactate dehydrogenase cytotoxicity assay kit (Shanghai Biyuntian Biotechnology Co., Ltd., China), and the procedure was performed according to the manufacturer's instructions. MDA level was determined using a lipid oxidation assay kit (Shanghai Biyuntian Biotechnology Co., Ltd., China) according to the manufacturer's instructions. The SOD activity was measured with a total SOD activity detection kit (Shanghai Biyuntian Biotechnology Co., Ltd., China). The total protein was extracted and determined using a Bicinchoninic Acid (BCA) protein assay kit (Shanghai Biyuntian Biotechnology Co., Ltd., China) according to the manufacturer's instructions. Then, the SOD activity was determined accordingly.

Determination of Caspase-3, Bcl-2 and Bax levels by Western blot

The expression of Caspase-3, Bcl-2, and Bax A was measured using SDS-PAGE electrophoresis (sodium dodecyl sulfate-polyacrylamide gel electrophoresis) combined with the Western blot technique. Briefly, after extraction, the proteins from each sample were resolved in 10% SDS-PAGE and blotted onto a polyvinylidene difluoride (PVDF) membrane at 150 mA for 50 min. Then, the PVDF membrane was blocked using 5% skim milk and incubated overnight at 4□ with primary antibodies against caspase-3, Bax, and Bcl (1: 500 dilution) (Beijing Boosen Biotechnology Co., Ltd., China). After incubation, the PVDF membranes were washed with PBST (phosphate-buffered saline Tween-20) and further incubated with diluted secondary antibodies (Dilution ratio: 1:1000, Proteintech Group, USA) for 90 min. After incubation and washed again with PBST, the membrane was developed using a chemiluminescence reagent (Shanghai Beibo Biotechnology Co., Ltd., China) and visualized using a chemiluminescence imager (Shanghai Yifute Photoelectric Technology Co., Ltd., China). Finally, the grayscale value of each target protein band was analyzed by Image-Pro Plus software (Beijing Zhongsheng Tiancheng Technology Co., Ltd., China) to calculate its relative expression using glyceraldehyde-3-phosphate dehydrogenase (GAPDH) as the internal control.

Statistical analysis

SPSS 24.0 (SPSS Inc., USA) was used to analyze the results. One-way analysis of variance was used to compare the difference among multiple groups, and Least-Significant Difference (LSD) was used to compare the difference between the two groups. The experimental data were expressed by mean ± standard deviation. $P < 0.05$ indicated significant difference and $P < 0.01$ indicated very significant difference.

RESULTS

Effects of curcumin and doxorubicin on H9C2 cells survival rate

Curcumin did not have any impact on the

survival rate of H9C2 myocardial cells (Table I). The survival rate of H9C2 cardiomyocytes was significantly decreased after treatment with different concentrations of doxorubicin (P<0.05). Ten μmol/L doxorubicin reduces cell survival to almost 50% after 12 h of culture. Therefore, this doxorubicin concentration was used as the modeling condition for doxorubicin-induced cardiotoxicity (Table I).

Table I. *Effects of different concentrations of curcumin and doxorubicin on the survival rate of H9C2 cardiomyocytes ($\bar{x}\pm s$).*

Group	OD value	Survival rate (%)
Control group (curcumin)	0.57±0.04	100
5μmol/L curcumin	0.58±0.03	101.7±4.47
10μmol/L curcumin	0.59±0.04	102.61±6.25
20μmol/L curcumin	0.58±0.04	101.57±3.89
35μmol/L curcumin	0.58±0.02	101.43±3.73
75μmol/L curcumin	0.57±0.03	100.02±5.31
100μmol/L curcumin	0.59±0.05	102.29±3.79
Control group (doxorubicin)	0.41±0.04*	100
1μmol/L adriamycin	0.33±0.04*	80.59±9.67*
5μmol/L adriamycin	0.21±0.03*	55.89±6.45*
10μmol/L adriamycin	0.18±0.01*	46.59±4.71*
15μmol/L adriamycin	0.16±0.02*	37.01±5.90*
20μmol/L adriamycin	0.13±0.01*	30.22±6.21*
25μmol/L adriamycin	0.10±0.01*	26.25±3.19*

*Note: * P < 0.05, compared with the control group.*

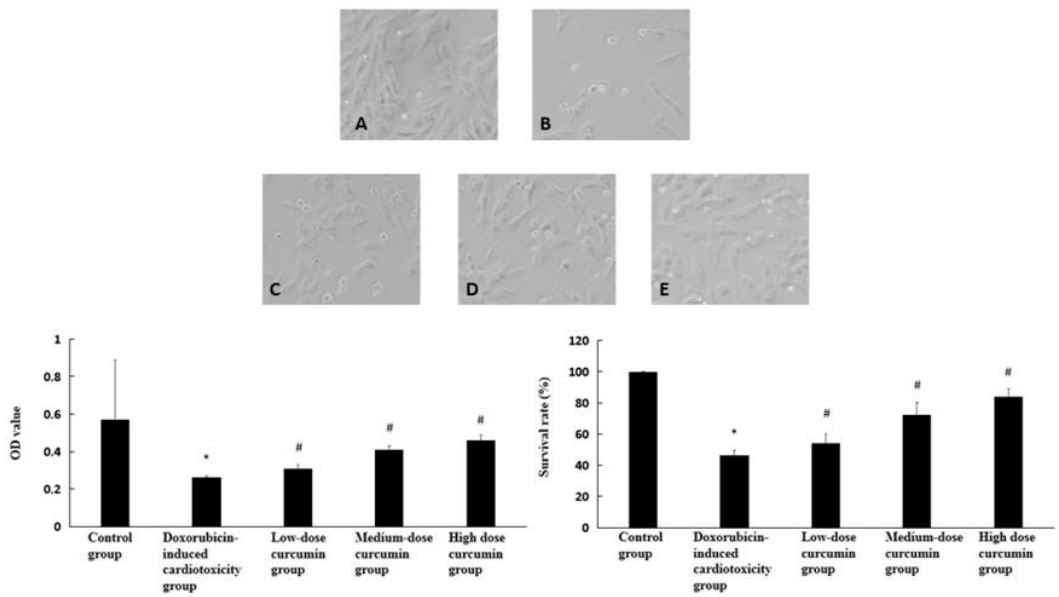

Fig. 1. *Effects of curcumin on the morphology of H9C2 cardiomyocytes after doxorubicin-induced cardiotoxicity (20×), **A**) control group; **B**) doxorubicin-induced cardiotoxicity group; **C**) low-dose curcumin group; **D**) medium-dose curcumin group; **E**) high-dose curcumin group). Effects of curcumin on the survival rate of H9C2 cardiomyocytes upon doxorubicin induction (x ±s). * P<0.05, compared with the control group; # P<0.05, compared with the doxorubicin-induced cardiotoxicity group*

We observed that after 12 h of culture, the cells in the control group showed good growth with a long spindle shape. In contrast, the cells in the doxorubicin-induced cardiotoxicity group became round, and the number of dead cells increased. Moreover, the number of survival cells in each curcumin group was higher than that in the doxorubicin-induced cardiotoxicity group (Fig.1).

The results of the MTT assay showed that, compared with the control group, the doxorubicin-induced cardiotoxicity group presents a significantly decreased cell survival rate ($P<0.05$). Furthermore, the cell survival rates of the low, medium and high dose groups of curcumin were considerably higher than those of the doxorubicin-induced cardiotoxicity group ($P<0.05$) (Fig.1).

Effects of curcumin on doxorubicin-induced oxidative stress

Compared with the control group, the doxorubicin-induced cardiotoxicity group showed increased levels of LDH and MDA and decreased levels of SOD activity ($P<0.05$). The levels of LDH and MDA significantly decreased ($P<0.05$, and respectively $P<0.01$) and SOD activity increased in a dose-dependent manner in the low-dose, medium-dose and high-dose groups of curcumin compared with the doxorubicin-induced cardiotoxicity group (Fig. 2 A, B, and C).

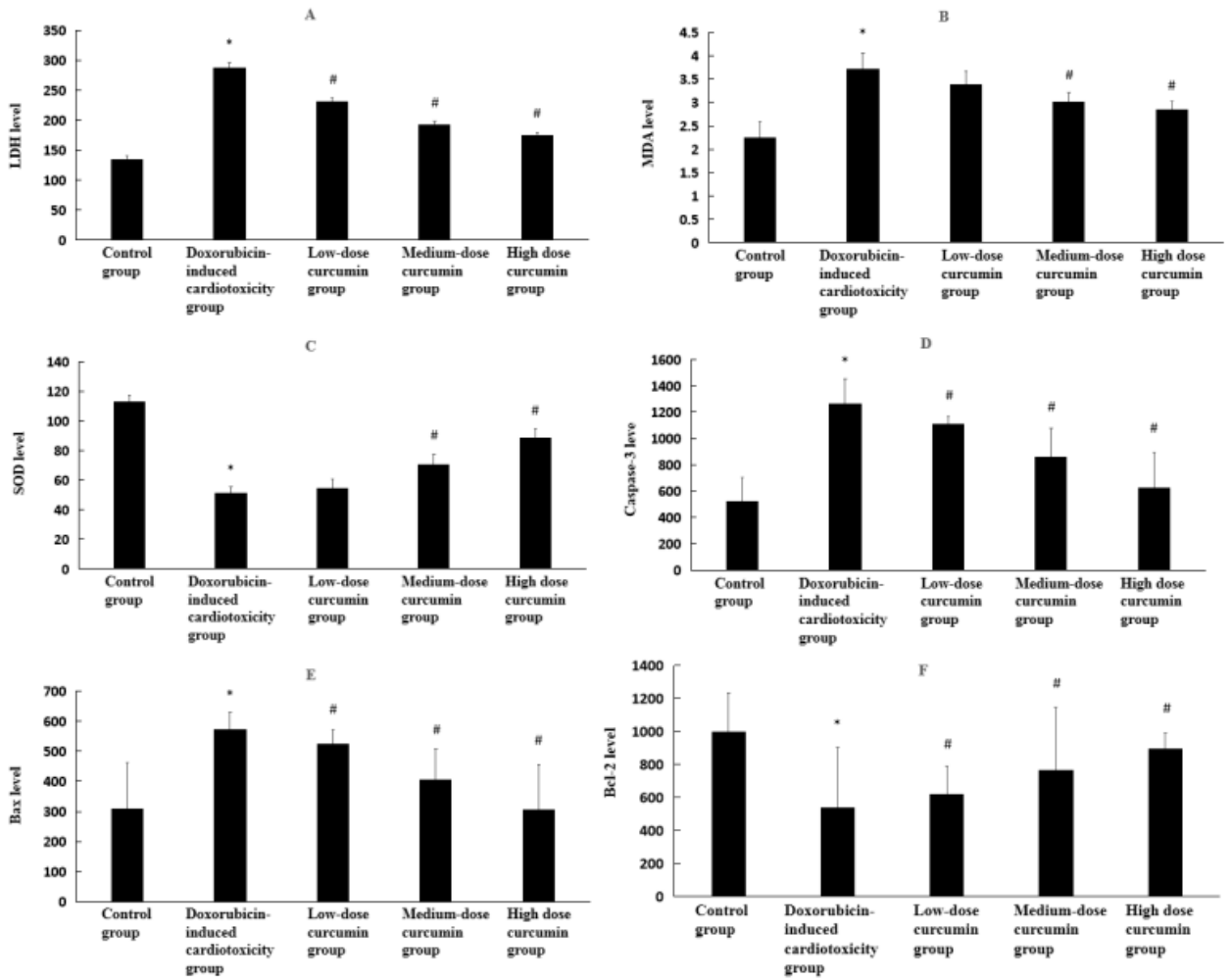

Fig. 2. *Effects of curcumin on LDH, MDA, SOD, Caspase-3, Bax and Bcl-2 proteins levels of H9C2 cardiomyocytes after doxorubicin-induced cardiotoxicity (x ±s).* ***A)*** *LDH level;* ***B)*** *MDA level;* ***C)*** *SOD level; D) Caspase-3 level;* ***E)*** *Bax level;* ***F)*** *Bcl-2 level.*P<0.05, compared with the control group; # P<0.05, compared with the doxorubicin-induced cardiotoxicity group.*

Effects of curcumin on the expression of Caspase-3, Bax, and Bcl-2 proteins

Compared with the control group, the doxorubicin-induced cardiotoxicity group showed increased protein levels of Caspase-3 and Bax and decreased levels of Bcl-2 protein ($P<0.05$). The levels of Caspase-3 and Bax proteins decreased ($P<0.05$) and the level of Bcl-2 protein increased ($P<0.05$) in the low-dose, medium-dose, and high-dose curcumin groups compared to doxorubicin-induced cardiotoxicity group in a dose-dependent manner (Fig. 2 D, E, and F).

DISCUSSION

Doxorubicin exerts a strong toxic effect on cardiac myocytes and can induce their death through a series of molecular mechanisms. This study confirms the protector effect of curcumin against doxorubicin-induced toxicity on cardiomyocyte cells by increasing the survival rate.

Many studies have confirmed that curcumin exerts a strong antioxidant effect, while the doxorubicin-induced cell toxicity is mainly determined by oxidative stress (10). Curcumin can reduce the generation of oxygen free radicals. The results of this study showed that curcumin reduces the LDH level in the cardiomyocytes in all the doses tested compared with the doxorubicin-induced cardiotoxicity group. Curcumin increased the level of SOD and decreased the level of MDA in the medium and high-dose curcumin groups, indicating that these doses could improve the oxidation and lipid resistance of cells.

Doxorubicin-induced cardiotoxicity is mainly mediated by apoptosis. Bcl-2 and Bax proteins are two proteins in the Bcl-2 protein family, reflecting anti-apoptosis and pro-apoptosis status, respectively (11). Caspase-3 protein is an essential member of the Caspase family with the ability to induce apoptosis by directly degrading intracellular structural and functional proteins (12). This study showed that curcumin could decrease the expression of Caspase-3 and Bax and increase the expression of Bcl-2 protein in a dose-dependent manner compared with the doxorubicin-induced cardiotoxicity group. These findings demonstrate that curcumin could inhibit doxorubicin-induced cardiac damage by modulating Bcl-2 and Caspase pathways. This study showed that curcumin could be used with success for the prevention and treatment of doxorubicin-induced cardiotoxicity.

ACKNOWLEDGEMENT

This work was supported by Heilongjiang Health and Family Planning Commission Scientific Research Project (2018073).

REFERENCES

1. Serini S, Vasconcelos RO, Gomes RN, Calviello G. Protective Effects of ω-3 PUFA in Anthracycline-Induced Cardiotoxicity: A Critical Review. Int J Mol Sci 2017; 18(12):2689.
2. Benjamin RS, Wiernik PH, Bachur NR. Adriamycin chemotherapy--efficacy, safety, and pharmacologic basis of an intermittent single high-dosage schedule. Cancer 1974; 33(1):19-27.
3. Cardinale D, Colombo A, Bacchiani G, et al. Early detection of anthracycline cardiotoxicity and improvement with heart failure therapy. Circulation 2015; 131(22):1981-88.
4. Nizhenkovska I, Narokha V, Kuznetsova O. Effects of nicotinic acid on protein oxidative modifications in experimental chronic heart failure. Farmacia 2018; 66(6):959-62.
5. Vejpongsa P , Yeh ET. Prevention of anthracycline-induced cardiotoxicity. J Am Coll Cardiol 2014; 64(9):938-45.
6. Santel T, Pflug G, Hemdan NY, et al. Curcumin inhibits glyoxalase 1: a possible link to its anti-inflammatory and anti-tumor activity. Plos One 2008; 3(10):e3508.
7. Kunnumakkara AB, Bordoloi D, Padmavathi G, et al. Curcumin, the golden nutraceutical: multitargeting for multiple chronic diseases. Br J Pharmacol 2017; 174(11):1325-48.
8. Qualls Z, Brown D, Ramlochansingh C, Hurley LL, Tizabi Y. Protective effects of curcumin against rotenone and salsolinol-induced toxicity: implications for Parkinson's disease. Neurotox Res 2014; 25(1):81-89.

9. Rana MN, Tangpong J, Rahman MM. Toxicodynamics of lead, cadmium, mercury and arsenic- induced kidney toxicity and treatment strategy: A mini review. Toxicol Rep 2018; 5:704-13.
10. Durgaprasad S, Pai CG, Vasanthkumar, Alvres JF, Namitha S. A pilot study of the antioxidant effect of curcumin in tropical pancreatitis. Indian J Med Res 2005; 122(4):315-18.
11. Chen LQ, Wei JS, Lei ZN, Zhang LM, Liu Y, Sun FY. Induction of Bcl-2 and Bax was related to hyperphosphorylation of tau and neuronal death induced by okadaic acid in rat brain. Anat Rec A Discov Mol Cell Evol Biol 2005; 287(2):1236-45.
12. Choudhary GS, Al-Harbi S, Almasan A. Caspase-3 activation is a critical determinant of genotoxic stress-induced apoptosis. Methods Mol Biol 2015; 1219:1-9.

LETTER TO THE EDITOR

FLT3 AND FLT3-ITD GENE MUTATIONS AND PROGNOSIS IN PATIENTS WITH ACUTE MYELOID LEUKEMIA

LG. CHEN, RZ. PEI, Y. LU, PS. ZHANG, XH. LIU, XH. DU, D. CHEN, JJ. CAO and SY. LI

Department of Hematology, Yinzhou Hospital Affiliated to Medical School of Ningbo University, Ningbo, China

Received May 6, 2019 - Accepted October 17, 2019

To the Editor,

Acute myeloid leukemia (AML) is one of the most common malignant tumors (1). Epidemiological statistics have found that although 70-80% of patients with AML have significantly improved response rates and survival rates after induction of chemotherapy, the 5-year overall survival rate is still only 40-50% (2, 3). Therefore, it is necessary to understand the molecular biological mechanisms of the disease in order to find new diagnostic and therapeutic strategies.

At present, stratified therapy for AML patients is of great significance (4, 5) according to prognostic risk. There are two main fms-like tyrosine kinase 3 (FLT3) mutations in AML, namely the FLT3-internal tandem duplication (FLT3-ITD) and FLT3 tyrosine kinase domain (FLT3-TKD) mutations. The FLT3-ITD mutation is more common in AML (6). However, little research has been done on FLT3. Therefore, the relationship between AML and FLT3 has increasingly become the focus of research (7, 8). In this study, real-time fluorescence quantitative PCR was used to detect gene mutation in patients with acute myeloid leukemia. Through the follow-up of patients, the mutations and prognosis of FLT3 and FLT3-ITD genes in leukemia patients were explored, to provide an important basis for guiding treatment of these patients.

MATERIALS AND METHODS

Patients

Ninety-two AML patients (non-M3) hospitalized in the Hematology Department of Yinzhou Hospital Affiliated to the Medical School of Ningbo University from August 1, 2015 to December 31, 2018 were selected. All patients in this study signed an informed consent and the study was approved by the Ethics Committee of Yinzhou Hospital Affiliated to the Medical School of Ningbo University.

The inclusion criteria were: Primary AML; AML secondary to MDS (myelodysplastic syndromes); FAB (French-American-British) type non-M3; aged over 14 years, without gender limitation. Exclusion criteria: FAB AML-M3; acute mixed cell leukemia; chronic myeloid leukemia patients with acute change. Forty-two males and 50 females with an average age of 43 years (15-77 years) met the inclusion criteria. Chromosome karyotype analysis, flt3-itd and NPM1 genotype mutation detection were performed on the 92 patients.

All cases were diagnosed and classified according to MICM (Morphology, Immunology, Cytogenetics and Mol ecular biology) criteria. Morphology was classified according to FAB criteria: M0, M1, M2, M3, M4, M5, M6. In addition, AML classification was not clear.

Detection of gene mutations

Bone marrow smear specimens were collected at

Key words: acute myeloid leukemia; FLT3; FLT3-ITD; gene mutation; C-KIT

Corresponding Author:
Dr Lieguang Chen, Department of Hematology, Yinzhou Hospital Affiliated to Medical School of Ningbo University, No. 251, Baizhang East Road, Ningbo 315040, China
e-mail: chen_lieguang2011@126.com

0393-974X (2019)

the patients' first visit through bone marrow aspiration, followed by genetic mutation testing. The bone marrow samples were diluted 1:1 with 0.8% physiological saline, and then 200 µl of the lysate (Shanghai Yubo Biotechnology Co., Ltd., China) was added to lyse the cells and then heated at 60°C for 30 min. The DNA was precipitated with 200 µl of absolute ethanol, and the tips were mixed and transferred to an adsorption column. After standing for 3 min, and centrifuging at 12,000 rpm for 30 s, the precipitate was discarded, and 450 µl of buffer was added and then repeatedly centrifuged for washing. After 12,000 rpm separation for 30 s, the liquid at the bottom of the column was discarded, 100 µl of distilled water was added, and heated at 60°C for 3 min. After centrifugation at 12,000 rpm for 1 min, the extracted DNA was diluted 10-fold, and the concentration of the extracted DNA was measured. The genomic DNA sample was diluted to 50-150 ng/µl with double distilled water and amplified with PCR.

PCR amplification

The PCR solution was extracted by the leukemia prognosis gene detection kit (FLT3-ITD, Shanghai Biyuntian Biotechnology Co., Ltd., China), and the mixture was shaken at room temperature and then centrifuged at 2,000 rpm for 10 s. A 2% agarose gel was prepared and ethidium bromide (EB) (0.5 µg/ml) was added. The sample to be tested was placed in a horizontal well for electrophoresis, and the DNA molecular weight marker (dl2000) was used as the molecular weight control of the electrophoresis. The electrophoresis results were observed with an ultraviolet spectrophotometer (Shanghai Beyotime Institute of Biotechnology, China).

Chromosome preparation

Fresh bone marrow was added with 2 ml of heparin, 0.8% sodium chloride injection, and 4 ml of human lymphocyte separation solution (Nanjing Shengxing Biotechnology Co., Ltd., China). The diluted sample was slowly added to the surface of the separation solution, and centrifuged at 1,500 rpm for 15 min to adsorb the white membrane, and mixed with 0.8% sodium chloride injection at 1,500 rpm for 5 min. After gently mixing the cell suspension with the pipette, it was dropped vertically onto the glass slide, heated and dried several times. The slide specimen was placed in an Earl solution (Shanghai Ruishi Biotechnology Co., Ltd., China), and the preheating temperature was 87.5°C. After incubating for 80 min, it was rinsed with tap water. It was stained with 10% giemsa staining solution (Nanjing Institute of Bioengineering, China) for 9 min, rinsed with tap water, dried and observed under a microscope.

Table I. *Reaction system.*

	Component	Volume
A	Total RNA	2 µL
	5*first-strand Buffer	4 µL
	M-Mu LV Reverse Transcriptase (200U/µl)	0.8 µL
	Oligo dT Primer (50µM)	2 µL
	dNTP Mixture (10mM each)	2 µL
	RNase Inhibitor (40U/µL)	0.5 µL
	RNase Free dH_2O	up to 50 µL
B	2*Super SYBR premixture	9 µl
	PCR Forward Primer (10µM)	0.5 µl
	PCR Reverse Primer(10µM)	0.5µl
	cDNA	4µl
	RNase Free dH_2O	up to 20 µl

***A)** Reverse transcription; **B)** Real-time fluorescence quantification*

Real-time quantitative PCR

Cellular RNA was extracted by adding RNA extractant Trizol (Biyuntian Biotechnology Co., Ltd., China). The absorbance of RNA at 260 and 280 nm was measured by a quantitative machine (Zhejiang Lecheng Electrical Factory, China), and the concentration was calculated and its purity was evaluated. Total RNA = 500/sample concentration. A reverse transcription system was prepared, as shown in Table I, using PCR for direct amplification in the finished CRNA (ABI, USA).

Follow-up

The median follow-up was 9.8 months (1.5-22.3 months) at the end of February 28, 2019 or at the time of death. Survival rate was the number of days from the initial diagnosis of AML to the end of follow-up.

Statistical analysis

Statistical analysis was performed using SPSS 22.0 statistical software. The Mann-Whitney nonparametric test was used for continuously variable data. The data is expressed in median. *Chi*-squared test was used for the categorical data. The survival curve was drawn by the Kaplan-Meier method. The Log-rank test was used to compare survival rates. The difference was statistically significant with $P < 0.05$.

RESULTS

Analysis of gene mutation results

According to the analysis of the data obtained from gene mutation detection, 18 (19.6%) of the 92 AML patients with positive nucleophosmin-1 (NPM1) gene mutations were detected. Among them, type A mutation was the most common (72.2%) (13 of 18 cases). The FLT3-ITD mutation was positive in 12 cases (13.0%) and the FLT3-TKD mutation was positive in 5 cases (5.4%). Moreover, 3 cases were of D835Y (aspartic acid mutation to tyrosine) mutations and 2 cases were of D835H (aspartic acid mutation to histidine) mutations. None of patients had both mutations. Six patients were positive for simultaneous NPM1 and FLT3 mutations, of which 4 were of NPM1 mutations with FLT3-ITD mutations and 2 were of NPM1 mutations with FLT3-TKD mutations. The incidence of C-KIT mutations was 14.1% (13 out of 92 cases), including 8 cases of D816V (aspartic acid converted to valine) mutations and 2 cases of D816R (aspartic acid converted to arginine) mutations. This was mainly found in M2 and M4 sub-types, including 7 cases of M2 and 5 cases of M4. As shown in Fig. 1, the results of agarose gel electrophoresis of PCR amplification products of NPM1, C-KIT, FLT3-ITD and FLT3-TKD genes showed that although the mutation occurred in the four repeated experiments, the size and expression level were not changed significantly.

Relationship between mutation types and chromosome karyotypes in AML patients

According to the analysis of the data, 21 of 81 cases with chromosome examination did not have mitotic phase, and 8 mutations occurred in 21 cases, including 3 cases of FLT3-ITD mutations, 2 cases of NPM1 mutations, 2 cases of CEBPA mutations and 1 case of C-KITD 816V mutations. Among the remaining 60 patients, 36 (60%) were normal karyotypes. Among the normal karyotypes, 18 cases had gene mutations, 5 cases had FLT3-ITD mutations (13.9%), 7 cases had NPM1 mutations (19.4%), 6 cases had CEBPA mutations (16.7%) and 1 case had C-KITD816V mutations (2.7%). One case was positive for both FLT3-ITD and NPM1. C-KIT D816V was positive in 4 cases, abnormal karyotype in 2 cases, no mitotic phase in 1 case and normal karyotype in 1 case. Among 18 cases of abnormal karyotype, 3 cases were positive for mutations. These results suggested that the proportion of gene mutations in the normal karyotype group was higher than that in the abnormal karyotype group (P=0.019), and NPM1 mutations also occurred in the normal karyotype group (P=0.029).

Prognostic analysis of FLT3-ITD mutations

As shown in Fig.2, the overall survival rate of the related genes for prognostic analysis was obtained by following-up the patients with AML and statistical analysis of the data. Two of the FLT3-ITD positive patients reached CR after one cycle of induction chemotherapy, and the FLT3-ITD positive group was lower than the negative group (Fig. 2A), but there was no significant difference. The median survival of FLT3-ITD mutation positive group (9 cases) was 7.73 (0.5-18.4) months. Compared with

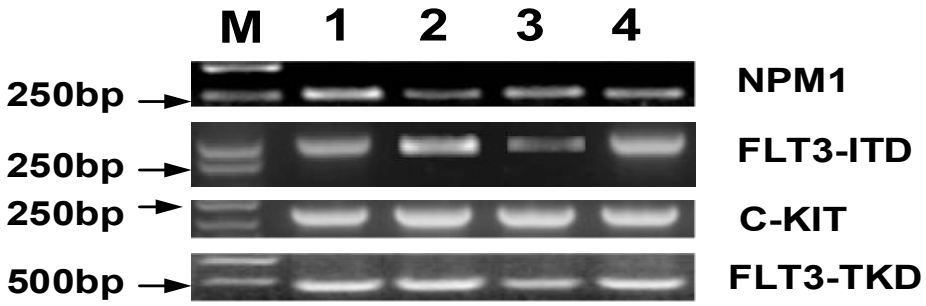

Fig. 1. *Agarose gel electrophoresis of PCR amplification products of gene mutations.*

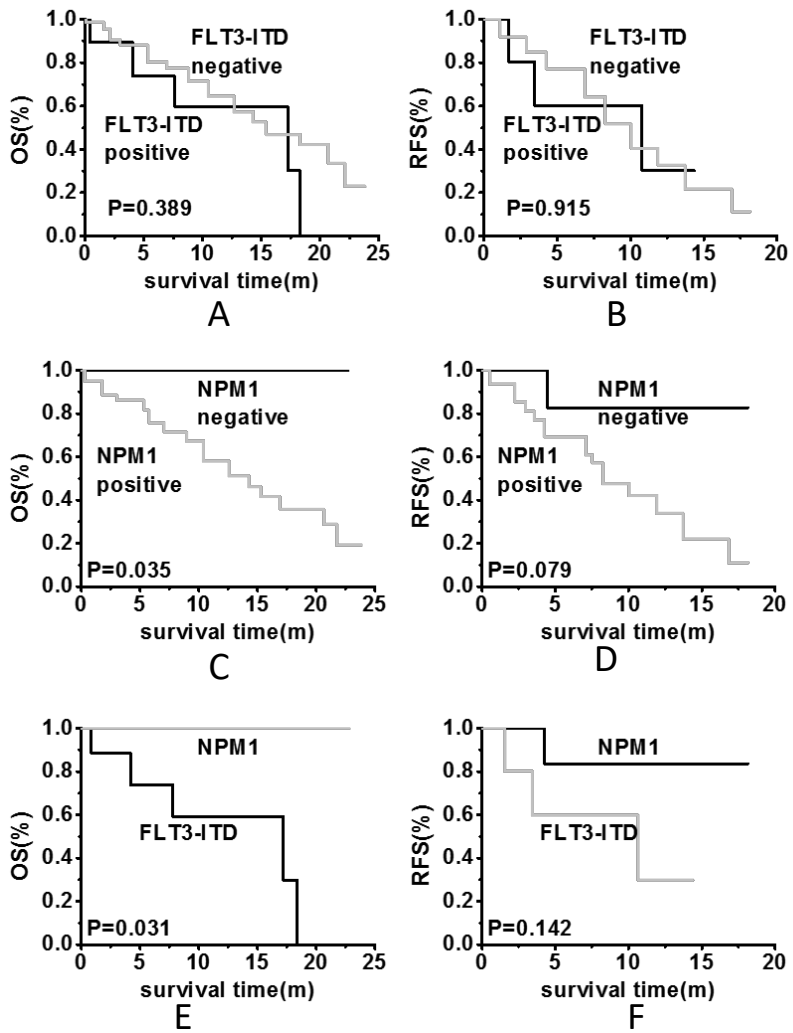

Fig. 2. *Survival curves of FLT3-ITD and NPM1 positive individuals and their comparison.* ***A)*** *Comparison of overall survival rates (OS) between FLT3-ITD mutation positive AML patients and negative AML patients;* ***B)*** *Comparison of relapse-free survival (RFS) between patients with FLT3-ITD mutation-positive AML and those with FLT3-ITD mutation-negative AML;* ***C)*** *Comparison of overall survival rates (OS) between NPM1 mutation positive AML patients and negative AML patients;* ***D)*** *Comparison of recurrence-free survival (RFS) between NPM1 mutation positive AML patients and negative AML patients;* ***E)*** *Comparison of OS between FLT3-ITD mutations patients and NPM1 mutation patients;* ***F)*** *Comparison of RFS between FLT3-ITD mutation patients and NPM1 mutation patients.*

10.47 (0.27-23.67) months in negative group, the median survival of FLT3-ITD mutation positive group (9 cases) was decreased, whereas there was no significant difference in OS rates between the two groups. Fig. 2B shows that 3 cases of FLT3-ITD mutation positive patients (6 cases) relapsed when FLT3-ITD mutations and non-relapse survival rates were detected separately. There was no difference in the recurrence rate between the two groups. The median time of RFS in the positive group was slightly shorter than that in the negative group, but there was no significant difference between the two groups. Survival analysis showed that there was no significant difference in the recurrence-free survival rate between the FLT3-ITD positive group and the negative group (P=0.915).

When the NPM1 positive patients were detected, CR rate of the NPM1 positive patients was significantly higher than that of negative patients after one cycle of chemotherapy (Fig. 2C). The median survival of the NPM1 positive group was not different from that of the negative group, while survival analysis showed that the overall survival (OS) rate of the positive group was higher than that of the negative group (P=0.035). showed that The recurrence rate was 12.5% in the NPM1 positive group and 54.8% in the negative group, while the recurrence rate of the NPMI positive group was significantly lower than that of the negative group (Fig. 2D). The median time of RFS in the positive

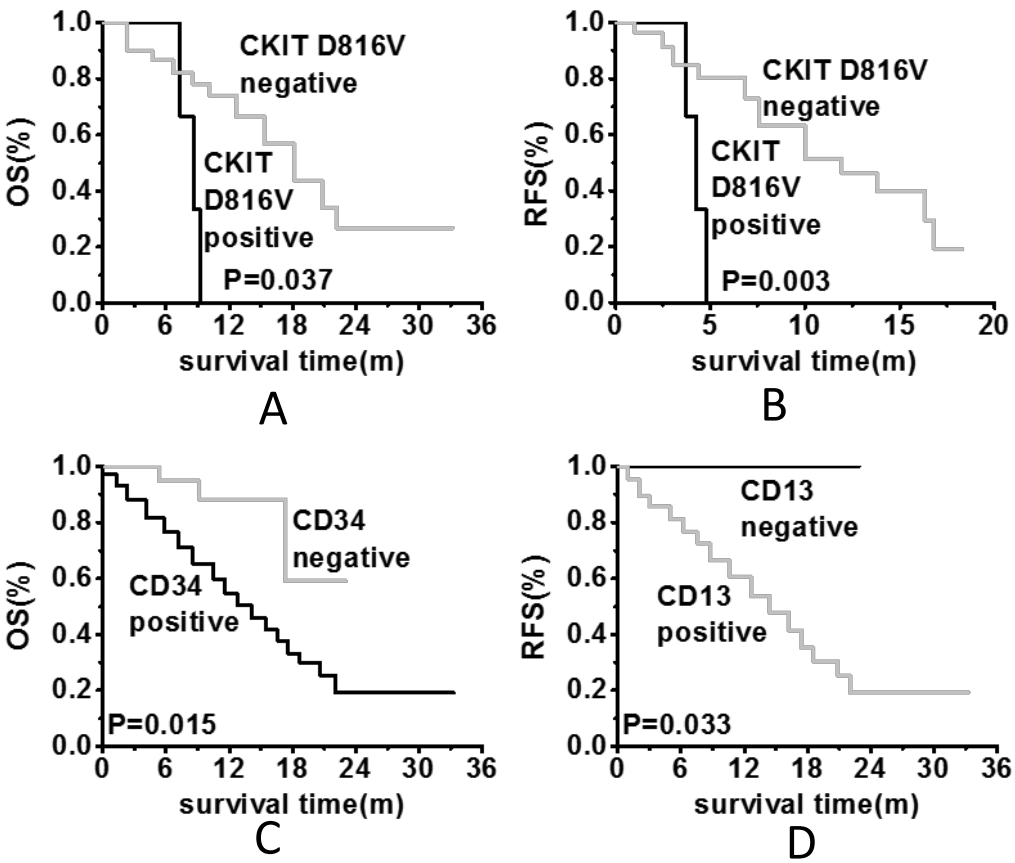

Fig. 3. *Univariate analysis of OS and RFS by gene mutations.* ***A****) Effect of C-KIT D816V mutation on the overall survival rate (OS rate);* ***B****) Effect of C-KITD816V mutations on recurrence-free survival (RFS);* ***C****) Effect of CD34 on the overall survival rate (OS rate);* ***D****) Effect of CD13 on recurrence-free survival (RFS).*

group was slightly longer than that in the negative group, but there was no significant difference between the two groups. Survival analysis showed that the non-recurrence survival of NPM1 positive group was longer than that of the negative group (P=0.079). the total survival of FLT3-ITD mutation patients (not up to CR) was significantly shorter than that of NPM1 mutation patients (P=0.031), but the RFS was not significantly different (Fig. 2 E, F). According to the above results, it can be concluded that the FLT3-ITD mutation had no effect on prognosis of patients. OS, RFS, CR and recurrence rates of patients with the mutation were not significantly different from those of patients without the mutation.

Prognostic analysis of OS and RFS in patients

The survival analysis of mutations in C-KIT D816, CD34 and CD13 genes can be seen in Fig. 3. Univariate analysis showed the total survival of patients with C-KIT D816V mutations (P=0.037) and CD34 positive (P=0.015) had a significant correlation with OS shortening, while those with C-KIT D816V mutations (P=0.003) and CD13 positive (P=0.033) showed a significant correlation with RFS shortening.

DISCUSSION

FLT3, a member of the tyrosine kinase receptor type III family, plays an important role in the proliferation and differentiation of early hematopoietic progenitor cells (9). NPM1 gene mutations can cause abnormal accumulation of nuclear phosphoprotein in cytoplasm (10). In this study, 18 (19.6%) of 92 AML patients with NPM1 gene mutations were detected, of which type A mutation was the most common. The incidence of C-KIT mutations was mainly found in M2 and M4 subtypes.

The FLT3-ITD mutation was a poor prognostic factor, and its adverse prognosis was reflected by a low remission rate, shortened non-recurrence survival and overall survival (11). The NPM1 mutation was a good prognostic factor. It was often co-expressed with FLT3-ITD. NPM1 mutation alone and FLT3-ITD negative patients were sensitive to chemotherapy and had a good prognostic effect. In this study, the impact of FLT3-ITD mutations on prognosis was not found. OS, RFS and recurrence rates were like those of mutation-negative patients.

To sum up, through the study of FLT3 and FLT3-ITD gene mutations and prognosis of patients with AML, it was found that the patients with FLT3-ITD and NPM1 mutations had typical clinical features. The NPM1 mutation suggested a good prognosis, and no FLT3-ITD mutation was found to affect prognosis, which provides an important basis for the treatment of AML patients.

REFERENCES

1. Garcia JS, Stone RM. The Development of FLT3 Inhibitors in acute myeloid leukemia. Hematol Oncol Clin North Am 2017; 31(4):663-80.
2. Chien W, Sun QY, Ding LW, et al. Diagnosis and relapse: cytogenetically normal acute myelogenous leukemia without FLT3-ITD or MLL-PTD. Leukemia 2017; 31(3):762-66.
3. Hospital MA, Jacquel A, Mazed F, et al. RSK2 is a new Pim2 target with pro-survival functions in FLT3-ITD-positive acute myeloid leukemia. Leukemia 2018; 32(3):597-605.
4. Konuma T, Mizuno S, Kondo T, et al. Allogeneic hematopoietic cell transplantation in adult acute myeloid leukemia with 11q23 abnormality: a retrospective study of the Adult Acute Myeloid Leukemia Working Group of the Japan Society for Hematopoietic Cell Transplantation (JSHCT). Ann Hematol 2018; 97(11):2173-83.
5. Falini B, Spinelli O, Meggendorfer M, et al. IDH1-R132 changes vary according to NPM1 and other mutations status in AML. Leukemia 2019; 33(4):1043-47.
6. Heydt Q, Larrue C, Saland E, et al. Oncogenic FLT3-ITD supports autophagy via ATF4 in acute myeloid leukemia. Oncogene 2018; 37(6):787-97.
7. Larrosa-Garcia M, Baer MR. FLT3 Inhibitors in acute myeloid leukemia: current status and future directions. Mol Cancer Ther 2017; 16(6):991-1001.
8. Weis TM, Marini BL, Bixby DL, Perissinotti AJ. Clinical considerations for the use of FLT3 inhibitors in acute myeloid leukemia. Crit Rev Oncol Hematol 2019; 141:125-38.
9. Grafone T, Palmisano M, Nicci C, Storti S. An

overview on the role of FLT3-tyrosine kinase receptor in acute myeloid leukemia: biology and treatment. Oncol Rev 2012; 6(1):e8.
10. Toruner GA, Thakral B. Relapsed NPM1 mutated acute myeloid leukemia with PDGFRA rearrangement. Blood 2019; 133(2):181.
11. Heath EM, Chan SM, Minden MD, Murphy T, Shlush LI, Schimmer AD. Biological and clinical consequences of NPM1 mutations in AML. Leukemia 2017; 31(4):798-807.

LETTER TO THE EDITOR

EVALUATION OF THE SYSMEX UF-5000 AUTOMATED URINALYSIS ANALYZER

Q. LI[1], J. XU[1], Y. TANG[1], X. WEN[1], P. GUO[1], Z. SONG[1], F. WANG[1], P. ZHANG[1], X. SHANG[1] and C. WANG[2]

[1]Department of Clinical Laboratory of Xiyuan Hospital, China Academy of Chinese Medical Sciences, Beijing, China; [2]Department of Clinical Laboratory, The PLA General Hospital, Beijing, China

Received June 14, 2018 – Accepted October 12, 2018

To the Editor,

Urinalysis is an indispensable and fundamental test offered by clinical laboratories to assess overall health and provide valuable diagnostic information in multitudinous diseases (1). Presently, there are multiple methods available for routine urinalysis, and the clinically common ones include urine physical appearance, visual microscopic examination (VME), dry chemistry and flow cytometry (2). A urine dry chemical analyzer can only be used for preliminary patient screening and not as the basis for a definitive diagnosis due to the many false positive results (3). VME is the gold standard test for the visible components, Unfortunately, it is time-consuming and labor-intensive.

The automated urinalysis analyzer is based on the principle of flow cytometry. With flow cytometry detection, the urine does not have to be centrifuged and the types and quantities of urine-formed elements are reported by comprehensively analyzing the fluorescence intensity and the intensity of the scattering light.

The Sysmex UF-500i Automated Urine Formed Element Analyzer (UF-500i) has been widely used in clinical laboratories over the years. Recently, a new-generation automated urinalysis system [the Sysmex UF-5000 Automated Urine Formed Element Analyzer (UF-5000)] was produced with an improved model (Sysmex Corporation, Kobe, Japan). We observed that the basic performance of the UF-5000, including the accuracy, repeatability, stability and blank count, was superior to the UF-500i through our pre-stage test. Furthermore, the detection speed is greatly increased compared to the UF-500i. To date, there has not been any published study comparing the two instruments. In this study, we conducted a comparison to evaluate whether there was a good correlation between the clinical results from the UF-5000 and those of the control groups and whether it was sufficient to satisfy the requirements of clinic trials.

MATERIALS AND METHODS

Instruments

The UF-5000 (Sysmex Corporation, Kobe, Japan) and the UF-500i (Sysmex Corporation, Kobe, Japan) were used for the automated analysis. An Olympus CX31 microscope (Olympus Corporation, Tokyo, Japan) was used for VME.

Collection of urine specimens

This experiment was approved by the medical ethics committee of the Xiyuan Hospital and the Chinese Academy of Chinese Medical Sciences. During the study, from April 2016 to July 2016, 269 urine samples from inpatients and

Key words: urinalysis, UF-5000, VME

Mailing address:
Chengbin Wang, MD, PhD,
Department of Clinical Laboratory,
The PLA General Hospital,
Beijing, 100853, China
Tel.: +86 13683347768
e-mail: wangcb301@126.com

0393-974X (2019)

outpatients, submitted for urinalysis to the Xiyuan Hospital Laboratory were used, and these included a diversity of abnormalities to ensure a wide range of data of the particles. All of the specimens included in this clinical research met the following standards: fresh urine (within 2 hours after urine collection) (4); clinically salvaged samples; the sample collection and processing met the requirements of standard laboratory operations and product manual (5); and the relevant information from the samples was complete. Beyond those standards, samples with a high concentration of pyuria, gross hematuria, a great quantity of mucus, and a fluorescent substance, due to chemical agent staining, preservative and urine sedimentation, were excluded (6). The sample collection was performed in strict accordance with the recommendations of the National Committee for Clinical Laboratory Standards (NCCLS) (7). A sterile container without preservatives was used for random, mid-stream urine collection, and the urine samples were transported to our laboratory within 2 h after the collection at room temperature.

The study was approved by the Medical Ethics Committee of Xiyuan Hospital, China Academy of Chinese Medical Science. The Waiver of Informed Consent is agreed.

Examination of the urine samples

The evaluation of the UF-5000 included qualitative items (white blood cell clumps (WBCC), non-squamous epithelial cells (NSE), hyaline cast (Hy.CAST), pathological cast (Path.CAST), X'TAL, yeast analogical cells (YLC), spermatozoa (SPERM), MUCUS and squamous epithelial cells (SEC) and quantitative items (leukocytes (WBCs), erythrocytes (RBCs), epithelial cells (ECs) and CASTs), including a total of 13 parameters.

The urine samples were analyzed by the two instruments and the VME method in parallel. Both machines were calibrated according to the manufacturer's recommendations. Quality control was carried out as follows: Urinalysis Control level 1 and level 2 (Sysmex Corporation, Kobe, Japan) were used daily as an internal quality control.

For the analysis, a 14-mL urine specimen was collected and transferred to a collection tube which was place into a compatible rack and was automatically run on the analyzer. Both machines provided automatic counts of WBCs, RBCs, ECs and CASTs (8).

For the standardization of the VME, we referred to the recommendations of the Chinese Association of Laboratory Medicine and the European Confederation of Laboratory Medicine (9). After performing the automated particle testing by the two instruments, approximately 10 mL of each residual urine specimen was centrifuged at 1500 rpm (400 g) for 5 min (9). After centrifugation, the pellet was carefully re-suspended into 200 μL of sample using a pipette, and later, 20 μL of the unstained sample was placed onto a microscope slide to reach a concentration of 50 particles. The slide was covered with a slide cover measuring 18X18 mm. First, the whole slide was observed with low-power fields (10×10 times) (LPFs), and thereafter with high-power fields (10×40 times) (HPFs). The cells were represented by the lowest and highest numbers as shown by the HPF, and the CASTs were represented by the lowest and highest numbers as shown by the LPF. Next, we observed at least 20 HPF and took the average. All of the microscopic examinations were performed by two qualified blinded medical technologists, and all of the samples were completely processed within 2 h after receiving them (10). HPFs of the WBCs, RBCs, and ECs and LPFs of the CASTs were assessed, and the results are expressed as the mean of the count obtained per HPF and LPF separately at first. The particle counts were finally recorded as particles per microliter (10). The conversion between 'per HPF' with 'per microliter' of WBCs, RBCs, and ECs and 'per LPF' with 'per microliter' of the CASTs for VME were 1/HPF=5.56/μL, 1/HPF=5.56/μL, 1/HPF=5.56/μL, 1/LPF=0.34/μL, respectively, which reflects the health-related values from the Chinese population.

For the qualitative items, which were reported by the UF-5000 but not by the UF-500i, the samples were only detected by the UF-5000 and VME method (11). For the SEC, which was quantitated by the UF-5000, the results were finally presented as particles per HPF, and the conversion was 1/HPF=2.90/μL.

Statistical analysis

We analyzed the data obtained from the 269 samples using the IBM SPSS Statistics, Version 17.0 (IBM Corporation, New York, United States).

For the quantitative items, because the data does not satisfy normal distribution, the differences between the methods were compared by Kruskal-

Wallis Test. *P* value less than 0.05 was considered to be statistically significant. The correlations and agreements between both instruments and the VME were assessed by Passing-Bablok regression analysis, an intraclass correlation coefficient (ICC) and Bland-Altman analysis. When comparing each of the two instruments with VME, in all cases the 95% confidence interval for the intercept did include 0 and the slope did include 1, demonstrating a good agreement among the three methods. The limits of agreement assessed by the Bland-Altman method were defined as the mean difference plus or minus 1.96*SD* of the differences. In addition, the regression equations were calculated for the quantitative items.

For the qualitative items, the positive predictive value (PPV), negative predictive value (NPV) and total predictive value (TPV) were calculated, and the agreement between the UF-5000 and VME was analyzed by calculating the Cohen's κ coefficient and its 95% *CI*. The κ values were interpreted as follows: slight agreement, 0.00 to 0.20; fair agreement, 0.21 to 0.40; moderate agreement, 0.41 to 0.60; substantial agreement, 0.61 to 0.80; or almost perfect agreement, 0.81 to 1.00 (12).

RESULTS

Kruskal-Wallis test analysis between methods for the quantitative items

Kruskal-Wallis test was performed, and there were no statistically significant differences between the methods for WBCs and ECs, and the specific pairwise agreement results are shown in Table I. There were no statistically significant differences for UF-5000 VS VME of the RBCs.

Passing-Bablok regression analysis, ICC and Bland–Altman analysis among three methods for the quantitative items

For the quantitative items, using Passing-Bablok regression analysis and ICC, we observed a satisfactory correlation and good agreements between the UF-5000 and VME, except for the CASTs (Table I).

Table I. *Kruskal-Wallis test, Passing-Bablok regression analysis, an intraclass correlation coefficient (ICC) and Bland-Altman analysis results* for the quantitative items

Cell type	group	Sig of Kruskal-Wallis Test	Sig of Pairwise comparison	Regression equation	95% CI of slope	95% CI of intercept	ICC	95%*CI* of ICC	The mean of bias(x)	Bias standard deviation(SD)	x-1.96SD	x+1.96SD
WBC	UF-5000 VS VME	0.904	0.418	y=-0.42+1.11x	1.08~1.17	-0.60~-0.25	0.996	0.995~0.997	6.73	38.06	-67.8676	81.3276
	UF-500i VS VME		0.057	y=-0.21+1.14x	1.09~1.22	-0.50~-0.01	0.993	0.991~0.994	11.45	50.02	-86.5892	109.4892
	UF-5000 VS UF-500i		0.296	y=-0.17+0.97x	0.94~1.00	-0.38~0.03	0.997	0.996~0.998	-4.72	32.02	-67.4792	58.0392
RBC	UF-5000 VS VME	0.810	0.984	y=-0.906+1.07x	0.98~1.14	-0.58~-1.38	0.970	0.962~0.976	13.74	137.23	-255.231	282.7108
	UF-500i VS VME*		0.000	y=-0.66+1.42x	1.24~1.68	-1.52~0.11	0.955	0.943~0.965	23.04	171.97	-314.021	360.1012
	UF-5000 VS UF-500i*		0.001	y=-0.76+0.85x	0.80~0.88	-1.07~-0.59	0.993	0.991~0.994	-9.29	72.16	-150.724	132.1436
EC	UF-5000 VS VME*	0.856	0.040	y=-0.765+1.07x	1.00~1.14	-0.90~-0.40	0.951	0.937~0.961	0.67	6.29	-11.6584	12.9984
	UF-500i VS VME		0.707	y=0.25+1.03x	0.99~1.07	-0.48~-0.08	0.961	0.951~0.969	0.23	5.05	-9.668	10.128
	UF-5000 VS UF-500i		0.105	y=-0.43+1.09x	1.00~1.16	-0.66~-0.20	0.948	0.933~0.959	0.44	6.57	-12.4372	13.3172
CAST*	UF-5000 VS VME*	0.000	0.000	y=-0.00+0.87x	0.68~1.00	0.00~0.00	0.548	0.426~0.645	0.11	1.27	-2.3792	2.5992
	UF-500i VS VME*		0.000	y=-0.00+5.07x	4.00~6.26	-0.04~0.00	0.339	0.160~0.480	1.29	2.60	-3.806	6.386
	UF-5000 VS UF-500i*		0.000	y=-0.00+0.173x	0.13~0.21	0.00~0.00	0.786	0.740~0.839	-1.18 ~ 1.85		-4.806	2.446

**: P<0.05*

The Passing-Bablok regression equations among the three methods for the WBCs, RBCs, ECs and CASTs are shown in Fig. 1.

In addition, Table I shows the bias and 95% limits of the agreement calculated by Bland-Altman between the three methods for the quantitative items and reveals that the UF-5000 showed a better agreement with the VME than the UF-500i except for the ECs. Fig. 2 shows the Bland-Altman plot for the quantitative items.

Predictive value and Kappa test for the qualitative items

For the WBCC, NSE, Hy.CAST, Path.CAST, X'TAL, YLC, SPERM, MUCUS and SEC, the overall coincidence rate between the UF-5000 and VME were good (99%, 95%, 96%, 97%, 98%, 98%, 99%, 94% and 96%, respectively), and the $\varkappa$ values indicated an almost perfect agreement (0.92, 0.84, 0.84, 0.81, 0.93, 0.80, 0.98, 0.83 and 0.83, respectively)($p<0.05$)

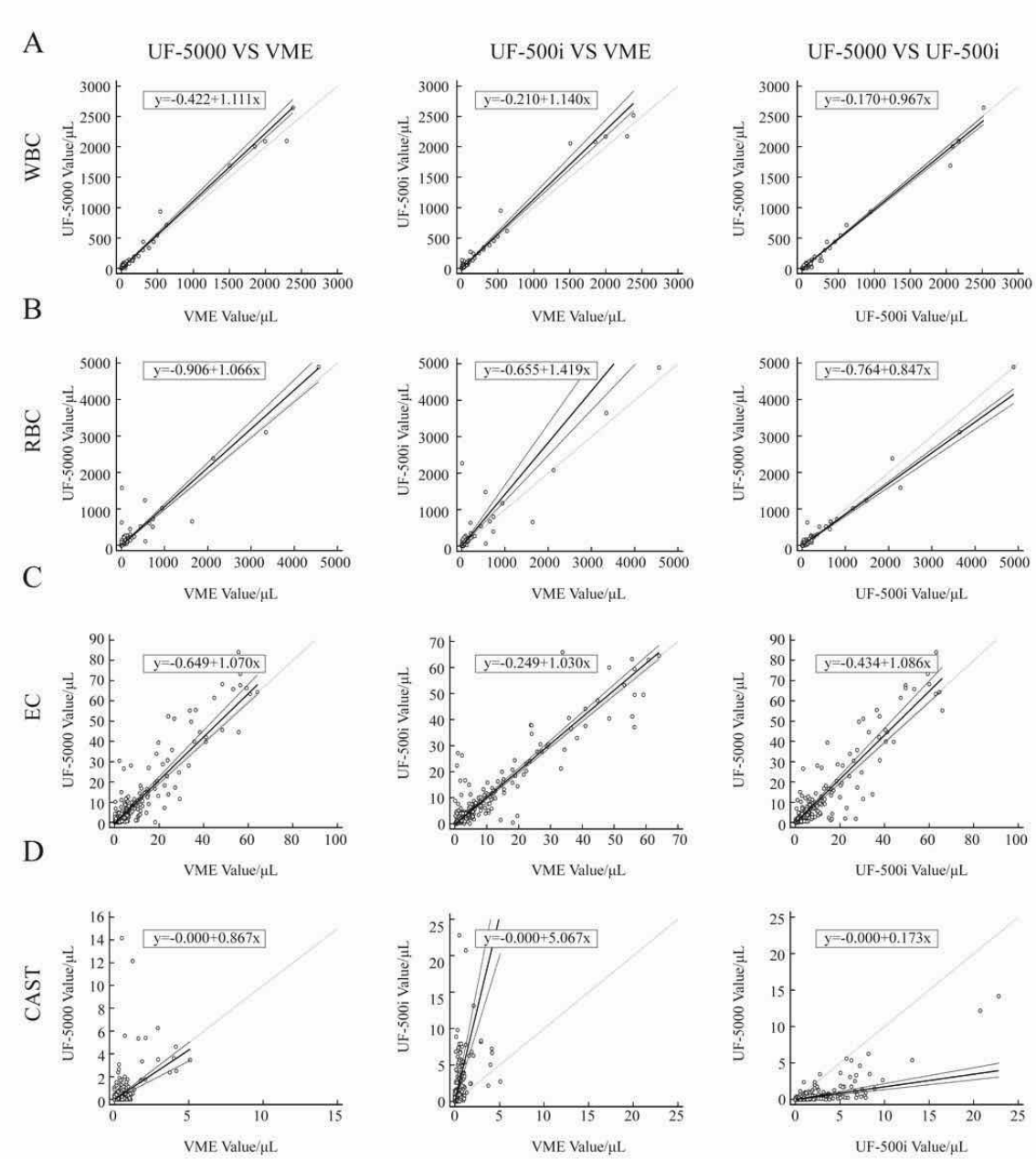

Fig. 1. *Regression correlation among the values measured by the UF-5000, UF-500i and VME for the WBCs, RBCs, ECs and CASTs in the urine samples, (**A**-**D**).*

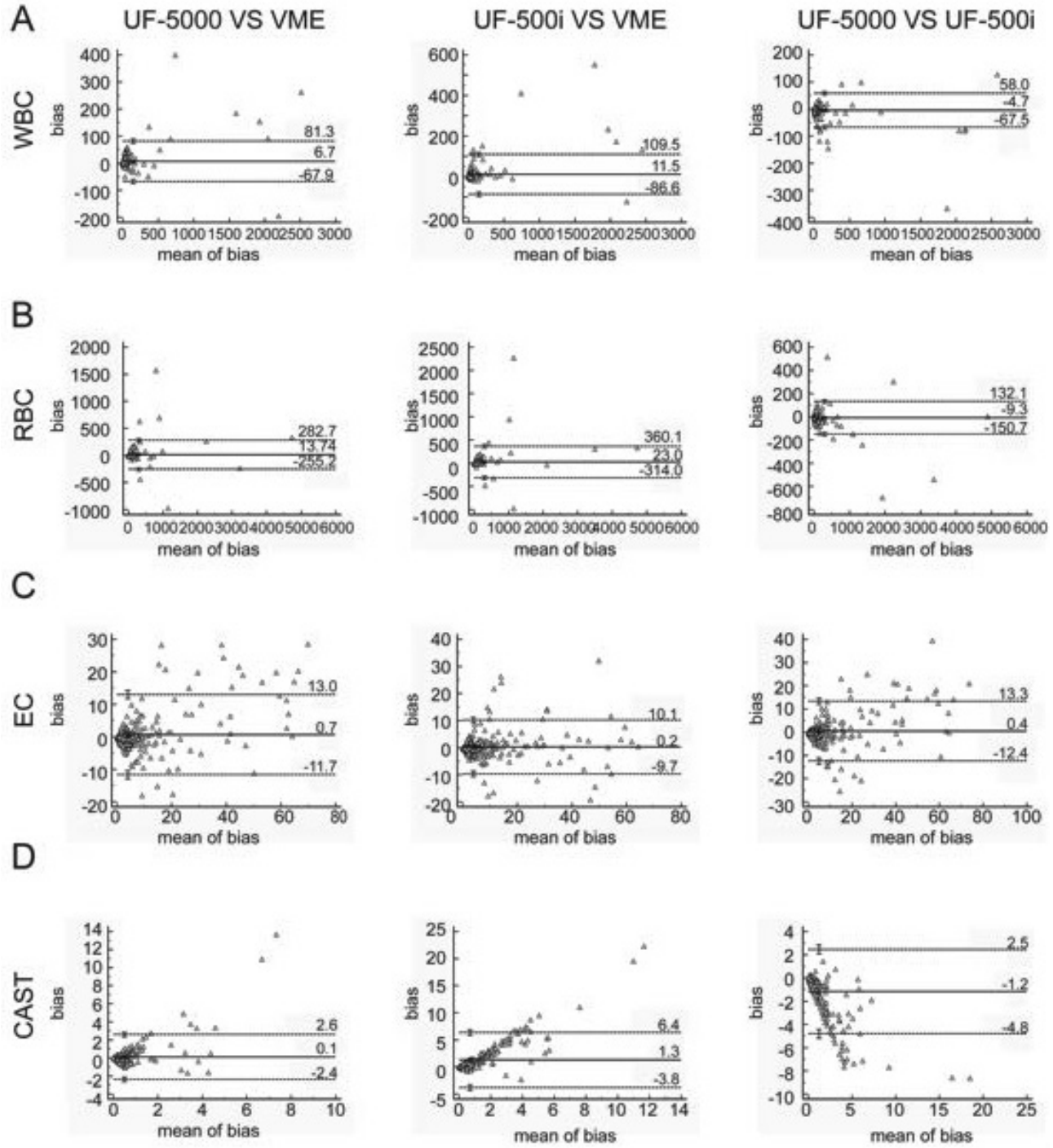

Fig. 2. *Agreement analysis between the three methods for the WBCs, RBCs, ECs and CASTs by the Bland-Altman method (A-D).* ***A****) The Bland–Altman analysis for the comparison of the WBC measurement by the UF-5000 and VME, UF-500i and VME, and UF-5000 and UF-500i, respectively.* ***B****) Bland–Altman analysis for the comparison of the RBC measurement by the UF-5000 and VME, UF-500i and VME, and UF-5000 and UF-500i, respectively.* ***C****) Bland–Altman analysis for the comparison of the EC measurement by the UF-5000 and VME, UF-500i and VME, and UF-5000 and UF-500i, respectively.* ***D****) Bland–Altman analysis for the comparison for CAST measurement by the UF-5000 and VME, UF-500i and VME, and UF-5000 and UF-500i, respectively. The mean difference and limits of the agreement are displayed as reference lines.*

DISCUSSION

The UF-5000, with an improved capability, is a new generation instrument. The UF-5000 provides a full printed report of the test results within 50 seconds and the excitation light source of the UF-5000 is upgraded to a blue semiconductor; thus, it provides more accurate data for urinalysis. For the quantitative items, we found that the differences among the three methods were not statistically significance for the WBCs, ECs. By a further pairwise comparison, there was no statistically significant difference between the UF-5000 and the VME for RBCs. However, there were still statistically significant differences between the UF-500i and VME for the RBCs. Similarly, the ICC values and the Bland-Altman analysis showed an excellent correlation for the UF-5000 with the VME for the WBCs, RBCs and ECs, but was dissatisfactory for the CASTs. The MUCUS in these samples possibly caused interference for the analyzers or the inconsistency is probably related to the variability of the morphology of the CASTs, resulting in possibly false high CAST counts. For the qualitative items, the PPV, NPV and TPV values between the UF-5000 and VME were greater than 80%, and the κ values were more than 0.8. These data suggested that the UF-5000 showed a good correlation with the VME for the qualitative items. In general, we conclude that the UF-5000 tested showed more consistent results with the VME than did the UF-500i. Furthermore, the UF-5000 has high applicability in screening urine for formed elements in the clinical setting. We could at least show that the UF-5000 performs as well as VME by collecting 269 samples. The relatively low number of samples could have affected the outcome, particularly the lack of large differences found, and this is a limitation of this study and needs to be improved.

ACKNOWLEDGEMENTS

This work was supported by the National Major Scientific Instruments and Equipment Development #: 2012YQ18011708; Military Medical Technology Research Pillar Program during the Twelfth Five-year Plan Period #: AWS11Z005-4 to Chengbin Wang. The Authors would like to express our thanks to Sysmex Medical Electronics (Shanghai) for providing the test instrument and all the assistants in our laboratory for their assistance. In particular, we thank the volunteers who participated in this study.

REFERENCES

1. Ipe DS, Horton E, Ulett GC. The basics of bacteriuria: strategies of microbes for persistence in urine. Front Cell Infect Microbiol 2016; 6:14.
2. Lee W, Ha JS, Ryoo NH. Comparison of the Automated cobas u 701 urine microscopy and UF-1000i flow cytometry systems and manual microscopy in the examination of urine sediments. J Clin Lab Anal 2016; 30(5):663-71.
3. Lee W, Kim Y, Chang S, Lee AJ, Jeon CH. The influence of vitamin C on the urine dipstick tests in the clinical specimens: a multicenter study. J Clin Lab Anal 2016; 31(5):e22080.
4. Kouri T, Malminiemi O, Penders J, Pelkonen V, Vuotari L, Delanghe J. Limits of preservation of samples for urine strip tests and particle counting. Clin Chem Lab Med 2008; 46(5):703-13.
5. Fully Automated Urine Particle Analyzer manual (UF-5000). Sysmex corporation. 2017.
6. Nagaraj N, Mann M. Quantitative analysis of the intra- and inter-individual variability of the normal urinary proteome. J Proteome Res 2011; 10(2):637-45.
7. National Committee for Clinical Laboratory Standards (NCCLS).
8. Wang J, Zhang Y, Xu D, Shao W, Lu Y. Evaluation of the Sysmex UF-1000i for the diagnosis of urinary tract infection. Am J Clin Pathol 2010; 133(4):577-82.
9. Ko DH, Ji M, Kim S, et al. An approach to standardization of urine sediment analysis via suggestion of a common manual protocol. Scand J Clin Lab Invest 2016; 76(3):256-63.
10. Jiang T, Chen P, Ouyang J, Zhang S, Cai D. Urine particles analysis: Performance evaluation of Sysmex UF-1000i and comparison among urine flow cytometer, dipstick, and visual microscopic examination. Scand J Clin Lab Invest 2010; 71(1):30-37.
11. Manoni F, Tinello A, Fornasiero L, Hoffer P, Temporin V, Valverde S, Gessoni G.. Urine particle

evaluation: a comparison between the UF-1000i and quantitative microscopy. Clin Chem Lab Med 2010; 48(8):1107-11.

12. van Delft S, Goedhart A, Spigt M, van Pinxteren B, de Wit N, Hopstaken R. Prospective, observational study comparing automated and visual point-of-care urinalysis in general practice. BMJ Open 2016; 6(8):e011230.

LETTER TO THE EDITOR

MONOCULAR ACCOMMODATIVE AMPLITUDES IN FEMTOSECOND LASIK FLAP CREATION FOR HIGH AND LOW-MODERATE MYOPIA

Q-B. LI[1] and X-T. LIU[2]

[1]Department of Myopia Laser Division, NingBo Eye Hospital, NingBo, China;
[2]Department of Clinical inspection section, NingBo Eye Hospital, NingBo, China

Received April 30, 2019 – October 30, 2019

To the Editor,

Laser *in situ* keratomileusis (LASIK) is a kind of corneal refractive surgery. Its operation mainly exerts on the corneal stromal layer. First, a lamellar corneal flap is created using a micro-corneal knife. Then, refractive ablation is performed on the corneal stromal bed using an excimer laser to effectively preserve the corneal epithelium, the anterior elastic layer and the whole cornea, making it more in line with the corneal physiology. Furthermore, this induces a good corrective effect on high ametropia and rapid postoperative recovery, therefore its application range in clinics has constantly expanded (1). However, LASIK surgery also brings many new problems. With the development of excimer laser refractive surgery, it was found in clinical practice that some patients developed intermittent blurred vision, visual fatigue and other symptoms (2). In addition, the postoperative improvement of the objective visual acuity of hyperopic patients was not superior to that of myopic patients, however, their subjective symptoms were better than those of myopic patients. Some scholars stated that LASIK surgery reduces the diopter and implicit oblique angle of hyperopic patients (3). However, few studies have been conducted on the different effects of LASIK surgery on the monocular accommodative power of patients with different degrees of myopia. This study aims to observe changes in monocular accommodative amplitude in patients with high and low-moderate myopia before and after LASIK surgery, and explore the feasibility of LASIK surgery in some patients from the perspective of accommodation.

MATERIALS AND METHODS

This study was conducted in accordance with the Declaration of Helsinki and with approval from the Ethics Committee of NingBo Eye Hospital. Written informed consent was obtained from the participants. Ethical batch number: (2013-qtky-003)

The study subjects were patients who received femtosecond LASIK flap creation at the Myopia Laser Department of our hospital from January 2014 to October 2014. A total of 136 eyes of 68 patients were included in the study. Of the 68 patients, 36 were male (72 diseased eyes) and 32 were female (64 diseased eyes); and the ages of ranged between 18-35 years. Preoperative uncorrected visual acuity ranged between 0.01-0.1. According to the spherical equivalent, these patients were divided into two groups: low-moderate myopia group (n=46, -6.00 D), and high myopia group (n=76, -6.25 D to 10.00 D). LASIK surgery was performed for patients who had a stable degree of myopia in the previous two years, and

Key words: high myopia; accommodative amplitude; femtosecond laser; excimer laser in situ *keratomileusis; vision*

Corresponding Author:
Dr Xiao-Tian Liu
Department of Clinical inspection section,
NingBo eye Hospital, NingBo, 315040, China
Tel: +86 15058839344/0574-87862233
Fax: +0574 87741727
e-mail: liuxiaotian0923@163.com

0393-974X (2019)

DISCLOSURE: ALL AUTHORS REPORT NO CONFLICTS OF INTEREST RELEVANT TO THIS ARTICLE.

voluntarily requested femtosecond LASIK flap creation. All patients had been wearing glasses for a long period of time, the degree of myopia in both eyes was the same, and the diopter maintained above 2a. All patients underwent preoperative examination: autorefraction, insertion of the phoropter under the small pupil for the determination of the diopter, slit lamp examination, fundus examination by three-mirror contact lenses, non-contact tonometer examination, corneal topography, corneal thickness measurement, ophthalmological A/B ultrasound and routine blood test, exclusion of other eye diseases, determination of history of surgery and trauma, systemic connective tissue disease and autoimmune diseases.

The instruments used for LASIK were the MEL80 excimer laser system (Zeiss, Jena, Germany) and Intralase femtosecond laser (Johnson, USA).

Before surgery, the conjunctival sac and eye skin were routinely rinsed, and a sterile drape was placed. Under local anesthesia, the eyelid was stretched using an eye speculum. Under axicon lens and negative pressure suction, the corneal flap was made using the Intralase femtosecond laser, with a thickness of 9-110 μm. The corneal flap was removed, and was precisely cut using the excimer laser system. Next, the space under the flap was washed, the corneal flap was reset, and the water was dried.

Before surgery, ofloxacin eye drops were used four times a day **(FOR HOW LONG)**?, and was stopped three days after the surgery. Immediately after surgery, patients wore a transparent eye patch for one day, and were instructed to visit the hospital for recheck the following day. On the day after surgery, patients began to administer 0.1% fluorometholone, four times a day **(FOR HOW LONG)**?. Then, the dose frequency was reduced to once a day each week, the administration lasted for one month. Artificial tear (such as Tears Naturale Forte and ETUDE) was applied four times a day for 3-6 months.

Visual acuity, dioptry, intraocular pressure and corneal topography were examined at 1 day, 10 days, 1 month, 2 months and 6 months after the operation. The best corrected visual acuity before the intervention, and the uncorrected visual acuity and best corrected visual acuity at six months after surgery were observed.

Binocular accommodative amplitudes were measured by an experienced optometrist before the operation and at 10 days, 1 month, 3 months and 6 months post-operatively. Ametropia in both eyes was completely corrected. A near visual acuity chart was placed 40 cm in front of the phoropter, and a near PD was adopted. Patients were instructed to observe the upper line of the line that had the best visual acuity, and report whether it was clear. If it was clear, accommodative amplitude was gradually increased by +0.25 D each time (negative relative accommodation) until the patient reported that the visual acuity chart became blurred or ghost images appeared. Then, the value of the spherical mirror of the previous gradient was recorded. This procedure was conducted three times, and the average value was calculated. Conversely, -0.25 D was added each time (positive relative regulation) until the patient reported that the visual acuity chart became blurred or ghost images appeared, and the value of the spherical mirror of the previous gradient was recorded. This procedure was conducted three times, and the average value was calculated. Final record = negative relative regulation + positive relative regulation. The above measurements were all performed by the same optometrist.

Statistical analysis

Data were analyzed using statistical software SPSS 15.0, and were evaluated using analysis of variance (ANOVA) and *t*-test. Inspection level was set as $\alpha = 0.05$.

RESULTS

Visual acuity

The best corrected visual acuity of the 68 patients (132 eyes) with high myopia, and the uncorrected visual acuity and best corrected visual acuity at six months after the operation were observed and recorded. This study divided vision range into 3 segments, i.e. ≤0.4, 0.5-0.8 and ≥1.0. The results showed that the BCVA is considered to have no significant difference before and after surgery within the vision range of each segment ($P>0.1$). The postoperative vision of ≤0.4 in the sixth month was decreased by 78.7% from the previous value; the postoperative vision of 0.5-0.8 in the sixth month was decreased by 7.3% from the previous value; the postoperative vision of ≥1.0 in the sixth month was increased by 91.9% from the previous value, which was significantly increased compared to that before operation ($P<0.001$) (Table I).

Monocular accommodative amplitude

According to the measurement method of binocular accommodative amplitude, the measurement data acquired before the operation, and at day 10, 1 month, 3 months and 6 months after surgery were compared between the low-moderate myopia group and high myopia group.

Statistical analysis showed that the monocular accommodation amplitude for 10 days after operation was significantly lower than that before operation (P<0.05). The numbers of the high myopia group and low to moderate myopia group reaching the preoperative level only accounted for 3.9% and 13%, respectively. The monocular accommodation amplitude for 1 month after the intervention was relatively increased and had no significant difference with preoperative monocular accommodation amplitude (P>0.05). The numbers of the two groups reaching the preoperative level only accounted for 86.6% and 89.1%, respectively, and basically

Table I. *Preoperative and postoperative uncorrected visual acuity (UCVA) and best corrected visual acuity (BCVA) (Percentage)*

Vision	n	Vision type	≤0.4	0.5-0.8	≥1.0
Before operation	136	UCVA	107(78.7)	29(21.3)	0(0.0)
		BCVA	3(2.2)	4(3.0)	129(92.8)
After operation	136	UCVA	0(0.0)	11(14.0)	125(91.9)
		BCVA	2(1.5)	10(7.4)	124(91.2)

Table II. *The monocular accommodation amplitude ($\bar{x}\pm s$) in different period and different myopia category, and the proportion of numbers reaching to the preoperative accommodation amplitude level ($\bar{x}\pm s$) at each time point after the intervention.*

	n	Before operation	After operation			
			10 days	1 month	3 months	6 months
High myopia group	76	8.28±1.21	7.42±1.09, 3(3.9)	8.16±1.14, 66(86.8)	8.98±1.15, 74(97.4)	8.95±1.13, 76(100)
Low to moderate myopia group	46	8.47±1.17	8.1±1.27, 6(13.0)	8.29±1.22, 41(89.1)	9.77±1.18, 43(93.5)	9.79±1.09, 46(100)
P		<0.05	<0.05	>0.05	>0.05	>0.05

recovered to the preoperative proportion; The numbers of the two groups reaching the preoperative level for 3-6 months were significantly increased and the average value exceeded the preoperative level (P>0.05) (Table II).

The results of this study revealed that before LASIK, the monocular accommodative amplitude was lowest in subjects in the high myopia group, followed by subjects in the moderate myopia group (P<0.05). At 10 days after the operation, this accommodative amplitude transiently decreased, and recovered to a certain extent; and the extent of increase was most significant in subjects in the low-moderate myopia group (P<0.05). At one month after sirgery, the monocular accommodative amplitude of subjects in the high myopia group was close to the preoperative level, but the difference was not statistically significant when compared with controls (P>0.05). At three months and six months after the operation, the monocular accommodative amplitude of subjects in the high myopia group exceeded the preoperative level, and the difference was not statistically significant when compared with subjects in the low-moderate myopia group (P>0.05). This was consistent with the results of an earlier study (4).

DISCUSSION

Accommodation, the important functions of eyes, is used to adjust the refractive power of the lens through ciliary muscle contraction in order to allow a close object to form a focus on the retina (5, 6). This study revealed that the monocular accommodative amplitude was lower in myopic eyes before LASIK than in normal eyes, and was lowest in the high myopia group. The accommodative amplitude in eyes with different diopter degrees all decreased in the early stage after the operation, and the extent of this decrease was most significant in the high myopia group. Eyes with high myopia had smaller accommodative amplitudes before the operation. The deeper the intraoperative corneal incision is, the more serious the postoperative corneal edema becomes, the poorer the retinal imaging quality becomes, and the greater the extent of decrease in accommodation power. This study reconfirmed that the mean value of accommodative amplitude was negatively correlated with ametropia (7, 8). However, most of the patients, who were 18-35 years old in this study, had strong accommodative function, and the adaptive and compensatory ability for increase in accommodation requirements was also good. Therefore, the accommodative power could be restored in the short term after the operation. For middle-aged patients, further studies are needed to determine whether postoperative accommodative power can be restored, and whether the recovery time of accommodative power in patients of different ages differs.

REFERENCES

1. Guber I, Mouvet V, Bergin C, Perritaz S, Othenin-Girard P, Majo F. Clinical outcomes and cataract formation rates in eyes 10 years after posterior phakic lens implantation for myopia. JAMA Ophthalmol 2016; 3(5).
2. Chen H, Liu Y, Niu G, Jingxue M. excimer laser versus phakic intraocular lenses for myopia and astigmatism: a meta-analysis of randomized controlled trials. Eye Contact Lens 2016; 25(1).
3. Stidham DB, Borissova O, Borissov V, Prager TC. Effect of hyperopic laser insitu keratomileusis on ocular alignment and stereopsis in patients with accommodative esotropia. Ophthalmology 2002; 109(6):1148-53.
4. Maddock RJ, Millodot M, Leat S, Johnson CA. Accommodation responses andrefractive error. Invest Ophthalmol Vis Sci 1981; 20(3):387391.
5. Schmid KL, Strang NC. Differences in the accommodation stimulus response curves of adult myopes and emmetropes: a summary and update. Ophthalmic Physiol Opt 2015; 35(6):613-21.
6. Zhou SB, Li H, Hong HF, Tan J. Comparison of the changes of anterior segment structurebefore and after the LASIK treatment. Chinese J Practical Ophthalmology 2014; 32(8): 984-987.
7. Sekundo W, Gertnere J, Bertelmann T, Solomatin I. One-year refractiveresults, contrast sensitivity, high-order aberrations and complications after myopic small-incision lenticule extraction (ReLExSMILE). Grafes Arah Clin Exp Ophthalmol 2014; 252(5):837-43.
8. Singman E, Matta N, Tian J, Silbert D. association between accommodative amplitudes and amblyopia. Strabismus 2013; 21(2):137-39.

LETTER TO THE EDITOR

LEFT SUBCLAVIAN ARTERY STENOSIS TREATED WITH COVERED STENT

S.J. YANG[1], Y.Q. GU[1,2], T. LUO[3], L.X. QI[1], C.C. ZHANG[1,2], Z. TONG[1], D.S. WANG[1] and Z.J. WU[2]

[1]Department of Vascular Surgery, Xuanwu Hospital of Capital Medical University, Beijing, China;
[2]Institute of Vascular Surgery, Xuanwu Hospital, Capital Medical University, Beijing, China;
[3]Department of Human Resources, Xuanwu Hospital, Capital Medical University, Beijing, China

Received May 23, 2019 – November 4, 2019

To the Editor,

The prevalence of subclavian artery stenosis (SAS) in the general population is approximately 2% (1). Chronic obstructive lesions of the proximal subclavian artery lead to retrograde blood flow in the ipsilateral vertebral artery, and result in symptoms, such as vertebrobasilar insufficiency, upper limb claudication, and transient ischemic attacks (2). The most common cause of such obstructive lesions is atherosclerosis

It has been reported that percutaneous transluminal angioplasty and stent (PTA/PTS) has been the first line of treatment for SAS, with the advantages of being minimally-invasive and safe, as well as having a high success rate and satisfactory effect. Becker (3) performed a simple arteroplasty, and reported a high restenosis rate of 20% in 1-5 years. Furthermore, the technical success rate of stenosis was 83-100%, while the success rate of the occlusion technique was 50-87% (4). In recent years, the risk of cerebral infarction is 1%, with the improvement of equipment and operative skills. Furthermore, the PTA immediate success rate has greatly improved compared to previous rates. However, we still face the challenge of restenosis.

The present case was investigated to assess the application of a covered stent, and determine its safety and effects on endovascular treatment for left SAS.

Case report

A 65-year-old male patient complained of dizziness accompanied by left upper limb weakness, no pain, numbness and sensory disorder for five years, but without nausea, vomiting, headache, hemiplegia or aphasia. The ultrasound results revealed left SAS and left carotid artery stenosis. The patient had a 10-year history hypertension and diabetes, however, denied any history of coronary heart disease (CHD). Examination results: double upper limb skin temperature was normal; the bilateral radial artery was palpable, while the left side was weaker than the contralateral side. Furthermore, a vascular murmur was audible on the left supraclavicular fossa, and the upper extremity systolic blood pressure difference (SBPD) was 30 MMHG.

Technique

The patient was administered 75 mg of clopidogrel one day prior to the intervention, and also received 100 mg per day of enteric-coated aspirin.

With local anesthetic of 1% lidocaine, percutaneous arterial access was achieved from the right femoral artery. Then, an 8 Fr Flexor sheath (Terumo) was placed, and intravenous heparin was administered (total dose, 4,000 units; average activated clotting time during the procedure, 254

Key words: subclavian artery; subclavian artery steal syndrome; bare stents; covered stents; arteriosclerosis

Corresponding Author:
Dr Tao Luo,
Department of Human Resources,
Xuanwu Hospital, Capital Medical University,
No. 45 of Changchun Street, Xicheng District,
Beijing 100053, China
Tel.: +86 136 9360 6065 - Fax: +86 010 8319 8627
e-mail: luotao889_dr@163.com

0393-974X (2019)

seconds). A pigtail catheter was advanced to the ascending thoracic aorta over a 0.035 angled glide wire (SSAGW; Meditech, Boston Scientific, Natick, MA, USA). Aortic arch angiography was performed, and revealed that the ostial of the left subclavian artery had severe stenosis.

A 5-Fr vertebral catheter (Cordis, Miami, FL, USA) was pushed forwards through the sheath into the left axillary artery. The wire was removed and exchanged for a 0.035, 260 cm stiff wire (Terumo). The 8 Fr-90 cm Flexor sheath (Boston Scientific) was then advanced into the left subclavian artery, and positioned just below the left subclavian artery. Then, the stiff wire was exchanged with a 0.018, 300 cm Steelcore wire (Guidant Vascular Intervention, Santa Clara, CA, USA). A 6-mm diameter, 40 mm long Mega Titan balloon (Cordis) was advanced to the proximal left subclavian artery, and inflated to 8 atm with successful dilatation of the stenosis. The balloon was removed, and an 8 mm in diameter and 25 m long Viabahn stent graft (WL Gore and Associates; Fig. X) was placed with the distal end just proximal to the left origin and extended proximally. Then, post-dilation was performed using an 8 mm in diameter and 40 mm long balloon (Meditech) inflated to 8 atm. The final angiogram revealed no residual stenosis, and the left vertebral artery became positive of blood supply (Fig. 1). There were no neurological or other complications. After the femoral artery was sutured by using Perclose (USA), the patient was safely sent back to the ward. Perioperation therapy included heparin anticoagulation and oral double anti-platelet drugs after discharge. The vascular murmur disappeared on the left supraclavicular fossa, and upper extremity SBPD was 0 MMHG. This study was conducted in accordance with the Declaration of Helsinki. Written informed consent was obtained from the patient.

DISCUSSION

SAS is most commonly caused by atherosclerotic occlusive vascular disease. However, it has also been described in patients with stenosis caused by fibromuscular dysplasia. Takayasu syndrome, radiation exposure, post-traumatic compression syndrome, polymyalgia rheumatica and SAS may also occur in patients who have undergone coronary artery bypass surgery with a left internal mammary artery graft, with ensuing angina or myocardial ischemia (5). The consequences of SAS include chronic arterial insufficiency, leading to vertebra-basilar insufficiency or arm claudication.

In 1980, Bachmann and PTA were used to treat subclavian artery stenosis or occlusion (6), and Mathias (7) separately reported percutaneous transluminal angioplasty as a method for treating subclavian artery stenosis for the first time.

Thereafter, multiple studies have confirmed the safety and effectiveness of endovascular treatment for this purpose (8-10). The prevalence of endovascular treatment for subclavian artery lesions and the advancement of interventional techniques during the last three decades have led to a 91-100% technical success of treatment for subclavian artery lesions (11). In recent years, more assistive technologies have been added to make the placement of stents more accurate (12).

In the present case, the femoral artery was used as the first choice approach, which has the advantages of puncturing, easy operation, and less complications. Furthermore, a guide catheter greater than 8-F can be placed during the operation. However, the femoral approach has disadvantages when the subclavian artery is occluded or severe stenosis is present as this would lead to difficulties in allowing the guide wire to pass through the occluded or narrow segment of the vessel. Furthermore, when the occluded segment is located at the opening of the subclavian artery, the guiding catheter cannot be maintained in the proximal subclavian artery. In addition, even though the guide wire cannot be supported through the diseased vessels, the vascular recanalization is difficult, and the success rate of stent implantation is low. For the brachial artery, the guiding catheter is well fixed in the axillary artery, and can provide good support and direction for the guide wire. The patency rate of the occluded vessel is high. The shortcomings of this method are when subclavian artery occlusion or severe stenosis is present, brachial artery pulsation is very weak, and the puncture of the surgical anatomy of the brachial artery is very difficult, as is the

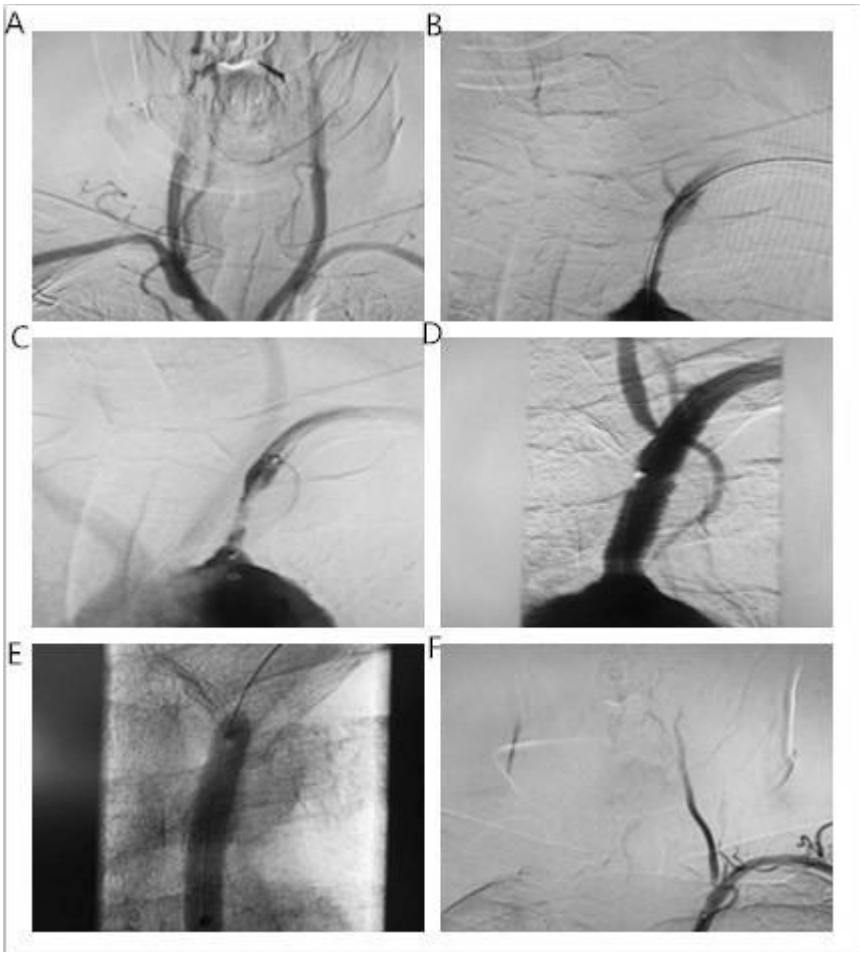

Fig. 1. ***A)*** *The aortic arch angiography revealed severe stenosis at the beginning of the left subclavian artery.* ***B)*** *The 8F-90cm long sheath and left subclavian artery.* ***C)*** *The INVATEC 6-40 mm balloon dilatation of left subclavian artery lesions.* ***D)*** *Release of the Viabahn 8-25 mm stent in diseased vessels.* ***E)*** *INVATEC 8-40 mm balloon endovascular dilatation.* ***F)*** *The left subclavian artery was found to flow well on angiography. Furthermore, there was no residual stenosis or leakage of the contrast agent.*

prevention of complications. In addition, the brachial artery is thinner than the femoral artery, the puncture complications are more serious, when compared to the femoral artery, and the median nerve and radial nerve can be easily damaged.

The advantages of Viabahn-coated covered stents are that they have a nickel-titanium alloy skeleton with ultra-thin ePTFE coating layer, the inside can override occlusion segment lesions, and it can effectively reduce artery wall shedding for irregular tissues, thereby reducing post-interventional necrosis of distal limb or toe due to embolic shedding. The following should be to achieve better operative success: stent diameter and vascular diameter matching; the coated stents must cover all lesions and be close to the remote anchoring area needed to allow movement into healthy blood vessels, in which a balloon pre-expansion part of at least 1 cm must be completely covered.

ACKNOWLEDGEMENTS

We are particularly grateful to all the people who have given us help on our article. This study was supported by National Fund for Nature (No. 81470587).

REFERENCES

1. Burihan E, Soma F, Iared W. Angioplasty versus stenting for subclavian artery stenosis. The Cochrane Database Syst Rev 2011; 10:CD008461.
2. Aiello F, Morrissey NJ. Open and endovascular management of subclavian and innominate arterial pathology. Semin Vasc Surg 2011; 24:31-35.
3. Becker GJ, Katzen BT, Dake MD. Nocoronary angioplasty. Radiology 1989; 170:921-40.
4. Patel SN ,White CJ, Collins TJ, et al. Catheter-based treatment of the subclavian and innominate arteries .Catheter Cardiovasc Interv 2008; 71:963-68.
5. Shadman R, Criqui MH, Bundens WP, Fronek A, Denenberg JO, Gamst AC, McDermott MM. Subclavian artery stenosis: prevalence, risk factors, and association with cardiovascular diseases. J Am Coll Cardiol 2004; 44:618-23.
6. Bachman DM, Kim RM. Transluminal dilatation for subclavian steal syndrome. Am J Roentgenol 1980; 135:995-96.
7. Mathias K, Staiger J, Thron A, Spillner G, Heiss HW, Konrad-Graf S. Percutaneous transluminal dilatation of the subclavian artery (author's transl). Dtsch Med Wochenschr 1980; 105:16-18.
8. Zhang JL, Tong W, Lv JF, Chi LX. Endovascular treatment and morphology typing of chronic ostial occlusion of the subclavian artery. Exp Ther Med 2017; 13:2022-28.
9. Zairi I, Mzoughi K, Jnifene Z, Boukhris M, Mrabet K, Kraiem S. Coronary-subclavian steal syndrome presenting with stable angina.Tunis Med 2017; 95:315-16.
10. Chung WJ, Soga Y, Tomoi Y, et al. SCALLOP Investigators. Clinical Impact of Intravascular Ultrasound Guidance During Endovascular Treatment of Subclavian Artery Disease. J. Endovasc. Ther 2017; 24:731-38.
11. Przewlocki T, Wrotniak L, Kablak-Ziembicka A, et al. Determinants of long-term outcome in patients after percutaneous stent-assisted management of symptomatic subclavian or innominate artery stenosis or occlusion. Euro Intervention 2017; 13:1355-1364.
12. Aiello F, Morrissey NJ. Open and endovascular management of subclavian and innominate arterial pathology. Semin Vasc Surg 2011; 24:31-35.

LETTER TO THE EDITOR

UPDATE ON THE CELLULAR, GENETIC AND CYTOKINE BASIS OF EPIRETINAL MEMBRANE PATHOGENESIS

E. TSOTRIDOU[1,2], E. LOUKOVITIS[1,3], K. ZAPSALIS[1,2], I. PENTARA[1,2], S. KORONIS[1], P. TRANOS[1], S. ASTERIADIS[1], M. BALIDIS[1], T. SOUSOURAS[1], T. VAKALIS[1], Z. ZACHARIADIS[1] and G. ANOGEIANAKIS[1,4]

[1]Ophthalmica Eye Institute, Thessaloniki, Greece; [2]Faculty of Medicine, Aristotle University of Thessaloniki, Thessaloniki, Greece; [3]Hellenic Army Medical Corps, Thessaloniki, Greece; [4]Association for Training in Biomedical Technology, Thessaloniki, Greece

Received July 3, 2019 – Accepted October 4, 2019

To the Editor,

Epiretinal membrane (ERM) is a layer of pathologic tissue which grows on the internal surface of the retina at the vitreoretinal interface (1). It was first described in 1865, and it can be either idiopathic, or secondary to some pathologic conditions (2). The progression of a secondary ERM is generally less aggressive and seldom causes traction retinal detachment as do primary ERMs (3). ERM consists of an inner cellular layer with one or multiple cell layers and an outer extracellular matrix (ECM) layer that contains bundles of extracellular fibrils, usually randomly oriented (1).

ERMs are characterized by a number of pathological changes that occur in the vitreoretinal junction and have varying degrees of clinical significance (4). On ophthalmoscopic examination, ERM presents as an obvious transparent, translucent, or even pigmented membrane, or as a glistening light reflection if it is thin. Although peripheral ERMs do exist, it is the macular ERMs that are, visually, more disturbing (1, 2). ERMs can involve the macular or perimacular regions and cause a reduction in vision, blurred vision, micropsia, metamorphopsia and occasionally monocular diplopia (2). They may also cause vitreoretinal traction or even tractional retinal detachment. The symptoms felt by patients can differ, depending on the duration and severity of ERMs (1). The incidence and the prevalence of ERMs increases with age. The ERM incidence is estimated close to 20% for the total population by the age of 70. The prevalence of macular ERMs in individuals under the age of 60 years is estimated at 2% and in individuals over 70 years at 12%. Other population studies indicate an overall prevalence of 7% to 11.8%, and a 5-year incidence of 5.3% (2). The purpose of the present mini review is to concentrate on the genes, cells and cytokines that are involved in the ERM pathogenesis, idiopathic and secondary.

Factors affecting prevalence

Of interest is the great discrepancy in the prevalence of idiopathic ERM among different ethnic groups which ranges from 1.02% to 28.9%. The prevalence of idiopathic ERM in the United States and Australia is higher than that in Asia, which indicates that genetic and lifestyle factors may play a role in ERM occurrence. Finally, the observed

Key words: Epiretinal membrane (ERM); ERM pathogenesis; ERM related genes; Idiopathic ERM; proliferative diabetic retinopathy (PDR-ERM)

Corresponding Author:
G. Anogeianakis MD, PhD
Ophthalmica Eye Institute,
Vas Olgas 196 & Ploutonos 27,
54655 Thessaloniki, Greece
Tel.: +306976637334
e-mail: anogian@auth.gr

0393-974X (2019)

DISCLOSURE: ALL AUTHORS REPORT NO CONFLICTS OF INTEREST RELEVANT TO THIS ARTICLE.

higher prevalence of idiopathic ERM in diabetes, hypercholesterolemia, and vascular narrowing or occlusion indicates the possible involvement of metabolic factors (1). However, despite its high prevalence, the pathophysiology of ERM has not been fully elucidated (2).

Types of ERMs

Depending on the initiating event of the ERM formation, ERMs can be classified as idiopathic or secondary. Fibro glial proliferation secondary to a break in internal limiting membrane (ILM) occurring during the process of posterior vitreous detachment is mainly associated with idiopathic ERM formation (5). On the other hand, secondary ERM results from an already existing ocular pathology such as proliferative diabetic retinopathy (PDR), retinal breaks, retinal detachment, central or branch retinal vein occlusion, proliferative vitreoretinopathy (PVR), ocular trauma, ocular inflammation (e.g., uveitis) and high myopia (5, 6). In addition, several ocular surgeries, such as lensectomy and retinal detachment surgery or argon laser photocoagulation, may also be associated with ERM formation. Nonetheless, as idiopathic and secondary ERM are characterized by different primary formation mechanisms, the features of these membranes may also differ (3, 5). Moreover, the molecular mechanism formation of both primary and secondary ERMs is still poorly understood (1).

Theories of ERM pathogenesis

Based on the evidence presented, the pathogenesis of ERM is associated with the migration of glial cells that are derived from retinal tissue to the surface of the retina and arise from microdefects in the ILM that occur during posterior vitreous detachment (PVD) (7). Another theory proposes that the pathogenesis of ERM is associated with the growth and fibrous metaplasia of the vitreous cells that remain on the retina surface after PVD. A third theory proposes that the retinal pigment epithelial (RPE) cells migrate to the vitreous cavity through the retinal break and settle on the retinal surface, forming the ERM that occurs after rhegmatogenous retinal detachment (2,7).

Cells and cytokines involved in ERM pathogenesis

ERMs are characterized by the cellular migration and proliferation on the inner retinal surface (1), ECM formation and tissue contraction (4). Histopathological studies demonstrated that various cell types such as RPE cells, glial cells, endothelial cells, fibrocytes, fibrous astrocytes, macrophages and myofibroblast-like cells, as well as trophic and transcription factors may be associated with the formation of ERMs, although the pathogenic mechanisms are still unknown. RPE cells are hexagonal quiescent cells that do not proliferate or migrate under physiological conditions and represent various cell types including glial cells that are involved in the fibrotic reaction of the detached retina (4, 6). These cells form a scar-like thin layer as an immune response to protect the retina (6).

Another type of cells, especially in secondary (PDR) ERM, are fibroblasts, whose origin is still not fully elucidated, but they synthesize the ECM. Moreover, they construct the structural framework of the membrane and cause tractional retinal detachment (8).

ERM progression is considered to be a fibrotic process due to the increased collagen deposition and membrane contraction. Collagen types I, II, III, IV, V, and VI are important components of ERM indicating the vital role of collagen in ERM construction. Type VI collagen in particular, which forms a fine fibrillar network in idiopathic ERM, has been identified as a crucial component of ERM (9).

Müller cells are also considered to have a central role in ERM contraction by producing various collagens and expressing a-SMA which is also involved in the membrane contraction (9). Müller cells are actively involved in idiopathic ERM formation by migration, proliferation, and transdifferentiation. Müller glial cells (MGCs) acquire migratory ability and exhibit a fibroblast-like phenotype, contributing to the formation of ERM, stretching the retina and causing retinal detachment and vitreous hemorrhage. MGCs also contribute to the diabetic ERM formation, a progress associated with reactive gliosis, fibrosis, and migration (8). Laminocytes are also another fundamental cell type involved in the pathology of idiopathic ERMs and

are dispersed in reduced numbers in eyes containing a PVD (4).

Both retinal Müller cells and hyalocytes can produce and activate transforming growth factor beta (TGFb) during the idiopathic ERM formation. TGFb upregulates the expression of a-SMA in the epiretinal cells, contributing to the ERM contraction. The retinal Müller cells that express a-SMA are responsible for the membrane contraction while the retinal Müller cells that do not express a-SMA could continue their production of collagens to form the ECM network of the idiopathic ERM (9). There is also evidence that during the formation of ERM cytokines, ECM proteins and growth factors may be involved in the intracellular signaling and histologic changes (6).

Therefore, cytokines, like insulin-like growth factor (IGF), are involved in the progression of ERMs. The IGF system which is associated with inflammation process, is also involved in the stimulation of ERM contraction and it is suggested that growth factors are involved in the progression of ERMs, especially during PDR (1, 4). Older reports indicated that specific cytokines play a role in ERM formation given that they are expressed in idiopathic ERMs. Among them are the vascular endothelial growth factor (VEGF), interleukin-6 (IL6), TGFb, the connective tissue growth factor, chemokine CCL2 and tumor necrosis factor alpha (TNFa) (4). On the other hand, other T-cell cytokines or T-cell-associated factors, such as IFNG, RORC, IL17A and TBX21, have no correlation with ERM formation (6).

Genes involved in ERM pathogenesis

Biological events are due to changes in the expression of crucial genes and extensive changes take place in gene expression, during the onset and progression of diseases. By comparing gene expression profiles under different conditions, genes that play crucial role in a particular disease process can be identified (3). Thus, analyzing gene expression can enhance the understanding of the formation of ERM. Tables I and II summarize the genes, cells and cytokines involved in Idiopathic and secondary ERM, respectively.

There are many studies about the expression of a variety of genes in ERM, idiopathic or secondary (6). There are reports which mention that at least 52 genes are highly represented in either PVR-ERMs or other secondary ERMs. 23 genes are expressed at higher levels in the PVR-ERMs and 29 genes at higher levels in other secondary ERMs, while, especially, 4 genes, ZNF713, FN1, MALAT1 and PARP8 are abundantly represented in secondary ERMs. Genes related to proliferation and cell adhesion are highly expressed in secondary (PVR) ERMs, while in other secondary ERMs genes related to ribosomes, metabolism, and signaling are preferentially upregulated. Ten of the cell adhesion genes that are expressed in secondary (PVR) ERMs are COL1A1, COL1A2, COL3A1, LGALS1, POSTN, SPARC, THBS1, TIMP3, FN1 and DCN. These observations are in good agreement with morphological studies indicating that the amount of ECM in ERMs is positively correlated with the disease process, and it is greater in secondary (PVR) ERM than in slowly progressing ERM. There are also several genes related to proliferation, (e.g., MALAT1, CD320, SERPINE1 and STAT3) that are upregulated in secondary (PVR) ERMs, while there are possible relationships to other genes/ proteins including an additional 60 genes that have not been detected in secondary ERMs (3).

The MALAT1 gene is also associated with ERM formation. It is a long, non-coding RNA that regulates the processing pre-mRNAs in mammalian cells and plays an important role in the progression of secondary (PVR) ERM. Apparently, it is the most highly expressed gene in secondary ERM. It regulates cell motility through the concomitant regulation of the expression of motility-related genes by transcriptional and/or post-transcriptional regulation. It is also associated with metastasis. MALAT1 has not been shown to be synthesized by secondary (PVR) ERM. Nonetheless, the need for extensive migration of secondary ERMs on the retina explains the strong expression of MALAT1 in secondary ERMs (3).

The expression levels of RELA (v-rel avian reticulo endotheliosis viral oncogene homolog A), GFAP (glial fibrillary acidic protein), TNC (tenascin C) and other cytokine-encoding genes such as IL6, TGFb2, VEGFA, and CXCL1 (chemokine C-X-C

motif ligand 1) are increased, especially in idiopathic ERM eyes irrespective of sex. RELA is a subunit of the nuclear factor kappa B (NF-κB) heterodimer, a transcription factor that can be activated by various stimuli, like bacterial and viral infections, hypoxia and proinflammatory cytokines, including IL1β and TNFα, which play a vital role in inflammation, immune response, cellular proliferation and apoptosis. NF-κB and IL8 are expressed in the vascular endothelial and glial cells and are also associated with ERM formation (6). Finally, it is possible that advanced age is associated with upregulation of RELA in endothelial and glial cells and in ERM formation.

Numerous NF-κB target genes, including proinflammatory cytokines, such as TNFα, IL1β

Table I. *Idiopathic ERM. Genes, cells and cytokines involved in pathogenesis*

GENES	**Cells**
CXCL1 (6)	Müller glial cells (8)
	Laminocytes (4)
	Hyalocytes (9)
GFAP (6)	Collagen type II (9)
IL6 (6)	Collagen type IV (9)
RELA (6)	Collagen type I (9)
TGFb2 (6)	Collagen type V (9)
TNC (6)	Collagen type III (9)
VEGFA (6)	Collagen type VI (9)

Table II. *Secondary ERM. Genes, cells and cytokines involved in pathogenesis*

GENES	**Cells**	**Cytokines**
CD320 (3)		
COL1A1 (3)	Fibroblasts (8)	Growth Factors (9)
COL1A2 (3)	Müller glial cells (8)	IGF (1,4)
COL3A1 (3)		TGFβ2 (9,12)
DCN (3)		Other Cytokines (9)
FN1 (3)		TGFb (11)
LGALS1 (3)		VEGF (11)
MALAT1 (3)		Fibrogenic (11)
NF-κB mRNA (10)		
POSTN (3)		
PPM1D (10)		
SERPINE1 (3)		
SP1 mRNA (11)		
SPARC (3)		
STAT3 (3)		
TGFb2 (6)		
THBS1 (3)		
TIMP3 (3)		

and IL6 (which are important contributors to the pathological process of DR and to the formation of ERMs) can be upregulated by activated glial cells. NF-κB can also contribute to the proliferation of glial cells. It is noteworthy that patients with secondary (PDR) ERMs have significantly higher NF-κB mRNA expression levels than patients with idiopathic ERMs.

Secondary (PDR) ERMs are related to the expression of Wild-type p53-induced phosphatase 1 (Wip1), which is encoded by the PPM1D gene and plays a key role in stress signaling, cell cycle progression, cell survival, inflammation and proliferation. However, although Wip1 may be associated with ERM formation, little is known about this relationship (10). SP1 mRNA is also highly expressed in secondary (PDR) ERM, while the SP1 protein is mainly co-localized with VEGF. SP1 regulates the promoter activity and expression of genes encoding angiogenesis-related factors and thus plays an important role in the angiogenesis of PDR, highlighting the role of this gene in ERM. SP1 can regulate the expression of a wide variety of genes, including TGFb, VEGF, fibrogenic cytokine, and many matrix genes. These cytokines can be detected in the vitreous fluid and secondary ERMs, especially these obtained from patients with PDR (11).

The expression levels of pro-inflammatory genes and the genes expressed during angiogenesis and wound healing process, like IL6, TGFb2, VEGFA, CXCL1, RELA, GFAP, and TNC are significantly higher in eyes with idiopathic ERM. Moreover, there is a positive correlation between TGFb2 and IL6, CXCL1 or RELA. TGFb2, which is associated with intraocular fibrosis, is upregulated in eyes with idiopathic and secondary ERM. It induces the transformation of hyalocytes, myofibroblastic cells and RPE cells.

The expression of TGFb1 is also elevated in ERM vitreous, but only the expression of TGFb2 is increased in idiopathic ERM. In addition, the correlation of TGFb2 is more significant in the case of idiopathic ERM than that of TGFb1. In the presence of TGFb2 there is strong contractile activity of collagen gels and αSMA (ACTA1) overexpression in hyalocytes. ERM foci are composed of αSMA-positive cells with a periphery of GFAP-positive cells (6). Thus, the expression level of ACTA1 (the gene encoding αSMA) may be very low. In addition, the gene expression levels of VEGFα seem to be significantly higher in ERMs (3).

Other reports suggest that GFAP-expressing glial cells (Müller cells or astrocytes) are associated with idiopathic ERM. Additionally, retinal glial cells were reported to produce VEGF. Furthermore, there is an apparent association between VEGFA and GFAP gene expression levels in idiopathic ERM eyes. TNC, a gene that encodes the extracellular protein TNC, is involved in inflammation, wound healing, and the sprouting of endothelial cells during angiogenesis. So it is possible that TGFb2 and three factors (IL6, CXCL1, and NF-κB) stimulate GFAP positive cells related to fibrosis, while angiogenic factors (VEGFA and TNC) may augment idiopathic ERM formation.

The levels of genes encoding cytokines also seem to change in ERM eyes. As mentioned above, genes like TGFb2, CXCL1, GFAP, VEGFA, IL6, RELA and TNC seem to be significantly upregulated in the idiopathic ERM eyes, while ACTA1 and IL17A are not detected in the irrigation solution obtained from idiopathic ERM. Finally, the levels of IFNG, CCL2, CCL5, CXCL10, TGFb1, TNF, TBX21, STAT3, RORC and POSTN don't differ in idiopathic ERM (6).

Management of ERM

In recent years, there has been much debate about the management of idiopathic and secondary ERMs, whereas it seems that several cytokines and genes may be therapeutic targets in the future. At present the options are limited and consist of prevention, watchful waiting or vitrectomy surgery, especially in idiopathic ERMs (1, 12). However, it is not known whether the surgery for idiopathic ERMs should be aimed at an early stage with minimal symptoms or it can be safely delayed. Vitrectomy and ERM peeling have been used in patients with symptomatic visual disturbances. Nonetheless, there are cases that ERMs recurred and a second surgical intervention is needed, mainly because of incomplete removal. Thus, the removal of ILM in concert with ERM peeling may be beneficial but remains controversial (12). Moreover, there are several pharmaceutical

treatments including the use of anti-inflammatory and vitreolytic agents that improve the visual function and prevent complications of idiopathic ERMs (1, 12). In addition, as the formation of ERMs is associated with the procedure of fibrosis the verification of the role of fibrosis may contribute to find new treatment options (1).

The emergence of certain genes and cytokines as important factors for the development and progression of ERMs has led to the development of new, modern therapeutic methods. Thus, therapeutic agents have been created against targets such as TGFβ2, which has a crucial role in the formation of both idiopathic and secondary ERM, to prevent the formation and progression of ERMs. Nonetheless, further study is needed to develop more effective treatment methods targeting several genes and cytokines (9, 12).

CONCLUSIONS

As mentioned above, of the three main theories proposed for the pathogenesis of ERM, two propose cellular migration and one cellular proliferation as the relevant mechanism. This is the reason the present mini review concentrated on the genes, cells and cytokines that are involved in the ERM pathogenesis.

Although the issue of ERM pathogenesis is still not resolved, certain features of ERM are already apparent from the findings to date: i) With the exception of the TGFb2 (5) gene there is no overlap between the genes identified so far as being involved in idiopathic and secondary ERM (Tables I and II). This may imply that the pathogenesis of each of these forms of ERM may be of different origin although they may share similar pathways of expression; ii)Although Müller glial cells and fibroblasts or collagen cells are involved both in idiopathic ERM and secondary ERM, based on our present knowledge, in each case, they use different sets of cytokines; iii) Very little is known about the pathogenesis of secondary ERM (Table II) or what triggers its pathogenesis.

REFERENCES

1. Bu S-C, Kuijer R, Li X-R, Hooymans JMM, Los LI. Idiopathic epiretinal membrane. retina 2014; 34(12):2317-35.
2. Stafiej J, Kaźmierczak K, Linkowska K, Żuchowski P, Grzybowski T, Malukiewicz G. Evaluation of TGF-Beta 2 and VEGFα gene expression levels in epiretinal membranes and internal limiting membranes in the course of retinal detachments, proliferative diabetic retinopathy, macular holes, and idiopathic epiretinal membranes. J Ophthalmol 2018; 2018:1-6.
3. Asato R, Yoshida S, Ogura A, et al. Comparison of gene expression profile of epiretinal membranes obtained from eyes with proliferative vitreoretinopathy to that of secondary epiretinal membranes. PLoS One 2013; 8(1).
4. Yu J, Feng L, Wu Y, et al. Vitreous proteomic analysis of idiopathic epiretinal membranes. Mol Biosyst 2014; 10(10):2558-66.
5. Yazici AT, Alagöz N, Çelik HU, et al. Idiopathic and secondary epiretinal membranes. retina 2011; 31(4):779-84.
6. Myojin S, Yoshimura T, Yoshida S, et al. Gene expression analysis of the irrigation solution samples collected during vitrectomy for idiopathic epiretinal membrane. Plos One 2016; 11(10).
7. Nam KY, Kim JY. Effect of internal limiting membrane peeling on the development of epiretinal membrane after pars plana vitrectomy for primary rhegmatogenous retinal detachment. Retina 2015; 35(5):880-85.
8. Luo W, Hu L, Li W, et al. Epo inhibits the fibrosis and migration of Müller glial cells induced by TGF-β and high glucose. Graefes Arch Clin Exp Ophthalmol 2016; 254(5):881-90.
9. Bu S-C, Kuijer R, Worp RJVD, et al. Immunohistochemical Evaluation of Idiopathic Epiretinal Membranes and In Vitro Studies on the Effect of TGF-β on Müller Cells. Invest Ophthalmol Vis Sci 2015; 56(11):6506-14.
10. Xu J, Zhong H, Cui L, et al. Expression of wild-type p53-induced phosphatase 1 in diabetic epiretinal membranes. Oncotarget 2017; 8(22):35532-41.
11. Yoshida-Hata N, Mitamura Y, Oshitari T, et al. Transcription factor, SP1, in epiretinal membranes of patients with proliferative diabetic retinopathy. Diabetes Res Clin Pract 2010; 87(3):26-28.
12. Akiyama K, Fujinami K, Watanabe K, Tsunoda K, Noda T. Internal limiting membrane peeling to prevent post-vitrectomy epiretinal membrane development in retinal detachment. Am J Ophthalmol 2016; 171:1-10.

LETTER TO THE EDITOR

EXPRESSION AND CORRELATION OF Rab23 WITH PATHOLOGICAL GRADES IN HUMAN GLIOMA CELLS

JJ. DONG[1], Y. LIU[2], YK. HAO[3], L. YAN[1], J. LIANG[4] and YD. MU[1]

[1]Department of Histology and Embryology, Mudanjiang Medical University, Mudanjiang, China; [2]Office of Educational Administration, Mudanjiang Medical University, Mudanjiang, China; [3]Department of Medical Function, Mudanjiang Medical University, Mudanjiang, China; [4]Stem Cell Institute, Mudanjiang Medical University, Mudanjiang, China

Received September 24, 2019 – Accepted November 4, 2019

To the Editor,

Glioma is the most common malignant tumor of the nervous system, and its pathological mechanism is complex and related to various genetic abnormalities and exposure to carcinogens (1, 2). The tumor is highly malignant, challenging to treat and easy to relapse, therefore new target treatments are increasingly being investigated in recent years (3). Rab23 is a member of the Ras proto-oncogene, and its coding protein is a member of the small GTPase superfamily, Rab family (4), whose mutation can cause open brain syndrome in mice (5). It is involved in the vesicular transport mechanism. It is also a negative regulator of sonic hedgehog signaling pathway and plays different roles in many types of tumors (6). In recent years, an increasing number of researchers have investigated the role of Rab23 as a proto-oncogene. In some cancers, such as gastric cancer, it was shown that Rab23 is closely related to tumor invasion. Rab-coupling protein (RCP), composed of Rab11 and Rab25, is involved in cancer cell invasion through transferring epidermal growth factor receptor (EGFR) on the surface of the cell membrane (7). Rab23, Rab11, and Rab25 are members of the Rab family which can also perform the vesicle transport function (8). The aim of this study was to investigate the involvement of Rab23 in the invasion process of glioma, starting from the hypothesis of a similar action with RCP in the tumor invasion. In this research, the expression of Rab23 in glioma tissues was studied at the gene level. Furthermore, the relationship between the Rab23 expression and glioma malignancy was analyzed, to provide the clinical basis for further research on the molecular mechanism of Rab23 in glioma.

MATERIALS AND METHODS

Case selection

A total of 46 glioma patients who were admitted to Hongqi Hospital Affiliated to Mudanjiang Medical University from January 2015 to July 2017 were selected and included in the study. These patients were pathologically confirmed to have brain glioma after surgery and had not undergone previous surgery, radiotherapy or chemotherapy.

The cases were diagnosed and classified using the World Health Organization (WHO) protocol in grade I - 7 cases, grade II - 15 cases, grade III - 16 cases, and grade IV - 8 cases. The cases were further divided into a low-grade glioma group (22 cases with grade I and II), and a high-grade glioma group

Key words: Rab23 gene; glioma; pathological grade; survival

Corresponding Author:
Dr Yindong Mu,
Department of Histology and Embryology,
Mudanjiang Medical University,
No.3.Tongxiang Road,
Mudanjiang, Heilongjiang Province, China.
e-mail: muyindongmyd2011@126.com

0393-974X (2019)

(24 cases with grade III and IV). In 25 cases, tumors were located in the frontal lobe, and in 21 cases they were diagnosed in the temporal lobe.

Thirty-five cases of normal brain tissue specimens were used as the negative control group (all brain tissues were surgically removed from patients with internal decompression of craniocerebral trauma). Tumor centers were selected as specimens to avoid bleeding and necrotic areas.

All patients were evaluated for functional impairment using the Karnofsky Performance Scale (KPS) index before surgery. The size of the tumors was determined by measuring the maximum diameter of the tumor with magnetic resonance imaging (MRI). The study was approved by the Ethical Committee of Hongqi Hospital Affiliated to Mudanjiang Medical University, and each patient signed an informed content to participate in the study.

Quantitative expression of Rab23 mRNA by Reverse Transcription-Polymerase Chain Reaction

Firstly, 100 mg of frozen brain tissues were taken and ground into powder in liquid nitrogen with a mortar. Then, RNA was extracted according to the standard operation steps. 50 μg of RNA was taken from each sample with the Super Script III reverse transcription kit (Invitrogen, USA), and cDNA was synthesized with random primers. Primers were designed by Primer premier 6.0 software (PREMIER Biosoft International, CA, USA) and synthesized by Sangon Bioth Co. Ltd. (Shanghai, China). Quantitative detection primers for Rab23 were designed as follows: upstream: 5'-GCGCGGGACGAAGAATAATCAT-3', downstream: 5'-TACACGCTTCCGCCAACAAACT-3'. The reaction product was electrophoresed on a 1.5% agarose gel for 30 min, and the absorbance value of the target gene was determined by the Eagle Eye II gel image software (Siemion, USA).

Quantitative expression of Rab23 protein by Western blot

The protein was extracted from tissue lysate and quantified using the bicinchoninic acid (BCA) method; 200 mg of frozen tumor samples were taken, and then the whole protein was extracted and maintained at -70°C for later use after concentration measurement. Each group was subjected to electrophoresis on 30 μg of 10% SDS-PAGE gel, and the internal reference (β-actin) was used as a positive control. Afterward, the proteins were transferred to the polyvinylidene fluoride (PVDF) membrane when they were semi-dry. Moreover, Tris Buffered Saline Tween (TBST), configured with 5% skimmed milk powder, was blocked at room temperature for 2 h, and then incubated with Mouse anti-Human Rab23 monoclonal antibody (dilution ratio was 1:1000) (Santa Cruz, USA) overnight. Then the membrane was washed and incubated with HRP-labeled goat anti-mouse IgG secondary antibody (dilution ratio, 1:2000) (Beijing Zhongshan Jinqiao Biotechnology Co., Ltd., China) at room temperature for 2 h. The samples were visualized using the electrochemical luminescence (ECL) kit (Thermo Fisher Scientific, USA) and the images were analyzed using an image analysis system (National Institutes of Health, USA).

Patients' follow-up evaluations

The patients included in the study were followed-up regularly every month after discharge from the hospital by telephone to confirm whether they were still alive. The end event was the death of patients. Overall survival (OS) was defined as the time from the initial pathological diagnosis to death (if the patients did not die during the follow-up period, it would be the time from diagnosis to the final follow-up, which was the censored data). Progression-free survival (PFS) was defined as the time from initial pathological diagnosis to tumor recurrence or subsequent growth of the residual tumor by MRI (if there was no progression, then it would be the time from diagnosis to death of patients or final follow-up). GraphPad Prism 8 software (Beijing Huanzhong Ruichi Technology Co., Ltd., China) was used to do the survival curve.

Statistical analysis

SPSS 19.0 statistical software (IBM, USA) was used for running the statistical test. The student's *t*-test was used for appraising the difference between the two groups. A value of $p<0.05$ was considered statistically significant.

RESULTS

The quantitative expression of Rab23 mRNA

The average expression level of Rab23 mRNA in the experimental group was 0.537±0.036, which was significantly higher than that in the control group (0.203±0.041) ($p<0.01$). After further analysis, it was found that the relative expression levels of the high-grade glioma group (0.635±0.065) were higher than those of the low-grade glioma group (0.397±0.025) ($p<0.01$). Furthermore, the Rab23 mRNA level of the experimental group increased with the increase of pathological grade, and the difference was statistically significant, as shown in Fig.1, A and B.

Quantitative expression of Rab23 protein

The average expression level of Rab23 protein in the low-grade glioma group (0.76±0.22) and in the high-grade glioma group (0.97±0.28) was significantly increased compared to the control group (0.46±0.25) ($p<0.01$) (Fig. 1, C and D). Moreover, the Rab23 protein level increased significantly in the high-grade glioma group compared with the low-grade glioma group ($p< 0.01$) (Fig. 1, C and D).

Association between the expression level of Rab23 mRNA and clinicopathological characteristics of the patients

It was observed that the expression level of Rab23 mRNA had no significant correlation with the age, sex, KPS scores, location or size of the tumor (Table I).

Relationship between Rab23 mRNA expression level and survival rates of glioma patients

Patients in the experimental group were divided into two groups according to the expression level

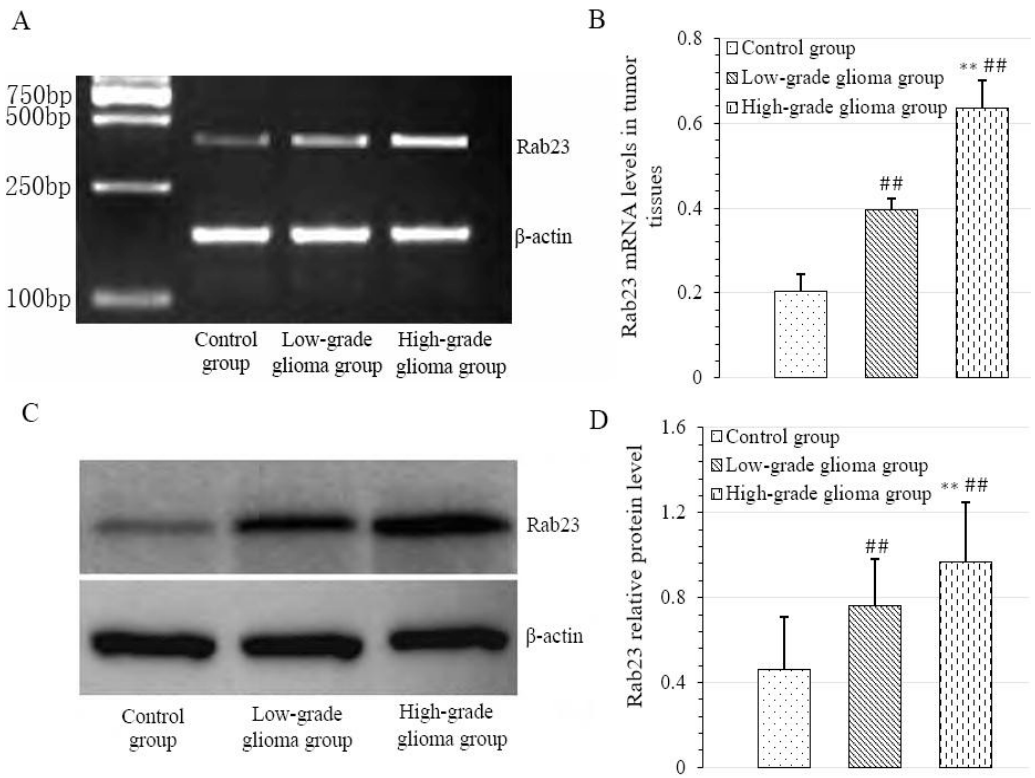

Fig. 1. *Expression levels of Rab23 protein. A) Expression levels of Rab23 mRNA detected by RT-PCR. **B**) Rab23 mRNA levels in tumor tissues of patients with different pathological grades of glioma, ## $p<0.01$ compared with the control group;** $p<0.01$ compared with Low-grade glioma group. **C**) Expression levels of Rab23 protein detected by Western blotting; **D**) The grey value of expression levels of Rab23 protein, ## $p<0.01$ compared with the control group; ** $p<0.01$ compared with Low-grade glioma group.*

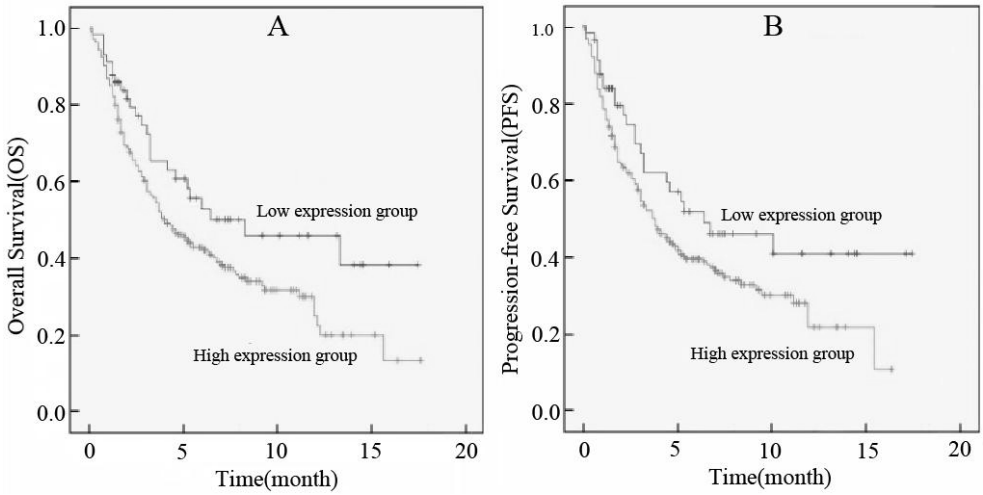

Fig. 2. *Survival curves: **A**) overall survival; **B**) progression-free survival.*

Table I. *Relationship between Rab23 mRNA expression levels and clinicopathological features of glioma in the experimental group.*

Category		Number of cases	Rab23 mRNA	T value	P value
Gender	Male	24	0.528±0.023	0.646	0.516
	Female	22	0.547±0.043		
Age	< 50 years old	27	0.482±0.047	1.336	0.172
	≥ years old	19	0.562±0.045		
Tumor size	< 5cm	12	0.561±0.057	0.786	0.462
	≥ 5cm	34	0.527±0.073		
Tumor site	Frontal lobe	25	0.573±0.064	1.013	0.134
	Temporal lobe	21	0.494±0.048		
KPS score	<70	25	0.502±0.031	0.952	0.372
	≥70	21	0.543±0.038		

of Rab23 mRNA: 26 cases in the high expression group (whose relative expression level was equal or more than 0.4) and 20 cases in the low expression group (whose relative expression level was less than 0.4). The analysis revealed that the low expression group presented a high overall survival and a high progression-free survival compared with the high expression group ($p<0.01$) (Fig. 2 A and B).

DISCUSSION

As a proto-oncogene, Rab23 has gradually attracted the attention of researchers. Rab23 was highly expressed in lung cancer tissues, while it was not expressed in normal lung tissues (9). Regarding the implication of RAB23 in the formation and progression of gastric cancer, Kim et al. (10) reported

that the expression level of Rab23 in atrophic gastritis and intestinal metaplasia mucosa was 10 times higher than that in normal gastric mucosa, and Hou et al. (11) showed an increased expression of Rab23 in metastatic gastric cancer cell line (Hs746T) compared with the non-metastatic ones (KATO III). The results of this study showed that the expression level of Rab23 in the experimental group was significantly higher than that in the control group. Meanwhile, the expression level of Rab23 protein and mRNA in high-grade glioma tissues was significantly higher than that in low-level glioma tissues, which indicated that the Rab23 expression might promote tumor invasion and metastasis, and its expression level could reflect the development and prognosis of glioma to some extent. In addition, it was also found that the expression level of Rab23 mRNA was not correlated with patients' age, gender, or tumor growth location, while positively correlated with the pathological grade of glioma. Moreover, the survival of patients with a high expression level of Rab23 was significantly shorter compared with those with a low expression level. This phenomenon indicated that the expression of Rab23 gradually increased with the formation of glioma and the development of malignancy. The results are consistent with a previous study that compared 73 glioma samples with 30 normal brain tissue samples and discovered that the expression level of Rab23 in glioma was significantly higher than that in normal brain tissues, and there was a significant negative correlation between Rab23 and miR-200b (12).

The current study showed that Rab23 could be used as a marker for clinical diagnosis and prognosis of glioma.

ACKNOWLEDGEMENT

This work was supported by Mudanjiang Science and Technology Planning Project (Z2018s043).

REFERENCES

1. Erdal S, McCarthy BJ, Gurule N, et al. Application of mutagen sensitivity assay in a glioma case-control study. Toxicol Rep 2018; 5:183-88.
2. Gutmann DH, Huang Z, Hedrick NM, Ding H, Guha A, Watson MA. Mouse glioma gene expression profiling identifies novel human glioma associated genes. Ann Neurol 2002; 51(3):393-405.
3. Gong HD, Li HZ, Li JK, Wang C. Myricetin inhibition on murine glioma gl261 cell line. Farmacia 2017;65(6):934-9.
4. Hosoda K, Feussner GK, Rydelek-Fitzgerald L, Fishman PH, Duman RS. Agonist and cyclic AMP mediated regulation of β1 adrenergic receptor mRNA and gene transcription in rat C6 glioma cells. J Neurochem 1994; 63(5):1635-45.
5. Tsutsumi M, Akimoto J, Nakajima N, Hashimoto R, Haraoka J. Two cases of posterior reversible encephalopathy syndrome resembling brainstem glioma. Clin Neurol Neurosurg 2012; 114(7):1062-65.
6. Ulasov IV, Nandi S, Dey M, Sonabend AM, Lesniak MS. Inhibition of sonic hedgehog and notch pathways enhances sensitivity of CD133(+) glioma stem cells to temozolomide therapy. Mol Med 2011; 17(1-2):103-12.
7. Caswell PT, Chan M, Lindsay AJ, McCaffrey MW, Boettiger D, Norman JC. Rab-coupling protein coordinates recycling of alpha5beta1 integrin and EGFR1 to promote cell migration in 3D microenvironments. J Cell Biol 2008; 183(1):143-55.
8. Lall P, Lindsay AJ, Hanscom S, et al. Structure-Function Analyses of the Interactions between Rab11 and Rab14 Small GTPases with Their Shared Effector Rab Coupling Protein (RCP). J Biol Chem 2015; 290(30):18817-32.
9. Huang S, Yang L, An Y, et al. Expression of hedgehog signaling molecules in lung cancer. Acta Histochemica 2011; 113(5):564-9.
10. Kim KR, Oh SY, Park UC, et al. Gene expression profiling using oligonucleotide microarray in atrophic gastritis and intestinal metaplasia. Korean J Gastroenterol 2007; 49(49):209-24.
11. Hou Q, Wu YH, Grabsch H, et al. Integrative genomics identifies RAB23 as an invasion mediator gene in diffuse-type gastric cancer. Cancer Res 2008; 68(12):4623-30.
12. Liu Q, Tang H, Liu X, et al. miR-200b as a prognostic factor targets multiple members of RAB family in glioma. Med Oncol 2014; 31(3):859-27.

LETTER TO THE EDITOR

INFLAMMATORY MARKERS AS PROGNOSTICATORS OF CARDIOVASCULAR DYSFUNCTION IN HYPOTHYROID PATIENTS

Z. NASEEM[1], M.A. IQBAL[1], S. AHMAD[2] and N. ROOHI[1]

[1]Physiology/Endocrinology Laboratory, Department of Zoology, University of the Punjab, Lahore, Punjab, Pakistan; [2]King Edward Medical University, Neela Gumbad, Lahore, Pakistan

Received August 2, 2019 – Accepted November 7, 2019

To the Editor,

Hypothyroidism is a condition characterized by reduced circulating levels of thyroid hormones, T_3 (tri-iodothyronine) and T_4 (tetra-iodothyronine) which are produced by the thyroid gland, and increased levels of Thyroid Stimulating Hormone (TSH) from the anterior pituitary (1). The cardiovascular system is among the main targets of thyroid hormones (2), therefore, most descriptive signs and symptoms of thyroid disorders are due to their effects on the cardiovascular system (3). Direct actions of altered thyroid hormones on heart and indirect impacts through inflammatory markers, such as C-reactive protein (CRP), Interleukin-6 (IL-6) and Homocysteine (Hcy), are of great health concern.

Particularly, CRP is a renowned biomarker to measure cardiovascular risks in both healthy as well as diseased subjects (4). Moreover, IL-6 is a chief mediator of tissue injury and infection, perpetuating lymphocyte infiltration in thyroid, manifesting its inflammation (5). Additionally, Hcy, having an atherogenic nature, stimulates inflammatory chemokine production and induces oxidative stress by lowering serum anti-oxidants (6). Hence, inflammatory markers may reveal the mechanism of disease progression, and can be used as a possible tool for predicting atherosclerosis and cardiovascular events (7).

The aim of the present study was to assess the risk of cardiovascular dysfunctions in hypothyroid patients through predictive inflammatory markers.

MATERIALS AND METHODS

The Institutional Ethics Review Committee provided the approval for this study. Subjects visiting the Institute of Nuclear Medicine and Oncology Lahore (INMOL), from January 2014 to December 2015, with apparent signs and symptoms of hypothyroidism, were interviewed after giving their written consent. Thyroid Function Test (TFT) was performed to ascertain the diagnosis of hypothyroid condition. Demographic features and detailed history of all the participants were taken by means of a pre-designed questionnaire. Patients having cardiovascular disease, diabetes mellitus and hypertension were eliminated from the study. Presence of familial history of cardiovascular disease (CVD) and diabetes mellitus was documented. A total of 140 individuals, satisfying the inclusion criteria comprising of sixty healthy controls (48 females and 12 males), thirty subclinical (21 females and 9 males) and fifty overt hypothyroid subjects (38 females and 12 males) were enrolled in the study. A selected set of subjects (n= 35; 28 females, 7 males), who underwent thyroxine treatment for a period of three months, was engaged for follow-up analysis. The average daily dose of thyroxine varied between 100-300 mg, according to the intensity of the disease.

Key words: inflammatory markers; CVD; hypothyroidism

Corresponding Author:
Associate Professor Nabila Roohi,
Physiology/Endocrinology Laboratory,
Department of Zoology, University of the Punjab,
Lahore, 54590, Punjab, Pakistan
Tel.: +923334053953
e-mail: nabilaruhi@gmail.com

0393-974X (2019)

For blood collection, subjects were categorized into four groups. The control group was comprised of healthy age and sex matched volunteers. Group I included newly diagnosed overt hypothyroid patients, and newly diagnosed subclinical hypothyroid patients were placed in Group II. Group III included subjects who had undergone treatment. Standard reference ranges for fT_4, fT_3 and TSH were 11.5- 23.0 pmol/L, 2.5 – 5.8 pmol/L and 0.3 – 5 mIU/L, respectively.

About 5 cc of venous blood from each patient was drawn after an overnight fasting of 12 hours. Following standard procedure, the serum was separated and stored at -80°C until further analysis of biochemical parameters. Thyroid profile was measured by Radioimmunoassay (RIA) using commercially available kits (Beckman Coulter of Czech Republic, at INMOL Lahore, Pakistan).

For assessing serum CRP concentration, commercially available kit of Calbiotech, USA was used. For measuring serum concentration of IL-6 and Hcy, commercially available ELISA kits (Glory Science Co., Ltd., USA) were used.

Statistical analysis

One-way ANOVA was applied to calculate the overall biochemical comparisons among control (Cn), subclinical (Sb), overt hypothyroid (Ot) and follow-up (Fll) groups. Newman-Keuls Multiple Comparison Test was applied to compare the group means. $P < 0.05$ was designated as statistically significant.

RESULTS

Free tetra-iodothyronine

Comparison of the overt group with the control group showed a highly significant ($P \leq 0.001$) reduction of 56% in the overt group, and after treatment the level of fT_4 increased significantly ($P \leq 0.001$) up to 100% as compared to the overt group. The overt group showed a significant ($P \leq 0.001$) decrease of 53% in contrast to the subclinical group (Table I).

Free tri-iodothyronine

Highly significant ($P \leq 0.001$) variation was seen in the overt group when compared with controls, showing a 42% decrease of fT_3 in the overt group. In comparison between the subclinical and overt groups, a significant ($P \leq 0.001$) reduction of 37% was observed in the overt group. Marked ($P \leq 0.001$) increase of 39% was noticed in the follow-up group in comparison with the overt group. A significant ($P \leq 0.01$) decrease of 19% was witnessed in follow-up group in comparison with control group (Table I).

Thyroid stimulating hormone

Comparison between the overt group and control group revealed significantly ($P \leq 0.001$) enhanced levels of TSH up to 1896% in the overt group. A significant ($P \leq 0.05$) rise of 371% was shown by the follow-up group in contrast with the control group. However, after treatment the value of TSH significantly ($P \leq 0.001$) declined up to 77% in the follow-up group related to the overt group. A significant ($P \leq 0.01$) increase of 346% was recorded in the subclinical group in comparison with control group. The overt group also presented a highly significant ($P \leq 0.001$) elevation of 346% compared to the subclinical group. However, comparison between the subclinical and follow-up groups showed a non-significant up-regulation of 5% in the follow-up group (Table I).

C-Reactive protein

Levels of CRP in intergroup comparison, were found to be increased non-significantly in the subclinical and overt groups up to 24% and 11%, respectively, as compared to the control group. However, in the follow-up group the concentration of CRP continued to be increased as compared to the overt group and showed a significant ($P \leq 0.05$) increase of 38% compared to the control group. Comparison between the subclinical group and the follow-up group showed an increase of 24% in the follow-up group. The overt hypothyroid group exhibited an increase of 11% compared to the subclinical group whereas comparison of overt group with follow-up group also presented non-significant increase of 11% in the follow-up group (Fig. 1A).

Interleukin-6

Pronounced increase ($P \leq 0.001$) of 26% was revealed in the overt group as compared to the control

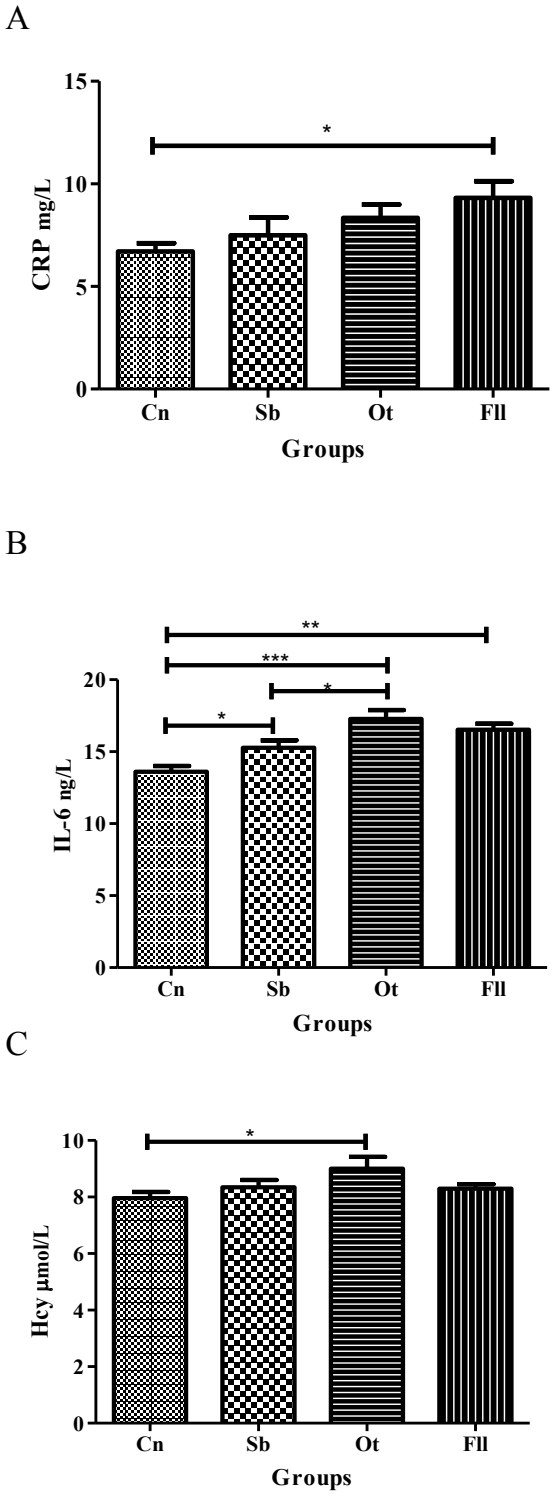

Fig. 1. ***A)*** *Mean±SEM of CRP mg/L in study groups.* significant at P ≤ 0.05.* ***B)*** *Mean±SEM of IL-6 (ng/L) in study groups. *, **, *** significant at P ≤ 0.05, 0.01, 0.001, respectively.* ***C)*** *Mean±SEM of Hcy µmol/L in study groups.* significant at P ≤ 0.05.*

group. The subclinical group also showed a statistically significant ($P \leq 0.05$) increase of 12% when compared with the control group, whereas comparison between the follow-up group and control group presented a significantly ($P \leq 0.01$) increased level of IL-6 up to 21% in the follow-up group. Comparison of the subclinical group with the overt group also showed 13% significant increase ($P \leq 0.05$) in the overt group. Whereas, comparison of the follow-up group with the subclinical and overt groups showed a non-significant increase of 8% in the follow-up group compared to the subclinical group and non-significant decrease of 5% in the follow-up group compared to the overt group (Fig. 1B).

Homocysteine

The analysis of variance showed statistically significant elevation ($P \leq 0.05$) of 13% in the overt group when compared with the control group. Comparison of the control group with the subclinical group showed a non-significant increase of 4% in the subclinical group. After medication, the concentration of Hcy was decreased up to 4% in the follow-up group compared to the overt group. A non-significant increase of 7% was observed in the overt group compared to the subclinical group. The follow-up group showed a decrease of 1% compared to the subclinical group, whereas the follow-up group exhibited a down-regulation of 8% after medication when compared with the overt group (Fig. 1C).

DISCUSSION

Serum levels of CRP were mildly elevated in both the subclinical and overt hypothyroid subjects. Additionally, no efficacy of thyroxine therapy on CRP was observed. Interaction of IL-6 on tumor necrosis factor-α (TNF-α) and IL-1 might result in elevated CRP level in hypothyroidism. Slowed metabolic rate in hypothyroidism, results in impaired biochemical processes involving reduced CRP clearance rate and, consequently, elevated serum CRP levels (8). Both subclinical and overt hypothyroid groups presented elevated IL-6 levels. Furthermore, mild reduction was demonstrated after thyroxine treatment. Long-term circulating IL-6 level is attributed to coronary

Table I. *A comprehensive presentation of studied parameter*

Parameters	Control	Subclinical	Overt	Follow-up	*P*-value
fT_4 (pmol/L)	16.76±0.39	15.53±0.6	7.416±0.92	14.88±0.85	< 0.0001***
fT_3 (pmol/L)	4.13±0.09	3.85±0.17	2.43±0.17	3.38±0.22	0.0001***
TSH (mIU/L)	1.8±0.16	8.04±0.40	35.93±2.18	8.48±2.26	< 0.0001***
CRP (mg/dL)	6.708±0.4	7.49±0.88	8.345±0.65	9.315±0.82	0.0275*
IL-6 (ng/L)	13.61±0.39	15.28±0.51	17.27 ±0.62	16.53±0.42	<0.0001***
Homocysteine (µmol/L)	7.96±0.22	8.35±0.26	9.01±0.41	8.30±0.16	0.064

fT_4: free tetra-iodothyronine; fT_3: free tri-iodothyronine; TSH: thyroid stimulating hormone; CRP: C-reactive protein; IL-6: Interleukin-6.

heart disease (CHD) (9). Studies have documented remarkable elevation in IL-6 in patients with Hashimoto's disease bringing about destruction of thyroid cells, hence participating in inflammatory events. This advocates that IL-6 can contribute to disease progression in thyroid dysfunction (10). IL-6 stimulates atherogenesis directly by endothelial-dependent mechanisms and indirectly by promoting hepatic production of CRP (11). Therefore, direct association present between IL-6 and CRP levels in hypothyroid condition indicates manifestation of cardiac pathogenesis in hypothyroid subjects. Plasma Hcy level was significantly elevated in overt hypothyroid state and stabilized moderately after thyroxine treatment. Elevated Hcy concentration results from compensated activity of flavoprotein methylene tetrahydrofolate reductase (MTHFR), an enzyme crucial for the catalysis of Hcy and its remethylation to methionine. Interplay of total cholesterol, low density lipoprotein cholesterol and Hcy with total antioxidant in hypothyroidism proposes overproduction of free radicals that contributes towards atherogensis (12).

Hypothyroidism is responsible for fluctuations in inflammatory elements in the body that may elevate the risk of cardiac disorders in hypothyroid patients.

ACKNOWLEDGEMENTS

The present work is a part of a Ph.D. thesis entitled "Identification of Potential Biomarkers of Cardiovascular Risk in Hypothyroid Patients From Lahore, Pakistan" submitted to the Pakistan Higher Education Commission. The authors gratefully acknowledge HEC for financial assistance of the present investigation vide pin No.112-35045-2BM1-513(50022879).

REFERENCES

1. Pirahanchi Y, Jialal I. Physiology, Thyroid Stimulating Hormone (TSH). In: StatPearls. Treasure Island (FL): StatPearls Publishing; 2019.
2. Fazio S, Palmieri EA, Lombardi G, Biondi B. Effects of thyroid hormone on the cardiovascular system. Recent Prog Horm Res 2004; 59:31-50.
3. Danzi S, Klein I. Thyroid hormone and the cardiovascular system. Minerva Endocrinol 2004; 29:139-50.
4. Buckley DI, Fu R, Freeman M, Rogers K, Helfand M. C-reactive protein as a risk factor for coronary heart disease: a systematic review and meta-analyses for the U.S. Preventive Services Task Forces. Ann Intern Med 2009; 151:483-95.

5. Gani DK, Lakshmi D, Krishman R, Emmadi P. Evaluation of C-reactive protein and interleukin-6 in the peripheral blood of patients with chronic periodontitis. J Indian Soc Periodontol 2009; 13:69-74.
6. Ruggeri RM, Barresi G, Sciacchitano S, Trimarchi F, Benvenga S. Trovato M. Immunoexpression of the CD30 ligand/CD30 and IL-6/IL-6R signals in thyroid autoimmune diseases. Histol Histopathol 2006; 21:249-56.
7. Wang H, Jiang X, Yang F, et al. Hyperhomocysteinemia accelerates atherosclerosis in cystathionine beta-synthase and apolipoprotein E double knock-out mice with and without dietary perturbation. Blood 2003; 101:3901-907.
8. Welsh P, Packard CJ, Sattar N. Novel antecedent plasma biomarkers of cardiovascular disease: improved evaluation methods and comparator benchmarks raise the bar. Curr Opin Lipidol 2008; 19:563-71.
9. Czarnywojtek A, Owecki M, Zgorzalewicz-Stachowiak M, et al. The role of serum C-reactive protein measured by high-sensitive method in thyroid disease. Arch Immunol Ther Exp 2014; 62:501-509.
10. Danesh J, Kaptoge S, Mann AG, Sarwar N, et al. Long-term interleukin-6 levels and subsequent risk of coronary heart disease: two new prospective studies and a systematic review. PLoS Med 2008; 5:78.
11. Taddei S, Caraccio N, Virdis A, et al. Low-grade systemic inflammation causes endothelial dysfunction in patients with Hashimoto's thyroiditis. J Clin Endocrinol Metab 2006; 91:5076-82.
12. Rahbani-Nobar M, Bahrami A, Norazarian M, Dolatkhah H. Correlation between serum levels of cholesterol and homocysteine with oxidative stress in hypothyroid patients. Int J Endocrinol Metab 2004; 2:103-109.

JOURNAL OF BIOLOGICAL REGULATORS & HOMEOSTATIC AGENTS Vol. 33, no. 6, 1897-1902 (2019)

LETTER TO THE EDITOR

ASSOCIATION BETWEEN MICROVASCULAR AND MACROVASCULAR DAMAGE IN PATIENTS WITH SYSTEMIC SCLEROSIS: AN UPPER LIMB ECHO-COLOR-DOPPLER AND NAILFOLD VIDEOCAPILLAROSCOPY STUDY

A. MONTELLA, C. CORALLO, M. PASTORELLI, M. CAPECCHI, M. VOGLINO, G. RUOCCO, G. WOLF and N. GIORDANO

Department of Medicine, Surgery and Neurosciences, University of Siena, Siena, Italy

Received May 8, 2019 – Accepted September 5, 2019

To the Editor,

Systemic Sclerosis (Scleroderma, SSc) is a multisystemic disease characterized by the accumulation of fibrous tissue in skin and internal organs, such as lungs, kidneys, esophagus and cardiovascular system (1). The disease is present in every ethnic group, with the highest incidence from the third to the fifth decade of life (1). Women are affected almost three times more than men (1). Although SSc etiology is still undetermined, several lines of evidence suggest an immunological onset of the disease (2). In fact, fibrosis is generally anticipated by endothelial damage and perivascular inflammation due to activated T-lymphocytes that stimulate fibroblast activity, with consequent excessive production of type I collagen (2).

Recently, due to the need for an early diagnosis, new classification criteria have been introduced, which require the evaluation of several parameters, including the presence of Raynaud's phenomenon and SSc related autoantibodies, coupled with nailfold videocapillaroscopic patterns (3). Naildold videocapillaroscopy is able to evaluate the progressive alterations of the microvasculature from the early stages to the late ones (4). In fact, there are three capillaroscopic patterns in SSc, identified by morphological and numerical abnormalities of microvasculature: early, active and late (4).

While microvascular alterations are well controlled, macrovascular damage has always been considered unusual in SSc and related to side phenomena (5). Therefore, it is typical to hypothesize that in SSc the body alterations are inversely proportional to the caliber of interested vessels (5). Nowadays, one of the most used method to observe macrovascular alterations is the echo-color-doppler because of its reproducibility, non-invasiveness and relative simplicity of execution (6). The aim of this study is to expand the knowledge of macrovascular damage in SSc, and to evaluate its relationship with the microvascular one.

MATERIALS AND METHODS

In this observational study, 32 SSc patients, admitted to the Scleroderma Unit of the University-Hospital of Siena in Italy, and 32 healthy controls were enrolled. The two groups were homogeneous for sex and age, without any risk factors for vascular diseases. SSc was diagnosed in accordance with the ACR/EULAR 2013 criteria (3). According to the extent of the skin involvement 20 patients were classified as limited cutaneous SSc (LcSSc) and 12 by diffuse cutaneous SSc (DcSSc). The local Ethics Committee of the University-Hospital of Siena approved

Key words: systemic sclerosis; nailfold videocapillaroscopy; echo-color-doppler; macrovascular damage; microvascular damage

Corresponding Author:
Nicola Giordano, MD
Department of Medicine,
Surgery and Neurosciences,
University of Siena,
53100 Siena, Italy
e-mail: nicola.giordano@unisi.it

0393-974X (2019)

DISCLOSURE: ALL AUTHORS REPORT NO CONFLICTS OF INTEREST RELEVANT TO THIS ARTICLE.

the study protocol, according to the Helsinki Declaration, and all participants signed an informed consent.

For each patient or control subject enrolled in the study, comorbidities and common risk factors for atherosclerosis (smoke, diabetes, hypertension, etc.) were first evaluated and the two groups resulted homogeneous. In addition to this, for SSc patients only, cutaneous and internal manifestations of the disease, pharmacological treatment, if present, and the disease duration were considered. The autoantibody pattern for the presence of anti-nuclear antibodies (ANA) and extractable nuclear antigens (ENA), in particular topoisomerase-I (Scl-70) and centromeric protein-B (Cenp-B) were evaluated. Moreover, naildfold videocapillaroscopy by using Videocap 3.0™ (DS Medica, Italy) evaluating the second to the fifth fingers of both hands was performed. Only data regarding giant capillaries were evaluated because they are the most typical capillaroscopic alterations in SSc. In particular, giant capillary number (GCN) and giant capillary diameter (GCD) were taken into consideration. Lastly, an echo-color-doppler of digital artery, evaluating from the second to the fifth fingers of both hands, and of the palmar, radial and ulnar arteries, in both upper limbs was carried out. The index of pulsatility (IP) and the index of resistance (IR) of those arteries were evaluated. Videocapillaroscopy and echo-color-doppler were performed both on affected patients and controls.

Statistical analysis

Statistical calculations were performed by using SPSS (ver 20.0) software™. Continuous data (disease duration, echo-color-doppler and videocapillaroscopy) are expressed as mean ± standard deviation (SD) and analyzed by *t*-test, while the qualitative data (presence of digital ulcers, therapy assumption, autoantibody profile) are expressed as percentage and analyzed by χ^2. The normality of the distribution of each parameter was verified with Kolmogorov-Smirnov test. To compare echo-color-doppler and videocapillaroscopy, a Pearson's correlation was used. Statistical significance was set at $p<0.05$.

RESULTS

The clinical and laboratory characteristics of the enrolled patients and control subjects are shown in Table I. Control subjects showed a negative autoantibody profile and did not take any medication. SSc patients instead exhibited positive autoantibody pattern, and underwent pharmacological treatment (Table I). There were no statistical differences in ANA positivity between LcSSc and DcSSc patients. ENA screening showed Cenp-B positivity only in the LcSSc group, and Scl-70 positivity only in the DcSSc group.

No statistical difference in drug use was found between LcSSc and DcSSc patients, although disease duration resulted higher in the DcSSc group in respect to the LcSSc group. Regarding microvascular parameters, healthy controls always showed a normal videocapillaroscopic pattern with only few giant capillaries that could be ascribed to microtraumas of the fingers related to daily life activities. On the other hand, 8 SSc (6 LcSSc and 2 DcSSc) patients exhibited an early scleroderma pattern, 18 (12 LcSSc and 6 DcSSc) an active scleroderma pattern, and 6 (2 LcSSc and 4 DcSSc) a late scleroderma pattern. No one was in the "very early" phase. GCN was related to the disease duration ($r=0.60$; $p<0,001$) (Fig. 1), as was their diameter ($r=0.68$; $p=0.01$) (Fig. 1). Furthermore, no statistical difference was found between the number of giant capillaries in the left and the right hands. Similarly, there was no difference between the number of giant capillaries in either LcSSc or DcSSc patients. However, LcSSc patients usually presented an early or active capillaroscopy pattern, while DcSSc patients showed an active or late capillaroscopy pattern.

Analyzing data related to the macrovascular situation, the echo-color-doppler IP and IR measurements were evaluated on the digital artery of the second finger, of the palmar artery, of ulnar artery and on radial artery, in both upper limbs. As shown in Table II, a statistical difference was found both in IP and in IR between SSc affected and healthy controls in every examined artery, bilaterally. In addition to this, echo-color-doppler parameters were also compared between LcSSc and DcSSc patients, but no statistical difference was found (Table II). Finally, microvessel- and macrovessel-related data were compared, considering the left and the right side independently. On the right side, IP and IR of

Table I. *Clinical and laboratory features of the enrolled patients and controls.*

Parameters	SSc patients (n=32)	Healthy controls (n=32)	p-value	LcSSc patients (n=20)	DcSSc patients (n=12)	p-value
age (years)	63±9	63±8	p=0.96	62±10	66±8	p=0.33
Sex						
male	2.00	3.00	p=0.51			
female	14.00	11.00	p=0.51			
Disease Duration				10.00±5	14.00±7	p=0.031
Autoantibodies						
ANA (%)				90.00	100.00	p=0.49
Scl-70 (%)				0.00	80.00	p=0.001
Cenp-B (%)				64.00	0.00	p=0.02
Therapy (%)						
Bosentan				64.00	60.00	p=0.89
Macitentan				0.00	23.00	p=0.13
Aspirin				27.00	60.00	p=0.21
Nifedipine				45.00	20.00	p=0.33
Mycophenolate				9.00	20.00	p=0.54
Videocapillaroscopy						
GCN right	6.2±4.3	0.4±0.7	p<0.001	5.8±4.6	7.5±3.7	p=0.49
GCN left	6.4±4.3	0.2±0.4	p<0.001	6.4±5	6.5±2.3	p=0.96
GCN total	12.7±8	0.5±1	p<0.001	12.2±9.1	14.00±6	p=0.66
PAPs (mmHg)	31.00±8	26.00±4	p=0.04	30.00±7	33.00±10	p=0.51
Digital Ulcerations (%)						
Active				18.00	40.00	p=0.35
Previous				36.00	100.0	p=0.01

SSc: systemic sclerosis; LcSSc: limited cutaneous systemic sclerosis; DcSSc: diffused cutaneous systemic sclerosis; GCN: giant capillary number

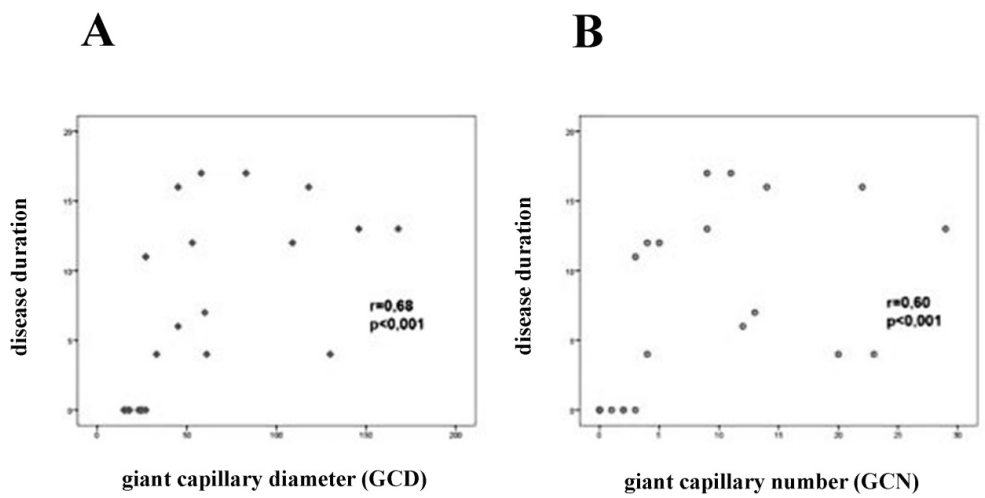

Fig. 1. *Correlation between giant capillary diameter (GCD) and disease duration (**A**) and between giant capillary number (GCN) and disease duration (**B**).*

Table II. *Evaluation of echo-color-doppler parameters.*

Parameters	SSc patients (n=32)	Healthy controls (n=32)	p-value	LcSSc patients (n=20)	DcSSc patients (n=12)	p-value
Radial art. right						
IP	4.85±3.60	2.24±0.50	p=0.01	5.92±3.85	2.49±1.15	p=0.07
IR	0.89±0.13	0.66±0.04	p<0.001	0.91±0.13	4.16±3.24	p=0.47
Radial art. left						
IP	5.74±5.00	2.19±0.45	p=0.01	6.46±5.61	4.54±3.24	p=0.32
IR	0.89±0.13	0.64±0.04	p<0.001	0.89±0.14	0.90±0.14	p=0.98
Ulnar art rigt						
IP	5.89±3.58	2.36±0.45	p=0.01	6.51±3.68	4.54±3.30	p=0.31
IR	0.92±0.13	0.63±0.05	p<0.001	0.94±0.12	0.88±0.16	p=0.48
Ulnar art. left						
IP	5.35±3.61	2.24±0.52	p=0.004	5.93±3.80	4.09±3.14	p=0.33
IR	1.11±0.77	0.65±0.05	p=0.03	1.23±0.92	0.85±0.14	p=0.21
Palmar art. right						
IP	4.00±3.60	1.29±0.30	p=0.009	4.85±4.08	2.14±0.85	p=0.17
IR	0.86±0.15	0.62±0.05	p<0.001	0.87±0.13	0.90±0.11	p=0.64
Palmar art. left						
IP	4.28±4.15	1.35±0.32	p=0.01	5.05±4.85	2.57±0.73	p=0.28
IR	0.86±0.15	0.64±0.05	p<0.001	0.84±0.15	0.90±0.13	p=0.47
II digital art. right						
IP	1.60±0.62	0.89±0.10	p<0.001	1.54±0.71	1.75±0.41	p=0.46
IR	0.66±0.23	0.51±0.06	p=0.02	0.73±0.13	0.50±0.32	p=0.06
II digital art. left						
IP	3.39±3.17	1.17±0.27	p=0.009	3.36±3.25	3.45±3,28	p=0.96
IR	0.77±0.19	0.61±0.08	p=0.02	0.79±0.15	0.73±0.29	p=0.68

SSc: systemic sclerosis; LcSSc: limited cutaneous systemic sclerosis; DcSSc: diffused cutaneous systemic sclerosis; IP: pulsatility index; IR: resistance index; Art: artery.

every examined artery were related both to GCN and GCD (Table III). The same results were shown on the left side, with the exception of IR of the second digital artery and GCD, and IR of the ulnar artery and GCN (Table III).

DISCUSSION

SSc pathogenesis has always been linked to microvascular alterations and autoimmunity, followed by fibroblast activation and fibrotic development (7). Videocapillaroscopy is an easy, reliable and non-invasive instrument to evaluate microvascular alterations not only in SSc, but potentially in every microvessel–related disease (8). Nowadays, it is assumed that this method of evaluation can not only precociously identify alterations of the microcirculation, but can also be used as a follow up instrument to control the evolution of vascular injuries (8), and our data globally confirm this information.

On the other hand, there is a great debate about large-vessel involvement in SSc since previous studies evaluating the presence of atherosclerosis and other risk factors for cardiovascular events among SSc patients have generated controversial results

Table III. *Echo-color-doppler parameters compared to videocapillaroscopic parameters.*

Parameters	SSc patients (n=32)	Healthy controls (n=32)	p-value	LcSSc patients (n=20)	DcSSc patients (n=12)	p-value
Radial art. right						
IP	4.85±3.60	2.24±0.50	p=0.01	5.92±3.85	2.49±1.15	p=0.07
IR	0.89±0.13	0.66±0.04	p<0.001	0.91±0.13	4.16±3.24	p=0.47
Radial art. left						
IP	5.74±5.00	2.19±0.45	p=0.01	6.46±5.61	4.54±3.24	p=0.32
IR	0.89±0.13	0.64±0.04	p<0.001	0.89±0.14	0.90±0.14	p=0.98
Ulnar art rigt						
IP	5.89±3.58	2.36±0.45	p=0.01	6.51±3.68	4.54±3.30	p=0.31
IR	0.92±0.13	0.63±0.05	p<0.001	0.94±0.12	0.88±0.16	p=0.48
Ulnar art. left						
IP	5.35±3.61	2.24±0.52	p=0.004	5.93±3.80	4.09±3.14	p=0.33
IR	1.11±0.77	0.65±0.05	p=0.03	1.23±0.92	0.85±0.14	p=0.21
Palmar art. right						
IP	4.00±3.60	1.29±0.30	p=0.009	4.85±4.08	2.14±0.85	p=0.17
IR	0.86±0.15	0.62±0.05	p<0.001	0.87±0.13	0.90±0.11	p=0.64
Palmar art. left						
IP	4.28±4.15	1.35±0.32	p=0.01	5.05±4.85	2.57±0.73	p=0.28
IR	0.86±0.15	0.64±0.05	p<0.001	0.84±0.15	0.90±0.13	p=0.47
II digital art. right						
IP	1.60±0.62	0.89±0.10	p<0.001	1.54±0.71	1.75±0.41	p=0.46
IR	0.66±0.23	0.51±0.06	p=0.02	0.73±0.13	0.50±0.32	p=0.06
II digital art. left						
IP	3.39±3.17	1.17±0.27	p=0.009	3.36±3.25	3.45±3,28	p=0.96
IR	0.77±0.19	0.61±0.08	p=0.02	0.79±0.15	0.73±0.29	p=0.68

SSc: systemic sclerosis; LcSSc: limited cutaneous systemic sclerosis; DcSSc: diffused cutaneous systemic sclerosis; GCN: giant capillary number; GCD: giant capillary diameter; IP: pulsatility index; IR: resistance index; Art. artery; Echo: echo-color-doppler.

(9). In fact, while the mechanisms of accelerated atherosclerosis are well established in other rheumatic disorders, it is reasonable to hypothesize that SSc also could accelerate the atherosclerotic phenomenon, but this still lacks robust data. At present, there are several lines of evidence in literature which suggest that the macrovascular involvement in SSc takes place especially in distal arteries (10), and our data confirmed this assumption. A question arises: how can we define the macrovascular involvement in the above-mentioned areas? In our opinion, it could be defined as the combination of the general endothelial damage specific to SSc and the chronic shear stress due to the increase of vascular resistances observed in microcirculation (11). This latter phenomenon alone represents an independent damage factor in SSc. Comparing micro- and macrovascular alterations in SSc, we found a direct correlation between these two compartments and believe that the two phenomena represent two faces of the same coin. In fact, in the "very early" stage of SSc it is plausible that alterations in microcirculation prevail (12). Then, with the evolution of the disease, micro- and macrovascular events increase equally in number and severity (12). Therefore, we strongly believe that when there is presence of macrovascular

damage in the early stages of SSc, this could be a precocious sign of a rapid progression of the disease. After all, even if it is not clear why and how, it is known that macrovascular damage is a phenomenon related and consequent to microvascular damage almost in every in chronic disease in general (12), and in SSc in particular.

Given the above, together with nailfold videocapillaroscopy, we suggest echo-color-doppler examination of upper limbs as an integrative evaluation method, because of its simplicity of execution, non-invasiveness and reproducibility. In this way, it could be possible to improve the accuracy of the assessment of the disease and to predict its rapid progression. This paper presents several limitations, the main one being primarily due to the limited number of patients enrolled which causes large confidence intervals of the statistical estimates. Furthermore, the relationship between the microvascular pattern and treatment could not be defined with certainty, as videocapillaroscopy was performed only once. There is therefore no temporal assessment of the disease during treatment. Obviously, for ethical reasons, we could not interrupt ongoing therapies, or start a new one if the patient's situation did not need it. Lastly, because of the small sample size, we could not analyze echo-color-doppler data in relation to every single SSc capillaroscopic pattern.

REFERENCES

1. Denton CP. Advances in pathogenesis and treatment of systemic sclerosis. Clin Med London 2016; 16:55-60.
2. Ruaro B, Soldano S, Smith V, et al. Correlation between circulating fibrocytes and dermal thickness in limited cutaneous systemic sclerosis patients: a pilot study. Rheumatol Int 2019; 39(8):1369-76.
3. Van den Hoogen F, Khanna D, Fransen J, et al. 2013 classification criteria for systemic sclerosis: an American College of Rheumatology/European League against Rheumatism collaborative initiative. Ann Rheum Dis 2013; 72: 1747-55.
4. Mihai C, Smith V, Dobrota R, Gheorghiu AM, Cutolo M, Distler O. The emerging application of semi-quantitative and quantitative capillaroscopy in systemic sclerosis. Microvasc Res 2018; 118:113-20.
5. Ingegnoli F, Smith V, Sulli A, Cutolo M. Capillaroscopy in routine diagnostics: potentials and limitations. Curr Rheumatol Rev 2018; 14(1):5-11.
6. Schioppo T, Orenti A, Boracchi P, De Lucia O, Murgo A, Ingegnoli F. Evidence of macro- and micro-angiopathy in scleroderma: An integrated approach combining 22-MHz power Doppler ultrasonography and video-capillaroscopy. Microvasc Res 2019; 122:125-30.
7. Cutolo M, Soldano S, Smith V. Pathophysiology of systemic sclerosis: current understanding and new insights. Expert Rev Clin Immunol 2019; 15(7):753-64.
8. Cutolo M, Melsens K, Herrick AL, et al; EULAR Study Group on Microcirculation in Rheumatic Diseases. Reliability of simple capillaroscopic definitions in describing capillary morphology in rheumatic diseases. Rheumatology (Oxford) 2018; 57(4):757-59.
9. Psarras A, Soulaidopoulos S, Garyfallos A, Kitas G, Dimitroulas T. A critical view on cardiovascular risk in systemic sclerosis. Rheumatol Int 2017; 37:85-96.
10. Rollando D, Bezante GP, Sulli A, et al. Brachial artery endothelial-dependent flow-mediated dilation identifies early-stage endothelial dysfunction in systemic sclerosis and corelates with nailfold microvascular impairment. J Rheumatol 2010; 37(6):1168-73.
11. Chatzizisis YS, Coskun AU, Jonas M, Edelman ER, Feldman CL, Stone PH. Role of endothelial shear stress in the natural history of coronary atherosclerosis and vascular remodeling: molecular, cellular, and vascular behavior. J Am Coll Cardiol 2007; 49(25):2379-93.
12. Camargo CZ, Sekiyama JY, Arismendi MI, Kayser C. Microvascular abnormalities in patients with early systemic sclerosis: less severe morphological changes than in patients with definite disease. Scand J Rheumatol 2015; 44(1):48-55.

LETTER TO THE EDITOR

FUNCTIONAL OUTCOMES AFTER SUPRACRICOID MODIFIED PARTIAL LARYNGECTOMY

C. SARANITI[1], R. SPECIALE[1], M. SANTANGELO[1], N. MASSARO[1], A. MANIACI[2], S. GALLINA[1], A. SERRA[3] and S. COCUZZA[2]

[1]ENT Department of the University of Palermo, Italy; [2]ENT Department of the University of Catania, Italy; [3]ENT Department, G.B. Morgagni Foundation, Catania, Italy

Received July 5, 2019 – Accepted September 9, 2019

To the Editor,

Open partial horizontal laryngectomy (OPHL) was developed in the 1950s by Hoffman-Saguez (1) and subsequently described by Mayer and Rieder (2) in 1959 (OPHL IIa). The resection performed by Hoffman-Saguez (1), Tucker's frontal laryngectomy (3) and Guerrier's (4) OPHL IIa are similar in terms of resected structures, but they differ in terms of reconstructive techniques: Hoffman (1) reconstructs the cartilaginous structure by preserving external perichondrium of thyroid cartilage while Tucker (3) proposes a closure with mobilized epiglottis displaced inferiorly into the laryngeal defect, and Guerrier (4) performs a pexy between preserved laryngeal structures (cricoid-epiglottis-hyoid; cricoid-hyoid). In 1987, Guerrier (4) described his technique as a combination of Tucker's technique (3), i.e. a frontal resection, and an OPHL IIa reconstruction. Therefore, the maximum extent of resection does not include the posterolateral portion of thyroid cartilage alae and does not require the detachment of pyriform sinuses. OPHL is a standard surgical procedure consisting of a resection followed by reconnection of preserved structures: cricoid-hyoid-epiglottis (CHEP) in OPHL IIa, or cricoid-hyoid (CHP) in OPHL IIb. The key objective is the preservation of neoglottic functions, such as laryngeal functions in terms of voice quality, swallowing and breathing. Moreover, no permanent tracheostomy is required after performing an OPHL. The crucial point in this surgical procedure is the preservation of no less than one functional and mobile crico-arytenoid unit, including arytenoid cartilage, cricoid lamina, posterior and lateral cricoarytenoid muscles, superior and recurrent laryngeal nerves, allowing the preservation of the pharyngolaryngeal sensitivity, protecting the airways and maintaining physiologic coordination during deglutition (5).

The purpose of this study was therefore to assess the neoglottic capabilities retrospectively, in relation to voice quality, swallowing and breathing, after having modified OPHL type II in relation to the Guerrier technique, in a group of selected T2 and T3 patients.

MATERIALS AND METHODS

A multicenter prospective randomized study was conducted on 59 patients who had previously untreated T2 and T3, glottic and transglottic squamous cell carcinoma, and whohad been treated with modified OPHL IIa or OPHL IIb (Guerrier's technique) in the University Departments of ENT of Palermo and Catania (Sicily-Italy) from December 2010 to December 2016 (Protocol of approval

Key words: OPHL type II; Guerrier; pexy; functional results

Corresponding Author:
Dr. Antonino Maniaci,
ENT Department of University of Catania,
95100, Via Santa Sofia, Catania, Italy
Tel.: +39 3204154576
e-mail: tnmaniaci29@gmail.com

0393-974X (2019)

DISCLOSURE: ALL AUTHORS REPORT NO CONFLICTS OF INTEREST RELEVANT TO THIS ARTICLE.

of the Ethics Committee No. 11/2017). Exclusion criteria included: no evident disease (NED) during the last follow-up (n = 0); patients with follow-up < 3 years (n = 7); loco-regional and distant (n = 1 pulmonary metastasis after 2 years) metastases and secondary to the residual tumor laryngeal after 6 years of age (n = 1); presence of a tracheostomy (n = 0). Of the 50 remaining patients, 25, (21 males, 4 females) aged 43-74 (median 59.1) years, were randomly selected, and underwent OPHL IIa with or without arytenoidectomy (ARY) (18 patients: 6 OPHL IIa; 12 OPHL IIa + ARY) or OPHL IIb with or without ARY (7 patients: 4 OPHL IIb; 3 OPHL IIb + ARY) with the modified Guerrier technique (Table I); mono or bilateral neck dissection was performed on each patient.

All patients underwent the same rehabilitation procedure, with obvious exception of those with severe early complications. Each patient started talking and swallowing within 7 days of surgery with rehabilitation, teaching them correct posture, while coordinating swallowing the saliva and correct breathing during conversation to mobilize the cricoarytenoid unit. The nasogastric tube (NGT) was removed as soon as a good level of swallowing of both solids and liquids was achieved. We considered a minimum follow-up of 36 months, and a maximum of 72 months.

All procedures performed in this study involving human participants were in accordance with the ethical standards of the institutional and/or national research committee and with the 1964 Helsinki declaration and its later amendments or comparable ethical standards. Informed consent was given by all patients involved in the study.

Pre- and intraoperative assessment

For pre- and intraoperative assessment, patients underwent laryngoscopy with flexible fiberoptic and CT and/or MR, to verify paraglottic and pre-epiglottic space invasion. Intraoperative assessment was performed by direct microlaryngoscopy under general anesthesia to assess the patient suitability for Guerrier's OPHL II. An important parameter was the extension of the superficial tumor no more than 5 mm on both the ventricles and the subglottis.

Surgical procedure

Guerrier's modified OPHL (4) follows the same surgical steps as in Labayle and Mayer-Piquet's OPHL II (2): an incision of cricothyroid membrane from below to the superior edge of the cricoids, then an incision from above to the glosso-epiglottic vallecula. When OPHL IIb is performed, the latter incision follows the resection of thyroid membrane at the level of the hyoid, or, in the case of OPHL IIa, after a horizontal section over the thyroid cartilage superior edge. Guerrier's modification refers to lateral section lines: performing vertical incisions on thyroid cartilage at the level of the oblique line, no detachment of the piriform sinuses from the thyroid wings or from the paraglotitic space is required (4).

Such procedure allows to maintain pervious and gaping pyriform sinus as well as allowing preservation of the superior laryngeal nerve, responsible for pyriform sinus and epiglottic sensitivity; both these factors are very important for successive laryngeal rehabilitation.

Analysis of neoglottis functionality

Patient neoglottis anatomy and physiology were assessed via videolaryngoscopy after treatment with the modified technique. Vibratory characteristics of the neoglottis, degree of arytenoid motion, and anterior-posterior valving of the arytenoid/epiglottal/base-of-tongue complex were analyzed. Neoglottis motility considering the same parameters as Zacharek (6) et al. and Schindler (7) et al., were assessed but each parameter was attributed a score between 1 and 3. Thus, vibration was described as excellent (grade 1), good (grade 2) and poor (grade 3); arytenoid motility was classified as normal (grade 1), hypomobile (grade 2) and absent (grade 3); antero-posterior movement was classified as complete (grade 1), incomplete (grade 2) and absent (grade 3). Such variables are mutually influenced by neoglottis incompetence, tissue stiffness and neoglottis mucosal thickness (7-8).

Swallowing functional analysis

A comprehensive analysis to assess swallowing ability was performed. For the objective assessment, Bastian's FEES (Flexible endoscopic assessment of swallowing) (9) with milk testing the premature spillage of food, laryngeal motility and laryngeal aspiration of each patient and videofluroscopic examination (VFS) with semi-liquid contrast medium were performed in both right and antero-posterior projection, to study swallowing functionality.

Each patient was assigned a value on the Donzelli scale (10) after three specialists (ENT, phoniatrician and

radiologist) had separately evaluated FEES and VFS results. An MD Anderson Dysphagia Inventory (MDADI) questionnaire was administered to assess physical, functional and emotional components of dysphagia and to quantify the subjective component with codified questions. Each question matches a pre-determined range from 1 to 5 to get an overall score between 20 and 100, which corresponds to the highest level of disability perceived by the patient swallowing (11).

Perceptual analysis of voice

For assessment of dysphonia, all patients were administered the Voice Handicap Index (VHI-10) questionnaire proposed for self-assessment of vocal disability. This is a questionnaire consisting of 30 items referring equally to three different aspects of vocal disorders: physical, functional and emotional. The patient may provide five possible answers, from never to always, assigning a score from 0 to 4. Summing the values assigned to the 30 responses, an overall score between 0 and 120 is obtained that corresponds to the highest level of phonatory disability perceived by the patient.

Finally, the GRBAS (grade, roughness, breathiness, asthenia, strain) scale regarding dysphonia was applied, assigning values from 0 to 3 to each patient.

Statistical analysis

Inter-rater reliability (IRR) was generated by randomly reanalyzing a sample of 50% of the total population data. Weighted kappa with quadratic weighting was calculated; k values were interpreted as follows: ≤ 0.20 poor agreement; 0.21-0.40 fair agreement; 0.41-0.60 moderate; 0.61-0.80 good; and 0.81-1.00 very good (12).

RESULTS

Laryngeal functionality analysis

Each patient was examined and assessed by three ENT specialists, who, individually, assigned the patient a score according to the scale we developed. The assessment for vibration assigned grade 1 to 44% of the patients (11 patients), grade 2 to 24% (6 patients) and grade 3 to 32% (8 patients) (k = 0.79) with an average value of 1.93 (range 1-3).

The evaluation of arytenoid mobility assigned grade 1 to 80% of the patients (20 patients), grade 2 to 16% (4 patients), and grade 3 to 4% (1 patient) (k = 0.86) with an average value of 1.27 (range 1-3). The anterior-posterior movement was assessed as grade 1 in 60% of the patients (15 patients), grade 2 in 33% (8 patients), and grade 3 in 7% (2 patients) (k = 0.91) with an average value of 1.47 (range 1-3).

Swallowing analysis

FEES analysis, according to the Donzelli scale, assigned grade 0 to 72% of the patients (18 patients) grade 1 to 28% (7 patients) (k = 0.77), with an average value of 1.27 (range 1-3). VFS evaluation assigned grade 0 to 72% of the patients (18 patients), grade 1 to 20% (5 patients) and grade 2 to 8% (2 patient) (k = 0.80), with an average value of 1.33 (range 1-3) (Table II). The study of swallowing function was completed by self-assessment of dysphagia using the MDADI questionnaire, and scores were stratified by the type of intervention. Generally, 60% of patients maintained a low level of swallowing disability with MDADI scores of 20–40. The most significant perceived swallowing disability, with MDADI scores > 61, was observed in three interventions (12%) (Table II). The feeding tube was removed within an average time of 12 (range 7-14) days and a median time of 12. Mean time to decannulation was 21 (range 7- 45) days with median time 20 days. No patient suffered from aspiration pneumonia.

Voice analysis

Assessment via the GRBAS scale underlined that 28% (7 patients) achieved grade 2, corresponding to moderate dysphonia, and 72% (18 patients) achieved grade 1, corresponding to slight dysphonia (k = 0.65). Generally, the average patient value was 1.27 (range 0-3) (Table III). The study of phonatory function using the VHI questionnaire demonstrated that a large number of patients, representing 32% of the study cohort, maintained a low level of vocal handicap (VHI score 0–30), while 7 of the 25 patients (28%) complained of a moderate-high degree of speech handicap (Table III).

DISCUSSION

OPHL type II a-b plays a significant role in

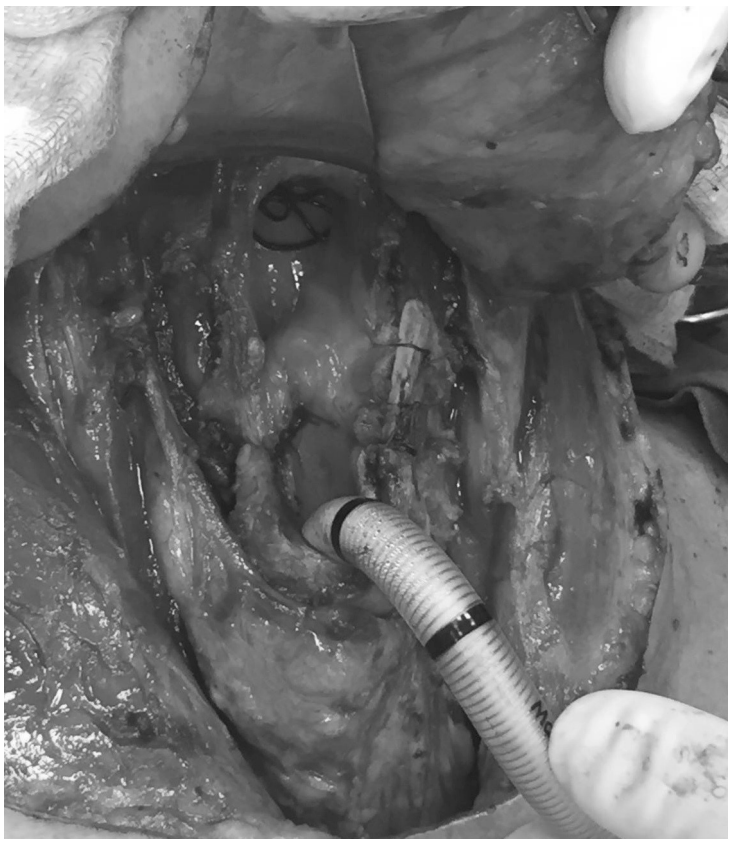

Fig. 1. *Surgical time of the modified technique. The limit of the lower section on cricoid cartilage represents the crucial point in both techniques.*

glottic and transglottic tumour treatment. Due to the major alterations to the normal anatomy of the upper digestive tract, the maintenance of adequate function can be difficult to achieve (6, 7). Guerrier's OPHL II can be performed when extension to the paraglottic space has been excluded by endoscopy and imaging (CT) (4). This extension is the critical point in OPHL II, both in the classic or modified Guerrier technique, above all in T3 tumours with mobile arytenoid. The crucial point in both techniques is the limit of the lower section on cricoid cartilage (Fig. 1). It is in these cases that the margins of the section could be close or involved, without necessarily involving cartilage. Original indications by Guerrier include T1a, T1b, and T2 (4). However, we excluded patients with T1 treated with transoral surgery, while T3 patients, glottis-supraglottis with extension into the pre-epiglottic space and with compromised cordal motility but with mobile arytenoid, were included. In our study the anatomy and physiology of each single component of the neoglottis were assessed according to a scale we developed. We evaluated neoglottis motility considering the same parameters as Zacharek et al. and Schindler et al. (6, 7). The overall results showed a well performing laryngeal physical examination demonstrated by an overall average value of 1.5 (range 1-3). The GRBAS values reported in our series a slight dysphonia in 72% of patients ($k = 0.65$) with a low level of vocal handicap (VHI score 0–30) in 32% of the study cohort (Table III). Video laryngoscope analysis showed an absolutely atypical mucosal vibration. Swallowing is a fundamental outcome for quality of life in patients undergoing supracricoid partial laryngectomy (9). Using FEES/VFS scoring and MDADI methods to evaluate swallowing function, the score showed

level 1 in 73% of the patients, and level 2 in 27%. VFS analysis showed level 1 in 72% of the patients, level 2 in 20% and level 3 in 8%, while the type of partial laryngectomy did not affect the deglutition results (Table II). We successfully decannulated all patients in a mean time of 21 days after surgery, and most patients had their gastric feeding tubes removed 20 days after surgery. In conclusion, these data show that Guerrier's OPHL II is a well-tolerated procedure with generally good functional outcomes, although some voice and swallowing complaints continue long-term. If patients are properly selected, this technique allows oncological radicality.

REFERENCES

1. Hofmann-Saguez MR. Conservative subtotal laryngectomy. Ann Otolaryngol 1950; 67:811-16.
2. Meyer EH, Rieder W. Technic of laryngectomy permitting the conservation of respiratory permeability (cricohyoidopexy). Ann Otolaryngol 1959; 76:677-81.
3. Tucker HM, Wood BG, Levine H, Katz R. Glottic reconstruction after near total laryngectomy. Laryngoscope 1979; 89:609-18.
4. Guerrier B, Lallemant JG, Balmigere G, Bonnet PH, Arnoux B. Our experience in reconstructive surgery in glottic cancers. Ann Otolaryngol Chir Cervicofac 1987; 104:175-9.
5. Holsinger FC, Laccourreye O, Weinstein GS, Diaz EM, McWhorter AJ. Technical refinements in the supracricoid partial laryngectomy to optimize functional outcomes. J Am Coll Surg. 2005; 201:809-20.
6. Saraniti C, Speciale R, Gallina S, Salvago P. Prognostic role of resection margin in open oncologic laryngeal surgery: survival analysis of a cohort of 139 patients affected by squamous cell carcinoma. Braz J Otorhinolaryngol 2018; doi: 10.1016/j.bjorl.2018.04.012.
7. Serra A, Maiolino L, Di Mauro P, Licciardello L, Cocuzza S. The senile functional evolution of the larynx after supracricoid reconstructive surgery. Eur Arch Otorhinolaryngol 2016; 273(12):4359-68.
8. Dispenza F, Saraniti C, Mathur N, Dispenza C. Modified fronto-lateral laryngectomy in treatment of glottic T1(a-b) cancer with anterior commissure involvement. Auris Nasus Larynx 2010; 37(4):469-73.
9. Di Santo D, Bondi S, Giordano L, Galli A, Tulli M, Ramella B, Bussi M. Long-term swallowing function, pulmonary complications, and quality of life after supracricoid laryngectomy. Otolaryngol Head Neck Surg 2019; 161(2);307-14.
10. Donzelli J, Wesling M, Brady S, Craney M. Predictive value of accumulated oropharyngeal secretions for aspiration during video nasal endoscopic evaluation of the swallow. Ann Otol Rhinol Laryngol 2003; 112:469-75.
11. Chen AY, Frankowski R, Bishop-Leone J, et al. The development and validation of a dysphagia-specific quality-of-life questionnaire for patients with head and neck cancer: the M.D. Anderson dysphagia inventory. Arch Otolaryngol Head Neck Surg 2001; 127:870-76.
12. Cohen J. Weighted kappa: nominal scale agreement with provision for scaled disagreement or partial credit. Psychol Bull 1968; 70(4):213-20.

JOURNAL OF BIOLOGICAL REGULATORS & HOMEOSTATIC AGENTS Vol. 33, no. 6, 1909-1912 (2019)

LETTER TO THE EDITOR

OPERCULECTOMY AND SPONTANEOUS ERUPTION OF IMPACTED SECOND MOLARS: A RETROSPECTIVE STUDY

C. MASPERO, A. ABATE, D. CAVAGNETTO, A. FAMA, A. STABILINI, G. FARRONATO and M. FARRONATO

Department of Biomedical, Surgical and Dental Sciences, University of Milan, Fondazione IRCCS Cà Granda, Ospedale Maggiore Policlinico, Milano, Italy

Received July 16, 2019 – Accepted September 16, 2019

To the Editor,

Failure of eruption of permanent second molars is a rare condition that affects 0.06% of the population (1). Andreasen and Kurol classified this failure into three clinical conditions: impaction as a result of a physical obstacle; primary retention, caused by eruption arrest prior to the penetration in the oral cavity; secondary retention referring to the cessation of eruption of a tooth after emergence without a physical barrier or ectopic position of the tooth (2). The etiology of failure of eruption is therefore connected to interference in the physiological growth and tooth development, such as space deficit, ankylosis, systemic factors, soft tissue anomalies and alteration of the eruptive axis, although in some cases the causes are unknown (3, 4).Treatment options for retained second molars are: follow-up evaluations, surgical uncovering with or without orthodontic assisted eruption and extraction. Patients undergo scheduled clinical and radiographic examinations that aim to promptly identify whether the evolution of each patient's condition requires surgical intervention to ensure proper eruption of retained teeth (5, 6).

Surgical uncovering (operculectomy) alone is performed if the tooth presents an adequate position, and an incomplete root, thus remaining potential for spontaneous eruption. Orthodontic-assisted eruption and surgical uprighting are indicated if the impacted tooth position is not likely to allow spontaneous eruption. Third molar extraction may be required. Extraction of a retained element is chosen in complex cases, such as presence of cystic neoformation, root resorption of one or more adjacent teeth or whether the retained tooth is ankylosed (7). Moreover, extraction is indicated if surgical uncovering prognosis is unfavorable, such as in cases with excessive root inclination.

The aim of the present study is to retrospectively evaluate the efficacy of operculectomy in the treatment of patients with primary retention of one or more second molars by comparing the outcome at 12-month follow-up between a group of patients treated with operculectomy and a group of patients' whose parents did not give consent to perform operculectomy, thus serving as controls.

MATERIALS AND METHODS

The present study was conducted in accordance to the Declaration of Helsinki. All patients both in the case and in the control group or their parents gave informed consent

Key words: operculectomy; impacted second molar

Corresponding Author:
Dr Cinzia Maspero,
Ospedale Maggiore Policlinico,
Via Francesco Sforza 35,
20122. Milano (Mi). Italy
Tel./Fax: +39 0255032520
e-mail: cinzia.maspero@gmail.com

0393-974X (2019)

to all the procedures reported. The sample of this study included 222 subjects with a diagnosis of delayed eruption of a second molar who were treated between January 2018 and March 2019 at the Orthodontic Department of the University of Milan (Ospedale Maggiore Policlinico, Milano, Italy). Clinical examination (tooth not present in the arch) and radiographic examination (orthopantomography and intra-oral radiography) were performed for each subject.

Inclusion criteria were: no previous orthodontic treatment, no other systemic or dental disease but one retained permanent second molar per arch when more than two-thirds of its root was formed and the other one is erupted, absence of interference from third molar and of second molar root anomalies.

Eighty-eight patients, 40 males and 48 females (mean age 15±1.6 years), met the inclusion criteria and were included in the final sample. The total number of impacted/retained second molars considered were 145, 75 in the treatment group and 70 in the control group. The conditions evaluated by comparison with the contralateral side on each radiography were: stage of dental maturity assessed according to the morphological description by Demirijan et al. (8); inclination of the retained second molars measured on the orthopantomograms as described by Evans (9). From the tangent to the tips of the cusps, a perpendicular line was constructed through the middle of the crown and root on the affected second molar and on the adjacent first molar. The angle between these lines was measured. The teeth are considered mesio-tilted when the angle is more than 40 degrees, vertically positioned if the angle is ranged between 40 and 20 degrees and distally inclined if the angle is less than 20 degrees.

Patients in the case group underwent surgical removal of the mucosa (operculectomy) covering the retained teeth (Fig. 1 a-c); the control group consisted of patients whose parents had refused consent to perform operculectomy. Treatment was defined unsuccessful if the second molar did not erupt within 1 year after surgical intervention. Occlusion was defined successful if the erupted tooth had occlusal surface within 2 mm from the occlusal plane.

RESULTS

Eruption occurred in 93.3% teeth in the treatment group (70/75) after surgical removal of the mucosa, while in the control group only 10% teeth erupted (7/70). In the case group, following operculectomy, the eruption in the upper arches occurred in 95.2% of cases (40 out of 42), while in the lower arches the eruption occurred in 90.9% of cases (30 out of 33). In the control group, the spontaneous eruption of the upper second molars occurred only in 8.5% of cases (3 sites out of 35), while in the lower ones the spontaneous eruption occurred only in 8.5% (3 sites out of 35). Flow chart of clinical outcomes are reported in Fig. 2. Percentages of eruption of the second permanent molars, in the case group and in the control group, divided between the upper and lower arches are shown in Table I. *Chi*-squared test showed a statistically significance difference between the treatment group and the control group $p < 0.05$. In the treatment group the probability of teeth eruption is 10 times higher than the probability in the control group, as reported in Table I. The amount of permanent second molars erupted after surgery, in the upper and lower arch, observed in the case group was 40/42 and 30/33, respectively. By contrast, in the control group,

Table I. *Frequency of eruption in the treatment group in and the control group.*

	Treatment Group	**Control Group**
Second molars that have erupted (mean between upper and lower arch)	93.3%	10%
Upper second molars that have erupted	95.2%	8.5%
Lower second molars that have erupted	90.9%	8.5%
Odds ratio between case and control group	10	1
p-value (*chi*-squared test)	p<0.001	

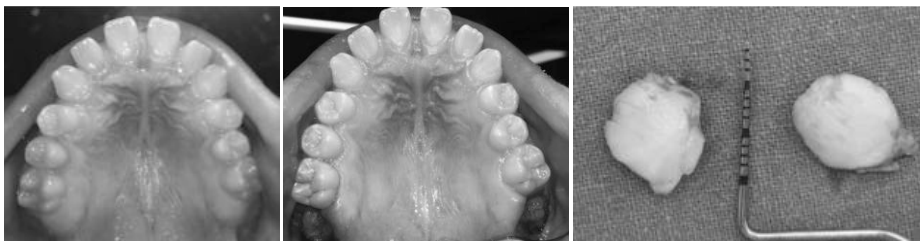

a b c

Fig. 1. ***a)*** *Pre-surgical occlusal vision.* ***b)*** *Post-surgical occlusal vision.* ***c)*** *Gingival operculum after surgical removal.*

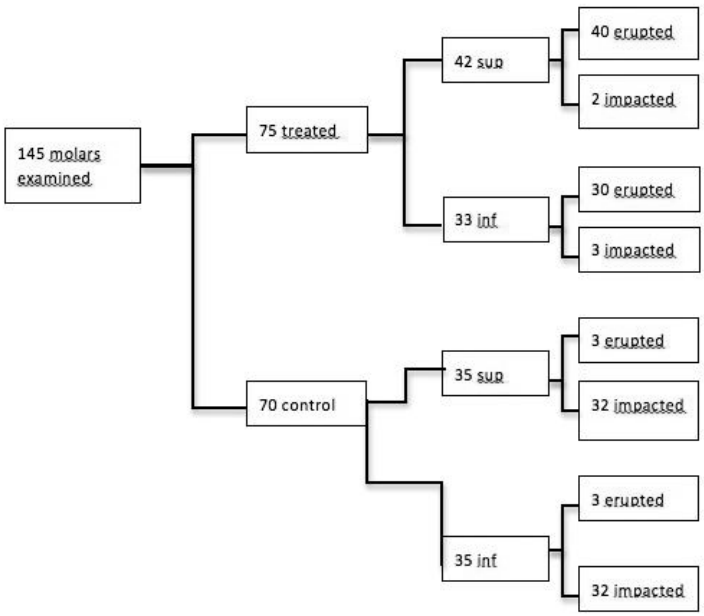

Fig. 2. *Flow chart of clinical outcomes in case group and control group.*

only 3 second molars out of 35 erupted in the oral cavity both in the upper and lower arch.

Of the non-erupted teeth 23 were positioned with a mesial inclination (41%), 13 were positioned vertically (34%), 8 showed a bigger crown compared to the contralateral (13%), and 10 showed an enlarged follicle compared with a normal crown follicle (12%).

DISCUSSION

The results of this study indicate that the retained permanent second molars still have the ability to erupt after surgical removal of the overlying mucosa and could represent a temporary problem and not a failure of eruption. These dental elements may be able to erupt spontaneously after the surgical removal of the overlying mucosa. If the dental element presents a real inclusion able to complicate the following therapy, clinicians should consider an orthodontic, orthodontic-surgical or purely surgical approach (10). In the cases of primary retention, among factors limiting the eruption of the considered element, the relationships between the dental sac and the overlying tissue seem to play an important role: a follicle malfunction or the presence of gingival tissue anomalies within the overlaying soft tissue (like a fibrous formation) can hinder the path of tooth eruption. The success rate in the case group was 93.3% (70/75). Spontaneous eruption in the control group after one year occurred in 10% of

patients (7/70). This value is in accordance with the results obtained by Kenrad et al. (90% success rate) (11). Upper second molars presented a higher rate of success compared to inferior ones, both in the case and in control groups, in particular if the tooth was in a vertical position or with a slight mesial inclination. The major advantages of this therapeutic approach are its conservative nature and its efficacy. Surgical exposure of a retained tooth allows in case of failure to intervene with other therapeutic options, as suggested by Farronato et al. (12). In treated cases, there were no complications following the operation and no periodontal problems occurred on the treated nor on the other dental elements.

At present, there are no guidelines for the treatment of eruptive problems of impacted second molars. For a correct treatment plan, it is advisable to proceed to an early and precise diagnosis, which allows to identify the causes involved. Surgical exposure is a simple, non-invasive and valid method which allows the eruption of second molars in the majority of cases. It does not preclude the possibility of subsequent treatments and aims to facilitate the natural eruption process. There is a statistically significant difference between treatment success in patients where the mucosa was removed and those where it was not removed.

REFERENCES

1. Baccetti T. Tooth anomalies associated with failure of eruption of first and second permanent molars. Am J Orthod Dentofacial Orthop 2000; 118(6):608-10.
2. Andreasen JO, Kurol J. The impacted first and second molar. Textbook and color atlas of tooth impactions Copenhange: Munksgaard; 1977.
3. Lucchese A, Sfondrini MF, Manuelli M, Gangale S. Fixed space maintainer for use with a rapid palatal expander. J Clin Orthod 2005; 39(9):557-58.
4. Maspero C, Maschio MM, Fama A, Zanoni F, Farronato M. Consequences in permanent dentition of untreated impacted deciduous teeth. Minerva Stomatol 2019; 68(1):57-59.
5. Lucchese A, Matarese G, Manuelli M, et al. Reliability and efficacy of palifermin in prevention and management of oral mucositis in patients with acute lymphoblastic leukemia: a randomized, double-blind controlled clinical trial. Minerva Stomatol 2016; 65(1):43-50.
6. Litsas G, Lucchese A. Dental and chronological ages as determinants of peak growth period and its relationship with dental calcification stages. Open Dent J 2016; 10:99-108.
7. Farronato G, Maspero C, Farronato D. Orthodontic movement of a dilacerated maxillary incisor in mixed dentition treatment. Dent Traumatol 2009; 25(4):451-6.
8. Demirijan A, Goldstein H, Tanner JM. A new system of dental age assessment. Human Biology 1973; 45:211-27.
9. Evans R. Incidence of lower second permanent molar impaction. Br J Orthod 1988; 15(3):199-203.
10. Farronato G, Galbiati G, Esposito L, Mortellaro C, Zanoni F, Maspero C. Three-dimensional virtual treatment planning: presurgical evaluation. J CraniofacSurg 2018; 29(5):e433-e437.
11. Kenrad J, Vedtofte H, Andreasen JO, Kvetny MJ, Kjær I. A retrospective overview of treatment choice and outcome in 126 cases with arrested eruption of mandibular second molars. Clinical oral investigations 2011; 15(1):81-87.
12. Farronato G, Giannini L, Galbiati G, Consonni D, Maspero C. Spontaneous eruption of impacted second molars. Progr Orthod 2011; 12(2):119-25.

JOURNAL OF BIOLOGICAL REGULATORS & HOMEOSTATIC AGENTS Vol. 33, no. 6, 1913-1919 (2019)

LETTER TO THE EDITOR

EFFICACY OF SODIUM HYALURONATE AND SYNTHETIC AMINOACIDS IN POST-EXTRACTIVE SOCKET IN PATIENTS WITH LIVER FAILURE: SPLIT MOUTH STUDY

N. COCERO, T. RUGGIERO, A. PEZZANA, M. BEZZI and S. CAROSSA

Oral Surgery Department, Department of Surgical Sciences, Dental School, University of Turin, Turin, Italy

Received June 12, 2019 – Accepted September 27, 2019

To the Editor,

In recent years, among the new biomaterials used in dentistry the focus has been on products based on amino acids and hyaluronic acid (1). In this study we evaluated the effectiveness of hyaluronic acid gel, a new medical device that acts on fibroblasts to improve wound healing, composed of hyaluronic acid (HA) and aminoacids (AA) collagen precursors, L-lysine, L-proline, L-leucine and glycine. The system is composed by Glycol propylene e carbopol, HA e AA; the HA molecular weight is 1.500 KDalton, and it works at pH 5.5 – 6.5

In vivo and *in vitro* studies show that fibroblasts treated with HA in amino acid solution display increased and proliferative activity, with increased collagen production and fibronectin synthesis. In addition, they increase the expression of transforming growth factor beta, the connective tissue growth factor, and of interleukins 6 and 8. These results suggest that hyaluronic acid is involved in many stages, including neoangiogenesis, fibroblast proliferation and differentiation, extracellular matrix deposition, cytokine production and release, and re-epithelialisation. In the field of dentistry, some studies have shown significant advantages of the product, especially in patients with periodontal disease who show significant bone defects and in patients undergoing surgery for the removal of benign tumors (2, 3).

The need to promote and accelerate the healing of wounds is even more necessary in patients in whom the healing process is inadequate (4). For this reason, in this study, we used SH-AAs in a group of patients with chronic liver disease. Liver failure is a clinical condition that enables a limited compensation of the function of the organ due to the progression of chronic diseases (5, 6). This type of patients are subject to abnormal wound healing due to their liver disease, which exposes them to conditions of malnutrition, hormonal disorders, bilirubin and ammonia intoxication and bleeding diathesis (7). Extraction complications are associated with a loss of organ functions, and abnormalities in drug metabolism, immune response and haemostatic process often occur (8). These conditions characterize chronic liver disease and can influence the physiological processes of post-extraction alveolus healing, thus exposing the wound to a higher risk of complications (9). The purpose of the study is to assess how the use of products based on sodium hyaluronate and aminoacids (HS-AAs) can improve epithelial regeneration and healing of the post-extractive tooth socket.

Key words: socket healing, tooth extraction, liver, amino-acid, sodium hyaluronate, dental care, SH-AA

Corresponding Author:
Dr T. Ruggiero,
Oral Surgery Department,
Department of Surgical Sciences,
University of Turin, Dental School,
Via Nizza 230, 1 - 0100 Turin, Italy
e-mail: tiziana.ruggiero@unito.it

0393-974X (2019)

DISCLOSURE: ALL AUTHORS REPORT NO CONFLICTS OF INTEREST RELEVANT TO THIS ARTICLE.

MATERIALS AND METHODS

Research design and management

A split mouth study was conducted in which each patient served as both case and control: one post-extraction alveolus was treated with an SH-AA gel (case site), whilst another was left to naturally heal following the formation of a clot (control site). The choice of alveolus to be treated was made in a controlled randomised manner by an internal use software. The inclusion criteria for the study were: i) patients with severe liver failure, awaiting a liver transplant; ii) platelets higher than 50.000 on the day of surgery; iii) need for extraction of dental elements, no longer recoverable bilateral homologues; iv) giving informed consent to the study. Exclusion criteria were: i) known allergy to one of the components of the compound; ii) inability to attend follow-ups; iii) systemic diseases, in addition to liver failure, which could affect the healing of wounds (e.g. diabetes, chronic renal failure, autoimmune diseases); iv) chronic mucocutaneous diseases; v) inability or unwillingness to provide their informed consent.

The study population was composed of 58 patients referred to the Oral Surgery Section of the Dental School of the University of Turin by the Liver Transplant Center from January 1 to December 31, 2017, as a part of the protocol for candidates to receive a liver transplant. One hundred and sixteen simple bilateral and symmetrical dental extractions were performed. Patients with liver failure prior to transplantation (OLT) had to meet the inclusion and exclusion criteria of the study and agree to be monitored. All patients were informed about the possible use of their data for clinical studies and signed an informed consent form. The patient data were anonymized before analysis. The analysis was performed in accordance with the local institutional review board standards and conformed to the Declaration of Helsinki of 1975 and subsequent modifications.

Surgical protocol

The included patients were registered in a computerized clinical file which recorded information on age, gender, smoking habits, alcohol consumption, systemic pathologies, and the use of any drugs. Each patient then attended a program of professional dental hygiene to nullify differences in preoperative hygiene conditions, after which a thorough clinical and radiologic evaluation and digital case history for each patient was filed containing oral and dental parameters: periodontal screening and recording code; conditions of untreatable teeth undergoing extraction (e.g., presence of infections, carious processes, or periodontal affection); difficulty of extraction (based on crown integrity, root morphology, space, and patient compliance); and symptoms.

Alveolar nerve block infiltration was administered with local or regional anesthesia, depending on the dental arch, using 2% mepivacaine. Mepivacaine does not contain epinephrine, therefore, it was used to prevent restriction of the blood supply (10). To prevent interference with the healing process, no intraligamentous or intrapapillary infiltrations were performed. Non-traumatic bilateral extractions were accomplished without elevation of full-thickness flaps to preserve the bone ridges and soft tissue at the two sites. Surgery was performed on the treatment and control sides at the same time. After socket curettage to remove granulation tissue, a millimeter probe was used to measure the socket diameters (maximum mesiodistal and buccolingual extensions).

The SH-AAs gel in a syringe (15 ml) was applied within the socket chosen as the study site, and the membrane was laid above within the socket wall. After 5 min of compression with sterile cotton, bleeding was evaluated as spontaneous, induced by palpation, or absent. Accurate postoperative recommendations were provided to the patients. No pharmacologic therapy was prescribed, and recourse to antibiotics was considered a negative postoperative parameter, a sign of postoperative complications from infection. Patients were taught to apply SH-AAs gel on the study site 3 times a day, every 8 hours, for 7 days. After the extractions, each patient underwent a precise follow-up program: 4 sessions conducted at 7, 14, and 21 days or until socket closure. Each session included measurements of the socket in the study and control sites. Pain was evaluated by the patients using a VAS, (11) which distinguished the study and control sockets, for 7 consecutive days, with day 0 considered the day of extraction, after resolution of the effects of the anesthesia. The patients' general satisfaction was evaluated with a questionnaire administered after extraction. Patients were asked to state any differences noticed in bleeding or pain between the 2 sites and to state which technique they would choose for a future extraction. Additional control sessions after postoperative day 21 until the achievement of socket

epithelialization and the need for antibiotic administration or for surgical re-intervention in cases of alveolitis were considered possible negative postoperative parameters.

Statistical analysis

For the statistical analysis of the oral vestibule and mesiodistal diameters at 0, 7, 14 and 21 days and on the accompanying pain over a period of one week, the data were expressed as means and standard deviations. Being a case-control trial, their comparison involved the Student's paired data *t*-test, which reduces the problem of biological variability between the various patients. The values of the probability of random difference p were considered significant for $p< 0.05$.

RESULTS

Oral vestibule diameters. The results of the oral vestibular diameters of the post extractive sites of the treated group (case site) and untreated group (control site) at time zero (T0), at 7 days (T1), at 14 days (T2) and at 21 days (T3) are shown in Table I. Fig. 1 shows the different trend in oral vestibule diameters at the 4 points (time zero, 1 week, 2 weeks, 3 weeks), respectively, for the case site and for the control site. The dashed line shows the inclination that the straight line would likely have taken had the SH-AAs gel treatment continued for more than one week.

Mesiodistal diameters. The results of the mesiodistal diameters of the post extractive sites of the treated group (case site) and untreated group (control site) at time zero, and at 7, 14 and 21 days are shown in Table I. Fig. 1 shows the diverse trend in mesiodistal diameters at the 4 time-points, respectively, for the case site and for the control site. The dashed line shows the inclination that the straight line would likely have taken had the HA-AA gel treatment continued for more than one week.

*Upper and lower arch comparison***.** There are no statistically significant differences when comparing the upper arch with the lower arch in either the case site or in the control site. The force of gravity seems to have no influence on the healing mechanisms, therefore, the application of the product promotes faster epithelialization, regardless of the position of the dental elements in the arch.

Comparison of single-/multi-rooted dental elements. Table II shows the variations in the oral vestibule and mesiodistal diameters in the time interval ranging from time zero to 21 days, divided between single-rooted and multi-rooted dental elements; p1 represents the probability associated with comparing the single-rooted dental elements in the case site and in the control site; the same is carried out for multi-rooted elements; this is to understand whether the application of the product gives the same results for both single-rooted and multi-rooted elements. p2 represents the probability by comparing single-rooted and multi-rooted dental elements of the case site; the same was carried out for the control site; this is to understand whether the alveolar dimensions and morphology could affect the speed of healing.

VAS Scale. The intention was to establish whether the use of the product could give benefits, not only in

Table I. *Alveolar diameter reduction. The values highlighted in bold represent the statistically significant associated probabilities.*

	Alveolar diameters		
ΔT	**Case site (mm)**	**Control site (mm)**	**Paired *t*-test**
T0	6.72± 1.95	6.60 ± 1.88	0.77
T1	3.89±1.73	4.64 ± 2.03	**<0.0001**
T2	2.09±1.31	3.07 ± 1.51	**<0.0001**
T3	0.58±1.11	1.21 ± 1.25	**<0.0001**
	Mesiodistal diameters		
ΔT	**Case site (mm)**	**Control site (mm)**	**Paired *t*-test**
T0	6.56 ± 2.04	6.51 ± 2.03	0.62
T1	3.61±1.84	4.69 ± 2.04	**$\leq 10^{-7}$**
T2	1.74±1.54	2.82 ± 1.70	**$\leq 10^{-7}$**
T3	0.44±1.02	1.16 ± 1.25	**2.31×10^{-3}**

T1:7 days, T2:14 days; T3:21 days.

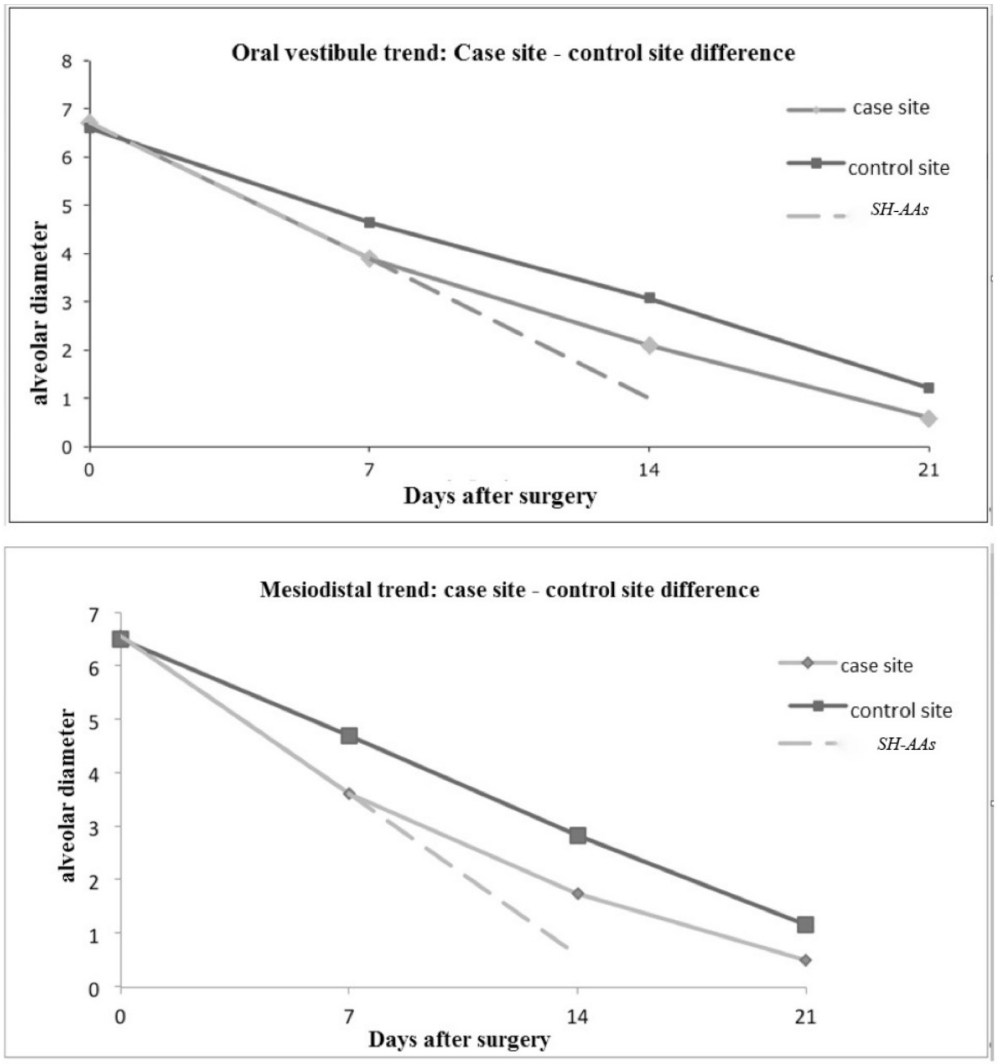

Fig. 1. *Trend in oral vestibule and mesiodistal diameters. The divergence between the two lines is significant in the first 7 days; subsequently, the lines are parellel. little squares: case site; big squares: control site; dashed lines: probable healing if patients continued application of SH-AAs.*

terms of healing, but also in terms of post-operative pain, given that a faster and better quality healing has a positive effect on this aspect also. During the first week after surgery, the patient was advised to report the intensity of pain by recording it on the VAS scale (assessed on a scale between 0 and 10 cm), referring to both the case site and to the control site. The trend in pain in both the case site and in the control site in the first 7 days are shown in Table II and Fig. 2. The values were statistically significant only in the first 3 days; from the fourth to the seventh days, the values were no longer significant .

DISCUSSION

The main purpose of SH-AA gel is to improve healing, from qualitative and temporal points of view. Sodium hyaluronate (SH) contributes by acting with an anti-edematous, encouraging vascularization and promoting epithelial healing (2). It is reasonable to think that if a surgical site epithelializes within a short space of time, it is less subject to healing problems. With greater reason, oversight has previously occurred for patients who had most need to be guided in their recovery, such as

Table II. *The comparison of single-/multi-rooted dental elements in speed healing and comparison single-rooted and multi-rooted elements.*

ΔT	Case site	Control site	Paired *t*-test	*t*-test on average values
Day 1	0.84 ± 0.29	1 ± 0.41	**$7.61x10^{-5}$**	**$3.54x10^{-4}$**
Day 2	0.51±0.50	0.86 ± 0.44	**$2.09x10^{-5}$**	**$1.30x10^{-4}$**
Day 3	0.19±0.40	0.49 ± 0.50	**$2.54x10^{-4}$**	**6.61×10^{-4}**
Day 4	0.12±0.33	0.16±0.37	0.53	0.59
Day 5	0.02±0.13	0.07±0.26	0.18	0.17
Day 6	0	0.04±0.019	0.16	0.16
Day 7	0	0.02±0.13	0.32	0.2

	Tooth	Vestibule/oral case site (mm)	Vestibule/oral control site (mm)	p1	Mesio/distal case site (mm)	Mesio/distal control site (mm)	p1
ΔT (0-21 days)	**single-rooted**	96±87%	89±14%	**$3x10^{-3}$**	98±6%	87±14%	**$4x10^{-3}$**
	multi-rooted	89±11%	78±12%	**$13x10^{-3}$**	88±17%	79±10	**$4x10^{-3}$**
	p2	**$2.65x10^{-3}$**	**$7.80x10^{-3}$**		**$5x10^{-3}$**	**$5.2x10^{-3}$**	

The values highlighted in bold represent the statistically significant associated probabilities.

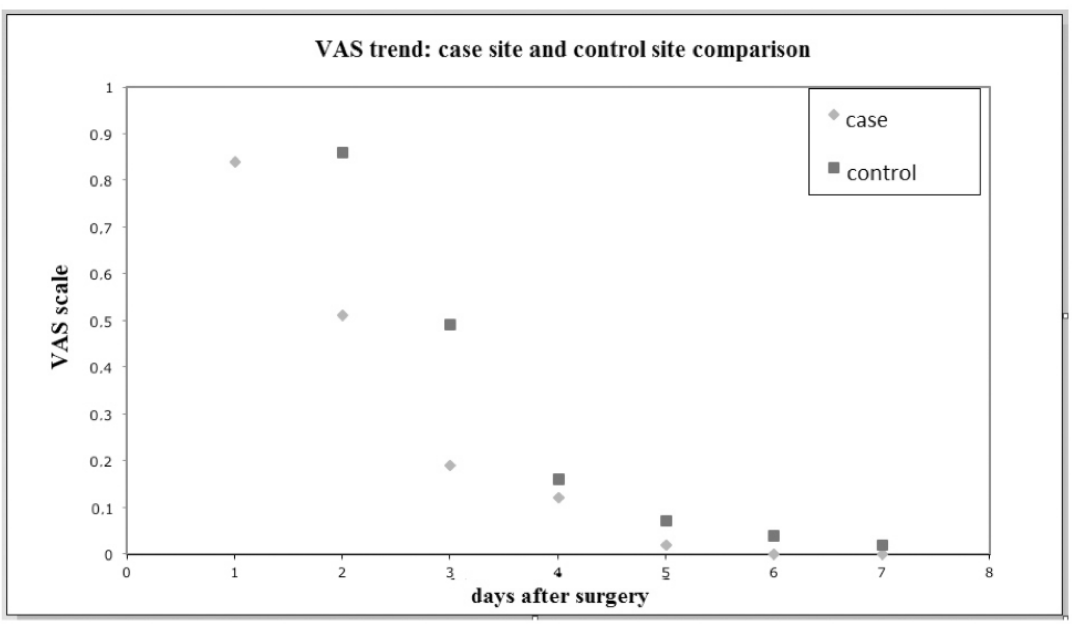

Fig. 2. *Trend in pain. The difference was statistically significant in the first 3 days but not from the fourth to the seventh days. little squares: case site; big squares: control site.*

those with liver disease (12). The clinical sensation, confirmed by this study, shows that the effectiveness of the product is maximal, especially in the first days, from both an epithelial healing point of view and from a VAS point of view. With regard to the trend in diameters, the statistical survey shows that the significance is valid in all 3 time-points taken into account (days 7, 14 and 21). Since the product was only applied for the first week, the intention was to understand in which time interval the product was most effective. What was expected (and confirmed by the statistical analysis) was that, in the first time interval, the difference would be maximal and would gradually decrease during subsequent time intervals. In the subsequent time intervals, the associated probabilities tend to become less significant, but always remain significant in all time intervals, except for between days 7 and 14 (Table I, Fig. 1). The comparison of single-/multi-rooted dental elements was carried out to understand whether there is also a correlation between alveolar size and shape. A small alveolus, with the same conditions, heals sooner than a large alveolus (Table II). This can be explained simply by the fact that larger alveoli, with a different alveolar morphology, require more "repairing cells" and, therefore, more time. Then, the intention was to understand whether this product is equally effective in single-/multi-rooted elements. Also in this case (Table II), the associated probabilities were statistically significant: the speed of epithelial healing is influenced by the use of SH-AAs, in both oral vestibule and mesiodistal diameters. The gel promotes an improvement that is always statistically significant from a healing point of view, but healing differs depending on whether the element is single- or multi-rooted, with a preference for small alveoli with single root. If a wound remains constantly covered by a protective gel it is less subject to the intraoral environment; if this product also acts as a healing mediator, it is clear that the risk of superinfection is lower. This translates into the fact that healing optimally starts with practical advantages in terms of post-operative sensitivity. The gel exerts its effect of reducing the perception of pain only in the first 3 days. During subsequent follow-ups the associated probability values between the case site and the control site are non-significant. This can be explained by the fact that the surgical damage to the patient is minimal, due to the minimally invasive nature of the surgical act of extraction.

REFERENCES

1. Price RD, Myers S, Leigh IM, Navsaria HA. The role of hyaluronic acid in wound healing: assessment of clinical evidence. Am J Clin Dermatol 2005; 6(6):393-402.
2. Colella G, Vicidomini A, Soro V, Lanza A, Cirillo N. Molecular insights into the effects of sodium hyaluronate preparations in keratinocytes. Clin Exp Dermatol 2012; 37(5):516-20.
3. Kim J-J, Song HY, Ben Amara H, Kyung-Rim K, Koo K-T. Hyaluronic Acid Improves Bone Formation in Extraction Sockets With Chronic Pathology: A Pilot Study in Dogs. J Periodontol 2016; 87(7):790-5.
4. Vazquez JR, Short B, Findlow AH, Nixon BP, Boulton AJM, Armstrong DG. Outcomes of hyaluronan therapy in diabetic foot wounds. Diabetes Res Clin Pract 2003; 59(2):123-27.
5. Jalan R, Fernandez J, Wiest R, et al. Bacterial infections in cirrhosis: a position statement based on the EASL Special Conference 2013. J Hepatol 2014; 60(6):1310-24.
6. Perdigão JPV, de Almeida PC, Rocha TDS, et al. Postoperative bleeding after dental extraction in liver pretransplant patients. J Oral Maxillofac Surg Off J Am Assoc Oral Maxillofac Surg 2012; 70(3):e177-84.
7. Pereira TDSF, Pelinsari FCM, Ruas BM, et al. Postoperative complications after dental extraction in liver pretransplant patients. Spec Care Dent Off Publ Am Assoc Hosp Dent Acad Dent Handicap Am Soc Geriatr Dent 2016; 36(5):277-81.
8. Cocero N, Pucci F, Messina M, Pollio B, Mozzati M, Bergamasco L. Autologous plasma rich in growth factors in the prevention of severe bleeding after teeth extractions in patients with bleeding disorders: a controlled comparison with fibrin glue. Blood Transfus Trasfus Sangue 2015; 13(2):287-94.
9. Helenius-Hietala J, Åberg F, Meurman JH, Nordin A, Isoniemi H. Oral surgery in liver transplant candidates: a retrospective study on delayed bleeding and other complications. Oral Surg Oral Med Oral Pathol Oral

Radiol 2016; 121(5):490-95.

10. Colbath AC, Wittenburg LA, Gold JR, McIlwraith CW, Moorman VJ. The effects of mepivacaine hydrochloride on antimicrobial activity and mechanical nociceptive threshold during amikacin sulfate regional limb perfusion in the horse. Vet Surg VS 2016; 45(6):798-803.
11. Aicher B, Peil H, Peil B, Diener H-C. Pain measurement: Visual Analogue Scale (VAS) and Verbal Rating Scale (VRS) in clinical trials with OTC analgesics in headache. Cephalalgia Int J Headache. 2012; 32(3):185-97.
12. Silva Santos PS da, Fernandes KS, Gallottini MHC. Assessment and management of oral health in liver transplant candidates. J Appl Oral Sci Rev FOB. 2012; 20(2):241-45.

LETTER TO THE EDITOR

MINOCYCLINE HYDROCHLORIDE *VERSUS* TRIAMCINOLONE ACETONIDE AS MINI-INVASIVE TREATMENT IN SYMPTOMATIC BAKER CYSTS: A PROSPECTIVE STUDY

A. PALADINI[1], N. MAGARELLI[2], D. BEOMONTE ZOBEL[2], I. PERCIVALE[1], G. BELMONTE[2], D. COVIELLO[2], A. CARRIERO[1] and G. GUZZARDI[1]

[1]Radiology Institute, Services Diagnosis and Therapies Department, Maggiore della Carità Hospital, University of Eastern Piedmont – UPO University, Novara, Italy; [2]Institute of Radiology, Fondazione Policlinico Universitario A. Gemelli IRCCS, Catholic University of the Sacred Heart, Rome, Italy

Received August 27, 2019 – Accepted October 1, 2019

To the Editor,

Popliteal cyst, also known as Baker's cyst (BC), is a fluid synovial lesion of the postero-medial part of the knee (1). It represents a distention of the gastrocnemio-semimembranosus bursa which communicates with the knee joint through a small capsular opening. The key pathogenetic role is played by a valve-type structure that allows unidirectional flow into the bursa (1). In 94% of cases BCs are secondary to intra-articular diseases: osteoarthritis, medial meniscal tear, ligament and chondral lesions (1), and inflammatory diseases (rheumatoid arthritis, seronegative and pyrophosphate arthropathy) (2). BC is often an accidental finding. Symptomatic BC typically presents with fullness and swelling (1). When the cyst breaks, it manifests with acute pain, itching and ecchymosis ("pseudothrombophlebitis syndrome") (3). Ultrasound (US) should be the first line examination as it has a very high sensitivity, but it cannot adequately visualize joint diseases (4). Magnetic resonance imaging (MRI) remains the reference standard method for the characterization of knee masses and the detection of related intra-articular pathologies (4) (Fig. 1). There are several therapeutic options: the traditional approach is to "watch and wait", while treating the underlying joint disease. Surgical and arthroscopic techniques are described in literature but both have risks associated with the presence of vessels and nerves in the popliteal region (4). US-guided non-invasive procedures are therefore catching on, with aspiration of fluid and injection of drugs aimed to avoid cyst recurrence. Intra-articular or intra-cyst corticosteroid injection is a relatively low-risk and successful procedure in patients with knee osteoarthritis (5-7). A plethora of sclerosing agents are reported in literature: ethanol, phenol, lyophilized mixture of group A *Streptococcus pyogenes*, 12.5% dextrose and morrhuate sodium and fibrin glue have all been used to sclerose para-articular cystic cavities (8-11). We prospectively compare two therapy cohorts: antibiotic (minocycline hydrochloride) and steroid (Triamcinolone acetonide).

MATERIALS AND METHODS

We performed a prospective cohort non-randomized study, enrolling 80 patients [55 men, 25 women, mean age = 63 years (44 to 73)], affected by symptomatic BCs between 2017 and 2018. All patients had low to moderate knee pain while walking, and lamented sensation of weight and fullness ("mass effect") in the knee (Table

Key words: Baker's cyst interventional, percutaneous; sclerosis; minocycline hydrochloride

Corresponding Author:
Dr. Nicola Magarelli
Institute of Radiology, Fondazione Policlinico Universitario A. Gemelli IRCCS, Catholic University of the Sacred Heart, Largo Francesco Vito 1, 00168, Rome, Italy
Tel.: +39 3382438340 - Fax: +39 0630155428
e-mail: nicolamagarelli@gmail.com

0393-974X (2019)

I). Before treatment all patients underwent an orthopedic visit to confirm that the symptoms were due to the cyst enlargement. All patients were studied with US (64) or MRI (16), both performed by a radiologist with over 10 years of experience in musculoskeletal radiology. Fourteen patients were excluded because affected by a small cyst (less than 2 cm) and other comorbidities possibly responsible for the symptoms (rheumatoid arthritis, previous traumas, severe arthrosis). Eight patients did not complete the scheduled follow-up and were not included in the final analysis. The 58 patients included in the statistical analysis were allocated without randomization for each treatment: 30 treated with cyst drainage and injection with minocycline hydrochloride [16 women, 14 men, mean age of 65yrs (48 to 79)]; 28 treated with drainage and injection with tacetonide [16 women, 12 men, mean age: 62 years (44 to 76)]. Treatment did not require any hospitalizations or one-day-care at the hospital, but only a simple ambulatory radiologic consult. Patients presented to our Hospital with radiological exams (if not performed in our center). All procedures were conducted with US guidance with the only nurse assistance.

After the skin disinfection and, where appropriate, local anesthesia (performed according to the patient's compliance with 5 ml of Lidocaine 2%), the best puncture site was selected with US. In most cases a fine needle (19G, length of 10 cm) was used, being atraumatic. In selected cases (3 patients) a bigger needle was used due to the high density of the cyst content. The US monitoring was continuous in order to spot the possibility of intracyst bleeding and the correct emptying of the fluid collection.

Patients treated with mynocicline hydrochloride, after emptying the cyst, were injected with a solution containing a dose of 3 mg of sclerotizing antibiotic per mL of drained fluid from the native cyst (for example a 20 mL cyst was treated with 60 mg of Mynocicline hydrochloride), dissolved in 3-5 ml (depending on the total quantity of drug injected) of saline water (Fig. 2 A and B).

Before treatment, the cyst volume was calculated with the ellipsoid volume formula ("length" × "width" × "depth" × 0.5233). Any pre- or post-treatment antibiotics were administered, and the only advice given was to rest after the procedure (avoiding intense physical activities) for at least 24 h. Minocycline hydrochloride was not drained after the injection but left in place inside the cyst.

In the Triamcinolone acetonide cohort (Triacort 40 mg), after completely emptying the cyst, 1 mL of drug (40 mg) was injected. In this cohort of patients the only advice given was to rest for the first 24 hours after the procedure. Observation after the procedure was 1 hour, checking for

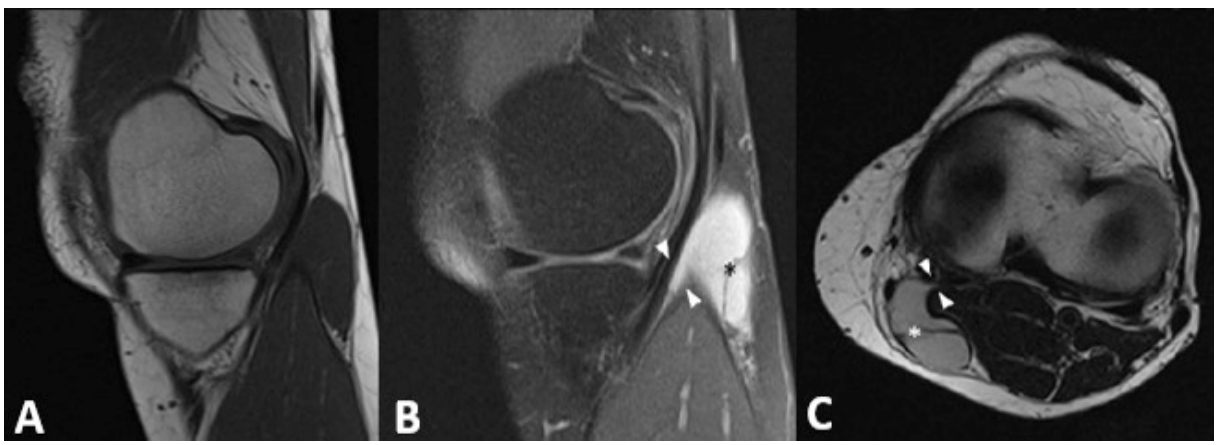

Fig. 1. *MRI sagittal spin echo-T1w (**A**), turbo spin echo-T2w Fat Sat **(B)** and axial turbo spin echo-T2w (**C**) images. Large ovular formation, which extends from the knee posteriorly between the tendons of the medial head of the gastrocnemius and the semimembranous, with low signal in T1w sequences and high signal in T2w, consisting in complicated Baker's cyst. Note the internal irregular septa (*) and the collar of the cyst (between the arrowheads) through which it is in communication with the joint cavity.*

side effects described in literature such as hypersensitivity to the active agent and/or other ingredients, moderate pain or drug leakage.

The study design included a clinical follow-up (for cases with recurring symptoms) and a radiological follow-up (persistence or recurrence of cyst formation) through US exam, the results of which were analyzed at 6 months after the treatment. Our primary end-point was a volume reduction of 40% or more than the initial volume 6 months after therapy.

Secondary end points evaluated were: VAS score reduction after treatment confronted with the initial score, cyst persistence, considered as a volume reduction <40%; and procedure duration: considering that all procedures, in both cohorts, were performed by the same radiologist.

This study was conducted according to the principles expressed in the Declaration of Helsinki. The trial protocol was approved by the ethics committee of Novara. All patients provided written informed consent for the collection of data and subsequent analysis.

Statistical analysis

For the purpose of the study we considered only patients fulfilling the overmentioned inclusion criteria. Data were analyzed using StataMP version 13.0 Windows. Patient samples were statistically analyzed at time 0, to assess the homogeneity of the sampled data and in order to find the comparable variables between the two samples. We outlined the following statistically significant variables, defined by the primary and secondary endpoints:

- treatment type/volume variability of the cyst, from t0 to t1.
- treatment type/VAS
- treatment type/number of recurrences.

Each quantitative variable was described as mean value and standard deviation. We used qualitative variables, frequency and percentages.

Statistical analysis was employed to compare the results of treatment with cortisone versus minocycline over Baker's cysts. Statistical analysis was performed with Student's *t*-test, and/or Wilcoxon test to analyze continuous variables, *chi*-squared test or Fisher exact test for dichotomous variables and/categorical variables and F text for variance analysis. Significance was attributed to values <0.05.

RESULTS

The results of this prospective study were analyzed after a clinical and radiological follow-up at 6 months after the procedure for each patient (Jan 2018 to April 2019). We excluded 8 patients who

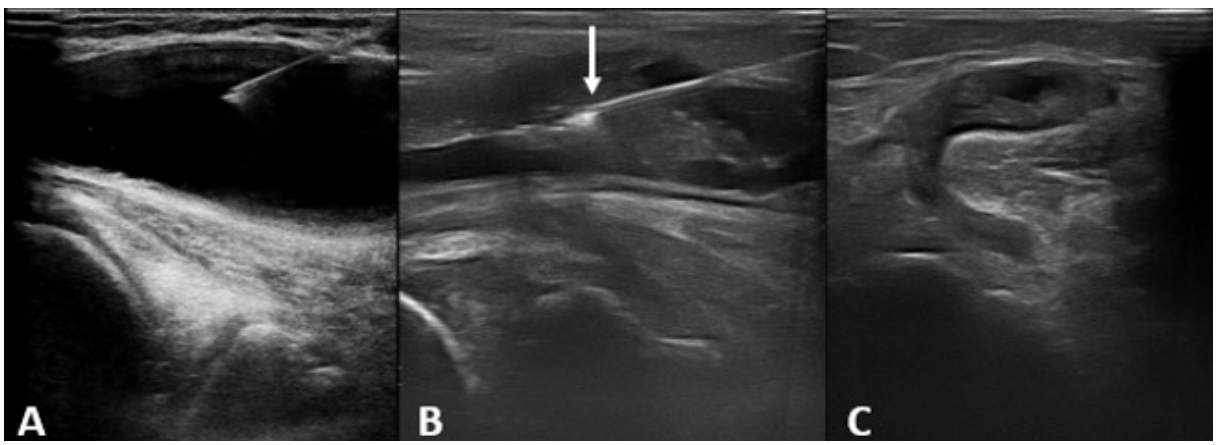

Fig. 2. *US Sagittal image of the postero-medial knee region shows a large simple Baker's cyst (**A**). Puncture of the Baker's cyst with standard length spinal needle (arrow) under real time US-guidance, fluid aspiration and injection of Minociclyne (**B**). US control study after 6 months shows complete resolution with negligible residual fluid and thickened walls (**C**).*

refused follow-up control. Some cases demonstrated persistence/recurrence of disease shortly after therapy: some of them were re-treated (3 from the antibiotic group, 2 from the steroid group), with good results, whereas some of them (2 from the antibiotic group, 1 from the steroid group) were not treated because of patient's decision or adjoining diseases. Final analysis shows two cohorts of patients with BCs, 30 of whom were treated with drainage and Minocycline hydrochloride infusion, and 28 treated with drainage and Triamcinolone acetonide injection. The procedure was well tolerated in all patients and no need of local anesthetic was necessary (except for 3 patients). During puncture and aspiration and post-procedure period no complications were documented.

In patients treated with Minocycline hydrochloride infusion, the primary endpoint (cyst volume reduction equal or >40% compared to initial volume) was obtained in 66.7% of cases with a mean reduction of volume up to 54% (Fig. 2C). In patients treated with Triamcinolone Acetonide, however, the primary endpoint was obtained in 35% of cases, in whom the reduction of volume reached 69%. Analysis of data showed a statistically significant volume reduction with therapy.

The secondary endpoint analysis showed a global reduction of VAS after treatment (with both antibiotic and cortisone) with a mean of 3.2 points. In patients treated with Minocycline hydrochloride, VAS reduction reached 3.3 as a mean, while patients treated with Triamcinolone acetonide reached

Table I. *Population distribution.*

Population		Minocycline cloridrate Tot. 30 (51.7%)	Triamcinolone acetonide Tot.28 (48.3%)	p*
Age	<50	4 (13.3%)	6 (21.4%)	0.312
	50-59	9 (30.0%)	7 (25.0%)	
	60-69	11 (36.7%)	5 (17.9%)	
	>70	6 (20.0%)	10 (35.7%)	
Gender	Female	16 (53.3%)	16 (57.1%)	0.798
	Male	14 (46.7%)	12 (42.9%)	
Local	Right	16	15	1
	Left	14	13	
VAS score	<3	12 (40.0%%)	3 (10.7%)	<0.05*
	3 4 5	7 (23.3%)	15 (53.6%)	
	>5	11 (36.7%)	10 (35.7%)	
Symptoms	Discomfort	10 (33.3%)	1 (3.5%)	<0.05*
	Physical limitation	4 (13.3%)	8 (28.6%)	
	Mild Pain	4 (13.3%)	0 (0.0%)	
	Moderate Pain	0 (0.0%)	0 (0.0%)	
	Pain at rest	0 (0.0%)	4 (14.3%)	
	Physical limitation and mild pain	6 (20.0%)	4 (14.3%)	
	Physical limitation and moderate pain	4 (13.3%)	8 (28.6%)	
	Physical limitation and pain at rest	2 (6.8%)	4 (14.3%)	

*$p<0.05$

3.1 VAS reduction. No statistically significant difference was found between the two methods as far as VAS was concerned. Analysis of persistence/recurrence of the disease after treatment was 33.3% in cases treated with Minocycline hydrochloride *versus* 64.3% in patients treated with Triamcinolone acetonide (Table II).

The last endpoint was procedural time, which showed a significantly longer duration [up to a mean of 15.5 min (12.9 to 18.1)] with Minocycline hydrochloride treatment compared to a mean of 8.6 min. (7.7 to 9.5) for the Triamcinolone acetonide treatment.

No major or minor complications were found in either cohort. More specifically, there was no local bleeding or pain during the procedure.

DISCUSSION

Besides the variability of therapeutic approaches (surgical or non-invasive), BC recurrence is a common event. It is important to establish a safe and easily reproducible therapeutic regimen. Previous retrospective studies or case reports demonstrated the efficacy of treatment with drainage and US-guided steroid or sclerosing agent injection (5-11). Short–term efficacy was evident from a clinical point of view (good results achieved the first few weeks after treatment), but the recurrence rate was high.

This is the first prospective study that compares a group submitted to aspiration and steroid injection (Triamcinolone acetonide 40 mg) to a group submitted to drainage and an antibiotic injection

Table II. *Relapses and VAS score analysis in both cohorts of atients treated with Minociclyne and steroid.*

Population		Relapse Tot. 28 (48.3%)	NO Relapse Tot.30 (51.7%)	p*
Age	<50	8 (28.6%)	2 (6.6%)	0.798
	50-59	5 (17.9%)	11 (36.7%)	
	60-69	8 (28.6%)	8 (26.7%)	
	>70	7 (25.0%)	9 (30.0%)	
Gender	Female	14 (50.0%)	18 (60.0%)	0.598
	Male	14 (50.0%)	12 (40.0%)	
Local	Right	17 (60.7%)	14 (46.7%)	0.306
	Left	11 (39.3%)	16 (53.3%)	
VAS score	<3	6 (21.4%)	9 (30.0%)	0.798
	3 4 5	11 (39.3%)	11 (36.7%)	
	>5	11 (39.3%)	10 (33.3%)	
Symptoms	Discomfort	2 (7.1%)	9 (30.0%)	<0.05*
	Physical limitation	4 (14.3%)	8 (26.7%)	
	Mild Pain	1 (3.5%)	3 (10.0%)	
	Moderate Pain	0 (0.0%)	0 (0.0%)	
	Pain at rest	3 (10.7%)	1 (3.3%)	
	Physical limitation and mild pain	7 (25.0%)	3 (10.0%)	
	Physical limitation and moderate pain	5 (17.9%)	6 (20.0%)	
	Physical limitation and pain at rest	6 (21.4%)	0 (0.0%)	

**p<0.05*

(Minocycline hydrochloride, a tetracycline family antibiotic). Minocycline hydrochloride is used as a sclerotizing agent, since its low Ph is active on endothelial cells covering the inside layer of the cyst, avoiding recurrence, especially when there is a coexistence of inflammatory joint diseases. The latter treatment has already been used in hepatic and renal cysts, showing better efficacy regarding recurrence and a better safety profile compared to alcohol, as a sclerotizing agent (12).

In our study both drugs showed an excellent safety profile (there were no major or minor complications) and efficacy in reducing the volume of cysts. Despite a longer procedural time, Minocycline hydrochloride treatment was more effective than Triamcinolone acetonide, because of a minor number of cases experiencing disease persistence or recurrence. It is unclear why in some patients the treatment is not effective: some Authors hypothesized that the presence of septal formations block the drug's diffusion; another possible cause for inefficacy might be explained by the presence of a wide communication between the cyst and the articular cavity, which may reduce the drug concentration in the cyst itself, spreading to the knee cavity. In conclusion, percutaneous sclerosis with Minocycline hydrochloride should be considered a very effective and promising non-surgical treatment for symptomatic BC.

REFERENCES

1. Herman AM, Marzo JM. Popliteal cysts: a current review. Orthopedics 2014; 37:e678-84.
2. Liao ST, Chiou CS, Chang CC. Pathology associated to the Baker's cysts: a musculoskeletal ultrasound study. Clin Rheumatol 2010; 29:1043-47.
3. Drescher MJ, Smally AJ. Thrombophlebitis and pseudothrombophlebitis in the ED. Am J Emerg Med 1997; 15:683-85.
4. Frush TJ, Noyes FR. Baker's Cyst: diagnostic and surgical considerations. Sports Health 2015; 7:359-65.
5. Köroğlu M, Callıoğlu M, Eriş HN, et al. Ultrasound guided percutaneous treatment and follow-up of Baker's cyst in knee osteoarthritis. Eur J Radiol 2012; 81:3466-71.
6. Bandinelli F, Fedi R, Generini S, et al. Longitudinal ultrasound and clinical follow-up of Baker's cysts injection with steroids in knee osteoarthritis. Clin Rheumatol 2012; 31:727-31.
7. Smith MK, Lesniak B, Baraga MG, Kaplan L, Jose J. Treatment of popliteal (Baker) cysts with ultrasound-guided aspiration, fenestration, and injection: long-term follow-up. Sports Health 2015; 7:409-14.
8. Linetsky F. Sclerotherapy for Baker's cyst. Pain Physician 2008; 11:375-76.
9. Németh P, Füzesi K. Sclerosing therapy: an alternative treatment for popliteal cyst in children. Pediatr Surg Int 1990; 5:134-35.
10. Tamai M, Kurokawa M, Hattori R. Sclerotherapy with OK-432 for Baker's cyst [in Japanese]. Japanese J Plastic Reconstructive Surg 2006; 49:693-97.
11. Shigeno Y, Harada I, Katayama S. Treatment of cystic lesions of soft tissue using fibrin sealant. Clin Orthop Relat Res 1995; (321):239-44.
12. Danza FM, Falcione M, Bordonaro V, Infante A, Paladini A, Bonomo L. Minocycline hydrochloride as a soft sclerotizing agent for symptomatic simple renal and hepatic cysts. Eur Rev Med Pharmacol Sci 2017; 21:408-15.

JOURNAL OF BIOLOGICAL REGULATORS & HOMEOSTATIC AGENTS Vol. 33, no. 6, 1927-1930 (2019)

LETTER TO THE EDITOR

IS HYALURONIDASE ABLE TO REVERSE EMBOLISM ASSOCIATED WITH HYALURONIC ACID FILLER? AN ANATOMICAL CASE STUDY

R. RAUSO[1], G. COLELLA[1], R. FRANCO[2], F. CHIRICO[1], A. RONCHI[2], F. FEDERICO[3], A. VOLPICELLI[3] and G. TARTARO[1]

[1]Maxillo-Facial Surgery Unit, University of Campania "Luigi Vanvitelli", Naples, Italy; [2]Pathological Anatomy Department, University of Campania "Luigi Vanvitelli", Naples, Italy; [3]University of Campania "Luigi Vanvitelli", Naples, Italy

Received September 17, 2019 – Accepted October 3, 2019

To the Editor,

Injectable dermal fillers generally provide excellent outcomes owing to relatively simple nonsurgical delivery, rapid results, and low costs (1). Although such fillers generally are considered safe, complications may occur. Skin necrosis is one of the most severe and feared early-occurring complications of hyaluronic acid (HA) fillers, resulting from interruption of the vascular supply to the area by direct injury of the vessel, compression of the area around the vessel, and/or obstruction of the vessel (embolization) by the filler material (1, 2). Once the HA material has entered an artery, the embolic material is commonly carried distally in the normal direction of blood flow, and progressively into smaller-sized vessels, until the material can no longer pass any further distally, which results in complete obstruction. In the absence of sufficient collateral blood supply, tissue ischemia (and eventually tissue necrosis) may result (1). If the filler had been injected at a high pressure and/or rapid rate, the embolus may paradoxically flow retrograde to the normal direction of blood flow. A large bolus, after pushing backward inside an artery into progressively larger vessels, may become "sidetracked" into other branches of the vessel. From there, filler material may be carried to distal sites through proximal vascular tributaries, creating a paradoxical ischemic area far from the original site of injection (3).

Hyaluronidase (Hyal) has been used for various purposes in clinical medicine, including dispersion of local anesthetics in retrobulbar block, hypodermoclysis, and the treatment of extravasation injuries (4). Hyal also has been effective *in vivo* for reducing the quantity of HA when aesthetic results are unsatisfactory (5). In cases of accidental intravascular injection, Hyal is generally used to break down the longer, viscous, cohesive HA chains into small segments, resulting in a dramatic decrease in viscosity, such that HA degradation products can pass through vessels and relieve vascular obstruction (6).

The goal of the present case study was to evaluate the capability of Hyal to degradate crosslinked HA that was injected into a human vessel. During a radial forearm free-flap harvesting procedure for reconstructive purposes, the authors collected a cephalic vein, filled it with HA, and soaked it in Hyal to assess the effect of this agent.

Case presentation

During harvesting of a radial forearm free flap, a 6-cm cephalic vein was collected from the left arm

Key words: hyaluronic acid; vascular impairment; hyaluronidase; dermal filler

Corresponding Author:
Prof Raffaele Rauso, MD, PhD, MSc
Maxillo-Facial Surgery Unit,
University of Campania "Luigi Vanvitelli",
Piazza L. Miraglia 2,
80138 Naples, Italy
e-mail: raffaele.rauso@unicampania.it

0393-974X (2019)

DISCLOSURE: ALL AUTHORS REPORT NO CONFLICTS OF INTEREST RELEVANT TO THIS ARTICLE.

of a patient who had provided written consent to participate in the present study. The vein was washed with saline and then filled with saline. Throughout the procedure, 3× loupe magnification was used to achieve detailed visualization. The saline-filled vein demonstrated absence of small side branches. A metallic clip was placed on one end of the vein; on the other end, a cannula was inserted and 0.5 mL of 20-mg/mL crosslinked HA filler was injected (Hyamira BASIC, APHARM s.r.l., Arona, Italy). After filling the vein with HA, a clip was placed on the other end to close the vein. Following this, 2 more metallic clips were placed, in the center of the vein, to divide it at the midpoint and obtain 2 vein specimens that each contained approximately 0.25 mL of HA. One specimen was soaked in 1.5 mL of Hyal (300 IU/mL) and the other in 1.5 mL of saline; the samples were named specimen A and specimen B, respectively.

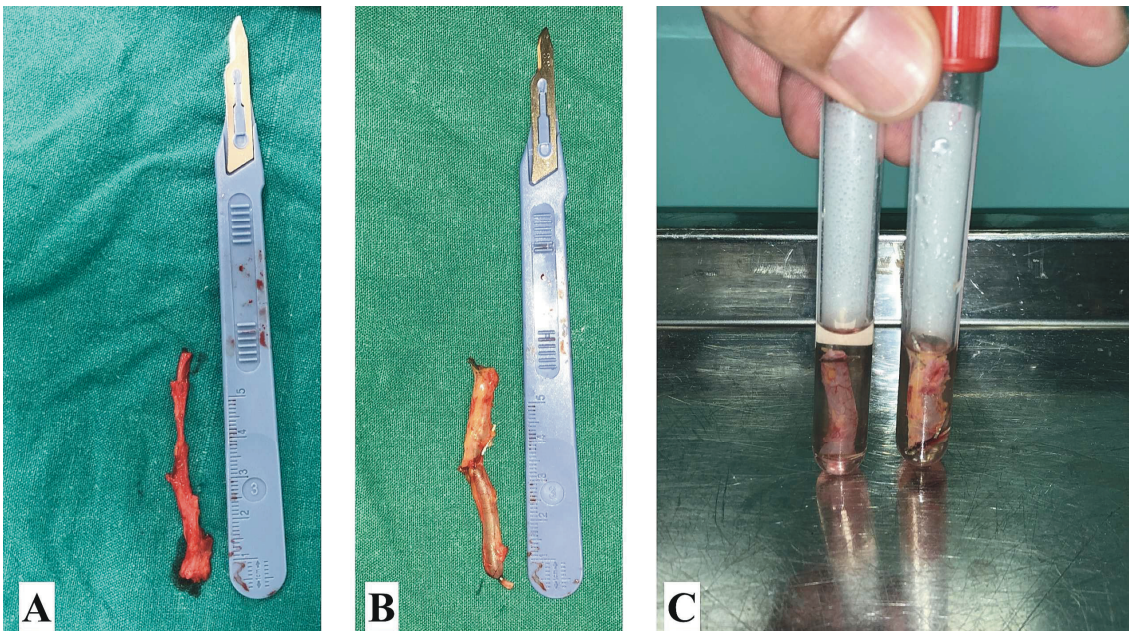

Fig. 1. ***A)*** *Cephalic vein harvested.* ***B)*** *Same vessel as in 1a, once washed and filled with HA. Metallic clips were placed at each end and in the center.* ***C)*** *The 2 samples, one containing saline and the other hyaluronidase, were sent to the Pathological Anatomy Department.*

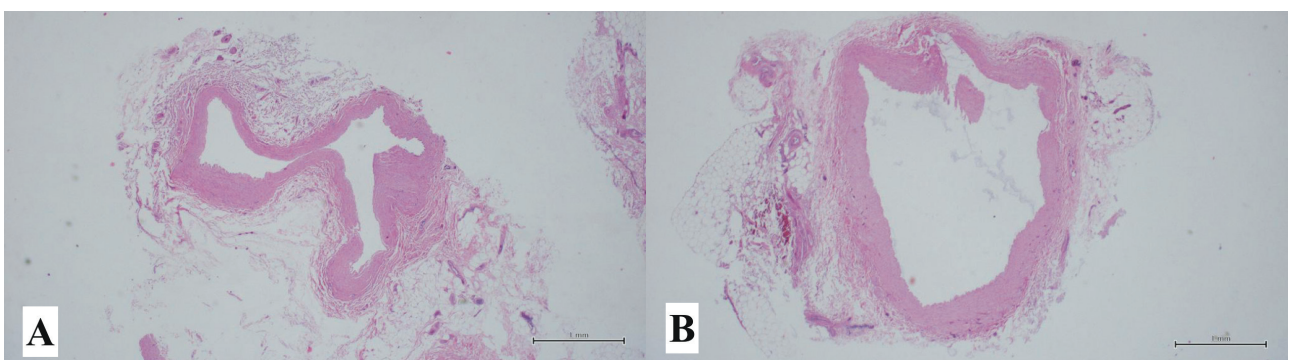

Fig. 2. *Histology of the specimens.* ***A)*** *the vein soaked in hyaluronidase;* ***B)*** *the vein soaked in saline.*

After 2 hours of soaking, specimens A and B were delivered to the Pathological Anatomy Department. The physician of that Department, who was blinded to the soaking agent used for each specimen, evaluated the amount of HA present in each specimen (Fig. 1 A-C). The metallic clips were then removed. All HA material in the vessel lumen was collected in a graduated vial and quantified. Subsequently, the vessels were cut and fixed in formalin. Paraffin-embedded sections were stained with Hematoxylin and Eosin. Semiquantitative analysis showed the presence of 0.15 mL of HA in specimen A and 0.25 mL of HA in specimen B. Histological differences between the 2 specimens were not detected, but the venous wall of specimen B (soaked in saline) appeared to have greater expansion than the wall of specimen A (Fig. 2 A,B).

DISCUSSION

Once it is evident that HA filler is blocking a vessel's blood flow, the goal is to restore circulation to the affected area so that ischemic necrosis can be prevented (7). Current strategies involve immediate use of mechanical means (massage), warm compresses and topical nitro paste (7). Injection of Hyal is another recommended strategy because it is believed to be clinically effective in reducing the ischemic lesion by enzymatically breaking down the embolus so that effective circulation can be restored (8). A 2011 study on a rabbit ear model of intra-arterial HA embolus showed that Hyal was effective in preventing ischemic necrosis of tissues when administered within 24 hours (9).

In 2014, DeLorenzi performed research similar to ours, in which he harvested facial artery and vein specimens from fresh human cadavers during a teaching session on anatomy. In his study, the specimens were analyzed 4 hours and 24 hours after immersion in Hyal. One end of the vessel was removed, and its contents were expressed, examined under loupe magnification, and photographed; this procedure was performed for both artery and vein specimens. No HA was detected in the artery or vein specimens (10). Results differed from those of the present study in that the vein soaked in Hyal by DeLorenzi showed complete reduction of HA rather than just the partial reduction that we observed. However, our study has some important differences from the work by DeLorenzi. Firstly, we used a vein collected from a living patient (not from a cadaver), which would be more likely to resemble real-world clinical practice. The capability of Hyal to work through a vein wall may differ for living patients and cadavers, although Hyal has been shown to increase vessel permeability (4). On the other hand, we used a vein instead of an artery, which may represent a limitation of the present study.

In 2017, DeLorenzi proposed a new protocol called the "new high dose pulsed hyaluronidase protocol for hyaluronic acid filler vascular events." The protocol involves administration of relatively high doses of Hyal into the ischemic tissue, repeated hourly until resolution (11). Repeated injections of Hyal are mandatory because this drug loses its effect after a few hours (12). Moreover, published literature indicates that the higher the concentration of HA, the lower its sensitivity to Hyal (13).

The present case study involved evaluating the effectiveness of Hyal injection through the vein wall in the setting of HA embolism. To the authors' knowledge, this is the first report of a vessel being harvested from a living patient for this purpose. However, there are limitations to using a vein instead of an artery and to testing only one concentration of HA filler (20 mg/mL). Regardless, this study shows that Hyal is effective for reducing the quantity of HA in a vein, but complete HA hydrolysis was not achieved (as it was by DeLorenzi) which emphasizes the importance of repeating Hyal injections in the first several hours following detection of vascular impairment.

REFERENCES

1. Bertossi D, Giampaoli G, Verner I, Pirayesh A, et al. Complications and management after a nonsurgical rhinoplasty: A literature review. Dermatol Ther 2019; 1:e12978.
2. Daines SM, Williams EF. Complication associated with injectable soft-tissue filler, a 5-year retrospective review. JAMA Facial Plast Surg 2013; 15(3):226-31.

3. Lazzeri D, Agostini T, Figus M, et al. Blindness following cosmetic injection of the face. Plast Reconstr Surg 2012; 129(4):995-1012.
4. Cavallini M, Gazzola R, Metalla M, Vaienti L. The role of hyaluronidase in the treatment of complications from hyaluronic acid dermal fillers. Aesthet Surg J 2013; 33(8):1167-74.
5. Pierre A, Levy PM. Hyaluronidase offers an efficacious treatment for inaesthetic hyaluronic acid overcorrection. J Cosmet Dermatol 2007; 6:159-62.
6. Doerfler L, Hanke CW. Arterial occlusion and necrosis following hyaluronic acid injection and a review of the literature. J Drugs Dermatol 2019; 18(6):587.
7. Goodman, GJ, Roberts S, Callan P. Experience and management of intravascular injection with facial fillers: results of a multinational survey of experienced injectors. Aesthetic Plastic Surgery 2016; 40(4):549-55.
8. Lee A, Grummer SE, Kriegel D, Marmur E. Hyaluronidase. Dermatol Surg 2010; 36(7):1071-77.
9. Kim DW, Yoon ES, Ji YH, Park SH, et al. Vascular complications of hyaluronic acid fillers and the role of hyaluronidase in management. J Plast Reconstr Aesthet Surg 2011; 64(12):1590-95.
10. DeLorenzi C. Transarterial degradation of hyaluronic acid filler by hyaluronidase. Dermatol Surg 2014; 40(8):832-41.
11. DeLorenzi C. New high dose pulsed hyaluronidase protocol for hyaluronic acid filler vascular adverse events. Aesthet Surg J 2017; 37(7):814-25.
12. Kim HJ, Kwon SB, Whang KU, Lee JS, Park YL, Lee SY. The duration of hyaluronidase and optimal timing of hyaluronic acid (HA) filler reinjection after hyaluronidase injection. Journal of Cosmetic and Laser Therapy 2018; 20(1):52-57.
13. Buhren BA, Schrumpf H, Hoff N-P, Bolke E, Hilton S, Gerber PA. Hyaluronidase: from clinical applications to molecular and cell mechanism. Eur J Med Res 2016; 21(5):1-7.

LETTER TO THE EDITOR

CROSS REACTIVITY BETWEEN RECOMBINANT PARVALBUMIN OF CARP AND COD AND RECOMBINANT GRASS MOLECULES

M. DE AMICI[1], G. CIPRANDI[2], S. CAIMMI[3], L. SACCHI[4], A. LICARI[3], F. BAROCCI[5], G. TESTA[3] and G.L. MARSEGLIA[3]

[1]Laboratory Immuno-Allergology of Clinical Chemistry and Department of Pediatrics, Foundation IRCCS Policlinic San Matteo, Pavia, Italy; [2]Allergy Clinic, Casa di Cura Villa Montallegro, Genoa, Italy; [3]Department of Pediatrics, Foundation IRCCS Policlinic San Matteo, University of Pavia, Pavia, Italy; [4]Laboratory for Biomedical Informatics "Mario Stefanelli", Department of Electrical, Computer and Biomedical Engineering, University of Pavia, Pavia, Italy; [5]Laboratory Medicine Unit, ASST Rhodense, Garbagnate Milanese, Italy

Received June 5, 2019 – Accepted October 3, 2019

To the Editor,

Pollen allergy is very common in clinical practice. Some allergenic proteins are highly conserved and are present in homologous forms that may be unrelated between them. These molecules are defined panallergens: they are responsible for IgE cross-reactivity between unrelated pollen and plant food allergen. Sensitization to panallergens might be problematic as it implicates the risk of developing multiple sensitizations. However, other molecules have an allergenic specificity and are defined as primary or "genuine" molecules (1, 2). Panallergen structures may be conserved among proteins with similar function (3). Recently, the European Academy of Allergy and clinical Immunology (EAACI) published evidence-based guidelines for Food Allergy and Anaphylaxis (4). The allergens were classified in different groups. Grass pollens, belonging to *Poaceae* family, are classified in many genera (5). There are several molecules belonging to *Phleum pratense* (Phl p) species. The different Phl p sensitization patterns depend on the geographic area. Patients sensitized to the epitopes Phl p1, Phl p 2, Phl p5, and Phl p 6 are considered primarily sensitized to *Gramineae*; whereas patients sensitized only to nCyn d 1 are sensitized to *Cynodon dactylon* or *Zea mays*; patients sensitized to Phl p 6 are sensitized to *Lolium perenne*. In clinical practice, sensitization to Phl p 5 is considered a marker for genuine grass sensitization. Phl p 7 and Phl p 12 are the main cross-reactive components: Phl p 7 is a calcium-binding protein and Phl p 12 is a profilin (6). Sensitization to Phl p 1, 2, and 5 predicts successful response to allergen immunotherapy (7).

Gad c 1 is the main allergen of cod (*Gadus callaria*) and is a heat-resistant and gastro-resistant parvalbumin. Gad c 1 is a sarcoplasmic protein belonging to the family of muscular calcium-binding proteins.

Cyp c 1 is the main allergen of carp (*Cyprinus carpio*) and is a parvalbumin. Cyp c 1 share 70% epitopic homology with cod (Gad c 1), tuna (Thu a 1), and salmon (Sal s 1) parvalbumins (8). In clinical practice, sensitization to the carp parvalbumin is detectable in over 95% of people with allergy to seafood. Therefore, Cyp c 1 sensitization is

Key words: cross-reactivity, pollen allergy-grasses, parvalbumin of carp

Corresponding Author:
Mara De Amici,
Foundation IRCCS Policlinico San Matteo,
Viale Golgi 19, 27100 Pavia, Italy
Tel.: +39 3351287476
e-mail: m.deamici@smatteo.pv.it

0393-974X (2019)

an excellent marker of seafood allergy. There is evidence that various species of fish significantly cross-react with grass pollen, especially in patients sensitized to cod parvalbumin (9). In this regard, molecular diagnostics is fundamental in poly-sensitized patients (10).

The current study investigated the possible relationship between cod/carp and grass sensitizations and the pattern of grass sensitization based on parvalbumin sensitization.

MATERIALS AND METHODS

In this study, 387 pediatric patients (228 males and 159 females, median age 11.9 years) were enrolled. The parents (or the guardians) signed an informed consent and the procedure was approved by the Ethics Committee of the Policlinico San Matteo. Thorough medical history was performed. Moreover, *in vivo* tests (skin prick test) and *in vitro* molecular analysis were performed. The subjects were included in the study if they had at least one sensitization to recombinant grass (Cyn d1, Phl 1, Phl 2, Phl 4, Phl 5, Phl 6, Phl 7, Phl 11, Phl 12) and/or cod and carp parvalbumin (Cyp c 1 and Gad c 1).

Serum IgE were measured by ImmunoCAP solid-phase allergen chip (ISAC) test according to the manufacturer's recommendations (Thermo-Fisher, Milan, Italy). The test comes in a four reaction sites glass holder, each of them of 7 x 7 mm. Each site contains 103 individual molecules immobilized on the surface of the slide in triplicate. Analysis of the results was automatically evaluated using a micro-array Image Analyser, using only 20 μL of the patient's serum. The ISAC score was reported as ISAC Standardized Units (ISU-E). Levels < 0.3 were defined as negative test results.

Statistical analysis was made using the statistical toolbox package from Matlab®. Data were described as mean, median, and 25th-75th percentile. The association of categorical variables was assessed by the Wilcoxon test. Categorical variables were compared using *Chi*-squared test. A value of $p < 0.05$ was considered statistically significant.

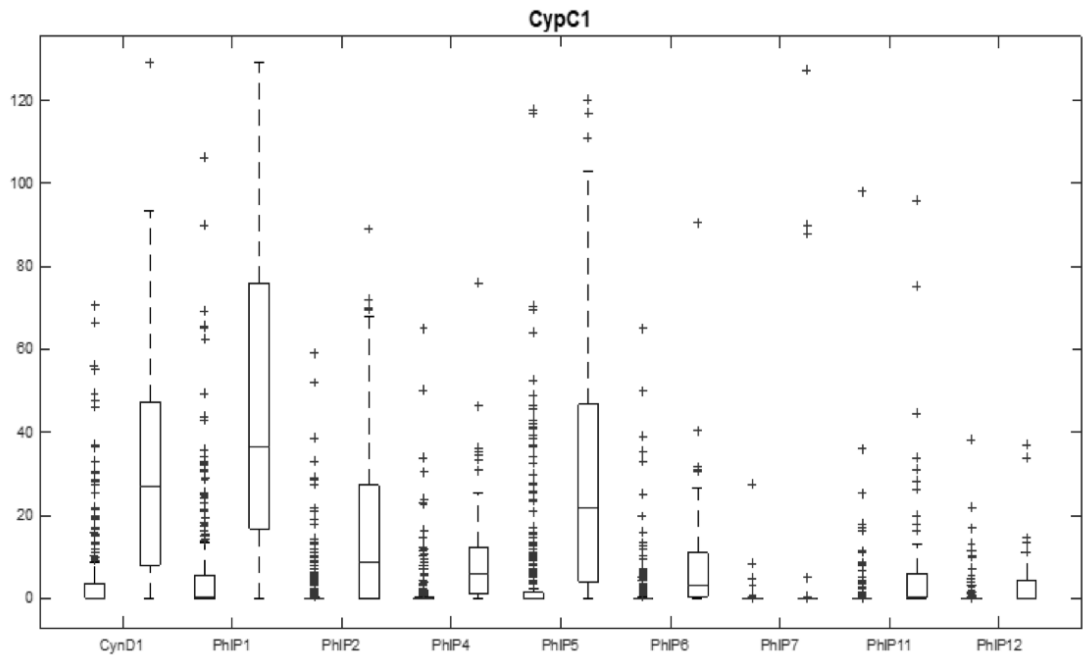

Fig. 1. *Difference in the recombinant grass molecules between the two groups of patients, with and without positivity to Cyp c 1.*

RESULTS

The patients were divided into 4 groups: 321 patients without Cyp c1 sensitization (Group 1), 66 patients sensitized to Cyp c1 (Group 2), 373 patients without Gad c 1 sensitization (Group 3), 14 patients sensitized to Gad c1 (Group 4). Groups 1 and 2 showed a significantly different profile of sensitization to the recombinant grass molecules (Fig. 1).

Groups 3 and 4 did not show any statistically significant difference in the sensibilization profile for any of the recombinant grass molecules. In detail, Wilcoxon test, performed between Group 1 and Group 2, showed significant results for all the molecules, with p-values <0.001 in all cases, except for Phl p 7 (p-value = 0.04). Considering Gad c 1 (Groups 3 and 4), we found no significant association with grass molecules. Notably, all the subjects tolerated fish. In other words, they were only sensitized and not allergic to seafood molecules.

DISCUSSION

Carp is rarely present in the Mediterranean diet, but the current globalization involves considerable variability in the diet of the population. Cross-reactivity between carp and grass allergens was found for Cyp c 1 molecule, although this phenomenon was exclusively immunological as all the subjects tolerated the seafoods to which were sensitized, i.e. they were not allergic. It would be helpful to investigate the immunological mechanisms involved in the cross-reactivity cod/carp-grass, considering the structural analogy between the grass family carp/cod parvalbumin.

In conclusion, a careful interpretation of clinical history and *in vitro* molecular analysis provides an accurate diagnosis of the causative allergen, so the patient can be correctly informed about his/her condition and advised appropriately in relation to the risk of potential cross-reactions to ensure a normal quality of life without dietary restrictions, if not justified.

ACKNOWLEDGEMENTS

The authors would thank Cristina Torre for the active collaboration in the laboratory of Immuno-allergology. IRCCS Policlinic San Matteo Pavia.

REFERENCES

1. Asero R. Looking for sensitization profiles in different populations by recombinant allergens. Int Arch Allergy Immunol. 2014; 164:106-8.
2. Muraro A, Roberts G, Worm M, et al. Anaphylaxis: guidelines from the European Academy of Allergy and Clinical Immunology. Allergy 2014; 69:1026-45.
3. Andersson K, Lidholm J. Characteristics and immunobiology of grass pollen allergens. Int Arch Allergy Immunol 2003; 130:87-107.
4. Ciprandi G, Scala E, Ariano R, et al. Phelumpratense molecular pattern across Italy. Eur Ann Allergy Clin Immunol 2017: 49:176-80.
5. Das Dores S, Chopin C, Villaume C, Fleurence J, Guéant JL. A new oligomericparvalbumin allergen of Atlantic cod (Gad m I) encoded by a gene distinct from that of Gad c I. Allergy 2002; 57(S. 72):79-83.
6. De Martino M, Novembre E, Galli L, de Marco A, Botarelli P, Marano E, Vierucci A. Allergy to different fish species in cod-allergic children: in vivo and in vitro studies. J Allergy Clin Immunol 1990; 86:909-14.
7. Werfel T, Asero R, Ballmer-Weber BK, et al. Position paper of the EAACI: food allergy due to immunological cross-reactions with common inhalant allergens. Allergy 2015; 70:1079-90.
8. Griesmeier U, Vazquez-Cortés S, Bublin M, et al. Expression levels of parvalbumins determine allergenicity of fish species. Allergy 2010; 65:191-98.
9. Mari A, Alessandri C, Bernardi ML, Ferrara R, Scala E, Zennaro D. Microarrayed allergen molecules for the diagnosis of allergic diseases. Curr Allergy Asthma Rep 2010; 10:357-64
10. Barocci F, De Amici M, Marseglia GL. Molecular evolution in food allergy diagnosis. Minerva Ped 2016; 68:374-81.

LETTER TO THE EDITOR

POTENTIAL ROLE OF TOPICAL ECTOINE FOR PREVENTION OF PEDIATRIC UPPER RESPIRATORY TRACT INFECTION: A PRELIMINARY OBSERVATIONAL STUDY

A. MOFFA[1], S. CARBONE[2], A. COSTANTINO[2], V. FIORE[1], V. RINALDI[2], P. BAPTISTA[3], M. CASSANO[1] and M. CASALE[2]

[1]Unit of Otolaryngology, University of Foggia, Foggia, Italy; [2]Unit of Otolaryngology – Integrated Therapies in Otolaryngology, Campus Bio-Medico University, Rome, Italy; [3]Unit of Otolaryngology, Clinical University of Navarra, Pamplona, Spain

Received September 14, 2019 – Accepted October 18, 2019

To the Editor,

Upper respiratory tract infections (URTIs) are very common in healthy infants and young children, are often recurrent, generally mild and often resolve spontaneously in a few days (1). URTIs commonly include pharyngotonsillitis, rhinosinusitis and otitis media. In most cases, the recurrent (r)-URTI treatment is symptomatic, but prevention is the highest challenge. Oral immunomodulator and saline nasal irrigations (SNIs) are among the different preventive strategies (2). Oral immunomodulators containing the lyophilized bacterial lysate of pathogenic bacteria of the respiratory tract stimulate immune defenses and reduce the frequency of respiratory infection. Typically, SNIs clean up the nasal cavities, removing mucus, crusts, cellular debris and various air contaminants such as common allergens and pathogens like virus and bacteria (3, 4). SNIs also improve mucociliary clearance, reduce local concentrations of pro-inflammatory mediators, such as histamine and prostaglandins, and humidify the nasal mucosa (5-7). Recently, some studies have used ectoine as coadjutant treatment for many upper airway inflammatory conditions, such as allergic rhinoconjunctivitis, rhinitis sicca and acute pharyngitis and/or laryngitis, significantly improving both the symptoms and the endoscopic evaluation (8). Ectoine is a natural extremolyte with anti-inflammatory and moisturizing properties. This molecule reduces inflammatory and oxidative stress induced by exposure to polluting dust and plays a protective and stabilizing role for many components of the cell wall (9). It binds strongly to water molecules and forms a hydrate "shield" that prevents dehydration and irreversible protein denaturation. Ectoine has versatile applications in medicine. It is used in cream for antiaging and dermatitis, in nasal spray for Acute Rhinosinusitis (ARS), and in nasal spray and eye drops for Allergic Rhinitis (AR). The aim of this study is to evaluate the effect of intranasal administration of ectoine saline solution nebulized through Spray-sol to prevent r-URTIs in children. Its effectiveness, tolerability, and safety were compared with those of normal saline inhalation solution.

MATERIALS AND METHODS

Study design

This prospective, observational study was carried out in accordance with the principles of Helsinki Declaration.

Key words: Spray-sol; single dose vial; nasal device; ectoine; upper respiratory tract infections; nebulization and children

Corresponding Author:
A. Moffa, MD.,
Unit of Otolaryngology,
University of Foggia,
71122 Foggia, Italy
Tel.: +39 388 3639207
e-mail: moffa.antonio1@gmail.com

0393-974X (2019)

All parents signed an informed consent form and were provided with the relevant information regarding the trial, which was designed as a prospective observational study. All patients were recruited at one pediatric outpatient clinic in Rome, and the same physician assessed every child at each visit. The data were collected in a strictly anonymous form and processed at the Unit of Otolaryngology – Integrated Therapies in Otolaryngology, Campus Bio-Medico University, Rome, Italy. Eligible patients were aged 3 to 10 years and were assessed by the physician for r-URTI according to the latest criteria (3). In particular, the definitions of recurrent acute otitis media and recurrent rhinosinusitis specify three episodes within 6 months or four episodes within 12 months, while a diagnosis of recurrent pharyngotonsillitis requires six episodes within 12 months. Specific exclusion criteria were anatomic sinonasal disorders, asthma, cystic fibrosis, known severe immune deficiency, and concomitant corticosteroid medication. A total of 24 children met the inclusion criteria and were randomized to receive either isotonic saline solution with single dose vials (S-group) or ectoine saline solution nebulized with a "Spray-sol" nasal device (E-group). All researchers were blinded to the saline solutions used. The study lasted 3 months, comprising an inclusion visit (V1, day 1) and 3 follow-up visits (V2, day 30; V3 day 60; V4 day 90), from January to April 2019, as the patients were enrolled between January and February. During this period, rhinologic and sleep symptoms, medication taken, number of URTI episodes, days of absence from school and compliance to the treatment were assessed. No laboratory testing was scheduled. Data were collected during the 3 follow-ups.

Study medications

Patients and parents in the E-group were instructed on the use ectoine saline solutions nebulized with Spray-sol, a commercially available product named Isonebial Kit (Steve Jones S.R.L., Sesto Fiorentino, FI, Italy) composed of: 20 single dose 5 ml vials with sodium chloride (0.9%) with the addition of ectoine, sodium phosphate, polyvinylpyrrolidone and water, a nasal device called Spray-sol and a Luer-Lock syringe of 5 ml. The saline inhalation solution contained 0.9% NaCl in water. Patients and parents in the S-group were instructed to use 5 ml of isotonic saline solutions contained in a single-dose vial, dividing the solution equally between the two nostrils. Patients applied both inhalation solutions 2 times per day for 3 consecutive months.

Patients and parents in the E-group had to use ectoine saline solutions with Spray-sol according to the following instructions:

- remove one single-dose vial and heat it between your hands before administering the solution;
- open the vial by turning the cap, connect it to the Luer-Lock syringe and aspirate the solution to be sprayed;
- fix the Luer-Lock syringe by screwing it into the appropriate Spray-sol nozzle;
- divide the contained solution equally in the syringe between the two nostrils;
- before storing the device, rinse the syringe under running water and wash Spray-sol.

Effectiveness variables

At enrollment, the following baseline parameters were obtained: sex, age, number of URTI during the 6 months preceding the first visit, story of allergies, and concomitant diseases (e.g., adenoid hypertrophy). On entry and at all subsequent visits, nasal symptoms and sleep quality were assessed by the physician using a qualitative predefined range: (i) No problem, (ii) Mild problem, (iii) Moderate problem, (iv) Serious problem). Some parameters of nasal symptoms had different scales, which are specified in Table I.

Based on the medical registers, the clinicians recorded the number of URTI episodes (rhinitis, rhinosinusitis, adenoiditis, otitis media, pharyngitis, and tonsillitis) carried out during each month of treatment. In addition, they asked the parents about the number of days of absence at school caused by these URTI. Most of the parameters (clinical status) were evaluated by physicians with the help of the parents during scheduled visits.

No restrictions were placed on the use of concomitant medication during acute illness. If necessary, both groups received standard treatment for acute illness of the upper airways occurring during the study period including: antipyretics, nasal decongestants, mucolytics and systemic antibiotics.

Tolerability and *adherence to the treatment/placebo*

Patients with their parents were evaluated for their attitude concerning tolerability and sensations reported

during and after application, using a standard 10-cm visual analogic scale (VAS) ranging from 0 (not comfortable) to 10 (very comfortable). The number of single dose vials in both groups provided was recorded in the protocol and the patients were asked to return empty bottles, which were weighed to assess compliance. Adverse events and consequent discontinuation were recorded.

Statistical analyses

All the qualitative parameters were converted to a numeric scale for evaluation purposes. The results were collected and stored in a Microsoft Excel spreadsheet. Statistical analyses were performed using the statistical package STATA version 13 (StataCorp LP, College Station, TX, USA). Graphs were prepared using GraphPad Prism 6.0 for MacOS (GraphPad, La Jolla, CA, USA). The results are expressed as mean and SD. Non-parametric Mann-Whitney test for non-paired data was used to compare different values. Our criterion for statistical significance was set at *p* values of less than 0.05 (2-tailed).

RESULTS

Of 24 patients enrolled, 23 were finally assessed (M: 12; 4.6±1.2 years). One patient (S-group) was not available for the second follow-up visit due to lower airway acute infective disease (judged as unrelated to prophylactic treatment) and was excluded from evaluation. There was no difference between the two groups according to episodes of URTIs in the six months preceding the enrolment with a mean of 4.27±1.0 URTIs (S-group) and 4.25±1.1 URTIs (E-group), respectively, (P = 0.83). Eight patients per group suffered from mild to moderate adenoid hypertrophy at the enrolment with no significant

Table I. *Rhinologic symptoms.*

	S-group	E-group	
Nasal secretions quality[a]	2.77±0.34	1.54±0.45	P < 0.001
Nasal secretions quantity[b]	2.95±0.47	1.58±0.51	P < 0.001
Nasal obstruction[c]	2.95±0.27	1.33±0.49	P < 0.001
Sore throat	2.14±0.45	1.37±0.48	P = 0.002
Dry cough	2.23±0.47	1.17±0.39	P < 0.001
Productive cough	2.77±0.52	1.33±0.39	P < 0.001
Sneezing	1.09±0.3	2.04±0.14	P = 0.74
Loss of smell/taste	1.64±0.64	1.17±0.25	P = 0.06

Results are expressed as mean±SD.

[a] *Nasal secretions quality: 1, absent; 2, serous; 3, purulent and serous; 4, purulent.*

[b] *Nasal secretions quantity: 1, absent; 2, poor; 3, moderate; 4, abundant.*

[c] *Nasal obstruction: 1, without any difficulty; 2, slightly difficult; 3, difficult; 4, impossible.*

difference between groups. The average duration of the trial was 3 months as defined in the protocol.

In several parameters, including sore throat, dry and productive cough, nasal secretions (quality and quantity), and nasal obstruction, the E-group had significantly lower occurrence and severity than the S-group (Table I). The E-group showed a significantly better sleep quality than S-group (1.07±0.11 *vs* 1.87±0.44; P < 0.001).

During the three months, URTIs episodes were significantly lower in the E-group in comparison to S-group (E-group: 0.75±0.96; S-group: 2±0.89; p = 0.003) (Fig. 1). Consequently, the E-group reported significantly fewer days of absence from school than the S-group (E-group: 1.75±3.14; S-group: 11.27±7.4 days; P < 0.001).

In terms of medication used, a higher percentage of children in the S-group than those in the E-group was using antipyretics, mucolytics, nasal decongestants, and systemic antibiotics, recording statistically significant difference only for topical nasal decongestant (Table II).

Children using the ectoine nebulized with Spray-sol reported higher significant tolerability than those treated with saline solution (E-group: 8.0±1.2; S-group: 6±1.1; p < 0.001). We did not hear substantial complaints about compliance, and good compliance seemed to be confirmed by the weight of the returned empty single-dose vials. No adverse events related to the investigated treatments were recorded in either group.

DISCUSSION

At the end of the three-month treatment period,

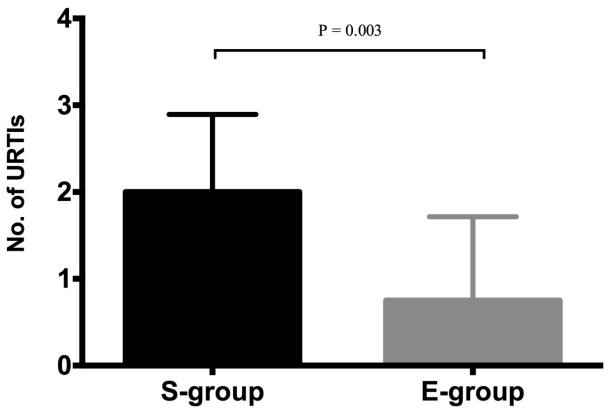

Fig. 1. *Number of URTIs during the overall treatment period (3 months).*

Table II. *Concomitant medication use.*

	S-group	E-group	
Mucolytics	0.9±3.1	0	P = 0.48
Topical decongestant	4.7±4.4	0	P = 0.001
Antipyretics	1.2±1.8	0.6±1.4	P = 0.37
Topicalcorticosteroids	2.7±3.9	0.2±0.9	P = 0.06
Systemicantibiotics	5.5±4.7	3.9±5.1	P = 0.46
Systemic anti-inflammatory	1.9±3.5	0.3±1.2	P = 0.15

Results are expressed as mean±SD.

the E-group showed a statistically significant improvement in rhinologic symptoms and sleep quality, a greater reduction in concomitant medication use and number of URTIs and days of absence from school than the S-group. Ectoine works via an entropy-driven mechanism called "preferential exclusion" or "preferential hydration" during which ectoine influences the characteristics of the "water shell" surrounding biomolecules in cell membranes. By excluding osmolytes from the direct hydrate shell of proteins and lipids, a preferential hydration of these molecules occurs, thereby stabilizing their native confirmation and making them less vulnerable to external stressors. In addition, it has been shown that ectoine limits the inflammatory cascade at the membrane level, playing a stabilizing role in receptor structures (10). In order to increase the amount of substance in nasal cavities, and to reach the most posterior and upper regions of the nasal cavities, a new nebulizer device called Spray-sol was designed. It shows low administration times (about 3-5 seconds for a complete and fine nebulization) and the ability to modulate applied forces. It is very easy to use, has a low cost, is single-patient, reusable and does not require electricity (11). Very often, children exchange nebulization with Spray-sol for a game time, as supported by the best compliance for the E-group in this study. This nasal device delivers particles with an average diameter between 10 and 20 μ, as does another common nasal device called "Rinowash" which is connected to an aerosol nebulizer with a pneumatic compressor. However, Spray-sol does not require energy, and takes few second as a spray device (12). Thanks to the small diameter of the particles and the availability to modulate the amount of substance, Spray-sol can quickly achieve not only the inferior turbinate and the floor of the nasal cavities, but also the middle meatus and nasopharynx, two anatomical regions mostly involved in child URTI. Despite these promising results, this study presents some limitations. It is necessary to consider that this was a preliminary observational study that included a relatively small number of patients in both groups, even if the results were very encouraging. In addition, our children were exposed to a relatively short period of treatment (three months); therefore, it would be interesting to investigate the preventive effects of ectoine nebulized by Spray-sol over a longer period.

CONFLICT OF INTEREST: M. Casale is the inventor but not the owner of the BI4630R/REPA/rst patent and PCT/IB2014/065121 of the Spray-sol device. All of the other authors report no conflicts of interest.

REFERENCES

1. Toivonen L, Karppinen S, Schuez-Havupalo L, et al. Burden of recurrent respiratory tract infections in children: a prospective cohort study. Pediatr Infect Dis J 2016; 35(12):e362-e369.
2. Marchisio P, Picca M, Torretta S, et al. Nasal saline irrigation in preschool children: a survey of attitudes and prescribing habits of primary care pediatricians working in northern Italy. Ital J Pediatr 2014; 15:40-47.
3. Slapak I, Skoupá J, Strnad P, Horník P. Efficacy of isotonic nasal wash (seawater) in the treatment and prevention of rhinitis in children. Arch Otolaryngol Head Neck Surg 2008; 134(1):67-74.
4. Casale M, Moffa A, Cassano M, et al. Saline nasal irrigations for chronic rhinosinusitis: From everyday practice to evidence-based medicine. An update. Immunopathol Pharmacol 2018; 32:2058738418802676.
5. Casale M, Vella P, Moffa A, et al. Hyaluronic acid and upper airway inflammation in pediatric population: A systematic review. Int J Pediatr Otorhinolaryngol 2016; 85:22-26.
6. Montella S, Cantone E, Maglione M, Iengo M, Santamaria F. Sodium hyaluronate improves quality of life and nasal endoscopy features in preschool children with upper respiratory tract infections. J Biol Regul Homeost Agents 2016; 30(1):303-8.
7. Cassano M, Russo GM, Granieri C, Cassano P. Cytofunctional changes in nasal ciliated cells in patients treated with hyaluronate after nasal surgery. Am J Rhinol Allergy 2016; 30(2):83-8.
8. Casale M, Moffa A, Carbone S, et al. Topical ectoine: A promising molecule in the upper airways inflammation - a systematic review. BioMed Res Int 2019; 7150942.
9. Sydlik U, Gallitz I, Albrecht C, Abel J, Krutmann J, Unfried K. The compatible solute ectoine protects against nanoparticle-induced neutrophilic lung

inflammation. Am J RespirCrit Care Med 2009; 180(1):29-35.

10. Tran BH, Dao VA, Bilstein A, Unfried K, Shah-Hosseini K, Mösges R. Ectoine-containing inhalation solution versus saline inhalation solution in the treatment of acute bronchitis and acute respiratory infections: a prospective, controlled, observational study. Biomed Res Int 2019; 2019:7945091.
11. Moffa A, Costantino A, Rinaldi V, et al. Nasal delivery devices: a comparative study on cadaver model. Biomed Res Int 2019; 2019:4602651.
12. Casale M, Pace A, Moffa A, Vella P, Sabatino L, Lopez MA, Salvinelli F. Post-operative nebulized sodium hyaluronate, versus spray after functional endoscopic sinus surgery for chronic rhinosinusitis. J Biol Regul Homeost Agents 2017; 31(4 Suppl 2):81-89.

JOURNAL OF BIOLOGICAL REGULATORS & HOMEOSTATIC AGENTS Vol. 33, no. 6, 1941-1944 (2019)

LETTER TO THE EDITOR

EVALUATION OF PULP NECROSIS OF A TOOTH WITH EXTENSIVE RESTORATION IN ABSENCE OF MICROLEAKAGES

F. FEMIANO, L. FEMIANO, V. GRASSIA, F. D'APUZZO, L. NUCCI and R. FEMIANO

Multidisciplinary Department of Medical-Surgical and Dental Specialties, University of Campania, Luigi Vanvitelli, Ex SUN, Naples, Italy

Received September 18, 2019 – Accepted October 20, 2019

To the Editor,

Dental caries is one of the most common problems in dentistry nowadays. In addition, recurrent or secondary dental caries has been proven to be one of the main complications following tooth restoration. The success of dental restoration depends on the total removal of the infected dentin and of good coronal and marginal seal. Unfortunately, it is not possible to be certain of the complete elimination of cariogenic microorganisms in the preparation of the cavity of a carious lesion. Several studies have shown that microorganisms left in the prepared cavity could survive for a long period of time, contributing to the increase of the bacterial load in case of a microleakage at the interface between the composite resin and the peripheral enamel edge of the cavity (1). Microleakage may be defined as the passage of saliva, bacteria, molecules or ions between a cavity wall and the restorative material applied to it. Many investigators have identified in microleakage of dental restoration, together with secondary caries, the primary cause of pulpal inflammation (2). However, the cause of pulpal inflammation and necrosis of a tooth with extensive restoration, after firstly excluding a traumatic dental injury is not always due to bacterial infection. The aseptic pulp necrosis, indeed, should not be underestimated. It may cause damage to the blood and nerve supply to the pulp before entering into the apical foramen (traumatic dental injury), or it may be the consequence of the compression of vessels in the dental pulp before the output from apical foramen (occlusal trauma). Excessive occlusal force has been postulated to cause changes in the pulp composition, such as hyperemia, pulpitis, pulp necrosis, pulp stones, and breaking of the periapical vessel (3).

Stress tolerance

Who and what can establish when mechanical stress with the consequential effort can be considered tolerable by a body? In mechanical engineering, the force can be considered tolerable in relation to the elastic properties of the object on which it acts. In dentistry, the force acting on a tooth is considered bearable when no structural damage has occurred to hard tissues and integrity of the pulp has been respected. *In vivo*, the tolerance of a tooth to stress is verifiable by the non-finding of objective clinical signs, such as fractures or cracks on the enamel surface, and, conversely, the finding of subjective signs, such as pulp positive response to cold stimuli (4).

Beyond stress tolerance

Teeth with extensive restorations, after occlusal forces of intensity well-tolerated by sound teeth, could cause responses of dental pulp with biological reactions of different severity up to aseptic necrosis.

Key words: extensive dental restoration; dental necrosis; irreversible pulpitis

Corresponding Author:
Prof. Felice Femiano,
Multidisciplinary Department
of Medical-Surgical and Dental Specialties,
University of Campania, Luigi Vanvitelli, Ex SUN,
Via De Crecchio 6, 83138 Naples, Italy
Tel./Fax: +39 081 5665500
e-mail: femiano@libero.it

0393-974X (2019)

In fact, a tooth is constantly subjected to mechanical, chemical and thermal stresses during physiological oral daily activities. If these actions are perceived as excessive by pulp receptors, a cascade of inflammatory responses occurs in the pulp complex in order to protect the pulp-dentinal organ (5). The sclerotic dentin and the secondary dentine represent the physiological reactions expressed to protect the dental pulp organ. Both types of dentine are elicited in response to physiological forces of mastication, changes in temperature or pH of the oral cavity, and in any actions considered to be of potentially harmful intensity if repeated over time, but still not capable of causing an acute injury. These reactions are identifiable in dentin at two ends of the tubule and respectively on the sub-enamel side or on pulp side along the entire perimeter of the pulp cavity with a kinetic proportional to the intensity of the event that has incised until being responsible for narrowing of the pulp cavity (6).

The pulp receives its blood supply through thin-walled arterioles entering through the apical and accessory foramina. These arterioles run longitudinally through the center of the pulp, branching out to its periphery where they form a capillary network in the subodontoblastic area. These capillaries do not enter the dentin; they drain into the venules that run alongside the arterioles and pass out through the same apical foramen (7).

The currently accepted mechanism of dentine hypersensitivity is the hydrodynamic theory firstly proposed by Brännström in 1964. According to this theory, when the exposed dentin surface is subjected to thermal, chemical, tactile, or evaporative stimuli, the fluid flow within the dentine tubules will be increased. This fluid movement within the dentine tubules causes an alteration in pressure and excites pressure-sensitive nerve receptors across the dentine. Thus, the response of the excited pulpal nerves, mainly in intradentine fibers, will depend on the intensity of stimuli in pain production. The variation of the pressure inside the tubules is correlated to the state of inflammation of the dental pulp. The essential condition for the Brännström theory for the hypersensitivity pain is the exposure of dentinal tubules and that they are evident (8).

A recent study of Linsuwanont P. et al. attributed the pain caused by thermal stresses to the mechanical deformation of the enamel, dentin, and pulp, causing the expansion of tissue fluids with the outward movement of the tubular fluid inside the dentinal tubules. This mechanism causes the distortion of the odontoblast cell membrane with excitation of pain receptors (indirect effect). The authors' explanation of their findings is that fluid movement occurred before any change in the temperature reached the dentine enamel junction, and that the pain is linked to the increase in temperature of the dentinal fluids before the structural alterations of dental hard tissues occur (9).

Mechanical insults to the coronal portion of the pulp can cause a localized acute inflammatory response. This immediate-type response involves the production of endogenous inflammatory mediators, including kinins, neuropeptides, and prostaglandins, which stimulate increases in vascular permeability, stasis, and leukocyte extravasation. Localized inflammation does not affect the state of the coronal pulp and, if it is possible to promptly intervene using non-steroidal anti-inflammatory drugs and reduce inductive stimuli, the *restitutio ad integrum* will be possible. In the most serious cases, when the stimuli are of greater intensity, in addition to the dilated vessels, a blood stasis due to slowing of the blood flow, and subsequently thrombosis, pulp necrosis and abscesses can be observed (10).

Traumatic injury

Traumatic dental injuries may inflict a variable degree of damage to the pulp and periradicular tissues, as well as to the surrounding soft tissues. The tissue damage initiates a sequence of events with the ultimate goal of healing. This sequence of events includes haemostasis, inflammation (whereby leukocytes migrate into the wound in order to protect the wound against infection and perform wound cleansing), proliferation (to close the wound defect with newly formed connective and epithelial tissue), and reorganization by remodeling. The healing process is basically the same in all tissues but it varies clinically depending on the type of tissue involved. If the inflammatory process is minimal, healing of

these tissues will take place, and this is considered to be favorable. However, if the inflammatory process is sustained by a continuous stimulus, such as the persistence of initiating stimuli or bacterial infection, no healing or an unfavorable response will take place, and an active inflammatory process will continue until the entire tooth is lost (11). Three mechanisms can induce vascular reactions during inflammation:

- an axonic reflex coming from the fibers of the trigeminal sensors;
- the release of vasoactive substances;
- inhibition of sympathetic vasoconstriction.

The proinflammatory cytokines, and in particular TGF-β, stimulate the odontoblasts to produce new dentin with a kinetic that is proportional to the stimulus received with progressive reduction of the pulp chamber. The triggered inflammatory state causes a rush of immune system cells (lymphocytes, polymorphonuclear cells, mast cells, and macrophages), and an excitation of unmyelinated fibers with a slowdown in blood flow by the opening of pulp arteriovenous shunts. This is responsible for vasal transudation with an increase in colloid-osmotic interstitial fluid. Blood stasis and vasal transudation contribute to increase pulp volume. This phase is referred to as pulp inflammatory hyperemia or reversible pulpitis because it is self-resolving with *restitutio ad integrum*, due to the arrest of inducing factors and a reduction in blood volume for reabsorption of interstitial edema induced by increased intravascular osmotic pressure with venous and lymphatic drainage. The reduction of the interstitial fluid pressure also contributes to the outflow of the transudate through the dentinal tubules with its dispersion in the oral cavity through the interprismatic spaces. This allows to preserve the vessel integrity as well as to maintain pulp vitality. The dental elements with losses of hard tissue requiring extensive adhesive restorations allow a reduced communication between the pulp area and the oral environment as a result of the considerable reduction of dentinal tubules with their adhesive seal in the outer side for restoration techniques. These anatomical conditions would make the dental element with extensive restorations less tolerant to physical stress due to the limitation of the draining effect of dentinal tubules in the case of an inflammatory response with a higher predisposition to pulpal suffering up to necrosis (12). This condition would explain why a dental element with extensive restoration exhibits a smaller pulp chamber than the neighboring dental elements (secondary dentin formation with faster kinetics), and that it is more exposed to pulp suffering with a poor clinical symptomatology until achieving aseptic necrosis for damage of pulpal vessels in the absence of a clinical history for high-intensity traumatic events.

CONCLUSIONS

The clinician must pay great attention to dental elements with extensive restorations since over time they could give negative responses to vitality tests. This complication may be mainly found in secondary caries for a micro-infiltration through the marginal gap due to a failure of the adhesive system or to a microfracture of cavity walls; in addition, it may be due to non-infectious causes, and factors not directly attributable to high intensity physical stress. The dental elements with extensive restorations do not have adequate recovery flexibility to inflammatory reactions induced by even modest physical stress for the narrowing of the pulp cavity and for a lower drainage power in presence of an inflammatory interstitial fluid.

REFERENCES

1. Jokstad A. Secondary caries and microleakage. Dent Mater 2016; 32(1):11-25.
2. Sasafuchi Y, Otsuki M, Inokoshi S, Tagami J. The effects on pulp tissue of microleakage in resin composite restorations. J Med Dent Sci 1999; 46(4):155-64
3. Lauridsen E, Hermann NV, Gerds TA, Ahrensburg SS, Kreiborg S, Andreasen JO. Combination injuries 1. The risk of pulp necrosis in permanent teeth with concussion injuries and concomitant crown fractures. Dent Traumatol 2012; 28(5):364-70
4. Shahrbaf S, vanNoort R, Mirzakouchaki B, Ghassemieh E, Martin N. Effect of the crown design and interface lute parameters on the stress-state of

a machined crown-tooth system: a finite element analysis. Dent Mater 2013;29(8):123-31.
5. Jontell M, Gunraj M, Bergenholtz G. Immunocompetent cells in the normal dental pulp. J Dent Res 1987; 66:1149-53.
6. Murray PE, Hafez AA, Smith AJ, Cox CF. Bacterial microleakage and pulp inflammation associated with various restorative materials. Dent Mater 2002; 18(6):470-78.
7. Liu Z, Zhao X, Zeng X, Xu S, Lu Y, Huang D. Effects of different resin adhesives on the microleakage in a new model with simulated subgingival condition and pulpal pressure. Dent Mater J 2018; 37(5):761-67. doi: 10.4012/dmj.2017-321.
8. Brännström M, Aström A. The hydrodynamics of the dentine; its possible relationship to dentinal pain. Int Dent J 1972; 22:219-27.
9. Linsuwanont P, Versluis A, Palamara JE, Messer HH. Thermal stimulation causes tooth deformation: a possible alternative to the hydrodynamic theory? Arch Oral Biol 2008; 53(3):261-72.
10. Tsatsas BG, Frank RM. Ultrastructure of the dentinal tubular substances near the dentino-enamel junction. Calcif Tissue Res 1972; 9:238.
11. Fan J, Caton JG. Occlusal trauma and excessive occlusal forces: Narrative review, case definitions, and diagnostic considerations. J Clin Periodontol 2018; 45(20):199-206.
12. Nakatsu S, Yoshinaga Y, Kuramoto, et al. Occlusal trauma accelerates attachment loss at the onset of experimental periodontitis in rats. J Periodontal Res 2014; 49:314-322.

JOURNAL OF BIOLOGICAL REGULATORS & HOMEOSTATIC AGENTS Vol. 33, no. 6, 1945-1947 (2019)

LETTER TO THE EDITOR

DENTAL ROOT SURFACE TREATMENT WITH ETHYLENEDIAMINETETRAACETIC ACID DOES NOT IMPROVE ENAMEL MATRIX DERIVATIVE PEPTIDE TREATMENT WITHIN INTRABONY DEFECTS: A RETROSPECTIVE STUDY

C. BERTOLDI, A. LABRIOLA and L. GENERALI

Department of Surgery, Medicine, Dentistry and Morphological Sciences with Transplant Surgery, Oncology and Regenerative Medicine Relevance, University of Modena and Reggio Emilia, Modena, Italy

Received September 25, 2019 – Accepted November 6, 2019

To the Editor,

The regenerative treatment of periodontal intraosseous defects is successfully achieved by different methodologies. Depending on the type of periodontal defect, and specifically its width and depth, the intraosseous component and the number of bony walls, it is possible to regenerate using different techniques (1, 2). Enamel matrix derivative peptide (EMP) is often used for periodontal regeneration, with the complementary treatment of exposed dental roots by ethylenediaminetetraacetic acid (EDTA) (3). All the minimally invasive surgical techniques are particularly suited to the use of EDTA and EMP, permitting a less invasive approach to the patients (1, 4). However, the role of EDTA, citric acid and other root surface modifiers is debated in periodontal regeneration (5). The aim of the present retrospective study is to compare the efficacy of EMP with or without the root conditioning by EDTA in the treatment of deep intraosseous defects using minimally invasive surgery technique.

MATERIALS AND METHODS

This retrospective study was performed at the Periodontology Unit of Dentistry and Oral-Maxillofacial Surgery of Modena University Hospital. The patients considered in the study signed informed consent detailing all procedures of the treatment, as requested by the Helsinki protocols. Subjects referred for dental and periodontal therapy were among those visited and treated from January 2002 to January 2005. The patients considered were suffering from moderate or severe chronic periodontitis. Moreover, they fulfilled the following systemic and local inclusion criteria: absence of relevant medical conditions (6), over 18 years of age, not pregnant or lactating. The full-mouth plaque score (FMPS) and the full-mouth bleeding score (FMBS), had to be maintained ≤25% (measured at 4 aspects per tooth).

Patients selected had at least one intrabony defect needing surgical treatment with the following properties: pocket depth (PD) ≥ 5mm with a radiologic intrabony component of at least 3 mm; defect angle of < 36° (1); the defects considered could not include furcations and each defect had to be mostly three-wall intraosseous defect; the patients enrolled in the study did not show bleeding on probing (BoP) in relation to the treated defect in any phase of the study.

Dental-periodontal procedures and clinical measurements

Subjects were included in the study after completion of cause-related therapy consisting

Key words: enamel matrix proteins; EDTA; periodontal pocket; minimally invasive surgical procedures; periodontal regeneration

Corresponding Author:
Prof. Carlo Bertoldi,
Dipartimento Chirurgico, Medico, Odontoiatrico e di Scienze Morfologiche con Interesse Trapiantologico, Oncologico e di Medicina Rigenerativa, Università di Modena e Reggio Emilia,
Via del Pozzo 71, 41124, Modena, Italy
Tel.: +39 0594224101 - Fax: +39 0594224795
e-mail: carlo.bertoldi@unimore.it

0393-974X (2019)

of scaling root-planing (S R-P), motivation, oral-hygiene instructions and the attainment of very high compliance and very low levels of plaque and BoP. When indicated, surgical periodontal therapy was performed on the remaining portions of the dentition of each patient before application of the regenerative treatment. The minimally invasive surgery principles and papilla preservation was always implemented on angular intraosseous defects (1). However, in the treatment group-1 (TG1) patients, the root surfaces were not previously conditioned. The treatment was performed using the only EMP (Emdogain, Biora AB, Malmö, Sweden) applied onto dental roots in treatment group-1 patients (TG1). In the treatment group-2 (TG2) patients, the root surfaces were previously conditioned by EDTA, immediately before the EMP application (PrepHgelA, Biora, AB, Malmö, Sweden).

Probing depth (PD) and gingival recession (GR) were taken at the experimental sites at baseline before the surgical treatment (T0) and after 12 months (T1). The greater values of these indices in relation to the periodontal defects were considered in this study during T0 and T1 measurements. Also, FMPS and FMBS were measured with the same timing. If BoP or plaque was found in relation to the sites considered during the study, the patient was eliminated from the study.

Statistical analysis

The 12-months primary outcomes of this study were: PD and GR comparison between TG1 and TG2. Secondary outcome was the evaluation of PD and GR changes during the study follow-up.

Statistical analysis was performed using the parametric paired *t*-test for the clinical data taken before and after the surgical treatment or the variance analysis parametric test for two groups patients at the same stage (T0 or T1), as the data were normally distributed. The χ^2 test (nominal data) was applied to compare the gender distribution between the two treated groups.

For all measured variables, the null hypothesis (H_0) of no difference among groups was rejected for a critical significance level of $p < 0.05$ (7).

RESULTS

Twenty-two patients, 10 women and 12 men, aged 29-68 years (mean ± SD – median, 51.7±11.2 – 52.5 years) fulfilled the entry criteria of the retrospective study. Eleven patients, 5 women and 6 men, aged 29-69 years (mean ± SD - median, 52.6±12.6 – 53 years) were enrolled in TG1 and eleven patients, 5 women and 6 men, aged 33-66 years (mean ± SD - median, 50.9±10.3 – 51years) were enrolled in TG2.

At baseline (T0), the full-mouth plaque and bleeding scores (FMPS and FMBS) were 16.9±2.7 – 16.7% and 6.6±2.2 – 6.3 % respectively in TG1 while resulted 15.6±2.7 – 16.1% and 8.6±3 – 8.7 % respectively in TG2. PD resulted 6.2±0.9 – 6 mm in TG1 and 6±0.8 – 6 mm in TG2. GR was 0.5±0.5 – 1 mm in TG1 and 0.6±0.5 – 1 mm in TG2. The difference between TG1 and TG2 at T0 was not statistically significant for age, FMPS, FMBS, PD, GR indices and gender, ($p>0.05$, variance analysis and χ^2 test for gender).

At the 12-month follow-up (T1), FMPS and FMBS were 15.7±3.3 – 14.8% and 5.1±2 – 4.8%, respectively, in the TG1, and were 14.3±2.2 – 13.9% and 7.4±1.8 – 8%, respectively, in the TG2. PD resulted 1.8±0.6 – 2mm in the TG1 and 1.5±0.5 – 2mm in the TG2. GR resulted 0.6±0.5 – 1mm in the TG1 and 0.7±0.6 – 1mm in the TG2. The difference between TG1 and TG2 was not statistically significant for FMPS, PD and GR ($p>0.05$) and was significant for FMBS ($p=0.01$ variance analysis test).

The baseline (T0) comparison with the end of follow-up (T1) showed a significant clinical improvement of FMPS, FMBS and PD in both TG1 and TG2 ($p<0.05$ paired *t*-test). On the contrary, GR showed a not significant increasing trend in both treatment groups ($p>0.05$ paired *t*-test).

DISCUSSION

Tissue regeneration depends on several variables, such as materials used (8), and devices used to apply these materials (6, 9, 10), but the defect properties and the surgical technique chosen to obtain the stability of the coagulum also play a fundamental role (2-4). Moreover, several

other factors could be involved in periodontal regeneration such as the patient's lifestyle and psychological profile or, directly, the wall-structure of the periodontal pocket and its self-maintaining space properties (1, 11). The study design requested stringent criteria for enrollment in the retrospective study to characterize as much as possible the periodontal defects considered. In this study, carried out on patients characterized by a good hygienic control, affected by deep and narrow periodontal defects with 2-3 bone walls and treated with an advanced model of minimally invasive surgical therapy, we found no significant differences in PD and GR between TG1 and TG2 either at baseline or 12 months after surgery. The patient-pool considered (TG1 and TG2), improved significantly their periodontal conditions in terms of FMPS, FMBS and PD. The significantly greater FMBS in TG2 than TG1 at T1 (however, it was clinically moderate in both TG1 and TG2) seems to have no clinical significance. The primary and secondary clinical outcomes of the study are comparable between the two treatment groups, both in the comparison analysis of the single phases (T0 and T1) and during the follow-up (TG1 and TG2 from T0 to T1). EDTA, citric acid and other root surface modifiers have been shown to be able to produce biologically acceptable root surface with enhanced fibrin clot adhesion, which is a critical step in the early wound healing process (12).

However, the 2-3-wall intrabony defects considered in the study are probably able to achieve enough fibrin clot adhesion and clot stabilization in order to obtain the clinical goal of the PD decrease without a substantial increase in GR that corresponds to the clinical attachment level gain. On the other hand, the EDTA treatment of dental root surfaces does not seem to be very efficient in ensuring the fibrin clot adhesion (12). However, in a different clinical setting in which the stabilization of the clot is not so well guaranteed by the morphology and the biology of the defect, the use of EDTA could have a clinical significance which was not observed in this study.

REFERENCES

1. Bertoldi C, Pellacani C, Lalla M, Consolo U, Pinti M, Cortellini P, Cossarizza A Herpes Simplex I virus impairs regenerative outcomes of periodontal regenerative therapy in intrabony defects: a pilot study. J Clin Periodontol 2012; 39:385-92.
2. Monari E, Cuoghi A, Bellei E, et al. Analysis of protein expression in periodontal pocket tissue: a preliminary study. Proteome Sci 2015; 13:1-11.
3. Amin HD, Olsen I, Knowles J, Dard M, Donos N. Interaction of enamel matrix proteins with human periodontal ligament cells. Clin Oral Investig 2016; 20:339-47.
4. Bertoldi C, Bellei E, Pellacani C, et al. Non-bacterial protein expression in periodontal pockets by proteome analysis. J Clin Periodontol 2013; 40:573-82.
5. Liu X, Mao M, Ma T. The effect of EDTA root conditioning on periodontal surgery outcome: A meta-analysis. Quintessence Int 2016; 47:833-41.
6. Consolo U, Bertoldi C, Zaffe D. Intermittent loading improves results in mandibular alveolar distraction osteogenesis. Clin Oral Implants Res 2006; 17:179-87.
7. Generali L, Cavani F, Serena V, Pettenati C, Righi E, Bertoldi C. Effect of different irrigation systems on sealer penetration into dentinal tubules. J Endod 2017; 43:652-56.
8. Bertoldi C, Zaffe D In vivo comparison of two bone substitutes in the distal femur of the rabbit. Int J Oral Maxillofac Implants 2012; 27:119-27.
9. Bertoldi C, Pradelli JM, Consolo U, Zaffe D Release of elements from retrieved maxillofacial plates and screws. J Mater Sci Mater Med 2005; 16:857-61.
10. Bertoldi C, Lusuardi D, Battarra F, Sassatelli P, Spinato S, Zaffe D. The maintenance of inserted titanium implants: in-vitro evaluation of exposed surfaces cleaned with three different instruments. Clin Oral Implants Res 2017; 28:57-63.
11. Bertoldi C, Venuta M, Guaraldi G et al. Are periodontal outcomes affected by personality patterns? A 18-month follow-up study. Acta Odontol Scand 2018; 76:48-57
12. Preeja C, Janam P, Nayar BR. Fibrin clot adhesion to root surface treated with tetracycline hydrochloride and ethylenediaminetetraacetic acid: A scanning electron microscopic study. Dent Res J 2013; 10:382-88.

LETTER TO THE EDITOR

COULD THE PRESENCE OF HEEL SPUR BE A PROGNOSTIC FACTOR FOR OUTCOME OF EXTRACORPOREAL SHOCK WAVE THERAPY FOR PLANTAR FASCIITIS?

A. NOTARNICOLA[1,2], G. MACCAGNANO[1,2], L. MORETTI[1], G. FARÌ[2,3], FP. BIANCHI[4], WORKING GROUP SWCB[5*], I. COVELLI[1,2] and B. MORETTI[1,2]

[1]Orthopedics Section, Department of Medical Sciences of Basis, Neurosciences and Organs of Sense, Faculty of Medicine and Surgery, University of Study of Bari, General Hospital, Bari, Italy; [2]Course of Motor and Sports Sciences, Department of Medical Sciences of Basis, Neurosciences and Organs of Sense, Faculty of Medicine and Surgery, University of Study of Bari, Bari, Italy; [3]Physical Medicine and Rehabilitation Section, Department of Medical Sciences of Basis, Neurosciences and Organs of Sense, Faculty of Medicine and Surgery, University of Study of Bari, General Hospital, Bari, Italy; [4]Department of Biomedical Sciences and Human Oncology, Faculty of Medicine and Surgery, University of Study of Bari, General Hospital, Bari, Italy; [5]Working Group Shock Waves Clinic of Bari

Received June 24, 2019 – Accepted November 14, 2019

To the Editor,

Plantar fasciitis affects 7-10% of adults during their lifetime (1). It is a degenerative-inflammatory disease of the plantar fascia, which is a connective fibrous structure originating from the medial tubercle of the calcaneus and that reach the metatarsal heads. The plantar fascia supports the longitudinal arch of the foot and acts as a powerful shock absorber (2). The formation of the calcaneal spur remains unknown. It is a neoformation of the lower part of the heel, from the origin of the flexor digitorum brevis muscle (3). Clinically, the spur may remain asymptomatic in 30% of population.

It is possible to recognize different types of spur according to shape (absent, horizontal, vertical, hooked) and size (<5mm, 5-10 mm,> 10 mm); neither the shape nor the dimensions may influence the clinical presentation and the response to conservative treatment (4). The treatment with shock waves (SW) is able to reach the cavitational effect due to a particular acoustic wave under the audible (<10 Hz) (5). Biological effects due to revascularization, inflammation modulation, analgesic and regenerative response? (6).

According to our observation, it remains unknown whether the concomitant plantar fasciitis with the calcaneal spur may influence the response and the efficacy of Extracorporeal Shockwave Therapy (ESWT). The aim of this study is to verify the clinical outcomes after ESWT in patients affected by plantar fasciitis with and without spur. Our hypothesis is nil, because the Authors are not able to indicate in advance whether the plantar fasciitis, associated with the spur, influences the clinical response compared to plantar fasciitis without spur.

Key words: spur; plantar fasciitis; shock waves; prognostic factors

Corresponding Author:
Angela Notarnicola, M.D. Ph.D.,
Orthopedics Section, Department of Medical Sciences of Basis, Neurosciences and Organs of Sense, Faculty of Medicine and Surgery, University of Study of Bari, General Hospital, Bari,
Piazza Giulio Cesare n.11, 70124, Bari, Italy
Tel./fax.: +39 0805592938
e-mail: angelanotarnicola@yahoo.it

0393-974X (2019)

DISCLOSURE: ALL AUTHORS REPORT NO CONFLICTS OF INTEREST RELEVANT TO THIS ARTICLE.

MATERIALS AND METHODS

For six months consecutively, 75 patients affected by plantar fasciitis, who had undergone shockwave therapy for plantar fasciitis (PF) were recruited in the study. The study model is a prospective observational cohort. The study was approved by the local Ethics Committee and written consent was obtained from the patients. The diagnosis of PF was confirmed by the criterium of tenderness extended along the plantar fascia, which increased after stretching of the plantar fascia due to passive toe dorsiflexion. All patients underwent pre-treatment lateral X-ray of the foot in order to reveal the heel spur (HS). According to the presence of HS, the study population was divided into two groups: deformity group if patients presented HS (with-HS group) concomitantly, and non-deformity group if patients did not present HS (no-HS group). The diagnosis of PF based on patient history, risk factors (pes planus, pes cavus, sedentary life style, obesity, prolonged walking/standing occupations), and physical examination (plantar fascia tenderness, heel pressure test). One doctor, with more than 6 years of experience in treatment of these diseases, performed the clinical evaluation of the study population. The heel pressure test was used for PF diagnosis. The pressure was applied to the medial plantar region of the heel. If pain was elicited, the test was accepted positive. Plantar fascia was palpated for tenderness bilaterally. Other specific tests for neuroma, nerve entrapment, and calcaneal stress fracture were performed in order to rule out these disorders. Comprehensive physical and neurological evaluations were performed in order to rule out lumbar radiculopathy and myofascial pain syndrome which are also responsible for plantar heel pain.

The following were used as inclusion criteria: plantar heel pain diagnosed as plantar fasciitis that was non-responsive to conservative treatment in the previous six months; requirement of lateral calcaneal X-ray for diagnosis and management of plantar fasciitis; patients aged 18-85 years; SW treatment carried out by our orthopedic and traumatology unit; and approval of inclusion in the study. Exclusion criteria were: history of previous ankle/heel fracture/surgery; PF rupture; neuropathy or radiculopathy associated with heel pain; secondary causes of heel pain due to other disease such as Achilles tendinitis, Morton neuroma; secondary causes of heel pain due to a chronic inflammatory disorders such as psoriasis, psoriatic arthritis, spondyloarthropathy, anklylosing spondylitis, other inflammatory spondylarthropathies, rheumatoid arthritis, or inflammatory bowel disease.

Each patient was evaluated at the start of treatment (T0), and three months (T1), 6 months (T2) and 12 months (T3) after the end of treatment. For each patient, the epidemiological variables (age, gender, presence/absence of spur), anthropometric variables (height, weight, BMI), smoking habit (yes/no), any previous treatments, site of the pathology (right/left/bilateral) were recorded using a specific form. At the different time-points, the VAS score, Ankle-Hindfoot Scale, Lower Extremity Functonal scale, and Foot function Index were recorded. The energy supplied for each of the three sessions was reported. Roles and Maudsley was measured at the last clinical evaluation. A lateral calcaneal X-ray and an echograph of the plantar fascia were analyzed at T0 for each patient enrolled.

Shock wave therapy

The ESWT was applied using a focalized shock wave device (Minilith, Storz, Switzerland) at the insertion of the plantar fascia under ultrasound guidance. The shock wave therapy was performed on the patient in the prone position and was administered once a week, for 3 sessions. All patients completed all 3 sessions. At each treatment session, 2000 pulses with an energy flux density of between 0.05 and 0.12 mJ/mm^2 and a rate of 4 pulses per second were applied (4 Hz). Gel was used between the cap and skin during the applications for ensuring conductivity. No local anesthetic was applied. A doctor, with more than 15 years experience in SW therapy, delivered the therapy. The shockwave treatment was combined with a self-administered eight-week plantar fascia-specific stretching program.

The compiled forms were put into a databases using Office Excel software and analyzed with Stata MP15 software. Continuous variables were

expressed in mean ± standard deviation and range or as median, interquartile range (IQR) and gamma, categorical variables as proportions. The Skewness and Kurtosis test was used for the distribution of continuous variables and, for those not normally distributed, a normalization model was constructed. To compare the continuous variables between groups, Student's *t*-test for paired data (parametric) was used; to compare the continuous variables between groups and times Analysis of Variance (ANOVA) for repeated measures was used; to compare the categorical variables between groups, the *chi*-squared test and Fisher exact test were used.

To evaluate the association between:

- Referred pain assessed on a VAS to T2 scale
- Ankle-Hindfoot Scale at T2
- Lower Extremity Functonal stairs to T2
- VISA-A Questionnaire at T2
- Foot function Index at T2

and the respective variable at T0, group (heel spur/no spur), gender (male/female), age, BMI, treated foot, smoke (yes/no), previous treatment (yes/no), energy delivered, for individual outcome, multivariate linear regression was used. The correlation coefficients were calculated with the indication of the 95% confidence interval (95% CI) and Student's *t*-test. A p-value <0.05 was considered significant for all tests.

Table I. *Characteristics of the sample at baseline, by group.*

Variabile	**No HS group (n=33)**	**With HS group (n=42)**	**Total (n=75)**	**Test**	**p**
Age; average±SD (range)	60.1±11.4 (34-82)	58.3±11.0 (32-81)	59.1±11.2 (32-82)	t=0.7	0.485
Females; n (%)	11 (33.3%)	21 (50.0%)	32 (42.7%)	χ^2=2.1	0.147
Height (m); average±SD (range)	1.7±0.1 (15-1.9)	1.7±91 (1.5-1.9)	1.7±0.1 (1.5-1.9)	t=1.3	0.211
Weight (kg); average ±SD (range)	76.5±10.7 (50-96)	83.5±14.5 (50-110)	80.4±13.3 (50-110)	t=2.3	0.022
BMI (kg/m2); average ±SD (range)	28.0±3.8 (21.2-36.6)	29.7±4.5 (17.9-39.7)	28.9±4.3 (17.9-39.7)	t=1.6	0.097
Treated foot; n (%) • Right • Left • bilateral	 19 (57.6%) 12 (36.4%) 2 (6.1%)	 21 (50.0%) 21 (50.0%) 0 (0.0%)	 40 (53.3%) 33 (44.0%) 2 (2.7%)	χ^2=2.1	0.170
Smoking; n (%)	6 (18.2%)	6 (14.3%)	12 (16.0%)	χ^2=0.2	0.648
Previous therapy; n (%) • rehabilitation • anti-inflammatory drug • Plantar • cortisone infiltration • Shock waves	18 (54.6%) 5 (15.2%) 3 (9.1%) 3 (9.1%) 2 (6.1%) 11 (33.3%)	30 (71.4%) 11 (26.2%) 6 (14.3%) 4 (9.5%) 3 (7.1%) 10 (23.8%)	48 (64.0%) 16 (21.3%) 9 (12.0%) 7 (9.3%) 5 (6.7%) 21 (28.0%)	χ^2=2.3 χ^2=1.3 χ^2=0.5 χ^2=0.0 χ^2=0.0 χ^2=0.8	0.131 0.274 0.723 1.000 1.000 0.362

RESULTS

The sample of the study is made up of 75 subjects, of whom 42/75 (56%) with calcaneal spur and 33/75 (44%) without calcaneal spur; the baseline characteristics of the patients, by group, are described in Table I. The ANOVA test for repeated measurements showed that there was a statistically significant differences in the comparison between variable times:

- VAS (F = 82.5; p = 0.000);
- Ankle-Hindfoot Scale (F = 81.7; p = 0.000);
- Lower Extremity Functonal scale (F = 79.8; p = 0.000);
- Foot function Index (F = 71.9; p = 0.000).

We did not observe statistically significant differences in comparison of the variables between groups and in the interaction between time and group (p> 0.05; Table II). The ANOVA analysis for repeated measures did not give evidence of significant differences in comparison of the variables between time and in the interaction between time and group (p> 0.05) and of the variable energy delivered per session between time, group and interaction between time and group (p> 0.05). Multivariate analysis showed a statistically significant difference of the VAS score at T2 with VAS score at T0 (coef. = 0.8; 95% CI = 0.4-1.1; t = 4.0; p = 0.000), with the age (coef. = 0.08; 95% CI = 0.02-0.14; t = 2.6; p = 0.011), with the right side *vs* left (coef. = 1.5; 95% CI = 0.2-2.8; t = 2.2; p = 0.029), with smoking habit (coef. = 1.9; 95% CI = 0.1-3.7 ; t = 2.1; p = 0.041). The multiple linear regression model showed an association of the Ankle-Hindfoot Scale value to T2 with the value of the same scale at T0 (coef. = 0.3; 95% CI = 0.1-0.5; t = 3.1; p = 0.0003), with age (coef. = - 0.7; 95% CI = -1.2—0.2; t = 2.9; p = 0.005), BMI (coef. = 1.3; 95% CI = 0.1 - 2.6; t = 2.2; p = 0.036) and smoking habit (coef. = - 27.2; 95% CI = -41.2—13 , 1; t = 3.9; p = 0.000). The results of the multivariate analysis showed a significant association between Lower Extremity Functonal scales at T2 and the score of the same scale at T0 (coef. = 0.5; 95% CI = 0.3-0.7; t = 4.1 ; p = 0.000), age (coef. = - 0.6; 95% CI = -1—0.2; t = 2.8; p = 0.007), smoking (coef. = - 16.7; 95% CI = -29.3—4.2; t = 2.7; p = 0.010). The Foot Function Index score at T2 is significantly associated with the value of the same scale at T0 (coef. = 0.7; 95% CI = 0.3-1.1; t = 3.6; p = 0.001), with age (coef. = 0.01; 95% CI = 0.001-0.01; t = 2.5; p = 0.014), with the side (coef. = 0.1; 95% CI = 0.003-0.2; t = 2.0; p = 0.045) and with smoking (coef0.2; 95% CI = 0.1-0.3; t = 2.0; p = 0.049). The statistical analysis of Roles and Maudsley results did not show statistical differences in the comparison between the two groups at T3 (t = 1.9; p = 0.339).

DISCUSSION

The Authors revealed a progressive improvement in all patients with tallodynia? already during the first months and at 1 year follow-up. Then they reported that in the treatment with SW, the calcaneal spur did not influence either negatively or positively the therapeutic reply. Although the SW treatment is initially applied in clinical cases of calcific metaplasia (7), according to our data we are able to confirm that this therapy should not be reserved for patients with spurs and that the clinical reply is not affected by its presence. This is consistent with the recent literature regarding the mechanisms of action of SW, from the desensitization of sensory unmyelinated fibers, to the modulation of neoangiogenesis, anti-inflammatory action and the synthesis of collagen in degenerated tissues (8).

Yalcin et al. (9) reported that ESWT was not able to reduce the calcaneal spur significantly. Indeed, in their work, they verified that it was not possible find a relationship between the clinical improvements after SW and the radiological changes (reduction of the angle of the spur in 17.6% of patients, reduction of the size of the spur in 21.3%, 1 case of spur failure).

We have to point out that our study can result potentially in conflict with a similar analysis conducted on the Achilles tendon model in the presence of Haglund's heel. Indeed, the presence of Haglund's deformity in the posterior heel may influence the response to SW, reducing the results in a statistically significant way (10). Moreover, there are new surgical strategies for the treatment of plantar fasciitis (11); the results of this clinical

Table II. *Average ± SD and variable VAS range, Ankle-Hindfoot Scale, Lower Extremity Functional scale and Foot function Index, by group and detection time.*

Time	No HS group (n=33)	With HS group (n=42)	Total (n=75)
Visual Analogue Scale			
T0	7.9±1.8 (3-10)	7.8±1.8 (3-10)	7.8±1.8 (3-10)
T1	4.8±3.3 (0-10)	4.8±2.9 (0-10)	4.7±3.1 (0-10)
T2	3.6±3.2 (0-10)	3.5±3.3 (0-10)	3.5±3.2 (0-10)
T3	3.8±3.3 (0-10)	2.9±3.5 (0-10)	3.3±3.4 (0-10)
Ankle-Hindfoot Scale			
T0	40.7±27.2 (16-85)	40.0±27.2 (16-85)	40.3±27.0 (16-85)
T1	71.5±29.8 (16-100)	73.6±25.3 (16-100)	72.7±27.2 (16-100)
T2	81.9±23.2 (16-100)	78.5±26.7 (16-100)	80.0±25.1 (16-100)
T3	78.6±25.7 (16-100)	80.5±27.9 (16-100)	79.7±26.8 (16-100)
Lower Extremity Functional scale			
T0	26.5±19.0 (0-60)	27.1±19.1 (0-60)	26.8±18.9 (0-60)
T1	48.7±25.3 (0-80)	51.2±20.4 (0-80)	50.1±22.6 (0-80)
T2	57.8±23.5 (0-100)	57.9±22.1 (0-80)	57.9±22.6 (0-100)
T3	55.4±25.5 (0-100)	61.4±23.4 (0-80)	58.8±24.3 (0-100)
Foot Function Index			
T0	71.2±14.6 (42-88)	69.5±14.5 (42-88)	70.2±14.4 (42-88)
T1	45.4±28.5 (0-88)	43.4±25.0 (0-88)	44.3±26.4 (0-88)
T2	24.9±28.2 (0-88)	33.5±28.9 (0-88)	34.1±28.4 (0-88)
Time 3	35.8±30.8 (0-88)	27.6±31.0 (0-88)	31.2±31.0 (0-88)
Roles and Maudsley			
T3	2.1±1.1 (1-4)	1.9±1.1 (1-4)	2.0±1.1 (1-4)

The times are at recruitment (T0) and at 3 (T1), 6 (T2) and 12 months (T3).

observational study show that patients affected by PF report a clinical improvement regardless of the presence or not of the calcaneal spur. Further studies will be able to verify whether there are differences due to the treatments combined with other methods (infiltrations, physical therapies, etc.).

ACKNOWLEDGEMENTS

The authors thank Brian John Molloy B.A. for language revision.

*The Working Group Shock Waves Clinic of Bari encloses P. Ribatti, C. Mennuni, S.Boodhoo, V. Pesce and S. Tafuri of the General Hospital, University of Study of Bari, Bari, Italy.

REFERENCES

1. Kirkpatrick J, Yassaie O, Mirjalili SA. The plantar calcaneal spur: a review of anatomy, histology, etiology and key associations. J Anat 2017; 230(6):743-51.
2. Petraglia F, Ramazzina I, Costantino C. Plantar fasciitis in athletes: diagnostic and treatment strategies. A systematic review. Muscles Ligaments Tendons J 2017; 7(1):107-18.
3. Weiss E. Calcaneal spurs: examining etiology using prehistoric skeletal remains to understand present day heel pain. Foot 2012; 22:125-29.
4. Ahmad J, Karim A, Daniel JN. Relationship and classification of plantar heel spurs in patients with plantar fasciitis. Foot Ankle Int 2016; 37(9)994-1000.
5. D Agostino MC, Frairia R, Romeo P, et al. Extracorporeal shockwaves as regenerative therapy in orthopedic traumatology: a narrative review from basic research to clinical practice. J Biol Regul Homeost Agents 2016; 30(2):323-32.
6. Saxena A, Fournier M, Gerdesmeyer L, Gollwitzer H. Comparison between extracorporeal shockwave therapy, placebo ESWT and endoscopic plantar fasciotomy for the treatment of chronic plantar heel pain in the athlete. Muscles Ligaments Tendons J 2013; 2(4):312-16.
7. Notarnicola A, Moretti L, Maccagnano G, Tafuri S, Moretti B. Tendonitis of the rotator cuff treated with extracorporeal shock wave therapy: radiographic monitoring to identify prognostic factors for disintegration. J Biol Regul Homeost Agent 2016; 30(4):1195-202.
8. Notarnicola A, Moretti B. The biological effects of extracorporeal shock wave therapy (eswt) on tendon tissue. Muscles Ligaments Tendons J 2012; 2(1):33-37.
9. Yalcin E, Keskin Akca A, Selcuk B, Kurtaran A, Akyuz M. Effects of extracorporal shock wave therapy on symptomatic heel spurs: a correlation between clinical outcome and radiologic changes. Rheumatol Int 2012; 32(2):3434-37.
10. Wu Z, Yao W, Chen S, Li Y Outcome of extracorporeal shock wave therapy for insertional Achilles tendinopathy with and without Haglund's deformity. Biomed Res Int 2016; 2016:6315846.
11. Oliva F, Piccirilli E, Tarantino U, Maffulli N. Percutaneous release of the plantar fascia. New surgical procedure. Muscles Ligaments Tendons J 2017; 7(2):338-40.

LETTER TO THE EDITOR

VISCOELASTIC PROPERTIES AND THERMODYNAMIC BALANCE IMPROVEMENT OF A HYALURONIC ACID HYDROGEL ENRICHED WITH PROLINE AND GLYCYNE

V. MARTINA[1], A. GALLO[1], E. TARANTINO[1], C. ESPOSITO[2], U. ZERBINATI[2], R. MOCCHI[3], D. MONTICELLI[4], T. LOTTI[5], M. TIRANT[5], N. VAN THUONG[6], R. RAUSO[7] and N. ZERBINATI[8]

[1]Department of Research and Development, MatexLab Spa, Brindisi, Italy; [2]Dermatology Department Centro Medico Polispecialistico, Pavia, Italy; [3]UB-CARE S.r.l. Spin-off University of Pavia, Italy; [4]Department of Biotechnology and Science of Life University of Insubria (Varese), Italy; [5]Department of Dermatology, University of Rome Guglielmo Marconi, Rome, Italy; [6]National Hospital of Dermatology and Venereology, Hanoi, Vietnam; [7]Maxillo Facial Surgery Unit, University of Campania "Luigi Vanvitelli", Naples Italy; [8]Department of Medicine and Surgery School of Medicine University of Insubria (Varese), Italy

Received June 14, 2019 – Accepted November 12, 2019

To the Editor,

Hyaluronic acid (HA), is a linear polysaccharide composed of repeating disaccharide units of d-glucuronic acid and N-acetyl-d-glucosamine linked by β-1-3 and β-1-4 glycosidic bonds that provides viscoelasticity to the dermis, fascia, and most fluid media in humans. HA is a primary component of the extracellular matrix (ECM) of the human connective tissues (1) which regulates and controls several tissue physiological functions *in vivo* (2) and is also present in high concentration in many specialized tissues of the human body.

HA regulates moisture, elasticity, and architecture of tissue, repairing tissue, promoting cell motility, and scavenging free radicals (3-5), thus has a very broad range of applications ranging from orthopedics to aesthetic medicine and surgery (6). The HA hydrogel evaluated in this study has been chemically modified with a crosslinking reaction made with cross-linking agents (PEGDE) based on epoxides, in a strongly basic environment with the formation of ether bonds C – O - C, which is among the most solid and, consequently, the most resistant to degradation (7).

The HA hydrogel evaluated has been enriched with two amino acids non-essential in particular glycine e and proline. Glycine e, proline and hydroxyproline contribute to 57% of total amino acids (AAs) in collagen, the largest and most abundant protein in the body. As proline is a promising and useful ingredient that improves wrinkles due to its ability to increase the elasticity of the stratum corneum, it will also be interesting to examine the additive and/or synergistic effects of proline combined with other anti-aging ingredients which function mainly in the dermis in some effective regimens. Indeed, proline, used with glycine e and leucine, protects skin from UV-damage by restoring the synthesis of HA and reducing the inhibition of elastase, and increases skin moisturization and elasticity (8). In the end, proline under stressful conditions imparts stress tolerance through maintaining cell turgor or osmotic balance, stabilizing cell membranes (9).

Key words: Neauvia, HA PEG crosslinked; proline and glycine e; viscoelastic property; thermodynamic balance

Corresponding Author:
Dr Nicola Zerbinati,
Department of Medicine and Surgery School of Medicine,
University of Insubria,
Varese, Italy
e-mail: nzerbinati@centro-medico.it

0393-974X (2019)

DISCLOSURE: ALL AUTHORS REPORT NO CONFLICTS OF INTEREST RELEVANT TO THIS ARTICLE.

MATERIALS AND METHODS

The cross-linked HA used is a hyaluronic acid hydrogel 24 mg/ml (MatexLab SPA, Brindisi, IT), which is of probiotic origin and cross-linked using PEGDE (Polyethylene glycol) diglycidyl ether). Rheological characterizations were performed on a Kinexus Instrument Rheometer (Malvern).

Sample preparation

To evaluate the variation of viscoelastic properties of HAP24 PEGde products with and without glycine e and proline (named HAP24-GLYPRO, HAP24, respectively) and only with glycine e (named HAP24-GLY), rheological tests were carried out both on the product immediately after extrusion (time 0) and after 30 min and 4 h of incubation where each sample was weighed (1 gr) and placed in contact with 500 µl of saline solution (0.9% NaCl in deionized water).

Viscoelastic properties

Rheological characterizations were performed on a Kinexus Instrument Rheometer at a temperature of 25°C. A 20-mm diameter plate was used combined with a Peltier lower plate. Before measurement, inertia and oscillatory mapping calibrations were performed. Then, samples were dropped onto the lower plate and then squeezed by the upper tool (plate). Product surplus was removed thanks to a spatula. After the gap was established, sample temperature was set to 25°C with a precision of 0.5°C.

HA hydrogel was subjected to periodic oscillation in a dynamic experiment (small amplitude frequency sweep tests) to evaluate the dependence of the viscoelastic parameters, such as the elastic and viscous moduli, *G*' and *G*'', upon the frequency. The mechanical response, expressed as shear stress τ of viscoelastic materials, is intermediate between an ideal pure elastic solid (obeying Hooke's law) and an ideal pure viscous fluid (obeying Newton's law) and, therefore, is out of phase with respect to the imposed deformation as expressed by

$$\tau = G'(\omega)\, Y_0 \sin(\omega t) + G''(\omega)\, Y_0 \cos(\omega t), \quad (1)$$

where $G'(\omega)$ is the shear storage modulus or elastic modulus and $G''(\omega)$ is the shear loss modulus or viscous modulus. *G*' gives information about the elasticity or the energy stored in the material during deformation, whereas *G*'' describes the viscous character or the energy dissipated as heat. The phase angle, δ, is equal to 90° for a purely viscous material, 0° for a pure elastic material, and $0° < \delta < 90°$ for viscoelastic materials (1, 9). The frequency range investigated was 0.1Hz–10Hz and fixed strain of 1%. In order to identify the linear viscoelastic response range of the materials, preliminary strain sweep tests were performed on the samples, at the oscillation frequency of 1 Hz and strain of 0.01-2000%. The tests were repeated at least three times on each sample. The tests were carried out at the controlled temperature of 25°C by using a thermostatic bath. In order to avoid water evaporation, the humidity of the chamber containing the samples was controlled by a humidity control accessory.

Statistical analysis

Results were obtained from three individual experiments. The results are expressed as mean ± SD.

RESULTS

The dependence of the elastic and the viscous moduli upon the amplitude strain and the oscillation frequency for the gels obtained by cross-linking of HA with PEGDE are reported. The amplitude strain spectra (Table I) shows a predominance of the elastic modulus (G') compared to the viscous modulus (G"), considered as a solid-like feature. In this way, the hyaluronic acid gel behaves as a three-dimensional network where the deformation feature is the main accommodation mode to the applied stress (Figs. 1, 2).

Moreover, the mechanical spectra (related to the frequency sweep) shows a predominance of the elastic modulus (G') compared to the viscous modulus (G") considered as a solid-like feature; indeed, the elastic modulus is one order of magnitude higher than the viscous modulus (Table II). Since G' is the modulus related to elasticity, when this value exceeds the viscous modulus (G"), which is related to flow, the material can be considered to have an associated structure and hence a yield stress. For a material to have a true yield stress then G' must exceed G" at infinitely low frequencies typical of an ideal gel, as occurred in these samples (Fig. 2).

Viscoelasticity values obtained from the amplitude strain spectra (Fig. 1) of the product containing the

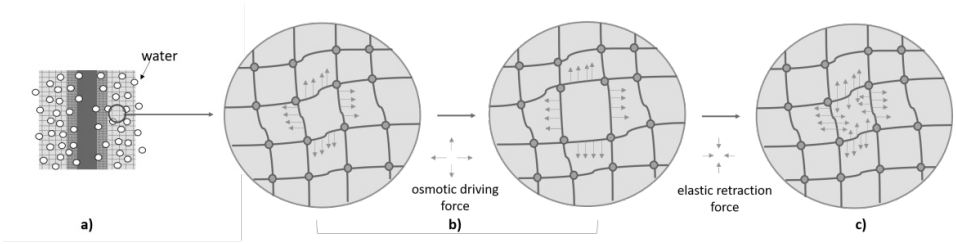

Fig. 1. ***a****) Schematic representation of the gel swelling phases,* ***b****) effect on the hydrogel of the action of osmotic force,* ***c****) effect on the hydrogel of the action of the osmotic force contrasted by the elastic network retraction force.*

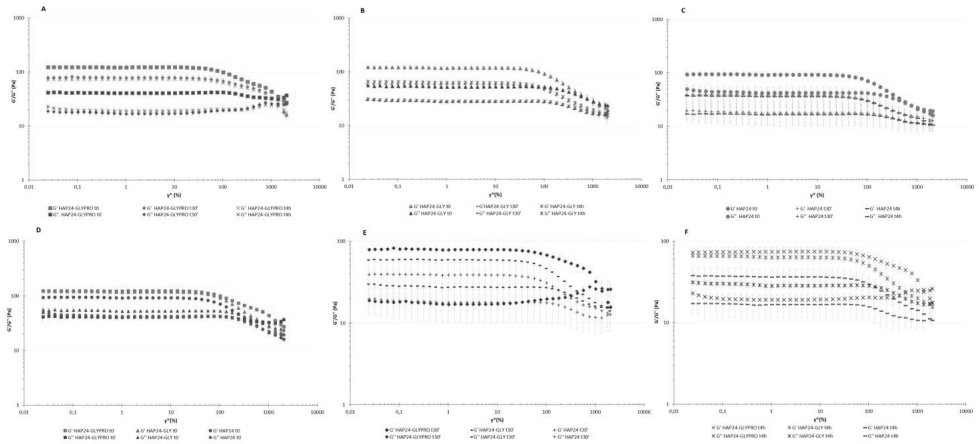

Fig. 2. *The amplitude strain spectra of samples characterized by frequency 1 Hz; stain 0.01-2000%; temperature 25°C. Viscoelastic parameters comparison of HAP24-GLYPRO at time 0, 30 min and 4 h (**A**); viscoelastic parameters comparison of HAP24-GLY at time 0, 30 min and 4 h (**B**); viscoelastic parameters comparison of HAP24 at time 0, 30 min and 4 h (**C**). Viscoelastic parameters comparison at time 0 of HAP24-GLYPRO, HAP24-GLY, HAP24 (**D**); viscoelastic parameters comparison at time 30 min of HAP24-GLYPRO, HAP24-GLY, HAP24 (**E**); viscoelastic parameters comparison at time 4 h of HAP24-GLYPRO, HAP24-GLY, HAP24 (**F**).*

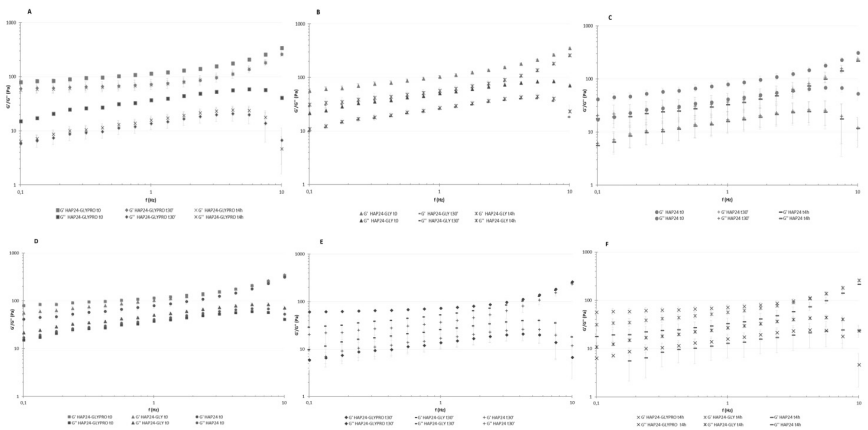

Fig. 3. *Mechanical spectra of samples characterized by frequency 0.1-10 Hz; stain 1%; temperature 25°C. Viscoelastic parameters comparison of HAP24-GLYPRO at time 0, 30 min and 4 h (**A**); viscoelastic parameters comparison of HAP24-GLY at time 0, 30 min and 4 h (**B**); viscoelastic parameters comparison of HAP24 at time 0, 30 min and 4 h (**C**). Viscoelastic parameters comparison at time 0 of HAP24-GLYPRO, HAP24-GLY, HAP24 (**D**); viscoelastic parameters comparison at time 30 min of Intense Lips, HAP24-GLYPRO, HAP24-GLY, HAP24 (**E**); viscoelastic parameters comparison at time 4 h of HAP24-GLYPRO, HAP24-GLY, HAP24 (**F**).*

Table I. *Viscoelastic parameters values of the gels at strain of 10%.*

	G' [Pa]			G" [Pa]			Ƞ* [Pa s]			δ [°]		
	Time 0	Time 30'	Time 4h	Time 0	Time 30'	Time 4h	Time 0	Time 30'	Time 4h	Time 0	Time 30'	Time 4h
HAP24-GLYPRO	125±3	80±9	76±9	42±2	17±3	19±2	21±1	13±2	12±2	18±1	12±1	15±2
HAP24-GLY	121±6	60±6	64±6	54±1	28±2	29±3	21±1	10±1	11±1	24±1	25±1	24±2
HAP24	94±13	39±16	37±9	43±7	18±8	17±6	16±3	7±3	6±2	25±1	25±1	24±3

Table II. *Viscoelastic parameters values of the gels at frequency of 0.5 Hz.*

	G' [Pa]			G" [Pa]			Ƞ* [Pa s]			δ [°]		
	Time 0	Time 30'	Time 4h	Time 0	Time 30'	Time 4h	Time 0	Time 30'	Time 4h	Time 0	Time 30'	Time 4h
HAP24-GLYPRO	105±6	69±15	67±8	32±1	11±3	13±3	31±2	20±4	19±2	17±1	10±1	11±2
HAP24-GLY	89±5	45±6	48±7	43±2	22±2	23±2	28±2	14±2	15±2	26±2	26±1	26±4
HAP24	68±9	31±14	28±8	35±6	14±6	13±5	21±3	10±4	9±3	27±1	24±1	25±6

amino acids glycine e and proline (HAP24-GLYPRO) and tested at different incubation times showed a gradual reduction of the elastic modulus observed over time (G ‘) and viscous module (G”). This phenomenon is due to the process of diffusion of water within the polymeric network of the gel following the contact of the hydrogel with the physiological solution (Fig 1).

In the product containing only glycine e (HAP24-GLY), the value of the elastic modulus (G ‘) at time zero remained unchanged (121 Pa) compared to that obtained in the product HAP24-GLYPRO (125 Pa), but the values of the viscous module (G “) tended to shrink slightly from a value of 54 to 42 Pa in the sample HAP24-GLY and HAP24-GLYPRO, respectively. This causes a reduction in the distance between the two modules, elastic and viscous, with a consequent liquid-like behavior of the HAP24-GLY gel in respect to the HAP24-GLYPRO gel; in fact, also the values of the δ angle went from a value of 24 to 18 degrees in the sample HAP24-GLY and HAP24-GLYPRO, respectively (Table I).

Moreover, in the HAP24-GLY product, due to the absence of proline, when subjected to swelling, a drastic reduction of the elastic modulus (G ‘) was observed (60 and 64 Pa at 30 min and 4 h of incubation, respectively), compared to the HAP24-GLYPRO product (80 and 76 Pa at 30 min and 4 h of incubation, respectively). These data are also confirmed by the significant increase in the values of the δ angle of the HAP24-GLY sample (25 and 24 Pa at 30 min and 4 h of incubation respectively) compared to the HAP24-GLYPRO sample (12 and 15 Pa at 30 m and 4 h of incubation, respectively) due to the increase in the liquid-like component.

The study of the viscoelastic behavior of the product hyaluronic acid hydrogel 24 mg/ml cross-linked with PEGde in the presence and absence of the amino acid glycine e and proline analyzed for the mechanical spectra (Fig. 2, Table II), related to the frequency sweep, highlighted a similar trend to the one previously described for the amplitude strain spectra.

DISCUSSION

The rheological response is due to the contributions of PEG cross-links for the presence of physical and chemical bonds crosslinks such as electrostatic interactions, hydrogen bonds and also some topological interactions among the HA macromolecules. Moreover, PEG cross-links bring about a reduction of the intrinsic mobility of the polymer chains with a predominance of the material elastic behavior (G’ > G’’). The ability of cross-linked HA to absorb water arises from hydrophilic functional groups attached to the polymer backbone

while their resistance to dissolution arises from cross-links between network chains. Water inside the hydrogel allows free diffusion of some solute molecules, while the polymer serves as a matrix to hold water together (10) (Fig. 3). Results of previous studies and from this one demonstrate that proline is able to regulate the water diffusion process inside the hydrogel, preventing an excessive swelling of the gel itself (11). Proline is one of the several small molecules classified as an osmolyte or an osmoprotectant. This osmolyte helps mitigate water stress and balance turgor pressure during stress (12). Finally, as our results clearly show, in the absence of proline and glycine (HAP24) in the product, the value of the elastic modulus (G ‘) already at time zero is drastically reduced (94 Pa) and decreases steadily after 30 min (39 Pa) and 4 h (37 Pa) compared to the G ‘values of the HAP24-GLY. This shows that glycine e also plays an important role in the control of cell volume and osmoregulation as it keeps the structure of the hydrogel constant and prevents uncontrolled swelling. The results obtained show that the addition of two amino acids osmolytes, proline and glycine e, in the Neauvia formulation ensures a better control of the hydrogel swelling capacity in the post-implant phase. At the same time, the proline and glycine e guarantee hydration and gives softness to the skin tissue, acting as humectant and emollient, respectively. All these factors lead to their choice for the stabilization of the structure of the hydrogel, especially in terms of viscoelastic properties and thermodynamic balance.

REFERENCES

1. Borzacchiello A, Russo L, Malle BM, Schwach-Abdellaoui K, Ambrosio L. Hyaluronic acid based hydrogels for regenerative medicine pplications. Biomed Res Int 2015; 11:217-18.
2. Borzacchiello A, Mayol L, Ramires PA, Pastorello A, Di Bartolo C, Ambrosio L, Milella E. Structural and rheological characterization of hyaluronic acid-based scaffolds for adipose tissue engineering Biomaterials. Epub 2007; 28:4399-408.
3. Hsu MF, Chiang BH. Stimulating effects of Bacillus subtilis natto-fermented Radix astragali on hyaluronic acid production in human skin cells. J Ethnopharm 2009;125:474-81.
4. Wen KC, Lin SP, Yu CP, Chiang HM. Comparison of Puerariae Radix and its hydrolysate on stimulation of hyaluronic acid production in NHEK cells. Am J Chin Med 2010; 38:143-55.
5. Park JI, Lee JE, Shin HJ, Song S, Lee WK, Hwang JS. Oral administration of glycine e and leucine dipeptides improves skin hydration and elasticity in UVB-irradiated hairless mice. Biomol Ther 2017; 25:528-34.
6. Kablik J, Monheit GD, Yu L, Chang G, Gershkovich J. Comparative physical properties of hyaluronic acid dermal fillers. Dermatol Sur 2009; 35:302-12.
7. Zerbinati N, Lotti T, Monticelli D, et al. In vitro evaluation of the sensitivity of a hyaluronic acid PEG cross-linked to bovine testes hyaluronidase. Mac J Med Sci. In Special Issue: Global Dermatology 2018; 2.
8. Kawashima M, Yokose U, Hachiya A, et al. Improvement of crow’s feet lines by topical Application of 1-cabamimidoyl-L-proline (CLP). Eur J Dermatol 2013; 23:195-201.
9. Ghorbanpour M, Khaltabadi FAM, Hadian J. Potential toxicity of nano-graphene oxide on callus cell of Plantago major L under polyethylene glycol-induced dehydration. Ecotox and Envl Safety 2018; 148:910-922.
10. D’Errico G, de Lellis M, Mangiapia G, et al. Structural and mechanical properties of UV-photo-cross-linked poly (N-vinyl- 2-pyrrolidone) hydrogels. Biomacro 2008; 9:231-40.
11. Inbar E, Schlisselberg D, Grotemeyer M, Rentsch D, Zilberstein D. A versatile proline/alanine transporter in the unicellular pathogen Leishmania donovani regulates amino acid homoeostasis and osmotic stress responses. Biochem J 2013; 449:555-66.
12. Liang X, Zhang L, Natarajan SK, Becker D. F. Proline mechanisms of stress survival. Antioxid Redox Signal 2013; 19:998-1011.

LETTER TO THE EDITOR

GENITOURINARY SYNDROME OF MENOPAUSE AND THE ROLE OF BIOSTIMULATION WITH NON-CROSS-LINKED INJECTABLE HYALURONIC ACID PLUS CALCIUM HYDROXYAPATITE

IP. GONZÁLEZ[1], G. LEIBASCHOFF[2], C. ESPOSITO[3], G. CIPOLLA[3], A. BADER[4], T. LOTTI[5], M. TIRANT[5], N. VAN THUONG[6], M. RAMO ABDULKADER[7], R. RAUSO[8], D. SERAFIN[9], A. VOJVODIC[10] and N. ZERBINATI[11]

[1]Urogynecology Unit, University Hospital San Jorge Pereira, Pereira, Colombia; [2]Department of Gynecology and Obstetrics, University of Buenos Aires, Buenos Aires, Argentina; [3]Dermatology Department, Centro Medico Polispecialistico, Pavia, Italy; [4]OB&GYN. European Society of Aesthetic Gynaecology "ESAG" London, United Kingdom;[5]Department of Dermatology, University of Rome Guglielmo Marconi, Rome, Italy; [6]National Hospital of Dermatology and Venereology, Hanoi, Vietnam; [7]Sharjah International Holistic Health Centre, Sharjah, United Arab Emirates; [8]Maxillo-Facial Surgery Unit, University of Campania "Luigi Vanvitelli", Caserta, Italy; [9]Department of Aesthetic and Reconstructive Gynecology, Multispecialised Medical Center, Gliwice, Poland; [10]Department of Dermatology and Venereology, Military Medical Academy, Belgrade, Serbia; [11]Department of Medicine and Surgery, School of Medicine, University of Insubria, Varese, Italy

Received June 14, 2019 – Accepted November 14, 2019

To the Editor,

Genitourinary Syndrome of Menopause (GMS) (1) includes a wide range of urogynaecology symptoms, such as dryness, irritation, itching, burning and dyspareunia, and is caused by estrogen depletion associated with the aging process. In GMS, the progression of vulvovaginal atrophy (VVA) ends with either hyalinization of connective tissues or loss of vaginal elasticity and function and consequent dryness that leads to dyspareunia and a reduction of sexual activity (2).

Even if the mechanisms involved are multi-factorial, it has been observed that stress urinary incontinence (SUI) is related to menopause due to a decrease in collagen and modification of its composition. Pharmacological options in the restoration of connective tissue aging-dependent changes can be preventive, restitutive, curative and palliative. Recitative treatments are defined as procedures aimed at restoring metabolism and function of connective tissue, the most important of which is bio-stimulation activating fibroblast anabolic functions, and particularly enhancing type III collagen, elastin and hyaluronic acid production from their precursors. Thus, in urogenital functional restoration, bio-stimulation could be considered as an innovative approach according to the principles of antiaging medicine. However, few studies support hyaluronic acid (HA) application during a simple outpatient procedure as possible therapeutic strategy (3). HA has a low potential risk for immunogenic reactions and shows no tissue or species antigenicity.

The aim of this double-blind randomized controlled clinical and histological study is to evaluate the efficacy of a treatment protocol based on the injection of a HA plus calcium hydroxyapatite in vaginal walls, based on filler propriety to activate collagen and promote elastin restoration at molecular level, improving vaginal epithelium thickness, elasticity, lubrication and function such as secretion and absorption.

Key words: genitourinary; menopause; vulvovaginal atrophy

Corresponding Author:
Dr Nicola Zerbinati,
Department of Medicine and Surgery School of Medicine,
University of Insubria (Varese), Italy
e-mail: nzerbinati@centro-medico.it

0393-974X (2019)

MATERIALS AND METHODS

The goal of this study was to evaluate the efficacy of a treatment protocol based on the injection of a non-cross linked hyaluronic acid (at a concentration of18 mg/ml) plus calcium hydroxyapatite in the lateral vaginal walls to activate collagen and promote elastin restoration at a molecular level, improving vaginal functions such as secretion, absorption, elasticity, lubrication and epithelium thickness, achieving a reduction in the symptoms related to the GSM, with no complications, side effects, local reactions or systemic complications for the patient.

A double-blind randomized controlled clinical trial was conducted from October 2017 to March 2018 at the Urogynecology Unit, San Jorge University Hospital, Pereira, Colombia. This study included 20 volunteer postmenopausal women who presented genitourinary symptoms related to GSM in the previous 24 months, such as SUI or mixed urinary incontinence detected by the International Consultation on Incontinence Questionnaire-Urinary Incontinence Short Form (ICIQ UI SF), or vaginal symptoms evaluated by the Vaginal Health Index (VHI) (4). Sexual function was evaluated using the Female Sexual Function Index (FSFI) score.

Exclusion criteria were patients not adequately classified, previous gynecological surgery, recurrent lower urinary tract infection, BMI > 35, cognitive or psychiatric disorders, pelvic floor dysfunction and pelvic organ prolapse > 2 according to the Pelvic Organ Prolapse Quantification System (POP-Q).

The demographic and clinical data of the study population are shown in Table I. All patients included in the study provided written informed consent and the procedure was compliant with the principles of the declaration of Helsinki, Belmont Report, Council for International Organizations of Medical Sciences rules, GPC/ICH and 008430 resolution of the Colombian government established on 4th October, 1993.

The 20 volunteer patients enrolled in this study were randomized prospectively in a 3-month follow-up into two groups:

- 10 patients in the Treatment Group (TG), were injected with not cross-linked hyaluronic acid (NCLHA) plus calcium hydroxyapatite in vaginal walls.
- 10 patients in the Control Group (CG) were injected with saline solution in vaginal walls.

The product is a sterile, pyrogen-free gel of NCLH, containing 18 mg/ml of pure HA, enriched with 0.01% of calcium hydroxyapatite (CaHA) plus Glycine and L Proline (Neauvia Hydro Deluxe, Matex Lab SA, Switzerland). For the randomization process, patients with similar urogenital symptoms were allocated into the two groups; the study was performed by two investigators and the treatment protocol was performed by the main investigator. The injection was performed in the lateral vagina wall, around the urethra-vesical junction, with a 27G/37mm disposable blunt microcannula. The procedure was made through the fan technique, and a quantity of 2 ml of the product was injected on each side.

Vaginal biopsies were obtained before the injections and after 3 months. The vaginal samples were sent for basic and special histological studies performed by a blinded pathologist in order to demonstrate vulvar and vaginal trophic changes after the treatment protocol. Two kinds of stains were used**,** Haematoxylin and Eosin (H&E**)** and modified Masson's trichrome. With the H&E, the nucleus and parts of the cytoplasm that contained ribonucleic acid were stained blue, while the rest of the cytoplasm were stained in pink because most of the proteins in the cytoplasm are basic, and eosin binds to those proteins thus staining them in pink. In wound healing, collagen fibers play a dominant role in maintaining structural integrity. The Modified Masson's trichrome was modified according to Kiernan. Stains were primarily used to show collagen and muscle in normal tissue, this stain is also used to distinguish collagen from muscle, to demonstrate an increased collagen deposition in tissue or to indicate fibrotic changes.

The primary endpoint of this study was a clinical assessment of changes related to vaginal tropism. The evaluation was made through clinical examination, change of scores in the VHI, and FSFI referred to desire, arousal, lubrication, orgasm and satisfaction. The secondary endpoint of the study was to assess the reduction of the symptoms related to the GSM, through the evaluation of ICIQ UI SF and the treatment satisfaction score after that was evaluated with a visual analog scale (VAS) from baseline conditions to the end of the treatment protocol.

Statistical analysis was performed using SPSS 11.5.1 software (SPSS, Chicago, Illinois. USA). The following quantitative variables were evaluated: mean, median,

and standard deviation in both groups. *Chi*-squared and Fisher's exact test were used to evaluate categorical variables of patients between the two groups (education level, marital status and parity).

RESULTS

The two groups were considered homogenous regardless of socio-demographic and clinical

Table I. *Demographic and clinical data of the patients.*

	Control Group (CG)n=10	**Treatment Group (CG)n=10**
Age (Years) SD	58.1 (±3.77)	57.9 (±3.22)
BMI (Kg/m2) SD	28.05 (±1.27)	28.35 (±1.55)
Parity SD	3.0 (±0,8)	2.7 (±0.8)
Marital Status %		
Married	60.0	50.0
Single	40.0	50.0
Education Degree %		
Illiterate	0	0
High School	67.3	60.3
University	32.7	39.7
CLINICAL CHARACTERISTICS		
Anterior Pelvic Organ Prolapse %		
Stage 0	0	0
Stage I	82.31	17.69
Stage II	42.33	57.67
Stage III	0	0
Mode of Delivery %		
Vaginal	40.7	59.3
Forceps	3.12	4.10
Cesarean Section	56.18	36.6
Urinary Incontinence		
Presence	83.33	83.33
No presence	16.7	16.7

Table II. *FSFI score at baseline and 12 weeks after the injection of NCLHA plus calcium hydroxyapatite (TG) or saline solution (CG), expressed as mean value SD.*

FSFI Domains	Desire	Arousal	Lubrication	Orgasm	Satisfaction	Pain
Baseline TG	2.5±1.2	3.1±1.6	3.8±1.7	3.5±1.6	4.4±1.3	3.8±1.9
12-Week Follow up TG	3.4±1.1	3.9±1.3	4.3±1.7	4.2±1.6	4.7±1.6	4.7±1.7
p	(p<0.01)	(p<0.01)	(p<0.01)	(p<0.01)	(p<0.01)	(p<0.01)
Baseline CG	2.6±0.9	2.1±0.7	1.2±0.4	1.8±0.4	2.8±0.4	3±0.4
12-Week Follow up CG	2.4±0.6	2.3±0.6	1.2±0.4	1.8±0.4	2.7±0.4	2.7±0.4

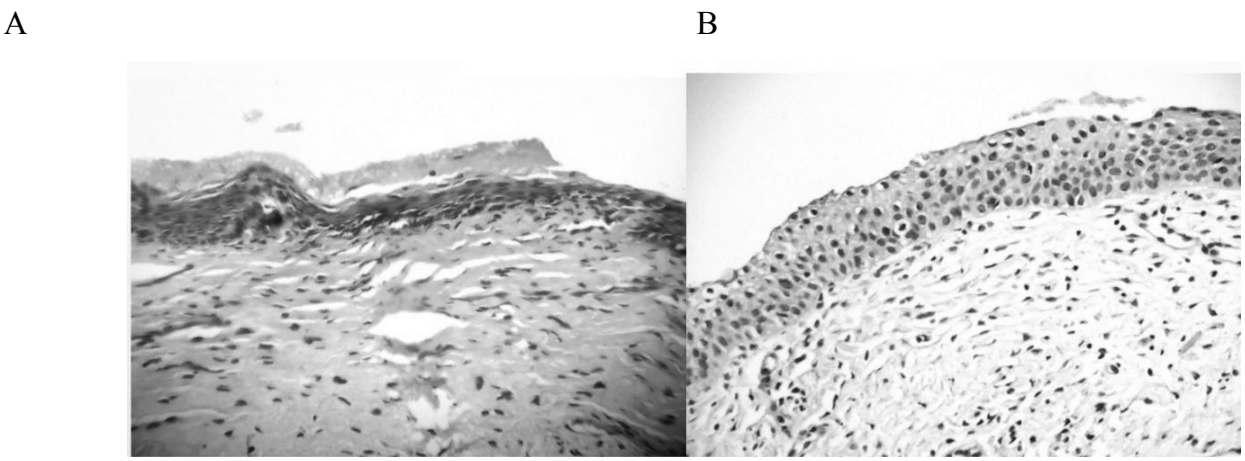

Fig. 1. *(H&E stain). Vaginal sample. Pre-treatment (**A**) and 3 months after the injection of NCLHA + CaHa (**B**). Before the treatment the epithelium of the vagina appeared flattened, atrophic, with few cell layers, small cells and dense stroma, while 3 months after the treatment with NCLHA plus CaHa, the epithelium of the vagina appeared thicker, with many cell layers, with stroma growth, enriched by many fibroblasts.*

variables. Between control and treatment group patients, no drop out during the study was recorded.

Urinary incontinence was detected in 80% of the patients (n=16) with stress component as a predominant symptom. Dyspareunia improvement was greater in the TG than in the CG. According to the VAS, the mean value in the TG at baseline was 6±1 while at the 12-week follow-up it was 3.65±0.79; the mean value in the CG was 5.6±1.2 while at the 12-week follow-up was 5.55±0.86. The VHI score in TG improved from baseline from 12.6±1.8 to 17.7±0.64 at the 12-week follow-up; meanwhile in CG, VHI values did not show any differences from 11.9±1.1 at baseline to 11.3±0.78 at the 12-week follow-up.

A B

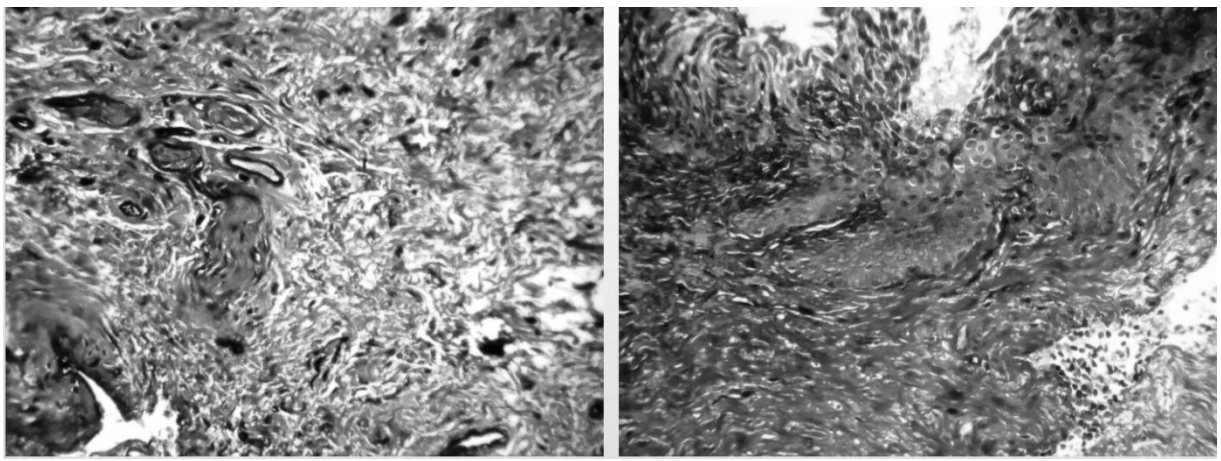

Fig. 2. *Modified Masson's trichrome stain vaginal sample. Pre-treatment (**A**) and 3 months after the injection of NCLHA + CaHa (**B**). Before the treatment the stroma appeared relatively dense with disorganized collagen, while 3 months after the injection protocol with NCLHA plus CaHA the epithelium appeared constituted by several layers of cells, and in the lamina propria an increase of collagen was clearly observable.*

ICIQ UI SF, used to evaluate urinary incontinence symptoms, showed a significant improvement in the TG at the end of the treatment protocol, the mean value was 14±2.2 at baseline and to 9.5±1.7 at the 12-week follow-up; the ICIQ UI SF did not improve in the CG, the mean value was 13.5±2.2 at baseline and 13.6±1.9 at the 12-week follow-up.

Sexual function, evaluated using FSFI score, showed an important improvement in the TG in all the points assessed: desire, arousal, lubrication, orgasm, satisfaction and pain, meanwhile the FSFI score did not show relevant differences in the CG. The results are shown in Table II.

Clinical evaluation according to the pre and post-operative pictures showed a significant improvement in the quality and tropism of the vaginal mucosa in all the TG. The histological evaluation of the samples from the patients in the TG demonstrated a significant improvement in the appearance of the epithelium. The results are shown in Figs. 1 and 2. Data analysis demonstrated an important clinical and histological improvement from baseline in all points assed in TG, while the patients in CG did not have any relevant clinical or histological improvement. No complications, side effects, local reactions or systemic complications were reported in either the TG or CG.

DISCUSSION

In the skin, the action of the CaHa in combination with or without HA scaffold is well described in literature (5, 6). Our results indicate a robust statistical significance of the improvements of symptoms, both objectively, by the use of the VHI, ICIQ UI ST, and subjectively, with a VAS of symptoms, 3 months after treatment in the treatment group. Clinical examination showed an important improvement in vaginal mucosa quality and tropism in all TG patients referring to FSFS, ICQ-SF, VAS scores and by pre- and post-operative pictures analysis. All TG patients reported an improvement in the sexual function and have also shown an improvement in urinary incontinence symptoms. A comprehensive analysis of VAS and VHI data showed how treatment satisfaction was greater in the TG compared to the CG. Moreover, important histological changes were demonstrated by the blinded pathologist in all the samples in the TG. Histological and histochemical

studies showed a significant recovery in the vaginal tissue (epithelium and stroma), and these changes appear to be related to the bio-simulative effect of NCLHA plus CaHA.

The injection of NCLHA plus CaHA in the anterior third of the vagina wall showed the ability to activate collagen and elastin production at a molecular level, restoring all the vaginal functions, such as secretion, absorption, elasticity and lubrication, as well as improving the vaginal epithelium thickness. Furthermore, once the thickness of the vaginal epithelium is re-established at the level of the anterior vaginal wall, the coaptative mechanism of the urethra is restored, and this causes a subjective and objective improvement in urinary incontinence. Moreover, also the application at the level of vulva allows to recover its shape and function which is altered in the GSM.

Treatment with NCLHA plus CaHA is affordable, safe, well tolerated and can offer patients important improvements in vaginal tropism and intrinsic and extrinsic continence mechanisms. Longer follow-up and a larger co-hort should be included in further well-designed studies in order to corroborate our findings.

REFERENCES

1. Portman DJ, Gass MLS. Vulvovaginal Atrophy Terminology Consensus Conference Panel. GSM: new terminology for vulvovaginal atrophy from the International Society for the Study of Women's Sexual Health and the North American Menopause Society. Menopause, New York, 2014; 21:1063-68.
2. Kingsberg SA, Wysocki S, Magnus L, Krychman ML. Vulvar and vaginal atrophy in postmenopausal women: findings from the REVIVE (REal Women's VIews of Treatment Options for Menopausal Vaginal ChangEs) survey. J Sex Med 2013; 10:1790-99.
3. Quaranta L, Ottolina J, Parma M, et al. An alternative approach for the treatment of vaginal atrophy. Minerva Ginecol 2014; 66(4):377-81.
4. Bachmann G, Phillips N. Dyspareunia: including this diagnosis in chronic pain reporting. Menopause. New York, 2016; 23(1):1-2.
5. Zerbinati N, D'Este E, Parodi PC, Calligaro A. Microscopic and ultrastructural evidences in human skin following calcium hydroxylapatite filler treatment. Arch Dermatol Res 2017; 309:389-96.
6. Zerbinati N, Calligaro A. Calcium hydroxylapatite treatment of human skin: evidence of collagen turnover through picrosirius red staining and circularly polarized microscopy. Clin Cosmet Investig Dermatol 2018; 11:29-35.

LETTER TO THE EDITOR

PEGYLATED HYALURONIC ACID FILLER ENRICHED WITH CALCIUM HYDROXYAPATITE TREATMENT OF HUMAN SKIN: COLLAGEN RENEWAL DEMONSTRATED THROUGH MORPHOMETRIC COMPUTERIZED ANALYSIS

N. ZERBINATI[1], R. RAUSO[2], M. PROTASONI[1], E. D'ESTE[3], C. ESPOSITO[3], T. LOTTI[4], M. TIRANT[4], N. VAN THUONG[5], R. MOCCHI[6], U. ZERBINATI[3], A. VOJVODIC[7] and A. CALLIGARO[8]

[1]Department of Surgical and Morphological Sciences, University of Insubria (Varese), Italy; [2]Maxillo Facial Surgery Unit, University of Campania "Luigi Vanvitelli", Naples; [3]Dermatology Department Centro Medico Polispecialistico, Pavia, Italy; [4]Department of Dermatology, University of Rome Guglielmo Marconi, Rome, Italy; [5]National Hospital of Dermatology and Venereology, Hanoi, Vietnam; [6]UB-CARE S.r.l. Spin-off University of Pavia, Italy; [7]Department of Dermatology and Venereology, Military Medical Academy, Belgrade, Serbia; [8]Department of Public Health, Experimental and Forensic Medicine, Unit of Histology and Embryology, University of Pavia, Italy

Received June 14, 2019 – Accepted November 15, 2019

To the Editor,

Functional fibroblast collapse is the most important factor of the extracellular matrix modifications of the connective tissue of aged skin (1). The progressive decreasing of the natural process of synthesis and renewal of extracellular matrix components, such as collagen and hyaluronic acid of the ground substance, constitutes the main cause of the loss of support, elasticity and hydration of the skin in older individuals, with the consequent appearance of lines and wrinkles. The use of implant materials such as gel-based on cross-linked hyaluronic acid were introduced and used with promising success. Due to the appreciated filling properties and immunological compatibility, hyaluronic acid-based fillers in dermatology and aesthetic medicine are today widely used for the restoration of lost volumes and the correction of wrinkles.

Thanks to technological achievements, a PEGylated HA-CaHA filler (Stimulate®, MatexLab SA, Lugano, Switzerland) has been recently introduced as a biocompatible, injectable filler for facial soft-tissue augmentation and wrinkle correction, with well described crosslinking properties (2) and characterized by interesting rheological and filling properties, which seems to offer considerable advantages in terms of biosafety and collagen stimulation (3).

In mammalian tissues, collagen molecules are ordered in a parallel orientation, providing a natural birefringence. This optical property is enhanced by Picrosirius red dye, a selective histochemical stain for collagen, due to a dye molecule alignment parallel to the axis of each collagen molecule constituting elementary collagen microfibrils. When viewed under polarized light, Picrosirius red stained collagenic structures change in colour depending on the size, type and the three-dimensional organization

Key words: PEGylated hyaluronic acid; calcium hydroxylapatite; neocollagenesis; Picrosirius red; circularly polarized light microscopy; Neauvia Stimulate®

Corresponding Author:
Dr Nicola Zerbinati,
Department of Medicine
and Surgery School of Medicine,
University of Insubria,
Varese, Italy
e-mail: nzerbinati@centro-medico.it

0393-974X (2019)

DISCLOSURE: ALL AUTHORS REPORT NO CONFLICTS OF INTEREST RELEVANT TO THIS ARTICLE.

of collagen molecules (4-6).

The current study used Picrosirius red in combination with circularly polarized light microscopy to examine the effects of PEGylated HA-CaHA filler treatment on the molecular organization of collagen, which is closely related to a possible stimulation of fibroblasts. In our histological preparations, the observed colour due to the birefringence is depending by the type of collagen, permitting the identification of newly formed collagen (4, 6).

MATERIALS AND METHODS

Five women scheduled for redundant abdominal skin removal received subdermal injection of a small volume (1 ml) of PEGylated HA-CaHA 1% filler (NEAUVIA Stimulate®) 2 months before surgery using a 25-gauge, 1-inch sharp needle and controlled slow withdrawal of the syringe. At the time of surgery, two specimens were obtained from the surgically excised skin, one 1 cm apart from the injection site, and another from an untreated zone at a distance of 10 cm to serve as a control. The study was conducted in accordance with the ethical principles that had their origin in the Declaration of Helsinki and all subjects provided written informed consent.

Biopsy specimens were fixed by direct immersion in a 4% paraformaldehyde/phosphate buffer solution for 24 h and then processed for light microscopy by dehydration, embedded in paraffin, and sectioned. The 5-µm thick sections were stained with hematoxylin and eosin (Merck, Darmstadt, Germany) to facilitate localization of the injected areas in the skin. Adjacent sections, with the same 5-µm thickness for all samples (control and treated), were stained with Picrosirius red dye solution 0.1% (Sirius red F3B, Sigma-Aldrich, St Louis, MO, USA) in a saturated aqueous solution of picric acid for 1 h, in the same staining solution and for the same length of time. To identify mature and newly-formed collagen, and therefore highlight possible regeneration/renewal of the connective tissue, a Zeiss Axioplan microscope (Carl Zeiss, Oberkochen, Germany) equipped with suitable circularly polarizing (in the condensor stage of the microscope) and analyzer (in the microscope tube above the objective lens) filters, was used. The filters were aligned so that the background in the field of view was as dark as possible. Morphometric computerized analysis of biopsy specimens from PEGylated HA-CaHA-treated and control tissues was performed using ImageJ software version 1.49h (Waine Rasband, National Institutes of

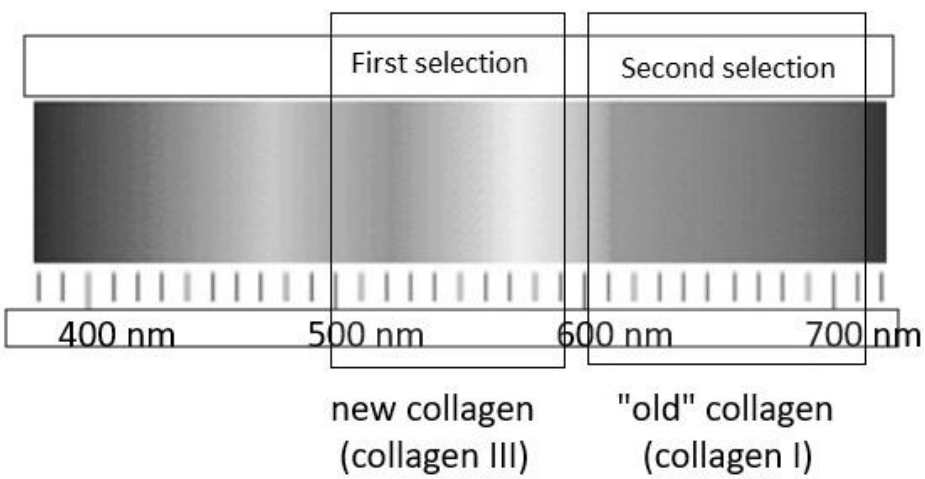

Fig. 1. *Two bands selected for segmentation of images as Fig. 2a (control) and Fig. 2d (following PEGylated HA-CaHA treatment). The second selection identifies the mature, stabilized, 'old' collagen fibers, the first one identifies the newly-formed fibers following stimulation of fibroblasts by PEGylated HA-CaHA treatment.*

Health, Bethesda, USA) on microscopic digital images recorded with a Nikon DS-Fi2 high definition 5-megapixel color CCD camera head (Nikon, Tokyo, Japan).

RESULTS

The original images of tissue sections acquired by circularly polarized light microscopy from untreated (control) and PEGylated HA-CaHA filler-treated skin (two months after injection) are respectively illustrated in Fig. 2, a and d. Pixel signals from both control and treated areas, which were extracted from the images and underwent morphometric analysis, permitted to provide a quantitative evaluation of the newly-formed collagen, representative of the regenerating effects of HA-CaHA filler treatment. Following the HA-CaHA filler treatment, the proportion of thin fibers formed by newly-formed collagen (type III) increased significantly ($p<0.01$) relative to the proportion of the thick mature old collagen (type I) fibers. In contrast, the collagen content of the control tissue consisted almost exclusively of thick mature collagen type I fibers. The comparative results are presented in Fig. 3.

DISCUSSION

Our results complement the findings from previous studies using HA-CaHA-based fillers (7-11) and demonstrate that PEGylated HA-CaHA significantly stimulates the formation of new collagen type III fibers. The association of Picrosirius red staining with

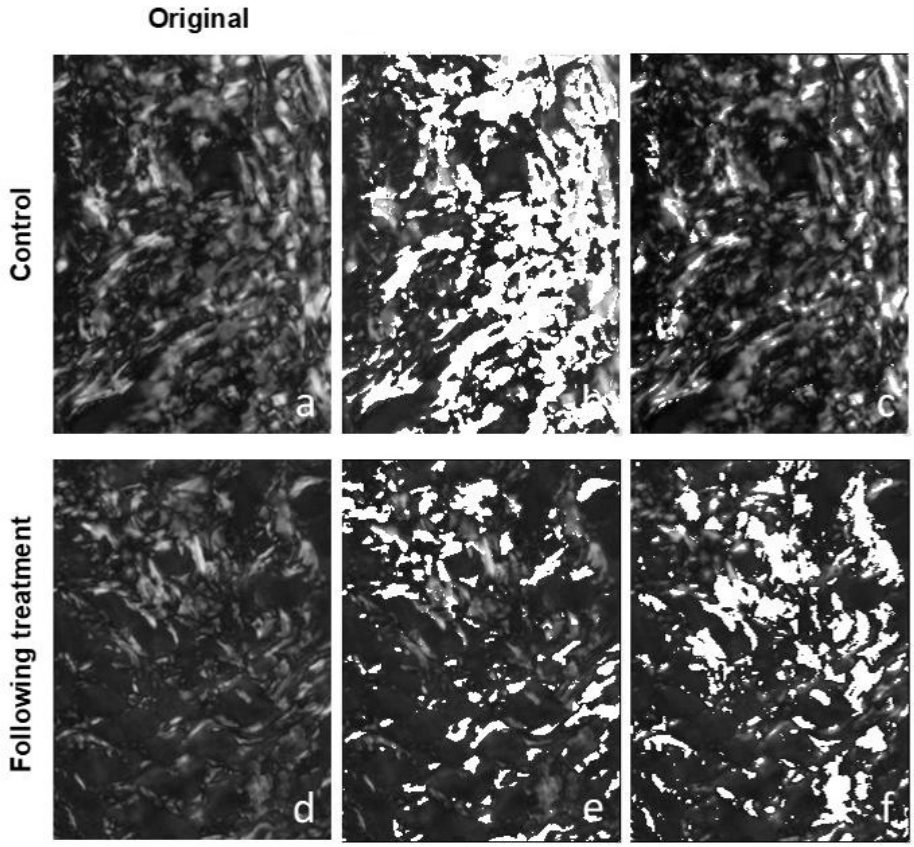

Fig. 2. *Histological subdermal sections stained with picrosirius red, observed under the microscope equipped with circularly polarized light.* ***a****) Control.* ***d****) Two months following pegylated HA-caha injection. Computerized image analysis was performed for both a) control and d) pegylated HA-caha-treated areas using imagej software (NIH).* ***a*** *and* ***d****) original photomicrographs of histological sections stained with Picrosirius red.* ***b*** *and* ***e****): segmentation of images a and d;* ***c*** *and* ***f****) segmentation of images a and d.*

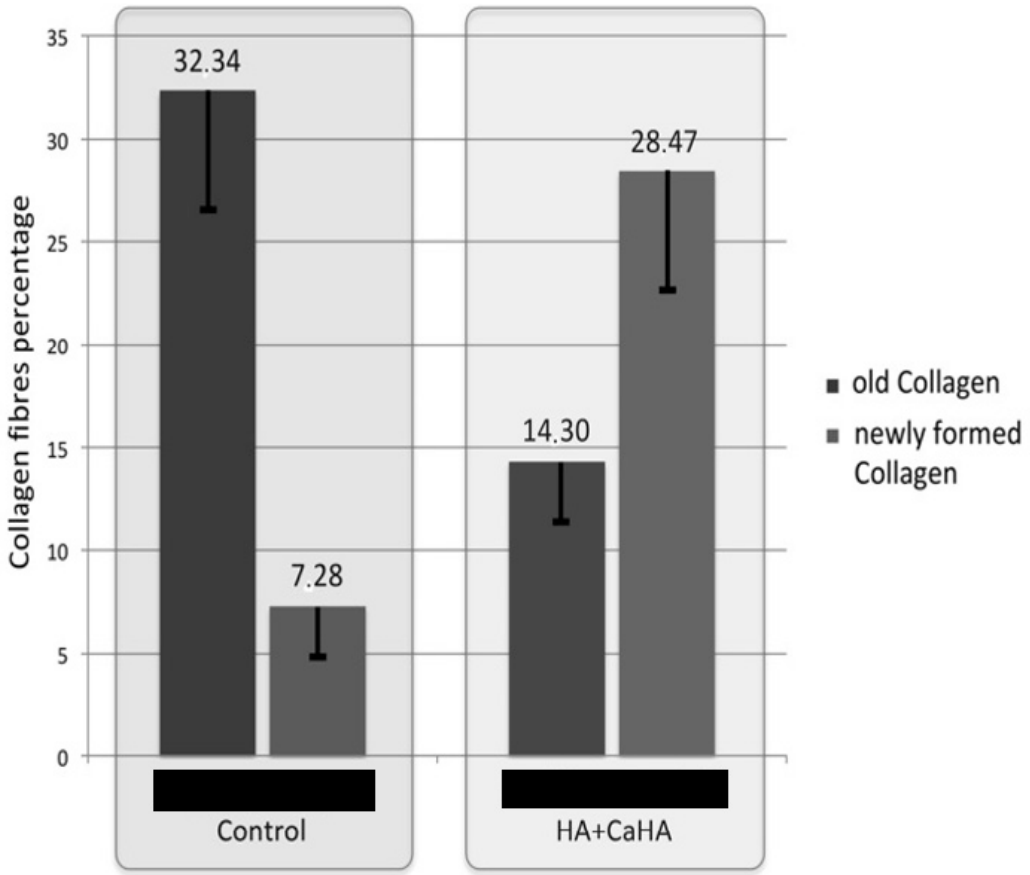

Fig. 3. *Morphometric evaluations of the regenerative effects of PEGylated HA-CaHA treatment. The statistically significant ($p<0.01$) increase in newly-formed collagen (type III) following treatment (lighter coloured bar) in comparison with the mature collagen type I (darker bar) is the result of a specific stimulation of fibroblasts to synthesize new collagen fibers for an effective renewal of the subdermal connective tissue.*

circular polarized light microscopy represents a useful method for the identification and characterization of collagen in human skin. This study demonstrated significant differences in collagen content between control skin and skin treated with subdermal injection of PEGylated HA-CaHA (26 mg/ml) + CaHA (1%) filler. It was possible to evaluate the content of mature collagen type I and the content of newly formed collagen type III. Differently from control samples, image analysis and computerized morphometry on samples from sites of PEGylated HA-CaHA filler injection demonstrated a predominance of birefringent fibres. It would now be of interest to use this sensitive method of visualizing new collagen to conduct further studies at longer time intervals between injection of PEGylated HA-CaHA and abdominoplasty surgery with biopsy withdrawal.

REFERENCES

1. Fisher GJ, Varani J, Voorhees JJ. Looking older: fibroblast collapse and therapeutic implications. Arch Dermatol 2008; 144:666-72.
2. Monticelli D, Martina V, Mocchi R, Rauso R,

Zerbinati U, Cipolla G, Zerbinati N. Chemical characterization of hydrogels crosslinked with polyethylene glycol for soft tissue augmentation. Maced J Med Sci 2019; 7(7):1077-81.

3. Hassan W, Dong Y, Wang W. Encapsulation and 3D culture of human adipose-derived stem cells in an in-situ crosslinked hybrid hydrogel composed of PEG-based hyperbranched copolymer and hyaluronic acid. Stem Cell Res Ther 2013; 4:32-43.
4. Zerbinati N, Lotti T, Monticelli D, et al. In vitro evaluation of the biosafety of hyaluronic acid PEG cross-linked with micromolecules of calcium hydroxyapatite in low concentration. J Med Sci 2018; 6(1):15-19.
5. Zerbinati N, Rauso R, Gonzalez P, et al. In vitro evaluation of collagen production on human fibroblasts treated with hyaluronic acid peg cross-linked with micromolecules of calcium hydroxyapatite in low concentration. J Biol Regul Homeost Agents 2017; 31(2 Suppl 2):87-90.
6. Cheng W, Yan-Hua R, Fang-Gang N, Guo-An Z. The content and ratio of type I and III collagen in skin differ with age and injury. Afr J Biotechnol 2011; 10:2524-29.
7. Yutskovskaya Y, Kogan E, Leshunov E. A randomized, split-face, histomorphologic study comparing a volumetric calcium hydroxylapatite and a hyaluronic acid-based dermal filler. J Drugs Dermatol 2014; 13:1047-52.
8. Van Loghem J, Yutskovskaya YA, Werschler WP. Calcium hydroxylapatite: over a decade of clinical experience. J Clin Aesthet Dermatol 2015; 8:38-49.
9. Courderot-Masuyer C, Robin S, Tauzin H, Humbert P. Evaluation of lifting and antiwrinkle effects of calcium hydroxylapatite filler. In vitro quantification of contractile forces of human wrinkle and normal aged fibroblasts treated with calcium hydroxylapatite. J Cosmet Dermatol 2016; 15:260-68.
10. Coleman KM, Voigts R, DeVore DP, Termin P, Coleman WP 3rd. Neocollagenesis after injection of calcium hydroxylapatite composition in a canine model. Dermatol Surg 2008; 34(Suppl 1):S53-55.
11. Berlin AL, Hussain M, Goldberg DJ. Calcium hydroxylapatite filler for facial rejuvenation: a histologic and immunohistochemical analysis. Dermatol Surg 2008; 34(Suppl 1):S64-S67.

JOURNAL OF BIOLOGICAL REGULATORS & HOMEOSTATIC AGENTS Vol. 33, no. 6, 1973-1979 (2019)

LETTER TO THE EDITOR

PROBIOTICS AND EPICOR® IN HUMAN HEALTH

F. INCHINGOLO[1*], L. SANTACROCE[2,3*], S. CANTORE[1,4], A. BALLINI[5,6,7], R. DEL PRETE[1], S. TOPI[3], R. SAINI[1], G. DIPALMA[1*] and R. ARRIGONI[8§]

[1]Department of Interdisciplinary Medicine, University of Bari "Aldo Moro", Bari, Italy; [2]Ionian Department, University of Bari "Aldo Moro", Bari, Italy; [3]School of Technical Medical Sciences, "A. Xhuvani" University, Elbasan, Albania; [4]Sorriso & Benessere Ricerca e Clinica S.r.l., Bari, Italy; [5]Department of Biosciences, Biotechnologies and Biopharmaceutics, Campus Universitario "Ernesto Quagliariello", University of Bari "Aldo Moro", Bari, Italy; [6]Department of Basic Medical Sciences, Neurosciences and Sense Organs, University of Bari Aldo Moro, Bari, Italy; [7]Department of Precision Medicine, University of Campania "Luigi Vanvitelli", Naples, Italy; [8]CNR Institute of Biomembranes, Bioenergetics and Molecular Biotechnologies (IBIOM), Bari, Italy

Received December 11, 2019 – Accepted December 16, 2019

**contributed equally to this work as co-first authors*
[§]*contributed equally to this work as co-last authors*

Altered gut microbiota may favor the production of effector over regulatory T cells, thereby disrupting the balance between them and contributing to the development of autoimmune disorders (1).

Probiotics are non-pathogenic microorganisms able to interact with the gut microbiota and provide health benefits; their use has recently been exploited to dampen immunological response in several experimental models of autoimmune diseases (2). Probiotics also have varying effects on the immune system during different stages of life and have different benefits for certain age groups, which is similar to how the microbiota in our gut is constantly changing over the course of life (1).

Lactobacilli and *Bifidobacteria* are the most common probiotics, and possess substantial health-promoting properties such as modulating the population and composition of gut microbiome and improving the intestinal barrier function (1-3). Furthermore, these microorganisms facilitate the production of metabolic parameters such as short-chain fatty acids (SCFAs) and reduce gut permeability which ultimately leads to improved immune responses and decreased inflammation (2).

Orally ingested probiotic bacteria are able to modulate the immune system. Conversely, alterations occur in the immunomodulatory properties of different probiotic strains. Prior studies achieved *in vitro* advise that EpiCor® fermentate has prebiotic-like properties, being able to positively benefit immonomodulation in non-vaccinated humans in terms of a meaningfully reduced incidence and length of cold and flu-like symptoms.

Therefore, the aim of the present study was to evaluate, in healthy adults, the effects of probiotic supplementation to the diet (*Hyperbiotics Immune*)

Key words: probiotic bacteria; prebiotics; synbiotics; human health; immunomodulation; translational medicine; dietary supplementation

Corresponding Author:
Andrea Ballini, D.M., M.Sc,
Department of Biosciences, Biotechnologies and Biopharmaceutics,
Campus Universitario "Ernesto Quagliariello",
University of Bari "Aldo Moro", 70124 Bari, Italy
Tel./fax: +39 0805448514
e-mail: andrea.ballini@me.com

0393-974X (2019)

on variations in the immune response through regulating some immunomodulation markers.

MATERIALS AND METHODS

Participants

This research was conducted in collaboration with the Elbasan University (School of Technical Medical Sciences, "A. Xhuvani"), Albania, and the University of Bari Aldo Moro as a randomized, double-blinded placebo-controlled study. The Institutional Ethics Committee of the Faculty of Technical Medical Sciences of Elbasan "Aleksandër Xhuvani" approved the application to conduct the clinical trial in the Faculty. Title of the Protocol: Probiotics efficacy and safety in humans. Protocol Identification: INTL_ALITCOOP/Probiotics/INRES2019_w/a/c.

A total of 20 healthy adult human volunteers (10 females and 10 males) with ages ranging from 30 to 50 years (mean age 42.7 years) were included in the study. Exclusion criteria were lactose intolerance, recent antibiotic treatment, frequent gastrointestinal disorders or metabolic diseases. The study was carried out according to the Helsinki declaration and informed written consent was obtained from all the subjects.

Experimental design

A randomized double-blind, placebo-controlled, parallel group design was used for this study. After completing baseline measures, participants were stratified by sex and randomized into one of two groups. The study consisted of three phases: a pre-treatment period (2 weeks/2 tablets twice per day), a treatment period (4 weeks/ 2 tablets once per day) and, finally, a wash-out period (2 weeks). The participants were asked not to alter their routine habits during the study and were randomly allocated to receive either a placebo (tablets looking similar but without probiotics) or tablets containing a specific targeted synbiotic (Hyperbiotics Immune), containing 5 different probiotic patented stains (*Lactobacillus plantarum*, *Lactobacillus acidophilus*, *Bifidobacterium infantis*, *Lactobacillus fermentum*, *Lactobacillus reuteri*), a prebiotic fructo-oligosaccharides (FOS), Vitamin C (500 mg), Echinacea (100 mg), and Chelated Zinc (10 mg), patented for LiveBac® manufacturing process, BIO-tract®, a protection and time-release delivery and EpiCor®, a fermented yeast superfood with antioxidant properties that have been clinically studied to support the immune system on multiple levels, soy free, gluten free, non-GMO. The tested formula contains 4 Billion Colony Forming Units per BIO-tract® pearl, which is equivalent to 60 Billion colony forming units (CFUs) of standard probiotic capsules.

Blood collection, immunoglobulin and leukocytes/lymphocytes (White blood cells, CD56+ natural killer cells) measurements

After an overnight fasting of at least 10 h, blood samples were taken using ethylenediaminetetraacetic acid (EDTA)-containing vacutainers from the volunteers just before and after the treatment period. All measurements were taken between the hours of 7:00 and 11:00 a.m. Blood was collected at baseline and at 8 weeks for immunoglobulin (IgA) and leukocytes/lymphocytes (White blood cells-WBC and CD56+ natural killer-NK cells) measurements.

Approximately 5 ml of blood were taken *via* vein puncture on each of the testing days from each participant and collected in a BD Vacutainer® (Becton Dickinson, Franklin Lakes, NJ, USA). The blood samples collected were centrifuged at 2500×g for 10 min, and the plasma was separated for serum biochemical analysis and stored at −80°C until analysis and compared if in the ranges of those for haematologically normal Caucasian adults.

Statistical analyses

The outcome values for Treated and Control groups were analysed using the a *t*-test for paired samples for pre–post differences with time as the factor and IBM Statistical Package for the Social Sciences (SPSS Inc. Version 16.0, Chicago, IL, USA) software to detect significant differences between pre-test and post-test scores.

RESULTS

To evaluate and study how and whether probiotics had a modulatory action on the human immune system, we performed a randomized study on 20 adult subjects aged between 30 and 50 years. The randomized study was completed through a computerized random number generator that selected 10 females and 10 males who were separated into two different groups. Group A was the experimental group (3 females and 7 males),

while group B was the control group (7 females and 3 males). The experimental group compared to the control group used probiotics during the study period. The study was divided into 3 phases. The first phase was before the treatment and lasted 2 weeks, the second phase lasted 4 weeks and was the treatment phase, and finally the last phase, the third, was the wash-out phase (2 weeks).

In light of the data analysis during the several phases of study, in the experimental group A it was highlighted that an increasing parameter was the WBC count, with a variation of 20%, compared to the values in the control group B in the different phases (Fig. 1 A-B). In particular, as shown in Fig. 1 B, we

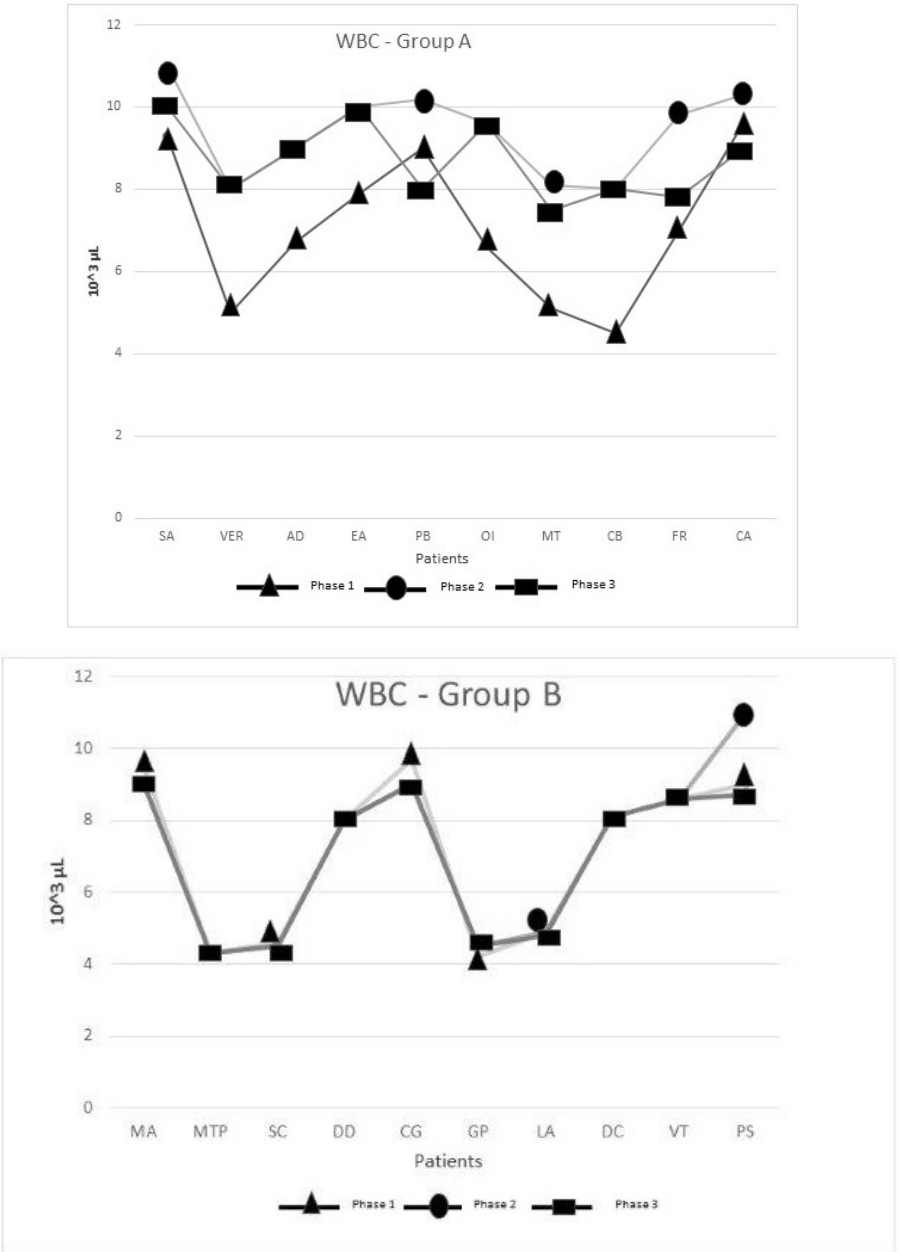

Fig. 1. ***A-B)*** *Comparative charts of Experimental/Treated (**A**) vs Placebo (**B**) groups. Blood levels were recorded from baseline to first two weeks (Phase 1) and after 4 weeks (Phase 2) and 2 wash-out weeks (Phase 3) of probiotic/placebo supplementation. In abscissa axis are shown both the patient's initials (proper name, family name) and in the ordinate axis the outcome (WBC count) value.*

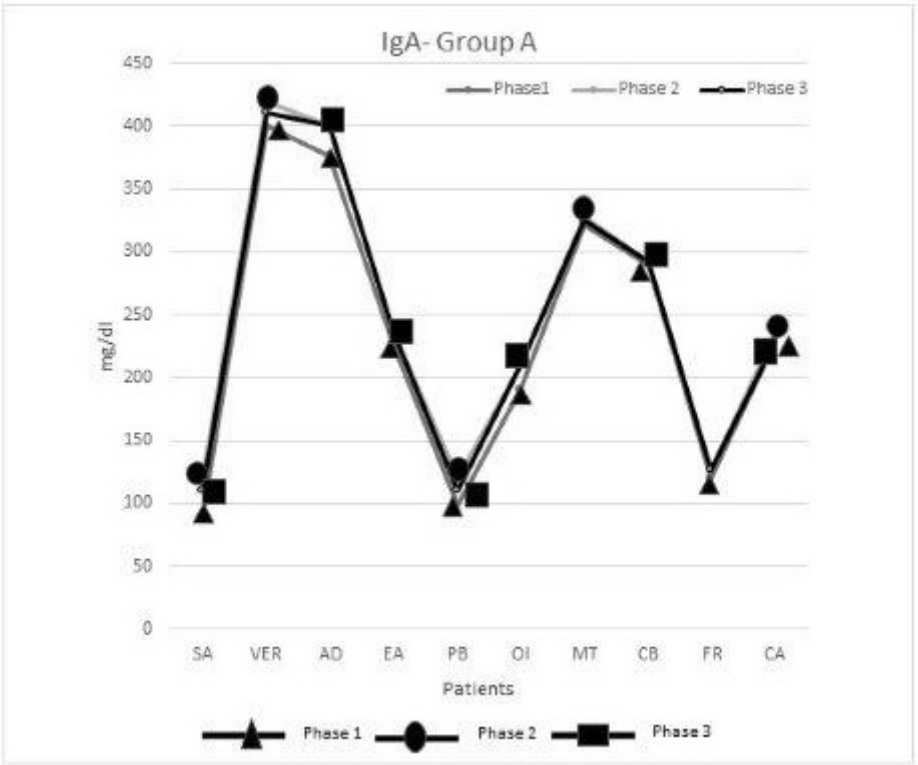

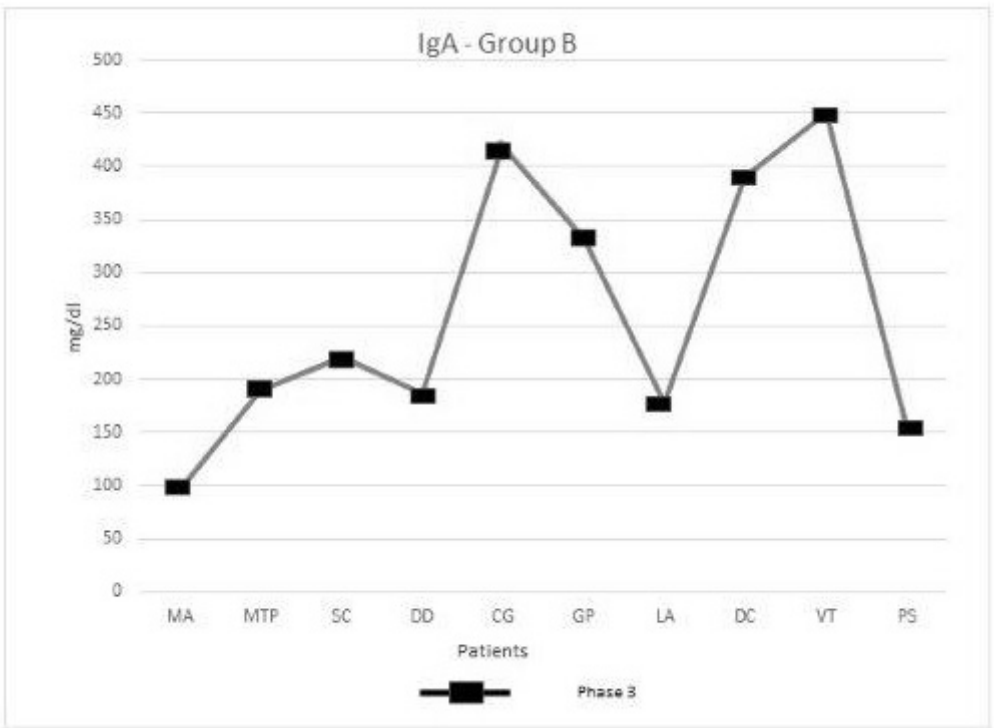

Fig. 2. ***A-B)*** *Comparative charts of Experimental/Treated (**A**) vs Placebo (**B**) groups. Blood levels were recorded from baseline to first two weeks (Phase 1) and after 4 weeks (Phase 2) and 2 wash-out weeks (Phase 3) of probiotic/placebo supplementation. In abscissa axis are shown both the patient's initials (proper name, family name) and in the ordinate axis the outcome (IgA levels) value.*

can state that in the control group the values remained unchanged, in fact, we found variations around 1%; only in the participating subject in phase 2, did we find an increase in WBC count which was, however, within the normal parameters in phase 3. Another value taken into consideration in both groups was IgA. Fig. 2 A-B shows a stationary condition in the control group B in the different phases with a variation of 0.2%, while there was an increase in the levels of IgA (≈ 5%) in the experimental group in phase 2 supportive of the data that the use of probiotics induces the increase of cells producing IgA.

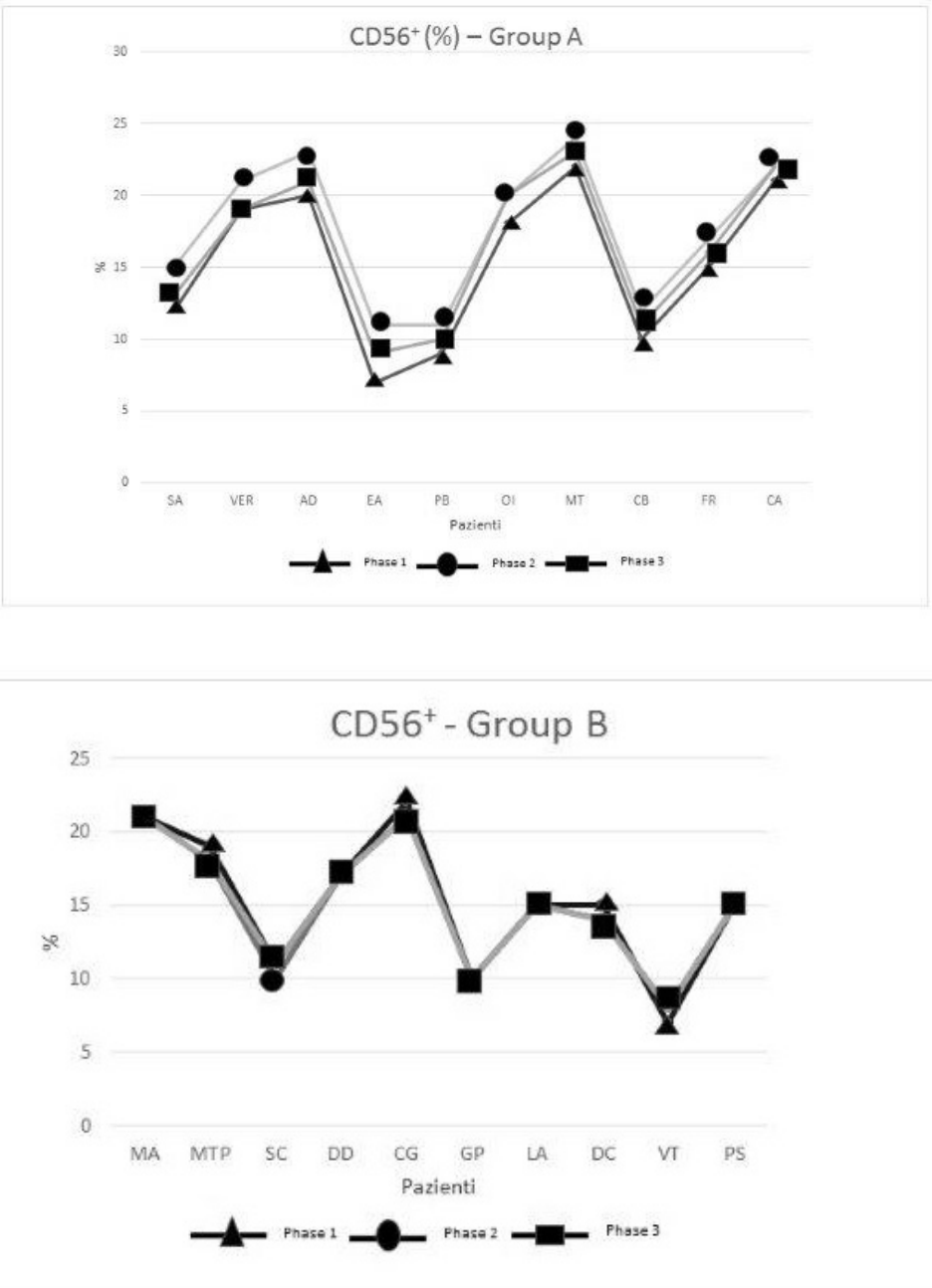

Fig. 3. ***A-B****) Comparative charts of Experimental/Treated (****A****) vs Placebo (****B****) groups. Blood levels were recorded from baseline to first two weeks (Phase 1) and after 4 weeks (Phase 2) and 2 wash-out weeks (Phase 3) of probiotic/placebo supplementation. In abscissa axis are shown both the patient's initials (proper name, family name) and in the ordinate axis the outcome (CD56⁺ count) value.*

Because several sub-populations belong to immuno-modulatory response, we took into consideration lymphocytes and, in particular, $CD56^+$ natural killer cells. Notably, in the experimental group (A) at different phases, an increase of 10%in the levels of natural killer $CD56^+$ cells can be seen, probably because the intake of targeted probiotics induces an increase in lymphocytes and NK-cells (Fig. 3 A-B). Moreover, no adverse events were reported as a result of the active or placebo treatment, or as a result of the study procedures.

DISCUSSION

The potential impact of the therapeutic effect of probiotics on a dysbiotic situation could not be seen without taking into consideration a change of lifestyle. Diet habits, stress, poor health conditions, and lack of exercise can significantly impact the microbiota stability (1-3).

In recent years, scientific studies have focused on the anti-carcinogenic effects of natural substances, such as probiotics (4). In particular, these studies were aimed at developing an effective drug with the lowest possible side effects (5). The most common risk factors for cancer include tobacco, alcohol, obesity, chronic virus infections, chemicals (6), environmental toxins, ionizing radiation and hormonal changes (7-10). In the current decade, intensive cancer research involving genomics and proteomics has improved the knowledge regarding cancer as well as promoting public awareness (11, 12). As not all probiotics are helpful in overall conditions, a careful selection of proper strains of bacteria established for the desired clinical outcome is of vital importance. Therefore, we selected a combination of *Lactobacillus plantarum*, *Lactobacillus acidophilus*, *Bifidobacterium infantis*, *Lactobacillus fermentum*, *Lactobacillus reuteri*) a prebiotic FOS, Vitamin C (500 mg), Echinacea (100 mg), and Chelated Zinc (10 mg), patented for EpiCor®, which have been shown in the current literature to improve health outcomes in humans, according to our findings (1). Our study has several limitations. Firstly, we have limited cases with many stronger outcomes. Secondly, there is a lack of fecal microbiome analysis. Since the gut microbiota of humans is highly variable, this may affect the response of subjects to the probiotic. The strength of this study lies in the selection of a product containing the strains of probiotics in addition to EpiCor® that have been indicated in previous studies to affect overall health. Probiotics act on a wide variety of cells in the intestine to modulate the immune system towards a pro-or anti-inflammatory action, depending on the strain, setting and immunological parameters measured, and the type of cells being acted upon. It is necessary to further evaluate potential changes in the gut microbiota composition that may occur following the immunomodulatory effects of these probiotic strains in humans.

REFERENCES

1. Ballini A, Santacroce L, Cantore S, et al. Probiotics efficacy on oxidative stress values in inflammatory bowel disease: a randomized double-blinded placebo-controlled pilot study. Endocr Metab Immune Disord Drug Targets 2019; 19:373-81.
2. Campanella V, Syed J, Santacroce L, Saini R, Ballini A, Inchingolo F. Oral probiotics influence oral and respiratory tract infections in pediatric population: a randomized double-blinded placebo-controlled pilot study. Eur Rev Med Pharmacol Sci 2018; 22:8034-41.
3. Ballini A, Gnoni A, De Vito D, et al. Effect of probiotics on the occurrence of nutrition absorption capacities in healthy children: a randomized double-blinded placebo-controlled pilot study. Eur Rev Med Pharmacol Sci 2019; 23:8645-57.
4. Beleford D, Liu Z, Rattan R, et al. Methylation induced gene silencing of HtrA3 in smoking-related lung cancer. Clin Cancer Res 2010; 16:398-409.
5. Boccellino M, Cuccovillo F, Napolitano M, et al. Styrene-7,8-oxide activates a complex apoptotic response in neuronal PC12 cell line. Carcinogenesis 2003; 24:535-40.
6. Di Domenico M, Pinto F, Quagliuolo L, et al. The Role of Oxidative Stress and Hormones in Controlling Obesity. Front Endocrinol (Lausanne) 2019 13; 10:540.
7. Boccellino M, Alaia C, Misso G, et al. Gene interference strategies as a new tool for the treatment of prostate cancer. Endocrine 2015; 49:588-605.

8. Ricci S, Pinto F, Auletta A, et al. The enigmatic role of matrix metalloproteinases in epithelial-to-mesenchymal transition of oral squamous cell carcinoma: Implications and nutraceutical aspects. J Cell Biochem 2019; doi: 10.1002/jcb.26905. [Epub ahead of print].
9. Vanacore D, Messina G, Lama S, et al. Effect of restriction vegan diet's on muscle mass, oxidative status, and myocytes differentiation: A pilot study. J Cell Physiol 2018; 233:9345-53.
10. Giudice A, Montella M, Boccellino M, et al. epigenetic changes induced by green tea catechins are associated with prostate cancer. Curr Mol Med 2017; 17:405-20.
11. Cardillo I, Spugnini EP, Galluzzo P, et al. Functional and pharmacodynamic evaluation of metronomic cyclophosphamide and docetaxel regimen in castration-resistant prostate cancer. Future Oncol 2013; 9:1375-88.
12. Boccellino M, Pinto F, Ieluzzi V, et al. Proteomics analysis of human serum of patients with non-small-cell lung cancer reveals proteins as diagnostic biomarker candidates. J Cell Physiol 2019; 234:23798-806.

SCIENTIFIC METHODS IN DENTAL RESEARCH: CRITICAL ANALYSIS OF THE LITERATURE AND EXPERT OPINION ON THE MATTER

G. SPAGNUOLO[1*], A. VALLETTA[1*], M. SIMEONE[1], F. RICCITIELLO[1], C. RENGO[2] and L. FORTUNATO[3]

[1]Department of Neurosciences, Reproductive and Odontostomatological Sciences, University of Napoli Federico II, Naples, Italy; [2]Department of Prosthodontics and Dental Materials, School of Dental Medicine, University of Siena, Siena, Italy; [3]Department of Health Sciences, Università Magna Graecia, Catanzaro, Italy

Received November 1, 2019 – Accepted November 28, 2019

[*]These authors equally contributed to this article

To the Editor,

Recently, dentistry topics have been well reported in the scientific literature (1), however, the general impact and presence of dentistry within top-class scientific journals is still weak. Typically, the scientific dental community is quite heterogeneous: in fact, it involves dentists, academics, scientists and students. On the contrary, the number of dental journals is scarce, as is their impact factor.

Researchers certainly know that the Impact Factor (IF) is one of the most influential indicators: recently, a worldwide debated topic was related to the aim of describing the overall quality of a scientific journal and whether the IF unquestionably defines the scientific reputation of a journal within the scientific community.

Currently, the highest impact factor reported in the ISI-category of 'Dentistry' has been attributed to the journal "Periodontology 2000" with IF 6.22. On the other hand, in the ISI-category of 'Oncology', the IF reaches higher values: for example, the journal "CA Cancer J Clin" reaches an IF 244.59. In this context, do we really assume that oncology-related topics are somewhat 30 times more interesting than dentistry?

Of course, different disciplines may have different ways to communicate, publish and share their topics; moreover, high-impact journals are more likely to be cited by several scientists in different fields. The interest in dentistry-related publications strongly depends on the quality of the data obtained, and on the potential clinical applications of such data; in this light, dentistry urges to link its topics to biosciences, to general medicine, and even to basic research (2).

In the present study, we searched the key word "dentistry" on PubMed, to assess whether the selected articles were related to dental sciences or to different matters.

MATERIALS AND METHODS

Searching strategy

We analyzed the impact of the key word "dentistry" in the title, in the abstract, and in the main text of articles published in top-journals previously selected: the main aim was to evaluate whether the topic discussed in these articles was relevant or not to dental fields. Searching for

Key words: dentistry; evidence-based medicine; dental journals; scientific research; dental education

Corresponding Author:
Prof. Leonzio Fortunato,
Head of the Dental School,
Department of Health Sciences,
Università Magna Graecia, Catanzaro, Italy
Tel.: +39 0961 712401 - Fax: +39 0961 712402
e-mail: prof.fortunatoleo@libero.it

0393-974X (2019)

the key word "dentistry" and "journal name" [journal] in PubMed, we analyzed all the items reported. Eight highly-impacted journals were considered in our research, as they represent a balanced selection of high-impact journals and those most recognized worldwide. We first debated to include top dental journals such as "Journal of Dental Research", "Dental Materials" and so on; however, we felt that those journals are certainly committed and well focused on dentistry. Thus, we decided only to investigate the following journals:

- JADA (Journal of the American Dental Association) ISSN: 0002-8177
- PLOS One (Public Library of Science) ISSN: 1932-6203
- Nature ISSN: 1476-4687
- Science ISSN: 1095-9203
- JAMA (Journal Of The American Medical Association) ISSN: 0002-9955
- PLOS Medicine ISSN: 1549-1277
- JCI (Journal Clinical Investigation) ISSN: 0021-9738
- Scientific Reports ISSN:2045-2322

The time frame of the selected articles ranged from 1973 to 2018.

The main criterium for selecting a scientific journal was its impact factor, and its overall impact to the scientific community: the 2017 Journal Citation Report (JCR) total Impact Factor of the journals selected in this investigation was 164.9.

RESULTS

The analysis of the 8 selected journals showed that the key word "Dentistry" was reported in 13,473 articles, however, only 767 articles reported such key word in the title and only 232 articles reported it in the abstract (Table I).

With the aim of understanding the overall impact of the dental sciences in the journal "Nature", we searched for the key word "dentistry" AND "Nature" [journal] on PubMed: 101 items were reported. Surprisingly, after a brief reading of the titles and the abstracts related to these 101 selected articles, we found that none of them really focused on dentistry until 1986.

The same research was carried out for the journal "JAMA" which reported the word "dentistry" in 225 published articles, only 5 of which reported such word in the title.

Our further analyses showed that the highest percentage of articles reporting the key word "Dentistry" belonged to the journal "JADA", undoubtedly one of the most important journals typically focused on dentistry; JADA reported 9,562 articles and 743 titles containing the key word "Dentistry".

The data obtained from the journal "PLOS One" were particularly suggestive about the substantiation of our starting hypothesis; in fact, we found 2,365 articles, but only six titles contained the key word "Dentistry".

We found extremely interesting the analysis made on the key word "dentistry" AND "Science" [journal] in PubMed: in fact, only 118 items were reported, and after a brief reading of the titles and the abstracts of these 118 selected articles, we deduced that none of them were really related to dentistry

Table I. *The key word "Dentistry" has been reported in the main text, in the title or in the abstract of scientific publications of the journals selected for this research.*

Journals	Dentistry - main text	Dentistry - title	Dentistry - abstract
JADA	9562	743	218
PLOS ONE	2365	6	12
NATURE	101	1	1
SCIENCE	118	12	0
JAMA	225	5	1
PLOS MEDICINE	35	0	0
JCI	145	0	0
SCIENTIFIC REPORTS	922	0	0

until the year 2012. In this case, the articles were mainly focused on molecular biology or forensic medicine, even to paleontology, but relatively few were closely related to dental fields.

Finally, no article and no title containing the key word "Dentistry" was found in the journals "JCI", "PLOS Medicine" and "Scientific Reports".

After this preliminary screening, we investigated the presence of the key word "Dentistry" in the abstract of those articles reporting the key word "Dentistry" in their title. Following a careful analysis, we found 232 abstracts containing the key word "Dentistry", although we must report that some articles reported no available abstract on PubMed and PMC.

In a further step, we critically read the whole text of articles containing the key word "Dentistry" both in the title and in the abstract. The results clearly show that the highest percentage of these articles was focused on "new concepts in dentistry" and "innovative techniques and materials", highlighting how the research and development (R&D) themes are undoubtedly the most appreciated by editors and readers.

Table II. *Topics summarized in macro-categories.*

	JADA	PLOS ONE	NATURE	SCIENCE	JAMA	PLOS MED	JCI	SCI REP
Evolution of dentistry	25	/	/	/	/	/	/	/
Women in dentistry	6	/	/	/	/	/	/	/
New concepts in dentistry	123	/	1	9	2	/	/	/
Guidelines in dentistry	29	2	/	/	/	/	/	/
Preventive and community dentistry	47	/	/	/	/	/	/	/
Oral diseases	12	/	/	/	2	/	/	/
Dentistry and systemic diseases	39	/	/	/	/	/	/	/
Innovative techniques and materials	91	/	/	1	1	/	/	/
Use of drugs in dentistry	20	/	/	/	/	/	/	/
Non-invasive dentistry	5	/	/	/	/	/	/	/
Aesthetic dentistry	21	/	/	/	/	/	/	/
International protocols	52	1	/	/	/	/	/	/
Adverse reactions and technical errors in dentistry	7	2	/	/	/	/	/	/
Dietology and dentistry	4	/	/	/	/	/	/	/
Anesthesiology	12	/	/	/	/	/	/	/
Clinical dentistry	30	/	/	/	/	/	/	/
Pediatric dentistry	5	1	/	/	/	/	/	/
Dentistry and laws	14	/	/	/	/	/	/	/
Ethics in dental research	7	/	/	/	/	/	/	/
Evolution of dental specialties	37	/	/	1	/	/	/	/
Public and private dentistry	8	/	/	/	/	/	/	/
Dentistry and social media	29	/	/	/	/	/	/	/

Moderate interest has also been reported for articles dealing with the "evolution of dentistry": these articles typically emphasize the history of dentistry and on the state of the art of the traditional techniques and technologies in the dental field.

Although we found that the topics related to "general dentistry" were mainly reported in JADA articles, we have tried to summarize the other topics most represented published in the selected journals. Table II shows the different topics distributed within the selected articles (Table II).

DISCUSSION

In our article, we have tried to understand whether dentistry-related topics are substantially represented in the top journals. For this purpose, we selected only articles reporting the key word "dentistry". After a careful analysis, we assessed that these articles mainly focused on matters belonging to the categories of "Evolution of dentistry and general concepts" and "Innovative techniques and materials". Such articles reported some interesting concepts related to innovation in dentistry, and the way in which dentistry has improved over past years thanks to the discovery of new biomaterials and novel techniques.

Few articles were focused on clinical research in dentistry, while several articles were focused on severe infections, bacteria superinfections, novel allergens, and acute respiratory diseases in dentistry, reporting authoritative considerations on air pollution and substances that daily pollute water and air.

The less-impacting articles were based on the use of 3D CAD/CAM-based digital technologies in implant dentistry (3).

We noticed that decayed teeth still represent a social and healthcare issue in many countries (4). We believe, on the other hand, that several impacting topics could be of interest for the general population, such as several diseases still frequently affecting oral health (5), or the use of stem cells for the growing branch of regenerative dentistry (6, 7). Of course, we do understand that dentistry is of interest mainly to dentists or to emerging dental journals (8), but the real challenge is to make dentistry attractive also with such closely related topics.

In our work, we have analyzed the prevalence and the overall coherence of the key word "dentistry" in some top-class journals. Nowadays, clinical dentistry is mainly focused on topics of general interest, such as bone scaffolds or osteonecrosis after oral surgery or the impact of syndromes on clinical management (9, 10). The interest of patients, on the other hand, is currently on aesthetic dentistry (11) and stem cells for biomedical applications (12).

A novel and safe evidence-based practice in dentistry would be the main and most reliable way for ensuring the scientific growth of this medical science in the near future. After our study, we provocatorily launched an overall alert on the scientific quality of dental research to the dental scientific community. In fact, despite dentistry being the subject for several research topics, it is possible that "dentistry-related" topics are still not interesting enough to reach a wider number of readers and to attract more attention from top-journals. Our opinion is that the truth is between the two: although the most debated topics in dentistry are still heavily related to clinical aspects, sometimes "exceptionally" overestimated and overestimated, it is equally true that some novel concepts, such as "regenerative dentistry" or "nanodentistry" have merits. Of course, we hope to see a general improvement of this trend in the near future.

REFERENCES

1. Kerativitayanan P, Tatullo M, Khariton M, Joshi P, Perniconi B, Gaharwar AK. Nanoengineered osteoinductive and elastomeric scaffolds for bone tissue engineering. ACS Biomat Sci & Eng 2017; 3(4):590-600.
2. Tse H. A possible way out of the impact-factor game. Nature 2008; 454:938-39.
3. Marrelli M, Maletta C, Inchingolo F, Alfano M, Tatullo M. Three-point bending tests of zirconia core/veneer ceramics for dental restorations. Int J Dent 2013; 2013:831976.
4. Cheifetz ID. AAOMS challenges AMA data series comments on OMS, dentistry. J Am Dent Assoc 2010; 141(6):617-18.
5. Inchingolo F, Tatullo M, Abenavoli FM, Marrelli M, Inchingolo AD, Inchingolo AM, Dipalma G. Non-

Hodgkin lymphoma affecting the tongue: unusual intra-oral location. Head Neck Oncol 2011; 3:1.
6. Paduano F, Marrelli M, Alom N, Amer M, White LJ, Shakesheff KM, Tatullo M. Decellularized bone extracellular matrix and human dental pulp stem cells as a construct for bone regeneration. J Biomater Sci Polym Ed 2017; 28:730-48.
7. Tatullo M, Marrelli M, Scacco S, et al. Relationship between oxidative stress and "burning mouth syndrome" in female patients: a scientific hypothesis. Eur Rev Med Pharmacol Sci 2012; 16(9):1218-21.
8. Paduano S, Uomo R, Amato M, Riccitiello F, Simeone M, Valletta R. Cyst-like periapical lesion healing in an orthodontic patient: A case report with five-year follow-up. G Ital Endod 2013; 27:95-104.
9. Giudice A, Bennardo F, Barone S, Antonelli A, Figliuzzi MM, Fortunato L. Can autofluorescence guide surgeons in the treatment of medication-related osteonecrosis of the jaw? A prospective feasibility study. J Oral Maxillofac Surg 2018; 76:982-95.
10. Inchingolo F, Tatullo M, Marrelli M, et al. Regenerative surgery performed with platelet-rich plasma used in sinus lift elevation before dental implant surgery: an useful aid in healing and regeneration of bone tissue. Eur Rev Med Pharmacol Sci 2012; 16(9):1222-26.
11. Inchingolo F, Tatullo M, Abenavoli FM, et al. Oral piercing and oral diseases: a short time retrospective study. Int J Med Sci 2011; 8:649-52.
12. Paduano F, Marrelli M, Amantea M, et al. Adipose tissue as a strategic source of mesenchymal stem cells in bone regeneration: A topical review on the most promising craniomaxillofacial applications. Int J Mol Sci 2017; 18.